



HAL
open science

Balearic Promontory architecture and history during the formation of the Mediterranean Salt Giant

Fadl Raad

► **To cite this version:**

Fadl Raad. Balearic Promontory architecture and history during the formation of the Mediterranean Salt Giant. Earth Sciences. Université de Montpellier, 2022. English. NNT : 2022UMONG018 . tel-03844128

HAL Id: tel-03844128

<https://theses.hal.science/tel-03844128v1>

Submitted on 8 Nov 2022

HAL is a multi-disciplinary open access archive for the deposit and dissemination of scientific research documents, whether they are published or not. The documents may come from teaching and research institutions in France or abroad, or from public or private research centers.

L'archive ouverte pluridisciplinaire **HAL**, est destinée au dépôt et à la diffusion de documents scientifiques de niveau recherche, publiés ou non, émanant des établissements d'enseignement et de recherche français ou étrangers, des laboratoires publics ou privés.

THÈSE POUR OBTENIR LE GRADE DE DOCTEUR DE L'UNIVERSITÉ DE MONTPELLIER

En Science de la Terre

École doctorale GAIA

Unité de recherche Géosciences Montpellier

Balearic Promontory architecture and history during the formation of the Mediterranean Salt Giant

Présentée par Fadl RAAD

Le 01 Avril 2022

Sous la direction de Johanna LOFI
et Agnès MAILLARD-LENOIR

Devant le jury composé de

William B. F. RYAN, Special Scientist, Lamont-Doherty Earth Observatory

Lies LONCKE, Maître de conférence, Université de Perpignan

Giovanni ALOISI, Directeur de Recherche, IGP Paris

Wout KRIJGSMAN, Professor, Utrecht University

Rachel FLECKER, Full professor, University of Bristol

Jacques DÉVERCHÈRE, Professeur, Université de Bretagne Occidentale

Johanna LOFI, Maître de conférence, GM, Université de Montpellier

Agnès MAILLARD-LENOIR, Maître de conférence, Université Toulouse III

Rapporteur

Rapporteuse

Examineur

Examineur

Examinatrice

Examineur

Directrice de thèse

Co-directrice de thèse



UNIVERSITÉ
DE MONTPELLIER



UNIVERSITÉ DE
MONTPELLIER

Géosciences
Montpellier



UNIVERSITÉ
TOULOUSE III
PAUL SABATIER
Université
de Toulouse

GÉOSCIENCES
ENVIRONNEMENT
TOULOUSE

SALT GIANT

This research is carried out under the SALTGIANT ETN, a European project funded by the European Union's Horizon 2020 research and innovation program under the Marie Skłodowska-Curie grant agreement number 765256

In memory of my mother Mariam

Mama, I had never imagined for one moment that this day would come and you are not there standing by my side. In every moment, in happiness and sadness, in highs and lows, in front of every decision and in every place I go, you were, you are and you will always be in my mind. I miss you and I will continue to make you proud, until we meet again.

Table of contents

Table of contents	ii
Acknowledgments.....	ix
The SaltGiant ETN	xiii
Abstract.....	xviii
Résumé	xx
Introduction	1
Chapter 1 - The Messinian Salinity Crisis: state of art.....	15
1.1 Timing and Chronology of the MSC events.....	18
1.2 The MSC Basins, Units and Surfaces	22
1.2.1 Pre-MSC (Lower Messinian) record	24
1.2.2 Onshore MSC Record	24
1.2.2.1 The Primary Lower Gypsum (PLG) and its time-lateral equivalents	25
1.2.2.2 The Resedimented Lower Gypsum (RLG).....	28
1.2.2.3 The Salt Unit.....	30
1.2.2.4 The Upper Evaporites Unit and Lago Mare.....	33
1.2.2.4.1 The Upper Evaporites (UE).....	34
1.2.2.4.2 The Lago Mare	34
1.2.3 Offshore MSC Record.....	35
1.2.4 The MSC offshore Surfaces	37
1.2.4.1 Margin Erosion Surface	37
1.2.4.2 Bottom Surface (BS) and Bottom Erosion Surface (BES).....	38
1.2.4.3 Intermediate Erosion Surfaces (IES).....	39
1.2.4.4 Top Surface (TS) and Top Erosion Surface (TES)	39
1.2.5 The MSC offshore Units	43
1.2.5.1 The Lower Unit (LU)	43
1.2.5.2 The Mobile Unit (MU)	44
1.2.5.3 The Upper Unit (UU)	46
1.2.5.4 The Complex Unit (CU).....	48
1.2.5.5 The Bedded Unit (BU)	48
1.3 Amplitude and Timing of the MSC drawdown: The major controversy	49
1.3.1 Amplitude of the MSC drawdown: Pros and Cons.....	49

1.3.2	Timing and duration of the MSC drawdown.....	50
Chapter 2	- Geological Setting and Tectonic Evolution of the Balearic Promontory	55
2.1	The Balearic Promontory in the context of the Western Mediterranean Basin's Geodynamics.....	56
2.1.1	Geodynamic settings of the Western Mediterranean basins.....	57
2.1.2	Formation and tectonic evolution of the Balearic Promontory.....	60
2.1.2.1	Oligo-Miocene Betic-Orogen Compressional Phase	61
2.1.2.2	Oligo-Miocene Extensional Phase.....	64
2.1.2.3	Late Miocene post-Orogenic Extensional Phase.....	66
2.1.2.4	Recent Reactivation of the Balearic Promontory	68
2.1.3	Stratigraphy and depositional environments of the Balearic Promontory.....	69
2.1.3.1	Onshore Stratigraphy.....	69
2.1.3.2	Offshore Stratigraphy.....	73
2.1.4	Present-day physiography of the Balearic Promontory.....	74
2.2	The Messinian Salinity Crisis in the Balearic Promontory.....	79
2.2.1	MSC in the offshore domain	79
2.2.2	MSC in the onshore domain.....	85
Chapter 3	- Data and Methods	89
3.1	Seismic reflection data and interpretation.....	90
3.1.1	The seismic reflection dataset	90
3.1.1.1	Industrial seismic profiles	93
3.1.1.2	Academic seismic profiles	98
3.1.2	Seismic Data Interpretation	102
3.1.2.1	Horizon picking and seismic facies analysis	102
3.1.2.2	Surface mapping and time-depth conversion.....	105
3.1.2.2.1	Creation of time maps	105
3.1.2.2.2	Time to depth conversion.....	108
3.2	Backstripping analysis	110
3.2.1	Isostasy, flexure and effective elastic thickness	110
3.2.2	Backstripping in the Balearic Promontory (Western Mediterranean).....	113
3.2.2.1	2D Restoration and Backstripping.....	115
3.2.2.1.1	Simple shear structural restoration (2D kinematic modelling) – step 3.....	116
3.2.2.1.2	Deflection due to mass movement along faults – step 4	117
3.2.2.2	Pseudo-3D Backstripping – step 5.....	119
3.2.2.2.1	Seismic-derived data input	120
3.2.2.2.2	Sediment unloading and decompaction.....	121

3.3	Modelling evaporites deposition	124
3.3.1	Modelling fluxes in the Central Mallorca Depression.....	126
3.3.1.1	Volume and budget calculations (Blocked outflow) – Approach 1.....	128
3.3.1.2	Two-way exchange between the CMD and Mediterranean – Approach 2	131
Chapter 4 - The Distribution, Nature and Origin of the MSC Units (BUs and Salt) of the Balearic Promontory: A Preliminary Scenario		135
4.1	Introduction: Messinian Salinity Crisis and Intermediate Basins.....	138
4.2	Geological background of the study areas.....	142
4.2.1	The Balearic Promontory: Tectonics, Architecture and Messinian Salinity Crisis...	142
4.2.1.1	MSC in the surrounding deep basins	143
4.2.1.2	MSC in the Balearic Promontory.....	144
4.2.2	The Sicilian Central Caltanissetta Basin: Geological context and MSC	148
4.3	Data and Methods	153
4.4	Results: MSC markers of the CMD/BP	154
4.4.1	Bedded unit 1 (BU1).....	155
4.4.2	Bedded Unit 2 (BU2)	157
4.4.3	Salt Unit.....	158
4.4.4	Bedded Unit 3 (BU3)	159
4.5	Interpretation/Discussion	160
4.5.1	Sicily vs Balearic Promontory: depositional units, surfaces and geometries.....	160
4.5.1.1	Geometry Similarities:.....	161
4.5.1.2	Facies Similarities:	162
4.5.2	CMD stratigraphy and relative chronology.....	169
4.5.2.1	Bedded Unit 1 (BU1)	169
4.5.2.2	Bedded Unit 2 (BU2)	171
4.5.2.3	Salt Unit.....	172
4.5.2.4	Bedded Unit 3 (BU3)	173
4.5.3	Depositional scenario in the CMD and associated regional consequences.....	174
4.6	Conclusions	177
Chapter 5 - Post-Messinian Salinity Crisis Tectonics in the Balearic Promontory: The Case Study of the Central Mallorca Depression		181
5.1	Introduction	183
5.2	Geological and Morphological Setting.....	185
5.2.1	Physiography of the Study Area.....	185
5.2.2	Regional Geological Setting and Late Oligocene to Miocene Tectonics	187
5.2.3	Onland Neogene Geological and Tectonic Record.....	188

5.2.4	Present-day Tectonics	190
5.3	Dataset and Methodology	191
5.3.1	Offshore Seismic Dataset	191
5.3.2	Backstripping.....	192
5.4	Results and Interpretation	194
5.4.1	Offshore Seismic Stratigraphy and Main Units	194
5.4.2	Offshore Deformation.....	196
5.4.2.1	Post-Messinian Deformation	196
5.4.2.2	Chronology of the Deformation.....	201
5.4.2.2.1	Remobilization of Former Structures.....	201
5.4.2.2.2	Plio-Quaternary Deformations	204
5.4.2.3	Role of Plio-Quaternary charge in the Vertical Movements.....	206
5.4.3	Land-Sea Correlation and Interpretation.....	207
5.4.3.1	Structural Continuity and Comparison	207
5.4.3.2	Structural Interpretation.....	210
5.4.3.3	Identification of the Units and Dating of Deformation.....	213
5.5	Discussion.....	216
5.5.1	Regional Extension of the Corridors	217
5.5.2	Regional Scheme, Relation with the Emile Baudot Escarpment.....	219
5.6	Conclusion.....	225
Chapter 6 - Paleo-Topography of the Balearic Promontory: A Regional Flexural Isostatic Restoration		229
6.1	Introduction	231
6.2	Geodynamic Setting	235
6.2.1	Tectonic Setting.....	235
6.2.2	Volcanism.....	236
6.2.3	Messinian Salinity Crisis Stratigraphy	236
6.3	Data and Methods	241
6.3.1	Paleo-shoreline Markers and Tested Scenarios.....	241
6.3.2	Flexural-Isostatic Backstripping	242
6.4	Results.....	248
6.4.1	Thermal Subsidence	248
6.4.2	Effective Elastic Thickness.....	249
6.4.3	Sensitivity of Paleo-Topography to EET	249
6.4.4	Sensitivity of Paleo-Shoreline Position to Water Level.....	250
6.4.5	Reference Model.....	255

6.5	Discussion.....	257
6.6	Conclusions	267
	Appendix 6-A.....	269
	Appendix 6-B.....	271
	Appendix 6-C.....	272
	Chapter 7 - Modelling of the evaporites deposition in the Central Mallorca Depression	
	277
7.1	Introduction	280
7.2	Geological Background	283
7.2.1	The Central Mallorca Depression: Present-day vs paleo-topography	284
7.2.2	Present-day Hydrography and Water Masses in the Central Mallorca Depression.....	285
7.2.3	Messinian Salinity Crisis in the Central Mallorca Depression	285
7.3	Data and Methods	287
7.3.1	Seismic dataset and volume calculations	287
7.3.2	Numerical model.....	288
7.4	Results	296
7.4.1	Volume considerations	296
7.4.2	Desiccation of an isolated basin.....	299
7.4.3	Full basin, inflow only.....	301
7.4.4	Two-way exchange.....	304
7.4.5	Precipitation of gypsum	306
7.5	Discussion.....	308
7.5.1	The pre-halite lower gypsum in the CMD: Stage 1 of the MSC	309
7.5.2	Halite in the CMD: Stage 2 of the MSC	313
7.6	Conclusions	320
	Chapter 8 - Conclusions and Perspectives	324
8.1	Conclusions	325
8.2	Perspectives	332
	References	344
	Annex A	418
	Annex B	468
	Annex C	482

Acknowledgments

I anticipate my gratitude to the jury members that are going to read this thesis. Bill Ryan, Lies Loncke, Giovanni Aloisi, Wout Krijgsman, Rachel Flecker and Jacques Déverchère; thank you all for accepting to be part of my defense jury and I hope you find it acceptable and not very long or difficult to read. I take the opportunity to thank Bill Ryan for his continuous constructive comments in the reviews of some of my published papers, and to Jacques Déverchère for the follow up during the annual ‘comité de thèse’ in the past three years.

This thesis has been a long journey and as any other journey, it had many ups and downs, sleepless nights and unforgettable moments. It is only with the presence and support of many people around me that I was able to achieve and terminate the journey.

First things first, the best seismic stratigrapher and supervisor ever, Johanna Lofi. I could have never asked for a better person, calm, knowledgeable and open minded, to follow and look after my project. I am so grateful for you Johanna, thankful for the countless things that I learned from you, and proud to be your first PhD student. You welcomed me with baby Lou at the beginning of the project, got your permanent position in between, and now ending the PhD with baby Malo arriving. I am extremely happy for all of your personal and professional achievements, and hope to work more together in the future.

To the most science-passionate person I’ve ever known, Agnes Maillard. I cannot express how much I enjoyed and appreciated working and discussing with you, and especially reading your comments on my work (I always have a smile on my face when reading them). As I always told you, I wish that we could continue collaborating as long as possible and I am sure that we could produce a dozen of articles per year. Thank you for everything Agnes.

Special thanks to Philippe Pezard. I enjoyed all our conversations and discussions that went beyond science, especially the football related ones. Our trip to Sorbas is something unforgettable for me with all the adventures that we had in those two weeks. I am very grateful for you to have taught me not only the principles of borehole logging, but also all the history of your career in the profession. I wish you as much CDDs as you desire, ‘à la libanaise’.

Many thanks to all the TMP team members, especially Giles and Laurent for the joyful logging moments and the support in my first logging missions. I am grateful to the administration team

at Geosciences Montpellier, especially Valerie Laurent and Helene Ournat for their perfect reception and help mainly in times where I did not understand a word of French.

Big thanks to all the PhD students and post-docs at Geosciences Montpellier for sharing a lot of funny moments in and outside the lab. Clement, Adeline, Marie, Juliette, Thierry, Gaetan, Leny, Sara, Maël, Maxime, Asma, Camille, Nestor, Enora, Romain and Romain, Anda, Laina, Timothée, Francesco, Hugo, Megan, Oswald, Lionel, Adrien, Severine, Agathe, Samantha and Megan. Thank you, all guys.

Thanks to the friends in Montpellier with whom I shared amazing moments outside work. In particular, Nico and Eleonora the Tower, for the countless funny moments at the 1030 apartment and the endless hikes together. Many thanks also to Andrea, Ruggero, Silvia, Celine, Gabrielle, Hugo, Camille, Lucia, Yousef, Delphine, Mattia, Sara, Silvio, Emanuele, Rossella. Big thanks to the duo Margeni, Virginie and Margherita.

To the Italian friends from Trieste, even though from distance but your presence was also crucial for me in the past years. Luigi and his lovely family, who I consider my Italian family, I am grateful for them forever. Rudolph, Gaiezza, Alicetta, Marpi, Ragù, Gerry, Massi, Berna, Francesco, Giulia, Alessandra, Marco and Marchetto, Nicolo. Thank you, all guys.

SaltGiant peeps. Best buddies and colleagues ever. You have been more like friends for me than simple co-workers. I am so happy to have met and shared all the moments together at workshops, courses and fieldtrips. Hanneke, Maria, Athina, Laetitia, Federico, Ronja, Siemon, Francesca, Jimmy, Simon, Beatriz, Mariam, Michel. You guys are the best. Big thanks to all SaltGiant PIs and POs. Vanni Aloisi, thank you for creating the fantastic project SaltGiant and for your immense energy and support towards the ESRs throughout the years. Julia Champagnac is also particularly thanked for her dedication and excellent administration of the SaltGiant project. Wout Krijgsman, Francesco Dela Pierre, Daniel Garcia-Castellanos, Paco Sierro, Antonio Caruso and Paul Meijer are particularly thanked for the endless, rich, and interesting discussions and good times spent during meetings, secondments, courses and workshops. I am filled with gratitude to Angelo Camerlenghi and Anna del Ben for their support and encouragement that helped me to enter the SaltGiant project.

I am also grateful to the Lebanese band of friends. ‘The Mastule’ Dana for the unforgettable summer vacations spent together. Jad and Loli my brothers. Farah for the lovely time spent together in Paris. Amjad, Ali, Mostafa, Benji, Ruba, Mofida, Ataya, Ahmad, Fadi, Bob, Abdallah. Thank you, all guys.

Last but not least my family. Zahraa, Hanin and baba. Without you none of my achievements would have been possible. Your love and support have given me most of the strength to carry on. Hanin and Zahraa, I wish that all your dreams come true. *Fesh ahmar menkon.*

Many thanks to my best cousin Hussein Mhanna. Hassoon, you are the reason why I ended up studying geology in the first place, so reaching this point in my career is thanks to you.

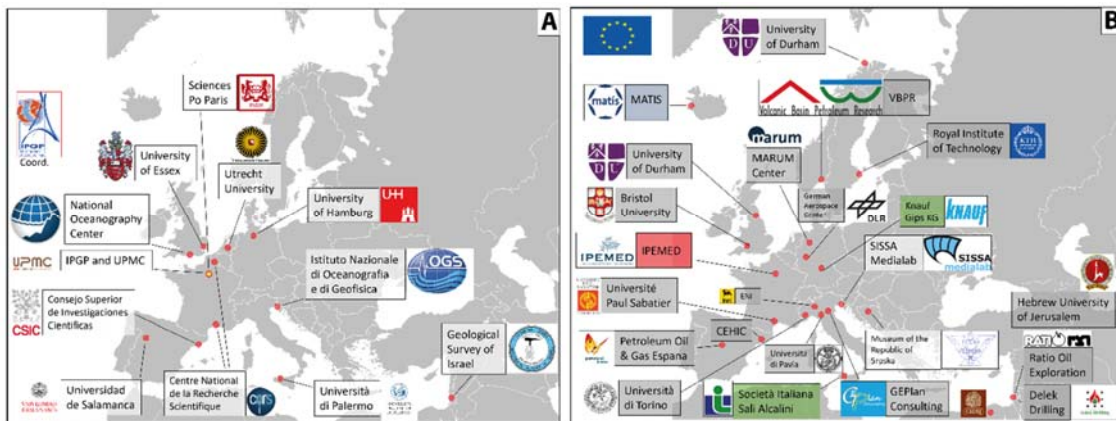
My work is also dedicated to my Aunts Farah and Nadira who passed away during my PhD. Amto Farah, with you going away I lost a mother for the second time in my life. I miss you and hope you are in a better place. Say hi to mama, amto Nadira, jeddo and teta and tell them that I miss them all.

Part of the seismic data covering the study area investigated in this thesis were provided courtesy of WesternGeco and Spectrum companies that I acknowledge. I acknowledge Schlumberger and Midland Valley Companies for providing the academic license of the softwares Petrel and MOVE, respectively.

The SaltGiant ETN



This PhD project is part of a broader project called SaltGiant. SaltGiant is a unique cross-disciplinary European Training Network (ETN) funded by the European Union's Horizon 2020 Research and Innovation Program. It initiated in 2018, with the aim of better understanding the MSC's Mediterranean Salt Giant (MSG). This ETN gathers scientists from different educational backgrounds and disciplines that work on the various aspects of the MSG. The coordinating institution of SaltGiant is the Institut Physique du Globe de Paris (IPGP), and chief of the project there is Giovanni Aloisi. The project includes 13 beneficiaries from all around Europe. The beneficiaries are local institutions/universities that, with the initiation of the project, recruited 15 Early Stage Researchers (ESRs) as PhD students, under the supervision of one or more local Project Investigators (PIs). SaltGiant has also 17 Partner Organizations (POs) which include academic organizations, private sector Oil&Gas companies, mining sector companies, museums and specialists in transferable skills from 12 different countries to stimulate interdisciplinary and intersectoral knowledge exchange between geologists, geophysicists, geochemists, microbiologist, geographers and historians in the network.



The 13 beneficiaries (A) and 23 academic and industrial Partner Organizations (B) of the SaltGiant project.

The multidisciplinary aspect of the projects is clearly reflected in its Work Packages (WPs). SaltGiant is divided in four WPs, each of them having a certain number of ESRs and has a different objective. The WPs are summarized hereafter:

WP1 – Formation of the MSG: This WP comprises ESRs 1 to ESR 7's projects. The aim of WP1 is to (1) develop a unified model that explains the formation of the MSG as a consequence of the tectonic and hydro-chemical evolution of the Mediterranean basin during the MSC, and to (2) provide scenarios for the cycling of carbon and sulfur in the Mediterranean during the MSC.

My PhD project belongs to this WP and I am the third of ESRs (ESR 3). My host institution, i.e., beneficiary, is the Centre National de Recherche Scientifique (CNRS). The local PI is Johanna Lofi, being the supervisor of ESR3 project. I am co-supervised by PO Agnes Maillard from Géosciences Environnement Toulouse. The ESRs of this WP include a micropaleontologist (ESR 1), two geophysicists (ESRs 2 and 3), two geologists (ESRs 4 and 5), a geochemist (ESR 6) and a physicist (ESR 7). Having the same final objective, which is reflected in the title of the WP itself, several interactions and collaborations took place between the ESRs of WP1. As the reader will see in the chapters of this dissertation, I collaborated with most of the ESRs of WP1. At the end of the projects, results from this work packages should be put together to try to come out with a new model for the MSC.

WP2 – Deep Life: This WP includes ESR 8 (chemist) and ESR 9 (biologist) projects. The aim of WP2 is to (1) explain the development of the exceptional and poorly understood deep microbial biosphere in the MSG, providing a terrestrial analogue for the hypersaline environments of Mars where life forms might have been preserved; and (2) to characterize the microbial pathway for the formation of H₂S (“sour gas”) via the microbial reduction of the gypsum mineral.

WP3 – Drilling Hazards: It includes ESR 10 to ESR 13, all geophysicists. The aim of WP3 is to develop a mechanistic and quantitative understanding of early salt deformation and sub-salt overpressure development that can be used by the oil industry to mitigate the risks associated with drilling in salt-capped hydrocarbon provinces.

WP4 – Geo-Economics and History of Science and Technology: WP4 includes ESR 14 (historian) and ESR 15 (economist) projects. The aim of WP4 is to (1) provide an integrated history of the discovery of the MSG, which contextualizes early research in this field in relation with paradigm shifts of mid-twentieth century geosciences, international oceanographic and prospecting campaigns, and geopolitical tensions in the Mediterranean in the cold war; and to (2) study the economic and geopolitical implications of the mapping of big salt deposits because of their association with natural gas fields.

During the past three and a half years, SaltGiant organized many events with the aim of training and encouraging the exchange between the 15 ESRs at the frontier between natural and social, fundamental and applied sciences, in the framework of one of Earth Science's most fascinating enigmas. This was achieved through short courses, field courses, workshops and symposiums in which all ESRs and PIs participated. The participants in these events, including myself, have benefited from these very prolific exchanges and have been able to acquire a broad training in terms of methods, both theoretical and applied.



Group photo of the SaltGiant team posing in front of the Messinian Salinity Crisis halite inside the Realmonte mine during a fieldcourse held in Sicily in May 2019.

My scientific interactions with SaltGiant ESRs:

In the framework of SaltGiant ETN, I had the chance to collaborate and interact with several ESRs. I list these collaborations hereafter:

- ESR2, Hanneke Heida (Geosciences Barcelona – Spain): My collaboration with Hanneke initiated with the kick-off of the project and lasted for the whole duration of the PhD. The first collaboration was a regional study that we conducted in the Western Mediterranean to restore its paleo-bathymetry during the Messinian Salinity Crisis

(MSC). This work is now published and will be a chapter of this thesis. Hanneke is also part of another collaboration that I started with ESR7 that I will mention below, and is also involved in a work that I conducted with my Agnes Maillard on the recent active tectonics in the central part of the BP. Throughout those interactions, Hanneke visited me and Johanna several time in Montpellier together with her supervisor PI Daniel Garcia-Castellanos. I myself also visited them several times in Barcelona where I spent almost 2 months for a secondment.

- ESR4, Athina Tzevahirtzian (Università di Palermo – Italy): I collaborated with Athina and her supervisor PI Antonio Caruso in a work in which we made a comparison between the MSC deposits of the Balearic Promontory (BP) and those of the Caltanissetta Basin (Sicily) which is Athina’s study area for her PhD project. This work is also published and will be presented as a chapter of this thesis. I spent one month as a secondment back in 2019 at the University of Palermo to work closely with Athina and Antonio.
- ESR5, Federico Andreetto (Utrecht University – Netherlands): Federico made an initiative to write a review paper about the terminal stage of the MSC, which is the focus of his PhD project. This review work involved a number of ESRs and PIs. I had several interactions with Federico during the time of writing of the review paper, in which I was leading the review of the offshore area. The review paper is now published and will be attached as an annex to this thesis.
- ESR7, Ronja Ebner (Utrecht University – Netherlands): The collaboration with Ronja and her supervisor PI Paul Meijer started in December 2020 and lasted till the end of my PhD project. We worked on the modelling of the MSC evaporites deposition, which is Ronja’s expertise, in the BP. We wrote a scientific article together on this work and it will be a chapter in this thesis. I was supposed to visit Ronja and Paul and work together for a short period in Utrecht, but due to the pandemic, we ended up doing the whole collaboration via daily online meetings.
- ESR10, Simon Blondel (Istituto Nazionale di Oceanografia e di Geofisica Esperimentale; Trieste – Italy): I was involved in a collaboration with Simon and his supervisor Angelo Camerlenghi to interpret together a seismic dataset that is in part covering the BP area, and which he re-processed in the framework of his PhD project. We submitted an abstract at the EGU in 2020, and the work is still in progress.

- ESR13, Gaia Travan (CNRS, Lille – France): Gaia and I worked together on a mapping project that I initiated in the Western Mediterranean area with the objective of making regional maps depth maps for the main seismic units of the area. I will present some of the results of this collaboration as an annex at the end of the thesis. We submitted an abstract together at the EGU 2021 in which Gaia benefited of this mapping to develop her study about salt tectonics in the Algerian Basin, which is the focus of her PhD project.

Abstract

The Messinian Salinity Crisis (MSC; 5.97– 5.33 Ma) is one of the most controversial geological events that influenced the evolution of the Mediterranean Basin in the late Miocene, leaving behind an immense volume of evaporites known as the Mediterranean Salt Giant (MSG). Today, more than 90% of the MSG evaporitic deposits are located offshore, buried below thick sediments that are Pliocene to Quaternary in age, and have thus been studied mainly by marine seismic reflection imaging. The Balearic Promontory (BP), a prominent topographic high in the Western Mediterranean basin, contains a unique and tectonically poorly deformed MSC record that resembles the evaporitic record of other peri-Mediterranean marginal and intermediate basins.

This PhD thesis was performed in the framework of the SaltGiant European Training Network (ETN), a cross-disciplinary project whose objective is to understand the formation of the MSG. The work of the thesis is focused on the MSC deposits of the BP. Multi-disciplinary approach was applied to answer some of the still open questions concerning the MSC event. As a first step, seismic interpretation of a wide seismic reflection dataset in the Western Mediterranean in general and in the BP in particular was performed, with the aim of refining the mapping of the Messinian units covering the area. To reconstitute the depositional history of the MSC evaporites of the BP, a detailed comparison with the Messinian evaporitic units of the Sicilian Caltanissetta Basin was carried out, in which a discussion on how this history matches the existing 3-stages chrono-stratigraphic ‘consensus model’ is illustrated. The next step consisted in the restoration of the paleo-bathymetry of the BP at the beginning of the MSC, focusing on the relatively less-deformed basin located in the central part of the BP and called the Central Mallorca Depression (CMD). To achieve this restoration, structural interpretation in the CMD area was done where the main post-MSC tectonic-related vertical movements that altered the MSC paleo-bathymetry were identified. Then 2D and pseudo-3D backstripping analysis were applied in collaboration with other colleagues from the SaltGiant project, to restore the paleo-bathymetry. In the final step, the paleo-bathymetry was used to model the deposition of the MSC evaporite volumes observed in the CMD using physics-based models built on strait hydraulic-control theory. The results show that the MSC units of the CMD could constitute an undeformed analog of those outcropping on-land in the Sicilian Caltanissetta Basin. Moderate post-MSC deformation acted along MSC strike-slip corridors in the CMD following the MSC evaporites deposition, thus altering only locally the paleo-bathymetry. A high amplitude

drawdown (>850m) is required during the halite stage of the MSC. The results raise a series of doubts about the current consensus model, still widely accepted. Doubts concern the synchronous onset of salt at the basin scale, the maximum depth of deposition of the Primary Lower Gypsum (PLG) and the timing of formation of the Resedimented Lower Gypsum (RLG). All the results and discussions hint to the need of revision of the current MSC consensus model, as well as the importance of initiating drillings offshore over the BP area, which would help revealing many of the mysteries still buried with the MSG.

Résumé

Entre 5.97 et 5.33Ma, à la fin du Miocène, un événement géologique exceptionnel aux conséquences majeures a affecté le bassin méditerranéen : la Crise de Salinité Messinienne (CSM). Cet épisode, dont le scénario exact reste encore énigmatique, est responsable du dépôt d'un volume considérable d'évaporites connu sous le nom de Géant Salifère de Méditerranée (GSM). Aujourd'hui, plus de 90 % des dépôts évaporitiques du MSG sont situés dans les bassins profonds de la Méditerranée et sont enfouis sous une épaisse couche de sédiments Plio-Quaternaire. Ces évaporites ont donc été étudiées principalement par imagerie sismique. Dans ce mémoire, nous nous intéressons aux dépôts de la crise enregistrés sur Promontoire des Baléares (BP), un haut topographique situé dans bassin de la Méditerranée occidentale. Du fait qu'il contient une succession de bassins en position intermédiaire stratégique, étagés entre les bassins marginaux du pourtour Méditerranéen et les bassins profonds, le BP se révèle un lieu unique avec des dépôts évaporitiques variés, ubiquistes et peu déformés tectoniquement, permettant d'accéder à une vision complète de l'enregistrement de la crise et pouvant mener à un scénario global cohérent.

Cette thèse de doctorat a été réalisée dans le cadre d'un projet transdisciplinaire : « European Training Network (ETN) SaltGiant », dont l'objectif est de comprendre le GSM. Une approche pluridisciplinaire a été appliquée sur la zone d'étude choisie pour apporter des contraintes afin de répondre à certaines des nombreuses questions encore sans réponses sur la crise de salinité messinienne. Le travail de base a consisté en l'interprétation d'un large ensemble de données de sismique réflexion en Méditerranée occidentale, particulièrement concentré sur les dépôts messiniens du BP. Ceci a permis de préciser la cartographie des unités messiniennes de cette région et de définir leurs inter-relations géométriques. Une comparaison détaillée de ces unités évaporitiques avec celles du bassin messinien sicilien de Caltanissetta a été menée afin de reconstituer l'histoire de leur dépôt pour la confronter au modèle chrono-stratigraphique « consensuel » à trois phases. Pour reconstituer la paléo-bathymétrie de la dépression centrale de Majorque (CMD), le bassin le moins déformé situé dans sa partie centrale du BP, une interprétation structurale a permis d'identifier les principaux mouvements tectoniques post-MSC, modérés et localisés dans des corridors de décrochement. L'analyse par backstripping 2D et pseudo-3D, en collaboration avec d'autres collègues du projet SaltGiant, a alors permis de restaurer la paléo-bathymétrie de la CMD. Enfin, ces résultats ont été utilisés comme

contraintes bathyétriques et de volumes pour modéliser le dépôt des évaporites observées, par des modèles physiques basés sur la théorie du contrôle hydraulique des détroits. Les résultats montrent que les unités messiniennes de la CMD pourraient constituer un analogue non déformé de celles qui affleurent à terre dans le bassin sicilien de Caltanissetta. Ils démontrent aussi qu'une baisse générale du niveau marin de grande amplitude (>850m) est nécessaire pour précipiter le volume de halite observé dans la CMD. Ces résultats, très bien contraints par ces études précises, remettent en cause certaines idées parfois encore largement acceptées. Ces doutes concernent en particulier l'apparition synchrone du sel à l'échelle du bassin méditerranéen, la profondeur maximale de dépôt du gypse inférieur primaire (PLG) et le moment de la formation du gypse inférieur resédimenté (RLG). En conclusion, ce mémoire montre la nécessité de réviser le scénario consensus actuel de la CSM, et l'importance de réaliser des forages en mer dans la région clef du BP, ce qui permettrait de révéler de nombreux mystères encore enfouis sous le géant salifère de Méditerranée.

Introduction

Among the Salt Giants of the globe, the Upper Miocene's Mediterranean Salt Giant is known to be one of the youngest. It formed during what is today known as Messinian Salinity Crisis (MSC; Selli, 1960), a crisis during which the Mediterranean Basin suffered extreme environmental and ecological conditions. They lead to the deposition of an immense evaporitic body having a volume of ~ 1.2 million km^3 (W. B. f. Ryan, 1976; Haq et al., 2020b) in a relatively short time span of ~ 0.64 Ma (Krijgsman et al., 1999; CIESM, 2008.; Manzi et al., 2013; Roveri et al., 2014a). It is thought that deposition of the Mediterranean MSC salt giant has greatly affected the global oceans, by sequestering ~ 5 - 10 % of their salt content into the Mediterranean Sea (eg. Garcia-Castellanos & Villaseñor, 2011). The causes of the MSC are associated mainly to a combination of orbital and tectonic drivers that restricted the connection and altered the amount of water delivered to the Mediterranean Basin from the Atlantic Ocean through the Gibraltar corridor (Duggen et al., 2003; P. Meijer & Krijgsman, 2005a; Gladstone et al., 2007; F. Hilgen et al., 2007; W. B. F. Ryan, 2009b; Govers, 2009b; Flecker et al., 2015).

Although documented earlier onshore (Selli, 1954; Ogniben, 1957; Ruggieri, 1967) the MSC deposits were recognized and appreciated broadly by the scientific community only after the pioneering of marine geology studies between the 60s and the 70s where the evaporites appeared to extend at a Mediterranean basin scale (Hersey, 1965; Mauffret, 1969; Montadert et al., 1970; W. B. F. Ryan, 1971). Then followed the Mediterranean cruise DSDP (Deep Sea Drilling Project) Leg 13, whose goal was 'to explore the origin and development of a small ocean basin, The Mediterranean' (Hsü, 1972; W. B. F. Ryan & Hsü, 1973), in which cores from the top of the MSC evaporites were recovered for the first time from the deep basins. Maybe the scientific community at that moment did not realize that they were in front of a new mystery and that a controversy was about to be unleashed following that discovery.

In the following years, conceptual models on how the MSC Mediterranean evaporites formed arose (eg. Drooger, 1976). The main points of disagreement between those models were the depth of the basin during the MSC and whether complete evaporation and desiccation was necessary to form the salts. Three models were proposed: the deep basin, shallow water model (Hsü, 1973), the shallow basin, shallow water model (Pautot et al., 1970; Nesteroff, 1973), and the deep basin, deep water model (Schmalz, 1969; Selli, 1973) which disputed the shallow water origin of the evaporites. The shallow basin model was disproved after a few years when

increasing evidence pointed towards the Mediterranean already being a deep basin in the Late Miocene, leaving the battlefield to the desiccation versus non-desiccation models, both still supported by the continuous collection of new data.

The sea level drop controversy and the depositional environments of the MSC's salt giant evaporites were not the only challenge to face, but there were also other questions to answer. To mention a couple, (1) the timing of the emplacement, and (2) the relationship and correlation between the shallow marginal evaporites and deep basin evaporites. Some authors proposed a diachronous inter-basinal onset of the MSC evaporites (Rouchy, 1982; Butler et al., 1995; J. M. Rouchy & Caruso, 2006), while others proposed a synchronous scenario (Gautier et al., 1994; Hilgen & Krijgsman, 1999; Krijgsman, Hilgen, et al., 1999b).

In 2007, several MSC experts gathered at a CIESM (Mediterranean Science Commission) meeting to try to define a stratigraphic consensus model consisting of three stages (CIESM, 2008a), inspired from the two-stage model of Clauzon et al. (1996), and later modified by Roveri et al. (2014). The stages can be summarized as follows:

- stage 1 (5.97-5.60 Ma): it marks the MSC onset in which up to 16 precession-driven cycles of gypsum-marls alternations, known as Primary Lower Gypsum (PLG), were deposited in shallow basins (Krijgsman, Hilgen, et al., 1999b; Lugli, Vinicio, et al., 2010).

- stage 2 (5.60-5.55 Ma): thick salt bodies (mainly halite) were deposited in intermediate and deep basins accompanying the maximum sea-level drawdown (of debated amplitude) (Lugli et al., 1999b). Shallower basins' PLG underwent erosion and redeposited as Resedimented Lower Gypsum (RLG) (Roveri et al., 2006). Margins also experienced intense erosion (of debated origin) during this stage.

- stage 3 (5.55-5.33 Ma): divided into 2 sub-stages, stage 3.1 (5.65-5.42 Ma), in which up to 10 precession-driven cycles of elastic-gypsum alternations, known as the Upper Evaporites (UE) or Upper Gypsum (UG) were deposited in intermediate and probably deep basins (J. M. Rouchy & Caruso, 2006; Manzi et al., 2009a); stage 3.2 (5.42 -5.33 Ma), also known as Lago Mare stage, where sediments containing brackish water fauna of Paratethyan origin were deposited in hyposaline conditions in shallow to deep basins (Bonaduce & Sgarrella, 1999; Stoica et al., 2016a).

The consensus model as well as the preceding proposed models were built based mostly on onshore studies performed in several peri-Mediterranean basins among which the key basin of Caltanissetta in Sicily. However, more than 90% of the MSC evaporites are still buried offshore (Ryan et al., 2009; Lofi et al., 2011a, b; Lofi, 2018) with very limited access through DSDP and ODP drillings and oil industry boreholes. With those evaporites remain buried a lot of

information on the MSC events. In fact, most of the arguments challenging the consensus model come from recent offshore studies performed either via seismic data, which quality keeps improving, and/or via borehole data, which penetrated for the first time the offshore deep basin sequence to its bottom (e.g., Meilijson et al., 2018, 2019).

In this framework, the Balearic Promontory (BP) appears as a unique place to further investigate the MSC records and better understand the MSC events. The BP is a SW-NE oriented prominent high lying in the core of the Western Mediterranean Basin. It consists of a series of perched sub-basins that during the MSC were lying at shallow to intermediate depths. Those sub-basins trapped a series of relatively thin MSC deposits known as the Bedded Units (BU; sensu Lofi et al., 2011) that show no apparent connection with the deep basin MSC evaporites (Mauffret, 1977; Driussi, Maillard, et al., 2015b). Unlike most of the onshore marginal to intermediate basins, which contain an incomplete and deformed MSC records, the BP underwent relatively few post-MSC tectonic deformation. Comparing and contrasting the onshore altered records with the offshore preserved records of the BP is thus of a relevant importance. Located between the Mallorca and Ibiza islands, the Central Mallorca Depression (CMD) notably offers a very good preservation of the record, including a salt (halite) layer. Thus, the BP in general, and the CMD in particular, present a unique opportunity to investigate the formation of the MSC evaporites and an interesting place to study for furthering our understanding and answering some of the key questions about the MSC events.

Thesis objectives

In the present PhD thesis work, I focused on the offshore record of the MSC deposits in the promising area of the Balearic Promontory. Very few attention was given so far in the literature to those deposits, where only 5 recent studies focused on the MSC record there (del Olmo, 2011b; Maillard et al., 2014b; D. Ochoa et al., 2015c; Driussi, Maillard, et al., 2015b; Roveri et al., 2019). The scientific questions that I will target and try to answer through my work are:

1) What is the nature of the evaporites of the BP and what is their relationship (spatial, geometric and temporal) with other Mediterranean marginal to deep MSC deposits?

2) Under what paleo-environmental conditions (water level and salinity) did the MSC evaporites emplace in the BP?

3) Is the chronostratigraphic 'consensus model' applicable/compatible with the observations from the MSC record of the BP?

To address these questions, I used multidisciplinary geophysical approaches:

- 1) I started with the interpretation of a widespread academic and industrial, low- and high-resolution seismic reflection dataset. The interpretation of the seismic dataset allowed me to distinguish and map the different seismic units belonging to the MSC on the BP;
- 2) In the absence of drills and cores, the lithology and stratigraphy of those seismic units can only be speculated. In order to discuss their possible nature, I performed a detailed comparison between the MSC record of the BP as imaged on the seismic data, and the MSC record outcropping onshore in some Mediterranean basins. A particular focus was given to the key Caltanissetta Basin (Sicily), a possible deformed analog of the BP;
- 3) The next step consisted in restoring the initial, pre-MSC, bathymetry of the BP, to reconstitute among others, the depositional environments of the evaporites. For this, I re-interpreted and compiled part of the seismic dataset of the entire Western Mediterranean area, in order to quantify the sediment load that was later used for a regional backstripping analysis lead by some colleagues from the University of Barcelona. With this step we obtained the paleo-bathymetry of the study area before the MSC;
- 4) In order to evaluate the post-MSC tectonic movements and how much those might have altered the paleo-bathymetry obtained from the previous step, I did structural interpretation in the CMD area and identified the main post-MSC tectonic-related vertical movements. The paleo-bathymetric map of the CMD is now considered as pretty much confident;
- 5) Based on this paleo-bathymetric map, the final step consisted in applying physics based numerical models to simulate and reconstitute the hydrographic conditions and connectivity of the CMD's water column to the Mediterranean during the deposition of the MSC evaporites. This was done in collaboration with colleagues from the University of Utrecht;

- 6) Finally, following my results and observations in the BP, I discuss their compatibility with the basin wide ‘consensus model’.

Outline of the thesis

The thesis consists in 8 chapters. At the beginning of each chapter, I will make a brief introduction of what the reader is expected to find and learn in that specific chapter. Where necessary I will specify who participated in the development of the work presented in it, and how.

Hereafter is a short outline of all the chapters of the thesis.

In chapter 1 of the thesis, I introduce the state of art of the Messinian Salinity Crisis since the discovery of the evaporites and until the most recent advancements. I start by explaining how the chronostratigraphic models of the MSC were first established and how did they evolve with time. I also present the MSC markers both in the onshore and offshore domain of the Mediterranean, highlighting the main controversies ongoing on the interpretation of the main MSC sedimentary units. Then I present the most debated argument in the MSC community, which concerns the timing and amplitude of the sea-level drawdown.

In chapter 2, I give a geological background on the study area, starting by restituting the Balearic Promontory in the geodynamic context of the Western Mediterranean area. Then I summarize its geological and tectonic evolution since its formation until the present-day, and how did this evolution affect the area in terms of present-day physiography. I end the chapter by introducing what is known about the MSC in the BP, both offshore and onshore.

In chapter 3, I present the dataset used in the development of my work and then explain in detail the theory and steps of the methodology applied throughout the PhD project.

Chapters 4 to 7 are the results of the PhD thesis project under the format of scientific articles, two of which are published (chapters 4 and 6), one is revised and under a second review round (chapter 5), and one is written and will be submitted immediately after I finish writing the

thesis. At the beginning of each of these chapters, I explain how the work developed, the collaborations, the main take-home messages and how does the work relate to the next chapter.

Chapter 8 is the last chapter in which I arrange my conclusions from the overall works. I provide answers to the research questions postulated at the beginning of the dissertation and discuss the implications of my results with regard to the MSC in a broader context, at the Western Mediterranean scale, trying finally to propose some future steps that I believe necessary to improve our understanding of the Messinian Salinity Crisis.

Introduction

Parmi les « géants salifères » présents sur terre, le « géant » méditerranéen datant du Miocène terminal est connu pour être l'un des plus jeunes et des plus surprenants. Il est reconnu comme une crise majeure pendant laquelle le bassin méditerranéen a subi des conditions environnementales et écologiques extrêmes : la crise de salinité messinienne (CSM; Selli, 1960). Les changements environnementaux ont conduit au dépôt d'un immense corps évaporitique d'un volume de ~1,2 million de km³ (W. B. f. Ryan, 1976 ; Haq et al., 2020) dans un laps de temps relativement court de ~0,64 Ma (Krijgsman et al., 1999 ; CIESM, 2008; Manzi et al., 2013 ; Roveri et al., 2014a). Les conséquences de cette crise sont majeures puisqu'on pense qu'elle aurait grandement affecté l'océan mondial, en séquestrant ~5-10 % de son contenu global en sel dans la mer Méditerranée (ex. Garcia-Castellanos & Villaseñor, 2011). Les causes de la CSM sont principalement dues à une combinaison de facteurs orbitaux et tectoniques aboutissant à une restriction des connexions entre l'Atlantique et la mer Méditerranée à travers les corridors du détroit de Gibraltar (Duggen et al., 2003; Meijer & Krijgsman, 2005; Gladstone et al., 2007; Hilgen et al., 2007; W. B. F. Ryan, 2009; Govers, 2009; Flecker et al., 2015).

Bien que documentés très tôt à terre (Selli, 1954 ; Ogniben, 1957; Ruggieri, 1967), les dépôts de la CSM n'ont été reconnus et considérés par la communauté scientifique qu'après les études pionnières de géologie marine entre les années 60 et 70 qui ont montré l'extension considérable des évaporites à l'échelle du bassin méditerranéen (Hersey, 1965 ; Mauffret, 1969 ; Montadert et al., 1970 ; W. B. F. Ryan, 1971). Des carottes du sommet de ces évaporites messiniennes furent récupérées pour la première fois dans les bassins profonds au cours du Leg 13 d'une campagne DSDP (Deep Sea Drilling Project), dont le but était "d'explorer l'origine et le développement d'un petit bassin océanique, la Méditerranée " (Hsü, 1972; W. B. F. Ryan & Hsü, 1973). A ce moment-là, la communauté scientifique n'avait peut-être pas réalisé qu'elle était face à un nouveau mystère et qu'une longue controverse allait être déclenchée suite à cette découverte. Dès les années suivantes néanmoins, des modèles conceptuels variés proposèrent d'expliquer la formation des évaporites méditerranéennes de la CSM (par exemple, Drooger, 1976). Les principaux points de désaccord entre ces modèles concernaient la profondeur du bassin pendant la crise et la nécessité ou non d'une évaporation avec dessiccation complète pour précipiter les sels. Trois modèles ont été proposés : le modèle du bassin profond en eaux peu profondes (Hsü, 1973), le modèle du bassin peu profond en eaux peu profondes (Pautot et

al., 1970; Nesteroff, 1973), et le modèle du bassin profond en eaux profondes (Schmalz, 1969; Selli, 1973), ce dernier contestant l'origine des évaporites en eaux peu profondes. Le modèle du bassin peu profond fut rapidement réfuté, dès lors que la géodynamique eut montré que la Méditerranée était déjà structurée en bassin profond au Miocène supérieur, laissant le champ de bataille aux modèles de « dessiccation » ou de « non-dessiccation », chacun soutenu par la collecte continue de nouvelles données.

La controverse sur la baisse du niveau marin et sur les environnements de dépôt des évaporites du « géant salifère » n'était pas le seul défi à relever, bien d'autres questions restaient en suspens. Pour n'en citer que quelques-unes, (1) la chronologie de la mise en place des différents événements, et (2) la relation et la corrélation entre les évaporites des bassins marginaux sur la périphérie de la Méditerranée avec celles des bassins profonds. Certains auteurs proposaient un début de la crise synchrone partout (Rouchy, 1982; Butler et al., 1995; Rouchy & Caruso, 2006), tandis que d'autres le considéraient diachrone (Gautier et al., 1994; Hilgen & Krijgsman, 1999; Krijgsman et al., 1999).

En 2007, plusieurs experts de la CSM se sont réunis lors d'une réunion de la CIESM (Commission Scientifique pour la Méditerranée) pour tenter de définir un modèle stratigraphique consensuel en trois étapes (CIESM, 2008), inspiré du modèle à deux étapes de Clauzon et al. (1996) modifié ultérieurement par Roveri et al. (2014). Les étapes peuvent être résumées comme suit :

- stade 1 (5,97-5,60 Ma) : il marque le début de la CSM, pendant lequel jusqu'à 16 cycles d'alternances gypse-marne, régis par la précession, ont été déposés dans des bassins marginaux peu profonds. Cet ensemble porte le nom de « gypse inférieur primaire » (PLG, Primary Lower Gypsum), (Krijgsman et al., 1999 ; Lugli et al., 2010).

- stade 2 (5,60-5,55 Ma) : des évaporites épaisses, principalement sous forme de halite, se sont déposées dans des bassins intermédiaires et profonds, durant la chute maximale du niveau de la mer (d'une amplitude discutée) (Lugli et al., 1999). Les PLG des bassins moins profonds ont alors subi une érosion et se sont redéposés sous forme de gypse inférieur re-sédimenté (RLG) (Roveri et al., 2006). Les marges de toute la Méditerranée étaient alors soumises à une érosion intense.

- stade 3 (5,55-5,33 Ma) : il est divisé en deux sous-stades : le stade 3.1 (5,65-5,42 Ma), au cours duquel jusqu'à 10 cycles d'alternance clastique-gypse régis par la précession, connus sous le nom d'évaporites supérieures (UE, Upper Evaporites) ou de gypse supérieur (UG, Upper

Gypsum), se sont déposés dans des bassins intermédiaires et profonds (Rouchy & Caruso, 2006 ; Manzi et al, 2009) ; le stade 3.2 (5,42 -5,33 Ma), également connu sous le nom de « Lago Mare », caractérisé dans des bassins peu profonds à profonds par des dépôts de sédiments à faune d'eau saumâtre d'origine paratéthysienne, dans des conditions hyposalines (Bonaduce & Sgarrella, 1999; Stoica et al., 2016).

Ce modèle consensuel ainsi que les précédents modèles proposés ont été construits en se basant principalement sur des études à terre réalisées dans plusieurs bassins marginaux méditerranéens, dont le bassin clé de Caltanissetta en Sicile. Cependant, plus de 90% des évaporites de la CSM sont enfouies au large (Ryan et al., 2009; Lofi et al., 2011a, b; Lofi, 2018) limitant leur accès aux forages DSDP et ODP et aux forages de l'industrie pétrolière, et par là même, empêchant d'avoir des informations directes sur les événements de la crise. La plupart des arguments qui aujourd'hui remettent en cause le modèle consensuel proviennent d'études offshore récentes réalisées via des données sismiques, dont la qualité ne cesse de s'améliorer, et/ou via des données de forage, qui ont pénétré pour la première fois la séquence du bassin profond jusqu'à sa base (cf Meilijson et al., 2018; 2019).

Dans ce cadre, le Promontoire des Baléares (BP) apparaît comme un lieu idéal pour étudier les enregistrements de la CSM et pour mieux en comprendre le déroulement. Le BP, englobant les îles Baléares, est une zone haute orientée SW-NE située au cœur du bassin de la Méditerranée occidentale. Entre les îles, il est constitué d'une série de sous-bassins perchés qui, pendant la CSM, se trouvaient à des profondeurs variant de faibles à intermédiaires. Ces sous-bassins contiennent des dépôts messiniens relativement minces connus sous le nom de Bedded Units (BU; sensu Lofi et al., 2011) apparemment déconnectés des évaporites du bassin profond (Mauffret, 1977; Driussi et al., 2015). Contrairement à la plupart des bassins marginaux aujourd'hui émergés, qui contiennent des enregistrements de la crise incomplets et déformés, le BP a subi relativement peu de déformations tectoniques post-CSM. Son étude permet donc non seulement de comparer les enregistrements terrestres altérés et les enregistrements offshore préservés, mais aussi de par sa position, d'imager le lien entre les dépôts marginaux et les dépôts profonds. Située entre les îles de Majorque et d'Ibiza, la Dépression Centrale offre notamment une très bonne préservation des dépôts, y compris une couche de sel mobile (halite). Ainsi, le BP en général, et la Dépression Centrale en particulier, représentent des lieux uniques pour étudier la formation des évaporites messiniennes, pour approfondir notre compréhension

de la crise et pour répondre à certaines des questions clés sur les événements complexes qui lui sont liés.

Objectifs de la thèse

Dans ce travail de thèse, je me suis donc concentré sur l'enregistrement offshore de la crise de salinité messinienne dans la zone prometteuse du Promontoire Baléares. Jusqu'à présent, très peu d'attention a été accordée dans la littérature aux dépôts liés à la crise dans cette région ; on dénombre seulement 5 études récentes sur la thématique (del Olmo, 2011; Maillard et al., 2014; Ochoa et al., 2015; Driussi et al., 2015; Roveri et al., 2019). Les questions scientifiques que je vais aborder et auxquelles je vais tenter de répondre à travers mon travail sont les suivantes:

1) Quelle est la nature des évaporites du BP et quelle est leur relation (spatiale, temporelle et géométrique) avec les autres dépôts (émergés, peu profonds et profonds) de la crise ?

2) Quelles sont les conditions paléo-environnementales (niveau d'eau et salinité) permettant le dépôt des évaporites observées sur le BP ?

3) Le 'modèle consensuel' chronostratigraphique est-il applicable/compatible avec ce que l'on voit des enregistrements de la CSM sur le BP ?

Pour répondre à ces questions, j'ai utilisé des approches géophysiques multidisciplinaires :

1) j'ai commencé par l'interprétation d'un vaste ensemble de données de sismique réflexion basse et haute résolution, tant académiques qu'industrielles. L'interprétation de ce jeu de données sismiques m'a permis de distinguer et de cartographier les différentes unités sismiques marqueurs de la CSM sur le BP ;

2) en l'absence de forages et de carottes, on ne peut que spéculer sur la lithologie et la stratigraphie de ces unités sismiques. Afin d'apporter de solides arguments quant à leurs possibles natures, j'ai effectué une comparaison détaillée entre l'enregistrement de la crise sur le BP vu par les données sismiques et les dépôts de la crise affleurant à terre dans certains

bassins ; une attention particulière ayant été accordée au bassin de Caltanissetta (Sicile), un possible analogue déformé du BP ;

3) l'étape suivante a consisté à restaurer la bathymétrie initiale, pré-CSM, du BP, afin de reconstruire, entre autres, les environnements de dépôt des évaporites. Pour cela, j'ai réinterprété et compilé une partie des données sismiques de toute la Méditerranée occidentale, afin de quantifier la charge sédimentaire, étape nécessaire pour une analyse régionale du 'backstripping' qui a été menée par des collègues de l'Université de Barcelone. Ce travail nous a permis de restituer la paléo-bathymétrie de la zone d'étude juste avant la CSM ;

4) afin d'évaluer les mouvements tectoniques post-CSM et leur impact sur la paléo-bathymétrie obtenue à l'étape précédente, j'ai effectué une interprétation structurale dans la Dépression Centrale du BP pour en déduire les principaux mouvements verticaux liés à cette tectonique. La carte paléo-bathymétrique de la Dépression Centrale est maintenant considérée comme bien contrainte ;

5) basée sur cette carte paléo-bathymétrique, l'étape finale a consisté à appliquer des modèles numériques basés sur la physique pour simuler et restituer les conditions hydrographiques et la connectivité de la colonne d'eau de la Dépression Centrale au reste de la Méditerranée pendant le dépôt des évaporites. Ce travail a été réalisé en collaboration avec des collègues de l'Université d'Utrecht ;

6) enfin, je discute la compatibilité de mes résultats et observations dans le BP, avec le 'modèle consensuel' à l'échelle du bassin.

Plan de la thèse

La thèse est divisée en 8 chapitres. Au début de chaque chapitre, une courte introduction expose ce que le lecteur est censé trouver et apprendre dans cette partie. Quand nécessaire, je préciserai qui a participé à l'élaboration du travail présenté, ainsi que les conditions de sa réalisation.

Ci-dessous, voici un bref résumé de chaque chapitre de la thèse.

Dans le chapitre 1, je décris l'état de l'art de la crise de salinité messinienne depuis la découverte des évaporites jusqu'aux avancées les plus récentes. Je commence par expliquer comment les modèles chronostratigraphiques de la CSM ont été établis et comment ils ont évolué avec le temps. Je présente également les différents marqueurs de la CSM tant dans les domaines

onshore qu'offshore de la Méditerranée, en soulignant les dernières controverses importantes quant à l'interprétation des principales unités sédimentaires. Ensuite, je développe le point de controverse le plus débattu dans la communauté messinienne, qui concerne le timing et l'amplitude de la baisse du niveau de la mer.

Dans le chapitre 2, le contexte géologique de la zone d'étude est présenté, en commençant par replacer le Promontoire Baléares dans la géodynamique de la Méditerranée occidentale. Son évolution géologique et tectonique depuis sa formation jusqu'à aujourd'hui est ensuite résumée et nous insistons sur l'impact de cette histoire complexe sur sa physiographie actuelle. Je termine le chapitre en présentant un bilan des connaissances de la CSM sur le BP, tant en mer qu'à terre.

Dans le chapitre 3, je présente le jeu de données utilisé dans le développement de mon travail, puis j'explique en détail la théorie et les étapes de la méthodologie appliquée tout au long de la thèse.

Les chapitres 4 à 7 sont les résultats de la thèse, présentés sous forme d'articles scientifiques, dont deux sont publiés (chapitres 4 et 6), un est en révision et fait l'objet d'une deuxième soumission à la revue *tectonophysics* (chapitre 5), et un est écrit et doit être soumis immédiatement après la rédaction de la thèse (chapitre 7). Au début de chacun de ces chapitres, j'explique comment le travail s'est déroulé, les collaborations engagées pour ce faire, les principaux messages à retenir et enfin comment les résultats amènent au chapitre suivant.

Le chapitre 8 est le dernier chapitre dans lequel j'organise mes conclusions à partir de l'ensemble des travaux. J'apporte des réponses aux questions fondamentales posées au début de la thèse et je dresse un bilan de l'état de connaissances ainsi atteint sur la CSM, en essayant finalement de proposer quelques étapes futures que je crois nécessaires pour améliorer notre compréhension de la crise environnementale majeure.

Chapter 1

The Messinian Salinity Crisis: state of art

In this chapter, I introduce the state of art of the Messinian Salinity Crisis since the discovery of the evaporites and until the most recent advancements. I start by explaining how the chronostratigraphic models of the MSC were first established and how did they evolve with time. I also present the MSC markers both in the onshore and offshore domain of the Mediterranean, highlighting the main controversies ongoing on the interpretation of the main MSC sedimentary units. Then I present the most debated argument in the MSC community, which concerns the timing and amplitude of the sea-level drawdown.

In its present day setting, the Mediterranean Sea ‘survives’ thanks to the connection with the Atlantic Ocean through the strait of Gibraltar. Cutting this connection would lead to severe consequences on the ecological and environmental systems of the Mediterranean area. This is what happened at the end of the Miocene epoch, when the Mediterranean area witnessed one of the most rapid environmental crises in the Earth sea’s history, today known as the Messinian Salinity Crisis (MSC; Selli, 1960). A combination of tectonic and orbital drivers lead to the alteration of the paleoceanographic and paleohydrological exchanges between the Mediterranean Sea and the Atlantic Ocean, affecting the paleoenvironmental and paleoecological conditions of the Mediterranean Basin (Duggen et al., 2003; F. Hilgen et al., 2007; Govers et al., 2009a; Flecker et al., 2015; Simon & Meijer, 2015). One of the most striking consequences of the MSC is the deposition of an immense evaporitic body known as the Mediterranean Salt Giant with a volume of ~ 1.2 million km³ (W. B. f. Ryan, 1976; Haq et al., 2020b) in a relatively short time span of ~0.64 Ma (Krijgsman et al., 1999; CIESM, 2008.; Manzi et al., 2013; Roveri et al., 2014a). Half a century and more than 1000 published scientific research articles since its discovery, yet what really happened during the MSC is still uncertain and highly debated. Reason for which it is considered one of the longest-living scientific controversies in the field of Earth Sciences (Camerlenghi & Aloisi, 2020).

First studies focusing on the MSC took place onshore where evaporites were thought to be coeval and derived from hyper- and hypo-saline environments that developed in the Upper Miocene all around the Mediterranean area (Ogniben, 1957; Selli, 1960; Ruggieri, 1967). In the following years and with the launching of the Deep Sea Drilling Project (DSDP) in the Mediterranean, the topmost part of the MSC evaporites of the deep basin was recovered and studied (Hsü, 1972, 1973), after which the first and still strongly supported theory of the Mediterranean Sea desiccation was postulated (Figure 1.1-A; Hsü et al., 1973). Naturally, such a theory, as most of the ‘catastrophic’ newly postulated theories throughout the geological history, was immediately opposed by ‘uniformitarians’, who proposed that the Mediterranean never dried completely but instead it was a full basin during the whole MSC (Figure 1.1-B; e.g., (Schmalz, 1969; Selli, 1973; Nesteroff, 1973; Hardie & Lowenstein, 2004; Roveri, Flecker, et al., 2014a). Accordingly, the MSC not only remains a hot topic in the scientific community but the complexity surrounding its aspects are interestingly increasing with years.

The following sub-sections will be focusing on the several aspects of the MSC that have been developed and improved since its discovery. First, the chronology of the MSC events according

to the existing models will be presented (section 1.1), followed by the different MSC surfaces and units of the Mediterranean Salt Giant, and their distribution in the various basins that trapped MSC evaporites around that Mediterranean (section 1.2). Finally, the chapter will be concluded by introducing the most debated question about the MSC, which is the base level drawdown (desiccation or non-desiccation; section 1.3). In each section, the controversies arising in some of the aspects will be highlighted, focusing particularly on controversies that will be targeted in this thesis.

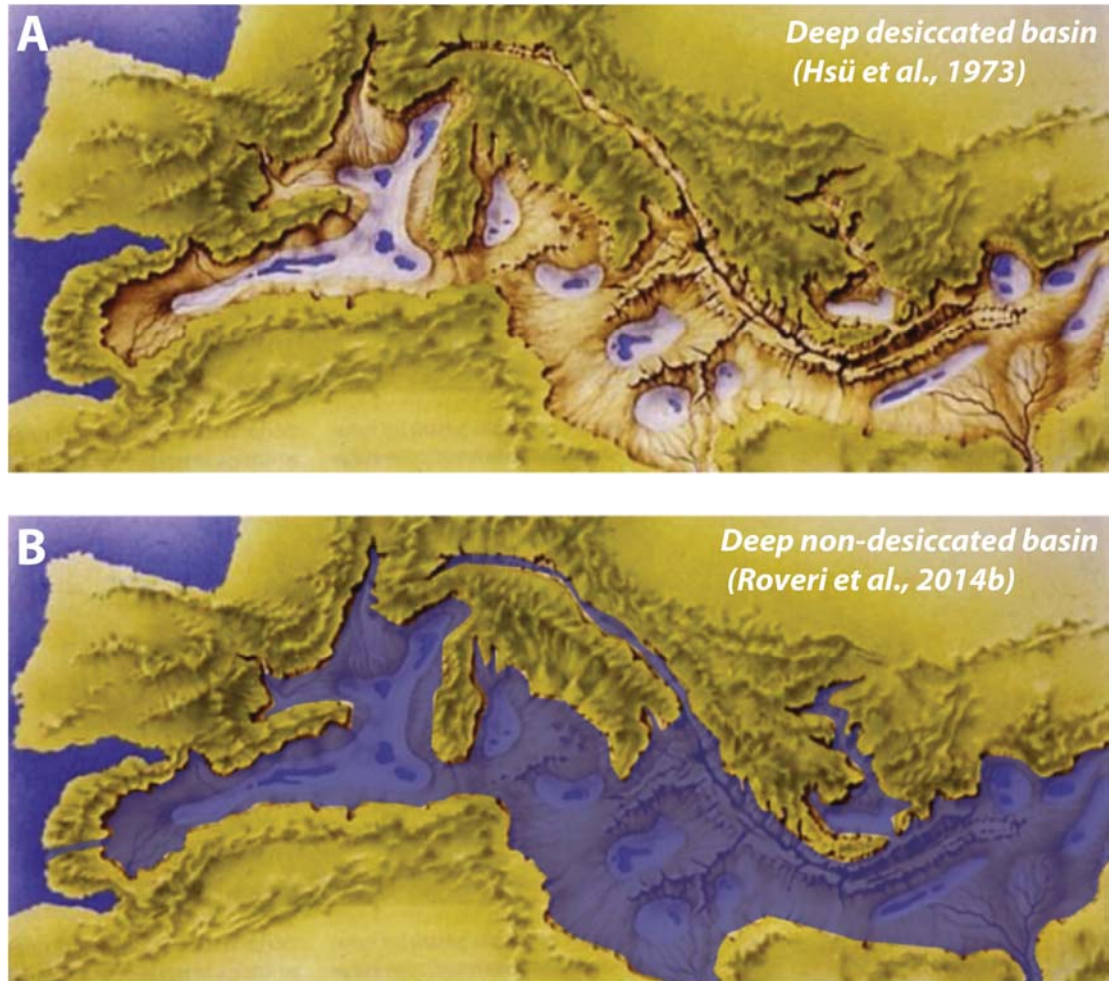


Figure 1.1. A representation of the two extreme models of the Mediterranean Basin during the Messinian Salinity Crisis. A: The long-living deep desiccated basin hypothesis. B: The deep non-desiccated basin theory. Modified from Krijgsman et al. (2018).

1.1 Timing and Chronology of the MSC events

The Messinian stage is marked by two Global Stratotype Section and Point (GSSP) boundaries with a total duration of 1.92 Ma (Figure 1.2). The Top Tortonian/Base Messinian GSSP has been defined at the Oued Akresh section (Western Morocco) at 7.25 Ma (F. Hilgen et al., 2000). The Top Messinian/Base Pliocene GSSP is defined at Eraclea Minoa (Sicily) at 5.33 Ma (Van Couvering et al., 2000). The Messinian Salinity Crisis (MSC) itself occupies only part (< half) of the whole Messinian stage duration (5.971-5.33 Ma; Figure 1.2).

Before the late 90s, the timing and evolution of the MSC events was based on observations and studies of single basins with few or no correlations between one basin and another. This resulted in completely different chronostratigraphic models in which the timing of the onset and evolution of the MSC events varied significantly between one study and the other (Figure 1.2). The key basin from which most of the observations and models derived is the Caltanissetta Basin in Sicily (e.g., Decima & Wezel, 1971; Butler et al., 1995; Krijgsman et al., 1999). This is because it was considered the only basin where a complete MSC record is outcropping. The only constant in the above-mentioned models was the timing of the end of the MSC dated at 5.33 Ma (Van Couvering et al., 2000) when the Zanclean reflooding occurred following the reestablishment of the Atlantic-Mediterranean connection (e.g., Garcia-Castellanos, Estrada, et al., 2009). However, this is not the case for the onset of the crisis, at least not until the introduction of the cyclostratigraphy as an astronomical dating instrument was applied to the lower Messinian deposits and MSC evaporites (F. J. Hilgen et al., 1995; Hilgen & Krijgsman, 1999; Krijgsman, Hilgen, et al., 1999b). For example, Butler et al. (1995) proposed an onset of the first evaporitic beds belonging to the MSC at 6.88 Ma based on magnetostratigraphic data in the Sicilian basins, whereas Riding et al. (1998) proposed an earlier onset around ~7 Ma based on the sedimentary record of the Betic cordillera (south-east Spain) (Figure 1.2). Moreover, most of those models proposed a diachronous onset for the evaporites deposition between the shallow marginal basins and the deep basins (Butler et al., 1995; Clauzon et al., 1996b; Riding et al., 1998; J. M. Rouchy & Caruso, 2006).

Krijgsman et al. (1999) were the first to correlate and compare the MSC onset from different basins (namely Sorbas-Spain, Metochia-Greece, and Gibliscemi-Italy basins) around the Mediterranean using cyclostratigraphic astronomical dating. The result was a synchronous onset of the MSC starting at ~ 5.96 (\pm 0.02 Ma) everywhere in the Mediterranean basins. This was done starting from the base of the Messinian stage at 7.25 Ma and counting the precessional cycles upwards (taking 21.7 kyrs as an average precessional cycle duration) in the pre-MSC

sedimentary series (pre-evaporitic marl-sapropel cycles), up to the first evaporitic bed. The authors went further proposing also a synchronous onset between the marginal and deep basin evaporites, probably because at that time the Sicilian evaporites were considered the equivalent of the deep basin.

Dating the onset and the end of the MSC was a good start. However, the more complicated task is to date the events within the 5.96-5.33 Ma interval. This is mainly due to the lack of absolute dating proxies within the very short duration interval of the MSC, together with the uncertainty about the importance of the hiatuses caused by erosion during periods of base level falls.

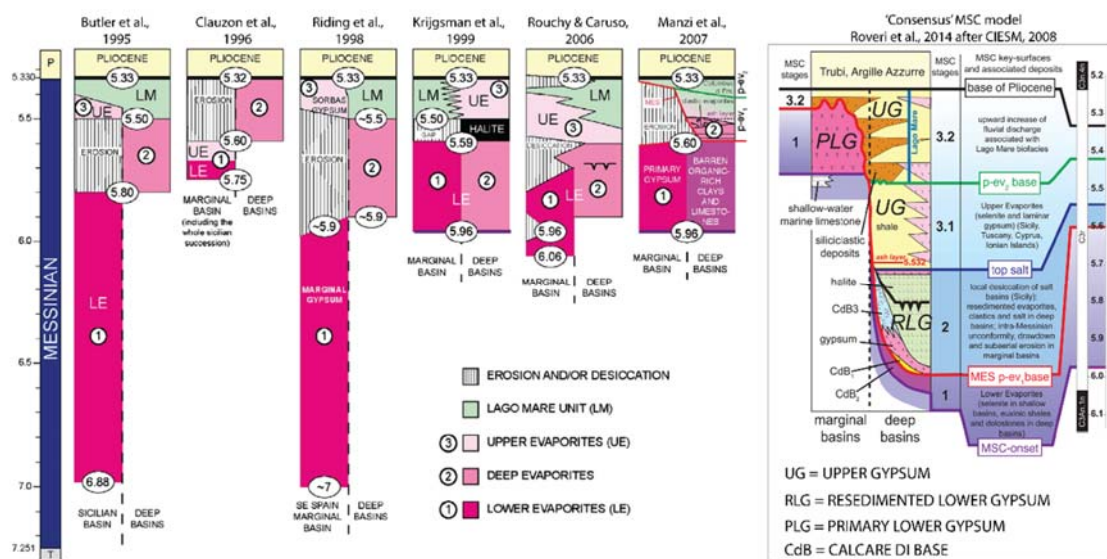


Figure 1.2. Figure showing different chronostratigraphic models proposed for the MSC events. Notice the different ages proposed for the onset of the MSC and the diachronous versus synchronous evaporites deposition between marginal and deep basins (see text for details). Modified from Roveri et al. (2014).

Seen the clear cyclicity of the pre-MSC marl-sapropel sediments, it was logical to assume/suggest cyclicity driven by precessional oscillations for the first evaporite cycles within the MSC interval as well. Reason for which Krijgsman et al. (2001) proposed that the evaporite beds correspond to precession maxima periods in which a relatively dry climate dominated the circum-Mediterranean area. Accordingly, counting the evaporite cycles in the same way for the pre-MSC sediments lead to a duration of ~380 ka (max of 16 cycles encountered; Vai, 1997; Krijgsman et al., 2001; Lugli et al., 2010; see also section 1.2.2.1) and the establishment of a 'Lower Evaporites stage' dated between 5.96-5.59 Ma (later the onset was revised to 5.97

Ma by Manzi et al. (2013). This phase was followed, in marginal basins, by a Messinian gap (5.59-5.55 Ma; Krijgsman et al., 1999; F. Hilgen et al., 2007; Cosentino et al., 2013) where erosion of the margins dominated with the formation of the Margin/Messinian Erosional Surface (MES; Lofi et al., 2011). Overlying the Messinian gap and its erosional surfaces are the Upper Evaporites and Lago Mare deposits. Those deposits are thought to display the same precession driven cyclicity as the lower evaporites stage and comprise up to 10 cycles (Decima & Wezel, 1971; Fortuin & Krijgsman, 2003; van der Laan et al., 2006; F. Hilgen et al., 2007; Manzi et al., 2007; see also sections 1.2.2.4 and 1.2.2.4.2), suggesting an overall duration of almost ~220 ka for the whole period postdating the Messinian gap up to the base of the Pliocene.

After several years of unending debates, for the first time the MSC community organized a workshop with the objective of putting together the ideas and try to come out with a common model that satisfy as much observations as possible. This workshop took place in Almeria, Spain in 2007 organized by the ‘Mediterranean Science Commission’ known as the CIESM, which come from the French term ‘Commission Internationale pour l'Exploration Scientifique de la mer Méditerranée’. The workshop’s outcome was published later in 2008 and for the first time the so-called ‘Consensus Model’ was introduced (Figure 1.2; CIESM, 2008). It was later slightly modified with yet another review publication that included most of the CIESM workshop participants by Roveri et al. (2014). The consensus model, which was inspired from the 2-stage model of Clauzon et al. (1996), divided the MSC events in 3 stages (Figure 1.2):

- Stage 1 (5.97 to 5.60Ma, ~370ky; Manzi et al., 2013): marks the onset of the MSC, where the lowermost primary evaporites (sub-section 1.2.2.1) were deposited in relatively shallow basins.
- Stage 2 (5.60 to 5.55Ma, ~50ky): Halite and potash salt bodies (sub-sections 1.2.2.3 and 1.2.5.2) were deposited in intermediate-depth to deep basins following the main sea-level drawdown. Shallower basins evaporites from stage 1 underwent intense erosion and reworked evaporites were deposited (sub-section 1.2.2.2).
- Stage 3 (5.55 to 5.33Ma, ~220ky): Typically divided in 2 sub-stages. Sub-stage 3.1 (from 5.55 to 5.42), in which upper evaporites were deposited (section 1.2.2.4), and stage 3.2 (5.42 to 5.33), that is known also as Lago Mare stage (section 1.2.2.4.2), where sediments with different lithologies rich in brackish water fauna content with paratethyan origin were deposited.

Since its publication, the consensus model has found fair acceptance in the literature of the MSC, because it at least tackled some of the debates, such as the one suggesting the deposition of the MSC lower evaporites postdates the main water level drawdown (Martín & Braga, 1994). On the other hand, the CIESM model was a kind of admission that some of the main questions and controversies about the MSC events, especially the amplitude of the drawdown, still cannot be answered with the present observations. This is mainly because the same observation can be interpreted in two or more plausible ways. Moreover, with time, many aspects started to appear dubious about the so-called consensus model and several research articles were published criticizing it, even from researchers who were part of the CIESM workshop.

Hereafter is the list of the most problematic issues that emerged about the CIESM model:

- Restricting the deposition of the stage 1 primary lower evaporites to marginal basins (i.e. <200m depth). There is no strong reason/evidence to support permanently this aspect, mainly because the offshore area of the Mediterranean is still not enough explored, and the few wells that have been drilled offshore in basins that were most probably lying at depths exceeding 200m during the MSC, have confirmed the presence of stage 1 lower evaporites (e.g., Ochoa et al., 2015; W. Martínez del Olmo & D. Martín, 2016).
- Limiting the salt sedimentation to stage 2 has no strong evidence as well. In fact, the immense salt body lying offshore the Mediterranean is still not well explored and studied. The few studies that were done on borehole data from the salt sequence in the Eastern Mediterranean's Levant Basin showed that the base of the salt could have started depositing since the beginning of the MSC (stage 1) and might have even continued through part of stage 3 (Meilijson et al., 2018; Meilijson, Hilgen, et al., 2019b).
- The origin of the Reworked Lower Gypsum (RLG; section 1.2.2.2) and limiting its occurrence only to stage 2 is also not clearly justified. In the CIESM model they explain its origin as due to the rheologic instability of the Primary Lower Gypsum (PLG) blocks combined with enhanced tectonic activity (Roveri et al., 2006). Admitting that this is the true origin of the RLG, there is no clear reason why such a phenomenon could not have appeared already in stage 1 or continued through stage 3.
- Dividing the stage 3 in 2 sub-stages (3.1 for upper evaporites and 3.2 for lago mare) appeared as an inaccurate aspect that needs to be revised. The lago mare stage was established because the first paratethyan ostracods bioevent in the Mediterranean is dated at 5.42 Ma. However, several studies reported the presence of brackish water

paratethyan ostracods already between two successive cycles belonging to the upper evaporites of stage 3.1 (e.g. Rouchy & Caruso, 2006). This aspect is discussed in details in Annex A.

More and more questions are arising and highlighting weak points in the so-called consensus model. Thus, it is a matter of time before this model falls, and then a new model that includes the most recent observations and updates will be needed in the MSC literature.

1.2 The MSC Basins, Units and Surfaces

Until the late 90s, the Mediterranean basins containing MSC evaporites were separated in Marginal and Deep basins (Figure 1.2; Butler et al., 1995; Clauzon et al., 1996; Riding et al., 1998; Krijgsman et al., 1999). This division is done mainly due to the important role that the pre-MSC paleo-topography and paleo-bathymetry play in the distribution of the MSC evaporites. Most of the marginal basins today are outcropping onland in areas tectonically active during and/or after the MSC (Figure 1.3; e.g. Sorbas Basin, Spain; Piedmont Basin, Italy). The MSC record in those basins is always incomplete because they were exposed to intense erosion during the main MSC sea-level drawdown and/or due to denudation as the basins were uplifted tectonically since the evaporites deposition. The deep basins, on the contrary, are mostly still lying offshore in the present day and still preserving the whole MSC record. Recently, a new schematic division of the MSC basins was established by Roveri et al. (2014) using the paleo-bathymetry as a main criteria. The authors differentiated between shallow (0–200 m water depth), intermediate (200–1000m) and deep basins (water depth > 1000m). In this view, these basins are thought to be physically disconnected from each other by topographic sills, and hold specific MSC records (Figure 1.4).

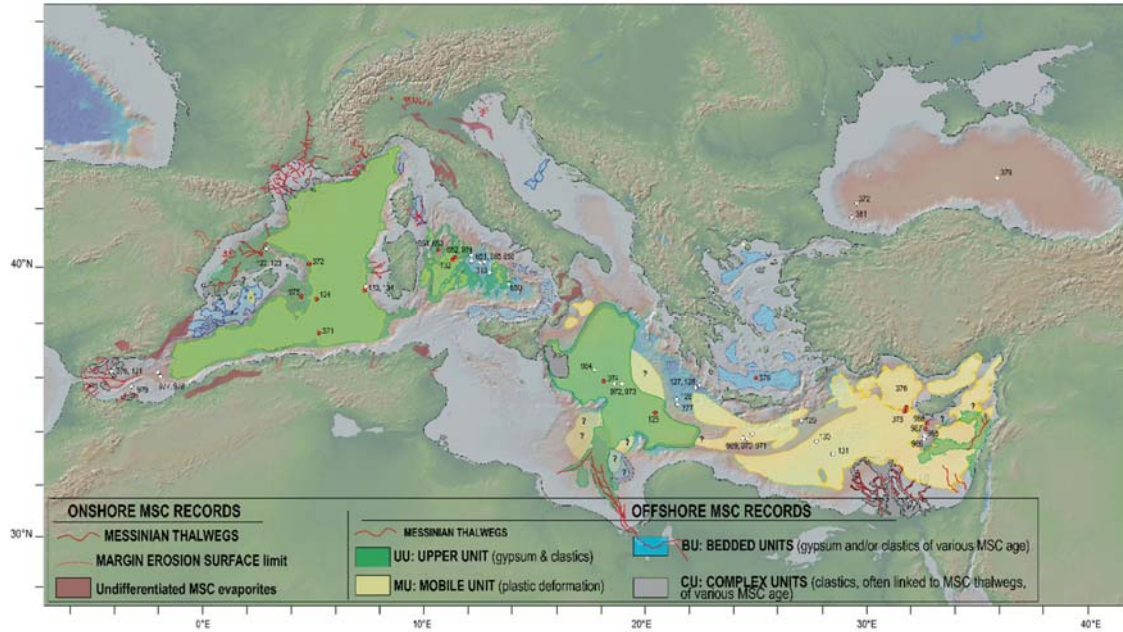


Figure 1.3. Present-day distribution of the MSC evaporites around the Mediterranean area. Dots represent the scientific DSDP and ODP sites that sampled (red) and did not sample (white) the MSC evaporites. Modified from Lofi, (2018).

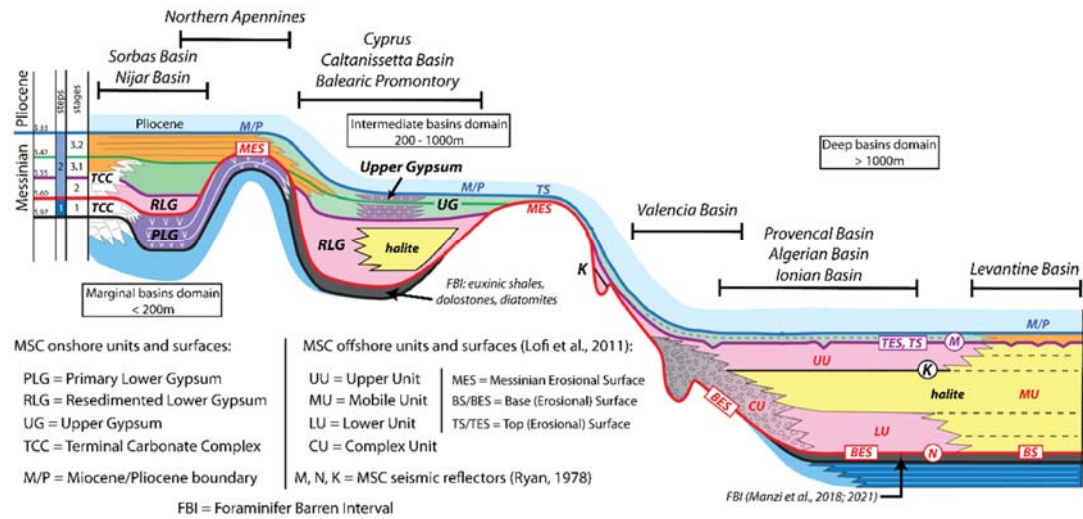


Figure 1.4. Schematic profile of the MSC basin deposits and their distribution between marginal, intermediate and deep basins as defined by the CIESM consensus model (details about model in the text) and later modified by Roveri et al. (2014). Note that so far there is no solid evidences for the correlations shown between the marginal, intermediate and deep basins, and the correlations done by Roveri et al. (2016, 2019) are considered speculations and were done to fit their three-step model. Modified from Roveri et al. (2016).

1.2.1 Pre-MSC (Lower Messinian) record

Prior to the onset of the MSC and the deposition of the first evaporitic beds, the Mediterranean recorded a progressive restriction of the Atlantic-Mediterranean gateways starting around 7.1 Ma (e.g., Bulian et al., 2021) until the beginning of the crisis. The cause of this restriction is commonly attributed to tectonic uplift processes possibly due to lithospheric slab detachment and roll back processes beneath the Gibraltar Arc in combination with slab tear propagation (Duggen et al., 2003; Villasenor et al., 2003; Govers et al., 2009a; Garcia-Castellanos & Villaseñor, 2011b). This stepwise restriction is associated with widespread deposition of diatom-rich sediments (e.g. Upper Abad marls – Southeastern Spain) and/or opal-rich deposits (e.g. Tripoli formation – Sicily) observed between 7.15 and 6.7 Ma (Roveri, Flecker, et al., 2014a). The widespread precipitation of authigenic calcite, dolomite and/or aragonite between 6.3 and 5.97 Ma, is another response to ongoing restriction. In addition, the drop in diversity until the complete disappearance of planktic foraminifera, especially during summer insolation minima at this time, indicates that surface waters reached salinities above the maximum tolerance of these organisms (F. J. Sierro et al., 1999; Blanc-Valleron et al., 2002; F. Sierro et al., 2003; Manzi et al., 2007a; Bulian et al., 2021b).

The pre-MSC records from all over the Mediterranean were subjected to integrated high-resolution cyclo-stratigraphic studies by Hilgen et al. (1995) and Hilgen et al. (2007). The authors applied astronomical tuning of the pre-evaporitic Messinian sapropel-marl cycles to the insolation peaks, showing good to excellent fit between the characteristic sedimentary cycle patterns and the astronomical target curve, including precession/obliquity interference patterns in insolation. This tuning was a key to date the widely accepted age of the onset of the MSC at around 5.96 Ma (section 1.1).

1.2.2 Onshore MSC Record

Except for the basins of Caltanissetta (Sicily) and Mesaoria (Cyprus), the rest of the onshore basins containing a MSC record are classified as marginal basins (Figure 1.4). Those basins have been tectonically active during and/or after the MSC, reason for which today most of their MSC record is outcropping and/or incomplete due to erosion.

The majority of the MSC studies and the built models come from studies of basins that are lying onshore. In particular, the Caltanissetta Basin in Sicily is considered a key basin from

which most of the model constraints come from, due to the resemblance of its MSC sequence to the one imaged in the deep Western Mediterranean Basin (J. M. Rouchy & Caruso, 2006; Roveri, Lugli, et al., 2014). In the following sub-sections, a summary of the main MSC units and their bounding surfaces that have been studied onshore will be described. Those are namely the Primary Lower Gypsum (PLG), the Resedimented Lower Gypsum (RLG), the Salt, the Upper Evaporites (UE) and the Lago Mare units (Figure 1.4).

1.2.2.1 The Primary Lower Gypsum (PLG) and its time-lateral equivalents

The onset of the MSC in the marginal basins is marked almost everywhere around the Mediterranean by primary in situ gypsum beds called the Primary Lower Gypsum (PLG - e.g. Yesares member in Sorbas Basin (Krijgsman et al., 2001b) ; Vena del Gesso formation in the Northern Apennines (Vai & Lucchi, 1977a)). The PLG unit deposited in stage 1 of the MSC and it includes up to 16 gypsum-mudstone precession driven cycles (Krijgsman et al., 1999; Lugli et al., 2010; Manzi et al., 2013), each cycle consisting of thick selenitic gypsum beds that vary from large massive bottom-grown selenites to gyparenites/gypssiltites and gypscumulites (Lugli, Vinicio, et al., 2010; Natalicchio et al., 2021) that deposited during the arid phase of the precessional cycles, separated by thinner organic-rich shale horizons that deposited during the humid phase of the precessional cycles (Figure 1.5).

Lugli et al. (2010) studied and correlated the PLG unit thicknesses and facies from different marginal basins of the Mediterranean. The five lowermost cycles consist of massive and banded selenite beds; cycles 1 and 2 are the thinnest (few meters) whereas cycles 3-5 are the thickest (up to 40 m). The uppermost cycles (6-16) show intermediate thicknesses with peculiar gypsum facies (branching selenite supercones; Lugli et al., 2010). According to those authors, the change in facies inside each cycle reflects the passage from arid to humid phase at the insolation minima and the insolation maxima respectively at a precession scale (Figure 1.5). The same authors also propose that the PLG formed exclusively in silled/closed basins at a maximum paleo-depth of 200m.

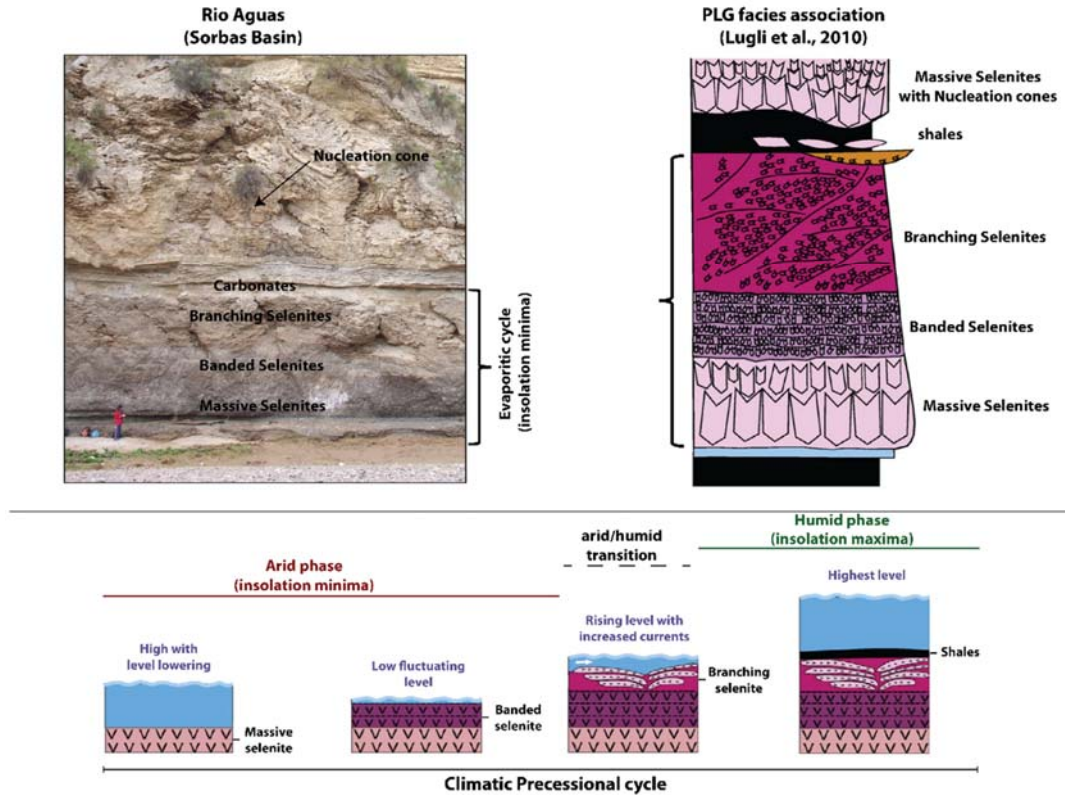


Figure 1.5. Facies representation of a typical PLG cycles following the facies association proposed by Lugli et al. (2010), and the hypothetical evolution of the brine level through a precessional cycle. Outcrop image credit to Sevasti Modestu featuring Johanna Lofi as scale. Facies drawing and model are modified from Lugli et al. (2010).

Towards the proximal domains of the marginal basins, the PLG thins out until pinching out on local highs or passes laterally into limestones known as the Terminal Carbonate Complex (TCC - Cornée et al., 2004; Roveri et al., 2009; Bourillot et al., 2010; Roveri et al., 2020). Other carbonate sediments known to represent the shallower lateral equivalent of the PLG are the Calcare di Base (CdB) limestones found in Sicily and Calabria basins (Ogniben, 1957). However, there is an ongoing debate whether the TCC and/or CdB mark the onset of the MSC or deposited in advanced stages of the crisis (see chapter 4 section 4.2.2 for more details; (Manzi et al., 2011; Caruso et al., 2015; Manzi, Gennari, et al., 2016)).

The distal time equivalent of the PLG in the marginal basins is expressed by marls, diatomites and thin laminated dolostones (e.g., Manzi et al., 2007) or organic rich shales (e.g., Dela Pierre et al., 2011). Those sediments were named Foraminifer-Barren Interval (FBI) by Manzi et al. (2018) (Figure 1.4).

A common feature overlying the top of the PLG unit and its proximal equivalent is a

widespread truncation by an erosional surface called the Margin/Messinian Erosional Surface (MES – Lofi et al., 2011) interpreted as the result of the subaerial exposure of the units following the MSC base level drawdown. According to most of the stratigraphic studies the MES's equivalent in a more distal domain is represented by a correlative conformity as no erosion involve the top of the FBI sediments (Dela Pierre, Bernardi, Cavagna, Clari, Gennari, Irace, Lozar, Lugli, Manzi, & Natalicchio, 2011; Manzi et al., 2011; Manzi, Gennari, et al., 2021).

The onset of the MSC, however, is not always coinciding with the base of the PLG, TCC and/or FBI as those units are sometimes locally missing (e.g., Dela Pierre et al., 2011; Manzi et al., 2016).

Main controversies and debates about the PLG

Two main open controversies/questions about the PLG unit will be targeted in this thesis:

- according to Lugli et al., (2010), the deposition of PLG took place exclusively within relatively shallow water depth (<200 m). Those authors base there hypothesis on the fact that the selenite crystals of the PLG contain filaments interpreted as cyanobacteria remnants (Vai & Lucchi, 1977a; Panieri et al., 2010) and thus limiting the paleo-water depth to the photic zone (~200 m) in which such micro-organism communities survive. However, this interpretation is debated as the same filaments are interpreted by other authors (Natalicchio et al., 2012; Dela Pierre et al., 2015; Pellegrino et al., 2021) as sulfide-oxidizing bacteria that can survive in wide range of water depth (Bailey et al., 2009; Natalicchio et al., 2021). Moreover, the occurrence of planktic diatoms trapped in the selenite crystals of PLG cycles 1 and 2 in the Piedmont Basin agrees with the notion that bottom-grown gypsum does not necessarily reflect shallow water conditions as those diatoms nowadays thrive in coastal to open waters (Pellegrino et al., 2021).
- Another open question is whether the PLG deposited everywhere on the Mediterranean Basin margins or the deposition was restricted to silled basins. Lugli et al. (2010) enhanced the necessity of a topographic sill in controlling the circulation in the basin during the PLG emplacement. However, the present-day distribution of the PLG is not limited to such basins as it can be found on open shelves in some offshore basins (e.g.

Elche Basin – offshore Alicante – Spain, Ochoa et al., 2015; Valencia Basin, del Olmo, 2011). Regarding the deeper domain (slopes and abyssal plains), several authors stated that, at a certain depth in those domains, the lack of oxygenation of the waters at sea bottom could hamper the formation of primary gypsum crystals (Babel, 2007; de Lange & Krijgsman, 2010a).

Another ongoing controversy, that is not be targeted in this thesis, is the low salinity values obtained from water inclusions in PLG gypsum crystals hinting for non-evaporative processes involved during the PLG stage (e.g. Piedmont Basin, Italy; Natalicchio et al., 2014; Calabria, Italy; Costanzo et al., 2019). However, the reliability of the salinities obtained from fluid inclusions measurements was recently questioned (Bigi et al., 2022).

1.2.2.2 The Resedimented Lower Gypsum (RLG)

The Resedimented Lower Gypsum (RLG) unit was introduced for the first time to the MSC literature by Roveri et al. (2006). It is found in the northern Apennines (Roveri et al., 2003; Manzi et al., 2005b), Sicily (Roveri et al., 2006), southern Spain (Fortuin et al., 1995; Fortuin & Krijgsman, 2003; Clauzon et al., 2015a), Cyprus (Orszag-Sperber et al., 2009; Artiaga et al., 2021) and Morocco (J.-J. Cornée et al., 2016). It consists mainly of relatively (relative to PLG) deep-water resedimented gypsum deposits resulting from the erosion and or/gliding of the PLG unit (Roveri et al., 2008a) during stage 2 of the MSC when the base level went down and margins were uplifted. According to Roveri et al. (2006), the emplacement of the PLG took place by several types of gravity-flows ranging from low-density turbidity currents to giant submarine slides involving huge slabs of massive selenite PLG bodies sliding from margins towards deeper waters. Thus, the RLG unit is thickest in the main depocenters and it thins out toward the margins, where it is also characterized by finer-grained facies dominated by gypsarenites and gypsum laminites. Rapid lateral facies and thickness changes within individual sub-basins suggest a strong topographic control and a syntectonic deposition (Figure 1.6). In particular, the evidence of huge mass-wasting involving the PLG massive selenite unit points to large-scale collapses (Manzi et al., 2021) of primary evaporitic basins, probably favored by the strong mechanical contrast between gypsum beds and intervening and/or underlying euxinic shales and marls, as also documented in the Apennine foredeep basin

(Roveri et al., 2003; Manzi et al., 2005b). However, deformation involving the massive selenite unit has also been related to dissolution of salt originally interbedded with gypsum (Rouchy & Caruso, 2006) thus questioning the tectonic/erosive origin of the RLG.

Main controversies and debates about the RLG

The main controversy about the RLG unit is related to the mechanism that formed it. It has been interpreted as (1) the result of intra- Messinian tectonic deformation (Decima and Wezel, 1971), (2) collapse features due to dissolution of more soluble evaporites interbedded in the gypsum beds (halite and K/Mg salts; Rouchy and Caruso, 2006), (3) subaerial fluvial deposits (Bache et al., 2012), or (4) mass transport deposits related to large-scale subaqueous instability processes (Fortuin et al., 1995; Roveri et al., 2006; Manzi, Roveri, et al., 2021).

Another problematic issue about the RLG unit that will be targeted in this thesis is the timing of its emplacement. The Roveri et al. group does not provide a reason for which the emplacement of RLG is limited to stage 2. Since they associate the active tectonics along growing thrust belts as the main trigger of its formation, one might question how and why did this happen contemporaneously in different basins of the Mediterranean that have nothing in common in terms of tectonic history and evolution.

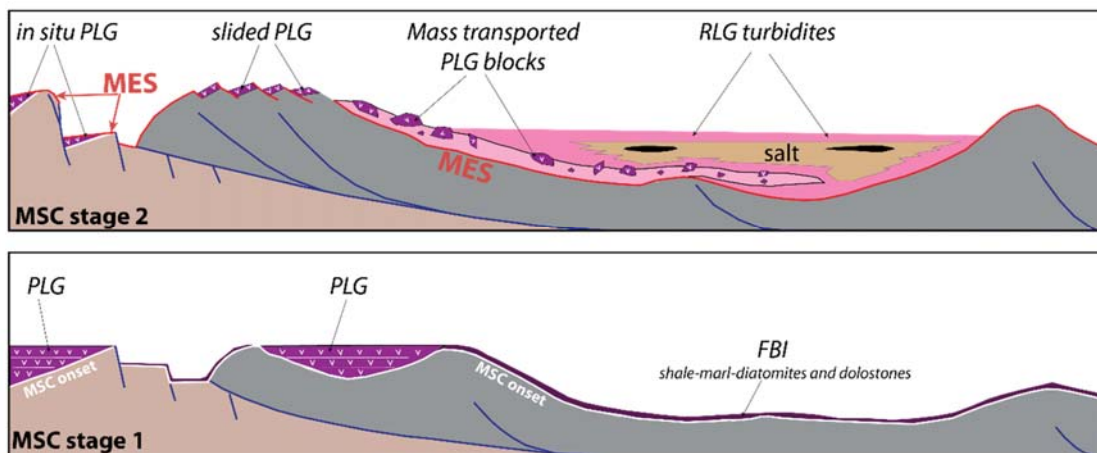


Figure 1.6. Schematic drawing of the RLG deposition during MSC stage 2 as proposed by Roveri et al. (2006). Modified from (Manzi, Roveri, et al., 2021).

1.2.2.3 The Salt Unit

According to the CIESM model, the salt deposition took place exclusively during stage 2, contemporaneously with the erosion of the PLG in the marginal basins and the deposition of the RLG (Figure 1.4). Onshore, the MSC salt is found only in Caltanissetta Basin (Sicily), Mesaoria Basin (Cyprus) and in Crotona Basin (Calabria-Italy). The common characteristic about these 3 basins is that they are classified as intermediate-depth basins (Figure 1.4) (Manzi et al., 2016) and are situated in tectonically active area. In all of the above-mentioned basins, the MSC salt is very rarely outcropping and it is accessible by mining activities and/or boreholes. Mesaoria and Crotona basins' MSC salt has been documented only by old industrial boreholes (Gass, 1960; Zecchin et al., 2013) and seismic profiles (Maillard et al., 2011; Zecchin et al., 2013), thus it has never been studied further. This is not the case for the Sicilian halite in Caltanissetta Basin, where the Realmonte salt mine, opened by Italkali company, in its southern part offered a unique opportunity to access the MSC salt and study it.

The salt of the Caltanissetta Basin is made of a massive halite body including also large amounts of, more soluble, potash salts mainly represented by kainite and minor inclusions of carnallite, bishofite, and sylvite (Figure 1.7) (Decima & Wezel, 1971; Lugli et al., 1999b). The salt body of the Realmonte mine has been divided into 4 depositional units (A to D; Figure 1.7-B); from bottom to top (Decima & Wezel, 1971, 1973b; Decima, 1976; Lugli et al., 1999b; García-Veigas et al., 2018b), those are:

- A- up to 50m-thick gray halite beds with white anhydrite nodules, passing upward to gray massive halite. The absence of bottom-grown crystals and the abundance of skeletal hopper crystals in this unit suggest formation in a significant water depth (Lowenstein & Hardie, 1985; Garcia-Veigas et al., 1995).
- B- up to 100m-thick massive halite with 6 light gray kainite layers that reach 12m thickness. The presence of rectangular crystal rafts in this unit suggest a shallow water deposition (Lowenstein & Hardie, 1985; Garcia-Veigas et al., 1995).
- C- up to 80m-thick white halite layers with high-frequency gray-mud inclusions. This unit is characterized by vertically elongated chevron halite crystals truncated by dissolution surfaces, which indicate shallow water conditions (Garcia-Veigas et al., 1995; Lugli et al., 1999b).
- D- up to 60m-thick gray halite with very frequent anhydrite laminate inclusions. Similar to unit C, this unit contains abundant chevron crystals truncated by dissolution surfaces,

indicating shallow water environment (Lowenstein & Hardie, 1985; Garcia-Veigas et al., 1995).

A striking geological feature that characterizes the MSC salt unit in the Caltanissetta Basin are the 6m high vertical fissures that cut the topmost part of unit B at its upper boundary (contact with unit C; Figure 1.7-C,D). They are filled with red mud and have been interpreted as desiccation cracks representing an exposure surface following the complete evaporation of the basin's water body Figure 1.7-D (Lugli et al., 1999b). The high-frequency halite-mud cyclicity characterizing unit C have been further studied by Manzi et al. (2012) and have been correlated to Quasi-Biennial Oscillations, the El Nino Southern Oscillations, the sunspot number solar cycles and lunisolar tidal cycles similar to the present-day quasi-periodic climate oscillations that characterize modern evaporitic analogues (Warren, 2010).

The geological stacking of the halite unit and its petrographic characteristics as described above, suggest a shallowing upward trend with the first salts (halite) depositing in deep-water conditions. The continuous evaporation of the basin lead to the deposition of the higher-salinity, more soluble salts (kainite) that were subsequently exposed to subaerial erosion which lead to the formation of the desiccation cracks.

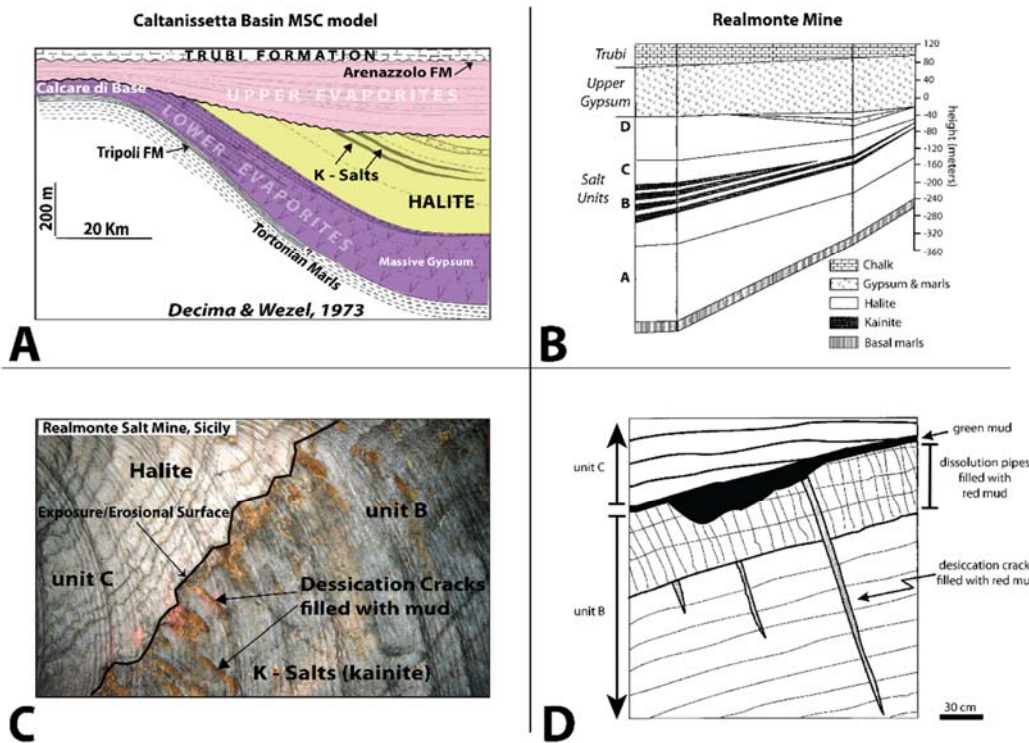


Figure 1.7. A: Sedimentary model of the Caltanissetta Basin highlighting the stratigraphic position and the geometrical relationship of the MSC halite with the other evaporitic deposits. Modified from Decima & Wezel, (1973). B: Stratigraphic column of the Realmonte mine in Sicily showing the position and thickness of the MSC halite units. Modified from Lugli et al. (1999). C: The MSC salt at the Realmonte Mine showing the exposure surface at the top of the K-Mg salts (unit B) with the desiccation cracks and the passage to halitic salts (unit C). D: A drawing of the contact between units B and C showing the sets of fissures initiating from the salt layers. Modified from Lugli et al. (1999).

Main controversies and debates about the salt unit

The main ongoing controversy about the formation of the MSC salt, and that will be targeted as an output of the work of this dissertation are:

- The onset of the salt's deposition. The salt bodies of the Caltanissetta Basin have been interpreted in 2 different ways: (1) for some authors it is, at least partly, the deep lateral equivalent of the PLG and thus it started depositing already in the earliest times (stage 1) of the MSC (Catalano & D'argenio, 1982; ROUCHY, 1982; Garcia-Veigas et al., 1995; J. M. Rouchy & Caruso, 2006); (2) for other authors it stratigraphically overlies

the PLG (Figure 1.7-A) and thus its deposition started only in later stages (stage 2) of the MSC (Decima & Wezel, 1971, 1973b; Roveri et al., 2008a). It is worth noticing that none of the boreholes drilled onland sampled the PLG below the salt unit.

- The above controversy extends, even with more complications, to the offshore salt unit that dominates the abyssal plains of the deep Mediterranean Basin. Between Sicily's salt and the deep basin salt, arises another question concerning whether the onset of salt deposition started contemporaneously everywhere or it was diachronous. This will be discussed further in section 1.2.5.2 when the offshore MSC units are presented.
- The amplitude and timing of the drawdown is another big unanswered question that is directly related to the emplacement mechanisms of the MSC salt unit. The clear erosional surface evidenced by the desiccation cracks described earlier (Figure 1.7) is a direct proof of the complete desiccation of the Caltanissetta Basin. Even though retrieving the paleo-depth of the basin during the MSC is very difficult because of the complex and very active tectonics that have been active since then, there are evidences indicating that the first post-MSC sediments that overly the MSC evaporites, contain fauna that live in depths of at least 1000m (CITA & COLOMBO, 2006; Sgarrella et al., 1997). According to the Roveri et al., group, the desiccation of the Caltanissetta Basin is only local and related to tectonics, and does not indicate that similar sea-level drawdown amplitude occurred elsewhere in the Mediterranean Basin. This is the most non-reasonable explanation, as this group just ignores all the rest of evidences coming from other basins of the Mediterranean and showing base level drawdown in the order of 1000+ meters (see section 1.3).

1.2.2.4 The Upper Evaporites Unit and Lago Mare

The Upper Evaporites and Lago Mare represent the final stage of the MSC in which the Mediterranean condition changed drastically from evaporitic phase (stage 3.1; upper evaporites) into brackish to fresh water conditions (stage 3.2; Lago Mare). Hereafter is a very brief description of the deposits that characterize both stages. An extended review with proper figures and detailed argumentation about those phases and their controversies will be presented in details in Annex A of this thesis.

1.2.2.4.1 The Upper Evaporites (UE)

Like the salt unit, the upper evaporites are found exclusively in intermediate-depth basins (Figure 1.4), namely Caltanissetta Basin (Decima & Wezel, 1973b; J. M. Rouchy & Caruso, 2006; Manzi et al., 2009a) and Cyprus (Rouchy et al., 2001; Manzi et al., 2016). They overly the salt unit and are proposed to have deposited during stage 3 of the MSC (Figure 1.7-A). The most complete section in which the upper evaporites unit outcrop is the Eraclea Minoa section in the Caltanissetta Basin (Sicily). There, the upper evaporites consist of ~200m thick, 6 to 7, precession driven, primary gypsum beds with repetitive internal organization of facies interbedded with marls and lenticular terrigenous sandstone bodies, gypsarenites and gypsrudites (Rouchy & Caruso, 2006; Van der Laan et al., 2006; Manzi et al., 2009). Towards the proximal parts of the Caltanissetta Basin, the terrigenous content of the upper evaporites decreases drastically as the gypsum beds from successive cycles become in contact. There, the upper evaporites onlap the underlying unit (PLG/RLG).

Onshore Cyprus, the upper evaporites unit is incomplete and comprises up to 6 gypsum beds, the lower three of which are mainly selenitic, while the upper three are predominantly laminated with an overall thickness of ~60m (J. M. Rouchy et al., 2001; Orszag-Sperber, 2006b; Manzi, Lugli, et al., 2016). The gypsum beds vary in thickness from 1 to 6m and are separated by laminated marls occasionally interbedded with conglomerates and sandstones. The sixth gypsum bed is interpreted by Rouchy et al. (2001) to be hollowed in the upper part with cavities filled with overlying sediments. According to both (J. M. Rouchy et al., 2001; Orszag-Sperber, 2006b), the top of the last gypsum bed of the Cypriot upper evaporites, coincides with a Mediterranean-scale sea-level drop, due to the presence of the above-mentioned cavities that are interpreted as the product of karstic dissolution following a prolonged period of subaerial exposure.

1.2.2.4.2 The Lago Mare

The Lago Mare cannot be considered a depositional unit but it is more a phase that the Mediterranean underwent at the end of the MSC in which brackish water conditions dominated the whole basin. It is present as variable lithologies between different basins that can vary from conglomerates (e.g., Adana Basin – Turkey; Cipollari et al., 2012; Faranda et al., 2013), to

sandstone (e.g. Caltanissetta Basin – Sicily; Decima & Wezel, 1973; Cita & Colombo, 1979), to mudstones (e.g. Mallorca – Spain; Mas & Fornós, 2020). The common feature, however, in those units is the appearance, following a completely barren MSC interval, of brackish water ostracods with Paratethyan affinity (Orszag-Sperber, 2006b). Whether the Mediterranean peribasins were connected in one whole water Mediterranean body fed by both the Atlantic and Paratethyan waters, or it was represented by separate water lakes alimeted by local rivers is the hardest question to answer when it comes to the Lago Mare phase (see Annex A). In the first case, the ostracods would simply transfer from the Paratethys to the Mediterranean through the watergate connecting the two water bodies (e.g., Marzocchi et al., 2016). In the latter case, the ostracods would be brought to the Mediterranean by migrating birds (Caruso et al., 2020).

1.2.3 Offshore MSC Record

The abyssal plains of the offshore domain of the Mediterranean are paved by prominent MSC deposits extending in almost all the basin, bounded by several erosional and/or conformable surfaces, and capped by a younger sedimentary unit that is Pliocene to Quaternary (PQ unit) in age (Figure 1.3 and Figure 1.8). The offshore MSC deposits constitute more than the 90% of the overall MSC deposits having an immense volume that reach ~ 1.2 million km^3 (W. B. f. Ryan, 1976; Haq et al., 2020b). Surprisingly enough, those deposits, particularly the Western Mediterranean ones, are still very poorly explored and or/ accessed, especially for the academic research. Most of the studies dedicated for the offshore MSC deposits are based on seismic reflection data (Lofi, 2011, 2018). The Deep Sea Drilling Project (DSDP; Figure 1.3) executed between the 70s and 80s of the past century, provided access to the topmost part of those deposits (Cita, 1973; Hsü et al., 1973b; W. B. F. Ryan & Hsü, 1973). A lot of industrial boreholes were drilled on the Spanish and Italian shelves of the Western Mediterranean, but unfortunately most of those boreholes are either beyond the extension of the MSC deposits or drilled through thin incomplete MSC sequence (e.g., del Olmo, 2011a, 2011b). Exceptionally, in the last decade, several industrial drillings went through the whole evaporitic sequence of the Levant Basin in the Eastern Mediterranean due to the increase interest in the oil and gas exploration of that area. Access to recovered cuttings and petrophysical well-logs from the MSC sequence in that area was provided to the scientific community which allowed to better study the deep basin evaporites (e.g., Feng et al., 2016; Meilijson et al., 2019; Manzi, Gennari,

et al., 2021). Traditionally, there was a distinction between the Western and Eastern Mediterranean MSC record where the Western Mediterranean records the so-called ‘trilogy’ with three distinct seismic units (MONTADERT et al., 1970), whereas the eastern Mediterranean, with the exception of the Ionian Basin, contains only a thick salt unit (Lofi, 2011).

In the following sub-sections, a summary of the main MSC units and their bounding surfaces that have been studied offshore will be described.

The MSC surfaces observed through seismic data offshore are (Figure 1.8):

- The Margin Erosion Surface (MES), observed on margins and slope in the absence of MSC units.
- The Bottom Surface (BS), or Bottom Erosion Surface (BES) when erosional, observed on slopes and in basins underlying existing MSC unit(s).
- The Intermediate Surface (IS), or Intermediate Erosion Surface (IES) when erosional, observed on slopes and in basins when sandwiched between 2 MSC units.
- The Top Surface (TS), or Top Erosion Surface (TES), observed on slope and in basins at the upper boundary between a MSC unit and post-MSC unit.

The units representing the MSC trilogy of the deep Western Mediterranean Basin are the Lower Unit (LU), the Mobile Unit (MU), and the Upper Unit (UU) (Figure 1.8). Other offshore units found in relatively shallower contexts such as shelves or intermediate to shallow basins are the Bedded Unit (BU) and the Complex Unit (CU).

This nomenclature was established and is continuously updated by the publications of Lofi, (2011, 2018b), in order to offer a global and consistent terminology for MSC markers (key bounding surfaces and depositional units) that can be used in the entire offshore Mediterranean area, in order to avoid nomenclatural problems. Since this nomenclature relies on seismic facies and geometrical relationship they cannot be used as a chronostratigraphic tool, and the same surface/unit from different places could have a different age.

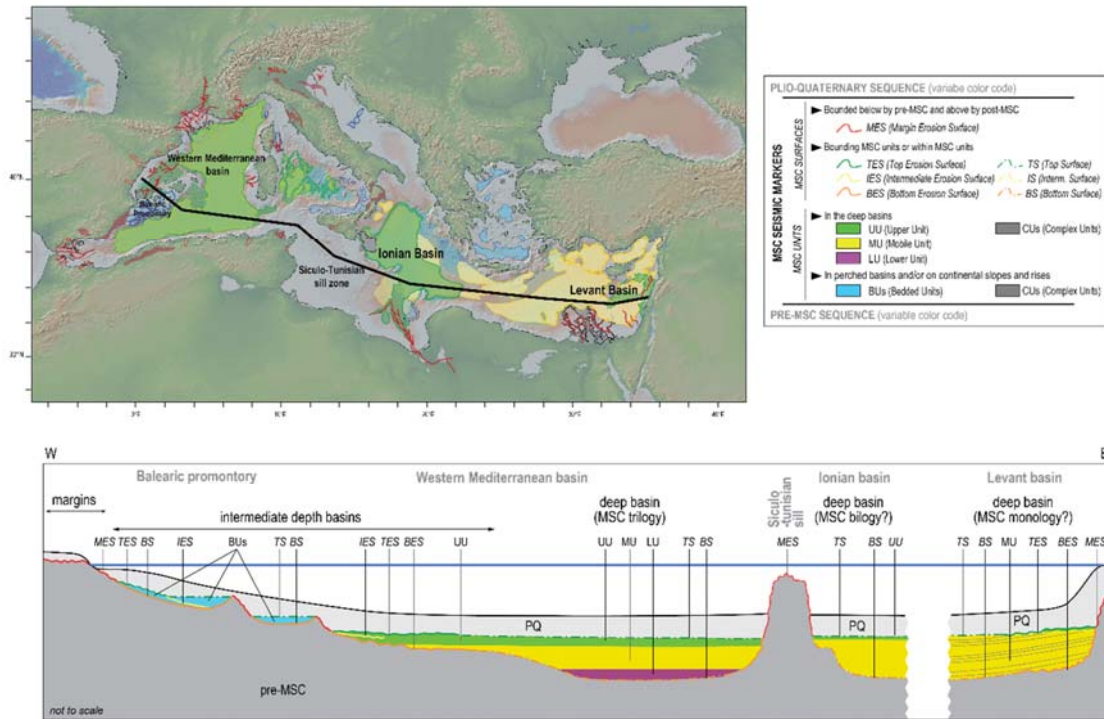


Figure 1.8. Schematic cross section of the Mediterranean basin illustrating the present-day distribution of the offshore MSC markers. Salt tectonics in the Western Mediterranean are not shown in the cross section (section 1.2.5.2). The Lower Unit's (LU) presence is only clearly documented in the Provencal Basin (section 1.2.5.1). The Complex Unit (CU) is not shown due to its complex, variable, geometrical and temporal relationship with the MSC units (section 1.2.5.4). Modified from (Lofi, 2018b).

1.2.4 The MSC offshore Surfaces

1.2.4.1 Margin Erosion Surface

The MES is the most important and widespread erosional feature. It consists in an erosion surface generally well identified on the upper margins (Figure 1.3 and Figure 1.8). The MES has been correlated with several exploration boreholes on the Mediterranean shelves, revealing an unconformity between pre-MSC and Pliocene deposits (Cravatte et al., 1974; Lanaja, 1987). Subaerial erosion features, such as fossil meanders and fluvial terraces (Stampfli & Höcker, 1989; Urgeles, Camerlenghi, Garcia-Castellanos, De Mol, Garces, et al., 2011) have been described from margin edges, suggesting fluvial erosion as an origin of the MES. It is thus

commonly interpreted as the result of subaerial erosion, essentially by river action and retrogressive erosion (Lofi, Gorini, Berné, Clauzon, Tadeu Dos Reis, et al., 2005; Loget & Van Den Driessche, 2006). In the proximal onshore domain, the MES is characterized by the presence of deep narrow incisions, which correspond to the entrenchment of streams in response to a large base level drop during the MSC (Chumakov, 1973; Clauzon, 1978).

Offshore, on the seismic profiles, the MES generally forms a prominent reflection with a strong erosional character as usually indicated by the truncation of the pre-MSC reflections (Figure 1.9, profiles A and B; zoom 03). The MES displays various morphologies, generally extremely rugged with deep incision beneath the inner and middle shelves (Figure 1.9, zoom 03) and becoming smoother basinward (Figure 1.9, profile A). The MES is also commonly evidenced by a high angular discordance between pre-MSC and Plio-Quaternary deposits (Figure 1.9, profile B; Lofi et al., 2011). Numerous investigations have enabled reconstructions of the detailed paleomorphologies of the MES at several margins, revealing the existence of Messinian paleo-fluvial networks: e.g. Egyptian margin (Barber, 1981), Gulf of Lions shelf (Guennoc et al., 2000), Ebro margin (Stampfli & Höcker, 1989; Urgeles, Camerlenghi, Garcia-Castellanos, De Mol, Garces, et al., 2011).

On large margins with thick and soft sediment cover, it has however been proposed that sub-aquatic processes such as gravity flows may have also contributed to the shaping of the MES at the beginning of the drawdown (Lofi, Gorini, Berné, Clauzon, Tadeu Dos Reis, et al., 2005; Cameselle & Urgeles, 2017a). In contrast, Roveri, Manzi, et al. (2014) suggested that the entire drainage networks visible on the seismic could be completely of subaqueous origin. The authors used numerical modelling to simulate dense shelf water cascading brines and conclude that the cascading water is at the origin of the incision of the MES (Figure 1.11).

1.2.4.2 Bottom Surface (BS) and Bottom Erosion Surface (BES)

The BS and the BES mark the base of the MSC deposits where present. In some places, the base of the MSC deposits is a conformable surface (BS), whereas in other places it is erosional/unconformable (BES).

In the Western Mediterranean, the BES passes basinward beneath the three Messinian units (UU, MU and LU) extending towards the depocenters, where it becomes a BS. Evidences for erosion of the pre-MSC deposits are frequent on the seismic data especially in the intermediate depth basins, such as the erosion beneath UU in the Valencia basin (Figure 1.9, profile C; Maillard et al., 2006) and beneath the Messinian Bedded Unit (BU) of the eastern Corsica Basin

(Thinon et al., 2016). In those areas, the BES displays locally small discontinuous gully type incisions. In the Gulf of Lions, there is also local evidence for erosion with truncations in the distal domain (Figure 1.9, profile A).

It is, however, often difficult to determine if the pre-MSC truncated reflections observed on the seismic profiles are related to the MSC event or instead reflect a pre-existing paleo-morphology predating the MSC.

In the eastern Mediterranean, the BS/BES generally extends beneath MU (Figure 1.10, zoom 02). There, the BES clearly shows evidence for erosion thanks to the truncation of the underlying reflections, related to MSC canyon systems (Bertoni & Cartwright, 2006). Locally, this surface passes at the bottom of some thin deposits supplied by the canyons and accumulated beneath MU. On the Cyprus arc a BS with no signs of erosion is observed at the base of MU, and shows large-scale deformation (Figure 1.10, profile F) reflecting the active tectonic context.

1.2.4.3 Intermediate Erosion Surfaces (IES)

The IES represent some intermediate unconformities contained in the MSC depositional units. Chronostratigraphically, they post-date the BS/BES and pre-date the TS/TES (Lofi, 2011). Several IESs, with clear erosional aspects (e.g., gullied morphologies), are documented within the thin MSC units (UU and BU) of the intermediate-depth basins (Figure 1.8; e.g., Valencia Basin, Maillard et al., 2006; east Corsica Basin, Thinon et al., 2016).

In the Levant Basin, a new intermediate surface truncating the upper boundary of the MU has been described by Gvirtzman et al. (2017). The authors labeled it as the Intra-Messinian Truncation Surface (IMTS; Figure 1.10, zooms 01 and 02).

1.2.4.4 Top Surface (TS) and Top Erosion Surface (TES)

The TS and the TES mark the top of the MSC deposits where present (Figure 1.8). In some places, the top of the MSC deposits is a conformable surface (TS), whereas in other places it is erosional (TES).

In the western Mediterranean basin, the TES passes basinward to the youngest MSC unit (UU) and extends toward the center of the basin, where it becomes a TS, except in areas affected by salt tectonics (Figure 1.9, profiles D and E). On slopes and at intermediate depths basins,

evidence for erosion of the top MSC deposits is however frequent on the seismic data. For example, in the Valencia Basin the erosional character of the TES incising the top of the UU is perfectly pronounced (Figure 1.9, profile C; [Frey-Martinez et al., 2004](#); [Maillard & Mauffret, 2006](#); [Urgeles et al., 2011](#)), where it is characterized by a sinuous central paleo-valley having tributaries that extend to the Provençal Basin ([Escutia & Maldonado, 1992b](#); [Maillard et al., 2006b](#); [Cameselle & Urgeles, 2017a](#); [Pellen et al., 2019b](#)).

In the eastern Mediterranean's Levant Basin, the TES, which was thought to be the erosional upper boundary of the MSC ([W. B. Ryan, 1978](#); [Lofi, Sage, Déverchère, et al., 2011](#)) was later relabeled as IES ([Madof et al., 2019](#)) or IMTS ([Gvirtzman et al., 2017](#)), following the discovery of a MSC unit above the MU (sections 1.2.5.2 and 1.2.5.3), called Nahr Mensahe corresponding to a very thin UU ([Madof et al., 2019](#); see section 1.2.5.3). [Madof et al. \(2019\)](#) argue that the top of this unit is erosional (TES; Figure 1.10, zooms 01 and 02), displaying meandering, reason for which they interpret it as of fluvial origin.

In the Ionian Basin, [Camerlenghi et al. \(2019\)](#) also evidenced the presence of a TES, imaged as V-shaped incisions and truncations (see also section 4.6 in Annex A). They interpret it as fluvial valleys carved in subaerially exposed UU by the Eso-Sahabi fluvial system, the closest fluvial drainage network to the area ([Micallef, Camerlenghi, Garcia-Castellanos, Otero, et al., 2018](#)) that drained Libya in the late Miocene ([Griffin, 2002](#)) and that has been traced across the Gulf of Sirt offshore ([Bowman, 2012](#)).

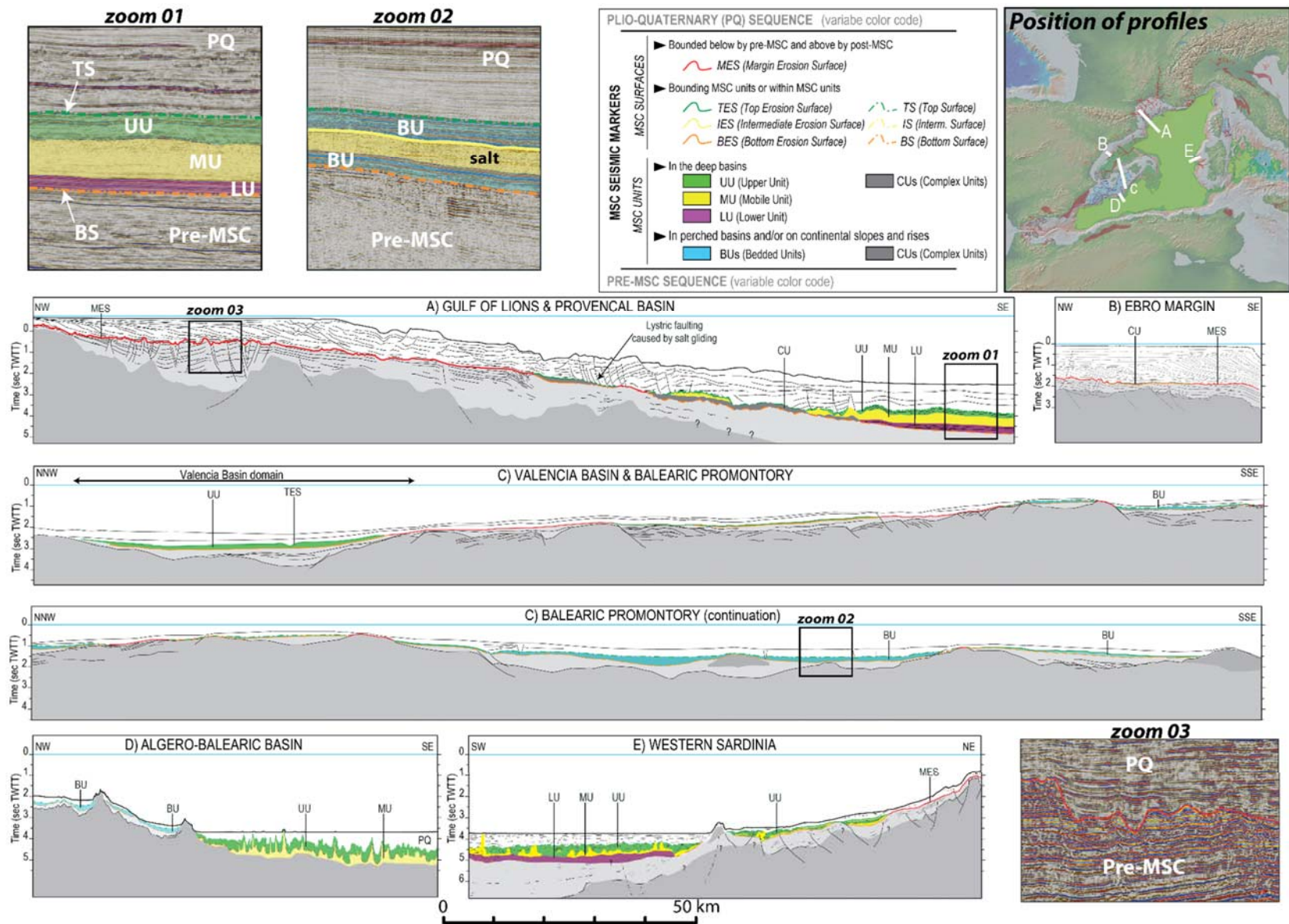


Figure 1.9. Present-day line drawings derived from seismic profiles illustrating the distribution of the MSC markers across several sub-basins of the Western Mediterranean. Modified from (Lofi, 2018b).

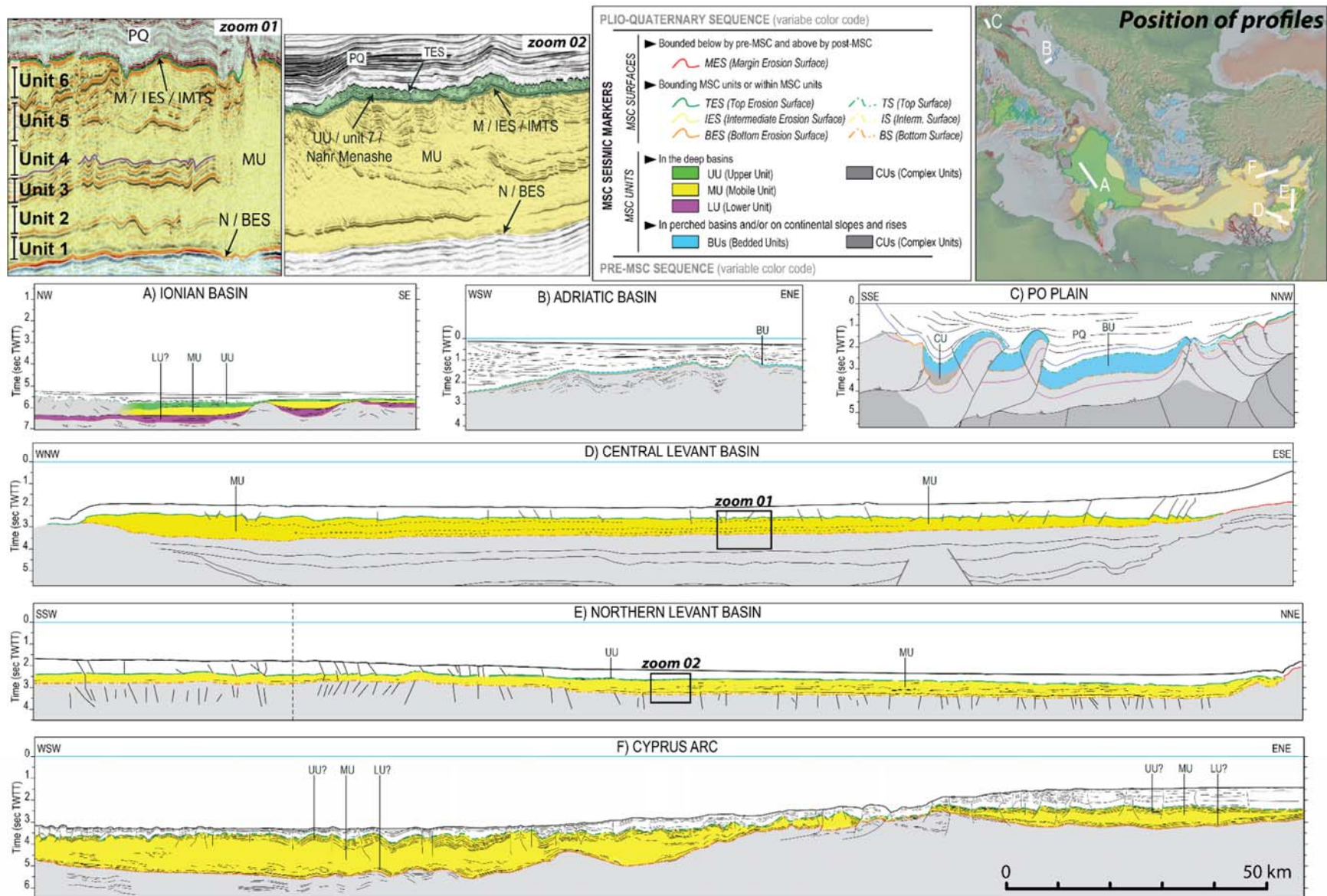


Figure 1.10. Present-day line drawings derived from seismic profiles illustrating the distribution of the MSC markers across several sub-basins of the Eastern Mediterranean. Modified from (Lofi, 2018b).

1.2.5 The MSC offshore Units

1.2.5.1 The Lower Unit (LU)

LU is the oldest unit of the MSC trilogy from a seismic stratigraphic point of view. It overlies the pre-MSC unit along a conformable surface called the Bottom Surface (BS; Figure 1.8; Figure 1.9, profiles A and E). In some places it is thought that it onlaps the BES/BS but this geometry has been observed only locally. On the seismic reflection profiles it appears as a group of continuous high amplitude reflections (Figure 1.9, zoom 01) (Lofi, Sage, Déverchère, et al., 2011). The present day distribution of the LU is still not clear. It is locally well imaged and mapped in the Provencal Basin (Lofi, Gorini, Berné, Clauzon, Tadeu Dos Reis, et al., 2005; Bache et al., 2009b), whereas in other basins of the Mediterranean its presence is yet not clearly evidenced. This could be due to the poor imaging below the MSC halite, especially in zone where the salt tectonics are very active (Obone-Zue-Obame et al., 2011). However, its presence have been inferred in the Algerian (Medaouri et al., 2014) and the Ionian (Camerlenghi et al., 2019) basins, where the presence of the salt tectonics, reduces the quality of the sub salt imaging and hampers the definitive proof of its presence. Its thickness in the Provencal Basin is debated according to the different existing interpretations. Lofi et al. (2011) proposed a maximum thickness of ~600m (0.35 sec TWTT for a velocity of 3500m/s) with LU onlapping the Miocene margin foot with no continuation on the slope, towards the proximal domains (Lofi et al., 2005). For Bache et al. (2009), the LU could be as thick as 1500m and passes laterally to clastic sediments extending on the margin slope. Bache et al. (2009) thus give a MSC syn-drawdown age to the submarine canyon cuts and fills identified on the Miocene slope by Lofi & Berné, (2008), previously considered by these latter as pre-MSC in age. There were several attempts to correlate the LU chronostratigraphically to the PLG (e.g. Krijgsman et al., 1999; Roveri et al., 2016), with some suggestions that it could be almost entirely evaporitic similar to the PLG sequence (Krijgsman, Hilgen, et al., 1999b). However, the nature and even the age of the LU are still unknown and all the hypothesis around them remain speculations until the unit is drilled. This is partly because the LU does not have a clear distinctive seismic imprint, contrary to the transparency of the MSC halite (see section 1.2.5.2), to confirm its nature definitively.

Offshore Israel in the Levant Basin (Eastern Mediterranean), the most recent studies from a number of industrial boreholes data by Manzi, et al. (2021) showed the presence of a 20m thick

cyclic (16 precessional cycles according to the authors) Foraminifer Barren Interval (FBI), similar to the FBI found elsewhere onshore (see section 1.2.2.1) marking the onset of the MSC in the deep basin. Assuming that the LU belongs to the MSC, then it could be the lateral time equivalent of the FBI of Manzi et al. (2021). However, studies from one of the boreholes investigated by Manzi et al. (2021), negated the presence of the FBI and suggested that it belongs to the pre-MSC sediments (Meilijson et al., 2018; Meilijson, Hilgen, et al., 2019b).

1.2.5.2 The Mobile Unit (MU)

The Mobile Unit (MU) is widespread in both Western and Eastern Mediterranean basins covering most if not all their abyssal plains (Figure 1.3) (Lofi, 2018).

In the Western Mediterranean, it is overlying the LU and clearly postdating it, along a sharp conformable contact (Figure 1.8 and Figure 1.9). Towards the margins and/or where the LU is absent, the MU overlies the pre-MSC sediments along an erosional surface known as the Bottom Erosional Surface (BES; Figure 1.9, profile A) (Lofi, Gorini, Berné, Clauzon, Tadeu Dos Reis, et al., 2005; Maillard et al., 2006b; Lofi, Sage, Déverchère, et al., 2011). On seismic profiles it is easily distinguished by having a global reflection free (transparent) seismic facies (Lofi, Sage, Déverchère, et al., 2011), and by its plastic deformation forming listric faults and complex salt structures such as salt diapirs (Figure 1.9, profile D) (Gauillier et al., 2006; Obone-Zue-Obame et al., 2011). In the Western Mediterranean, the MU has never been drilled, except for one DSDP borehole site 134 West to Sardinia Island (location on Figure 1.3) where there are only two cuttings from the drilling and are both consisting of pure halite (W. B. F. Ryan & Hsü, 1973; Sage et al., 2005; Lugli et al., 2015), thus there is no direct data for studies about its nature and characteristics. However, seen its plastic deformation and seismic facies, together with similarities in seismic facies with the drilled halite in the Eastern Mediterranean, it is thought to be dominantly made of halite (Nely, 1994). The thickness of the MU reaches a maximum thickness of about ~1000m (~0.5sec TWTT for an acoustic velocity of 4500m/s; Figure 1.9, profile A; Lofi et al., 2011) in the deepest parts of the Western Mediterranean Basin. It thins towards the margins of the basins where it pinches out (Figure 1.8 Figure 1.9). The present-day pinch out of the MU as imaged today on the seismic reflection profiles is clearly shifted towards the deeper parts of the basins due to the gliding of the salt along the lower slopes (Figure 1.9, profile A). This gliding is nicely evidenced by the presence of listric normal

growth faults (Gauillier & Bellaiche, 1996; dos Reis et al., 2005; Gauillier et al., 2006), the most proximal of which is considered the original paleo-pinchout of the MU (Lofi, 2011).

In the eastern Mediterranean Basin, particularly in the Levant Basin, the MU was traditionally thought to be the only MSC unit bounded by the pre-MSC sediments below and by the PQ unit above, along 2 erosional surfaces, the BES and the Top Erosional Surface (TES) (Lofi, 2011), respectively (Figure 1.10, profiles D to F; those surface were originally called N and M reflectors by W. B. Ryan, 1978). More recently, with the new high-resolution 3D seismic data and exploratory wells acquired by oil and gas companies, a new thin MSC unit (called Nahr Menashe by Madof et al., 2019 or unit 7 by Gvirtzman et al., 2017) overlying the MU came to the lights and thus the TES became an Intermediate Erosional Surface (IES; sensu Lofi et al., 2011) or intra-Messinian truncation surface (IMTS; sensu Gvirtzman et al., 2017) (Figure 1.10, zoom 02).

The MU in the Eastern Mediterranean is made mostly of halite and is considerably thicker than the one in the western basin, as it reaches thickness of ~3km in some places, with an average thickness of ~2km (Bertoni & Cartwright, 2007; Gvirtzman et al., 2017; Kirkham et al., 2019; Haq et al., 2020b).

The transparency of the seismic facies of the MU is interrupted by five high amplitude internal reflections (Bertoni & Cartwright, 2007; Gvirtzman et al., 2013, 2017). For this reason, Gvirtzman et al. (2013) divided the MU into 6 sub-units (1 to 6, from bottom to top; Figure 1.10, zoom 01). Later studies showed that layers of claystones (Gvirtzman et al., 2013; Feng et al., 2016) and/or argillaceous diatomites (Meilijson, Hilgen, et al., 2019b) are at the origin of the intra-MU reflections.

A much thinner salt unit (~250m), with very similar seismic characteristics, has been described in relatively shallower contest and completely disconnected from the deep basin MU (Acosta, Canals, et al., 2004b; Maillard et al., 2014b; Driussi, Maillard, et al., 2015b). It is found on the Balearic Promontory in a basin that has a present-day depth of about 1000m (Figure 1.9, zoom 02). This unit will be described and discussed in chapter 4.

Controversies around the MU come mainly from the Levant Basin where the halite constituting most of the unit is better studied. The main questions are somehow similar and related to the ones encountered when the onshore Sicilian salt of the Caltanissetta Basin was presented in section 0.

- The onset of the deposition of the halite is put at the beginning of stage 2 by (Manzi et al., 2018a; Manzi, Gennari, et al., 2021), and underlain by an FBI interval that represents the stage 1 equivalent of the deep basin. On the contrary, Meilijson et al. (2018) argue that the same FBI does not belong to the MSC and that the base of the halite (MU) represents the real onset of the MSC, inferring the beginning of salt deposition in the deep basin already taking place during stage 1.
- The origin of the erosional surface of the upper boundary (TES/IMTS) is the second debate about this unit. In their model, Gvirtzman et al. (2017) argue that no need for a drawdown and exposure of the halite in order to create the observed truncation at its top. Instead, they present a full basin model with a salinity-stratified water column in which the truncation of the salt is caused by relatively fresh water overlying the dense brine in depth. On the contrary, other authors suggest the truncation causing the erosional unconformity could be originated either by salt dissolution in under-saturated shallow diluted water (Kirkham et al., 2019) or by subaerial exposure (W. B. Ryan, 1978), both processes requiring a significant base level drop.

1.2.5.3 The Upper Unit (UU)

The Upper Unit (UU) is the youngest and the most widespread unit of the deep basin's MSC trilogy. It is present in most of the Mediterranean sub-basins, in deep to intermediate water basins, extending beyond the limit of the MU (Figure 1.3 Figure 1.8) (Maillard et al., 2006b; Lofi, Sage, Déverchère, et al., 2011). In the depocenters of the deep basins it overlies the MU along a conformable surface corresponding to an Intermediate Surface (IS; Figure 1.8). Whereas towards the margins of the deep basin the contact with the MU becomes erosional (IES), and beyond the pinch out of the MU it overlies the pre-MSC sediments along the BES (Figure 1.8) (Lofi, 2011, 2018b). Overlying the UU everywhere, is the Pliocene-Quaternary (PQ) sedimentary unit easily distinguished from the MSC deposits due the important acoustic impedance between its lowermost sediments and the UU. The contact between the UU and the overlying PQ unit, i.e., the Miocene-Pliocene boundary (originally called the M reflector by W. B. Ryan, (1978), is sharp and conformable in the deep basin, but becomes erosional towards the intermediate and marginal depths, which gave birth to another erosional surface called the Top Erosional Surface (TES; Figure 1.9, profile C). On the seismic profiles the UU appears as

a group of parallel and relatively continuous reflections (up to 9 reflections) having intermediate to very high amplitude (Figure 1.9, zoom 01). Its thickness spans from 0 (pinch out point on the pre-MSC slopes) to up to ~700m (0.4 sec TWTT using a mean acoustic velocity of 3500m/s) (Lofi, Sage, Déverchère, et al., 2011). According to Lofi et al. (2011) UU is aggrading and onlapping the margin foots, reason for which they interpret the onlaps of the UU as a succession of paleo-shorelines marker during a gradually rising base level.

The topmost part of the UU has been drilled during the DSDP and ODP expeditions (W. B. F. Ryan & Hsü, 1973; Hsu et al., 1978; Kastens & Mascle, 1990; EMEIS et al., 1996), thus revealing part of the identity of the UU. It is made of layers of gypsum and anhydrite intercalated with dolomitic marls, which explain its internal seismic facies. However, LOFI, (2011) highlighted lateral and vertical seismic facies changes in the UU in some areas which could reflect important local changes in the composition of the UU, passing for example from clast rich deposits close to the river thalwegs, to more evaporite rich deposits more distally. Indeed, fluvial deposits in DSDP site 122 were recovered from the topmost part of the UU of the Valencia Basin (Mauffret, 1977; Escutia & Maldonado, 1992). Most of the topmost parts of the recovered UU cores from the DSDP and ODP drillings showed brackish water fauna content with paratethyan affinity similar those described in the upper evaporites and lago mare stages (e.g. Cita et al., 1990; Iaccarino & Bossio, 1999) (see section 1.2.2.4 and Annex A).

In the Levant Basin offshore Israel, a unit similar and equivalent to the UU following the terminology of Lofi et al. (2011) overlies the MU above an erosional surface (IES/IMTS; Figure 1.10, zoom 02). This ~100m thick unit is named unit 7 by Gvirtzman et al. (2017) (Figure 1.10, profile E and zoom 02; see sub-section 1.2.5.2) and is made mainly of clastic anhydrite beds. Madof et al. (2019) described a similar, but thicker (~300m) unit offshore Lebanon using 2D and 3D seismic reflection data. They called it the ‘Nahr Menashe’ (from jewish ‘the forgotten river’) formation and interpreted it as a fluvial deposit resulting from subaerial erosion during stage 3 of the MSC. The Nahr Menashe sequence has been correlated by the same authors with the Abu Madi formation located within the Messinian canyons offshore Egypt (Loncke et al., 2006; Abdel-Fattah, 2014; Pigott & Abdel-Fattah, 2014).

The nature, origin, and probable depositional environments of the UU and its time equivalents, as well as the controversies about them are thoroughly discussed in chapters 4 and 7 of Annex A.

1.2.5.4 The Complex Unit (CU)

As clearly expressed by its name, the Complex Unit (CU) is the most complicated unit among the MSC offshore units due to the non-uniformity of its seismic facies and seismostratigraphic position relative to other MSC unit. On seismic reflection profiles, it generally appears as fan shaped sedimentary body having chaotic seismic facies with incoherent reflection configuration, more or less transparent (Lofi, 2011). Being mostly found at the foot of the margins, most of the authors interpreted the CU(s) as the product of margin erosion during MSC base level drawdown(s), e.g., Gulf of Lions (Figure 1.9, profile A) (Lofi, Gorini, Berné, Clauzon, Tadeu Dos Reis, et al., 2005), Valencia Basin (Figure 1.9, profile B) (Maillard et al., 2006b) and Levant Basin (Bertoni & Cartwright, 2007). The most intriguing CU is the one recently evidenced by Micallef et al. (2018) at the foot of the Malta Escarpment, interpreted as the result of erosion of the Sicily-Tunisian sill following the Zanclean reflooding (Micallef et al., 2019; Garcia-Castellanos et al., 2020b).

1.2.5.5 The Bedded Unit (BU)

The Bedded Unit (BU) is the less studied of the offshore MSC units. Its presence in the Mediterranean is restricted to present-day intermediate to shallow water depths (Figure 1.9, profiles C and D; Figure 1.10, profiles B and C; e.g., Po Plain – Adriatic Basin, Ghielmi et al., 2013; Balearic Promontory, Maillard et al., 2014; East Corsica – Tyrrhenian Basin, Thinon et al., 2016). Its distribution, however, might be underestimated (Figure 1.3) (Lofi, 2018b), because it is often present as a relatively thin unit that cannot be resolved without high-resolution seismic imaging. On seismic reflection profiles it most commonly appears as a series of parallel stacked continuous reflections (Figure 1.9, zoom 02), bracketed between two erosional surfaces, on the bottom (BES) and on the top (TES) (Lofi, Sage, Déverchère, et al., 2011). Often its internal facies allows the division of BU into two or more sub-units (Maillard et al., 2014b; Thinon et al., 2016). BU's thickness could be up to 350m (0.2 sec TWTT using a mean internal velocity of 3500 m/s; LOFI, 2011). Until now, the connection between the different BU(s) in the Mediterranean with the marginal outcropping MSC basins and with the deep basin evaporites is unclear (Figure 1.9, profiles C) (Driussi, Maillard, et al., 2015b; D. Ochoa et al., 2015c). Thinon et al. (2004) stated that there is a potential resemblance between the BU eastern Corsica and the UU of the deep basin due to similar geometries found in both

units. On the Balearic Promontory, the BU has been drilled in 2 old industrial boreholes and shown to consist of stage 1 PLG cut by a very clear erosional surface at the top (TES) (D. Ochoa et al., 2015c).

The BU in the Balearic Promontory will be one of the targets of this thesis. It has been studied recently by some authors. Its aspects, characteristics and interpretation will be described better in section 2.2.1, and then will be improved as a result of the work presented in chapter 4.

1.3 Amplitude and Timing of the MSC drawdown: The major controversy

The most disputed argument about the MSC is the amplitude of base level drawdown and whether the Mediterranean ‘desiccated’ or not. Not only how much the base level changed, but to add more complications, also the timing and duration of the changes are highly controversial.

1.3.1 Amplitude of the MSC drawdown: Pros and Cons

The idea of a quasi-desiccated Mediterranean (Figure 1.1-A) with a base level drop of 1500+m is supported by several observations (Figure 1.11, scenarios 2 and 3). (1) The widespread incision of erosional surfaces (MES, BES, IES, TES) interpreted as of subaerial origin cutting through the evaporites onshore (PLG and salt), the pre-MSC sediments in the offshore margins, and even the evaporites of the deep basins (W. B. Ryan, 1978; Lugli et al., 1999b; Lofi, Gorini, Berné, Clauzon, Tadeu Dos Reis, et al., 2005; Maillard et al., 2006b; Bertoni & Cartwright, 2007; Urgeles, Camerlenghi, Garcia-Castellanos, De Mol, Garces, et al., 2011; Estrada et al., 2011b; Lofi, Sage, Déverchère, et al., 2011; Pellen et al., 2019b; Madof et al., 2019; Camerlenghi et al., 2019) (2) The deepening of the incisions and adjustment of river profiles around the Mediterranean Basin, mainly the Nile and the Rhone rivers (Chumakov, 1973; Clauzon, 1978) (3) The presence of clastic fans (e.g., CU and Naher Menashe unit) at the output of the valleys incised by the erosional surfaces (Lofi, Gorini, Berné, Clauzon, Tadeu Dos Reis, et al., 2005; Maillard et al., 2006b; Bache et al., 2009b; Pigott & Abdel-Fattah, 2014; Micallef, Camerlenghi, Garcia-Castellanos, Otero, et al., 2018; Madof et al., 2019) (4) The aggrading geometry of the offshore deep UU onlapping the margins (Lofi et al., 2011; Lofi, 2018) (5)

The presence of benthic brackish shallow water fauna in the DSDP drilling on top of the UU (CITA et al., 1978; Iaccarino & Bossio, 1999) (6) The deep incision at the strait of Gibraltar indicating a reflooding which requires an important water level difference between the Atlantic and Mediterranean (P.-L. Blanc, 2002; Garcia-Castellanos, Estrada, et al., 2009; Micallef, Camerlenghi, Garcia-Castellanos, Otero, et al., 2018; Garcia-Castellanos et al., 2020b) (7) The bathymetric contrast between the last MSC sediments and the overlying Pliocene sediments, together with the fact that all the MSC units lack any evidence of marine fauna which could indicate normal marine connections and conditions (CITA & COLOMBO, 2006; Cita et al., 1990; Sgarrella et al., 1997; Bonaduce & Sgarrella, 1999; Caruso et al., 2020).

The opposite anti-desiccation (Figure 1.1-B) school claims that the base level did not vary during most of the MSC except for a very moderate drop of about 200 meters during stage 2 at the acme of the MSC and following the deposition of the immense halite body in the deep basins (Figure 1.11, scenario 1). They relate this drop to the glacial peaks TG12 and TG14 that might have contributed to a further restriction between the Mediterranean and Atlantic (Manzi et al., 2012; Roveri, Flecker, et al., 2014a; Manzi et al., 2018a). The arguments that support the full non-desiccated basin are (1) the sub-aqueous facies of some of the evaporites onland (RLG) and offshore (UU recovered from DSDP drillings) (Roveri et al., 2001; Hardie & Lowenstein, 2004; Roveri et al., 2006; Lugli et al., 2013, 2015; W. Martínez del Olmo & D. Martín, 2016) (2) The sulfate values measured in the Upper Evaporites reflect a clear Atlantic water signal (García-Veigas et al., 2018b) (3) The presence of Paratethyan fish fossils in marginal basins (Bannikov et al., 2018; Schwarzhans et al., 2020) (4) the mismatch between $87\text{Sr}/86\text{Sr}$ (Strontium) isotope ratios measured on marginal ostracods and Sr values expected from endorheic lakes fed with local freshwaters (Roveri, Flecker, et al., 2014a; Andreetto et al., 2020b) (5) The homogeneity of the paratethyan ostracods in the marginal basins all over the Mediterranean (Gliozzi et al., 2007; Stoica et al., 2015; Sciuto et al., 2018).

1.3.2 Timing and duration of the MSC drawdown

The second complication about the base level drawdown is its timing and its duration. There are two school of thoughts on when the drawdown happened, both relative to the emplacement of the deep basin salt (Figure 1.11). The first (Figure 1.11, scenario 3) postulates that the deep

basin salt deposited only after the end of the base level drawdown (Bache et al., 2009b, 2015; Pellen et al., 2019b). The main reason behind this interpretation is the large volume and geometries of the CU and LU in the Provencal Basin (Bache et al., 2015). However, (1) those volumes and geometries are still debated (Lofi et al., 2005; Lofi and Berné, 2008); (2) numerical modeling of the hydrological budget of the Mediterranean basin shows that in order to deposit the observed volume of halite in the Mediterranean, the Atlantic-Mediterranean gateway needs to be open and to permit the inflow of saline water from the Atlantic with a blocked outflow (P.-L. Blanc, 2002; P. Meijer, 2006; Krijgsman & Meijer, 2008; Topper & Meijer, 2013); (3) drillings from the eastern Mediterranean sampled and showed that at least the lowest part of the salt deposited in deep water context (Manzi et al., 2018a; Meilijson et al., 2018). Moreover, (4) evidence of a permanent, although decreasing, connection between the Atlantic and the Mediterranean during the whole stage 1 is obtained from geochemical isotopic data measurements and modelling in the PLG (Lugli, Vinicio, et al., 2010; Topper et al., 2011; Flecker et al., 2015; García-Veigas et al., 2018b). Those facts argue against the validity of this model, so unless it succeeds in showing that all the halite/MU and the upper evaporites/UU were deposited during stage 3.1 (~130 ka) before the establishment of the brackish water conditions of stage 3.2, the model needs to be revised.

According to the second school of thoughts, the halite emplacement started already in deep water conditions during the base level drop and ended when the basin was almost desiccated (W. B. F. Ryan, 2009b; Lofi, Sage, Déverchère, et al., 2011).

In both scenarios presented above, the base level rise happened slowly and progressively allowing the deposition of both the MU and UU (Bache et al., 2009b) or only the UU (Lofi, Sage, Déverchère, et al., 2011).

The duration of the drawdown is another important question that is still debated in the MSC community. It might be the second most debated argument after the amplitude of the drawdown due to the implications that this duration has on the connectivity of the Mediterranean Basin with the Atlantic and the Paratethys during the upper evaporites (stage 3.1) and lagoon (stage 3.2) phases (Flecker et al., 2015; Stoica et al., 2015; Marzocchi et al., 2016). This controversy will not be discussed at this point, as a complete review about it is presented in Annex A as a part of a review article published recently in collaboration with most of the colleagues in the Salt Giant project.

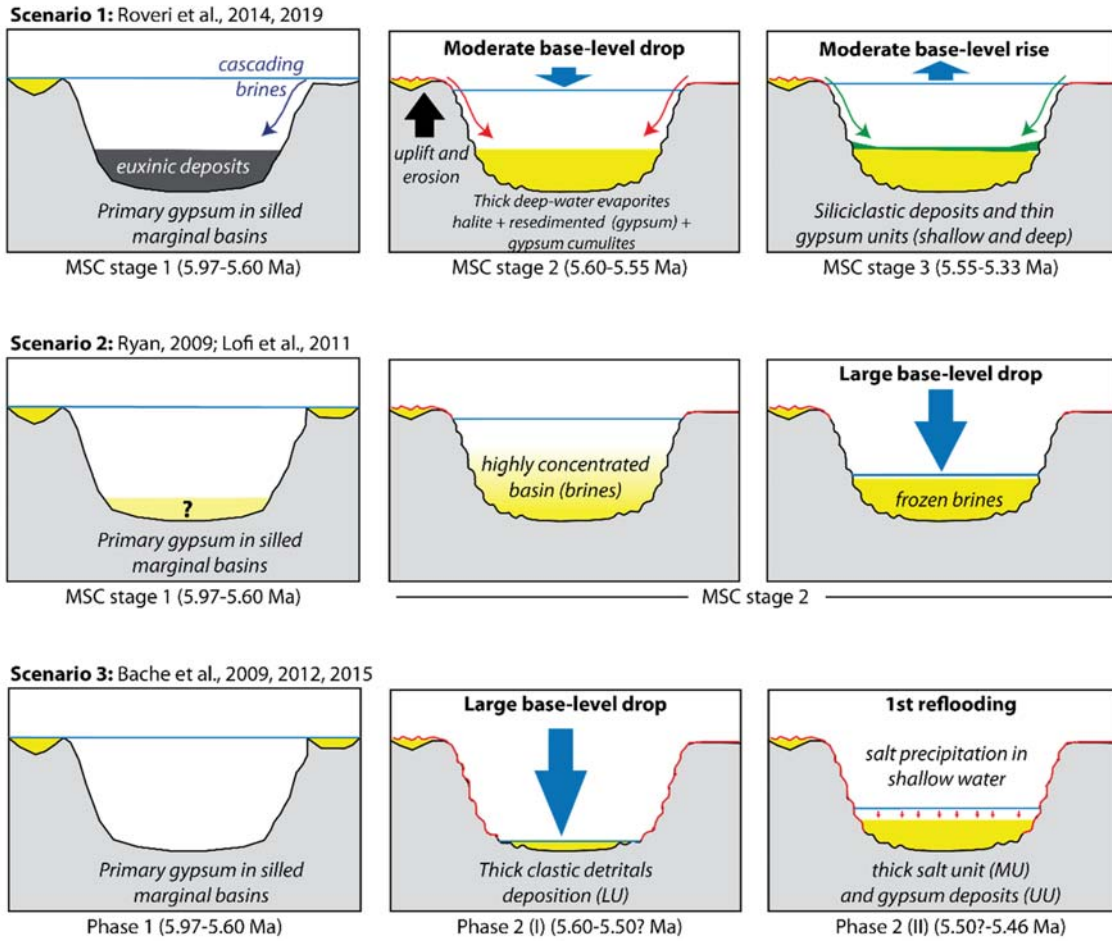


Figure 1.11. Existing conceptual models of the timing of the base level drawdown during the MSC, with respect to the timing of the salt (MU) emplacement. Scenario 1 proposes deep-water salt emplacement accompanied with erosion of the margins and ending with a moderate base level drop. Scenario 2 proposes the same salt emplacement beginning in deep water and ending with a large base level drop of > 1500m. Scenario 3 proposes that the deep basin salt deposited in shallow water only after the end of a large base level drawdown.

Chapter 2

Geological Setting and Tectonic Evolution of the Balearic Promontory

In this chapter, I present the geological background of the study area, starting by restituting the Balearic Promontory in the geodynamic context of the Western Mediterranean area. I also summarize its geological and tectonic evolution since its formation until the present-day, and how did affect the area in terms of present-day physiography. I end the chapter by introducing the state of art of the Messinian Salinity Crisis from previous studies both offshore and onshore the Balearic Promontory.

2.1 The Balearic Promontory in the context of the Western Mediterranean Basin's Geodynamics

The Mediterranean Basin is considered a unique natural laboratory for the study of geodynamics, structural geology and interaction between deep and surface processes. This is due to the fact that in a relatively small area all the ingredients for plate tectonics and deformation are present, with an immense quantity of acquired data/information. Traditionally the Mediterranean Basin is divided into 3 major regions: Eastern, Central and Western Mediterranean.

The Western Mediterranean Basin in particular is characterized by a very complex geologic, geodynamic and structural settings. It opened, as a series of back-arc basins, in an overall convergence context between the African and Eurasian plates during the Cenozoic era, when the Alpine chains were created (Doglioni et al., 1997; Carminati et al., 1998; Gelabert et al., 2002b; Cavazza et al., 2004; Carminati et al., 2012). The complexity, thus, lies behind the fact that extension (due to slab retreat) and compression (due to continental collision) acted contemporaneously (Malinverno & Ryan, 1986b; Royden, 1993; Lonergan & White, 1997b), resulting in the formation of both mountain ranges, namely the Alps, Maghrebides, Apennines and the Betic-Rif Cordillera, and continental extension in the Alboran and northern Tyrrhenian basins, with oceanisation in the Liguro-Provençal, Algerian, and southern Tyrrhenian basins (Figure 2.1).

In its present-day setting, the Western Mediterranean is divided in a series of basins (Figure 2.1), from West to East, those are: (1) The Alboran Basin (average depth ~750m) located near the Gibraltar strait, between the Betic and Rif chain belts, (2) The Algerian Basin (average depth ~2400m) to the south of the Balearic Islands, (3) The Valencia Basin (average depth ~900m) to the north of the Balearic Islands, (4) The Liguro-Provençal Basin (average depth ~2000m) which extends from the Gulf of Genoa to the region between the Balearic Islands and Sardinia, (5) and the Tyrrhenian Basin (average depth ~2000m) which is the basin located between the Corso-Sardinian block and western Italy (Figure 2.1). The Balearic Promontory (average depth ~650m) is a prominent high in the Western Mediterranean separating the Valencia Basin from the Algerian Basin, and is represented by the Balearic Islands and their surrounding offshore sub-basins. The timing and modality of the opening and/or formation of those basins in the geodynamic context of the Western Mediterranean tectonic evolution are complex and some of them are highly debated.

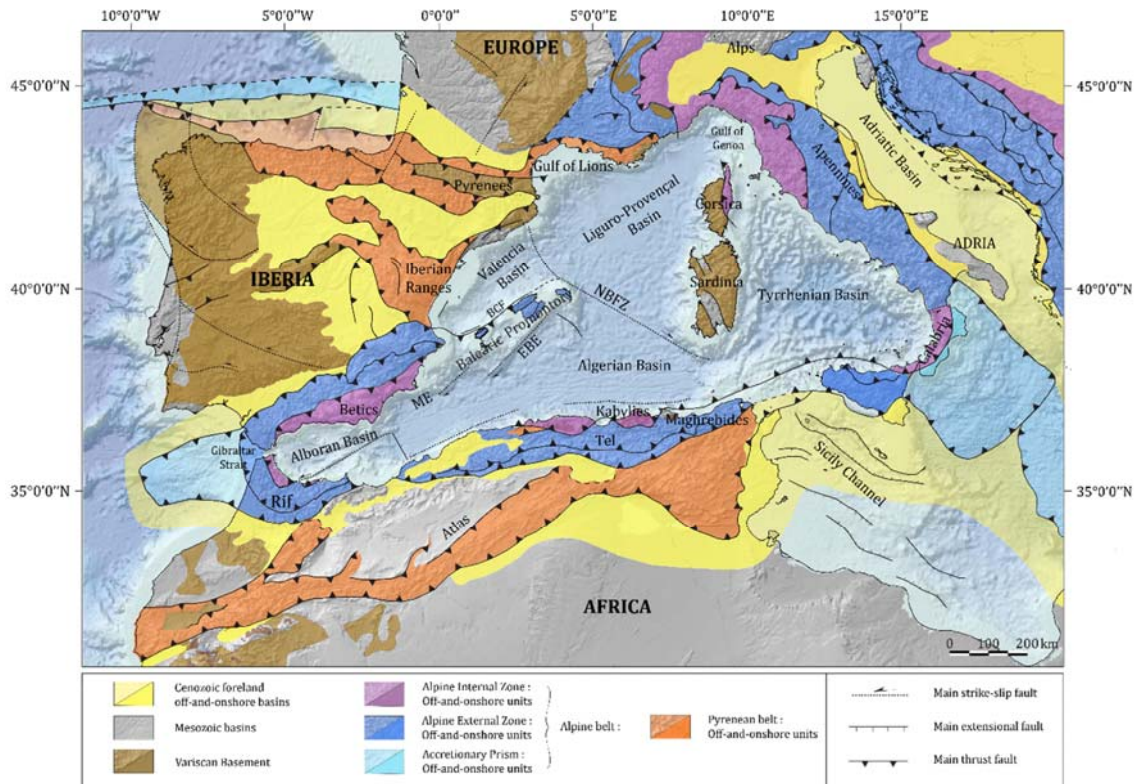


Figure 2.1. Structural map of the Western Mediterranean and North African regions showing the major Cenozoic structural trends in the area (modified from [Etheve et al., 2016](#)). A digital elevation map is displayed in the background. EBE= Emile Baudot Escarpment; ME= Mazarron Escarpment; BCF= Betic Cordillera Front; NBFZ= North Balearic Fracture Zone.

2.1.1 Geodynamic settings of the Western Mediterranean basins.

The convergence between Africa and Europe in the Upper Cretaceous (~80 Ma; e.g., [Dewey et al., 1989](#)), led to the closure of the Tethys and the consequent subduction and collision between the two plates (Dewey et al., 1989; Olivet, 1996; Rosenbaum et al., 2002a; Cavazza et al., 2004; Schettino & Turco, 2006a). Extension occurred in the overriding plate in response to the retreating subducting lithospheric slab that was then fragmented in 2 segments observed at present-day below Gibraltar and Calabria (Cohen, 1980; Lonergan & White, 1997b; Gutscher et al., 2002; Wortel & Spakman, 2000; El-Sharkawy et al., 2020). The slab roll back is attested by the dispersal of the AlKaPeCa block (Alboran- Kabylies-Peloritan-Calabria) (Bouillin et al., 1986).

In the late Eocene, a first rifting episode resulting from the counter clockwise rotation of the Corso-Sardinia block with respect to the Ibero-European plate, resulted in the formation of the

Gulf of Lions and the Liguro-Provencal Basin (Rehault et al., 1984a; Gueguen et al., 1998a; Speranza et al., 2002a). The rifting episode was followed by a drifting period during the Lower Miocene (Vigliotti & Langenheim, 1995; Olivet, 1996; Speranza et al., 2002a) that has been divided into a hyper-extensional phase (exhumation, 23-18 Ma) followed by an accretion phase (18-15 Ma) (Jolivet et al., 2015). Although the exact nature of the crust is still largely debated, the proposed mechanisms of the formation of the Gulf of Lions and the Liguro-Provencal Basin are widely accepted in literature.

To the southwest of the Liguro-Provencal Basin lies the Valencia Basin, the two separated by the North Balearic Fracture Zone (NBFZ; Figure 2.1). The Valencia Basin is an aborted rift that also opened along a NW-SE direction in the Late Oligocene / middle Miocene times (Clavell & Berastegui, 1991; Maillard, MAUFFRET, et al., 1992; Roca & Guimerà, 1992b; Roca, 2001) and its opening is thought to be linked to the opening of the Liguro-Provencal Basin (Maillard, MAUFFRET, et al., 1992; Roca & Guimerà, 1992b). A major unconformity (called ante-rift or Oligocene discontinuity) marks the contact between the resulting syn-rift sediments and the previous sedimentary record (Mesozoic to lower Oligocene in age) (Etheve et al., 2016). If the extension on the northern margin of the Valencia Basin is clearly observed, its southern margins are partly structured by the Betic Cordillera (northern part of the Balearic Promontory (Figure 2.1) (Bourrouilh, 1973; Gelabert et al., 1992; Sàbat et al., 2011), which is the reason why the Valencia Basin can also be interpreted as a foreland basin (Fontboté et al., 1990; Gelabert et al., 1992).

The Algerian Basin is located to the South of the Liguro-Provencal Basin and is separated from the southern part of the Balearic Promontory by the Emile Baudot and Mazarron Escarpments (EBE; Figure 2.1). Though the age and even the nature of the Algerian basin are poorly constrained, most authors propose an oceanic accretion phase dated from late Burdigalian or Langhian (19-15Ma) to Tortonian (8Ma), younging westward (Mauffret et al., 2004; Jolivet et al., 2009; Crespo-Blanc et al., 2016; Leprêtre et al., 2016; Romagny et al., 2020; Haidar et al., 2021).

The Algerian Basin is located to the South of the Liguro-Provencal Basin and is separated from the southern part of the Balearic Promontory by the Emile Baudot and Mazarron Escarpments (EBE; Figure 2.1). Although the age and even the nature of the Algerian basin are poorly constrained, most authors propose an oceanic accretion phase dated from late Burdigalian or Langhian (19-15Ma) to Tortonian (8Ma), younging westward (Mauffret et al., 2004b; Jolivet

et al., 2009; Crespo-Blanc et al., 2016; R. Leprêtre, 2018; Romagny et al., 2020; Haidar et al., 2021).

The evolution and kinematics of the Algerian Basin are highly debated, and no consensus exists at present. Two main different end members exist regarding the formation of the Algerian Basin. The first model (Figure 2.2-A) proposes a NW-SE opening of the entire Western Mediterranean. This scenario assumes that the opening of the Algerian basin is due to the south or southeastward retreat of the E-W oriented Maghreb subduction, implying that there is limited or even no westward movements. Such scenario implies that Alboran was already located at the level of Gibraltar when the Algerian basin opened (Carminati et al., 1998; Gueguen et al., 1998a; Wortel & Spakman, 2000; Gelabert et al., 2002b; Faccenna et al., 2004a; Schettino & Turco, 2006a; Jolivet et al., 2009; Frizon de Lamotte et al., 2011). This type of model is, however, not compatible neither with the observed directions of the southern Balearic margin represented by the Emile Baudot and Mazarron Escarpments (Figure 2.1), nor by the Gibraltar Arc slab (Crespo-Blanc et al., 2016).

The second model (Figure 2.2-B) proposes an E-W opening (Mattauer, 2006; Camerlenghi et al., 2009), with the Hannibal High area as accretion center (Mauffret et al., 2004b) or by fan-shaped accretion for the east Algerian basin followed by westward propagation along the slab tear (Haidar et al., 2021). The opening is associated with slab rupture and removal under the North African margin (Figure 2.2) (Gutscher et al., 2002; Duggen et al., 2004; DUGGEN et al., 2005). Models generally propose that the east Algerian Basin opened towards the SE and the west Algerian Basin opened westward, or at least propose a first phase of SE-NW opening to account for the collision of Kabylies (Rosenbaum et al., 2002a; Driussi, Briais, et al., 2015; R. Leprêtre, 2018). Only the initial position of Alboran as part of the AlKaPeCa Block is discussed, implying a varying westward migration from 200 km (Jolivet et al., 2006b) to 700km (600-700 km; Van Hinsbergen et al., 2014; Mattauer, 2006). Whichever the case, the resulting displacement generates a left-lateral deformation along the western and central Algerian margins accommodated by possible STEP faults (Medaouri et al., 2014; Haidar et al., 2021) and right-lateral deformation along the Balearic Promontory (Mauffret et al., 2004; Camerlenghi et al., 2009). The accommodation of the Alboran domain migration is thought to be accommodated along the Emile Baudot Escarpment (Acosta, Muñoz, Herranz, et al., 2001b), proposed to be a transform margin between the oceanic crust of the Algerian margin and the thick continental crust of the Promontory (Driussi, Briais, et al., 2015).

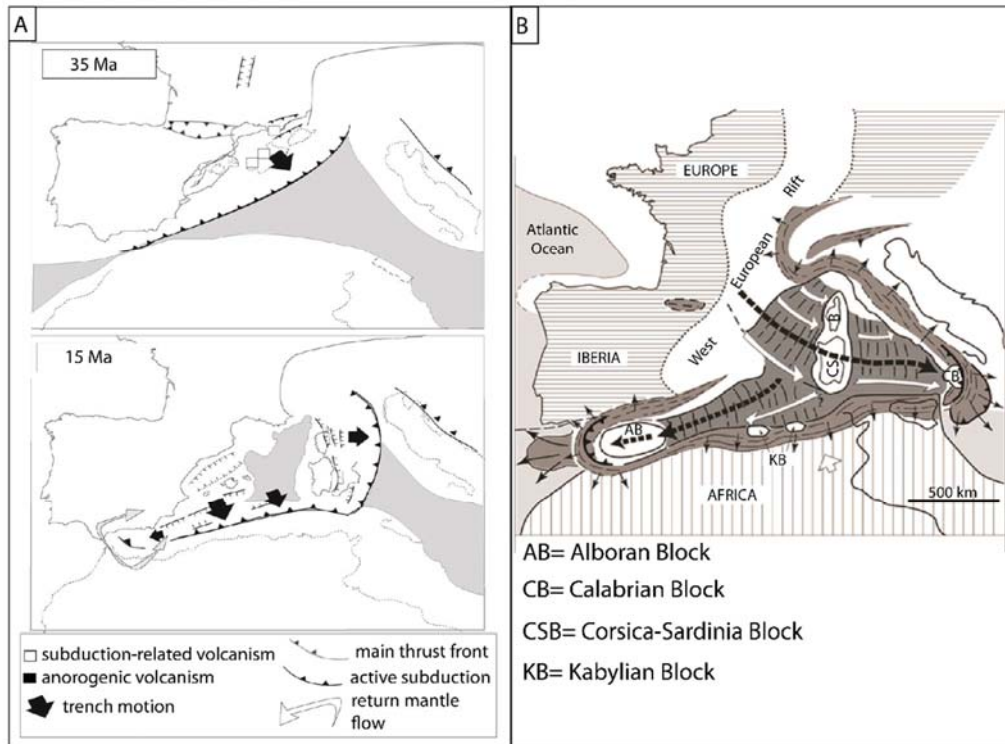


Figure 2.2. The two existing geodynamic models for the opening of the basins of the Western Mediterranean. A. NW-SE extension with roll back of the slab that goes from Gibraltar to Corsica. Modified from [Faccenna et al. \(2004\)](#); E-W extension in the Algerian basin with roll back confined to the Balearic and Corso-Sardinian segments. Modified from [MATTAUER \(2006\)](#).

The Tyrrhenian Sea is the youngest among the Western Mediterranean sub-basins. It is a Neogene back-arc basin that opened by E-W continental rifting and oceanic spreading related to the eastward migration of the Apennine subduction system (Figure 2.1) between middle Miocene and Pliocene times (Malinverno & Ryan, 1986b; J. Mascle & Réhault, 1990; Gueguen et al., 1998a; Jolivet & Faccenna, 2000; Jolivet et al., 2006b; Carminati et al., 2012).

2.1.2 Formation and tectonic evolution of the Balearic Promontory

The Balearic promontory is one of the continental blocks which detached from the Eurasian margin behind the retreating Tethyan subducting slab: the Corsica-Sardinia block, the Balearic Islands blocks, and the AlKaPeCa blocks (Alboran- Kabylies-Peloritan-Calabria; Figure 2.1

and Figure 2.4) (Bouillin et al., 1986). It is thus the result of the complex interaction of both shortening and extensional events during the Oligo-Miocene epochs.

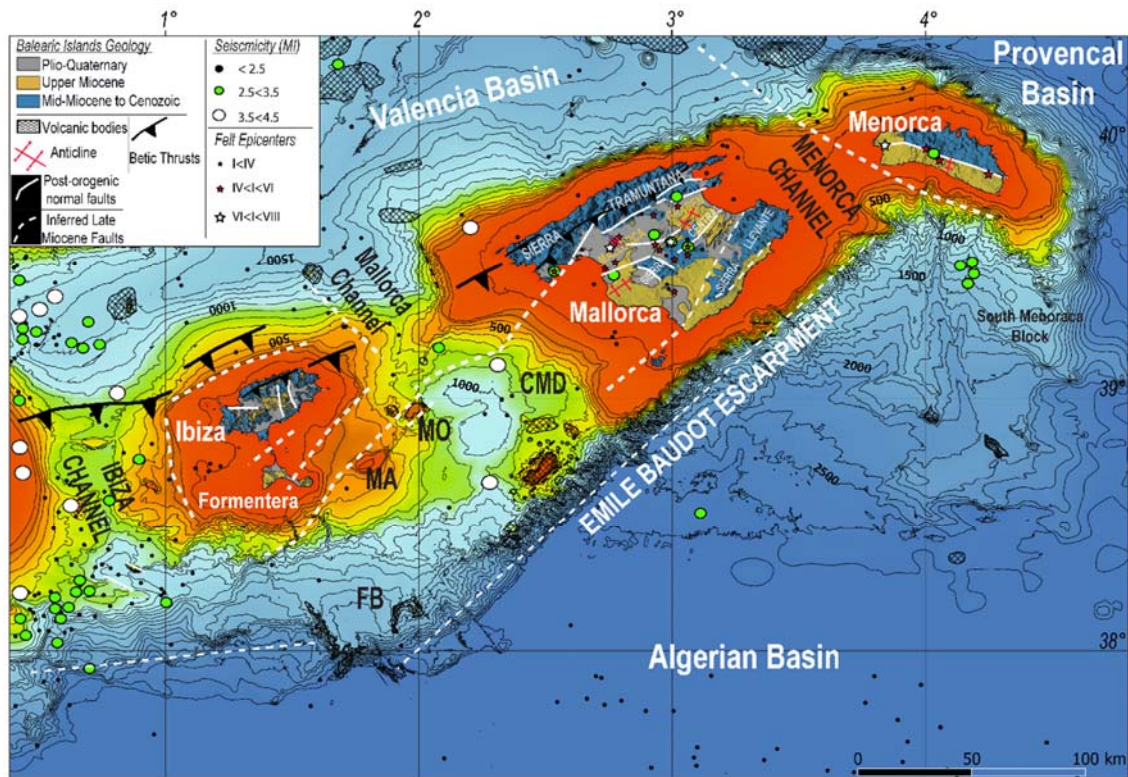


Figure 2.3. Map of the Balearic Promontory showing the main betic and post-orogenic structures, as well as the registered seismicity onshore and offshore the islands. Epicenters of the recorded earthquakes are from International Seismological Centre (2020), on-line Bulletin (<https://doi.org/10.31905/D808B830>) and Sánchez-Alzola et al. (2014). Faults and other structural features are taken and modified from Sàbat et al. (2011); Sánchez-Alzola et al. (2014); Etheve et al. (2016). Onland geology the Balearic Islands is modified from geological map of Spain 1:50000 (IGME). The bathymetric data for the offshore domain is downloaded from the European Marine Observation and Data network (EMODnet) database available online (www.emodnet-bathymetry.eu). Offshore: CMD = Central Mallorca Depression; FB = Formentera Basin; MA = Mont Ausias Marc; MO = Mont des Oliva.

2.1.2.1 Oligo-Miocene Betic-Orogen Compressional Phase

Lying as a prominent high in the core of the Western Mediterranean, the Balearic Promontory is considered the northeastern extension of the one of the Betic Cordillera (Bourrouilh, 1973) (Figure 2.1). Thus it formed as a result of the compressional deformation associated with the formation of the Betic ranges in the SE Spain, contemporaneously with the opening of the

Valencia and Algerian Basins (Ramos-Guerrero et al., 1989; De Galdeano, 1990; Roca, 2001). This phase led to the formation of the sierras (mountain ranges) onland the Balearic Islands (e.g., Sierra Tramuntana-Mallorca; Figure 2.3). Observations onland the islands of Ibiza and Mallorca showed that the betic thrusts are well expressed where the Mesozoic units overlap the Cenozoic units, along thrusts trending ESE-WNW (Figure 2.3) (FOURCADE et al., 1982; Sabat et al., 1988; Canas & Pujades, 1992; Sàbat et al., 2011; Etheve et al., 2016; Booth-Rea et al., 2017). Thrusting was also observed offshore the northwestern margins of Ibiza and Mallorca (Maillard, MAUFFRET, et al., 1992; Roca & Guimerà, 1992b; Maillard & Mauffret, 1993a). The geometry and nature of the sedimentary units affected by the thrusts show that the thrusting associated to the compressional phase was active from the Oligocene to the middle Miocene (Ramos-Guerrero et al., 1989; Fontboté et al., 1990; De Galdeano, 1990; Roca, 2001; Sàbat et al., 2011). Compression initiated in the late Oligocene in the southern parts of the Promontory (Figure 2.5) and propagated northward later during the Burdigalian (Bourrouilh, 1973; Gelabert et al., 1992; Bove et al., 1994). During the compression event, the islands experienced clockwise rotation as evidenced by paleo-magnetic measurements onshore Mallorca (Freeman et al., 1989; Parés et al., 1992).

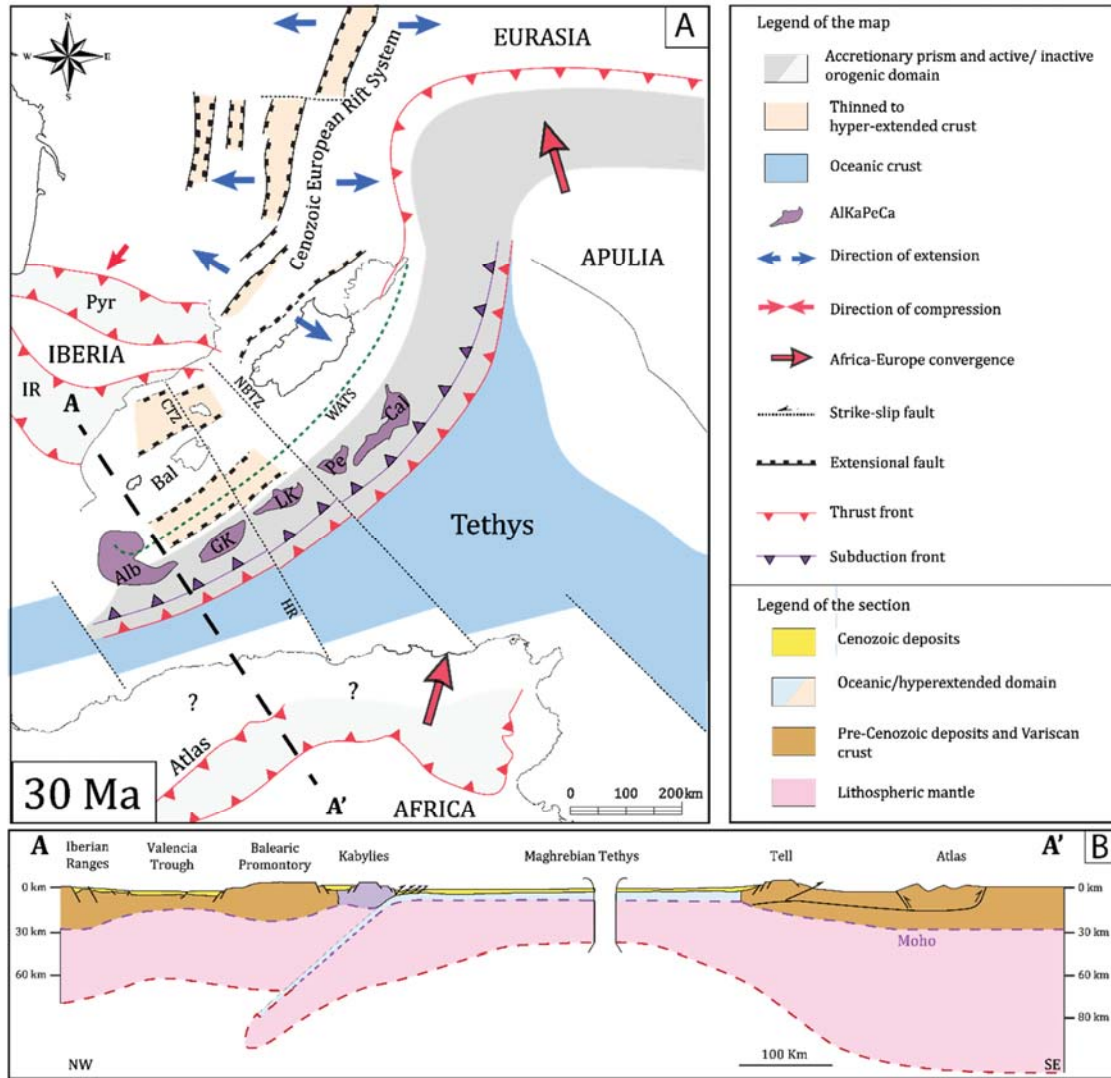
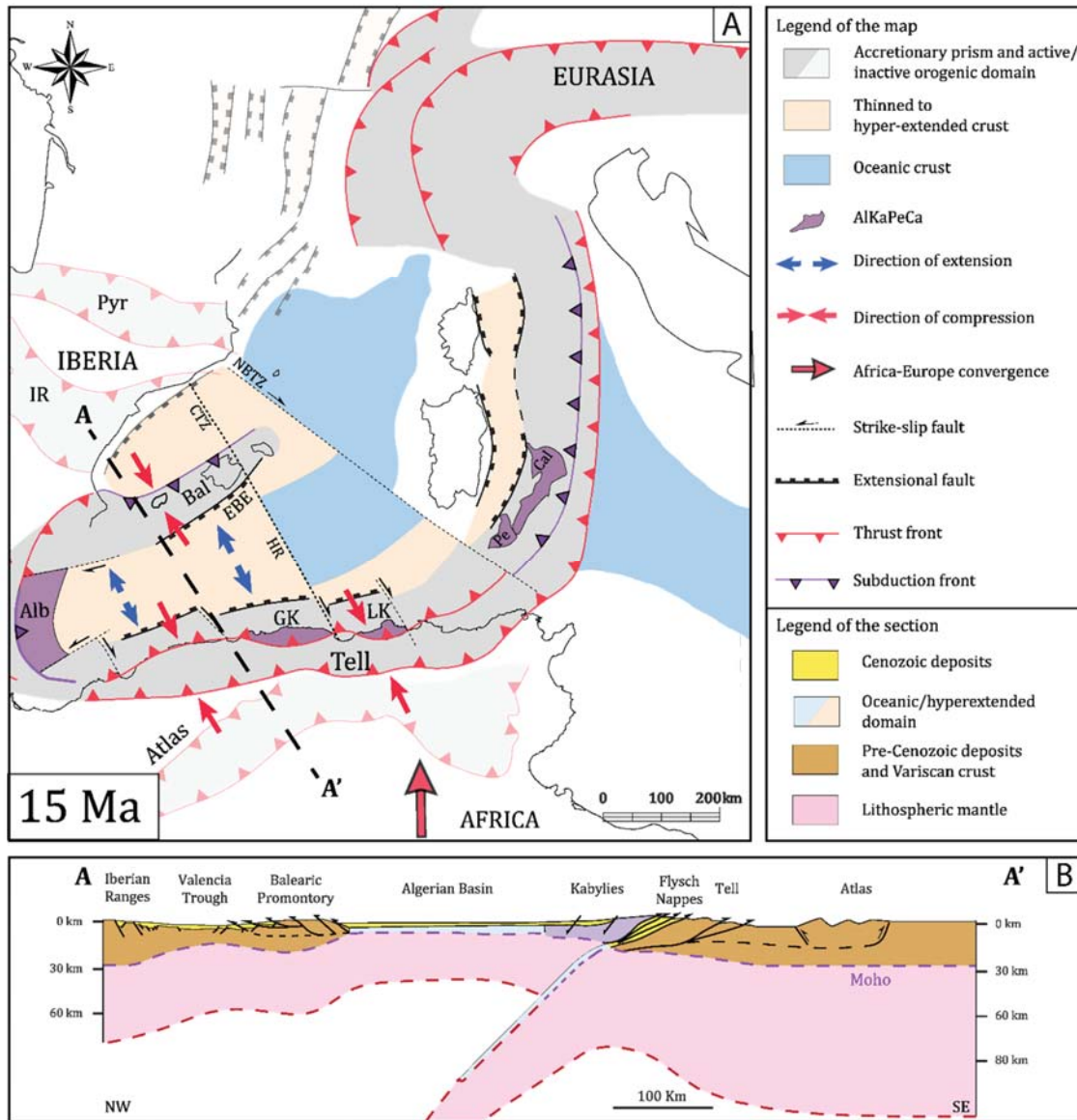


Figure 2.4. Palinspastic structural reconstruction (A) and related cross section (B) of the Balearic Promontory in the context of the Western Mediterranean at 30 Ma showing the configuration of the promontory during the late Oligocene–early Miocene extensional deformation observed in Ibiza Island. Alb=Alboran Domain, Bal=Balearic Promontory, Cal=Calabria, CTZ=Central Transform Zone, GK=Great Kabyllie, HR=Hannibal Ridge, IR=Iberian Ranges, LK=Lesser Kabyllie, NBTZ=North Balearic Transfer Zone, Pe=Peloritani, Pyr=Pyrenees, WATS=Western Alpine Tethys Suture. Modified from Etheve et al. (2016).

2.1.2.2 Oligo-Miocene Extensional Phase

Coeval to the orogenic compressional phase on the Balearic Promontory, a rifting phase had already initiated in the Valencia Basin (Fontboté et al., 1990; Maillard, MAUFFRET, et al., 1992; Roca & Guimerà, 1992b). Evidence of extension in the Valencia Basin were mainly described on the northern margin of Valencia. On the promontory, Oligo-Miocene normal faults belonging to this extensional phase were also described in the area north of Mallorca (Maillard, MAUFFRET, et al., 1992; Moragues et al., 2021). Even though many studies showed that the extensive phase related to the opening of the Valencia Basin is hardly observable onland and in the submerged areas of the Balearic Promontory, both Gelabert et al., 1992 and Moragues et al., 2021 described lower to middle Miocene normal faulting with tilted blocks in the Sierra de Tramuntana (Mallorca), all of them associated with anticlines and/or other compressive structures. Also Etheve et al. (2016) described extensional structures both onshore and offshore the island of Ibiza belonging to this phase, demonstrated to be clearly ante-thrust (Figure 2.4).



2.1.2.3 Late Miocene post-Orogenic Extensional Phase

Following the compressional phase and the establishment of the sierras on the islands, a post-orogenic extension phase (by collapse) initiated at the end of the Serravalian (Roca, 1992; Cespedes et al., 2001; Booth-Rea et al., 2017; Moragues et al., 2021). The Serravalian dating of this phase implies that it is synchronous to the opening of the Algerian Basin.

This extensional phase is at the origin of the different WNW-ESE structures onland Mallorca (Figure 2.3), e.g., the Mallorca Graben (Sàbat et al., 2011) and the Central Mallorca Depression between the islands of Ibiza and Mallorca (Roca, 1992; Acosta et al., 2003; Sàbat et al., 2011). The upslope domain of Ibiza and Mallorca margins are also structured by recent normal faulting that postdates the rifting phase of the Valencia Basin, and crosscuts the pre-existing thrusts, thus most probably belonging to the same extensional event (Maillard, MAUFFRET, et al., 1992; Sàbat et al., 1997a; Driussi, Briaies, et al., 2015; Etheve et al., 2016, 2018a). The direction of the late Miocene extension is perpendicular to the WSW-ENE faults that delimit the Mallorca Graben (Figure 2.6), thus globally NW-SE (Sàbat et al., 2011). More complex processes to explain this extension were recently proposed resulting in strike-slips and transfer faults with coeval NW-SE extension (Etheve et al., 2016; Moragues et al., 2021) that would make it compatible with the Westward motion of the Alboran Block and Algerian basin opening.

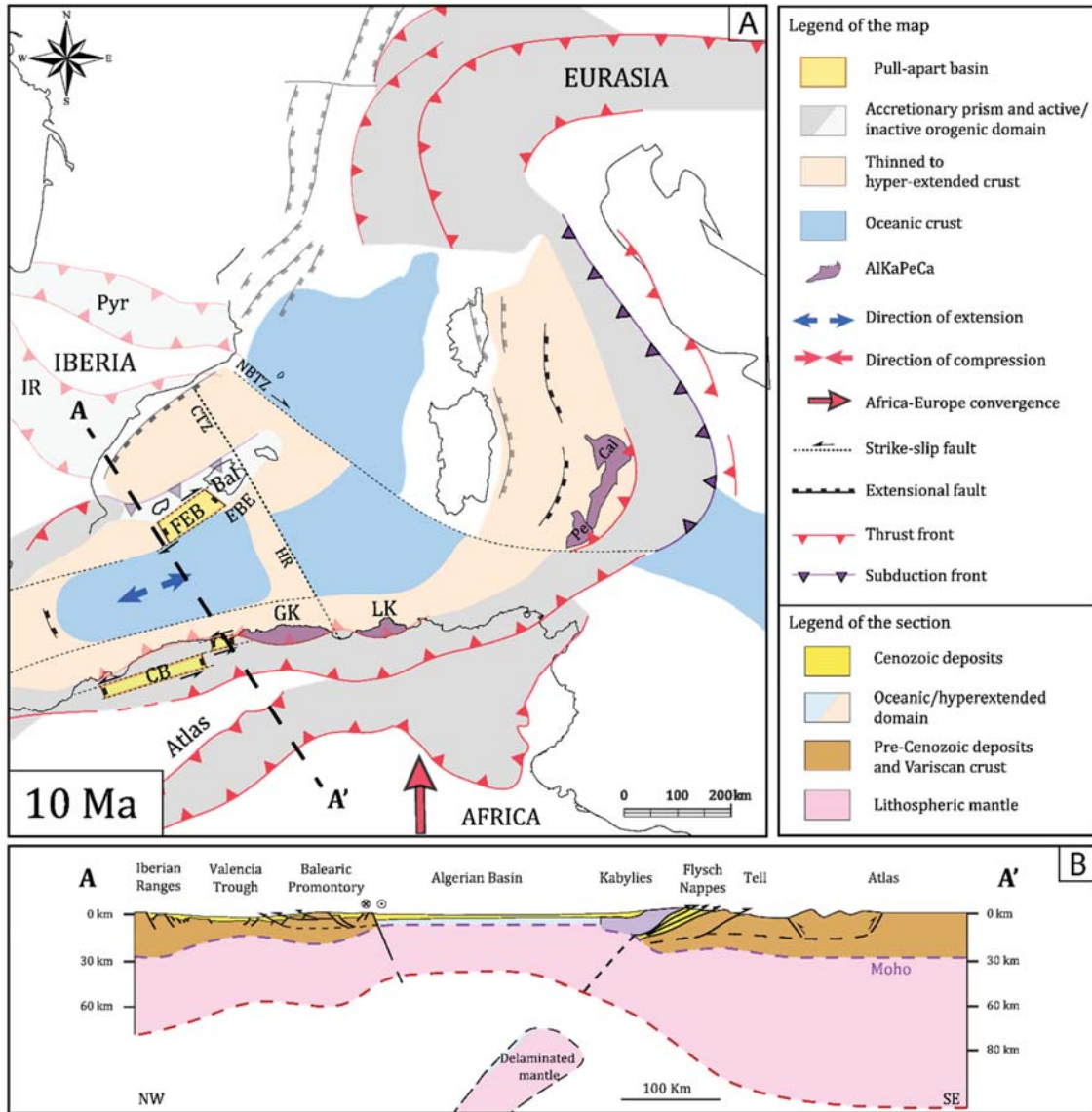


Figure 2.6. Palinspastic structural reconstruction (A) and related cross section (B) of the Balearic Promontory in the context of the Western Mediterranean at 10Ma showing the configuration of the promontory during the post-orogenic extensional phase. Alb=Alboran Domain, Bal=Balearic Promontory, Bet=Betics, Cal= Calabria, CB=Cheliff Basin, CTZ=Central Transform Zone, EBE=Emile Baudot Escarpment, FEB =Formentera Basin, GK= Great Kabylie, HR=Hannibal ridge, IR=Iberian Ranges, LK = Lesser Kabylie, NBTZ = North Balearic Transfer Zone, Pe= Peloritan, Pyr= Pyrenees. Modified from Ettheve et al. (2016).

2.1.2.4 Recent Reactivation of the Balearic Promontory

The Algerian-Balearic region was reactivated since 8 Ma due to the continuous convergence between Africa and Eurasia, and is nowadays subjected to a NW compression of several mm/y, as also evidenced by the inversion of the Algerian margin (Nocquet & Calais, 2003; Déverchère et al., 2005; Domzig et al., 2006). On the opposite side of the Algerian margin, onshore observations showed that all the Betic Cordillera is undergoing uplift due to this compression, with a perpendicular extension observed mainly towards the southern parts of the internal betics zone (Sanz de Galdeano & Alfaro, 2004; Serpelloni et al., 2007). Focal mechanisms along the main active faults in this area evidenced a major transpressive deformation component (MONTENAT et al., 1990; Alfaro et al., 2002). This activity, however, does not extend all along the Balearic Promontory, but instead its termination appears to be located somewhere between Alicante shelf and Ibiza Channel. In fact recent studies showed that the Ibiza Channel area has been highly active through the Pliocene-Quaternary period and up to the present, as evidenced by both the high deformation of the Pliocene-Quaternary sedimentary units, and the high seismicity affecting the area (Figure 2.3) (Alfaro et al., 2002, 2012; Maillard & Mauffret, 2013a; Acosta et al., 2013). Whereas, going towards the northeastern part of the Balearic Promontory this activity notably decreases with rare registered earthquakes having a magnitude that generally does not exceed 3.5 of the Richter scale (Figure 2.3) (Silva et al., 2001; Serpelloni et al., 2007; Sanchez-Alzola et al., 2014). Nevertheless, evidence of this relatively gentle deformation exist both offshore and onshore.

Offshore, between Ibiza and Mallorca (i.e., Central Mallorca Depression), gentle folds on the seabed are interpreted as the result of compressional deformation (Sàbat et al., 1997a). Acosta et al. (2003, 2004) evidenced also the presence of right lateral NE-SW strike-slip structures that are locally deforming the seafloor and that are visible particularly both on Mont Ausias Marc and Mont dels Oliva in the Central Mallorca Depression (Figure 2.3). Those authors show systems of near-vertical surficial normal and/or strike-slip faults affecting the Plio-Quaternary unit, together with numerous pockmarks widespread over the area. Moreover, the abundance of volcanic zones and mass failure structures suggest active tectonic processes (Acosta, Muñoz, Herranz, et al., 2001b; Acosta, Muñoz, P., et al., 2001; Acosta et al., 2003; Acosta, Ancochea, et al., 2004a; Acosta, Canals, et al., 2004b; Lastras et al., 2004; Camerlenghi et al., 2009b).

Onshore the Balearic Islands, very few seismic activity has been registered with Mallorca

having the highest number of earthquakes in the past decades (Figure 2.3) (Sanchez-Alzola et al., 2014). There is no focal mechanism available onshore due to the low magnitude of the earthquakes, which makes it difficult to constrain the type and direction of the ongoing deformation. Nevertheless, analysis of strain rates, allowed Sanchez-Alzola et al. (2014) to propose a gradual variation of the stress regime across the Promontory, with a NW–SE shortening in Menorca and eastern Mallorca, E–W extension in central Mallorca and WNW–ESE extension in Formentera and Ibiza.

The presence of gentle folds onshore the island of Mallorca (Figure 2.3), suggest that compression and/or transpression might have been active during the Pleistocene epoch. Moreover, some post-orogenic structures that developed as normal faults during the Miocene extensional phase (sub-section 2.1.2.3), such as the Sencelles Fault, were subsequently reworked as left-lateral strike-slip fault during the Pliocene epoch (Mas Gornals et al., 2014). A subsequent change to N-S compressional and E-W extensional regimes from Pliocene times to present-day, supported by evident compressional deformation during Quaternary times on the Sencelles Fault, has been proposed (Silva et al., 2001; Giménez & Gelabert, 2002; Giménez, 2003; Mas Gornals et al., 2014).

2.1.3 Stratigraphy and depositional environments of the Balearic Promontory

2.1.3.1 Onshore Stratigraphy

Numerous studies were performed onshore and determined the stratigraphic sequences of the Balearic Islands (Colom, 1980; Fourcade et al., 1982; Pomar et al., 1983; Rodriguez Perea, 1984; Ramos-Guerrero et al., 1989; Durand-Delga et al., 1993; Pomar et al., 1996; Ramos-Guerrero et al., 2000; Martín-Closas & Guerrero, 2005; de Neira & Gil, 2009; Sàbat et al., 2011; Rangheard et al., 2011; Durand-Delga & Rangheard, 2013; Díaz de Neira & Gil-Gil, 2013; Sàbat et al., 2018). The geological maps and corresponding stratigraphic columns/records are presented in Figure 2.7 and Figure 2.8.

Onland Mallorca, late Paleozoic (Carboniferous) sediments outcrop along the northwestern coast of the Tramuntana ranges, and they represent the oldest sedimentary record of the island (Rodriguez Perea, 1984; Sàbat et al., 2011). A Permian red shales and conglomerates series

overly the carboniferous and constitute the lowermost basement of Mallorca (Cuevas, 1958; MATAILLET & J, 1978). The Mesozoic series appears to be complete on the island of Mallorca without hiatuses/gaps between the Lower Triassic and the Upper Cretaceous (Sàbat et al., 2011). The Triassic record display typical Germanic facies including (from bottom to top, Figure 2.7): red sandstones and lutites of the Buntsandstein facies, dolomites and limestones of Muschelkalk facies (Colom, 1980) and marls, evaporites and alkaline basalt of the Keuper facies (BOUTET et al., 1982). Overlying this series are shallow water marine dolomites and limestones dated Late Triassic to Early Jurassic, indicating an increase in subsidence during this period. The Jurassic and Lower Cretaceous series are composed of pelagic sediments showing strong variations in thicknesses on the island. The Lower Cretaceous deep basinal sediments are interrupted by a long hiatus from the Late Cretaceous to Early Eocene times (Figure 2.7), probably related to crustal thickness during the development of the ALKaPeCa orogenic domain (Figure 2.4) (Bouillin et al., 1986; Ramos-Guerrero et al., 1989; Van Hinsbergen et al., 2014). The hiatus is overlain by Eocene syn-orogenic continental paralic sediments that evolve towards shallow marine transgressive sediments in the Middle Eocene. Late Oligocene to Early and Middle Miocene syn-orogenic sediments overlie the Mesozoic and Paleogene series along an unconformable surface. They correspond to a thick detrital series, reflecting coastal and deep sea fan and talus depositional environments (Rodríguez Perea, 1984; Piñol et al., 1991). Marine environments represented by calciruditic and calcarenitic platform deposits were re-established during the Burdigalian, followed by marine flysch deposits during the Langhian (Rodríguez Perea, 1984; Ramos-Guerrero et al., 1989). During the Serravallian, topographic lows (e.g., Mallorca Graben, Figure 2.3) resulting from the post-orogenic extension (sub-section 2.1.2.3) were filled by continental conglomerates, calcarenites and calcisiltites of lacustrine and alluvial fan facies (García-Yagüe & Muntaner, 1968; Pomar et al., 1983; Fornos & Pomar, 1983; Baron & Gonzalez, 1985; Sàbat et al., 2011). The Late Miocene is represented by reefs and associated shallow-water carbonates (Fornos & Pomar, 1983; Baron & Gonzalez, 1985; Pomar, 1991, 2001). Overlying the carbonatic reefs are the Messinian Salinity Crisis deposits (see section 2.2.2) followed by the Pliocene sediments along the Messinian/Margin Erosional Surface. The Pliocene sediments are made up of open marine platform facies and the Quaternary is formed by littoral and transitional deposits (see chapter 5, section 5.2.3 for details about the Plio-Quaternary sediments onland Mallorca) (Colom, 1980; Baron & Gonzalez, 1985; Pomar, 1991; Capó & Garcia, 2019a; G. Mas & Fornós, 2020).

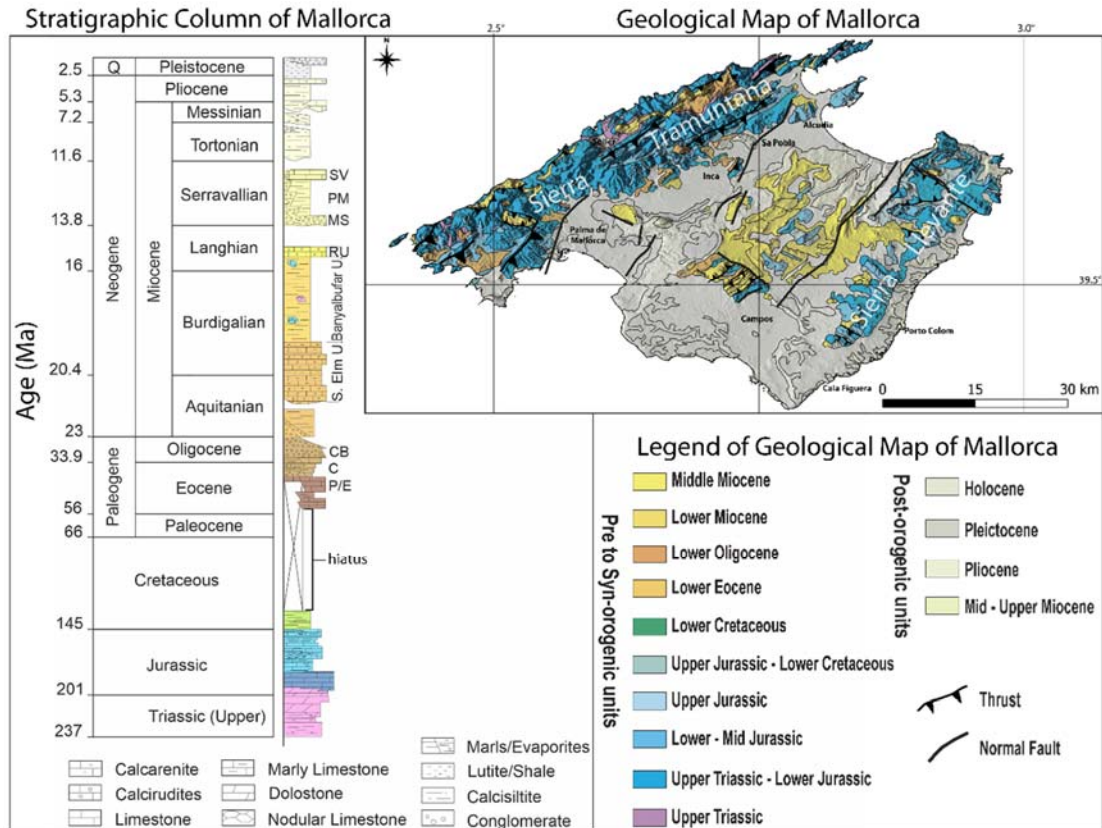


Figure 2.7. Geological map and stratigraphic column of Mallorca Island. The geology onland Mallorca is modified from the geological map of Spain 1:1000000; IGME. The stratigraphic column is modified from Moragues et al. (2021).

The stratigraphy of Ibiza Island is similar to the one described for Mallorca. Here, however, the Permian unit is absent as no Paleozoic outcrops are documented on the island (FOURCADE et al., 1982; Durand-Delga et al., 1993). The Triassic series is almost complete with the exception of the Triassic Buntsandstein, and is composed of red sandstones, limestones and gypsum (Germanic series), overlain by Jurassic and Cretaceous carbonatic units having variable thicknesses. Few Miocene deposits, upper Burdigalian to lower Langhian in age, composed mainly of marls and conglomerates, outcrop unconformably on the Mesozoic basement to the northeast and west of the island (Simo, 1982; Durand-Delga et al., 1993; Etheve et al., 2016). The Serravallian to Pliocene deposits, composed mainly of marine deposits, appear as sub-horizontal layers that unconformably overlay the previous syn-orogenic deformed rocks (Simo, 1982; Etheve et al., 2016).

Menorca's geology and stratigraphy is considered relatively erratic with respect to the other Balearic Islands. Bourrouilh, (1973) highlighted a presence of fossils considered incompatible

with those observed on Mallorca and Ibiza. These fossils correspond to those observed in the Hercynian part of Sardinia. However, Sàbat et al. (2018) highlighted that the Sardinian Paleozoic sediments, as well as its compressional deformation structures, do not temporally correlate with those of Menorca. Moreover, Paleozoic units are abundant and form the majority of the island's basement (Bourrouilh, 1973; Linol et al., 2009; Sàbat et al., 2018). They consist almost entirely of non-metamorphic terrigenous clastic deposits embracing Devonian to Upper Permian (Figure 2.8) (Bourrouilh, 1983; Sàbat et al., 2018). A sedimentary unit composed of a mega-conglomerate, supposedly Tortonian in age, and overlain by Upper Miocene to Pliocene carbonates covers the basement in the southern part of the island (Pomar, 2001). It is worth noticing that the WSW-ENE trend of the main structures of the BP seems absent in Menorca.

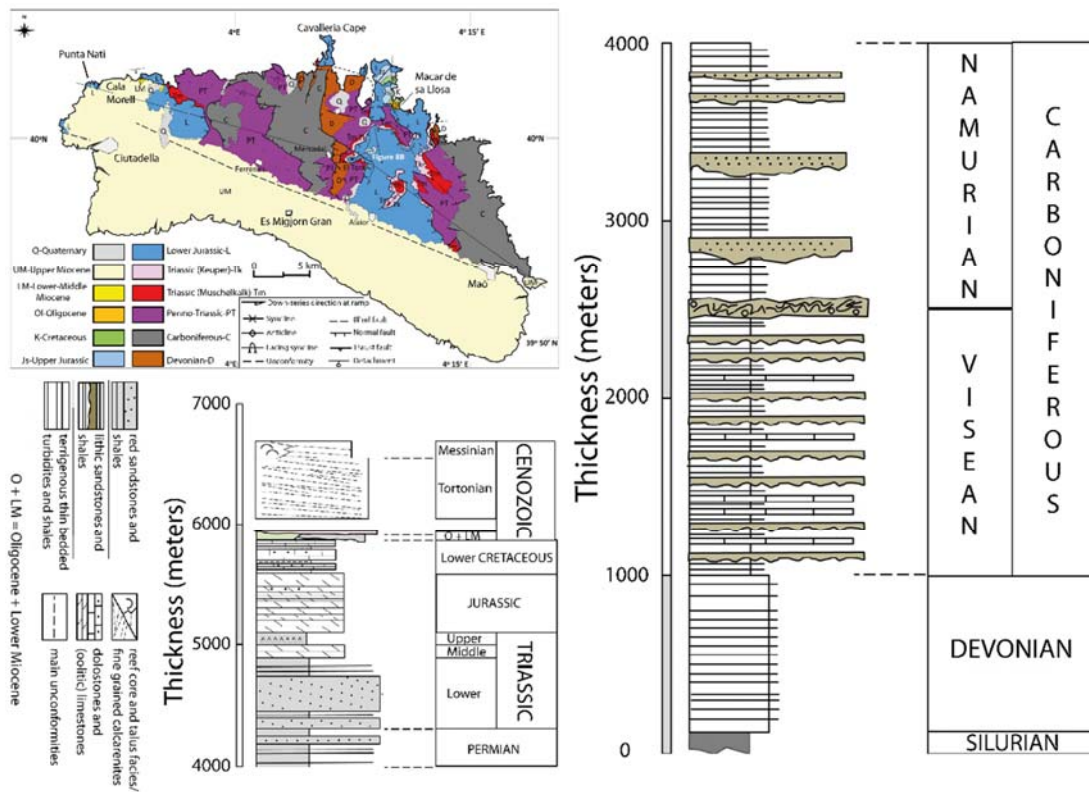


Figure 2.8. Geological map and stratigraphic column of Menorca Island. Modified from Sàbat et al. (2018).

2.1.3.2 Offshore Stratigraphy

The offshore geology and stratigraphy of the Balearic Promontory is poorly explored. Only few old industrial deep drillings exist on the westernmost side of the promontory, more precisely on the Alicante Shelf (Figure 2.14) (Lanaja, 1987; del Olmo, 2011b; D. L. Ochoa, 2016). The rest of the Promontory's offshore area is explored only by seismic reflection data. The seismostratigraphic, and eventual onshore-offshore correlations of the stratigraphic record will be described in Chapters 4 and 5.

The available drillings close to Alicante reached the Mesozoic deposits which appear to be widely present (Figure 2.9). The Mesozoic record is composed of alternating dolomites and evaporites from the Triassic period (e.g., Calpe borehole, Figure 2.9) and/or carbonates (limestones) from the Cretaceous period (e.g., Muchamiel borehole, Figure 2.9). In both Muchamiel and Calpe boreholes, the entire Eocene to Middle Miocene record is missing. In Calpe borehole, a continuous Tortonian-Quaternary sequence overlies the Triassic deposits. It constitutes of a Tortonian-Messinian claystone dominated sequence, a late Miocene evaporitic interval (section 2.2.1), a marly dominated Lower Pliocene interval and a Plio-Quaternary unit consisting of claystones. In Muchamiel borehole, a marly and clayey Lower Miocene sequence overlies unconformably the Cretaceous carbonates. The Upper Miocene record includes calcareous claystones at the base and gypsum/anhydrite beds at the top (section 2.2.1). The Plio-Quaternary cover comprises soft claystone and micritic limestone sediments (Lanaja, 1987; D. L. Ochoa, 2016).

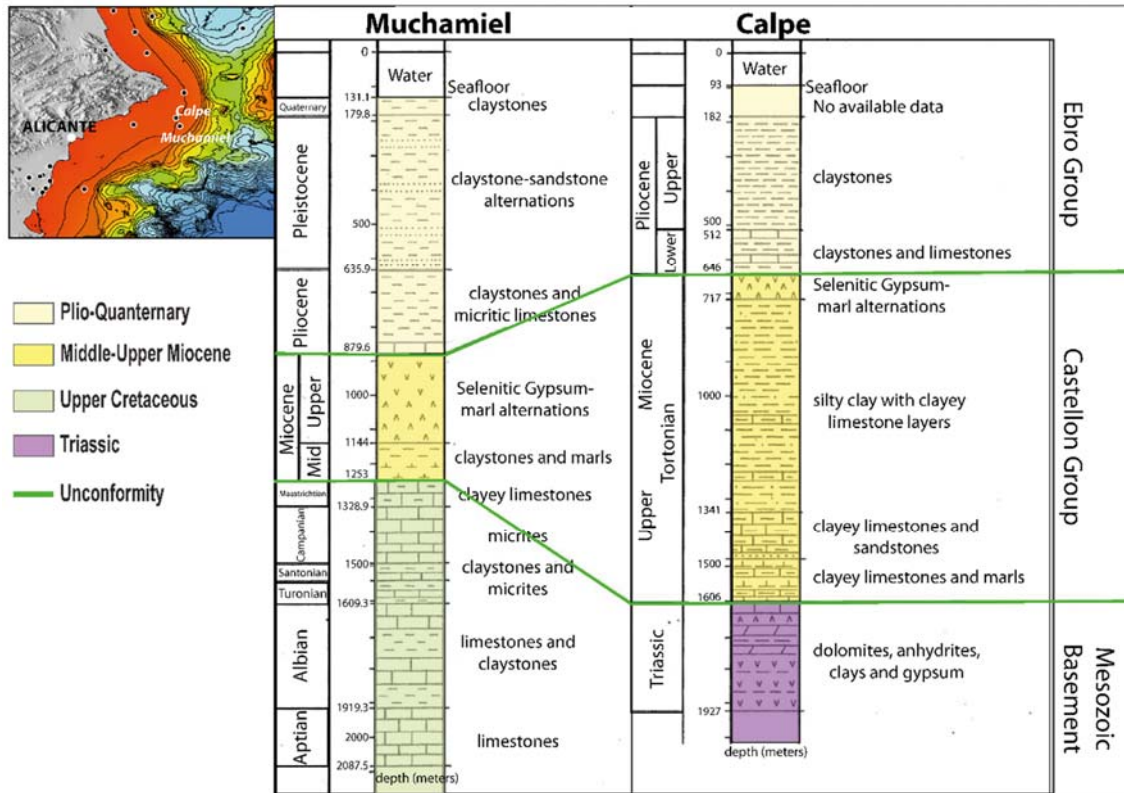


Figure 2.9. Offshore stratigraphy encountered in the only 2 deep boreholes drilled on the Balearic Promontory. Modified from Lanaja, (1987).

2.1.4 Present-day physiography of the Balearic Promontory

The Balearic Promontory separates the Valencia Basin from the Algerian basin. It is bounded to the northeast by the Liguro-Provençal basin (Figure 2.1). The promontory is about 450 km long and 110 km wide. It extends from the Alicante shelf near Cap Nao in southeastern Spain to the Liguro-Provençal basin along a NE-SW direction.

The Balearic Promontory is composed of four main big islands: (1) the largest of which Mallorca; (2) Ibiza on the eastern side of the promontory; (3) Menorca on the western part of the Promontory and (4) Formentera to the south of Ibiza (Figure 2.3). Ibiza, Formentera and Menorca present a topography with smooth morphologies having altitudes not exceeding 500m (Figure 2.10). Mallorca has a more rugged morphology with 3 mountain ranges (Tramuntana, Central and Llevant ranges) whose altitudes exceed 1000 m (Figure 2.3). The 4 islands are surrounded by continental shelves; the Mallorca-Menorca and Formentera-Ibiza blocks having a depth that does not exceed 100m (Figure 2.10 and Figure 2.11). The two blocks are separated

by an elliptical depression around 1050m deep, called the Central Mallorca Depression (Acosta et al., 2003). The Ibiza-Formentera block, together with the shelves surrounding Mallorca, have a NE-SW direction corresponding to the onland mountain ranges as well as the general direction of the Betic Cordilleras (Figure 2.3 and Figure 2.10) (Acosta, Muñoz, Herranz, et al., 2001b). On the contrary, the shelves surrounding Menorca are oriented in a NW-SE direction, which is considered perpendicular to the general orientation of the promontory.

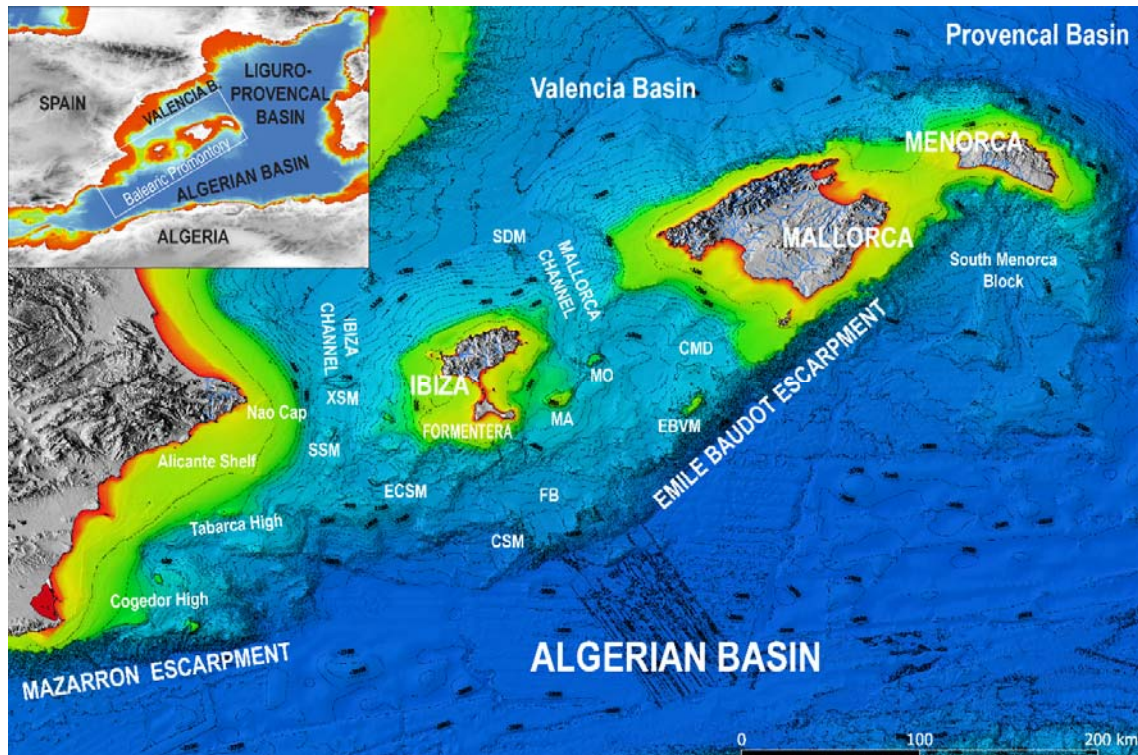


Figure 2.10. Topographic map of the whole Balearic Promontory area illustrating the main offshore features. The bathymetric data for the offshore domain is downloaded from the European Marine Observation and Data network (EMODnet) database available online (www.emodnet-bathymetry.eu). The digital elevation model in the onshore domain is downloaded from the Spanish Centre for Geographic Information (<https://www.ign.es/web/ign/portal/qsm-cnig>). CMD = Central Mallorca Depression; FB = Formentera Basin; MA = Mont Ausias Marc; MO = Mont des Oliva; EBVM = Emile Baudot Volcanic Mount; SDM = Sa Dragonera Mount; CSM = Chimene Sea Mount; ECSM = El Cid Sea Mount; SSM = Split Sea Mount; XSM = Xabia Sea Mount. Thin blue lines onshore the Balearic Islands represent the present-day river catchments.

Two wide channels incise the Balearic Promontory and connect it to the Valencia Basin to the north and to the Algerian Basin to the south (Figure 2.10).

The first channel, called Ibiza Channel, separates the Alicante shelf from the Ibiza-Formentera block along an N-S elongated axis, and it reaches depths of about 900m (Figure 2.10) (Acosta

et al., 2003; Lastras et al., 2004). Three seamounts (Xabia, Split and El Cid Seamounts) are located inside the Ibiza Channel, all of which are considered to be of tectonic origin. In particular, Xabia seamount is interpreted as a tilted Cenozoic horst (Lastras et al., 2004), however, Maillard & Mauffret, (2013) inferred that these seamounts could result from recent compression that possibly inverted former horsts, in accordance with the anticlines observed on the Alicante shelf (Tabarca and Cogedor highs) (Alfaro et al., 2002).

The second channel, called Mallorca Channel, separates Ibiza-Formentera block from the Mallorca-Menorca block (Figure 2.10) (Acosta, Muñoz, Herranz, et al., 2001b; Acosta, Muñoz, P., et al., 2001). It is a V-shaped channel oriented along a NW-SE axis towards the Valencia Basin with a depth varying between 400 m and 800 m (Figure 2.10). The channel is intruded by a volcanic seamount in the vicinity of Valencia Basin called the Sa Dragonera Seamount. To the southeast, the Mallorca Channel terminates in a pseudo-circular basin, ~75 km wide and ~60 km long, called the Central Mallorca Depression (CMD) that has a maximum depth of ~1050 m. The western side of the Central Mallorca Depression features 2 seamounts, Mount Ausias Marc and Mount dels Oliva (Figure 2.10), both interpreted as isolated blocks from the Ibiza-Formentera shelf (Acosta, Canals, et al., 2004b). To the south, the Central Mallorca Depression is closed by the Emile Baudot Volcanic Mounts (Figure 2.10 and Figure 2.11) and with no connection to the Algerian basin (Acosta, Ancochea, et al., 2004a; Acosta, Canals, et al., 2004b). On the contrary, the southwestern part of the depression extends into a deeper basin called the Formentera Basin (Figure 2.10), with the 2 basins separated by a local but gentle topographic high. The Formentera Basin is bounded to the east and to the west by volcanic mounts known as the Chimene Sea Mounts, incised by a local sub-marine active channel (Camerlenghi et al., 2009b). Both the Chimene and the Emile Baudout volcanic bodies are composed of cone-shaped volcanic edifices that are Pleistocene in age (Acosta, Ancochea, et al., 2004a; Camerlenghi et al., 2009b). The Balearic channels of Ibiza and Mallorca play a main

role in the regional water exchange and circulation of the Western Mediterranean water masses (see chapter 7, section 7.2.2).

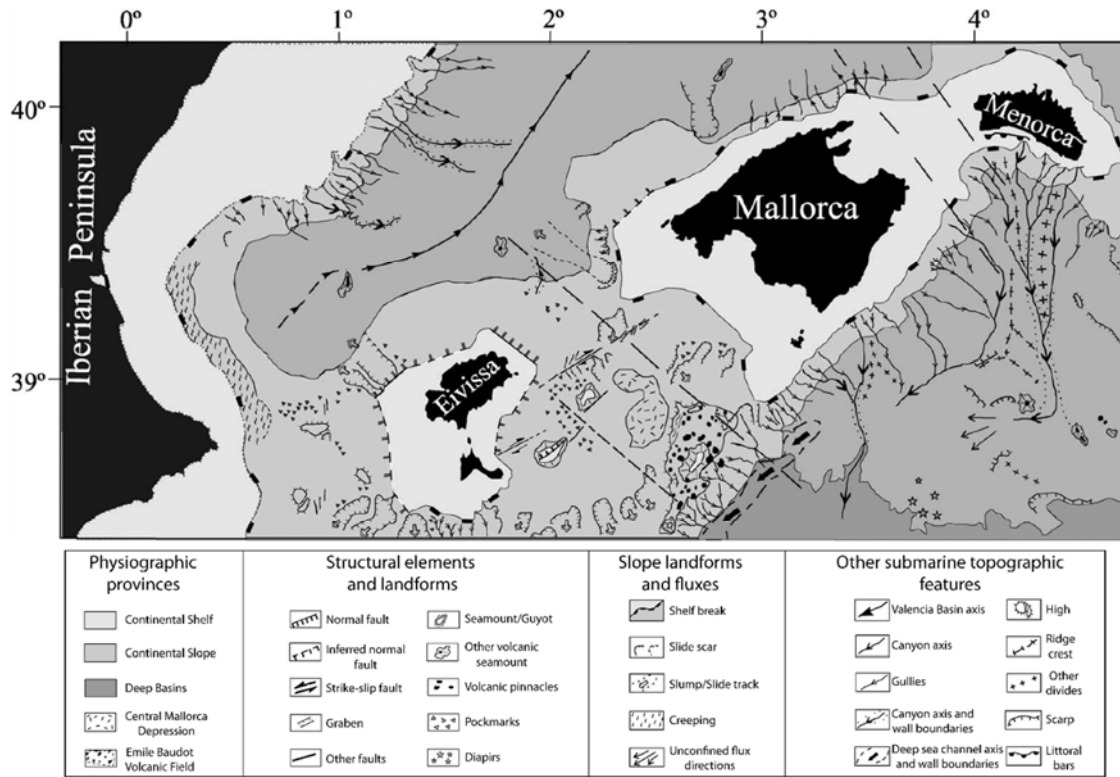


Figure 2.11. Physiographic provinces and geomorphologic features of the offshore area of the Balearic Promontory. Modified from Acosta *et al.* (2003).

To the south, the Balearic Promontory is bounded with the 2 long and sharp escarpments, the Emile Baudot and Mazarron escarpments, separating it from the Algerian Basin (Figure 2.10). The Emile Baudot is a ~180 km long, NE-SW oriented, escarpment that extends from the South Menorca Block to the southern end of the Ibiza Channel and includes the volcanic edifices described above. The bathymetry along the escarpment varies between 850 m and 1750 m, and its slope vary between 6.2° and 7.9° (11% to 14%) (Acosta, Muñoz, Herranz, et al., 2001b; Acosta, Ancochea, et al., 2004b). The crests and slopes of the escarpment are highly eroded and are characterized by the presence of numerous thalwegs (Figure 2.11) (Acosta, Muñoz, Herranz, et al., 2001b).

The Mazarron Escarpment is the westernmost feature of the southern Balearic margin. It is globally E-W oriented, parallel to the Tabarca and Cogedor highs, extending between the western flank of Ibiza Channel and the offshore part of the Vera Basin southeast Spain. The

escarpment is ~140 km long, having an average depth of ~2200m and its slopes vary between 14° and 31° (from 25% to 60%) (Acosta et al., 2013). It corresponds to the southern limit of the Alicante shelf and it is also highly incised by numerous narrow canyons (Figure 2.10). The northern slopes of the Balearic Promontory are relatively gentle descending towards the Valencia Basin, except for the northern Menorca scarp that descends abruptly towards the Liguro-Provençal Basin through the NBFZ (Figure 2.10).

The offshore area of the Balearic Promontory consists of a series of sub-basins that resulted from the complex tectonic history described in the previous sections that the promontory underwent since its formation. In the present-day physiography described above, only two sub-basins appear as depressions with a proper accommodation space; those are the Formentera Basin (1700m) and the Central Mallorca Depression (1050m; Figure 2.10). However, when looking to the depth maps of the basement in the area, at least three more sub-basins that have the shape of depressions appear on the southwestern present-day shelf of the promontory (Alicante shelf; Figure 2.12). Those sub-basins are the Elche Basin, El Cid Basin and Bajo Segura-San Pedro Basin. As will be shown in the next section of this chapter (section 2.2), those sub-basins trapped evaporitic deposits during the Messinian Salinity Crisis (Figure 2.14), but then were buried with Pliocene to Quaternary sediments after the crisis with a progressive retreat of the shelf towards the present day coastline.

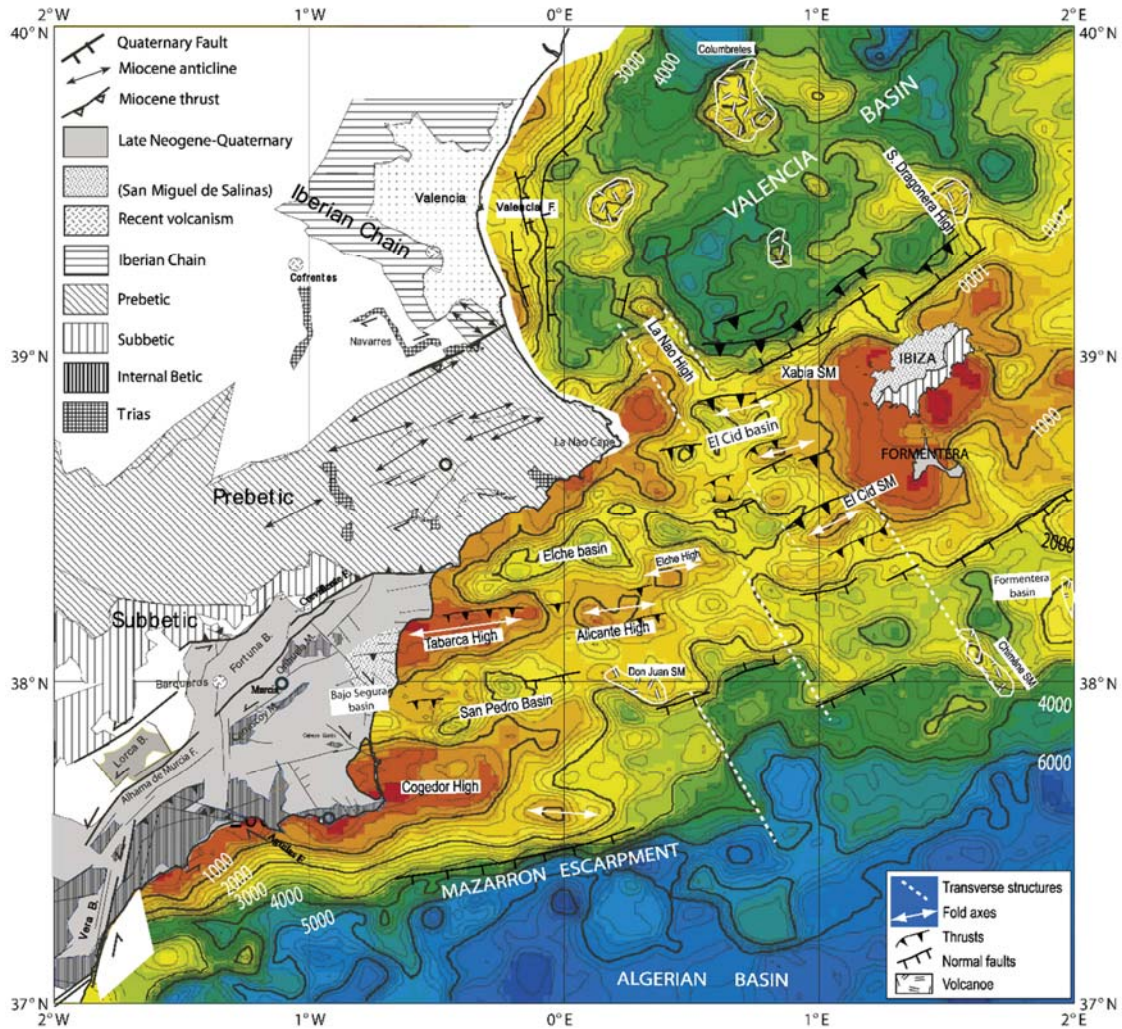


Figure 2.12. Structural map of the basement in the Southern part of the Balearic Promontory. Isobaths of the basement are in meters, with contour interval=200 m. Notice the presence of a series of sub-basins close to the present-day Spanish coastline. When looking to the present-day bathymetry of the promontory those basins do not exist anymore and constitute the present day shelf (Figure 2.10). Modified from Maillard & Mauffret, (2013).

2.2 The Messinian Salinity Crisis in the Balearic Promontory

2.2.1 MSC in the offshore domain

A relatively thin MSC record covers most of the offshore area of the Balearic Promontory, apparently disconnected from the other MSC units in the surrounding basins (Mauffret, 1977; Driussi, Maillard, et al., 2015b). This record has been studied mainly through seismic reflection

dataset with very limited and local access through old industrial borehole data (Figure 2.14) (del Olmo, 2011a, 2011b).

The MSC deposits were mapped accurately for the first time over the entire Balearic Promontory by Mauffret (1976) using seismic reflection profiles (Figure 2.13). Mauffret, (1976) highlighted the existence of several seismic facies linked to the MSC deposits that are overlain by the transparent Plio-Quaternary seismic unit, similar to most of the other parts of the Mediterranean where a MSC record is present (see section 1.2.3), without further analysis. More than two decades after Mauffret's work, the morphometric and structural studies done by Juan Acosta (Acosta, Muñoz, Herranz, et al., 2001b; Acosta, Muñoz, P., et al., 2001; Acosta et al., 2003; Acosta, Canals, et al., 2004b) (see section 2.1.4) brought back to the light the MSC deposits of the Balearic Promontory. On their high-resolution seismic dataset, Acosta et al. (2004) evidenced the presence of an unconformity, characterized by a U to V-shaped features, truncating the top of the MSC seismic units on the uppermost slopes of the Balearic Promontory, mainly offshore Mallorca and Ibiza islands (Acosta, Canals, et al., 2004b). They interpreted this unconformity to be the Margin Erosion Surface (MES; section 1.2.4.1), and associated it to subaerial erosion during the desiccation phase of the MSC. Their data allowed also the identification and mapping of a 'stratified unit' forming a trough-like structure, which is limited to the topographic lows of the Central Mallorca Depression (CMD). They interpreted this unit as Upper Evaporites unit (1.2.2.4.1), that however shows no lateral geometrical continuity with the UU (section 1.2.5.3) of the deep basin (Acosta, Canals, et al., 2004b).

Offshore the Alicante shelf to the southwest of the Promontory, old industrial seismic and borehole data from the Bajo Segura-San Pedro Basin (Figure 2.14) document the offshore continuation of the Primary Lower Gypsum (PLG; section 1.2.2.1) evaporites of the onland San Miguel de Salinas (Figure 2.14) (Soria et al., 2007, 2008; del Olmo, 2011b). Here, cuttings from the Torre Vieja M. C-1 borehole (Figure 2.14) evidenced the presence of porites, stromatolitic and oolitic limestones, consistent with the pre-MSC reef complex outcropping elsewhere in peripheral MSC basins (e.g., Palma Basin reefs; see section 2.1.3.1), overlapped by the MSC stage 1 PLG (del Olmo, 2011).

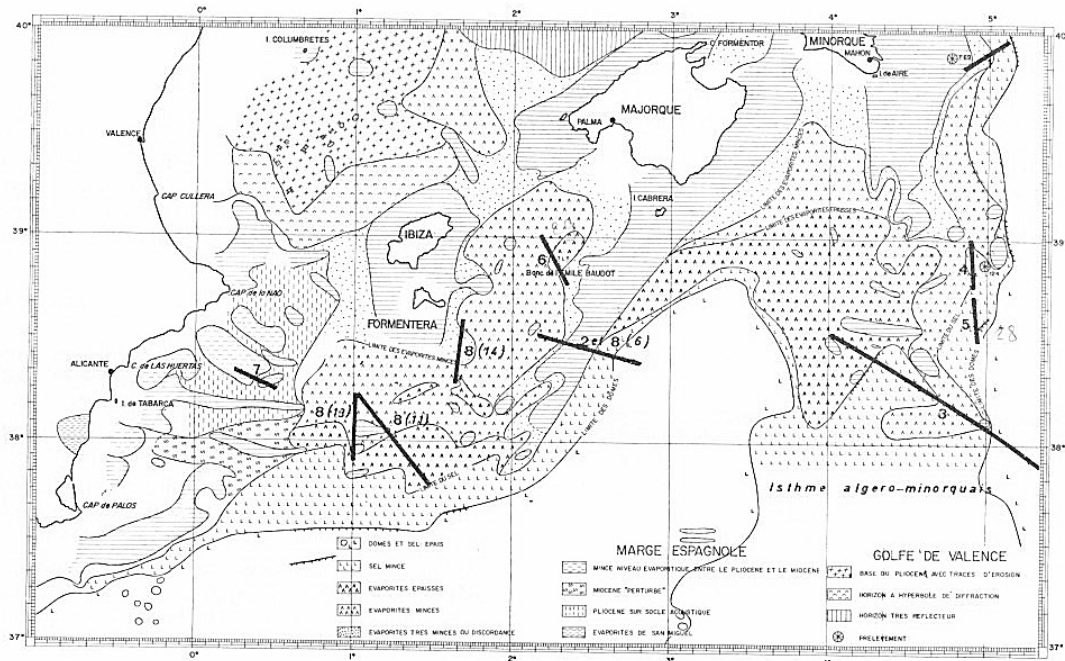


Figure 2.13. The first map of the extension of the MSC evaporites in the Balearic Promontory and Western Mediterranean in the late 70s by Mauffret, (1976).

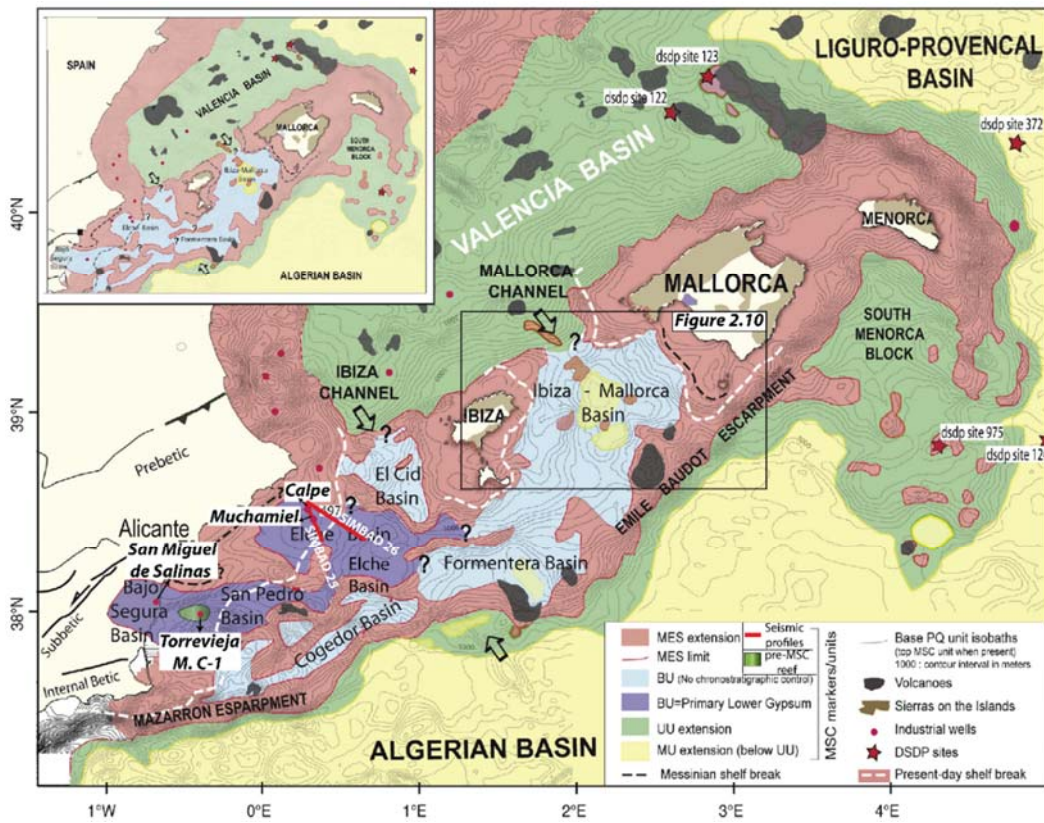


Figure 2.14. Map showing present-day extent of the MSC deposits over the Balearic Promontory sub-basins, as well as the units of the surrounding deep basin. Modified from Driussi et al. (2015).

With time, high-resolution seismic data was acquired on the promontory, allowing to perform new studies focusing on the MSC deposits. In particular, following the SIMBAD high-resolution seismic reflection campaign organized by Maillard & Gaullier, (2013), several publications came out and improved the knowledge about the MSC record on the Balearic Promontory. The first study was performed by Maillard et al. (2014), who focused exclusively on the MSC units of the CMD. They distinguished two different sub-units within the MSC deposits of the CMD (Figure 2.15). A Slope Unit (SU) located on the Mallorca and Ibiza slopes, clearly truncated by an erosional event on its top, which confirms the observation of Acosta et al. (2004), and a Bedded Unit (BU; sensu Lofi et al., 2011; Section 1.2.5.5) lying in the depocenter of the depression that contains a thin (~300m) salt unit (Figure 2.14 and Figure 2.15). The authors discussed the different chrono-stratigraphic possible positions for those two units in the CMD (Figure 2.15-C) in the framework of the MSC scenarios, attempting also to correlate the Palma de Mallorca gypsum (see section 2.2.2) to the offshore SU and BU (Figure 2.15-C). They favored a scenario in which the MSC deposits are diachronous, with progressively younger units forming towards the depocenter of the CMD in a progressive base level drawdown setting, as evidenced by the onlap of the BU on the SU (Figure 2.15-B).

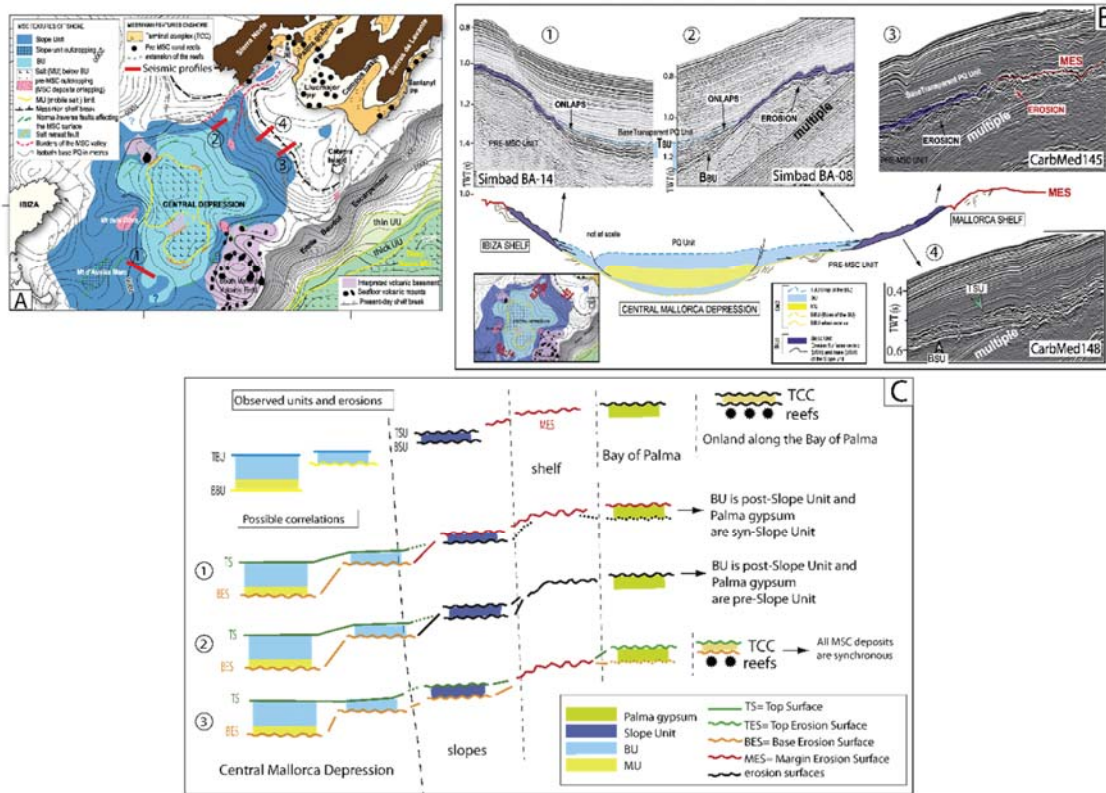


Figure 2.15. A: MSC units in the Central Mallorca Depression following the interpretation of Maillard et al. (2014). B: Seismic zooms showing the relationships between the different MSC units and the erosional surfaces, from the deep part of the CMD to the margins (modified from Maillard et al., 2014). C: Schematic diagram showing possible correlations between the different MSC markers, extending from onland Mallorca to the offshore CMD, and interpretations of the erosional surfaces (Maillard et al., 2014).

In the second study, Driussi et al. (2015) combined the widespread high and low-resolution seismic reflection dataset to map precisely and analyze the MSC deposits on the BP. They show that a “MSC unit”, 0-200m thick, extends all over the BP and lies in a series of perched sub-basins separated by highs partly controlled by post-MSD tectonically (Figure 2.14). Those authors confirm the existence of another thin MSC salt unit in the deeper Formentera Basin, as observed by Mauffret 1976, completely disconnected from the CMD and the deep basin MSC halite (Figure 2.14).

The third and last work of this research team and in which the SIMBAD campaign seismic dataset was used on the Balearic Promontory was performed by Ochoa et al. (2015), who focused on the MSC unit of the Alicante Shelf in the Elche Basin (Figure 2.14), where two old industrial boreholes offering access to the MSC unit exist. Based on the Calpe and Muchamiel (Figure 2.14 and Figure 2.16) borehole cuttings and logs tied to the high-resolution SIMBAD profiles, Ochoa et al. (2015) demonstrated that the “MSC unit” of Driussi et al. (2015) in Elche

and Bajo Segura sub-basins corresponds to the MSC stage 1 PLG (Figure 2.16). They called it the Bedded Unit (BU; section 1.2.5.5), in which they identified 12 precessionally driven PLG cycles in Calpe, and 14 in Muchamiel boreholes, and correlated them to the San Miguel de Salinas gypsum in the vicinity onland in the Bajo Segura Basin (Soria et al., 2008). The BU-PLG here is clearly cut on the top by the TES (Figure 2.16; section 1.2.4.4), whereas no erosion is identified at its bottom. Two important outputs from Ochoa et al. (2015)'s work were: (1) updating the distribution map produced previously by Driussi et al. (2015) by identifying the MSC unit of the San Pedro and Elche sub-basins as the present-day offshore extension of the PLG on the promontory, and (2) showing that PLG gypsum precipitation and/or preservation could occur in non-silled basins at water depth exceeding 200m, thus contrasting the ongoing idea of Lugli et al. (2010) (see section 1.2.2.1).

Following Ochoa's conclusion about the PLG paleo-depth and disproving the need of a sill for the formation of PLG, Roveri et al. (2019), bothered by the idea, proposed that only the shallower domains of the Elche and Bajo Segura sub-basins contained PLG, whereas the deeper parts of these basins are located beyond some volcanic 'sills' and contain stage 2 Resedimented Lower Gypsum (RLG; section 1.2.2.2). Roveri et al. (2019) did not provide any new seismic profiles to support their new interpretation and mapping, instead they re-interpreted the seismic profiles published previously by Ochoa et al. (2015) and erroneously citing the work of Driussi et al. (2015) that shows the continuation of the MSC unit from the shallow to the intermediate domain of the sub-basins.

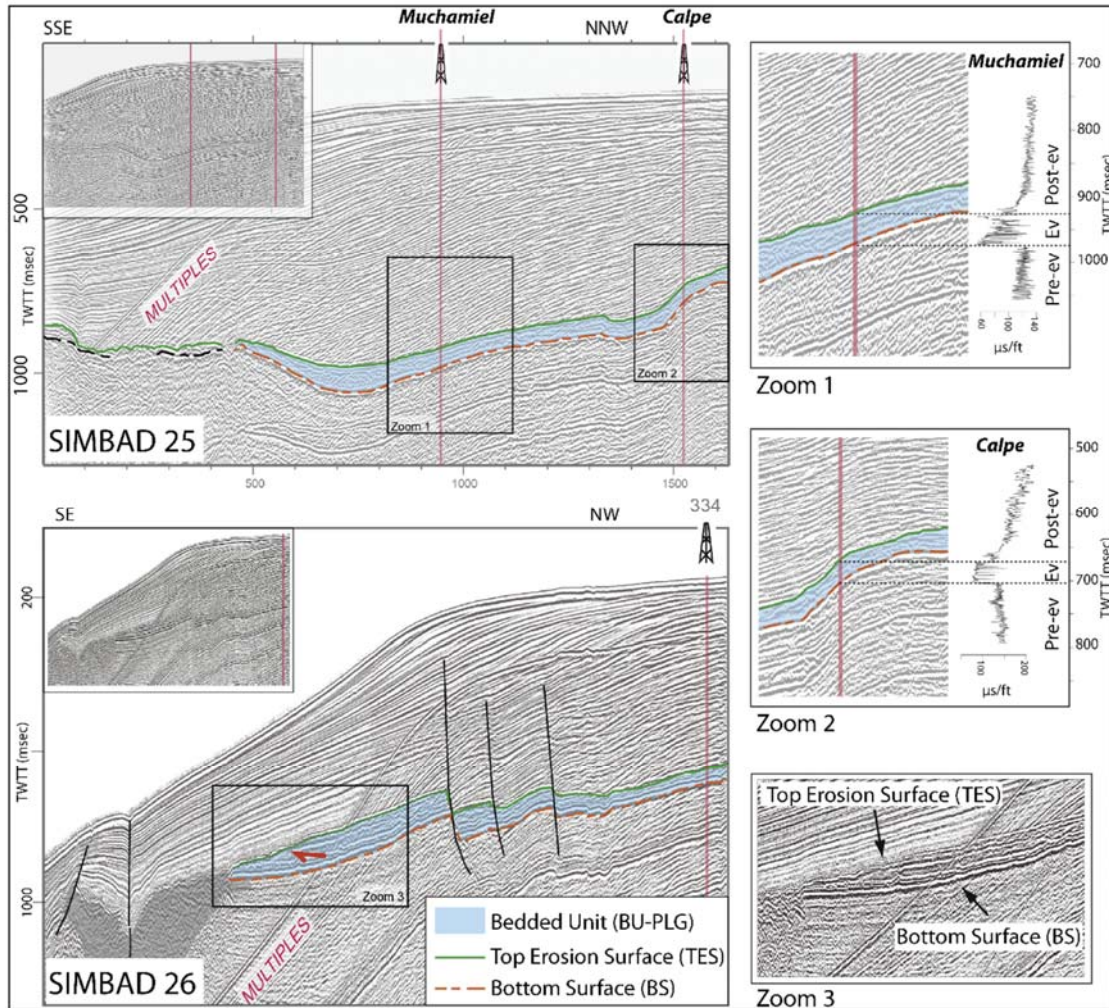


Figure 2.16. Seismic profiles SIMBAD 25 and 26 across the southwestern margin of the Balearic Promontory tied to Calpe and Muchamiel boreholes in the Elche sub-basin (position of seismic profiles and boreholes in Figure 2.14). Zooms 1 and 2 show seismic facies and corresponding well-log facies from Muchamiel and Calpe boreholes respectively. Zoom 3 shows non-erosive basal contact and a clear erosive contact at the top of the BU-PLG unit. Post-ev = Post-evaporitic, Ev = Evaporitic, and Pre-ev = Pre-evaporitic sequences. Modified from Ochoa et al. (2015).

2.2.2 MSC in the onshore domain

Onland Mallorca, two outcropping MSC-related units are lying above late Tortonian-Messinian reefal carbonates (Reef Complex Unit) (Pomar et al., 1983, 1996; Suarez-Gonzalez et al., 2019) and beneath the Pliocene deposits in the marginal part of the Palma Basin: those are the Santanyí limestones and the Ses Olles Formation (Mas Gornals & Fornós, 2012, 2013; G. Mas & Fornós, 2020). The Santanyí limestones are microbialites and oolite-dominated sediments in which a baleen whale neurocranium has been found (Mas Gornals et al., 2018).

Above the Santanyí limestones lies the Ses Olles formation which consists of marls, sandy-marls and marly-calcareous lacustrine deposits rich in in-situ freshwater, brackish water Paratethyan-like mollusks and ostracods, and littoral benthic foraminifera (Mas Gornals et al., 2014; G. G. Mas, 2015; G. Mas & Fornós, 2020). The lower contact of the Ses Olles Formation with the Santanyí limestones is sporadically marked by a well-developed reddish paleosol, indicating a period of subaerial exposure that must have occurred before the emplacement of the Ses Olles Fm. The upper contact of the Ses Olles Formation with the Pliocene corresponds to an erosional ravinement surface draped by a transgressive lag of coastal deposits usually containing coquinas and/or conglomerates (Mas Gornals et al., 2014; G. G. Mas, 2015; G. Mas & Fornós, 2020).

In the depocenter of the Palma Basin, old drills evidenced the presence of Primary Lower Gypsum (PLG; see section 1.2.2.1), consisting of up to 13 typical precession-driven gypsum-marl alternations (Baron & Gonzalez, 1985; Rosell et al., 1998b; García-Veigas et al., 2018b; G. Mas & Fornós, 2020), belonging to stage 1 of the MSC.

The Santanyí limestones formation of the Palma Basin was interpreted either as the Terminal Carbonate Complex (TCC, *sensu* Esteban, 1979; Section 1.2.2.1) laterally equivalent to the PLG (G. Mas & Fornós, 2020), or as time-equivalent to the pre-MSC Reef Complex Unit (e.g., [Arenas & Pomar, 2010](#); [Suarez-Gonzalez et al., 2019](#)). However, none of the boreholes drilled onland Mallorca records the PLG overlying the Santanyí limestones (Baron & Gonzalez, 1985), reason for which most of the studies suggested that the TCC is, at least partly, the lateral time equivalent of the PLG (Figure 2.17) (Baron & Gonzalez, 1985; Mas Gornals & Fornós, 2012; Maillard et al., 2014b; G. Mas & Fornós, 2020).

According to Mas and Fornós, (2020), the emplacement of the Ses Olles Fm. pre-dated the MSC peak and the erosional surface marking the Miocene/Pliocene boundary is associated with a 270 kyr hiatus linked to the main MSC base-level drawdown (Figure 2.17), thus adapting the two-step reflooding model of [Bache et al. \(2012\)](#) (see section 1.3 and Annex A). This interpretation is, however, in disagreement with the presence of the unconformity and the paleosol at the base of the Ses Olles Fm., which instead points to the deposition of the Ses Olles Fm. (and therefore to the arrival of the Paratethyan fauna in Mallorca) at some point during the terminal stage (Stage 3 of [Royer et al., 2014](#)).

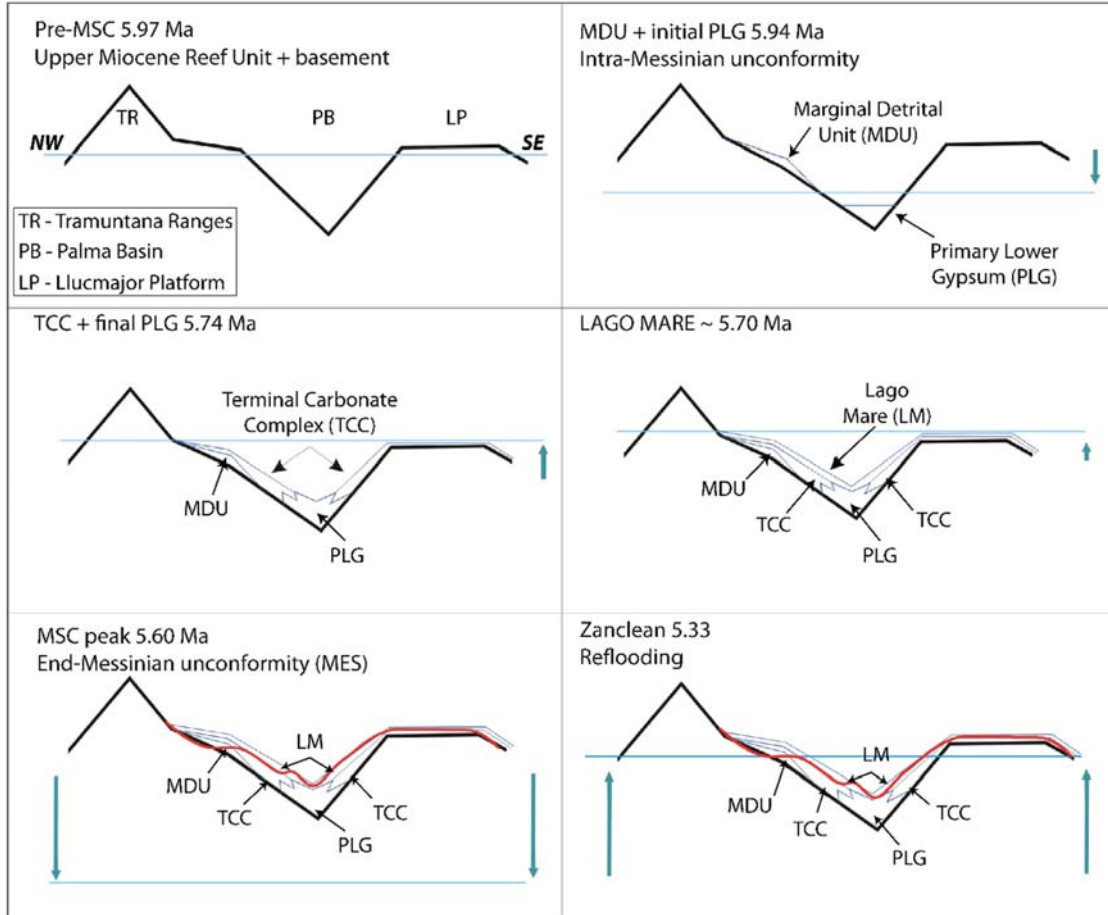


Figure 2.17. Schematic reconstruction of the evolution of sea-level and the main palaeogeographic changes, from pre-crisis Messinian to the Zanclean reflooding in the Palma basin following the interpretation of Mas and Fornos, (2020), adapting the two-step reflooding of Bache et al. (2012). Modified from Mas & Fornos, (2020).

Onland Ibiza, Late Miocene units outcrop only locally in the north of the island and show common characteristics with the units known in Mallorca, such as the reef complex and the Santanyi limestones (Durand-Delga et al., 1993; Pomar et al., 1996; Lezin et al., 2017). Important continentalization episode has been recently identified on top of these units with erosion and karstification, paleosols and gravity-driven instabilities that are thought to record the major sea-level fall of the MSC (Odonne et al., 2019; Maillard, Gaullier, et al., 2020a).

Chapter 3

Data and Methods

In this chapter, I will describe in detail the dataset used and the methodologies applied for the systematic development of this work. The starting point and main input is the seismic reflection dataset (section 3.1.1), which interpretation (section 3.1.2) was in part the basis for the successive steps of methods and analysis, namely the backstripping analysis (section 3.2) and the evaporites' deposition modelling (section 3.3).

The seismic dataset that is presented in the chapter was in part provided to me by Johanna Lofi and Agnes Maillard (my supervisor and co-supervisor, respectively), and in part I was able to obtain myself by contacting private companies such as Spectrum and Schlumberger who kindly accepted to provide me a remarkable number of seismic profiles through academic confidential contracts. The description of the seismic dataset will be focused on the seismic surveys covering the Balearic Promontory. Some seismic interpretation covering wider areas of the Western Mediterranean will be presented, as it was used as an input for the backstripping analysis (section 3.2.2.2) and for a general mapping of the main seismic horizons and units of the Western Mediterranean (Annex B and Annex C).

The seismic interpretation performed in the thesis was done mainly by me at the University of Montpellier under the supervision of Johanna and Agnes.

The pseudo-3D backstripping analysis technique (section 3.2.2.2) was performed and led by Hanneke Heida and Daniel Garcia-Castellanos, SaltGiant colleagues from the University of Barcelona.

The 2D backstripping (section 3.2.2.1) was performed by me in collaboration with Hanneke Heida and under the supervision of Daniel Garcia-Castellanos.

The evaporites deposition modelling (section 3.3) was performed by Ronja Ebner and me under the supervision of Paul Meijer, both SaltGiant colleagues from the Utrecht University. The theory behind the models as well as the coding were led by Ronja and Paul.

3.1 Seismic reflection data and interpretation

3.1.1 The seismic reflection dataset

Seismic reflection surveying is one of the most widely used and well-known geophysical methods. Its big success is mainly due to the fact that the seismic reflection images produced are very similar, although fundamentally different, to the geological section. In addition, they can represent penetration scales ranging from tens of meters up to several kilometers (eg. down to the Moho). Since the 1960s, the Western Mediterranean has been investigated by numerous reflection seismic surveys for research and industrial objectives.

The seismic data used in this thesis consist of low-, intermediate and high-resolution 2D seismic reflection profiles covering most of the Western Mediterranean area with denser coverage on the Balearic Promontory (Figure 3.1). They include both academic and industrial profiles (Table 3.1). This multi-resolution dataset allows crossing of seismic profiles that have different resolution and permits a better recognition, interpretation and mapping of the seismic sequences, features, units and surfaces (e.g. Figure 3.2).

The following two sub-sections include a brief description of the available seismic surveys with some examples of non-interpreted versus interpreted profiles from most of the surveys (Figure 3.3 to Figure 3.7).

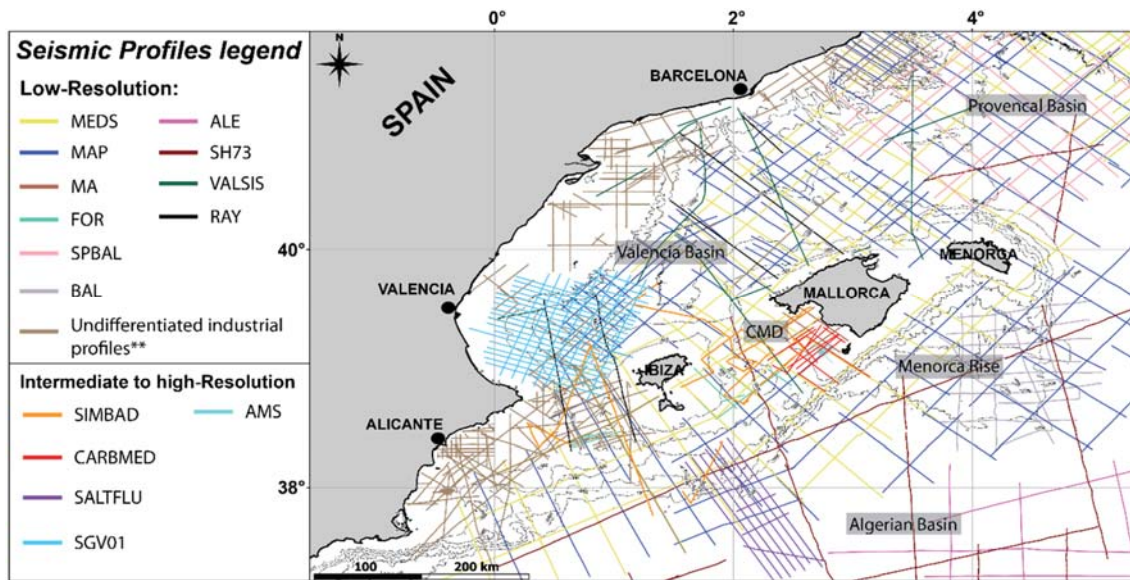


Figure 3.1. Map showing the position of the different seismic surveys used in this dissertation. Thin black isolines in the background represent the bathymetry of the area (every 500 meters). CMD= Central Mallorca Depression. ** The undifferentiated industrial seismic profiles include vintage re-processed (in 2011) profiles from several surveys that were provided by the Spectrum Geo Limited Company. No information were available about those surveys.

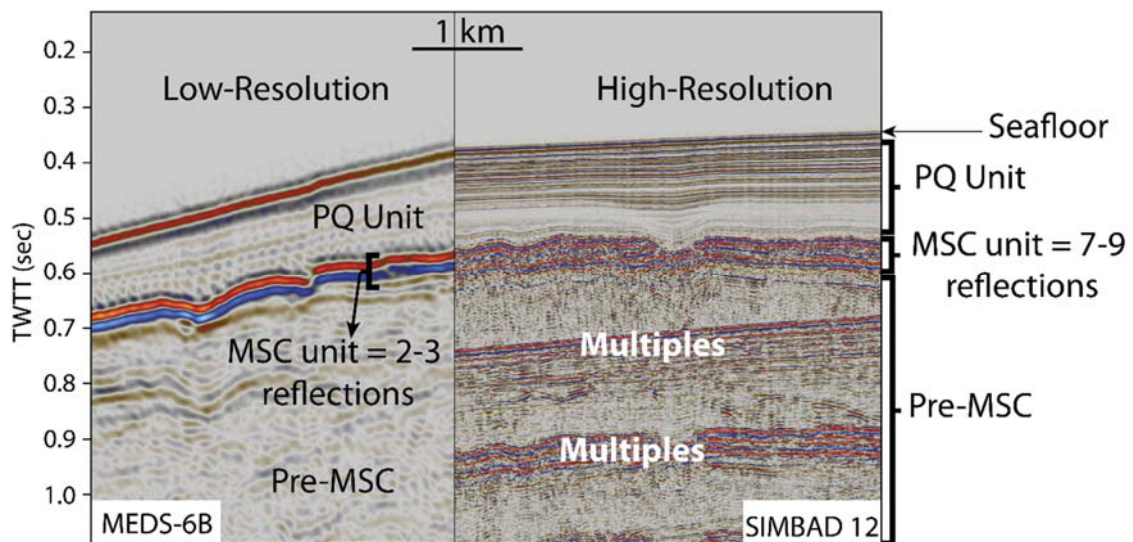


Figure 3.2. Low-resolution vs high-resolution seismic image crossing the same point. Notice how the MSC unit appears on the SIMBAD high-resolution profile as a package of up to 9 reflections with lateral changes in internal seismic facies, whereas on the MEDS profile it appears as two continuous high amplitude reflections without any lateral change in internal facies.

Seismic Survey	Resolution	Acquired by/Owner	Year	Seismic Source	Navigation Type	Cumulative Distance (Km)	Basin
MEDS	Low	Western Geophysics	1976*	Canon Maxipulse	Satellite	5913	Valencia, Algerian & Provençal basins - Balearic Promontory
MAP	Low	ENIEPSA	1978*	2 VAPORCHOC	Satellite Doppler	9059	Valencia, Algerian & Provençal basins - Balearic Promontory
MA	Low	CAMPSA	1970	600 cu. in. airgun	--	200	Central Mallorca Depression
FOR	Low	CAMPSA	1979	2 VAPORCHOC	Satellite Doppler	1132	Balearic Promontory
BAL	Low	University of Bologna	1984	--	--	1539	Menorca Rise
ALE	Low	Total	1977	Canon Maxipulse	Satellite	2039	Algerian Basin
SH73	Low	Sonatrach	1974	8 SEISPROBE air gun	--	3120	Valencia, Algerian & Provençal basins - Balearic Promontory
VALSIS	Low	UPMC	1988	10 BOLT Airgun 5861Cu.in	GPS	810	Valencia Basin & Central Mallorca Depression
RAY	Low	Mandrel Industry	1972	Airgun 3300 cu.in	Satellite	586	Valencia Basin & Balearic Promontory
SPBAL	Intermediate	MINCOTUR	2001	4240 cu. in. Bolt LL airgun	GPS	2700	Provençal Basin
SGV01	Intermediate	Fugro-Geoteam	2001	32 Sordera G-guns	GPS	2800	Valencia Basin and Balearic Promontory
SALTFLU	Intermediate	OGS	2012	2 GI-gun Sercel	GPS	1055	Algerian Basin and Balearic Promontory
SIMBAD	High	University of Toulouse	2013	1 mini-GI airgun	GPS	945	Balearic Promontory
CARBMED	High	University of Hamburg	2006	2 GI-airgun	GPS	280	Central Mallorca Depression
AMS	High	University of Hamburg	2006	--	GPS	211	Central Mallorca Depression

Table 3.1. Summary of the available information about the profiles of the seismic surveys shown in Figure 3.1. *The vintage seismic profiles from surveys MEDS and MAP acquired in the late 70s were reprocessed in 2011 (see section 3.1.1.1 for more details).

3.1.1.1 Industrial seismic profiles

- MEDS and MAP surveys: these are vintage multichannel profiles acquired in the late 70s (Table 3.1) covering a very wide area of the Western Mediterranean (Figure 3.1). The profiles of the MAP and MEDS surveys have been reprocessed in 2011 by Spectrum Geo Limited and Western Geco companies, respectively. Access to the reprocessed SEG-Y format profiles of the two surveys has been provided through an academic confidential agreement between the above-mentioned companies and Geosciences Montpellier in the frame of this PhD dissertation. The provided profiles are time-migrated seismic profiles with a very good quality (Figure 3.3 and Figure 3.4). They are low frequency-deep penetration profiles that often allows identifying the complete sedimentary sequences down to the top of the acoustic basement and even deeper in some cases (e.g. Figure 3.3). However, the low resolution of those profiles does not allow distinguishing details about the internal facies of thin (<50 msec) sedimentary units (Figure 3.2).
- SGV01: 2D multichannel seismic survey offshore the Valencia margin (SE Spain) (Cameselle, 2015) that partly covers the southwestern part of the BP (Figure 3.1). These data were acquired in October 2001 by Fugro-Geoteam aboard the RV Geo Baltic. Subsequent processing was performed by Robertson Research International Ltd (Robertson Research International Ltd., 2002). They are provided as post-stack time migrated profiles with a very good quality seismic image, which allows a good identification of tectonic structures, geometries and seismic facies.
- FOR, MA, SH and RAY: those surveys consist of vintage low-resolution profiles acquired between the 70s and 80s of the last century. Most of them are made available by the Spanish Geological Survey SIGEOF (www.igme.es) as .TIFF image format. Part of the profiles has been transformed by Driussi, (2014) from .TIFF format associated with their navigation files into SEG-Y format using the IMAGE2SGY software in MATLAB, a free SEG-Y tool developed at the Institute of Marine Sciences of Barcelona (Farran, 2008). The quality of those profiles is variable from ‘fair’ to ‘good’ (Figure 3.5). In some cases, the geographic position of some profiles belonging to those

surveys was deviated from its real/original location. This could be due to two reasons: (1) the error produced during the image to segy conversion process, or (2) the navigation system used to acquire the profiles in the past was less accurate than the global positioning systems (GPS) used today (Table 3.1).

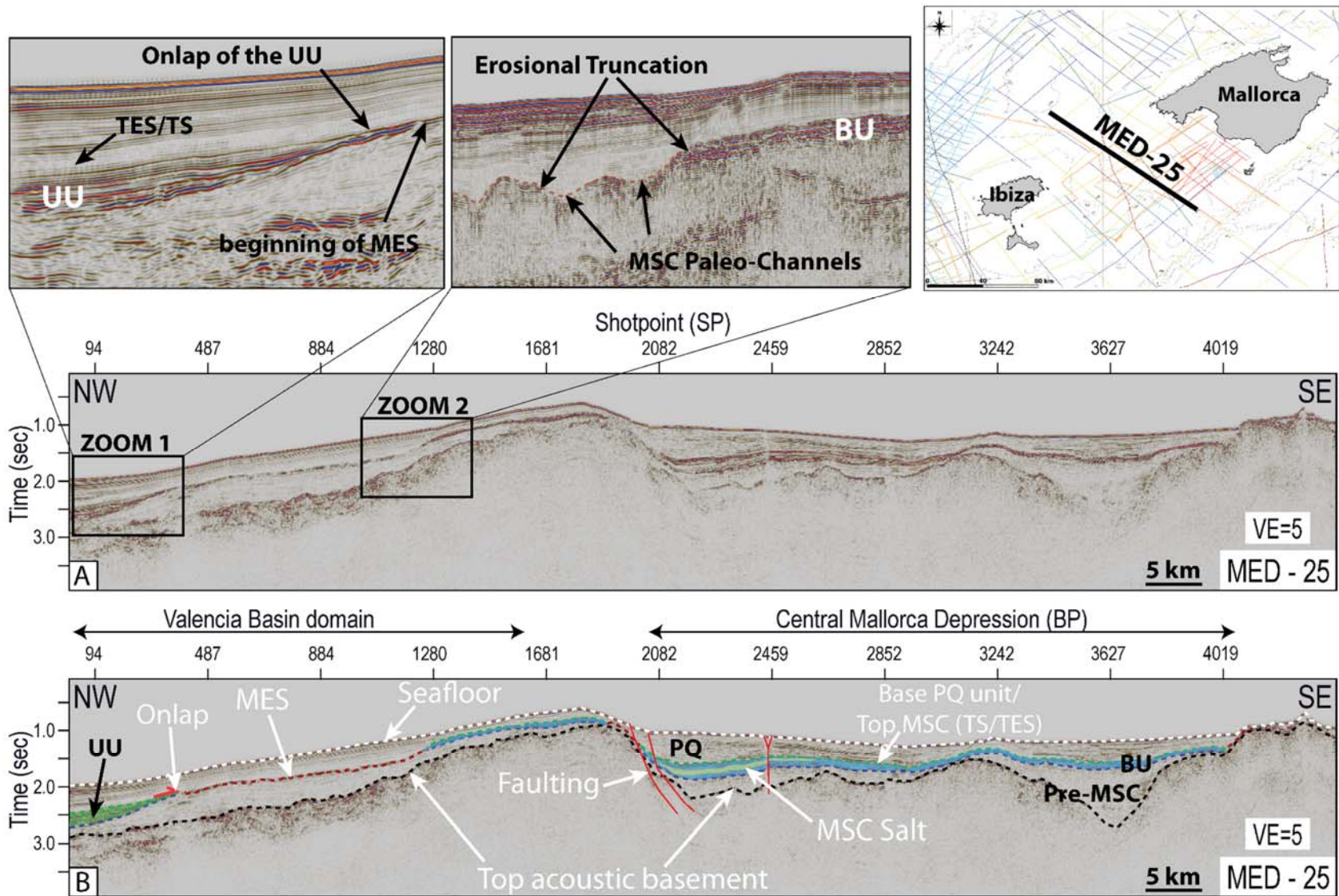


Figure 3.3. (A) Uninterpreted and (B) interpreted seismic profile illustrating the resolution and penetration of the low-resolution MED survey (MED – 25). Main seismic horizons, units and structures encountered in the Balearic Promontory as well as the transition from Valencia Basin to the Balearic Promontory are well imaged.

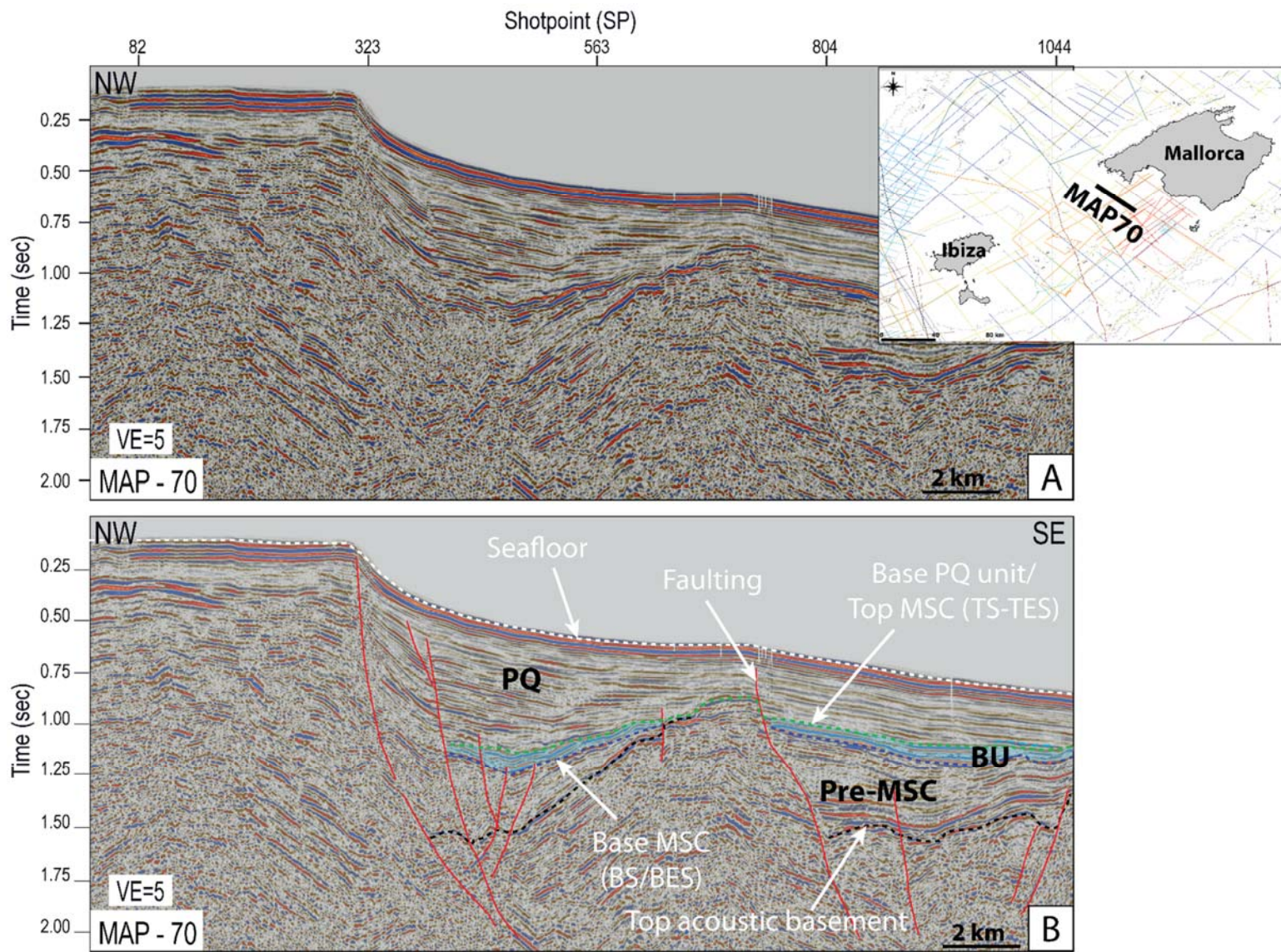


Figure 3.4. (A) Uninterpreted and (B) interpreted seismic profile illustrating the resolution and penetration of the low-resolution MAP survey (MAP – 70). The main seismic horizons and units encountered in the Balearic Promontory are visible. Quality is lower compared to the MED survey.

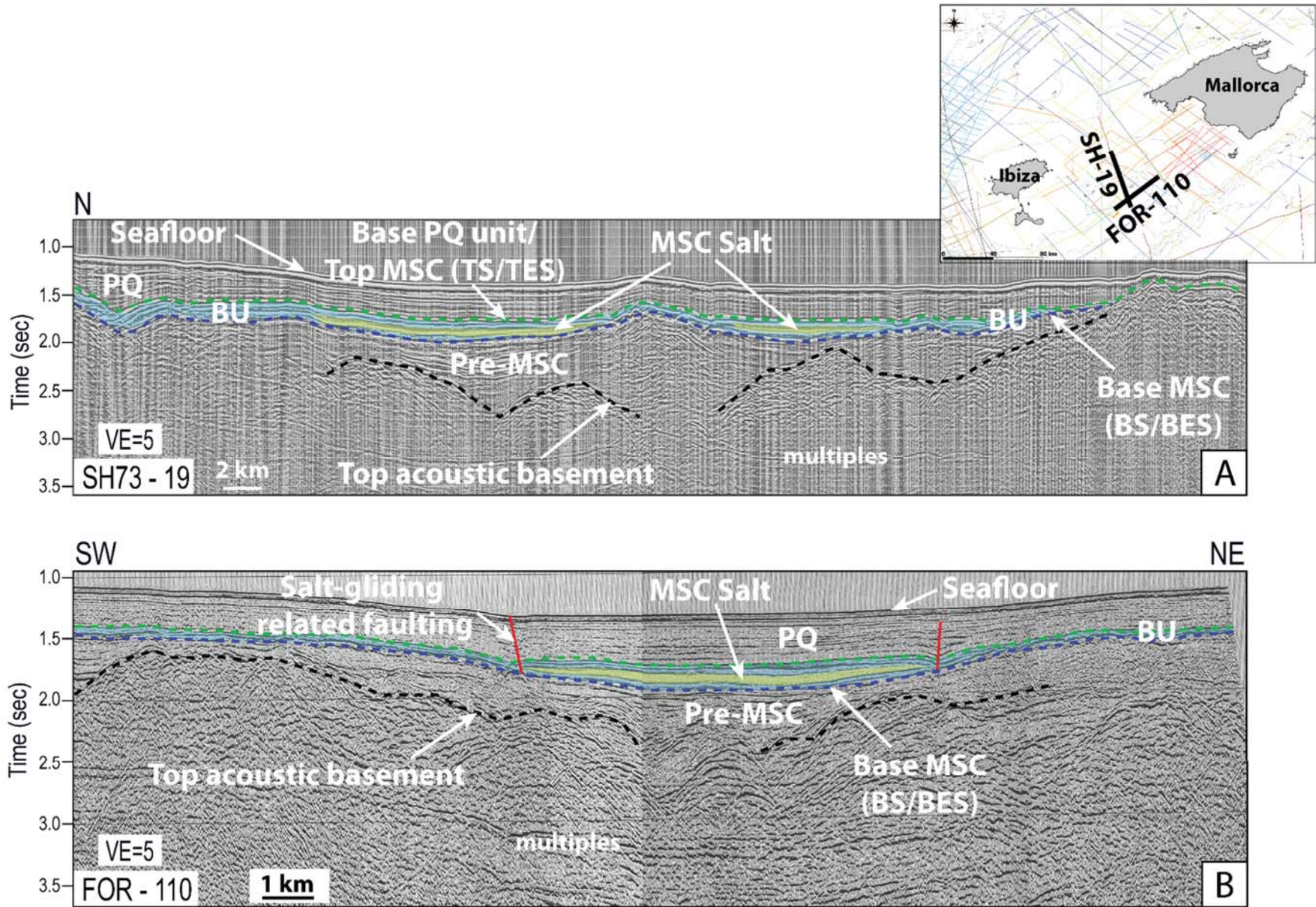


Figure 3.5. Two seismic profiles illustrating the resolution and penetration of the vintage low-resolution (A) SH73 survey (SH73 – 19) and (B) FOR survey (FOR – 110). The main seismic horizons and units encountered in the Balearic Promontory are imaged.

3.1.1.2 Academic seismic profiles

- VALSIS and BAL: these are vintage academic low- to intermediate-resolution multichannel profiles. VALSIS dataset (Mauffret et al., 1992; Pascal et al., 1992; Torné et al., 1992a) is made available online by the French Oceanographic Cruises (www.campagnes.flotteoceanographique.fr) in SEG-Y format. The BAL single-channel survey (Curzi et al., 1985) was available in .TIFF format and then transformed into SEG-Y format by Driussi (2014). The quality of the seismic images of both surveys can be considered ‘fair’.
- SALTFLU: multi-channel intermediate-resolution seismic dataset consisting of ten 2D profiles acquired in 2012 by the OGS Explora within Eurofleets Project SALTFLU. They were made available in the framework of the Saltgiant project by the National Institute of Oceanography and Experimental Geophysics (OGS - Italy) as pre-stack time migrated profiles in SEG-Y format (Blondel et al., 2020). The quality of the seismic images of the profiles is very good, allowing decent recognition and interpretation of seismic facies and geometries of the pre-MSC, MSC and PQ sedimentary units on the Balearic Promontory (Figure 3.6). In the deep Algerian Basin the profiles are highly disturbed by intense salt tectonics and penetration with good imaging is limited to the post-salt (Figure 3.6, SP 9179).
- CARBMED and AMS: those high-resolution multichannel profiles were acquired in the framework of the CARBMED project during RV Meteor cruise M69/1 in 2006 (Hübscher et al., 2010) which was aiming to study the Quaternary carbonates in the Western Mediterranean Sea. They were made available by the University of Hamburg as post-stack time migrated profiles in SEG-Y format. The quality of the seismic image of this dataset is very good as they allow distinguishing and interpreting details of the internal seismic facies and geometries of the MSC and PQ sedimentary units. The profiles of this survey were shifted vertically in time from their original position probably during the seismic processing phase. To fix the problem, they were crossed with several profiles from the different seismic surveys and shifted back to their original vertical position using the seismic interpretation software Petrel.

- SIMBAD: this survey consists of 26 high-resolution multichannel seismic profiles that were acquired on the Balearic Promontory during the “SIMBAD” cruise onboard the R/V “Tethys II” (INSU-CNRS/CIRMED) in 2013 (Maillard & Gaullier, 2013). The profiles are mainly situated in the Central Mallorca Depression and are considered the most valuable profiles for this work as they allow excellent facies and geometry identification of the MSC unit of the BP (Driussi, 2014; Maillard et al., 2015; Driussi et al., 2015; Ochoa et al., 2015). The seismic image of the profiles is very good; however, the main limitations are the locally limited penetration and the presence of multiples on the profiles, which sometimes mask the underlying seismic signal (Figure 3.7).

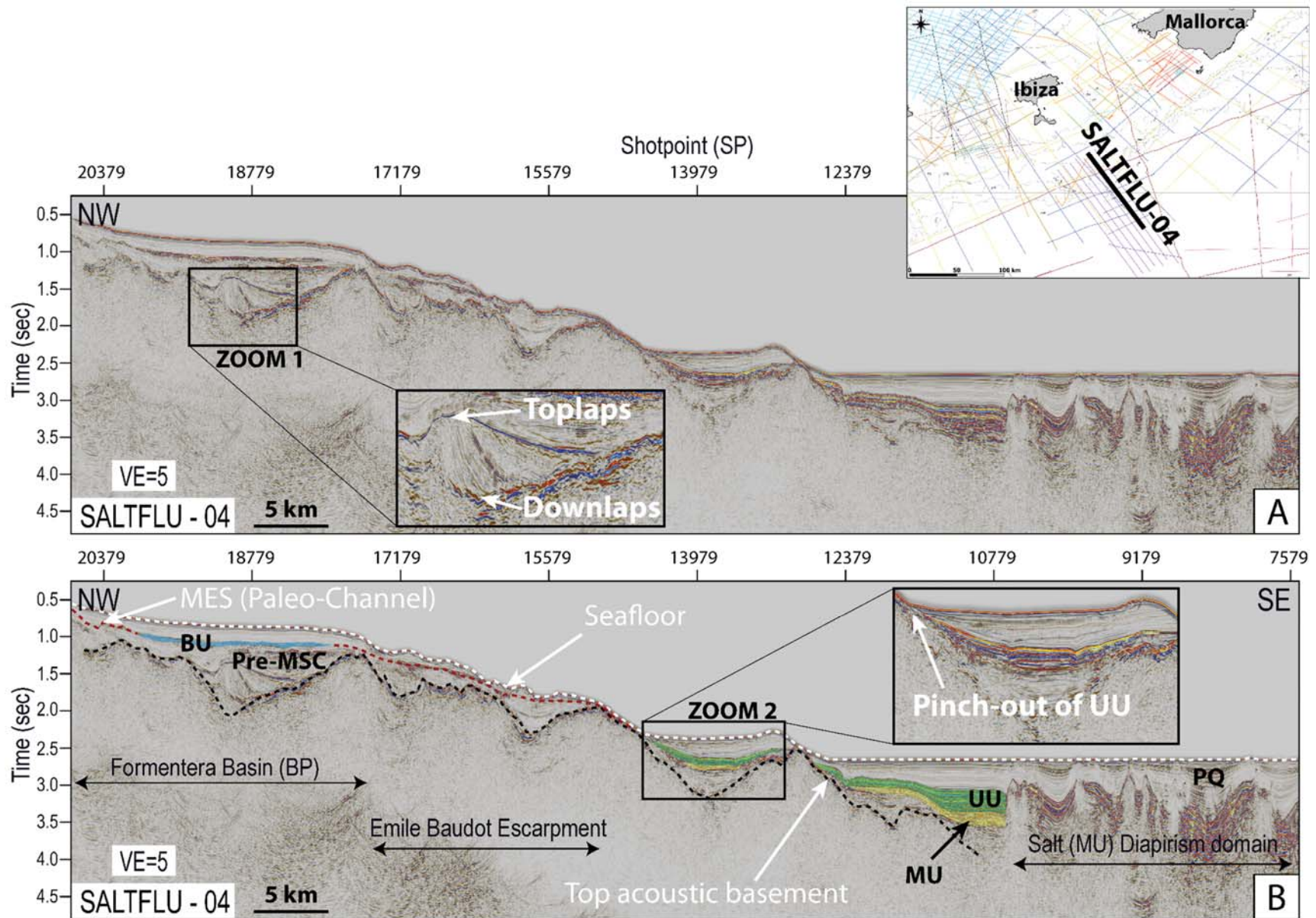


Figure 3.6. (A) Uninterpreted and (B) interpreted seismic profile illustrating the resolution and penetration of the SaltFlu survey (SaltFlu – 04) and showing the transition from the deep Algerian Basin (SE) to the Balearic Promontory (NW).

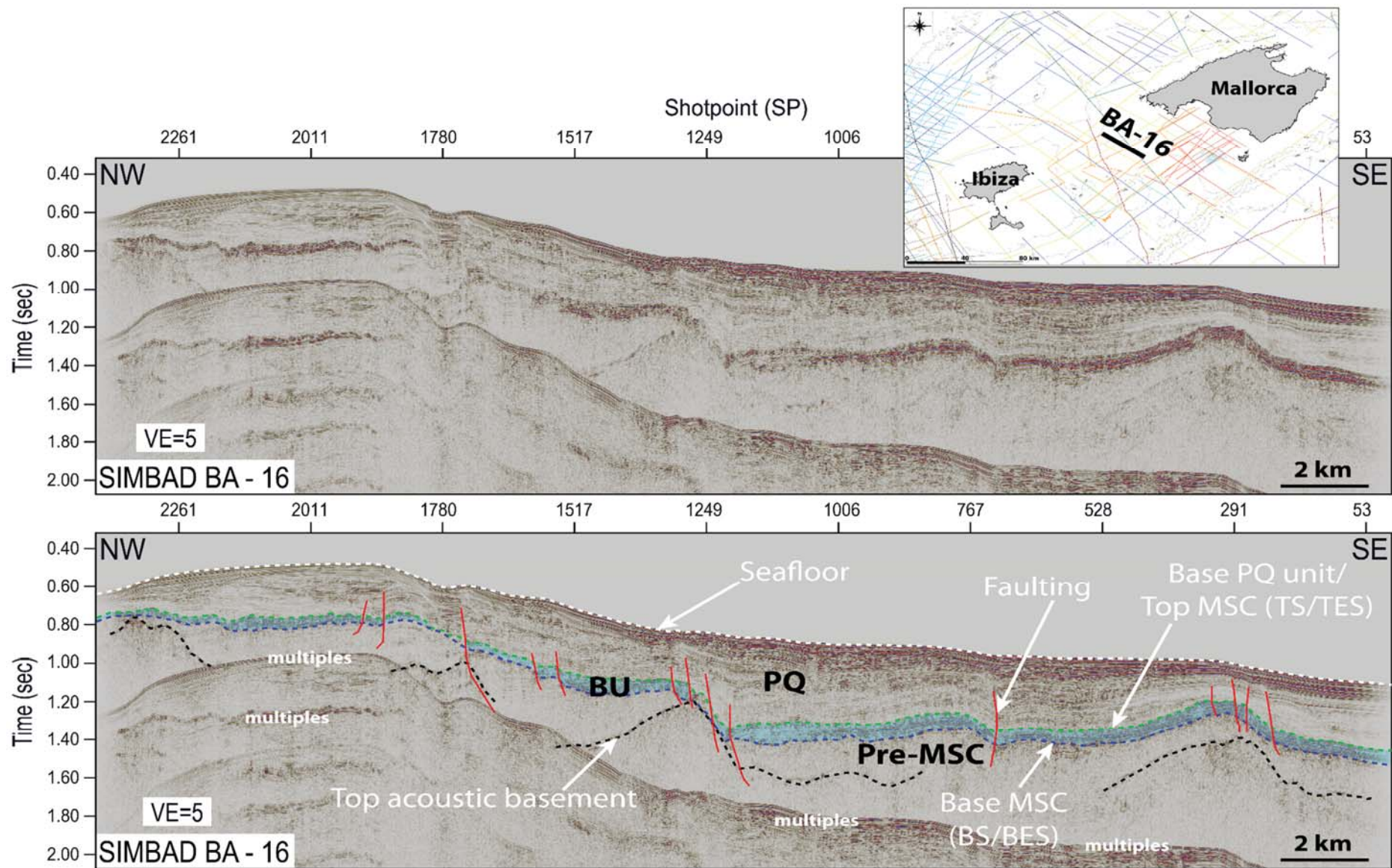


Figure 3.7. (A) Uninterpreted and (B) interpreted seismic profile illustrating the resolution and penetration of the high-resolution SIMBAD survey (BA – 16) and showing the main seismic horizons and units encountered in the Balearic Promontory.

3.1.2 Seismic Data Interpretation

Seismic stratigraphy involves the subdivision of seismic sections into sequences of reflections that are interpreted as the seismic expression of genetically related sedimentary sequences (Kearey et al., 2002). Conventional seismic interpretation consists of mapping geological structures by picking and tracking the reflectors of interest throughout the seismic profiles. Those reflectors are called horizons and are surfaces that separate different lithological units with different petrophysical characteristics. They can be recognized based on their terminations and geometries (Mitchum & Vail, 1977). Horizon picking involves identifying and recording the position of specific reflection events, while tracking implies to follow the same reflector over the seismic profile (Bakker, 2002).

3.1.2.1 Horizon picking and seismic facies analysis

The interpretation of the seismic profiles of the Balearic Promontory was performed using the software Petrel® by Schlumberger®, and the software SMT Kingdom Suite®. The horizon picking was done using a combination of 2D manual picks and automatic 2D tracking, depending on the quality of the seismic profile, the density of the seismic coverage in a specific area and the lateral continuation of certain horizons.

The performed seismic interpretation procedure followed the conventional concept of seismic stratigraphy as introduced by Mitchum & Vail, (1977). This procedure is based on the identification of reflection terminations, erosional truncations, onlaps, downlaps and other configurations that allow the identification and definition of the seismic units and their boundaries (Figure 3.8; e.g. zoom 2 in Figure 3.3). For the description of the internal configuration of the seismic units (seismic facies), the concept used is the one introduced by Roksandić, (1978) (Figure 3.9). Figure 3.10 is a synthesis of the main seismic facies that characterize the most common seismic units encountered on the seismic data in the BP. The seismic facies of the seismic units of the BP will be described and discussed in more details in chapter 4 section 4.4 and chapter section 5.4.1.

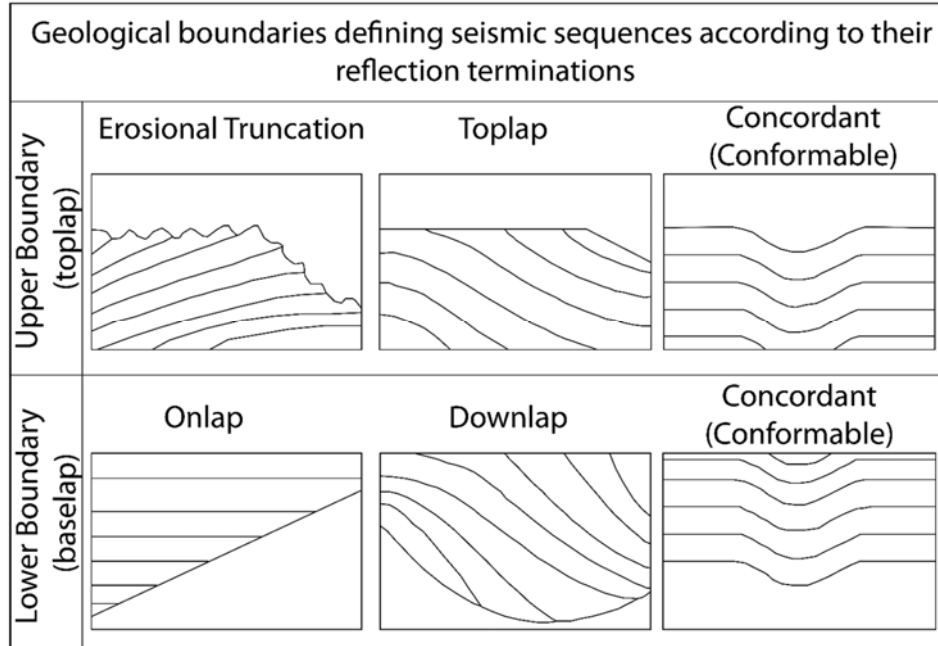


Figure 3.8. Different types of geological boundaries defining seismic sequences according to reflections terminations (modified from Mitchum & Vail, 1977).

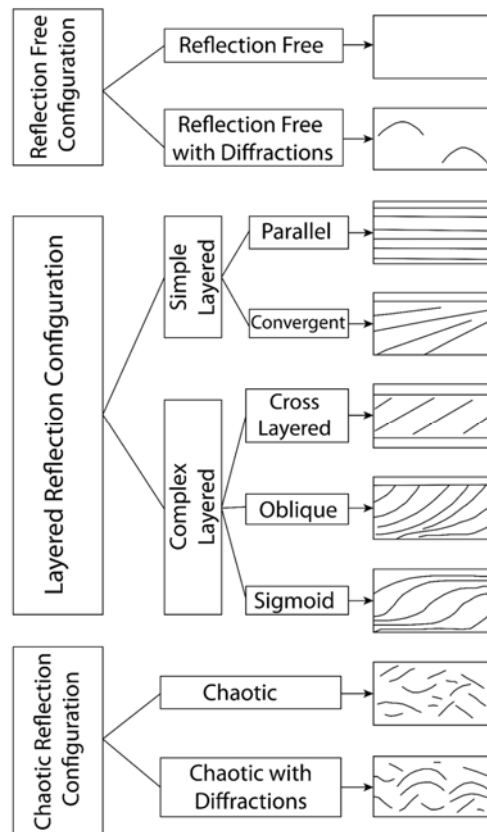


Figure 3.9. Different internal bedforms that typifies different seismic facies within sedimentary sequences identified on seismic reflection images and classification of internal reflection patterns of seismic data (modified from Roksandić, 1978).

Some of the main horizons interpreted and mapped in the BP are considered regional seismic stratigraphic markers throughout the whole Western Mediterranean basin (see also Annex B and Annex C of the thesis). Those are in brief:

- The seafloor, which is a very high amplitude reflection that marks the boundary between the water column and the first seabed sediments (e.g., Figure 3.6-A). It is usually characterized by positive polarity on conventional seismic data (SEG normal polarity).
- The base of the Pliocene-Quaternary (PQ) unit, which often marks the Miocene-Pliocene boundary (5.33 Ma; Van Couvering et al., 2000). It is characterized everywhere in the Western Mediterranean by a high amplitude and positive polarity strong reflection, underlying a reflection-free (transparent) seismic unit (e.g., Figure 3.3-B; PQ unit; sensu Lofi et al., 2011a). This horizon was also known as the M reflector (Ryan, 1978), and used to be considered a regional unconformity belonging to the MSC throughout the Mediterranean area.
- The base of the MSC, which marks the beginning of the first deposits belonging to the MSC. On the BP, it is easily distinguishable due to the high amplitude contrast between the MSC unit, where present, and the underlying pre-MS unit (Figure 3.10). It was also known as the N reflector (Ryan, 1978), and used to be considered a regional unconformity marking the onset of the MSC throughout the Mediterranean area.
- The top of the acoustic basement, which coincides with the deepest continuous but irregular, high amplitude and positive polarity reflection in the sedimentary column (Figure 3.6 and Figure 3.7).

A compilation and mapping of the above-mentioned horizons have been done for the whole Western Mediterranean region combining the dataset shown in Figure 3.1 with other dataset in collaboration with colleagues from the University of Brest and the University of Lille. The work was done in the framework of two separate collaborations. The results of both compilations are presented in Annex B and Annex C, respectively.

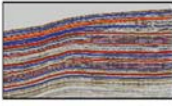

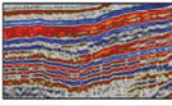
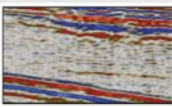
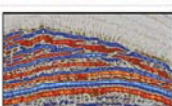


	Seismic Unit	Age	Thickness (TWTT)	Seismic Facies	Facies description
Pliocene - Quaternary	Upper PQ	5.33-0 Ma	200-300ms		- High amplitude, parallel to convergent, continuous reflections)
	Lower PQ		150-300ms		- Very low amplitude parallel reflections (transparent PQ sensu Lofi et al., 2011)
Messinian Salinity Crisis	distal BU	5.97-5.33 Ma	30-60ms		- up to 7 high-amplitude, low frequency reflections - Reflections are parallel with conformable upper boundary
	Salt		50-100ms		- reflection free - local low-frequency internal parallel reflections
	Proximal BU		30-60ms		- up to 9 high-amplitude, high frequency reflections - Reflections are parallel with erosional truncation on their top
	Pre-MSC	***	100-700ms		- mostly reflection free - local low-amplitude convergent reflections
	Acoustic Basement	***	---		- Top: Very high amplitude, low frequency reflection - Internal facies: Chaotic with diffractions

Figure 3.10. General facies description of the main seismic units encountered in the seismic stratigraphic sequence of the Balearic Promontory. *** The ages of the pre-MSC unit and the acoustic basement are unknown in most of the study area due to the lack of offshore boreholes.

Surface mapping and time-depth conversion

Creation of time maps

- The picked horizons were interpolated with the aim of creating time horizon maps (in TWTT). This step was also done using the seismic interpretation software Petrel® that offers a very user-friendly interface with sophisticated interpolation algorithms and visualizing options for the resulting maps. The gridding method used for the creation of the time structural maps is the Convergent Interpolation algorithm which is a fast algorithm

that builds the model in stages by iterating or ‘converging’ from an initial to a final solution (Figure 3.11). It is considered a control point orientated algorithm, which converges upon the solution iteratively adding more resolution with each gridding iteration. Each iteration of Convergent interpolation is broken into three separate, sequential steps:

- Refine - Change grid resolution.
- Snap – Grid (or re-grid) the data.
- Smooth – Minimize grid curvature using a constrained operator.

The final model is always refined to the desired grid interval. The grid interval chosen in this work varies from one zone to another in the study area in function of the density of the seismic profiles coverage and in function of the finality of the use of the interpolated map. On the Balearic Promontory, a gridding interval of 2x2 km is chosen most of the times seen the overall good density of seismic coverage.

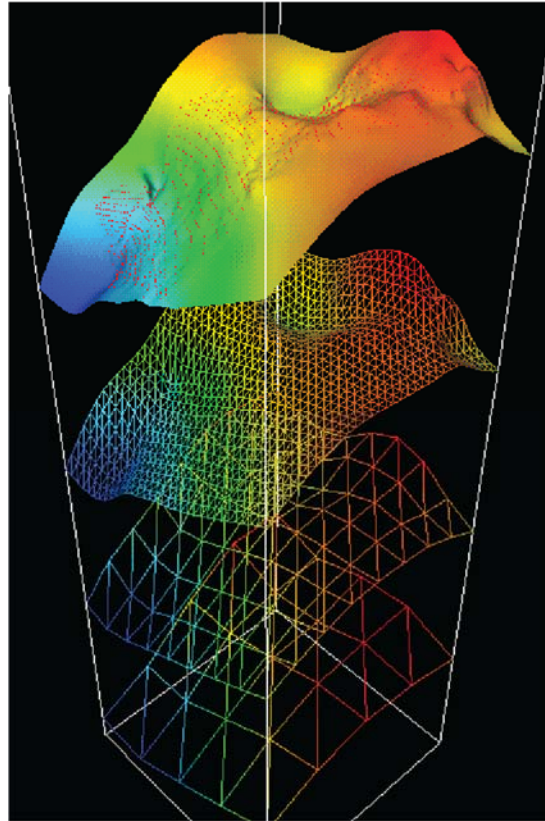


Figure 3.11. Graphic illustration of the convergent interpolation gridding algorithm (Petrel®). The top surface is the final solution and shows input data as red dots. The bottom surface is the initial iteration, which is fitted to the data points. Four iterations were performed to build this model, each at a different grid interval. The interval of each iteration is shown as the grid lattice graphic for all but the last (final) iteration. Starting with an initial coarse grid, a factor resolution change is applied between iterations. Between the last and next to last iterations, an exact factor is applied to achieve the final grid resolution.

A quality check was done after the creation of each interpolated surface, especially in areas that are complex from a structural point of views (e.g. faulted areas). The quality check is a part of a workflow (Figure 3.12) that is repeated several times in order to obtain a surface as realistic as possible and that fits well the structures imaged in the seismic profiles.

Where possible, the obtained maps were compared, for a final quality check, with published maps (e.g. Leroux et al., 2019).

The creation of the time maps allowed also the calculation of thickness maps of the seismic units (Figure 3.13), by simply subtracting two consecutive surfaces. This was followed by the time to

depth conversion (see next section 3.1.2.2.2) and volume estimation of some of the sedimentary seismic units.

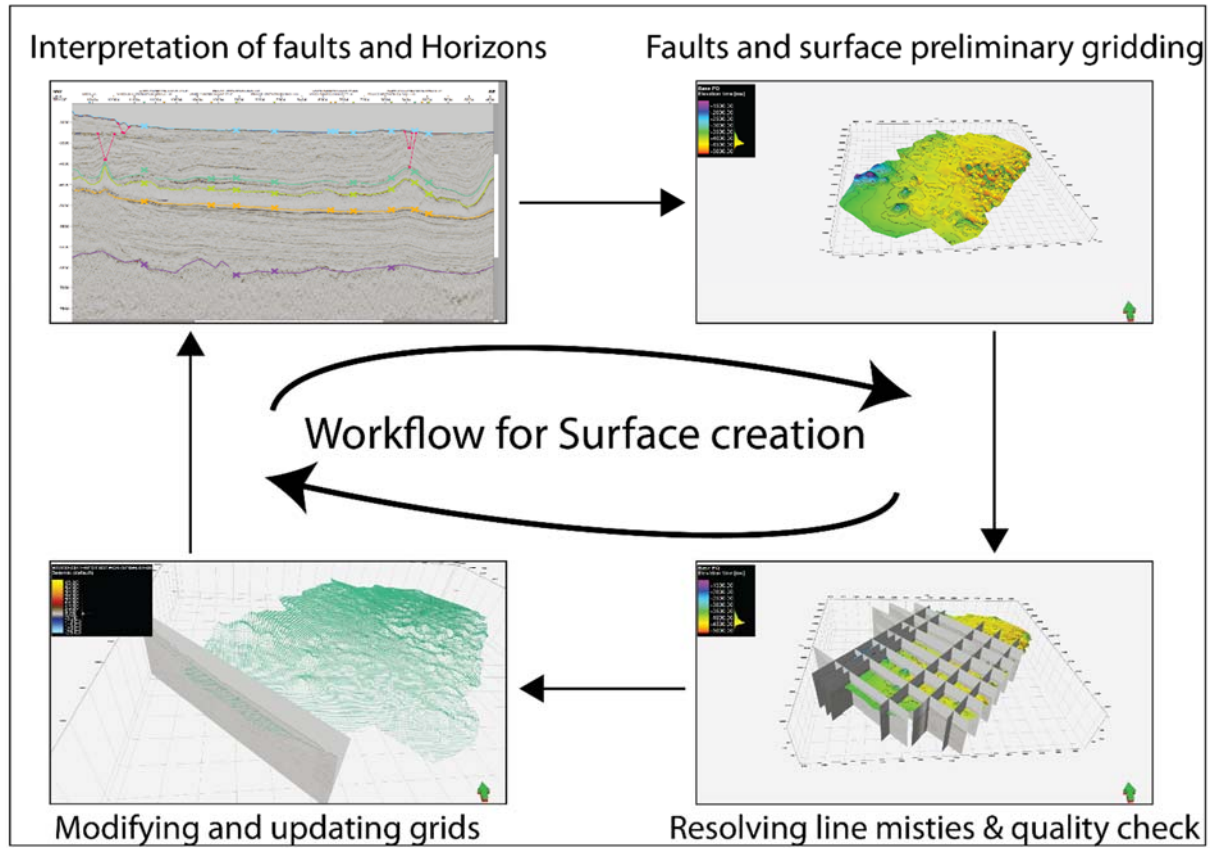


Figure 3.12. The workflow for the creation of the time structural maps of the interpolated seismic horizons.

3.1.2.2.2 Time to depth conversion

Time to depth conversion of horizons and/or grids is a delicate operation because seismic velocities of sedimentary units are not uniform in depth and space. A good depth conversion can be done with proper seismic data processing, which can only be done on single profiles starting from the raw seismic data. This has not been possible in this study as all the seismic surveys were provided as TWTT profiles (see section 3.1.1). Moreover, neither velocity analysis/profiles nor relevant borehole data were available in the study area. Consequently, time-depth conversions were performed using average velocities and/or empirical velocity functions for the different seismic units. This method consists in multiplying the isopach map in TWTT of each seismic unit with its mean (estimated) internal seismic velocity in order to have the isopach in meters. The isobath map in meters of each horizon/surface is obtained by adding the isopach map(s) of the overlying seismic units.

For each seismic unit, average internal velocities are estimated based on the internal lithologies, age and amount of compaction, which at some point have to be assumed. Moreover, the velocities used in this work depend on the local seismic stratigraphy of the single basins of the Western Mediterranean. Table 3.2 is a compilation of the average velocities used for the time-depth conversion in this study. The choice of those seismic velocities will be discussed and justified in each chapter where they are used.

Seismic Unit	Deep Western Mediterranean Basins					Balearic Promontory				
	Water Column	PQ unit	UU	MU	Pre-halite unit	Water Column	PQ unit	BU(s)	Halite unit	Pre-MSC unit
Average Velocity (m/s)	1500	2290 ^a ; or depth [m] = 1135.1 × TWTT[s]1.343 ^b	3100	4800	2440	1500	2290 ^a ; or depth [m] = 1135.1 × TWTT[s]1.343 ^b	3500 or 4500	4800	2440
Reference	Pascal et al., 1992	^a Lanaja, 1987 ^b Urgeles et al., 2011	Dal Cin et al., 2015	Samperi et al., 2020	Ochoa et al., 2015	Pascal et al., 1992	^a Lanaja, 1987 ^b Urgeles et al., 2011	**	Samperi et al., 2020	Ochoa et al., 2015

Table 3.2. Seismic velocities used for the time-depth conversion. ** The velocities used for the BU(s) of the Balearic Promontory are discussed and justified in chapter 7 section 7.3.1.

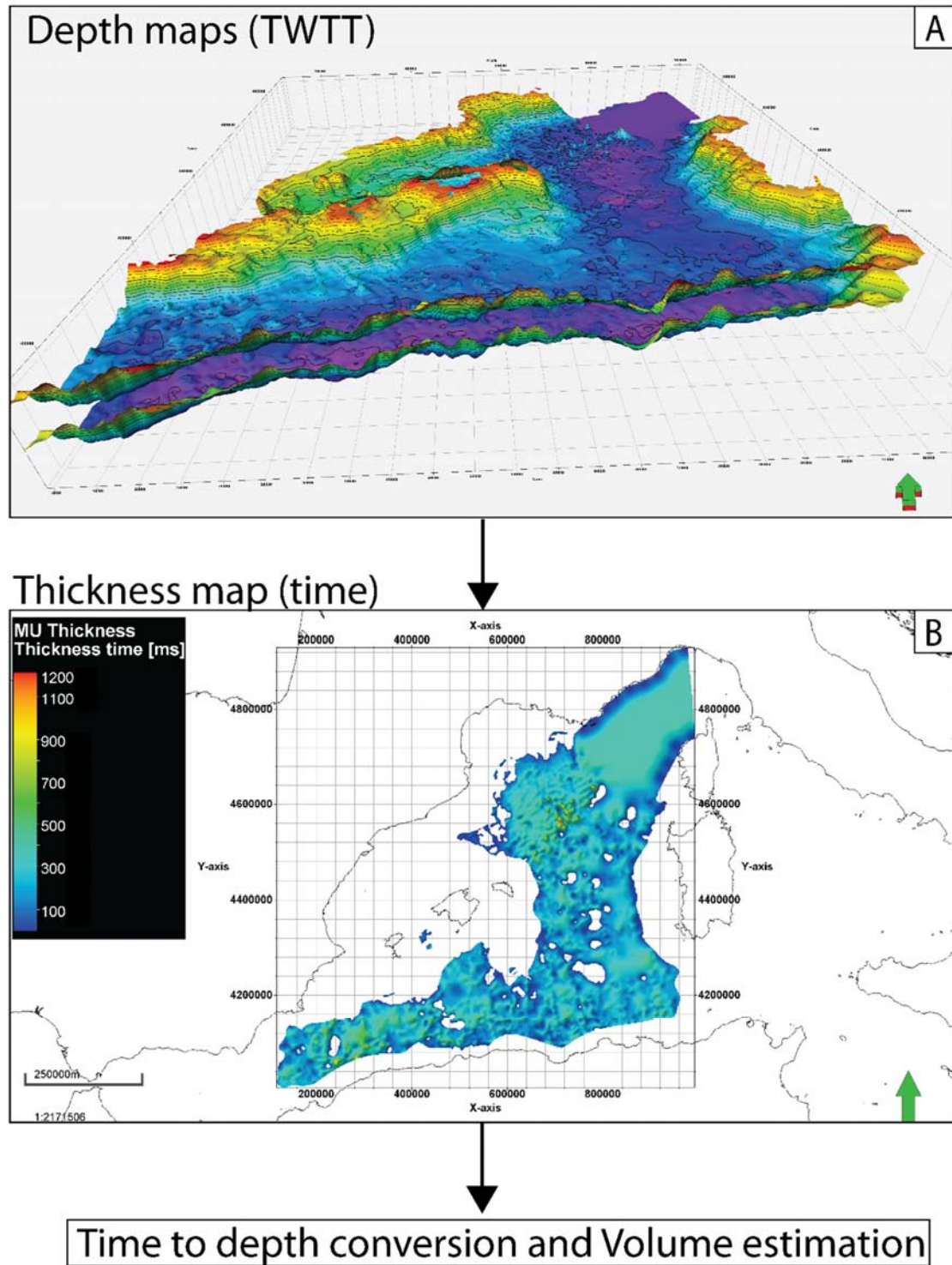


Figure 3.13. Workflow for the creation of the thickness maps and volume calculation of the studied seismic units. In this example, the thickness of the Mobile Unit in the Western Mediterranean is shown. In (A), upper horizon: the time maps of the top salt (top MU) + MES (where MU is not present) horizons and lower horizon: base salt + MES (where MU is not present) horizons. In (B), the isopach map (in msec twtt) of the MU. The resulting thickness maps in meters of the units are shown in Figure 3.21.

3.2 Backstripping analysis

Correcting the stratigraphic record for the vertical motions caused by water and sediment loading and compaction, allows identifying the form of the tectonic driving forces and the thermal subsidence components that affect a sedimentary basin. This is done by applying the backstripping technique (named backstripping because it is based on the removal of loads) developed by Watts & Ryan, (1976). By restoring the original sediment thickness of a layer at the time of its deposition, taking into account post-deposition compaction and water level changes, and then isostatically unloading it, it is possible to determine the depth at which the basement would be in the absence of water and sediment loading. The goal of the backstripping analysis applied in this thesis is to obtain an approximate idea about the paleo-bathymetry of the Balearic Promontory sub-basins at the beginning, during, and at the end of the MSC.

3.2.1 Isostasy, flexure and effective elastic thickness

A quick review of the concept of isostasy is needed before introducing the backstripping technique and its application in the framework of this dissertation.

Isostasy is a fundamental concept in earth sciences, describing the equilibrium state the crust and mantle tend to in the absence of disturbing forces, with the lighter crust floating on the denser mantle. This equilibrium state is disturbed by geological processes changing surface loads, such as mountain building, erosion and surface transport, volcanism and even the waxing and waning of ice sheets. The concept of isostasy was developed over the course of the 19th and 20th centuries, leading to the development of theories of isostasy based on two fundamentally different ways in which such disturbances are compensated.

The Pratt-Hayford model assumes that topographic features are underlain by regions of different density, so that the pressure at a certain compensation depth is equal for different regions (Figure 3.14) (Hayford, 1909). This implies that the density of oceanic crust (underlying topographic basins and thus consisting of a column of smaller thickness) is higher than that at sea level, while the positive topography of mountain ranges is underlain by crust of lower density (Watts, 2001). While this model was very effective at explaining geodetic observations in the United States, it assumes a base crust at a constant depth, and does not offer

a mechanistic explanation for how a disturbance of isostasy can be restored. The topography is driven by the density of the crust, but the density of the crust cannot adjust to restore isostatic equilibrium after a change to surface loading by erosion or sedimentation.

The Airy-Heiskanen model assumes that mountains and ocean basins are underlain by crusts with uniform density, where isostasy is reached by the formation of a crustal “root” under a mountain range where the lower density crust compensates for the excess mass of the mountain range. Inversely, a thinned crust or “anti-root” associated with higher density mantle compensates for mass deficiency at, for example, sedimentary basins (Figure 3.15). In this model, changes in the surface load are compensated by sinking of the crust into the mantle (subsidence) or a rise of the crust-mantle boundary (uplift) to restore isostatic equilibrium.

The Airy-Heiskanen model offers a useful first-order approach towards understanding the response of the crust to surface load changes due to its buoyancy relative to the underlying viscous mantle. It is controlled by the density contrast between the crust, mantle, the load being added or removed and the environment (air or water).

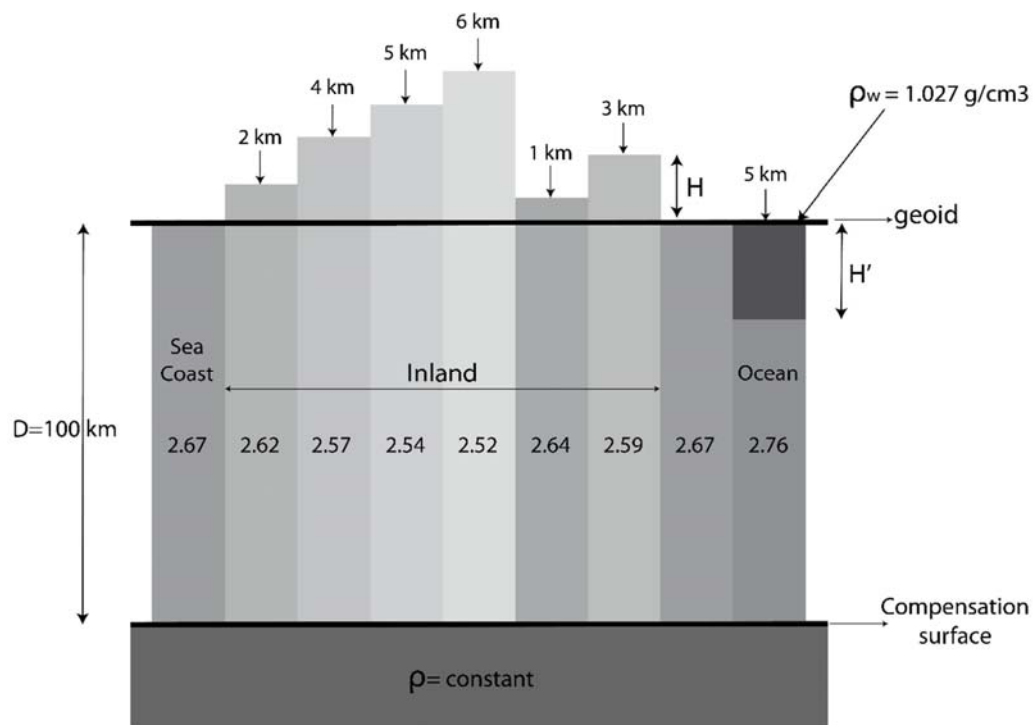


Figure 3.14. Pratt-Hayford isostatic compensation model. Modified from Sansò & Sideris (2013).

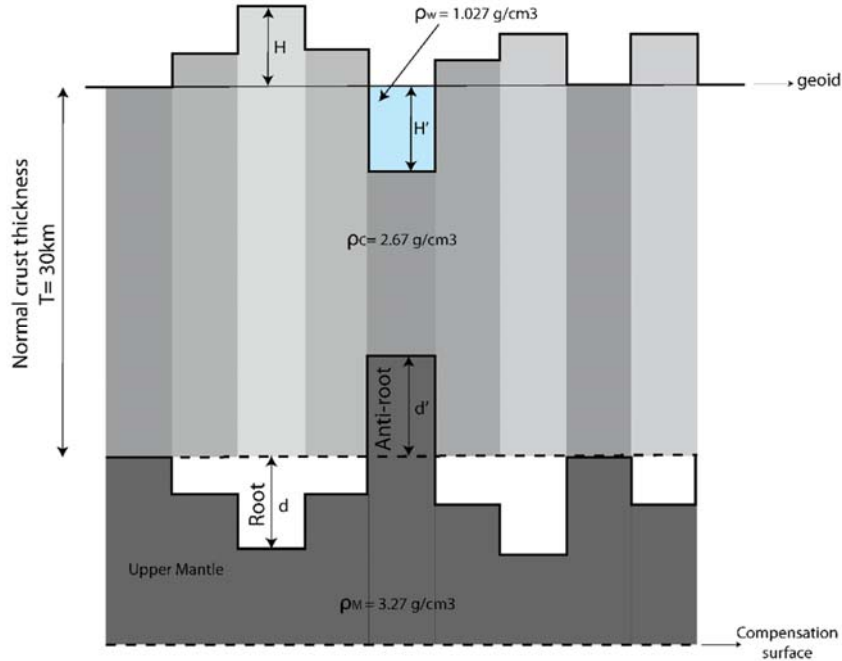


Figure 3.15. Airy-Heiskanen isostatic compensation model. Modified from Sanso & Sideris, 2013. P is density, H is height and d is depth.

Isostasy assumes that any surface load is completely compensated by displacement of mantle material to reach a situation of equilibrium. In reality, the crust has a load-bearing capacity, which will (partially) support surface loads on geological timescales. The capacity of the crust to support loads is related to its thickness, age, rheology, thermal structure and preexisting weaknesses. This complex set of parameters is captured in the “Effective Elastic Thickness” (EET), which equals the thickness of a purely elastic plate representing the earth’s crust. Thus, EET controls the magnitude of vertical motions as a response to tectonic and sedimentary loads (Burov & Diament, 1992; Watts, 2001), and is a crucial input parameter for flexural-isostatic modelling.

In this study, flexural-isostatic modelling was performed for the Western Mediterranean area. EET was estimated from the Yield Strength Envelopes of the lithosphere obtained from thermal and structural information (see chapter 6, section 6.4.2 for more details). This resulted in a wide choice of EET ranging from 10 to 45 km in the offshore domain. However, in general, low EET values are estimated for the Western Mediterranean (<20km) (Tesauro et al., 2009a; Kaban et al., 2018a). For the modelling applied in this work we therefore used the value of

EET = 15 km, also used by [Urgeles et al. \(2011\)](#) for 1D backstripping close to the Ebro Delta offshore Spain.

3.2.2 Backstripping in the Balearic Promontory (Western Mediterranean)

Since the deposition of the MSC evaporites, the BP has evolved undergoing vertical motions caused by different drivers. The vertical movements affecting the base level in the BP and surrounding basins since the MSC are:

- subsidence/uplift due to sedimentation (load)/erosion respectively
- subsidence due to sediment compaction
- subsidence/uplift caused by water level variations due to eustatic changes and/or sea-level drawdown during the MSC
- subsidence due to thermal cooling
- tectonic subsidence/uplift due to vertical movements along faults

Figure 3.16 is a synthetic visual presentation of the post-MSC vertical movements across a profile crossing the CMD (BP) and showing the positive and/or negative vertical movements caused by each of the above-mentioned components. The only vertical component that will not be taken into account in the modelling calculations is the thermal subsidence due to thermal cooling, because the used numerical models does not have an implemented tool for such calculations (which would require specific data at the same resolution of the seismic dataset). However, the thermal subsidence component will be considered attentively in the discussion after the calculation of the 3D backstripping (chapter 6 section 6.4.1). For the Balearic Promontory area, which is considered a thick continental crust domain (Figure 3.16; see also [Driussi et al., 2015](#) and references therein), this component can be considered negligible.

Backstripping can be applied in 1D (e.g. along a borehole log), 2D (e.g. along a seismic profile) and in 3D (e.g. along grids of sedimentary unit surfaces). Both 2D (section 3.2.2.1) and 3D backstripping (section 3.2.2.2) analysis were applied in this work to obtain the paleobathymetry at the beginning of the MSC in the BP. The applied analysis is the flexural backstripping, in which the sediment thickness data are used to determine the subsidence along a 2D profile and/or isopach maps of the basin.

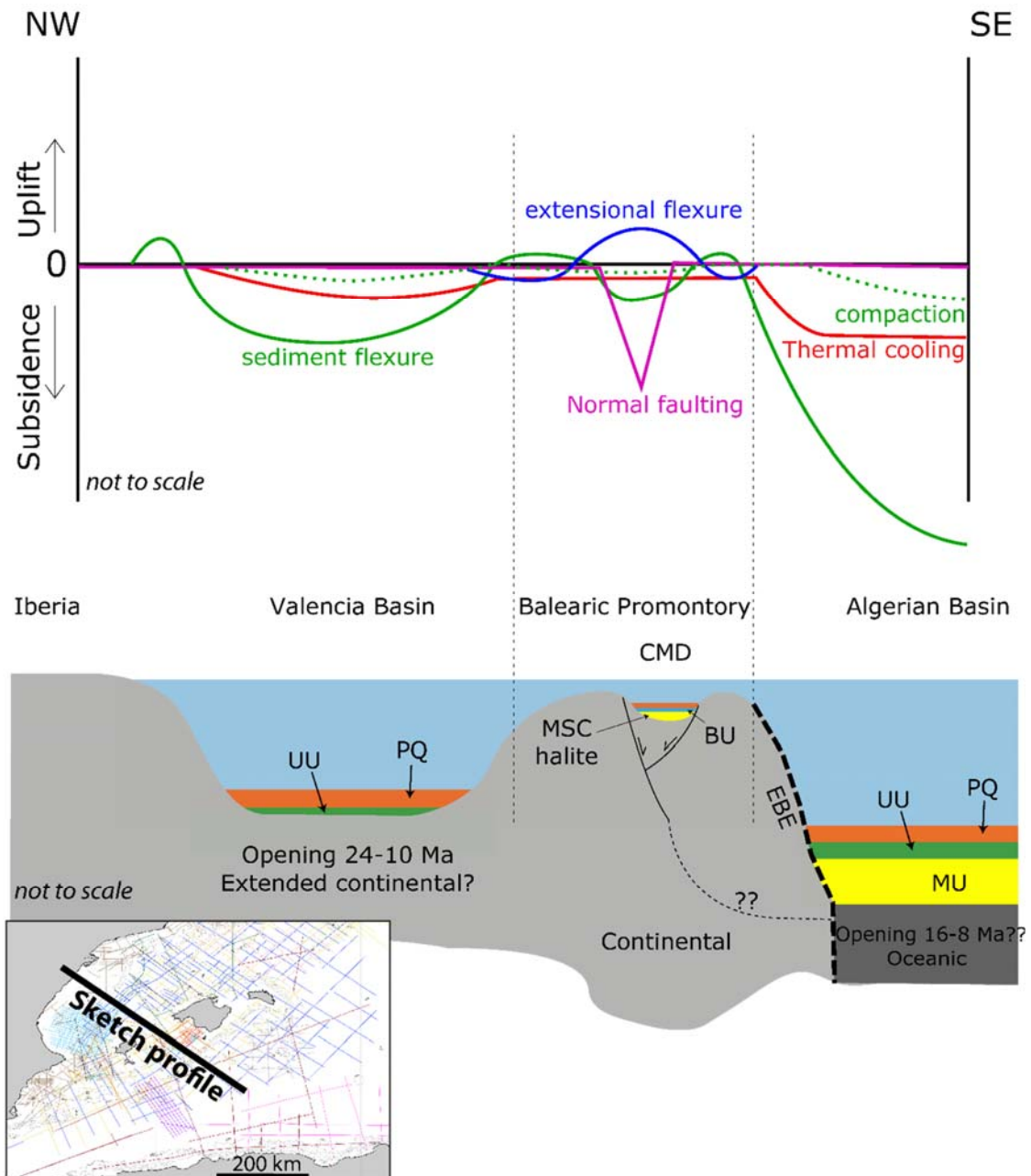


Figure 3.16. Top: synthetic sketch illustrating the positive (uplift) and negative (subsidence) vertical movements that acted on the Balearic Promontory area and its surrounding basins since the formation of the MSC evaporites. Bottom: sketch along a 2D section across the basin. The main vertical components to be considered in the CMD (BP) area are mainly: the syn- and post-MSC normal faulting together with the deflection caused by the load movement during this faulting; the flexure caused by sedimentation and compaction. EBE= Emile Baudot Escarpment.

3.2.2.1 2D Restoration and Backstripping

In this method, sediment thickness data as seen on a seismic reflection profile are used to determine the subsidence along the profile. This technique requires information on the spatial variations that occur in the sediments distribution (age, composition, thickness) and in the strength of the underlying lithosphere.

The 2D seismic profile used for the 2D restoration is the 192km-long profile MED25 (Figure 3.3). The choice of backstripping this particular profile is that it crosses some critical zones that are important for the paleo-bathymetry interpretation. Those zones are:

- the onlap of the UU of the VB on the BP slope to the north (zoom 1 in Figure 3.3)
- the sill separating the VB from the CMD.
- the salt unit of the CMD (Figure 3.3, SPs 2082-2500).

Another reason of the importance of the MED25 choice is that it is crossing perpendicularly the main tectonic feature (set of faults) that have been active during the post-MSD period (Figure 3.3, SP 2080), which allows the restoration of the movements along those features. Calculating and restoring the movements on those faults allows by their turn to calculate the isostatic response (subsidence and uplift) caused by the mass movements along those faults.

Therefore, five steps were followed for a complete backstripping of the MED25 profile (Figure 3.17):

Step 1- Interpretation of the horizons, units and faults on the profile;

Step 2- 2D time-depth conversion of the horizons;

Step 3- 2D simple shear post-MSD move on fault restoration (kinematic restoration) including the decompaction of the post-MSD sediments;

Step 4- 2D forward modelling of the mass movement along the faults (isostatic deflection);

Step 5- Addition of the vertical movements caused by sedimentation (isostatic response) and decompaction of pre-MSD sediments.

Steps 1 and 2 have been already described in section 3.1.2. Steps 3 and 4 will be described hereafter (sections 3.2.2.1.1 and 3.2.2.1.2, respectively). The final step (step 5) is derived from the 3D

backstripping result that will be introduced in the next section 3.2.2.2. The overall result of the 2D restoration and backstripping will be presented and discussed in Appendix 6-C of the thesis.

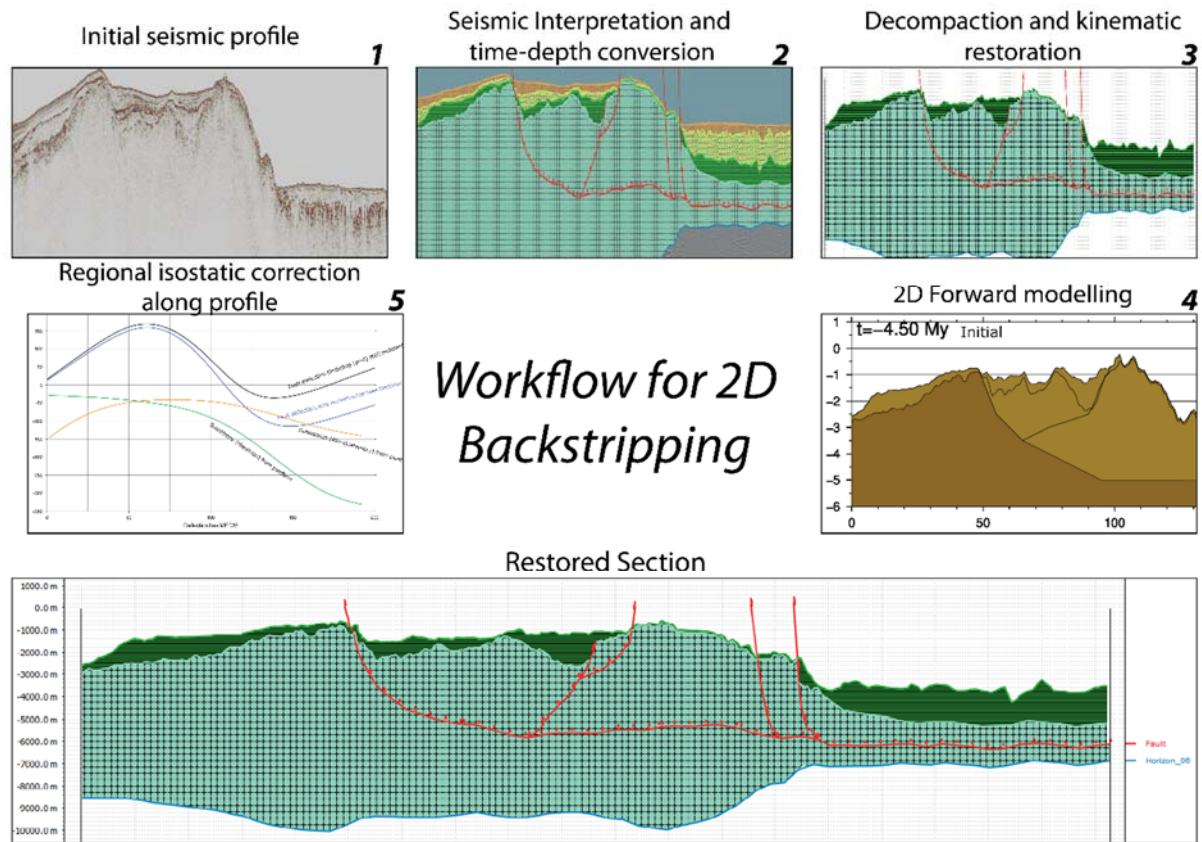


Figure 3.17. Workflow for the 2D backstripping technique followed to restore the Paleo-bathymetry at the beginning of the MSC along the MED25 profile. See text in section 3.2.2.1 for details about each step.

Simple shear structural restoration (2D kinematic modelling) – step 3

The kinematic structural restoration of the post-MSC movements on the fault was performed using the software MOVE® by Midland Valley®.

Prior to the move-on-fault operation, the post-MSC (PQ unit) was de-compacted after the removal of the overlying water column. For the MSC units along the profile, no decompaction was made as those are assumed to be made mainly of evaporites, which's porosity is considered negligible (Samperi et al., 2020 and references therein).

The used decompaction curve is the one proposed by Slater & Christie, (1980) which assumes an

exponential porosity decrease with depth (Equation 3.1).

$$\Phi = \Phi_0(e^{-cy})$$

(Equation 3.1)

Where Φ is the porosity at depth; Φ_0 is the initial porosity at surface; c is the porosity-depth coefficient; and y is the depth in meters. According to those authors the values for shale are $\Phi_0 = 0.67$, $c = 0.00051$, and for sand $\Phi_0 = 0.49$, $c = 0.00027$ (Sclater & Christie, 1980). The decompaction of the PQ unit is done adapting the shale curve, as the seismic profile is passes through the deep depocenter of the CMD (Figure 3.3) and probably shale is the dominant composition.

Following the decompaction of the PQ unit, the kinematic restoration was performed. The used algorithm is the Simple Shear Algorithm, which models geometrically the relationship between the geometries of the faults and the deformation of the hanging wall, thus restoring the sedimentary units to their initial geometric state at the time of deposition. In the simple shear algorithm, the deformation of the hanging wall is modelled by moving each point in the hanging wall by the same horizontal distance, following a path parallel to the fault. Each point on the hanging wall surface can be considered to fall along a pin that does not change its length as it is moved over the fault (Figure 3.18).

This algorithm is most applicable in extensional regimes (Fossen, 2016), which justifies its applicability for the post-MSC restoration along the used profile MED25 in the CMD zone (see chapters 2 and 5 for details about the post-MSC tectonic regime in this area). Extension creates a hypothetical void or gap between the hanging wall and footwall blocks. The area of extension equals the area of the void (Figure 3.18 A-B). The shear vector controls how hanging wall elements collapse down onto the fault plane, removing the void space (Figure 3.18-C).

Deflection due to mass movement along faults – step 4

Another vertical movement that needs to be corrected for a proper paleo-bathymetry estimation is the isostatic deflection component due to the mass movement along faults (Figure 3.16). In an

extensional regime, the fact that mass is removed from the fault zone and pushed to an adjacent zone would cause uplift in the fault zone and subsidence in the adjacent zone (Figure 3.19).

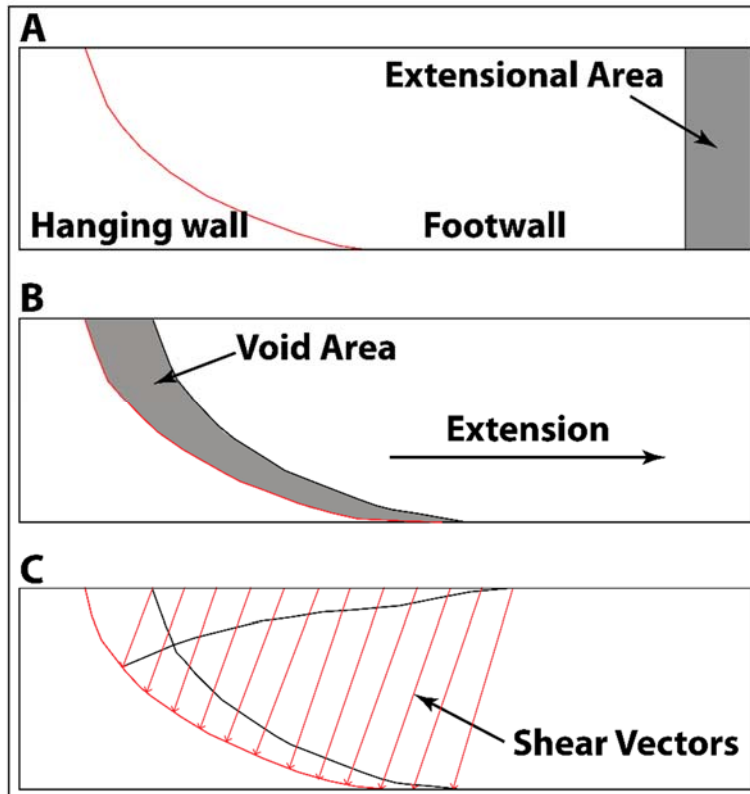


Figure 3.18. Sketch showing extensional faulting and the control of shear vectors on hanging wall collapse. In this example, shear is orientated antithetic to the fault plane.

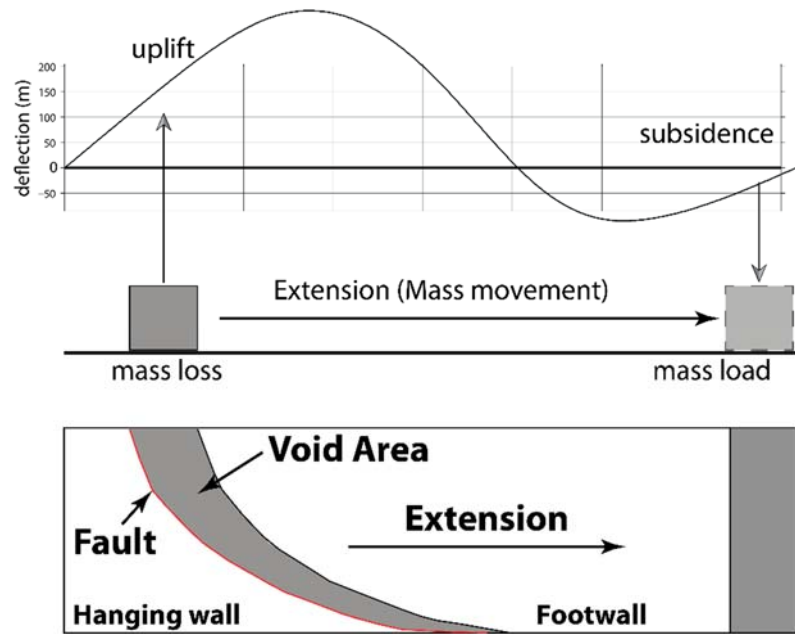


Figure 3.19. Schematic illustration of the isostatic deflection in an extensional regime. The mass movement/loss along the fault would cause uplift in the fault zone, whereas in the adjacent zone (load mass) subsidence would dominate. The uplift/subsidence values shown in the upper panel are only a demonstration and do not apply as values obtained along the profile MED25.

The deflection calculation along the profile is done by 2D forward modelling using the software tAo developed by [García-Castellanos et al. \(1997\)](#) to model the evolution and processes in foreland basins. tAo is a 2D (cross-section) numerical model that calculates 1D lithospheric flexure for different rheologies, in combination with fault kinematics, other isostatic loads, and erosion/deposition (available as an open source <https://sites.google.com/site/daniggcc/software/tao?authuser=0>).

The subsidence/uplift of the basement is calculated using the moving load mechanism. In this mechanism, an increase in the load is calculated at each time step as function of the load displacement rate. The height of the load is conserved during its movement. Thus, the model requires a starting topography and a displacement rate. The used topography is the structurally restored section MED25 (see previous step in section 3.2.2.1.1). The displacement rate used in the forward model is 0.1mm/yr as calculated by [Sabat et al. \(2011\)](#). Since the interest of the reconstruction is to correct the post-MSC movements, the two time steps used as an input are 6 Ma (~ the beginning of the MSC) and 0 Ma (present). The adopted fault geometry is based on the interpretation of the seismic profile rooting at 5 km and dipping towards the SE, with a conjugate

fault dipping NW (Figure 3.16). This geometry is in accordance with the structure model proposed by Sabat et al. (1997) in the CMD.

Pseudo-3D Backstripping – step 5

The pseudo-3D (planform) flexural-isostatic modelling was applied on a basin-wide scale on an area that includes most of the Western Mediterranean basin (Figure 3.20). The aim of this modelling is to correct for the vertical motions caused by sedimentation and rebound due to the removal of water load during periods of water level drawdown of the MSC. The compaction of pre-MSC sediments is taken into consideration in the modelling.

The modelling was performed using the open source software TISC (<https://sites.google.com/site/daniggcc/software/tisc?authuser=0>) developed by Garcia-Castellanos, (2002).

Several analysis were done during the 3D flexural modelling in the Western Mediterranean that allowed covering several scenarios of base level variations and their interpretation at different steps of the MSC. Those analysis and their corresponding interpretations and scenarios will be detailed and discussed in chapter 6. For the objectives of this dissertation, the important output that was aimed at is the restitution of the pre-MSC paleo-bathymetry. Therefore, hereafter the method used will be explained without justifying the water level at each step of the MSC, thus assuming that no significant base level drawdown happened during the MSC.

Seismic-derived data input

The first inputs needed into the model are the present-day bathymetry, the present-day thickness of the offshore sediments (Pre-MSC sedimentary unit above the acoustic basement, LU, MU, UU and PQ unit) and the depth to the basement. Figure 3.20 shows the complete seismic-derived dataset used to extract and interpolate these inputs. This data (Figure 3.20) correspond to already interpreted horizons provided in excel tables as horizons (x, y, z format; x and y being the geographic coordinates and z the depth of the horizons). They derive from several works that have

been published previously (Maillard, MAUFFRET, et al., 1992; Roca & Guimerà, 1992b; Maillard & Mauffret, 1993a; Mauffret et al., 1995; Leroux, Aslanian, Rabineau, et al., 2019), as well as the interpretation of some of the re-processed seismic dataset shown in (Figure 3.1) and/or presented in section 3.1.1. The data resulting from the interpretation of a 3D seismic cube in the Ebro Delta by Urgeles et al. (2011) was also provided and integrated to the overall compilation of the seismic data (position of the cube in Figure 3.20). The resulting thickness maps of the Pre-MSC sedimentary unit, MU, UU and PQ units are presented in Figure 3.21. The method to calculate the thicknesses and/or depths of the offshore sedimentary units/horizons is the same described in section 3.1.2.

The window in which the backstripping analysis is applied is restricted to the area between longitudes -1° to 9° and latitudes 36° to 44° of Figure 3.20. The onshore sedimentation is considered relatively limited in thickness and in spatial distribution with respect to the offshore part of the area, the reason for the assumption that their effect on a regional scale is limited for the MSC and PQ deposits.

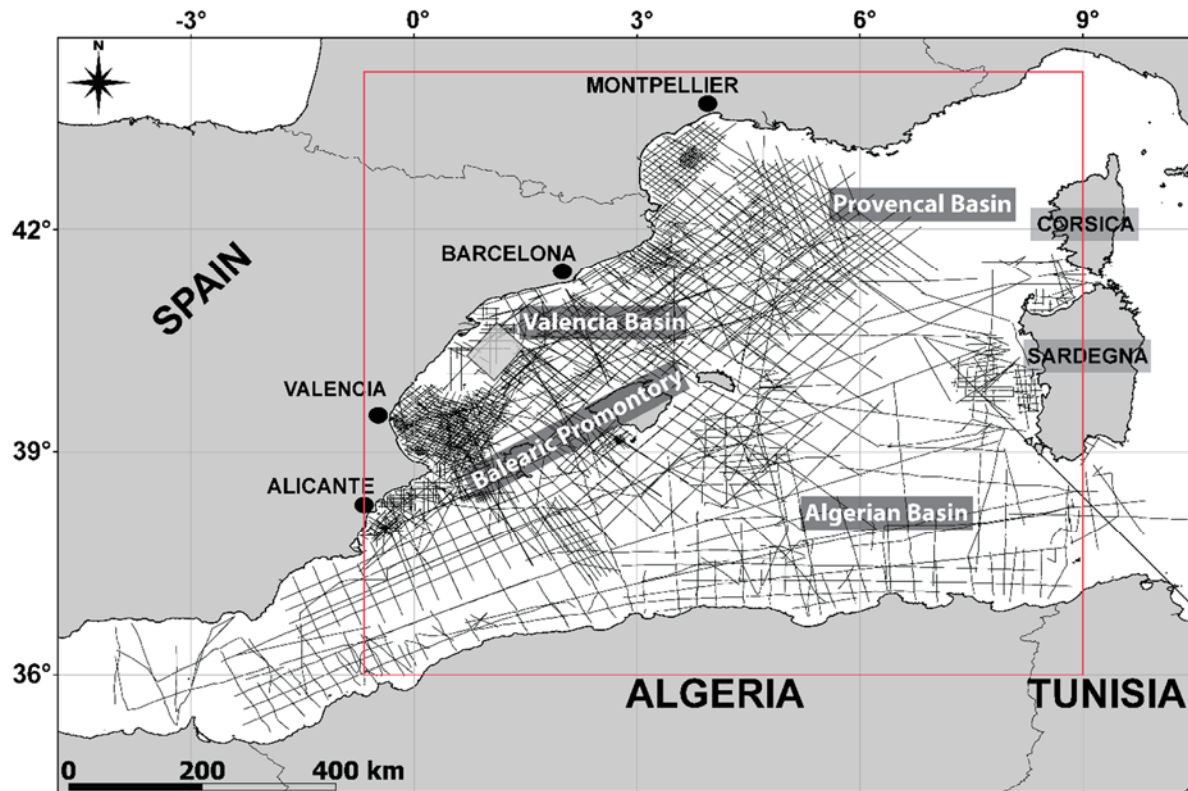


Figure 3.20. The seismic data used for the pseudo-3D (planform) backstripping in the Western Mediterranean (black lines). The grey box represents the position of a 3D seismic cube survey that was also integrated to the dataset. This dataset includes all the seismic profiles shown in figure 3.1. The area (red box) in which the analysis took place is between longitudes -1° to 9° and latitudes 36° to 44° (WGS 1984).

Sediment unloading and decompaction

Once the sediment coverage was defined, the sediment unloading and decompaction took place. As already mentioned, this was done as a pseudo-3D planform model. The present-day basin state with the depth of the key horizons and the thickness of the mapped stratigraphic units were defined in 200×200 grids covering an area of 860×890 km, corresponding to the area shown in Figure 3.21. The performed backstripping accounted for the subsidence caused by sedimentation since the onset of the MSC and the compaction of the pre-MSC sedimentary unit (Figure 3.22). The flexural calculation adopts an elastic thin plate, assuming that loads are supported by a strong lithosphere overlying a low-viscosity asthenosphere, which behaves like a fluid. The effect of compaction on the pre-MSC unit is calculated following the same porosity-depth exponential equation as for the 2D backstripping (Equation 3.1).

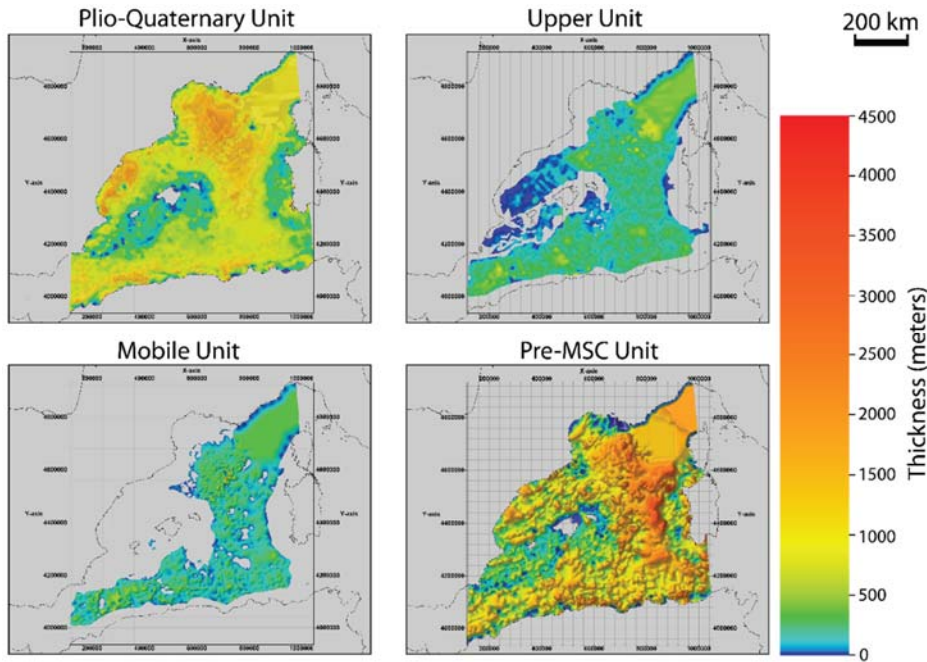


Figure 3.21. Thickness maps of the sedimentary units used as an input for the flexural-isostatic reconstruction

For the Western Mediterranean pre-MSC sediments, [Bessis, \(1986\)](#) presented a porosity-depth curve based on three wells in the Gulf of Lions. The curve fits with a relationship of $\Phi_0 = 0.75$ and $c = 0.00115$, which suggests a slightly faster compaction than the shale curve of [Sclater & Christie \(1980\)](#) used earlier for the PQ unit in the 2D backstripping method in the CMD (see section 3.2.2.1.2). Figure 3.22 illustrates the backstripping workflow to reach the paleo-bathymetry at the onset of the MSC. At each step, a sedimentary unit is unloaded, followed by the decompaction of the pre-MSC sediments and the determination of the corresponding basement uplift.

Two main aspects to keep in mind after obtaining the paleo-bathymetry are:

- the post-MSC tectonics are not considered. Those would require a specific attention and a proper 3D kinematic modelling, especially in areas that have been very active tectonically during the Pliocene to recent time (e.g. the southwestern part of the BP, northern Africa, north Ligurian margin).
- the thermal cooling is not integrated into the backstripping calculations. This component is expected to be important in the Provencal and Algerian basins, whereas it can be considered minor in areas with continental crust such as the Balearic Promontory.

Both aspects will be considered and further discussed in chapter 6 sections 6.4.1 and 6.5.

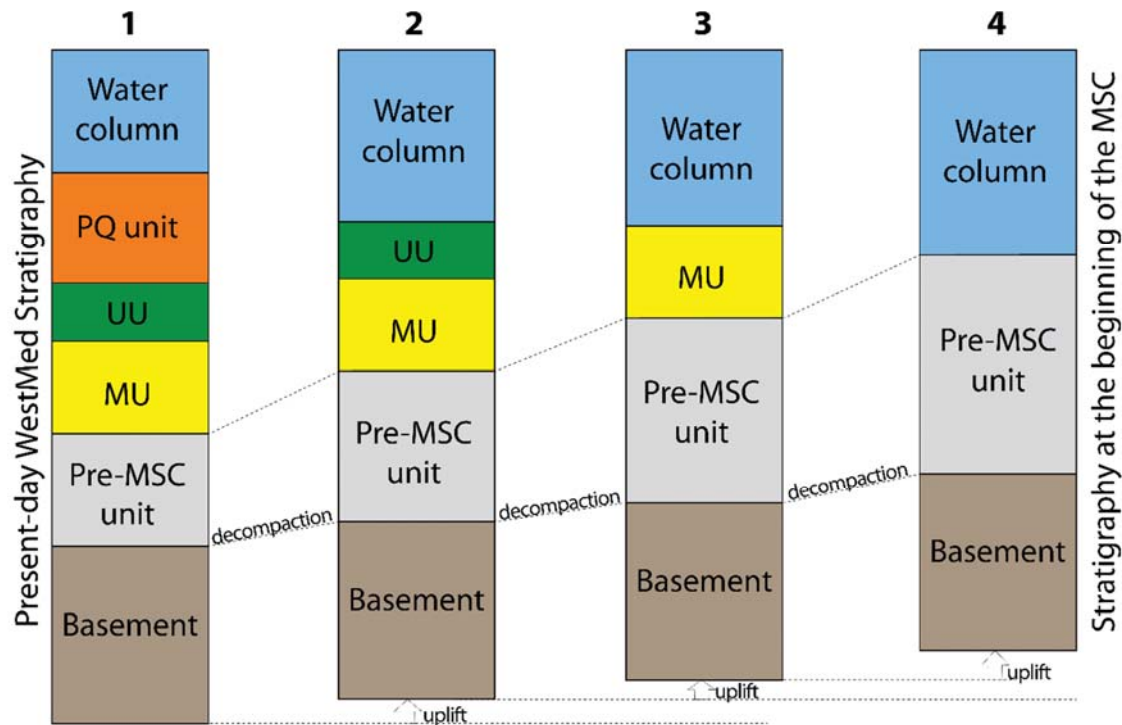


Figure 3.22. Systematic backstripping steps followed to obtain the paleo-bathymetry at the beginning of the MSC in the Western Mediterranean. In this process, no sea-level drawdown is considered because the objective is to obtain the paleo-Bathymetry prior to the beginning of the MSC (see text in section 3.2.2.2). 1: The present day stratigraphy in the study area; 2: Removal of PQ unit and decompaction of the pre-MSC sediments; 3: Removal of the UU and decompaction of the pre-MSC sediments; 4: Removal of the MU and decompaction of the pre-MSC sediments thus restoring the basin into its state at the beginning of the MSC.

3.3 Modelling evaporites deposition

Understanding the mechanisms and the conditions under which the MSC evaporites deposited have been a challenge for a long time. One way to look and better understand the formation of these evaporites is by observing and comparing them to present-day and/or ancient evaporitic analogues. However, the MSC evaporites have some unique aspects that are not found in any other ancient or present-day evaporitic basins (see also chapter 1). Modelling the MSC evaporites' deposition using physics-based numerical models is thus considered another way

to look at and understand their formation. Such models have shown to be an efficient instrument and they allowed tackling some of the questions and uncertainties surrounding the MSC salt giant. Most of the models applied to the study of the MSC are built based on the physical and hydrological properties of gateways, such as straits, connecting adjacent water bodies (Figure 3.23) (e.g., [Blanc, 2000](#); [Meijer, 2006](#); [Ryan, 2008](#)). These models rely mainly on climatic, oceanographic and topographic data, and as a result, they aim at evaluating the accuracy and feasibility of the proposed MSC evaporites processes and mechanisms. Their main applications were dedicated to model water fluxes and exchanges between the Mediterranean Basin and the Atlantic Ocean through the Gibraltar Strait, and the inter connection between the Western and Eastern Mediterranean basins through the Sicily Tunisian sill (Figure 3.23).

Figure 3.23-A illustrates how the dynamics of the fluxes at the Gibraltar Straits' sill are controlled by 2-layer or 2-way fluxes in and out from the Mediterranean Basin. These fluxes control the main characteristics of the Mediterranean, namely the Salinity and the amount of exchange of water with the Atlantic. The traditional way to model this kind of exchange, is to start from the assumption of mass and salt conservation statements for the Mediterranean Basin (hydraulic control theory; [Knudsen, 1900](#)). This can be written as follows:

$$Q_A * S_A = Q_M * S_M$$

(Equation 3.2)

Where Q_A and Q_M (in m^3/s) are the influx and outflux of the Mediterranean, respectively; S_A is the salinity of the Atlantic water and S_M is the salinity of the Mediterranean water (both in kg/m^3).

(Equation 3.2 simply describes the fluxes of salt from and into the Mediterranean basin. This version of the Knudsen theorem already uses the assumption that the differences between the densities of the flows can be neglected. From this, follows that for a certain salinity in the Mediterranean basin, the flux of salt into the basin ($Q_A * S_A$) must be the same as the flux out of it ($Q_M * S_M$). The loss of freshwater to the atmosphere is not part of this budget since it is not removing salt from the volume.

Depending on the objectives of the modelling, several derivations can be done starting from (Equation 3.2) (e.g. Meijer, 2006; 2012; Topper & Meijer, 2013). It is the case for the modelling applied to the CMD in this work. The derivations are presented in section 3.3.1.2.

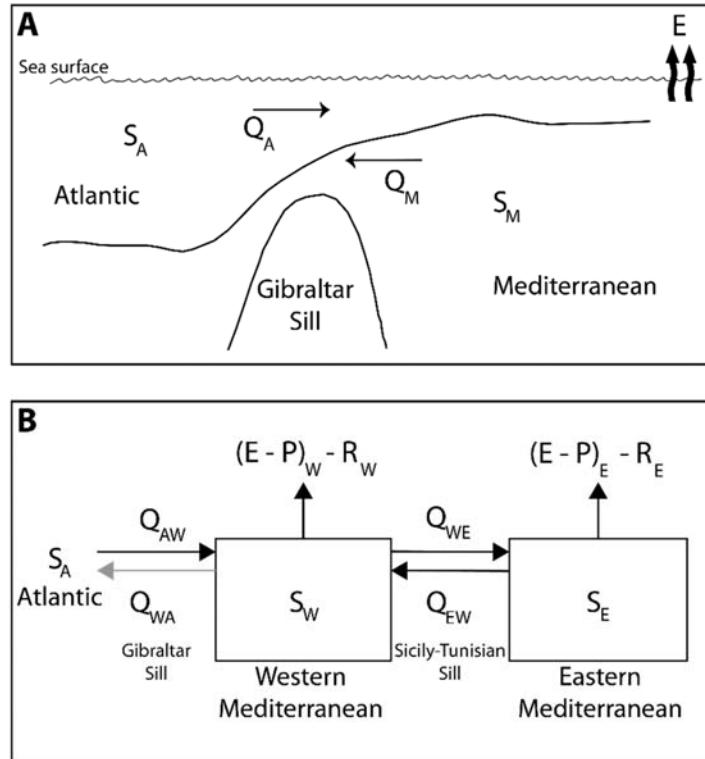


Figure 3.23. A- Schematic presentation of the two-way water fluxes over the Gibraltar sill. Q and S are the water fluxes and salinity, respectively. Modified from Bryden & Stommel, (1984). B- Diagram representing as boxes the connection between the Atlantic Ocean with the Western Mediterranean and the Western Mediterranean with the Eastern Mediterranean. Q_{WA} : outflux from the western basin to the Atlantic Ocean. S_A : salinity of the Atlantic water entering the western Mediterranean; S_W and S_E , average salinity of the western and eastern sub-basins, respectively; Q_{AW} , volume flux of Atlantic water into the western basin; Q_{WE} , volume flux from the western to the eastern basin; Q_{EW} , volume flux from the eastern to the western basin; $(E-P)_W$ and $(E-P)_E$, evaporation minus precipitation of the western and eastern basins, respectively, and R_W and R_E , river discharge into the two basins. Q_{WA} and Q_{AW} represent the Atlantic–Mediterranean connection; Q_{WE} and Q_{EW} the Sicily-Tunisian Strait. Modified from Meijer, (2012).

3.3.1 Modelling fluxes in the Central Mallorca Depression

Unlike all the modelling previously performed in the MSC literature, the applied modelling in this thesis is at a small scale, focusing on the connection between the Central Mallorca Depression and the surrounding Western Mediterranean Basin. The CMD is a key basin to model the evaporites formation for several reasons, and the choice to apply this kind of modelling there is justified as follows:

- it has undergone few post-MSC tectonic deformations (see chapter 5) and thus the restored pre-MSC paleo-bathymetry in the CMD is very reliable. This means that the volume, the depth of the sills and the hypsometry of the CMD are well constrained for the pre-MSC and can be used as input to the models with as less assumptions as possible.
- it contains a continuous MSC sequence including a halite unit that is lying at a depth that is considered deeper than marginal basins and way shallower than the deep basins, with no connection to neither the marginal nor the deep basins (see also chapter 2, section 2.2).
- a high density of high-resolution seismic data is available in the CMD, which makes the calculation of the volume of different MSC evaporitic units easy and relatively precise (Figure 3.1).

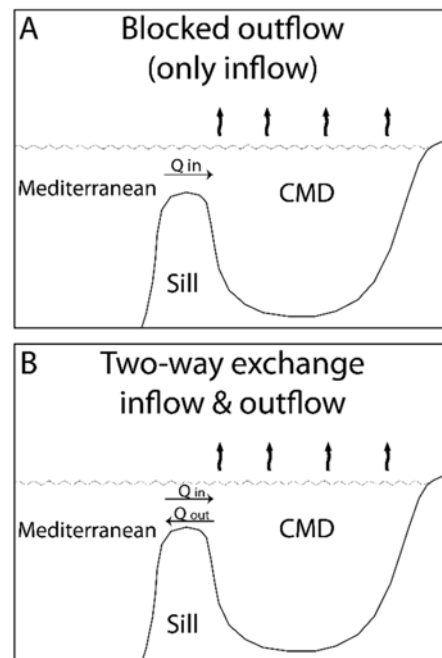


Figure 3.24. The two ways used to approach the connection between the CMD and the open Mediterranean. A: the basin is connected to the open Mediterranean in a way that inflow compensates the loss of freshwater due to evaporation. B: there is a two-way exchange over the sill. The inflow now compensates the freshwater budget as well as the saline outflow. Q_{in} is the influx from the Mediterranean to the CMD and Q_{out} is the outflow from the CMD to the Mediterranean.

The two main inputs used in the evaporites' deposition modelling in the CMD are the volumes of the MSC evaporites estimated from the seismic profiles (section 3.1.2.2.2) and the calculated pre-MSC paleo-bathymetry/paleo-hypsometry of the basin (section 3.2.2). Details about the calculation of the volumes of the evaporites and how were they differentiated between gypsum, halite and other clastic components will be described in chapter 7 section 7.3.1. They cannot be detailed at this stage of the dissertation because they are dependent on the interpretation of the bedded units that will be the focus of chapter 4.

In the modelling, the CMD is treated as a basin connected to the open Mediterranean through a sill (Figure 3.24). On the paleo-bathymetry of the CMD shown in Figure 3.25, it is connected to the deep Algerian Basin and the Valencia Basin by 2 different sills (sill 01 and sill 02 respectively in Figure 3.25). Sill 01, however, is the deepest sill (~900 m in paleo-depth > ~700 m for sill 02), thus we assume that the main fluxes and exchanges take place through the deeper sill (see discussion in chapter 7).

In this view and with the above mentioned basin settings, different approaches (approaches 1 and 2) were tested to account for the evaporite deposition in the CMD. Approach 1 (section 3.3.1.1) is the simplest and consists in the calculations of water budgets and volume of evaporites, first in a cutoff scenario in which the CMD is completely disconnected from the Mediterranean. In a second time a scenario where only an inflow from the Mediterranean towards the CMD is considered (Figure 3.24-A) with blocked outflow. In approach 2 (section 3.3.1.2) a two-way connection, with both an inflow and outflow (Figure 3.24-B), is considered.

It aims to testing the factors (mainly fluxes) controlling the salinity changes and evolution, and comparing those to the observed volumes of evaporites calculated in the CMD.

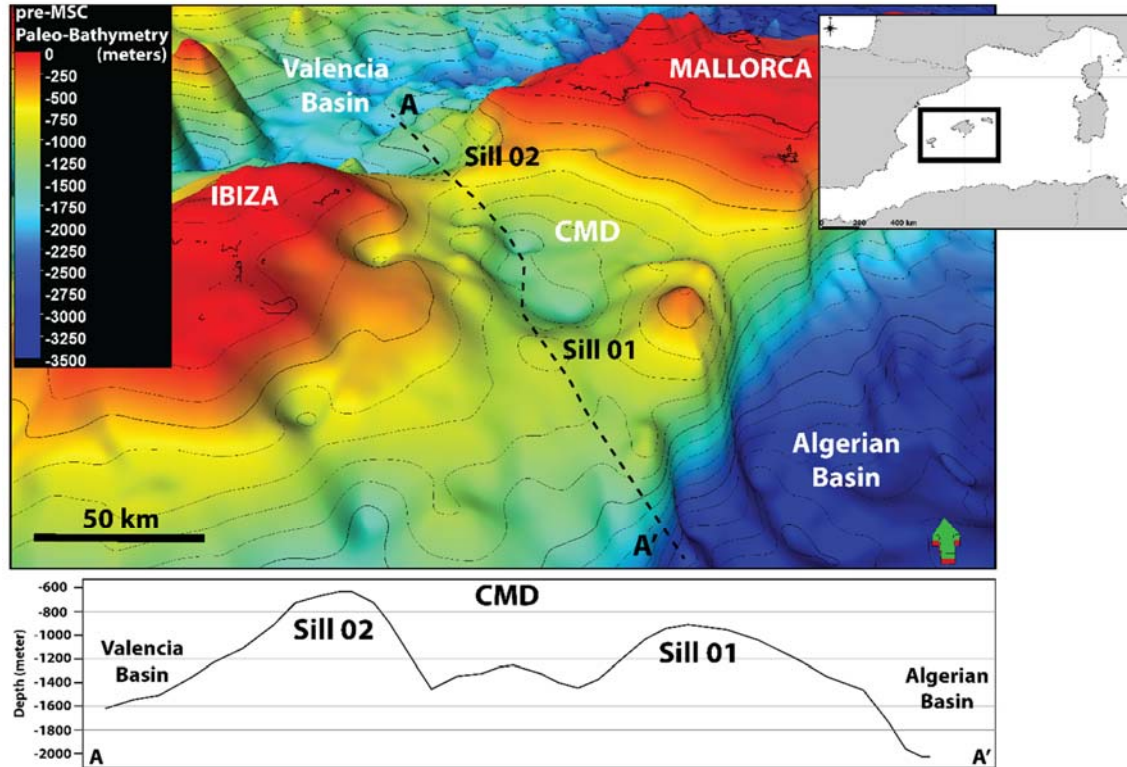


Figure 3.25. 3D paleo-bathymetry of the CMD at the beginning of the MSC. The depth scale applies only to the offshore area. The CMD is connected to the deep basin through 2 sills. Sill 01 is the deepest one and is the one that is used in the modelling as a connection between the CMD and the open Mediterranean (Figure 3.24). A-A' is a 2D profile highlighting the pre-MSC geometry of the CMD and sills.

3.3.1.1 Volume and budget calculations (Blocked outflow) – Approach 1

The first calculations performed focus on the relation between water volume and the volumes of the evaporitic deposits.

The salinity of the basin (kg/m^3) was handled in a way that allows to distinguish between ions that precipitate as gypsum ($\text{SO}_4^{2-}, \text{Ca}^{2+}$) and those that precipitate as halite (Na^+, Cl^- ; Topper & Meijer, 2013), here referred to as 'groups'. The parameters used for gypsum and halite in the modelling are shown in Table 3.3.

	Gypsum	Halite	Reference
Density (kg/m ³)	2300	2200	Leeder, 1999
Fraction of ion group (-)	1.27/ 35	27.21/ 35	Leeder, 1999 Topper & Meijer (2013)
Saturation Concentration (kg/m ³)	5.25	271.1	Leeder, 1999 Topper & Meijer (2013)
Volume in CMD (m ³)	3.80E+11	9.63E+10	--

Table 3.3. Table showing the parameters used in the modelling for Halite and Gypsum with the corresponding references.

The precipitation of gypsum and halite is not tied directly to a salinity threshold but rather to the concentration ($c_{saturation}$) of their ions in the basin's water body. This way, the minimum volume of water (V_{min}) needed to precipitate the observed volume of deposits ($V_{deposit}$) can be calculated using the equation below (Equation 3.3)

$$V_{min} = (V_{deposit} * \rho_{deposit}) / c_{saturation}$$

Equation 3.3

Where, ρ is the density of the evaporitic deposit in (kg/m³) (Table 3.3).

The two possible ways of increasing ion concentration to reach saturation are:

1. Adding ions to a basin that has a constant water body volume. This would happen in a basin where saline inflow (Equation 3.4) is balancing a negative freshwater budget.

$$c(t) = c_0 + \frac{Q_{in} * c_{in}}{V_0} * t, \text{ where, } Q_{in} = E * A - R, A = const$$

Equation 3.4

With c being the concentration, Q the flux, V the volume, t the time, E the evaporation rate, R the river inflow and A the surface area of the basin.

2. Decreasing the initial water volume, V_0 , but keep as a constant the mass of ions solved in it. This would happen in a terminal basin with a negative freshwater budget (Equation

3.5).

$$c(t) = \frac{c_0 V_0}{V_0 - Q_{out}} * t \quad , \quad \text{where } Q_{out} = E * A - R \quad , \quad A = const$$

Equation 3.5

With c being the concentration, Q the flux, V the volume, t the time, E the evaporation rate, R the river inflow and A the surface area of the basin.

Once the concentration at which a group is saturated in water (c_{sat}) is reached, the excess ions of that group precipitate and thus do not further increase the concentration.

Table 3.4 shows the main values of the geometric settings of the CMD used as an input for the model.

	CMD	Reference
Area (m ²)	11.83E+9	--
Max pre-MSC paleo-depth (m)	1500	Figure 3.25
Sills pre-MSC paleo-depth (m)	Sill01 = 900 Sill02 = 700	Figure 3.25
River inflow (m ³ /s)	≤ 10	^a Garcia et al., (2017)
Evaporation rate (m/a) (for the model)	0.25 – 1.5 ^a 1.04 ^b	^a Estrany et al., (2011) ^b Topper & Meijer, (2013)
Precipitation rate (mm/a)	300	^a Garcia et al., (2017)

Table 3.4. Table showing some of the inputs of the CMD settings used in the models.

3.3.1.2 Two-way exchange between the CMD and Mediterranean – Approach 2

To model the two-way fluxes between the CMD and the Mediterranean (Figure 3.24-B), the starting point is the Knudsen theory described in (Equation 3.2).

For a basin, that does not experience a drawdown (water volume conserved), the inflow must be equal to the total outflow including the loss of freshwater to the atmosphere. Since the fresh

water budget (fwb) is dependent on the surface area of the volume, the fluxes would be affected by a drawdown. This is described as follows (Equation 3.6)

$$Q_{in} = Q_{out} - fwb = Q_{out} + |(P - E) * A + R|, \quad \text{for } fwb < 0$$

Equation 3.6

Where Q represent the fluxes, P the precipitation rate, E the evaporation rate, R the river inflow and A the surface area of the basin.

Equation 3.6 describes not a constant salinity, but the conservation of water volume. Combining (Equation 3.2 and Equation 3.6 together, the following derivation could be done (Equation 3.7-A and B)

$$Q_{in} = \frac{(P - E) * A + R}{1 - \frac{S_{in}}{S_{out}}}$$

Equation 3.7-A

$$Q_{out} = \frac{(P - E) * A + R}{\frac{S_{out}}{S_{in}} - 1}$$

Equation 3.8-B

Equation 3.7-A and Equation 3.8-B calculate the inflow and the outflow in dependency of the salinity ratio and the surface area for given net evaporation ($P - E$) and river inflow R . The calculated inflow can be seen as the sum of all inflows, assuming all inflows have the same salinity. The same applies to the outflow. For the case of the CMD, this theory can be applied when the inflow salinity from the northern sill (sill02 in Figure 3.25) is the same as the one from the southern sill (sill01 in Figure 3.25).

The results of the modelling presented above will be shown and discussed in chapter 7 of the dissertation.

Chapter 4

The Distribution, Nature and Origin of the MSC Units (BUs and Salt) of the Balearic Promontory: A Preliminary Scenario

Marine and Petroleum Geology 124 (2021) 104777



Contents lists available at [ScienceDirect](https://www.sciencedirect.com)

Marine and Petroleum Geology

journal homepage: www.elsevier.com/locate/marpetgeo



Research paper

The Messinian Salinity Crisis deposits in the Balearic Promontory: An undeformed analog of the MSC Sicilian basins??[☆]



Fadl Raad^{a, *}, Johanna Lofi^a, Agnès Maillard^b, Athina Tzevahirtzian^c, Antonio Caruso^c

^a Géosciences Montpellier, CNRS, Université de Montpellier, Université des Antilles - Bâtiment 22, Université de Montpellier 2, Place E. Bataillon, Montpellier Cedex 05, 34095, France

^b Géosciences Environnement Toulouse (GET), Observatoire Midi Pyrénées, Université de Toulouse, CNRS, IRD, 14 avenue E. Belin, Toulouse, F-31400, France

^c Dipartimento di Scienze della Terra e del Mare (DiSTeM), Università degli Studi di Palermo, Via Archirafi 20-22, 90123, Palermo, Italy

In this chapter I perform a detailed comparison between the MSC record of the BP as imaged on the seismic data, and the MSC record outcropping onshore in the Caltanissetta Basin (Sicily). I started this work as a first step of my PhD project after interpreting the seismic data available in the BP and updating the distribution maps of the MSC seismic units existing in literature. The second part of the work was mostly bibliography in which I looked for published articles about the MSC evaporites of the Sicilian MSC basins and I identified common characteristics with those observed in the BP. No new field data is presented in the onshore part of this work.

This work was conducted by me, with the supervision and inspiration of my supervisors Johanna Lofi and Agnes Maillard, and in collaboration with SaltGiant colleagues Athina Tzevahertzian and Antonio Caruso from the University of Palermo. Athina and Antonio accompanied me to the field in Sicily when I visited them for a secondment. They provided me with some of the outcrop photos that are shown in the work, and they revised my bibliographic work and interpretation of the Sicilian MSC deposits. The work is published in Marine and Petroleum Geology journal.

Take-home messages of the chapter:

- *The MSC deposits of the BP have a tripartite character (lower evaporites, salt, upper evaporites) that matches with the existing 3-stages chrono-stratigraphic 'consensus model'*
- *The MSC deposits of the Central Mallorca Depression are an undeformed analogue of those of the Caltanissetta Basin*
- *The MSC halite of the BP shows no connection with the deep basin salt, thus rising doubts on its synchronous onset*

Abstract: The Messinian Salinity Crisis (MSC) is a controversial geological event that influenced the Mediterranean Basin in the late Miocene leaving behind a widespread Salt Giant. Today, more than 90% of the Messinian evaporitic deposits are located offshore, buried below the Plio-Quaternary sediments and have thus been studied mainly by marine seismic reflection imaging. Onshore-offshore records' comparisons and correlations should be considered a key approach to progress in our understanding of the MSC.

This approach has however not been widely explored so far. Indeed, because of the erosion on the Messinian continental shelves and slopes during the MSC, only few places in the Mediterranean domain offers the opportunity to compare onshore and offshore records that have been preserved from erosion. In this paper, we compare for the first time the MSC records from two basins that were lying at intermediate water depths during the MSC and in which salt layers emplaced in topographic lows: the Central Mallorca Depression (CMD) in the Balearic Promontory, and the Caltanissetta Basin (CB) in Sicily. The reduced tectonic movements in the CMD since the late Miocene (Messinian) till recent days, favored the conservation of most of the MSC records in a configuration relatively close to their original configuration, thus allowing a comparison with the reference records outcropping in Sicily. We perform seismic interpretation of a wide seismic reflection dataset in the study area with the aim of refining the mapping of the Messinian units covering the Balearic Promontory (BP) and restituting their depositional history based on a detailed comparison with the Messinian evaporitic units of the Sicilian Caltanissetta Basin. We discuss how this history matches with the existing 3-stages chrono-stratigraphic model. We show that the Messinian units of Central Mallorca Depression could be an undeformed analog of those outcropping on-land in the Sicilian Caltanissetta Basin, thus questioning the contemporaneous onset of the salt deposition on the Mediterranean scale. We show a change in seismic facies at a certain range of depth between stage 1 MSC units, and wonder if this could reflect the threshold/maximum depth of deposition of bottom growth PLG selenites passing more distally to pelagic snowfall cumulate gypsum. Moreover, we confirm that PLG could be deposited in water depths exceeding 200m.

4.1 Introduction: Messinian Salinity Crisis and Intermediate Basins

The Messinian Salinity Crisis (MSC) is a prominent and still misunderstood event that influenced the Mediterranean Basin in the late Miocene, leaving behind a Salt Giant with a volume of about $1.2 \times 10^6 \text{ km}^3$ (W. B. F. Ryan, 1976; Haq et al., 2020b) deposited in a relatively short time interval of $\sim 0.64 \text{ Ma}$ (Krijgsman, et al., 1999a, b; CIESM, 2008; Manzi et al., 2013). The first studies dedicated to the MSC took place onshore (Selli, 1960) while offshore works (W. B. F. Ryan, 1971) followed the first scientific drillings of the deep-sea drilling project DSDP (Hsü, 1973). Since then and until today, numerous studies have been conducted in order to better understand the series of events that modified the basin during the Messinian and, despite these efforts, most of the controversies still persist (see review in Roveri, Flecker, et al., 2014)). A consensus model for the MSC was proposed after the CIESM publication in 2008, inspired from the 2 stage model of Clauzon et al. (1996), where the MSC has been divided in 3 stages:

- stage 1 (from 5.97 to 5.60Ma, i.e. $\sim 370 \text{ ky}$): this stage marks the MSC onset, where the lowermost primary evaporites were deposited in shallow water basins.
- stage 2 (from 5.60 to 5.55Ma, i.e. $\sim 50 \text{ ky}$): at this stage, salt bodies (mainly halite) were deposited in deep basins accompanying the maximum sea-level drawdown (of debated amplitude). Shallower basins evaporites underwent erosion and reworked evaporites were deposited.
- stage 3 (from 5.55 to 5.33Ma, i.e. $\sim 220 \text{ ky}$): this stage was later on divided into 2 sub-stages, stage 3.1 (from 5.65 to 5.42), in which upper evaporites were emplaced and stage 3.2 (from 5.42 to 5.33), that is known also as Lago Mare stage, where sediments with brackish water fauna content were deposited.

This model has been widely built based on onshore studies performed on several key peri-Mediterranean outcrops among which the ones from Sicily. This model has recently been challenged at least for the Eastern Mediterranean Basins by studies from recent oil industry offshore drillings (e.g. Meilijson et al., 2019).

Today, more than 90% of the MSC evaporites are lying offshore (Figure 4.1-A; W. B. F. Ryan, 2009; LOFI, 2011; Lofi et al., 2011; LOFI, 2018). Offshore drillings remain very limited (DSDP and ODP drillings and oil industry wells) and the offshore MSC records thus still largely un-sampled. The most efficient approach in the offshore domain remains the seismic

reflection method.

There is an agreement about the important role of the pre-MSC topography on the distribution of the MSC sediments, although paleo-geographic reconstructions are still not well constrained (G. Mascle & Mascle, 2019). In their review, Roveri, Flecker, et al. (2014) proposed a schematic classification of the Messinian sub-basins in the Mediterranean, where they differentiate shallow (0–200 m water depth), intermediate (i.e. relatively deep-water, 200–1000m) and deep basins (water depth > 1000m). In this view, these sub-basins are thought to be physically disconnected from each other by topographic sills, and hold specific MSC records.

The shallow marginal basins have been largely studied onland as they are outcropping in areas tectonically active during and/or after the MSC (e.g. Southeastern Spain, Apennines, and Piedmont).

The Messinian sedimentary record in these basins is nevertheless always incomplete because it has been exposed to erosion during the MSC sea level fall and/or due to tectonics. The main feature in the onshore outcrops is the presence of thick gypsum beds that mark the onset of the MSC (e.g. Yesares member in Sorbas Basin (Krijgsman et al., 2001b); Vena del Gesso formation in the Northern Apennines (Vai & Lucchi, 1977a); Cattolica Gypsum group in the central Sicilian Basin (Decima & Wezel, 1971)). They are called Primary Lower Gypsum (PLG), corresponding to MSC stage 1 and are usually interpreted as precession driven beds (Lugli, Vinicio, et al., 2010). A few studies have also recognized the presence of PLG in the offshore domain (e.g. Northern Adriatic Sea (Ghielmi et al., 2013); Balearic Promontory (D. Ochoa et al., 2015c)).

The deep MSC basins are only observed offshore and they contain salt sequences > 1 km thick (see review in LOFI, 2011; Lofi et al., 2011; LOFI, 2018). In the Western Mediterranean, the Algero-Provencal Basin is known to contain the full MSC sedimentary sequence or the so-called trilogy (MONTADERT et al., 1970).

Following the nomenclature of Lofi et al. (2011), the 3 main seismic units forming this deep basin succession are: 1- the lower unit (LU), never sampled; 2- the mobile unit (MU), thought to be mainly made of Halite based on its transparent seismic facies and plastic deformation; 3- the upper unit (UU) which uppermost part is made of clastic sediments, dolomitic marls, clastic gypsum and anhydrite (Hsü et al., 1973b). The deep basin trilogy of the western Mediterranean Basin has never been drilled except for its topmost part, and thus lacks chronostratigraphic and lithostratigraphic control. The MSC record in the eastern Mediterranean (Levant Basin) differs from the trilogy described in the western basin (Lofi, 2011; Lofi, Sage, Déverchère, et al., 2011;

Lofi, 2018b) as it consists of up to 2km thick halitic MU with distinct internal reflection packages (Bertoni & Cartwright, 2006; Feng et al., 2016; Meilijson, Hilgen, et al., 2019b), overlain by a thin UU (Gvirtzman et al., 2017; Madof et al., 2019) made of clastic rich anhydrite that has been recently drilled (Gvirtzman et al., 2017).

The intermediate basins are lying between the shallow and deep basins (e.g. Cyprus and Caltanissetta Basins). The MSC record in these basins differs from the one described in shallow (containing mainly PLG) and deep (thick salt layer) basins, and can contain various deposits: 1- euxinic shales/dolostones of stage 1 that are considered the later distal equivalent of the PLG (e.g. Piedmont Basin (Dela Pierre, Bernardi, Cavagna, Clari, Gennari, Irace, Lozar, Lugli, Manzi, & Natalicchio, 2011)), 2- Resedimented Lower Gypsum RLG of stage 2 (e.g. Sicily (Roveri et al., 2006)) and 3- Upper Evaporites UE of stage 3 (e.g. Cyprus (Manzi, Lugli, et al., 2016)).

When lying offshore today, intermediate basins can also contain various seismic units that are Messinian in age, including 1- bedded units (BU) (e.g. Balearic promontory (Maillard et al., 2014b; Driussi, Maillard, et al., 2015b); Adriatic Basin (Ghielmi et al., 2013); Eastern Corsica Basin (Thinon et al., 2016)), 2- a relatively thin salt layer (e.g. Balearic Promontory (Maillard et al., 2014b)), and 3- an UU (e.g. Valencia Basin (Maillard et al., 2006b)) lying above a Complex Unit (CU) (Valencia Basin (Cameselle & Urgeles, 2017a)).

In this work, we consider as intermediate any basin that during the MSC was lying deeper than marginal basins (~200m water depth) and shallower than the deep basins, containing either none of the deep basin MSC trilogy members or only some of them (Figure 4.1-B).

Some or part of the intermediate basins are outcropping nowadays (e.g. Sicily and Mesoria Basins) and are thus considered as key areas to provide a stratigraphic link between marginal and deep basins. Offshore intermediate basins have not been intensively studied so far, although they may permit a comparison with some key onshore outcrops. Another importance of the offshore intermediate basins is that they may contain sedimentary records that are missing in the onshore outcrops that have undergone post-MSC erosion.

In this paper, we compare two basins that are thought to be lying at intermediate depths during the MSC and in which salt layers are encountered: the Central Mallorca Depression (CMD) on the Balearic Promontory (Maillard et al., 2014b), and the Caltanissetta Basin (CB) in Sicily (Roveri, Flecker, et al., 2014a). The first one is lying offshore between Ibiza and Mallorca islands, in a passive tectonic setting, and is studied via seismic profiles. The second one is lying

onshore in an active tectonic context, and its outcrops have been studied widely as references for understanding the MSC. First, we present a detailed study of the seismic records of the CMD. We then discuss similarities, in terms of geometry, facies, distribution and thickness between the Messinian deposits in both basins and we tempt to demonstrate that the CMD may be considered as an undeformed analog of the Sicilian CB. Finally, we propose a depositional scenario for the CMD and discuss the implications of the observations on the MSC event.

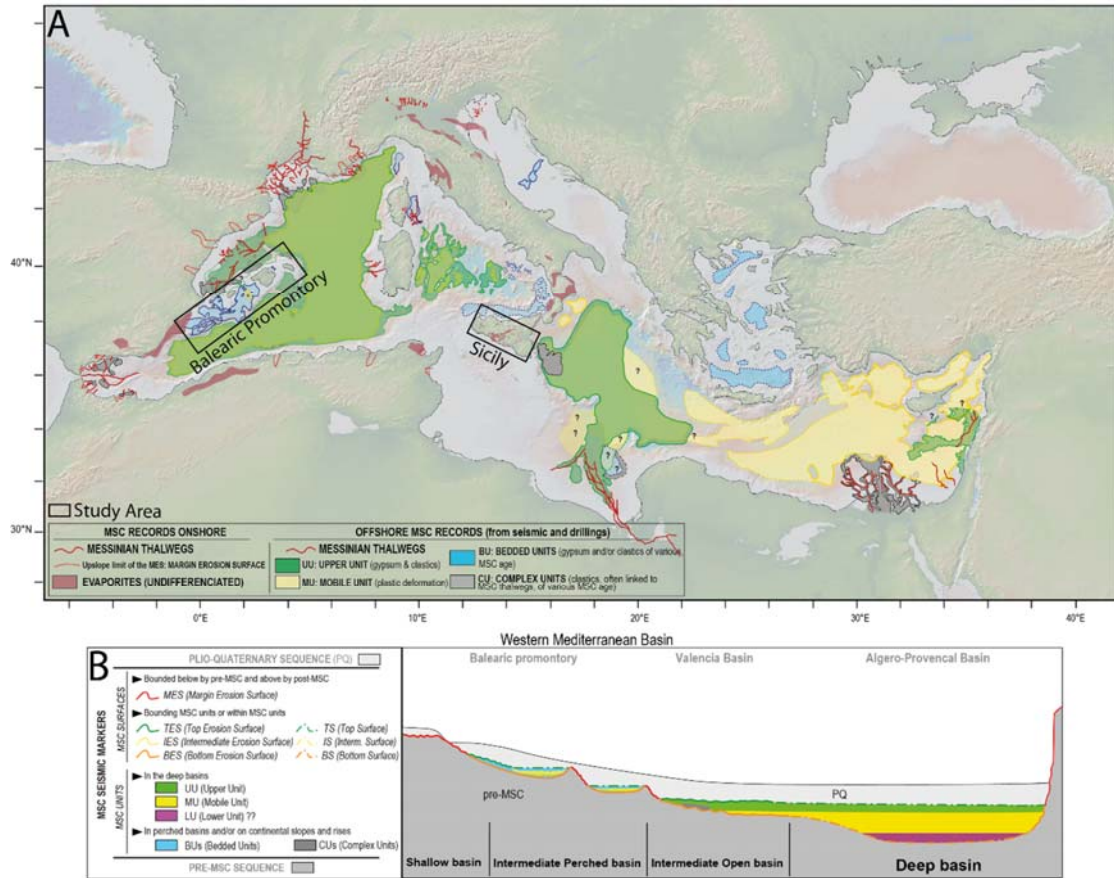


Figure 4.1. A: Extension map of the MSC seismic units around the Mediterranean illustrating our study area (modified from LOFI, 2018). Relief map is taken from Geomapapp (www.geomapapp.org). B: schematic present-day cross section of the Western Mediterranean basin. It shows a conceptual present-day distribution of the MSC offshore markers along a transect from shallow into deep basin passing through the intermediate basin (salt tectonics and post MSC movements are not included) (modified from (Lofi, 2018b).

4.2 Geological background of the study areas

4.2.1 The Balearic Promontory: Tectonics, Architecture and Messinian Salinity Crisis

Surrounded by 2 deeper basins, the Balearic Promontory (BP) is a continental high that includes the Balearic Islands. It is made of 2 main morphologic blocks (Acosta et al., 2003): the Mallorca-Menorca block and the Ibiza-Formentera block (Figure 4.2). The two blocks are separated by an elliptical depression, approximately 1050m water deep, called the Central Mallorca Depression (CMD). To the south, the BP is delimited by 2 steep escarpments marking the border with the Algero-Provençal deep Basin (>2400m depth): the Mazarron and Emile Baudot Escarpments, separated by the Ibiza Channel that, with the Mallorca Channel, connects the BP to the Valencia Basin (>1200m depth) (Figure 4.2).

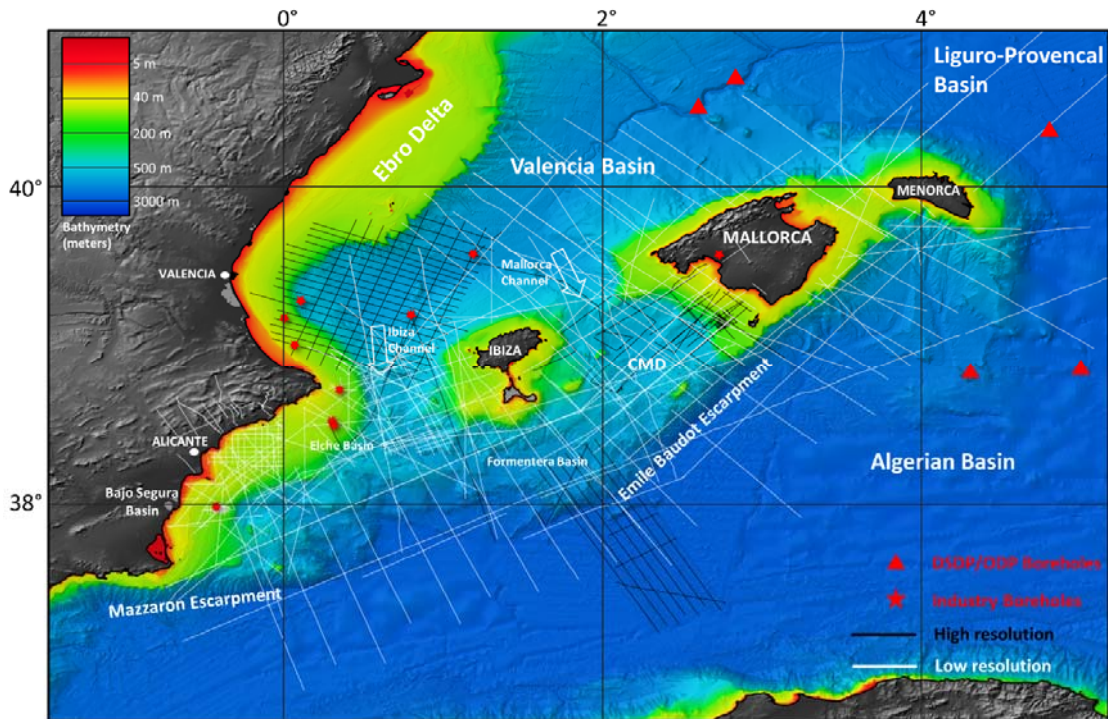


Figure 4.2. Bathymetric map showing the seismic dataset used for this study. CMD= Central Mallorca Depression. Bathymetry is downloaded from the European Marine Observation and Data network (EMODnet) database available online (www.emodnet-bathymetry.eu). White thick arrows indicate marine channels. Boreholes shown in the map represent a set of both industrial (IGME) and exploratory drillings (ODP and DSDP). Onshore digital elevation model has been produced using Copernicus data and information funded by the European Union- EU-DEM layers (www.eea.europa.eu).

The BP is known to be the north-eastern prolongation of the compressional Betic Cordillera thrust system (Roca, 2001). It is thought that the compression started in the late Oligocene to the south and then prolonged further to the north during the Burdigalian (Gelabert et al., 1992; Sàbat et al., 2011), while the surrounding Valencia and Algerian Basins underwent rifting in the back-arc context of the retreating Apennines-Maghrebian subduction. From late Serravallian and up to recent times, the BP underwent mild post-orogenic extension, resulting in a NE-SW normal fault system expressed plainly by the Palma Graben in Mallorca (Roca & Guimerà, 1992b; Sàbat et al., 2011).

This tectonic evolution of the BP thus resulted in a very complex structure including highs and lows resulting from compression and extension. The present-day BP contains a series of perched sub-basins lying at different depths, stepped from the present-day coastline near Alicante (Spain) down to the deep basin (Figure 4.3-A, B). Most of these sub-basins were probably already existing during the Messinian and inherited their structure from the tectonic evolution of the promontory. Today they are forming a series of topographic lows (Figure 4.3-B), more or less connected, lying at various water depths (Driussi, Maillard, et al., 2015b). During the MSC, these lows have been filled with deposits up to 500m thick (Maillard et al., 2014b; D. Ochoa et al., 2015c; Driussi, Maillard, et al., 2015b).

4.2.1.1 MSC in the surrounding deep basins

South of the BP, the MSC record in the Algerian Basin is represented by the deep basin trilogy ie. LU, MU and UU (Lofi, 2011; Lofi, Sage, Déverchère, et al., 2011; Lofi, 2018b). The UU and MU pinch out on the Mazarron and Emile Baudot escarpments (Camerlenghi et al., 2009b) and they show no connection with the MSC units of the BP (Figure 4.3-A and Figure 4.4-A). North-East of the BP, in the Provencal Basin, the MSC trilogy is also present (MONTADERT et al., 1970; Lofi, Gorini, Berné, Clauzon, Tadeu Dos Reis, et al., 2005). Towards the Valencia Basin, the LU and MU thin out progressively and pinch out in the area where a volcanic ridge separates the Provencal from the Valencia Basin (Figure 4.3-A; Maillard et al., 2006; Maillard & Mauffret, 2006; Pellen et al., 2019). The UU extends into the Valencia Basin, thinning out from the NE to the SW where it pinches out and passes into a Margin Erosional Surface (MES) on the Catalan/Ebro Margins and volcanic structures (Maillard et al., 2006b; Urgeles, Camerlenghi, Garcia-Castellanos, De Mol, Garces, et al., 2011), whereas towards the east it

drapes the lower margin of the BP (Driussi, Maillard, et al., 2015b) and it passes into a MES. In the western extremity of this basin, Cameselle & Urgeles, (2017) evidenced the existence of a widespread CU unconformably overlain by, here very thin, UU (Figure 4.3-A). They interpreted the CU as mass transport deposits resulting from large-scale destabilization of the continental slope during the initial rapid sea-level drawdown and exposure of the shelf and upper slope. Other CU exist locally at the downslope mouth of Messinian valleys (Maillard et al., 2006b)

Recently, Pellen et al. (2019) interpreted an additional MSC unit (unit SU12) lying below the MES on the Ebro Margin, and below the LU in the Valencia and Provençal Basins, which is thought to have been deposited during the MSC base-level fall. Maillard et al. (2006) proposed that following this important base level drop, the Valencia Basin was subaerially exposed and a widespread erosion surface was created (Bottom Erosional Surface, BES). The UU successively was emplaced under shallow water during a relative rise in base level as attested by their aggrading and onlapping geometry (Lofi, 2011; Lofi, Sage, Déverchère, et al., 2011). An erosional surface at the top of the UU (Top Erosional Surface, TES) could be a result of dilution during the Lago-Mare phase, possibly associated to a base level drop preceding the Zanclean reflooding (Escutia & Maldonado, 1992b; Maillard et al., 2006b; Garcia-Castellanos, Estrada, et al., 2009). For Cameselle & Urgeles, (2017) this erosion is minor and can be found only locally due to the dilution during the Lago Mare event.

4.2.1.2 MSC in the Balearic Promontory

Several studies showed the presence of a thin MSC unit offshore the BP, disconnected from the other MSC units in the surrounding basins (Maillard et al., 2014b; Driussi, Maillard, et al., 2015b; D. Ochoa et al., 2015c). Based on seismic profile interpretation, Driussi et al. (2015) identified a “MSC unit” (Table 4.1) extending all over the BP (their figure 4) from the present-day coastline down to the deepest part in the Formentera Basin (~1750m). This seismic unit is characterized by 2 to 7 sub-parallel continuous reflections of medium amplitude. It locally includes an internal facies made up of very thin reflections (Ft) with lower amplitude, found usually at the top of the MSC unit. The “MSC unit” is locally lying on an erosional unconformity (BES) and is eroded at the top (TES) towards the borders of the CMD.

Several works then proposed that this “MSC unit” is made of several sub-units and that not all of them have the same MSC age, depending on their location on the promontory (Maillard et al., 2014b; D. Ochoa et al., 2015c; Roveri et al., 2019).

Ochoa et al. (2015), based on borehole cuttings and logs tied to high-resolution seismic reflection profiles, demonstrated that the “MSC unit”, which they called Bedded Unit (BU, *sensu* Lofi et al., 2011) (Table 4.1), in Elche and Bajo Segura sub-basins corresponds to the PLG (Figure 4.3-B; see also their figures 2 and 8). This PLG is equivalent to the first stage evaporites found onland, for example in the Sorbas and Bajo Segura Basins (Soria et al., 2008) or in the Palma Basin boreholes (Figure 4.4-A; Baron & Gonzalez, 1985; Rosell et al., 1998; Maillard et al., 2014; García-Veigas et al., 2018). In this area, the seismic facies of the PLG consists of sub-parallel continuous 2 to 7 reflectors forming a Bedded Unit (BU), with very strong acoustic impedance at the base and at the top (see their figure 8). It is clearly cut by the TES, whereas no erosion is identified at the bottom. Based on their results, these authors suggested that PLG gypsum precipitation and/or preservation could occur in non-silled basins at water depth exceeding 200m. Both Ochoa et al. (2015) and Driussi et al. (2015) questioned the connectivity between the different shallow sub-basins (e.g. Bajo Segura and Elche Basins) and the ones currently lying deeper, because of the presence of local structural highs separating them, and because the density of seismic profiles is not high enough to show the connectivity. More recently, Roveri et al. (2019) hypothesized that only the shallower domains of the Elche and Bajo Segura sub-basins contained PLG, with the deeper parts of these basins located beyond some volcanic sills containing Resedimented Lower Gypsum (RLG) (their figure 14 a, b). However, no data support their new interpretation and mapping. At the present time, it is thus not clear whether the BUs filling the sub-basins lying deeper correspond to PLG, RLG or another MSC deposit.

In a study dedicated to the CMD, Maillard et al. (2014) distinguished two different sub-units within the MSC unit of Driussi et al. (2015) (see their figure 7): 1- a Slope Unit (SU) located clearly on the Mallorca and Ibiza slopes and 2- a Bedded Unit (BU) lying deeper and containing a thin salt unit (Table 4.1). The authors discussed the possible chrono-stratigraphic models for those 2 MSC units in the CMD (see their figure 12). They question whether the SU, being older than the BU, could be synchronous or could post-date the emplacement of the PLG of the Palma Basin. Based on low-resolution high-penetrative seismic profiles, Maillard et al. (2014) also argued that the salt layer in the CMD might be thicker than what is observed on the high-resolution seismic lines. Another salt unit is recognized in the southernmost part of Formentera

sub-basin (Figure 4.3-A, B and Figure 4.5-D; Driussi et al., 2015). It is lying on a present-day depth of ~450m below seafloor, whereas the salt in the CMD lies on 520m below seafloor.

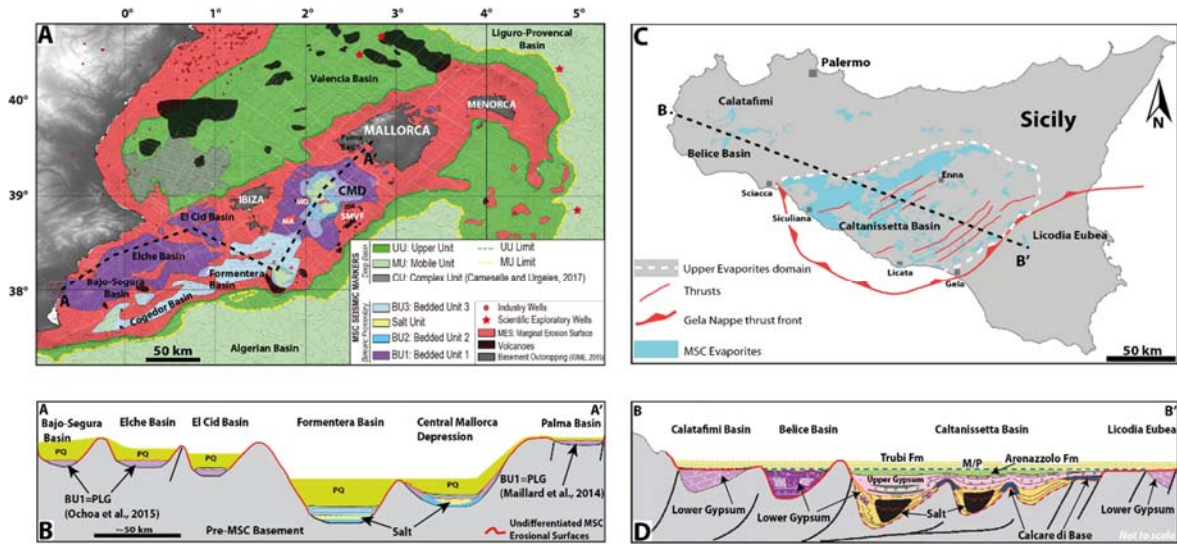


Figure 4.3. A: Map showing the present-day extent of the MSC units in the Balearic Promontory (BP) and the surrounding deep basins. Light grey lines are isochrones (every 200ms TWTT) of the offshore depth of the base Plio-Quaternary unit. Black dotted line shows the position of the section shown in 4.3-B. Thin white lines in the background are the positions of the seismic profiles used for the interpretation. MA=Mount Auzias; MO=Mount Oliva; SMVF=South Mallorca Volcanic Field; CMD=Central Mallorca Depression. Note that on the BP salt units are present in different perched basins (CMD, Cogedor Basin and Formentera Basin) lying at different depths. Notice also that bedded unit (BU1) extension in Elche and Bajo Segura basins is more important than what has been mapped by Driussi et al. (2015). B: Schematic profile across the perched basins of the BP showing the present day setting of the different bedded and salt units overlain by the PQ unit; the colors of the MSC units are the same used in 3A's legend. The pre-MSC basement was drawn from the compilation and mapping of the Base Messinian horizon from the seismic dataset. Black dotted line shows the position of the section shown in 4.3-D. PQ= Pliocene-Quaternary unit. C: Simplified map of the extent of the MSC evaporitic sediments in the different Sicilian basins (modified from Caruso et al., 2015). D: Schematic geological cross section across the Sicilian MSC basins showing the settings of the evaporitic units filling the sub basins topped by the base Pliocene Trubi sediments (modified from Roveri et al., 2006). Notice how in both the BP and Sicilian basins, the different sedimentary units belonging to the MSC are contained in a series of sub-basins lying at different depths with only the deepest basins containing salt.

Lofi et al. (2011a, b)	Maillard et al. (2014)	Driussi et al. (2015)	Ochoa et al. (2015)	Roveri et al. (2019)	This study
BU	BU	Ft	BU	BU - RLG	BU3
	Salt	Salt	Salt	Salt	Salt
	SU	MSC unit	BU - PLG	BU - PLG	BU2
					BU1

Table 4.1. Synthesis of the Messinian units in the Balearic Promontory from all the offshore studies dedicated to the MSC.

Onland Mallorca, the MSC record is expressed by the Santanyi limestones, that represent the Terminal Carbonate Complex (TCC), made of carbonatic microbialites, oolites and marls (Mas Gornals & Fornós, 2012). These authors suggest that the TCC is the lateral time equivalent of the PLG drilled in the bay of Palma. None of the boreholes drilled onland Mallorca records the TCC and PLG together (Baron & Gonzalez, 1985), which supports this interpretation. Overlying the TCC, and below the lower Pliocene sediments, a lacustrine-continental sedimentary unit known as the Ses Olles Formation that contains brackish to fresh water faunal assemblages, thus interpreted as representing the Lago Mare episode (Mas Gornals & Fornós, 2013). According to these authors the Lago Mare unit is cut by an erosional surface created during the major base-level drawdown, suggesting that the Lago Mare phase is related here to stage 1 of the MSC. This is not in agreement with the current crono-stratigraphic model (CIESM, 2008a; Roveri, Flecker, et al., 2014a).

Onland Ibiza, Late Miocene units outcrop only locally and show common characteristics with units known in Mallorca, such as the reef complex or a unit interpreted as the TCC (Durand-Delga et al., 1993; Pomar et al., 1996; Lezin et al., 2017). Important continentalization episode has been recently identified on top of these units with erosion and karstification, paleosols and gravity-driven instabilities that are thought to record the major sea-level fall (Odonne et al., 2019; Maillard, Gaullier, et al., 2020a).

4.2.2 The Sicilian Central Caltanissetta Basin: Geological context and MSC

Unlike the BP, the Sicilian Basins have been very active tectonically since the MSC.

Belonging to the Central Mediterranean domain, Sicily's structural and geological evolutions derive from the convergence between the African continental margin and the Eurasian plate (Catalano et al., 2012; Henriquet et al., 2020).

During the lower Miocene, the SE-wards shift of the Calabrian accretionary wedge above the slab, including AlKaPeCa blocks (i.e. Alboran, Kabylies, Peloritani, Calabria; Bouillin et al., 1986), lead to the growth of the Sicilian collisional complex (Catalano et al., 1996). The latter corresponds to a well-exposed fold-and-thrust belt (FTB) (Albanese & Sulli, 2012), the Maghreb-Apennine thrust belt, crossing from east to west the Sicily Island with the Gela Nappe along the thrust front (Lickorish et al., 1999).

The Caltanissetta Basin, located in the arcuate part of the Gela Nappe (Figure 4.3-C), represents the main foredeep of the frontal thrust belt system (Butler & LICKORISH, 1997). It consists of a single thrust sheet and comprises a series of continuously tightening folds (Lickorish et al., 1999). Its late Neogene evolution is related to the opening of the Tyrrhenian Sea (KASTENS et al., 1988). The CB is organized in an alternation of depocenters and highs that are mostly related to active thrusting synclines (Grasso & Butler, 1991; Butler et al., 1995; Catalano et al., 2012).

During the MSC, evaporites including halite were deposited in the CB and are mostly outcropping today, which made it a reference basin for the study of the MSC event. A complete sequence has been also found in a great number of cores in the CB, where the sequences are schematically formed of Tripoli Formation (30-90m), Calcare di base alternated to primary selenitic gypsum (> 300 m), halite and kainite (~ 500m) and Upper Gypsum (100-200m) (Rouchy and Caruso, 2006; Caruso et al., 2015). This tripartite character of the MSC sequence recalls the deep basin trilogy, thus the MSC succession of the central Sicilian CB was initially assimilated to an uplifted part of the deep basin succession, although not necessarily as the deepest areas (Decima & Wezel, 1971; Hsu et al., 1978; B. C. Schreiber, 1978; ROUCHY, 1982; J. Rouchy & Saint Martin, 1992; Garcia-Veigas et al., 1995; Clauzon et al., 1996b; J. M. Rouchy & Caruso, 2006). However, different opinions exist about the marginal vs. deep basinal character of Sicily during the Messinian (Butler et al., 1995; Clauzon et al., 1996; Krijgsman, HILGEN, et al., 1999; Krijgsman, Hilgen, et al., 1999; Clauzon et al., 2005) which resulted in

a number of chrono-stratigraphic models and related MSC scenarios (Figure 4.4-E to G; e.g. Decima & Wezel, 1971; Garcia-Veigas et al., 1995; Butler et al., 1995; J. M. Rouchy & Caruso, 2006; Roveri et al., 2008). Recently, some authors classified the CB as an intermediate basin with a complex stratigraphy as a result of its growth on an orogenic wedge (Roveri et al., 2008a; Roveri, Lugli, et al., 2014).

According to the mentioned works, the MSC deposits in CB (Figure 4.4-D) can be summarized as follows:

- Lower Evaporites (LE) or Lower Gypsum (LG) (Decima & Wezel, 1973b): this unit is made of massive bedded gypsum intercalated with clay beds with a thickness up to 140m (Lugli, Vinicio, et al., 2010). Roveri et al. (2006) divided this unit into primary PLG and resedimented RLG. The PLG consists of thick selenitic gypsum beds that vary from large massive selenites to gypsarenites, separated by thinner organic-rich shale horizons. The change in facies inside each cycle is thought to reflect the passage from arid to humid phase at the insolation minima and the insolation maxima respectively at a precessional scale (Lugli, Vinicio, et al., 2010). The PLG in the Sicilian MSC basins (Figure 4.6-A to C) records the same cyclicity (up to 13 cycles; Figure 4.6-C) as other PLG found in other marginal basins such as Sorbas Basin and the northern Apennines. According to Lugli et al. (2010) the cyclicity encountered in the PLG reflects the paleo-depositional environment, suggesting a general shallowing-upward trend with a change in the general hydrology of the basin. Moreover, these authors state that in the Sicilian Basins, PLG is found exclusively in silled shallow basins (<200m depth) at the borders of the main foredeep depression and has been deposited during stage 1 of the MSC (CIESM, 2008a), whereas the lateral equivalent of the PLG in the deeper parts of the basins is represented by levels of marls, diatomites and thin laminated dolostone (calcare di base 2, see next paragraph) ~20m thick (Manzi et al., 2011). The base of the PLG unit is conformable with pre-MSC deposits, whereas its top is cut by an erosional surface (Figure 4.6-A to C).

The RLG, bounded by the regional MES at the bottom (Roveri et al., 2008b), is found in the main foredeep. It consists of resedimented gypsum that varies from huge and undeformed PLG blocks to gypsarenites and gypsum laminates that has been re-deposited during stage 2 of the MSC. There is a controversy of whether the origin of the RLG is related to the combination of salt deformation followed by collapse

dissolution (J. M. Rouchy & Caruso, 2006) or due to sub-aqueous gravity flows in the foredeep due to erosion or thrusting of large PLG masses (Roveri et al., 2008b).

- **Calcare di Base (CdB):** this unit is made of complex carbonate formation with different facies (Decima et al., 1988; J. M. Rouchy & Caruso, 2006; Ziegenbalg et al., 2010) that are found most commonly on structural highs separating perched basins. The most widespread facies are m-thick micritic limestones (calcite and/or aragonite) of evaporative and/or bacterial origin, often found as brecciated deposits and interbedded with shales and clastic gypsum (Caruso et al., 2015; Perri et al., 2017). The CdB shows common unfossiliferous and evaporitic character marked by halite and gypsum pseudomorphs (Ogniben, 1957; PEDLEY & MANISCALCO, 1999), which suggest a shallow depositional environment close to the coastline (Butler et al., 1999; Suc et al., 1995). However, the origin and the position of the carbonates belonging to the CdB is still very highly debated. Caruso et al. (2015) consider the CdB as the lateral equivalent to the PLG, slightly diachronous, thus formed during stage 1 of the MSC. These authors argue that the transition from the pre-MSC sediments (Tripoli Formation) to the CdB is continuous without any evident unconformity and they relate the brecciation process observed to local collapses with limited transport.

On the other hand, Manzi et al. (2011) divided the CdB into 3 different types, with only type 2 (primary dolomitic limestones) belonging to the first stage of the MSC. Whereas CdB types 1 and 3 belong to the second stage of the MSC, with type 1 formed as the diagenetic product of bacterial sulfate reduction (BSR) of original clastic gypsum in presence of hydrocarbons, and type 3 made of brecciated limestones that formed due to regional mass transports.

- **Salt:** this unit is made mainly of halite and even large amounts of K-Mg salts and it is found mainly in the central CB (Figure 4.4-D), where its thickness reaches 400-600m at the Realmonte mine (Decima & Wezel, 1971, 1973b; Lugli et al., 1999b). There, it shows a clear shallowing upward trend until reaching an exposure surface (Figure 4.4-E to G and Figure 4.7-B) expressed by ~1.5m desiccation cracks (Lugli et al., 1999b), which suggest that the salt deposition started in a deep stratified water body that experienced a drawdown until the subaerial exposure and truncation (Lugli et al., 1999b; B. Schreiber et al., 2006). It is also characterized by a very high frequency halite-clay cyclicity (cm to dm thick) that has been correlated to Quasi-Biennial

Oscillation, the El Nino Southern Oscillation, the sunspot number solar cycle and lunisolar tidal cycle (Manzi et al., 2012). The precession cycles of the deep basin salt of the eastern Mediterranean suggested by Manzi et al. (2018) and more recently by Meilijson et al. (2019) have not been observed in the salts of the CB.

- Upper gypsum (UG) or Upper evaporites (UE): like the salt, this unit is present mainly in the CB (Figure 4.4-D) where it can reach thicknesses up to 300m. The most complete section outcrops at Eraclea Minoa along the south-western coast of Sicily (Figure 4.8-C). It is made of a rhythmic alternation of clays and marls interbedded with sandy and fine grained carbonates and seven gypsum bodies made by multiple strata of finely-laminated gypsum (balatino) and gypsarenites/selenites (Caruso & Rouchy, 2006; Grossi et al., 2015).

The chrono-stratigraphic tuning of the UE differs between the different authors. J. M. Rouchy & Caruso, (2006) recognized 6 precession-driven sedimentary cycles, with a possible 7th basal cycle, represented by a deformed gypsum deposit overlaid by the Arenazzolo sandstones (see next paragraph, Arenazzolo member). The Arenazzolo/Trubi contact marks the Messinian/Zanclean boundary (GSSP at Scala dei Turchi - Eraclea Minoa) and the return to normal marine conditions (Van Couvering et al., 2000; Pierre et al., 2006). Whereas Manzi et al. (2009) interpreted nine to ten sedimentary cycles, including the Arenazzolo member. According to these authors, each one of the cycles reflects oscillations in the basin's base level and its water concentration associated to transitions from wet to dry environments, marked by an erosional surface at the end of each cycle. However, there is a disagreement about whether these oscillations started with brackish conditions (e.g. Decima & Wezel, 1971) or with marine conditions (e.g. ROUCHY, (1976) and then evolved to hyperhaline conditions. For Rosell et al. (1998) the primary selenitic crystals on the top of each cycles reflect marine conditions, whereas Butler et al. (1995) considered them as salt-lake deposits. Londeix et al. (2007) suggested that the pollen content of the clay layer, preceding the last gypsum bed of the different cycles at Eraclea Minoa, indicates variable conditions that vary from distal to coastal. The base of the UE is marked by an unconformity (Decima & Wezel, 1973b; Butler et al., 1995; Garcia-Veigas et al., 1995). The UE lie on the salt in the distal part of the basin, whereas towards the proximal parts it shows onlap terminations on the underlying unit (ie. LE and/or CdB), where the

terrigenous content decreases and becomes enriched in coarser material, due to changes in the fluvial discharge and drainage (Roveri et al., 2008b).

- Arenazzolo member: this unit overlays the UE and is topped by the Pliocene marking the Messinian/Zanclean contact. It comprises a stratified arkosic sand with alternating thin layers of different grain-size which yielded a well-diversified fauna corresponding to brackish-water ostracods species (Lago Mare), mostly of Paratethyan origin (Bonaduce & Sgarrella, 1999; J. M. Rouchy & Caruso, 2006). Some authors distinguished the Lago Mare unit from the Arenazzolo member with the later lying unconformably on the earlier (CITA & COLOMBO, 2006; Bache et al., 2012). According to these authors there is a transition in the depositional environment from brackish shallow-water conditions during the Lago Mare to a high-energy littoral environment. Above the Arenazzolo lies unconformably the Trubi Formation that reflects open deep-water condition as shown by foraminiferal fauna (CITA & COLOMBO, 2006; Pierre et al., 2006) and dinoflagellate cyst flora (Londeix et al., 1999, 2007). Bache et al. (2012) suggested a 2 step reflooding after the MSC acme in order to explain these transitions.

In this paper, for our comparison with the CMD record, we will be focusing mainly on the Caltanissetta Basin where most of the stratigraphic models of the MSC are based on (Figure 4.4). In particular we will consider the geometries, facies, distribution and thickness of the MSC units.

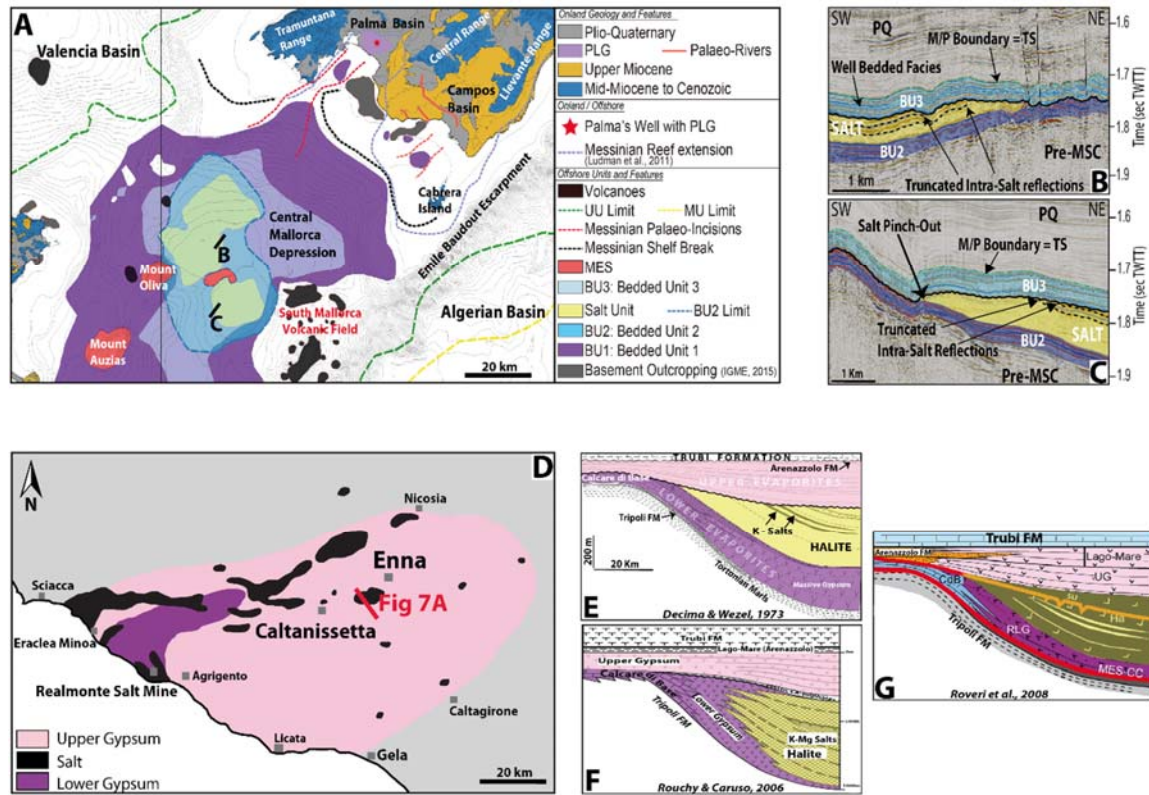


Figure 4.4. A: Detailed map of the MSC units and features in the Central Mallorca Depression (CMD). Note how the salt in the depocenter of the depression is distributed in 2 patches separated by a local topographic high. Isobaths (every 50m) represent the present-day bathymetry. Onland geology mapping of south Mallorca and North Ibiza is modified from geological map of Spain 1:50000 (IGME). Volcanoes and outcropping basement are from the geological map of Spain 1:1000000. BU1-PLG unit in the Palma Basin is mapped after Maillard et al. (2014). B-C: Parts of seismic profiles illustrating the geometrical relationship between the MSC units in the CMD: they show how the salt is lying between two MSC bedded units (BU2 and BU3) and contains internal reflections truncated at the top by an erosional surface. D: Map showing the distribution of the evaporitic units in CB (modified from Caruso et al., 2015). E-G: Sedimentary models showing the settings and geometrical relationships of the MSC evaporites in the CB published by different authors since the beginning of the studies of the MSC in that area (modified from Decima & Wezel, 1973; J. M. Rouchy & Caruso, 2006; Roveri et al., 2008b). Note how in both study areas the settings and the geometrical relationships between the sedimentary units are similar, where we have a salt unit eroded at the top and sandwiched between two other units belonging to the MSC.

4.3 Data and Methods

In this study we use a series of 2-D seismic reflection profiles covering the whole BP area with the highest density of data in the CMD compared to the other sub-basins (Figure 4.2). Part of this dataset consists of low-resolution seismic lines including old oil industry data that has been recently re-processed, provided by Spectrum Company, with a standard processing flow until

pre-stack time migration. Other old non-reprocessed seismic data was also provided by the Instituto Geologico y Minero de Espana (IGME). The high-resolution seismic lines are mainly covering the CMD and have been acquired during the SIMBAD survey (Maillard & Gaullier, 2013). High- and low-resolution lines were crossed for a better recognition, interpretation and mapping of the MSC units and surfaces.

The interpretation of the profiles was performed using the software Petrel® by Schlumberger®. Analysis of the seismic profiles following a seismic stratigraphic procedure in terms of reflection terminations, erosional truncations, onlaps, downlaps and configurations, allowed the identification of seismic units and their boundaries (Mitchum & Vail, 1977). The seismic horizons were then exported in digital format and imported to the geographic information system QGIS for the mapping of the MSC markers.

For the MSC seismic units and surfaces we adopt the nomenclature proposed by LOFI, (2011) and Lofi et al. (2011).

The mean acoustic velocities used for the time-depth conversion and thickness estimates are: 1500 m/s for the seawater; 2300 m/s for the Pliocene-Quaternary sequence derived from detailed curves based on wells (Maillard et al., 2014; Driussi et al., 2015 and references therein); 4500 m/s for the MSC pre-halitic unit (bedded units BU1 and BU2), based on the sonic log data tied to seismic profiles from Ochoa et al. (2015); 4780 m/s for the salt unit, based on laboratory measurements done on samples of halite from the MSC salts from Sicily published by Samperi et al. (2020); 3500 m/s for the MSC post-halitic bedded unit (BU3) assuming that it contains more terrigenous sediments than the pre-halitic bedded units (see results and discussion for more details).

4.4 Results: MSC markers of the CMD/BP

Seismic units and their bounding surfaces are well expressed and preserved in the CMD (Figure 4.5-B, C). Four MSC seismic units and several conformable or unconformable bounding surfaces were identified from high-resolution seismic profile's interpretation, based on their seismic facies and on their geometrical and seismostratigraphic positions and relationships.

They are described hereafter.

4.4.1 Bedded unit 1 (BU1)

This unit is widespread, mainly on the present-day shelves and slopes of the BP, ranging from a minimum present-day depth of ~170m below sea level beneath the shelves to a maximum of ~1200m beneath Mallorca slope (Figure 4.3-A and Figure 4.5-C, SP 2077). Its extension has been underestimated in previous studies (Driussi, Maillard, et al., 2015b; D. Ochoa et al., 2015c), as our new seismic dataset shows its wider presence on the Alicante shelf and on the shelf between Menorca and Mallorca islands. On oil industry profiles, BU1 is contained in 1 or 2 reflections, whereas on high resolution seismic profiles, it is made of up to 8, medium to high-amplitude, relatively low frequency, reflections (Figure 4.6-D to F). In the proximal domain, BU1 is overlain by the lower Pliocene unit and underlain by pre-MSC units (Figure 4.5-A, SP 791 to 1266; Figure 4.5-C, SP 1 to 662), respectively made of very low and low amplitude reflections. In more distal domains, BU1 is overlain by another MSC unit (BU3, described later in this section) and still underlain by pre-MSC sedimentary unit (Figure 4.5-A, SP 146 to 791; Figure 4.5-B, SP 150 to 833; Figure 4.5-C, SP 1016 to 2077).

The upper boundary of BU1 is marked by a regional erosional surface (TES or IES) (Figure 4.5-A, SP 791 to 1266; Figure 4.5-C, SP 309 to 2077; Figure 4.6-D to F) evidenced by truncated reflections (Figure 4.6-F). This erosion locally draw ~10 to 30ms TWTT deep V to U-shaped incisions (Figure 4.5-C, SP ~1500). The lower boundary of BU1 is generally concordant with the underlying pre-MSC units (BS), except locally, where the unit is internally deformed with an apparently unconformable base, probably due to seismic artefacts (Figure 4.6-E). Both the upper and the lower boundaries show an abrupt amplitude change, evidencing high impedance contrasts between the BU1 and the overlying Pliocene and underlying pre-MSC units (Figure 4.5-A to C and Figure 4.6-D to E).

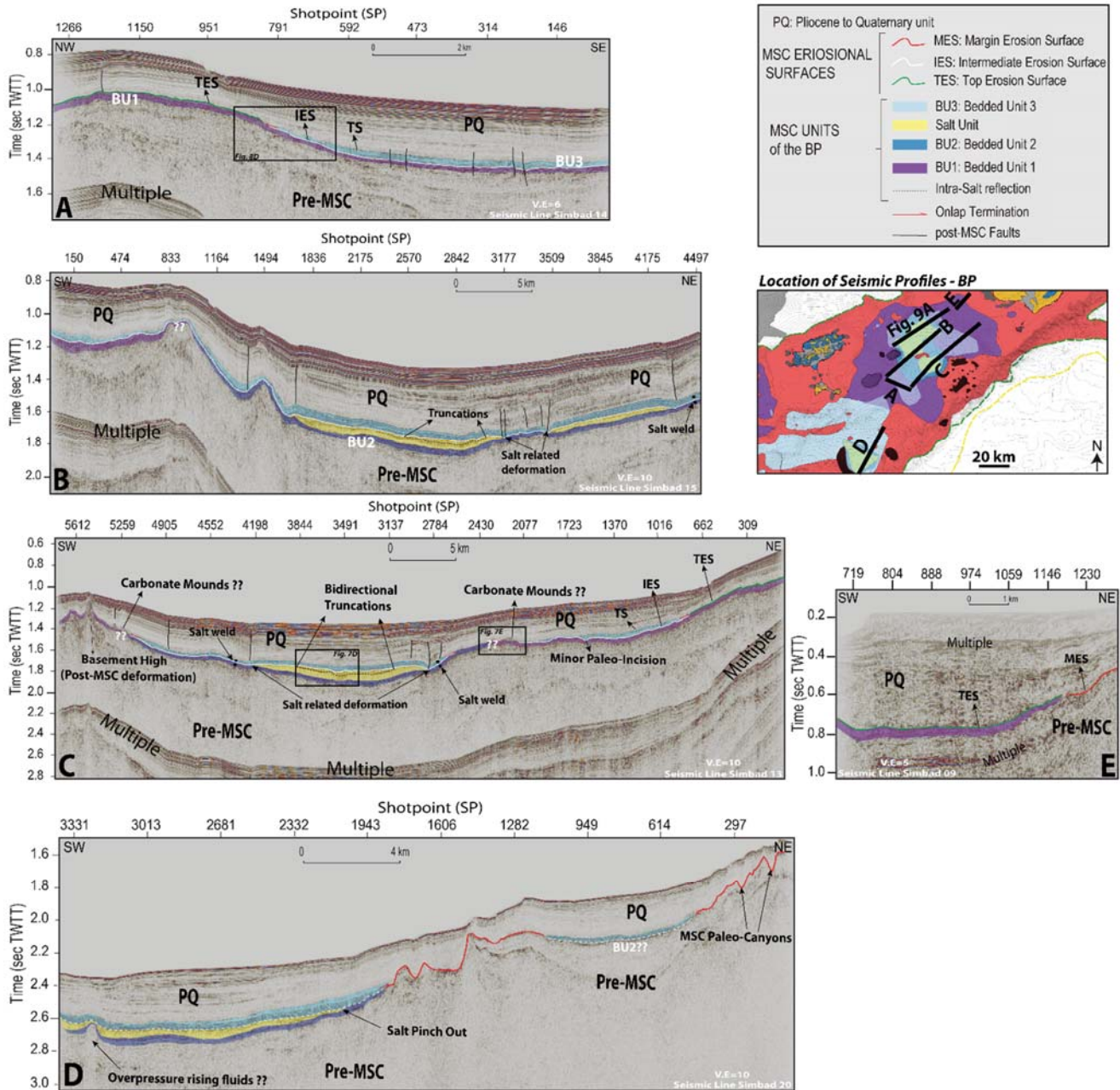


Figure 4.5. Seismic profiles covering different parts in the BP area. A: interpreted seismic profile Simbad 16 imaging the MSC seismic units in the southern part of the CMD, at the base of the Ibiza slope, where BU3 onlaps BU1. B-C: Interpreted seismic profiles Simbad 15 and Simbad 13 crossing the depocenter of the CMD showing all the MSC units and erosional surfaces. Note the bilateral truncation of the internal reflections intercalated in the salt unit due to an erosional event. D: Interpreted seismic profile in the southern depression of the Formentera Basin showing the presence of salt lying between 2 bedded units. E: Part of interpreted seismic profile Simbad 09 showing the thinning of BU1 passing into a Marginal Erosional Surface (MES) on the present-day southern shelf of Mallorca

BU1 is characterized by several internal seismic facies alternating high amplitude continuous parallel reflections (bedded facies) (Figure 4.6-D, F; Figure 4.6-E, SP 1376 to 1565) and medium amplitude deformed reflections (chaotic facies), observed especially on the slopes (Figure 4.6-E; SP 1565 to 1908). Reflection free facies is also locally found.

The thickness of BU1 is relatively constant along the BP (Figure 4.6-D to F), with an average thickness of ~ 110m. It is thinner (~60m; Figure 4.5-E) near the coastline of Mallorca, between Palma and Campos Basins, as a result of the partial erosion of the unit. Where not/slightly eroded or deformed, BU1 reaches a thickness of up to ~130m on the slopes (Figure 4.6-E, SP 1467). BU1 is however, most of the times, absent on the shelves where only the MES is observed (Figure 4.3-A and Figure 4.4-A; Figure 4.5-E, SP 1230). BU1 apparently thins out downslope (Figure 4.5-A, SP 592 to 1150), but its lateral continuity is unclear (Figure 4.7-E). On the seismic profile Simbad 14 (Figure 4.5-A) however, it seems continuous downslope.

4.4.2 Bedded Unit 2 (BU2)

On oil industry seismic profiles it appears as a single reflection. On high-resolution profiles, it consists of up to 5 medium- to high-amplitude, relatively low frequency reflections. BU2 is overlain by the salt unit (see description of this unit later in this section) in the depocenters (Figure 4.5-B, SP 1836 to 4497; Figure 4.5-C, SP 2784 to 4198; Figure 4.5-D, SP 1943 to 3331), whereas on the slopes, where there's no salt, it is lying below another MSC unit, labelled BU3 (Figure 4.5-B, SP 833 to 1823; Figure 4.5-C, SP 4198 to 5259). BU2 is everywhere lying above pre-MSC sediments (Figure 4.5-B to D).

In relatively proximal zones, the upper boundary of BU2 appears to be an erosional surface with some incisions (~5-10ms TWTT; Figure 4.9, SP 991), whereas in the deeper depocenters it is conformable with the overlying salt unit (Figure 4.5-B, SP 1836 to 2842). The lower boundary of BU2 is concordant with the pre-MSC units, but the low acoustic impedance contrast between those units makes it difficult to firmly identify the base of BU2.

The internal reflection pattern of BU2 is characterized by parallel reflections laterally continuous in the distal domain but their lateral continuity weakens moving towards the proximal domain (Figure 4.5-C, SP 2430 to 5259).

The maximum observed thickness of BU2 is 50ms TWTT (~ 110m to 65m depending on its internal lithology; see discussion for details). This thickness may be underestimated as the base

of BU2 is uncertain, especially in the deepest part of the CMD. The lateral extent of BU2 toward shallower depths is also not clear and its relationship with the BU1 not properly imaged (Figure 4.7-E). It is not excluded that BU2 could be the distal continuation (and thus the time equivalent) of BU1, accumulated in a more proximal domain (Figure 4.5-C and Figure 4.9-A), but additional profiles would be needed to confirm this geometry.

Figure 4.5-C (SPs 2077 to 2430; SP 5259) features an approximately 1.5km wide mounded structure overlain by the lower Pliocene and apparently lying directly above BU1 (Figure 4.7-E). It is observed on the borders of the depocenter, close to the pinch-out of BU3. The seismic signal around this feature does not allow us to figure out if any of the BUs has onlap termination on the structure. Onlap terminations and draping of the base reflections of the PQ unit on this mounded feature can be observed.

4.4.3 Salt Unit

This unit displays a classical dominantly reflection free (transparent) facies (e.g. LOFI, 2011; Lofi et al., 2011). Internal low-amplitude low-frequency continuous reflections are commonly observed in this unit (Figure 4.5-B, SP 2570 to 3177; Figure 4.5-C, SP 3137 to 3844; Figure 4.9-A, SP 1274 to 2122). The salt unit lies everywhere below BU3 and above BU2 (Figure 4.4-B and C; Figure 4.5-B to E).

The upper boundary of the salt is an unconformable surface marked by a truncation of the topmost internal reflections (Figure 4.4-B, C; Figure 4.9-A). The base of the salt is clearly concordant with BU2.

Its maximum thickness is ~240m, reached in the deepest part of the CMD.

The base of the salt (top BU2) remains locally uncertain because of the poor imaging below the salt on high-resolution seismic data, but crossing with confidential re-processed oil industry profiles confirmed its location at 1.8 - 1.9 sec TWTT in the CMD (Figure 4.5-B, C) and not deeper as questioned by Maillard et al. (2014). Toward the borders, the salt thins out as a wedge. Due to the ductile deformation of the salt, its pinch-out termination is often associated with listric faults and brittle deformation of the overlying BU3 and PQ units (Figure 4.5, SPs 1836, 3177 and ~4250). These listric faults, together with the deformation of the units overlying the salt, suggest that originally the salt extension was locally wider, and that it later glided towards the depocenter, leading to formation of salt welds (Figure 4.5-C). Moreover, the current thinning of the salt (wedge geometry) towards the borders of the salt basin is not an

expression of progressive onlap of younger layers. It results from an erosion evidenced by the truncation of the intra-salt reflections, more and more into deeper (older) levels towards the margin.

Seismic profile Simbad 13 shows that the top of the salt exhibits locally a concave U-shaped depression lying above down-warped internal seismic reflections (Figure 4.5-C, SP 3491). The relief extends for about 1.5 km horizontally along the seismic profile. Down-warped reflections are also observed in the BU3 and PQ deposits overlying the depression but the deformation is progressively attenuated upwards (Figure 4.7-D).

4.4.4 Bedded Unit 3 (BU3)

On oil industry profiles it is made of 2 reflections, whereas on high resolution profiles it consists of up to 9 low- to medium-amplitude, high frequency reflections (Figure 4.8-F). BU3 is everywhere conformably overlain by the lower Pliocene. In proximal domains, it unconformably overlies either the MES (Figure 4.5-D, SP 1943) or BU1 or BU2 (Figure 4.5-A, B). Internal reflections of BU3 show onlap terminations on the erosion surface (IES) bounding above BU1/BU2 (Figure 4.8-D, E). More distally, in the depocenters, BU3 conformably overlies the salt unit (Figure 4.5-A to D and Figure 4.8-D, E). On the border of the salt basin, BU3 is often affected by brittle deformation related to the ductile deformation of the underlying salt (Figure 4.5-C, SPs 2784 and 4198).

The spatial extent of BU3 is limited to some of the BP sub-basins (Figure 4.3-A). BU3 shows no lateral continuity or geometrical connection with the UU accumulated in the deeper basins surrounding the BP (Figure 4.3-A).

The internal facies of BU3 consists dominantly of parallel and clearly continuous reflections in the distal part of the CMD and Formentera Basin (Figure 4.5-A to D and Figure 4.8-F). It becomes hummocky and relatively chaotic towards the proximal areas (Figure 4.8-E). In shallower sub-basins, such as El Cid and Cogedor Basins, BU3 overlies BU1 and appears as a very thin unit, with less beddings and irregular top (Figure 4.6-D, SP 3848).

The thickness of BU3 is variable. In the CMD it reaches a maximum thickness of ~120m in the structural lows and/or in flat regions at the foot of slopes (Figure 4.8-F). In the southwestern basins of the BP, e.g. El Cid Basin, BU3 appears very thin on high-resolution seismic lines and thus cannot be distinguished from BU1 on the low-resolution seismic lines. Consequently, its

presence might be underestimated in the south-western part of the BP, where we have scarce high-resolution seismic coverage (Figure 4.3).

The PQ unit overlies BU3 in the distal domain (Figure 4.5-B to D). In proximal domains it overlies BU1 where present (Figure 4.5-E, SP 719 to 1146) or the MES where BU1 is absent (Figure 4.5-D, SP 297; Figure 4.5-E, SP 1230). The basal part of the PQ unit is characterized everywhere on the BP by a very low amplitude reflectivity (Figure 4.5 and Figure 4.6-D to F), except locally (e.g. Figure 4.5-B, SP 3845). The pattern of the basal reflections of the PQ unit in the CMD shows a clear sheet-like shape, draping the topography of the underlying Messinian units (Lüdmann et al., 2012). On the Mallorca slope it is deformed by the post-MSC gliding affecting BU1 (Figure 4.6-E; Maillard et al., 2014).

4.5 Interpretation/Discussion

4.5.1 Sicily vs Balearic Promontory: depositional units, surfaces and geometries

Several sedimentary models were proposed to account for the MSC deposits observed in the Sicilian Basins (Figure 4.4-E to G), starting from the oldest models by Decima & Wezel, (1971) and Garcia-Veigas et al. (1995), to more recent models by J. M. Rouchy & Caruso, (2006) and Roveri et al. (2008b). In all these models the depocenter of Caltanissetta Basin contains a halite unit sandwiched between two MSC units, the LE and the UE. Our seismic observations evidence that the MSC units in the BP, especially in the CMD, show a similar configuration: in the depocenter there is a salt unit (Figure 4.4-A) sandwiched between two other MSC units, BU2 below and BU3 above (Figure 4.4-B, C).

The distribution of the MSC deposits in Sicily has been described schematically by Roveri et al. (2006) (Figure 4.3-D). In their model, only the marginal sub-basins such as Calatafimi Basin contain in situ PLG deposited in shallow context, whereas deeper basins such as Belice Basin contain only RLG (Figure 4.3). The even deeper sub-basins of Caltanissetta are the only basins where salt and the upper evaporites are found (Figure 4.3-D and Figure 4.4-D). A very similar distribution is remarked in the BP, where the shallow perched sub-basins usually contain exclusively BU1, locally topped by a very thin BU3 with an irregular but non-erosional top

(Figure 4.6-D). The deeper sub-basins (Formentera Basin; Figure 4.5-D and CMD; Figure 4.5-B, C) contain BU2 and a thick BU3, together with the salt unit in between (Figure 4.3-A).

Herein we discuss a possible analogy between Messinian Sicilian basins and BP sub-basins, assuming that the MSC seismic units of the BP, described in the previous section, could be the equivalent of the Sicilian MSC units described in section 4.2.2.

Observations of Messinian sub-basins from both BP and Sicily show a high analogy between the evaporitic units in terms of geometry, facies and distribution. In our comparison we will focus mainly on the CMD and CB.

4.5.1.1 Geometry Similarities:

- a- In the north-eastern part of the CB, seismic profiles imaging MSC sediments in a relatively undeformed or slightly deformed perched sub-basin (Figure 4.9-B, C), show that this depression has a concave-like geometry. The MSC unit is thicker in the depression's depocenter and includes salt, whereas towards the borders of the depressions, the salt pinches-out and there is a notable thinning of the MSC units. This geometry is very similar to the one observed in the CBD (Figure 4.5-C and Figure 4.9-A).
- b- The top of the PLG in Sicily is cut by a regional erosional surface in the shallower parts of the basins (Figure 4.6-A, C) and is locally overlain by the lower Pliocene Trubi Fm. Similarly, in the proximal part and the slopes of the BP, the top of BU1 is cut by a regional erosional surface (TES in Figure 4.6-E) and is overlain by the lowest Pliocene unit.
- c- Towards the depocenter, in the CB, the UE overly the LE and the contact between those 2 units is often marked by an erosional surface (Figure 4.8-A, B; and Roveri et al., 2019). In the distal areas of the BP, BU3 overlies BU1 and the contact between the two units is also erosional (IES in Figure 4.8-D, E).
- d- The MSC salt in the CB is lying between 2 units (i.e. LE and UE; Figure 4.4-E to G and Figure 4.7-A) and is found in the depocenters. Towards the margins, the salt unit pinches out where LE and UE become in contact along an erosional surface. Exactly the same configuration is observed in the CMD, where the MU is underlain by

BU2 and overlain by BU3 in the depocenter (Figure 4.5-B, C). Toward the margin of the depression, the salt pinches out where BU2 and BU3 are in contact along an IES (Figure 4.4-B, C).

- e- In the depocenters of CB, the UE lie on the salt, where the transition is defined by a meter-thick laminar cumulate gypsum horizon (Figure 4.4-F). In a more proximal location, on the borders of the basin, clear onlap terminations of the UE against the LE (PLG and/or CdB) is observed (Figure 4.8-A, B; Decima & Wezel, 1971; J. M. Rouchy & Caruso, 2006; Roveri et al., 2008b).

A similar geometrical relationship exists in the CMD, where the post-salt BU3 lies above the salt unit (Figure 4.4-B, C) in the depocenter and onlaps BU1/BU2 (Figure 4.5-B, SPs 309 to 2077, and 4198 to 4905) in the proximal domains of the basin (Figure 4.5-A, SP 791; Figure 4.5-C, SPs ~800 and ~5100; Figure 4.8-D, E).

4.5.1.2 Facies Similarities:

a- PLG vs BU1

The PLG in the CB has been described and correlated across the Mediterranean by Lugli et al. (2010). It consists of processional driven cycles of primary gypsum separated by shale horizons. Ochoa et al. (2015) demonstrated that the BU1 of the Elche sub-basin also corresponds to the PLG. It is made of cyclical gypsum/marl alternations (up to 14 cycles; Figure 4.6-F) and displays a bedded seismic facies (see section 4.4.1, BU1), as expected from such internal lithologies. This bedded seismic facies is typical of the BU1 and is observed at the scale of the promontory, suggesting that BU1 is the equivalent of the PLG everywhere on the BP, and not only in the Elche Basin. The erosional surface at the top of BU1 (Figure 4.6-D to F) supports for its interpretation.

b- BU2 vs RLG

The RLG in Sicily consist of resedimented gypsarenites, gypsum laminates, and PLG gypsum blocks. As already discussed in section 4.2.2, the origin of the large dislocated blocks of RLG in the CB is controversial. However, both interpretations of RLG blocks imply an active syn-tectonic activity in the basin for the block-sliding. This is not the case in the BP, where the syn and post-tectonic movements are relatively negligible. In the MSC records of the BP, we thus do not expect the presence of large olistostromes,

which could have been at the origin of internal chaotic seismic facies as stated by Roveri et al. (2019). Thus, due to the geometrical position of BU2 below the salt, and the relatively continuous reflections it contains, it could be the equivalent of the RLG of CB made of gypsarenites and gypsum cumulates (sensu J. M. Rouchy & Caruso, 2006) resedimented from BU1 as well as primary. However, in the CMD, the relationship between BU1 and BU2 remains unclear. Both are clearly pre-dating the salt emplacement, and BU2 seems at least partly lateral time equivalent of BU1, but with a change in internal facies, that could be due to a change in the internal content in gypsum (Figure 4.5-B, C). At this stage, a firm link between BU2 and RLG is difficult to establish.

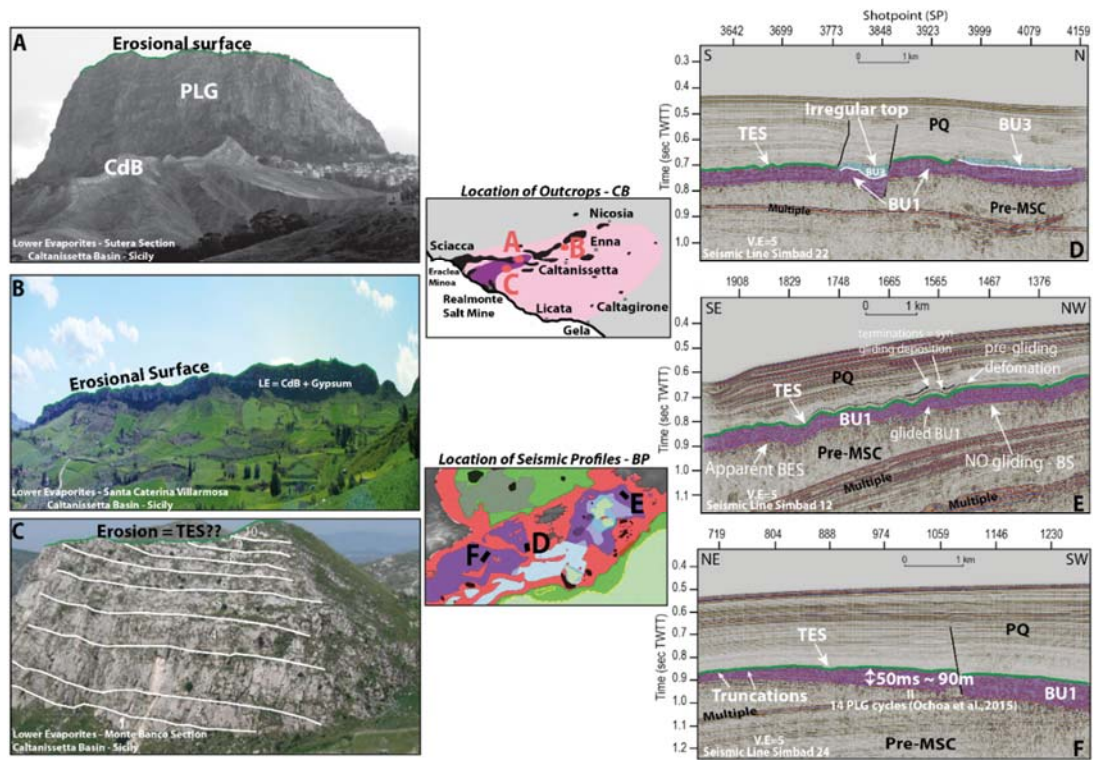


Figure 4.6. Figure illustrating the comparison between the Lower Evaporites (LE) and Bedded Unit 1 (BU1) in CB and BP, respectively, both belonging to stage 1 of the MSC. A: Lower evaporites section in Sutura (CB – Sicily) showing a Primary Lower Gypsum (PLG) eroded at the top by an erosional surface (TES?) (modified from Manzi et al., 2011). B: Section of Santa Caterina Villarmosa showing the LE unit, cut by an erosional surface. C: Monte Banco section made of up to 10 PLG cycles eroded at the top (modified from Bonanni, 2018). See Figure 4.4-D for the legend of the outcrops' location map. D: Interpreted part of seismic profile Simbad 22 showing the bedded facies of BU1 on the southern slope of Ibiza, where it is truncated at the top by the TES. Here another MSC bedded unit (BU3) appears to lie locally above BU1. The irregular top of BU3 is probably due to syn-depositional faulting. E: Part of interpreted seismic profile Simbad 12 showing different facies of BU1: its facies appears perfectly bedded when undeformed, whereas its facies becomes more chaotic when deformed by gliding. Note that the gliding affecting the unit is post MSC, which means it could not be compared to the RLG. F: Part of seismic profile Simbad 24 located on the Alicante Shelf of south-east Spain, showing BU1 abruptly truncated at the top and thinning due to erosion towards the NE. Note that the seismic facies and the thickness of BU1 is similar in all sub basins in the BP, suggesting that it is everywhere made of stage 1 PLG cycles truncated at the top. See Figure 4.3-A for the legend of the seismic profiles' location map.

c- MU vs Halite

The salt sequence in the CB consists mainly of Halite and K-Mg salts that show a clear shallowing upward trend until reaching an exposure erosional surface expressed by desiccation cracks (Figure 4.7-B; see section 3 and Lugli et al. (1999)). In the CMD the salt sequence is characterized by a globally transparent seismic facies with internal reflections in its upper part (Figure 4.4-B, C; Figure 4.7-D). Those intra-salt reflections suggest that it is not made of pure/unique salt. The uppermost reflection is truncated

abruptly at the top, which could be due to subaerial exposure or dissolution in shallow water. The erosional surface observed in the Realmonte mine of the CB (Figure 4.7-B) is found inside the salt unit and not at the top of it as in the salt observed in the CMD. The presence of a major erosion on the top of the salts in CB could not be excluded, as also described in the model of Decima & Wezel, (1973) (Figure 4.4-E). In fact, there could be several minor erosional/exposure surfaces inside the salt unit of the CMD as well, with only the major one visible at a seismic scale.

a- UE vs BU3

The thickness of the UE unit reaches its maximum in the depocenter of CB. Its sedimentary facies is characterized by thick mudstone, sandstone and marl intercalations (Figure 4.8-C; see section 4.2.2). Towards the margins of the basin this unit thins out until overlapping the LE, and the terrigenous layers tend to decrease and be rich in coarser material (Figure 4.8-A).

This is an adequation with the characteristics of BU3. This unit reaches its maximum thickness in the distal part of the perched basins, especially in Formentera Basin and the CMD (Figure 4.8-F) and thins out towards the proximal part of the basins (Figure 4.8-D, E), where it onlaps the underlying unit. Moreover, the seismic facies of BU3 changes laterally from the distal to the proximal domains, passing from a well bedded horizontal unit (Figure 4.4-B and Figure 4.8-F) into a more discontinuous, less bedded one (Figure 4.8-E). This facies change could be due to the finer granulometry of the clastic intercalations between gypsum beds in the depocenter (shales to sandstone?) and coarser grain in more proximal context (conglomerates?).

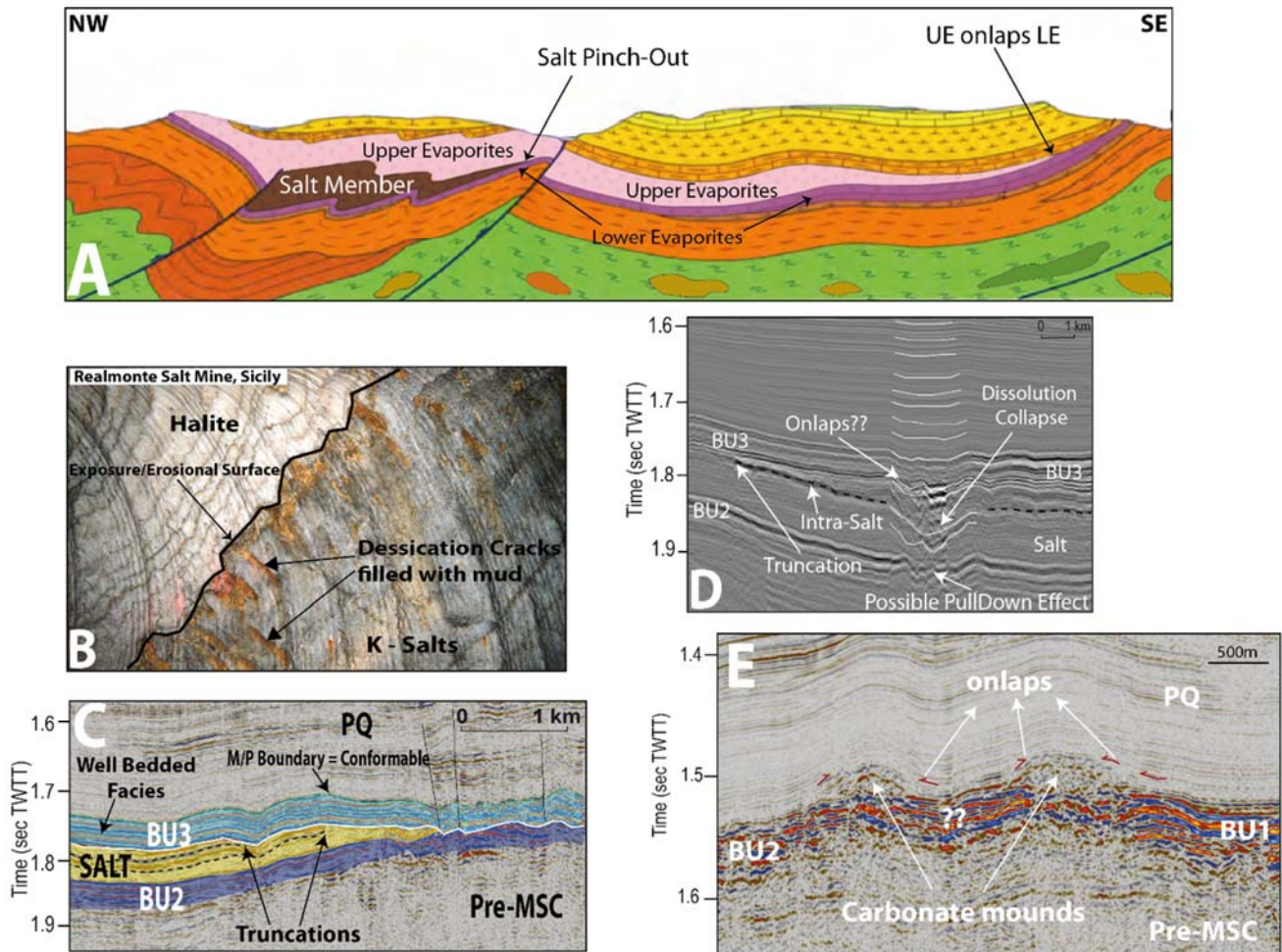


Figure 4.7. Figure showing the geometrical settings and facies of the salt unit in CB and BP. A: Geological cross section between the towns of Caltanissetta and Enna in CB (position in Figure 4.4-D; modified from Carta Geologica Italiana, Caltanissetta, foglio 631). The section shows how the salt formation (here deformed by regional tectonics) belonging to the MSC is lying in between the lower and upper evaporites in the center of the section and it pinches-out in NW and SE directions, where the LE and UE become in contact. Note the onlap of the UE on the LE in the southeastern border of the basin. B: The MSC salt at the Realmonite Mine, CB, Sicily, showing an exposure surface at the top of the K-Mg salts with the desiccation cracks and the passage to halitic salts. C: Part of the seismic line Simbad 15 showing the truncation of the internal reflections at the top of the salt and illustrating an erosional surface which we interpret as an exposure surface or a dissolution surface in shallow water. Note how the salt unit in the BP, equivalent to CB's salt, is sandwiched between two other MSC units in the central basin: where the salt pinches-out, the underlying BU2 and overlying BU3 units become in contact. D: Zoom from seismic profile Simbad 13, showing a concave feature on the top of the salt, and associated down-wrapped reflections below and above, possibly related to salt dissolution at depth and associated cover collapse. E: Zoom showing the facies of the interpreted carbonate mounds (see text for details). It also shows the uncertainty about passage from BU1 to BU2.

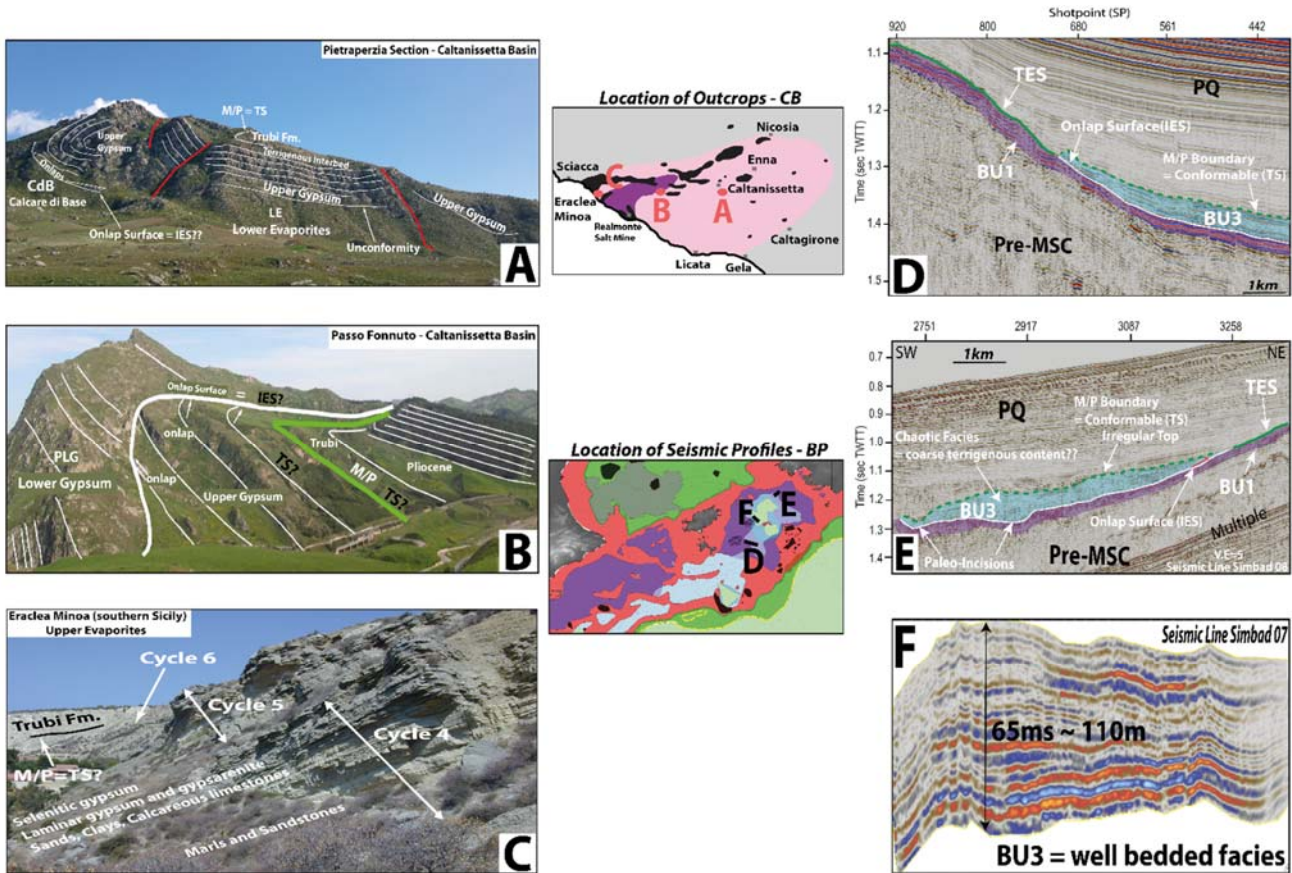


Figure 4.8. Figure showing the similarities between UE and BU3 in CB and CMD, respectively. A: Pietraperzia section (central CB – Sicily); Deformed upper gypsum cycles with terrigenous content in the uppermost cycle, showing onlap termination on the CdB along an erosional surface IES. B: Passo Fonnuto section (CB – Sicily; modified from Roveri et al., 2019); UE onlapping LE along an erosional surface. Note that the lower Pliocene formation (Trubi) is conformable with the UE (TS?). C: The upper evaporites cycles of the Eraclea Minoa section (CB – southern Sicily); the cycles are made of selenitic and clastic gypsum intercalated with levels of marls, limestones and clays. This facies is considered to be the most complete and has been deposited in the depocenter of the CB. For the legend of the outcrops' location map see Figure 4.4-D. D: Zoom from seismic profile Simbad 14 showing the onlap of BU3 on BU1 along an erosional surface (IES) on the southern border of the CMD. Note the poor beddings of the horizons of the PQ unit and the continuous (conformable) transition from the MSC to PQ. E: Part of seismic line Simbad 08 showing the onlap geometry of BU3 on BU1 on the northern border of the CMD along an erosional surface (IES). Note how the IES is characterized by Messinian paleo-incisions whereas the top of BU3 is conformable with the PQ unit. BU3's facies is poorly bedded here probably due to coarse terrigenous content, explaining its thickening. F: Figure showing the perfectly bedded facies of BU3 in the deep depocenter of CMD where it reaches its maximum thickness. It's worth noticing how both BU3 and UE change their facies from the depocenter into the borders of the basins and how both units onlap an older MSC unit along an erosional surface.

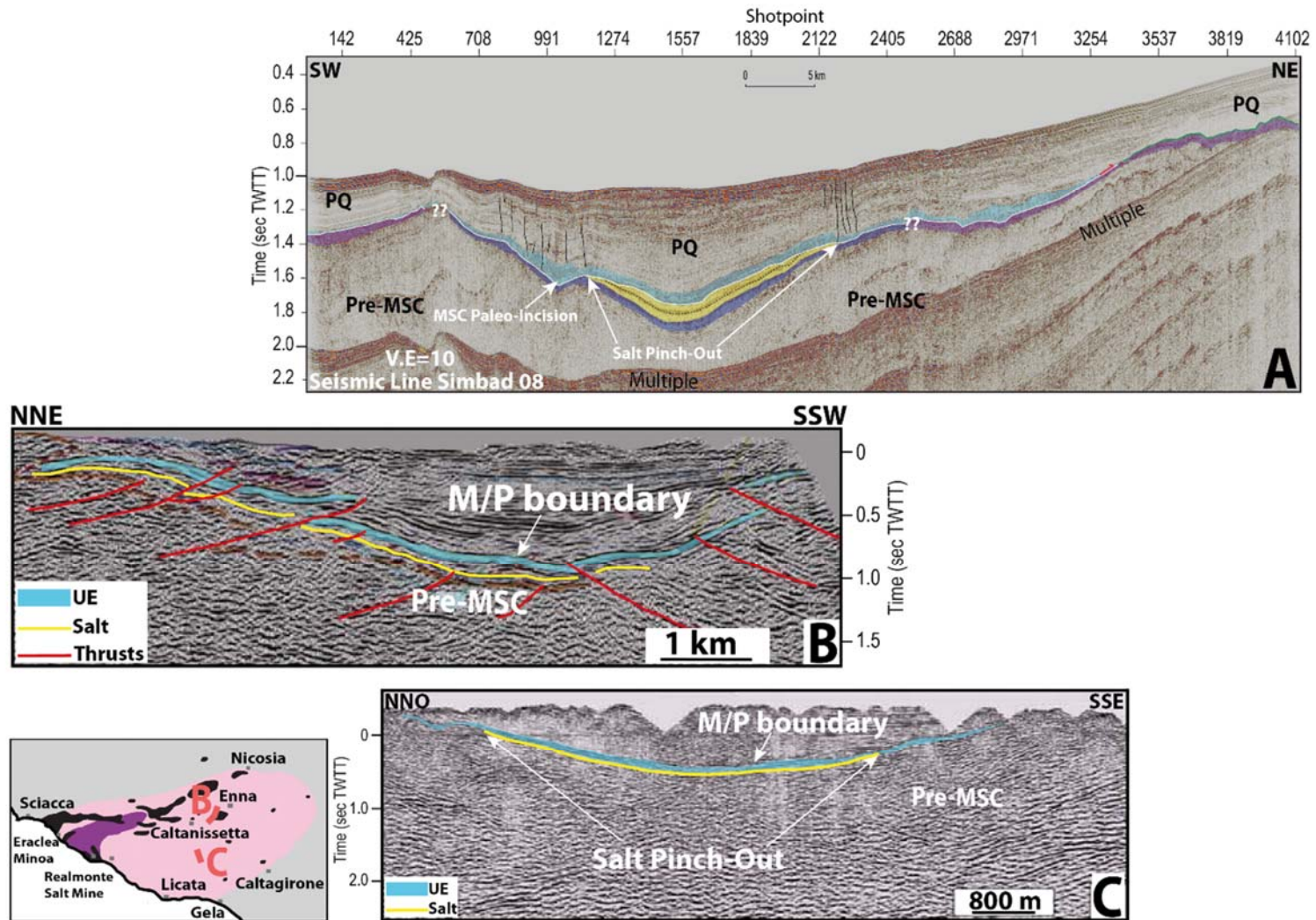


Figure 4.9. Interpreted profiles from both BP and CB showing the similarity in the shape and geometry of the sub-basins, especially here where a post-MSC flexure affected locally the CMD. A: Seismic profile Simbad 08 crossing the CMD from the southern to the northern part through the depocenter (position and legend in Figure 4.5). Note that the salt is exclusively found in the deepest part of the CMD, whereas to the borders it pinches-out. B: Onland seismic profile near Capodarso (CB – Sicily, modified from Catalano et al., 2012). C: Onland seismic profile in the central part of CB (modified from Catalano et al., 2012). See Figure 4.4-D for the legend of the location map. Note how in both the CMD and CB, the MSC sediments are contained in a concave-shaped depression with only the deepest part containing salt.

4.5.2 CMD stratigraphy and relative chronology

In the offshore domain of the BP, ODP and DSDP scientific drillings do not exist. Oil industry drillings exist only on the Alicante shelf, on the southwestern part of the BP. They only offer borehole logs and cuttings providing discontinuous lithological record of the MSC depositional unit (D. Ochoa et al., 2015c, 2018). Thus, the seismic method and onshore-offshore correlation approach are the only possible way to understand the history of deposition of the MSC deposits at a regional scale. Hereafter we discuss the significance and the chronology of the MSC units in the BP focusing on the CMD area based on the new interpretation of the seismic dataset. Most importantly, these units show similarity with the Sicilian CB (section 4.5.1).

4.5.2.1 Bedded Unit 1 (BU1)

Based on the following observations, we interpret BU1 as corresponding to the Primary Lower Gypsum (PLG) deposited during the first stage of the MSC:

- The proximal part of BU1 lies on a depth similar to the one of the PLG drilled onland in the Palma Basin (~120-200 m below sea level; Rosell et al., 1998; García-Veigas et al., 2018). They also show similar thicknesses (80-90m; Rosell et al., 1998);
- the seismic facies of BU1 is everywhere similar (see section 4.4 and Figure 4.6-D to F) to the BU drilled on the Alicante shelf and interpreted as PLG (D. Ochoa et al., 2015c), which suggests that the petro-physical characteristics of the unit are similar;
- Along the BP, BU1 is truncated almost everywhere by a regional erosional surface at the top, sometimes expressed by a valley-shaped incisions (Figure 4.5-C), suggesting a subaerial exposure of the unit during the MSC base level fall. This erosion could thus be the analog of the one at the top of the PLG in other peri-Mediterranean MSC basins (e.g. Sorbas and Appenines; Roveri et al., 2001, 2019). The erosional top of the BU1 becomes less important moving distally, which could reflect a shorter exposure time for subaerial erosion in distal areas and progressive transition to subaqueous erosion towards more distal areas;

- BU1 shows a high positive contrast in seismic impedance with the overlying PQ unit, suggesting BU1 is made of harder rocks than the marls above, in agreement with the presence of gypsum layers. BU1 locally shows internal reflection free facies (e.g. Figure 4.5-E, SP 719 to 804) possibly reflecting the presence of thick gypsum cycles such as cycles 3 to 5 that are, summed together, up to 60m thick and that have been correlated on the Mediterranean scale (Lugli, Vinicio, et al., 2010). This has been also hypothesized by Roveri et al. (2019) based on synthetic seismic models (see their figure 10).
- BU1 is locally deformed, showing internal chaotic facies (Figure 4.5-C, SP 309), probably due to the gliding of the entire unit (Figure 4.6-E, SP 1565 to 1908), at the gypsum/pre-MSC interface. Since the deformation also affects the lowermost overlying Pliocene strata (Figure 4.6-E), the gliding occurred after the MSC. It could have been triggered by several factors, among which the increase in slope angle with time, as a result of margin subsidence, favoured by the rheological contrast between the gypsum layers and underlying clastic sediments (probably marls). Gliding along gypsum interfaces has also been described by Bourillot et al. (2010) in the PLG of the Sorbas Basin. Locally, the internal chaotic facies could also be due to the presence of gypsum supercones similar to the one described in the PLG of Sorbas Basin (branching selenite facies, sensu Lugli et al., 2010).

Roveri et al. (2019) stated that BU1 in the CMD (SU) may correspond to chaotic deposits emplaced by gravity flows containing small to giant PLG gypsum blocks. We believe that their hypothesis is not correct, since RLG is known to be deposited in the second stage of the MSC, whereas the gliding affecting BU1 appears clearly to be post MSC (Figure 4.6-E). Moreover, the RLG is thought to be transported from margins and re-deposited basinwards (Roveri et al., 2008b) which is not the case for BU1 which shows an in-situ (< 1km) gliding without transport and re-sedimentation. Moreover, except very little in the Palma Bay, no gypsum exists all around the CMD's margins, so there is no possible source that such RLG might derive from.

4.5.2.2 Bedded Unit 2 (BU2)

The relatively high amplitude of some internal reflections of BU2 (Figure 4.5-C, SP 4198 to 5259) suggests that this unit contains gypsum. Since the geometrical and temporal relationship between BU1 and BU2 is not clear, we consider hereafter two possible alternative interpretations for BU2:

- BU1 passes laterally to BU2 in the distal domain with a change in facies, and thus BU2 is the lateral and time equivalent of BU1, deposited in MSC stage 1. This is supported by several observations: 1- Locally, where BU1 is absent, we find BU2 currently lying at a depth that coincide with the depth of BU1; 2- No onlaps are observed between BU2 and BU1 and BU2 is never observed overlying BU1. In such case, several interpretations for BU2 are possible. It could be made of marls and thin carbonatic layers deposited in deep water conditions (equivalent in time to PLG being deposited in the shallower domain) in the distal parts of the basin, similar to the one locally described in the CB by Manzi et al. (2011). It could be also made of shales similar to the one described in other Messinian evaporitic basins such as the Piedmont Basin by Dela Pierre et al. (2011). However, such shales and/or marls have usually a very low sedimentation rate, especially in areas not very active tectonically. Considering the thickness of BU2 (maximum 65m for such lithologies), it is unlikely that they could have been deposited during stage 1 of MSC (duration of 0.37Ma). More in accordance with the observed seismic facies, BU2 could also be made of pelagic primary gypsum cumulates depositing on the deep sea-bottom as a snow fall (Warren, 2016) or on the shallower slopes and then resedimented in deeper areas (de Lange & Krijgsman, 2010a). An alternation between gypsum cumulates and shales/marls is however not excluded. The downslope thinning of BU1 is compatible with what has been observed for the PLG in the Piedmont Basin by Dela Pierre et al. (2011).

- BU1 does not pass laterally to BU2, and BU2 is postdating BU1. This implies that BU2 is post-dating stage 1 of the crisis, emplaced probably in stage 2. The lateral discontinuity of the reflections of BU2 is the only observation that makes us doubt its continuity with BU1 (Figure 4.5-B, SP 833 and Figure 4.5-C, SPs 2430 and 5259). In this case, BU2 could be the product of erosion and re-sedimentation of BU1, possibly mixed with primary gypsum, as for the RLG in the CB (Roveri et al., 2008b). In such

a case, the absence of chaotic facies and diffractions in BU2 would imply that this type of RLG is likely made of gyps-turbidites rather than dislocated PLG blocks.

We, moreover, interpret the mounded features described in section (4.4.2, BU2; Figure 4.5-C) as microbial carbonate mounds. These carbonates could have been formed at the paleo-shoreline during the maximum retreat of the sea-level in the acme of the MSC (during deposition of BU3?), and they could be the equivalent of CdB or CdB1 described by Caruso et al. (2015) and Manzi et al. (2011), respectively. Similar isolated carbonate buildups with identical seismic facies has also been identified and described elsewhere in non-MSC context (e.g. offshore Ireland by Hovland (2008), their figure 5.3; offshore Philippines by Burgess et al. (2013), their figures 6B and 8C; and offshore Indonesia by Ruf et al. (2008), their figure 7).

4.5.2.3 Salt Unit

The salt unit fills the deepest parts of the CMD where it reaches its maximum thickness (~240m). Salt tectonics is clearly observed (Figure 4.4-B, C; Figure 4.9-A). The MU post-dates BU1 and BU2 since it is lying above the latter and pinches out laterally on it, which proves that it was deposited in a later stage of the MSC.

We propose that the salt unit is likely mainly made of halite like the other MSC salt bodies in the Mediterranean (e.g. CB, Lugli et al., 1999; Levant Basin, Feng et al., 2016). The continuous reflections in this unit might reflect a change in lithology from halite to Mg- and K-salts, as observed in the Sicilian salt (Decima & Wezel, 1971) of the CB. This would indicate increased brine concentration toward the top of the unit and could be related to a shallowing upward depositional environment (Lugli et al., 1999b).

Clastic intercalations have also been encountered in the MSC halite (MU) of the Levant Basin in the eastern Mediterranean. The intercalations consist of layers of claystones (Gvirtzman et al., 2013; Feng et al., 2016) and/or argillaceous diatomites (Meilijson, Hilgen, et al., 2019b). Such intercalations give birth to high-amplitude high-frequency reflections on the seismic profiles (Feng et al., 2016, their figure 2), due to the important change in the petrophysical characteristics between halite and clay/diatomites. In the CMD, the internal reflections in the salt unit are characterized by low-amplitude and low-frequency. This suggest only a slight change in the petrophysical characteristics of the material at the origin of the reflection and we

thus believe that the reflections within the salt of the CMD are due to change of evaporite type rather than to the presence of clastics.

The top of the salt in the CMD is marked by the truncation of intra-salt reflections (Figure 4.7-B, C). This erosional unconformity could be originated either by salt dissolution in under-saturated shallow diluted water (Kirkham et al., 2019) or by subaerial exposure (W. B. Ryan, 1978), both processes requiring a significant base level drop. Toward the borders of the salt basin, the fact that the truncation cuts into progressively older stratigraphic levels in the landward direction suggests that the salt was initially extending further landward and has subsequently been removed from shallower depths, supporting the hypothesis of an important drop in the base level associated with this erosional event. A similar geometry has been evidenced on in the deep Levant basin where intra-salt truncations are interpreted as of subaerial origin (W. B. Ryan, 1978), in agreement with the presence further north of fluvial deposits deposited at the top of the salt (Madof et al., 2019). In the CMD, we interpret the down-warped seismic reflections in the salt and overlying units as possibly imaging a solution-subsidence structure (Figure 4.7-D) related to the dissolution of the subjacent salt. Overburden collapse structures related to dissolution of subjacent evaporites have also been evidenced in the Levant Basin by Bertoni & Cartwright, (2005) and Huebscher et al. (2009). We tentatively suggest that in the CMD, such a dissolution may have been initiated during the lowstand phase contemporaneous with the erosion of the top of the salt.

4.5.2.4 Bedded Unit 3 (BU3)

We interpret this unit as the possible equivalent of the stage 3 MSC deposits of the CB (upper evaporites and the Lago Mare sub-stages). In the CMD, the important acoustic impedance contrast between BU3 and the overlying lower PQ unit (probably marls and calcisiltites similar to the lower Pliocene unit of Palma Basin; Capó & Garcia, 2019) reflects an important change in lithology. The internal stacking bedded facies of BU3 in the depocenter of the CMD (Figure 4.8-F) is coherent with an internal lithology consisting of alternations of gypsum and fine clastic sediments similar to the one described at Eraclea Minoa in CB. The low frequency characterizing the facies of BU3 (Figure 4.8-F) with respect to the high frequency ones encountered in BU1 could reflect the thicker layers of clastics included in it, similar to the clays and marls of the UE (Figure 4.8-C). If present, the Lago Mare phase representing the end of

the MSC could be contained in the uppermost reflection of BU3 or included in the lowermost PQ horizon due to its reduced thickness.

The aggrading pattern of BU3 suggests that, following the erosion of the top salt layer under lowered base-level, BU3 deposited in a topographic low forming a perched lake system. The onlap of the internal reflection of BU3 on the margin may reflect a rise in base-level, as the sediments infill the lake and the mean shoreline of the perched basin shoals through aggradation. This is in accordance with what proposed for the UE of the CB by Butler et al. (1995).

Similarly to the centi-metric to deci-metric scale erosions described in the UE in CB due to the precession driven sea-level oscillations (J. M. Rouchy & Caruso, 2006), internal erosions within BU3 might exist, but they are not visible at the seismic scale. The top of BU3 marking the Miocene-Pliocene (M/P) boundary is conformable in the CMD with no evidence of erosion on the seismic scale (Figure 4.4-B, C) suggesting that the perched lake always remained under water. The M/P boundary in CB is however interpreted as unconformable (see section 4.2.2, Arenazzolo member; Cita & Colombo, 1979). In other shallower sub-basins in the BP, a very thin BU3 appears locally. The irregular top could be due to mild syn-tectonic faulting affecting the unit (Figure 4.6-D).

4.5.3 Depositional scenario in the CMD and associated regional consequences

Maillard et al. (2014) proposed several possible correlations between the different MSC markers of the BP, extending from onshore to offshore. Roveri et al. (2019) subsequently adapted one of the proposed scenarios (see their figure 14) to fit their 3-stages model. However, two crucial features were not considered in both previous works: the BU2 lying below the salt and the clear erosional surface truncating the top of salt.

The approach that we use in this work and the similarities that we discussed between the CMD and CB, help us not only to constrain our understanding of the MSC in the BP, but also it could be a reciprocal way to answer some uncertainties about the MSC in CB.

Thus, hereafter we propose a new scenario (Figure 4.10) for the MSC in the CMD following our observations, interpretation, and comparisons and adapting the CIESM, (2008) time chronological model for the MSC:

- MSC stage 1 (5.97-5.60 Ma): during this stage, the Terminal Carbonate Complex (TCC), known also as Santanyi Limestones formation, has been deposited on Mallorca carbonate shelves contemporaneously with the Primary lower gypsum (PLG) in the Palma de Mallorca Basin (Mas Gornals & Fornós, 2012). Concurrently in the CMD, BU1 and BU2, which we interpret respectively as PLG and primary gypsum cumulates/marls, were deposited in continuity with the PLG of the southern Spanish basins, as equivalent to the lower evaporites unit of the Sicilian MSC basins.
- MSC stage 2 (5.60-5.55 Ma): in this stage, a major base-level drop took place. The TCC and PLG already deposited in the proximal parts were undergoing an important subaerial erosion. In the depocenter of the CMD, salt bodies deposited in the 2 disconnected depressions, probably from high-concentrated salt brines. At the acme of this stage, the base-level dropped until the exposure and erosion of the top of the salt layers, marked by the truncation of the salt's internal reflections. This erosion could also be due to dissolution of salt in shallow waters. The salt's internal reflections likely reflect the change in the salt facies from halitic to kainite salts. At the border of the depression, microbial carbonate mounds deposited near to the paleo-shoreline. This carbonate formation might have continued also in the next stage. Moreover, the bidirectional truncation of the intra-salt reflections suggests that salt may have been eroded on the higher flanks of the basin during the acme of the crisis, and then re-deposited in the deepest part of the depocenter. This observation is evidenced by the presence of a pure salt transparent facies above the intra-salt reflections in the depocenter. This process might have acted also in the salts of CB, where above the desiccation cracks at the top of the K and Mg-salts lies a pure halitic unit that could have deposited due to the washing of salts deposited initially at the flanks of the depression and re-deposition in the deepest area, as also indicated by the Strontium isotopes values in this unit (García-Veigas et al., 2018b).
- MSC stage 3 (5.65 to 5.33): during this stage, BU3 was deposited in the CMD. The bedded pattern of BU3 and its seismotratigraphic position suggest that it is likely

affected by cyclicity similar to the one observed in the UE of the CB. The Lago Mare deposits were deposited in the CMD, as well as in the Palma Basin at the very end of this stage. This could have happened perched brackish lakes lying at different levels and that has received high volumes of fresh water from increased water runoff, similar to what observed in the Arenazzolo member in CB by Cita & Colombo, (1979).

Onland Mallorca, as well as at Eraclea Minoa in CB, the M/P boundary is marked by an unconformity reflecting the return of normal marine conditions following the Zanclean re-flooding. This unconformity is not observed on the seismic scale in the CMD. The lowermost horizons of the PQ unit in the CMD drapes the slopes up to the shelves, which indicate deposition in normal marine conditions (Figure 4.5-C; Lüdmann et al., 2012).

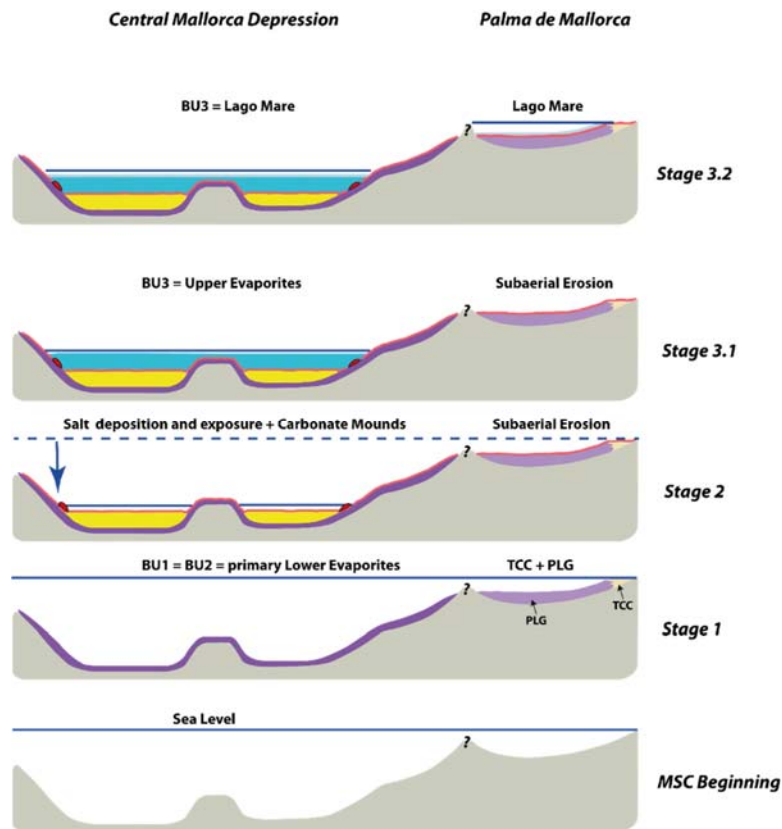


Figure 4.10. Proposed scenario of the MSC event in the CMD inspired from our new dataset interpretation and comparison with CB, adapting the consensus age model of the CIESM, (2008). Stage 1: deposition of BU1 and BU2 contemporaneously with TCC and PLG in the Palma Basin. Stage 2: Major sea-level drawdown during which the units deposited in stage one, were exposed to intense subaerial erosion and the deposited in the depocenter from two high-concentrated salt brines. At the paleo-shoreline, mounded carbonates equivalent to the CdB1 in CB probably formed in this stage. Stage 3.1: Deposition of BU3 in the CMD, the equivalent of the Upper Gypsum of the CB. Stage 3.2: Deposition of Lago Mare sediments from brackish-water lakes formed at different heights, probably due to increased rivers run-off.

4.6 Conclusions

The interpretation of a wide seismic reflection dataset covering the Balearic Promontory area allowed us to refine the mapping of the MSC unit's distribution and establish better the connection between the MSC sub-basins of the promontory. We were able to distinguish 4 different seismic units based on their seismic facies and on their geometrical and stratigraphic relationships. Those seismic units are, from the oldest to the most recent one: BU1/BU2, Salt Unit and BU3. They are very well defined in the Central Mallorca Depression, where we have the best coverage among the basins in terms of density of high-resolution seismic data. The settings and geometrical relationships of the MSC units in the CMD show a strong analogy with the MSC sediments of the Caltanissetta Basin in Sicily, in terms of stratigraphic geometries, distribution and facies. In both the BP and Sicily, the Messinian deposits are situated in a series of sub-basins that were lying during the late Messinian at different water depths. The deepest basins accumulated a relatively thin (~300-500m) salt unit, sandwiched between two other MSC units. The comparison of the MSC units in the BP with the ones outcropping in Sicily allowed to constrain and propose a new 3-stages scenario for the MSC in the CMD.

- The BU1 deposited first and is interpreted as equivalent to the bottom growth selenitic PLG found in CB and correlated on the Mediterranean scale (Lugli, Vinicio, et al., 2010). BU1 is widespread and its present-day depth below sea level ranges from ~170m beneath the shelves to ~1200m beneath the Mallorca slope. The erosion surface at the top of BU1, restricted to the borders of the basins, is interpreted as of subaerial origin, when the base level of the Mediterranean was lowered.
- The unit BU2, lying below the salt unit, is here considered as the temporal lateral equivalent of BU1 made of primary gypsum cumulates (snowfall) possibly mixed with clastic sediments.
- Following the deposition of BU1/BU2, the salt unit filling the depocenters of the CMD accumulated in topographic lows forming perched sub-basins. It likely started depositing in relatively deep water and ended in shallow water. This unit is interpreted as halite rich where displaying transparent seismic facies, while the internal reflections

may reflect K and Mg- salts. Their truncation strongly suggests a phase of subaerial exposure or dissolution under shallow water-column, contemporaneous with the Mediterranean base level lowering during the second phase of the crisis. The geometry of the intra-salt reflection truncations suggests that the salt layer in its entirety may have deposited higher up on the margin slopes before removal by erosion/dissolution.

- Above the salt, the youngest MSC unit, BU3, is considered as the equivalent of the Sicilian Upper Evaporites, including the Lago Mare event. This last deposited in perched lakes fed with fresh waters and topographically disconnected from the surrounding deeper basins in which the base level was lower.

This work suggests that the CMD can be considered as an undeformed analog of the Sicilian CB. During the MSC drawdown phase, temporary perched lakes developed in sub-basins forming topographic depressions lying at intermediate water depths. During the acme of the crisis, the sea-level drawdown was thus important enough to disconnect the BP sub-basins from the Valencia Basin and the rest of the Mediterranean.

The Sicilian MSC records (salt and the evaporites lying below and above it), classically provide key chronostratigraphic constrains for the MSC scenarios. They are often considered as representative of the deep basin records in particular to date the onset of the salt deposition at the Mediterranean scale. In our study, the clear absence of geometrical connection between the thin salt bodies found in the BP sub-basins and the thick salt layer from the deep Liguro-Provencal and Algerian Basins, however, indicate that salt deposition in perched basins is thus not necessarily contemporaneous with the deep basin salt, as also suggested recently by Meilijson et al. (2019) based on Eastern Mediterranean deep basin drillings. For the same reason, we also question the age and the origin of the thick, so-called, Lower Unit (LU), considered sometimes to be the equivalent of the outcropping Lower Evaporites. The CB salt and more generally its MSC records, should thus be used with care when trying to extrapolate the chrono-stratigraphy to the deep basin records.

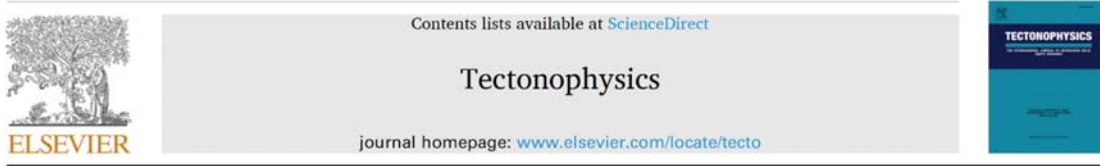
The change in facies between BU1 and BU2 described in this work and interpreted respectively as the passage at a certain depth range from primary bottom growth selenitic PLG to primary pelagic snowfall gypsum cumulates, is of an important significance as it might represent the maximum depth of formation of bottom growth selenitic gypsum in a non silled basin. In the BP, this depth is clearly exceeding the 200m threshold proposed by Lugli et al. (2010) and is

in agreement with the work of Ochoa et al. (2015), thus suggesting that PLG is not strictly related to shallow perched basins.

Chapter 5

Post-Messinian Salinity Crisis Tectonics in the Balearic Promontory: The Case Study of the Central Mallorca Depression

Tectonophysics 829 (2022) 229295



Plio-Quaternary strike-slip tectonics in the Central Mallorca Depression, Balearic Promontory: Land–sea correlation

Agnès Maillard^a, Fadl Raad^{b,*}, Frank Chanier^c, Hanneke Heida^d, Johanna Lofi^b, Guillem Mas^e, Daniel Garcia-Castellanos^d

In the previous chapter, I showed and discussed the nature of the evaporitic units belonging to the MSC in the Balearic Promontory. Since my ultimate objective is to try to understand under which conditions and what were the mechanisms that lead to the deposition of those evaporites, I had to take a step back and work on obtaining the pre-MSC paleo-bathymetry, which is essential for the modelling of the evaporites deposition.

So the starting point was a study in which I aimed on evaluating the relevance of the post-MSC tectonics in altering the bathymetry since the deposition of the evaporites. The chosen area for this study is the Central Mallorca Depression sub-basin. The reason for choosing the Central Mallorca Depression as an area is because it is the part of the promontory that underwent less tectonic deformation since the deposition of the MSC evaporites.

I started the work together with my co-supervisor Agnes Maillard who took the lead, being the expert in the tectonics of the Balearic Promontory and surrounding area. In the framework of this study, I went for a fieldwork in Mallorca with Agnes, accompanied by Guillem Mas-Gornals who showed us the onland MSC records of the island as well as the main post-MSC faults deforming this record onland.

The outcome of this work is the scientific article presented below in this chapter and published recently in the Tectonophysics journal.

The main take-home message that I want to give the reader from this chapter is:

- *Moderate post-MSC deformation acted along MSC strike-slip corridors in the CMD following the MSC evaporites deposition, thus altering only locally the paleo-bathymetry.*

Abstract: The Balearic Promontory (Spain) is of key importance to understand the tectonic kinematics of the westernmost Mediterranean, because its continued marine sedimentation has recorded the contrasting effects expected from competing geodynamic models proposed for the region. Near the center of this promontory, between the islands of Mallorca and Ibiza, the Miocene to Pleistocene stratigraphy of the Central Mallorca Depression presents an ideal record of the tectonic deformation that has received only limited attention. We use a widespread dataset of 2D seismic reflection profiles to identify, interpret and map the main prominent reflectors and extrapolate the thickness of the pre-Messinian and Pliocene-Quaternary sedimentary units. We then quantify the timing and style of deformation related to the various fault systems. Our results reveal for the first time a series of aligned small depressions bounded by extensional and strike-slip faults and filled with Plio-Quaternary sediment, perfectly aligned with the sub-basins of the onshore Mallorca Graben. A subsidence analysis confirms this correlation. We identify non-cylindrical deformation within the Plio-Quaternary unit that is remarkably similar to that observed onshore, suggesting continuous fault zones from the Central Mallorca Depression to Mallorca Island. We interpret an intra-PQ unconformity as the marker of a transition from extensional to strike-slip tectonic regime. The strike-slip stage is represented by both transpressional and transtensional structures, interpreted as restraining/releasing bends respectively and step overs along the faults. We show that these offshore faults in the Central Mallorca Depression overlap well with seismic epicenters and suggest major active strike-slip corridors that have an onshore continuity both until eastern Mallorca and in the southwestern Ibiza margin. The role of previous tectonic inherited structures (rifting, Betic thrusts, post-orogenic collapse) on the deformation reported here is discussed and we propose a tentative sketch that integrates our results in a Miocene to Present-day evolution at regional scale.

5.1 Introduction

In its present-day setting, the Western Mediterranean Basin is undergoing a diffuse compressional deformation due to the continuous convergence between the African and Eurasian plates (Stich et al., 2003; Serpelloni et al., 2007). The deformation is localized, mainly in the thrust belts of North Africa and the active northern African margin near Algiers, and partly in the external Betic Cordillera (Sanz de Galdeano & Alfaro, 2004; Serpelloni et al., 2007). Located between two extensional basins: the Valencia Basin (VB) to the north and the Algerian Basin to the south (Figure 5.1), the Balearic Promontory (BP) is considered the NE extension of the external Betic Cordillera (Figure 5.1).

The BP area recorded several tectonic phases since its formation and is tectonically active in the present (Fontboté et al., 1990; Gelabert et al., 1992; Sàbat et al., 1997a; Acosta, Muñoz, P., et al., 2001; Acosta et al., 2003; Sàbat et al., 2011; Sanchez-Alzola et al., 2014), as evidenced by numerous earthquakes taking place both onshore and offshore (Figure 5.1). This activity is not equally partitioned along the BP, as its southwestern part (Spanish margin offshore Alicante) has a relatively higher seismic activity than the rest of the BP, and it evidences clear active compressional deformation (Figure 5.1) (Alfaro et al., 2012; Acosta et al., 2013; Maillard & Mauffret, 2013b; Sanchez-Alzola et al., 2014). The central and northern parts of the BP are less seismically active, but some earthquakes have been recorded (Silva et al., 2001; Sanchez-Alzola et al., 2014). Mallorca accommodates most of this tectonic activity onland, except for 2 seismic events on Menorca Island (Figure 5.1). The highest magnitude recent seismic event recorded on Mallorca is the 1851 Palma earthquake (VIII, MSK intensity), known to have been generated along the active Sencelles fault (Figure 5.2-D) (Silva et al., 2001, 2002).

Several studies have been carried out to understand the structure and Cenozoic evolution of Mallorca and Ibiza Islands on the BP, in the framework of the Western Mediterranean dynamics (Gallart, Vidal, et al., 1995; Sàbat et al., 1995; Gelabert et al., 2002b, 2004; Sàbat et al., 2011; Driussi, Briais, et al., 2015; Etheve et al., 2016; Booth-Rea et al., 2017; Moragues et al., 2021). However, few studies focused on post-Messinian tectonics and/or concentrated on local faults activities (Silva et al., 2001; Giménez & Gelabert, 2002; Giménez, 2003; Mas Gornals et al., 2014). Only recently [Capó & Garcia, \(2019\)](#) studied in detail the Pliocene-Quaternary (PQ) sedimentary cover and evolution of the Mallorca Island.

So far, little attention was given to the offshore part of the BP, especially to the depression lying between Mallorca and Ibiza islands, known as the Central Mallorca Depression (CMD), which has accommodated a relatively important number of seismic events (Figure 5.1 and Figure 5.2-D). Since the detailed structural and morphometric works of Acosta et al. (Acosta, Muñoz, Herranz, et al., 2001b; Acosta, Muñoz, P., et al., 2001; Acosta et al., 2003; Acosta, Ancochea, et al., 2004b; Acosta, Canals, et al., 2004b), works focusing mainly on the Messinian Salinity Crisis (MSC) (Maillard et al., 2014b; Driussi, Maillard, et al., 2015b; Raad et al., 2021) and/or mass transfer deposits (Betzler et al., 2011; Lüdmann et al., 2012) were carried out in the offshore part of the BP.

In this study, we focus on the Central Mallorca Depression area offshore, and on the Mallorca Graben onshore (Figure 5.1). The aim of our study is to: 1- show the deformation style along the faults systems since the late Miocene up to present day and interpret their chronology; 2- compare and correlate the offshore structures to the onshore faults systems and PQ sedimentary units and trace their continuation along the whole study area; 3- integrate the offshore post-Messinian tectonic and seismic activity to the observations onland Mallorca and interpret the style of the deformation; 4-understand the role of the various tectonic inheritances and provide an integrated offshore/onshore sketch of the late Miocene to Quaternary tectonic evolution of the area. The final purpose is to propose a tectonic evolution of the BP during the Pliocene to Quaternary period, coherent with the western Mediterranean kinematics.

Thanks to previous works associated with new data, we evidence a post-MSC deformation linked to important structural heritages. We show complex and continuous active fault systems deforming the recent Plio-Quaternary (PQ) strata of the CMD.

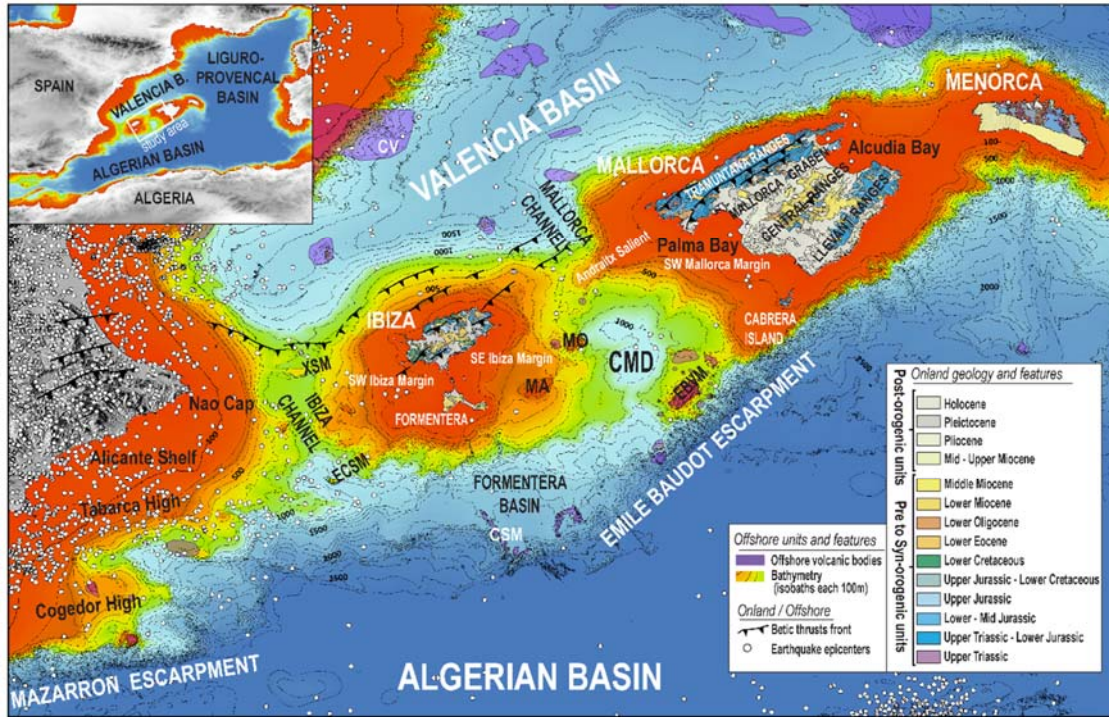


Figure 5.1. Map of the Balearic Promontory. The study area is located between Ibiza and Mallorca Islands. The bathymetric data for the offshore domain is downloaded from the European Marine Observation and Data network (EMODnet) database available online (www.emodnet-bathymetry.eu). The onland geology of Menorca, Mallorca and Ibiza islands is modified from the geological map of Spain 1:1000000; IGME. Epicenters of the recorded earthquakes are from International Seismological Centre (2020), On-line Bulletin (<https://doi.org/10.31905/D808B830>; [Storchak et al., 2017, 2020](#)). Onshore digital elevation model has been produced using Copernicus data and information funded by the European Union- EU-DEM layers (www.eea.europa.eu). CMD= Central Mallorca Depression; MA= Mont Ausias Marc; MO= Mont des Oliva; EBVM= Emile Baudot Volcanic Mounts. CSM= Chimene Sea Mount; CV= Columbretes Volcano; XSM= Xabia Sea Mount; ECSM= El Cid Sea Mount.

5.2 Geological and Morphological Setting

5.2.1 Physiography of the Study Area

The study area is located in the central part of the BP, between the islands of Mallorca and Ibiza-Formentera (Figure 5.1). It includes the SW shelf and slope of Mallorca, the Central Mallorca Depression (CMD, sensu Acosta et al., 2004a) and the E and SE slope of Ibiza. To the north, the CMD is partly connected to the deep Valencia Basin (water depth up to 1500 m) through the Mallorca Channel (Figure 5.1). To the south, it is limited by the steep Emile Baudot

Escarpment (EBE), dipping abruptly towards the Algerian abyssal plain where water depth exceeds 2800 m. The seafloor morphology of the study area has been widely investigated (Acosta et al., 2003; Acosta, Canals, et al., 2004b; Acosta, Ancochea, et al., 2004b; Camerlenghi et al., 2009b). The water depths in the CMD range from 700 to 1050 m. The Mont Ausias Marc and Mont dels Oliva are flat carbonate seamounts that are thought to be isolated parts of the Ibiza-Formentera shelf (Acosta et al., 2004a). The western Mallorca margin displays two prominent ridges: the Andraitx Salient in the prolongation of the Mallorcan Tramuntana Ranges (Figure 5.1) which is partly closing the CMD to the North; the second ridge is along strike with the Llevant Ranges and the Cabrera Island (Figure 5.1), and is aligned with the EBE including the Emile Baudot Volcanic Mounts (EBVM) which is composed of several cone-shaped volcanic mounts of Pleistocene age (Acosta et al, 2001a; Acosta et al., 2004b).

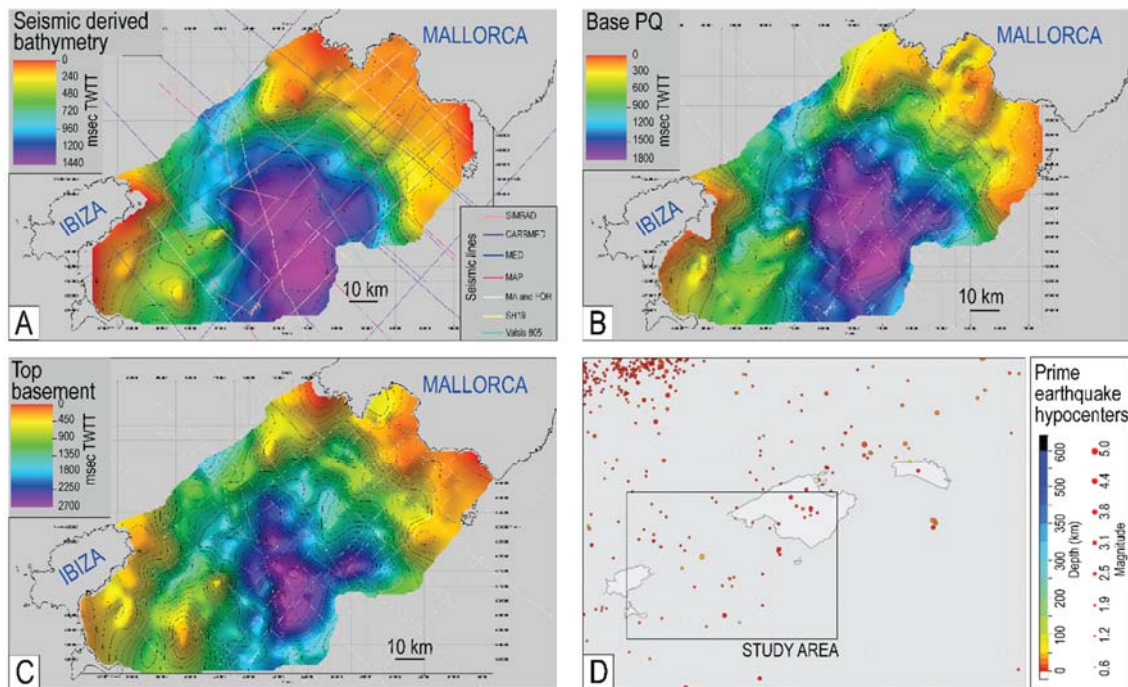


Figure 5.2. A: Location of the seismic dataset used in the study area superimposed on the seismic data-derived bathymetry map. B and C: Time structure maps showing the present-day depth of the Base PQ and the Top acoustic basement, respectively. Thin white lines represent the position of the same seismic profiles shown in A. D: Map showing the position of all prime earthquake hypocenters registered in the BP area and its surrounding (courtesy of International Seismological Centre (2020), On-line Bulletin <https://doi.org/10.31905/D808B830>; Storchak et al., (2017); (2020)).

5.2.2 Regional Geological Setting and Late Oligocene to Miocene Tectonics

The BP is bounded to the North by the VB, an aborted rift linked to the opening of the Liguro-Provençal oceanic Basin, which underwent extensional tectonics from Late Oligocene / middle Miocene times (Clavell & Berastegui, 1991; Maillard, MAUFFRET, et al., 1992; Roca, 1992, 2001). The EBE bounds the BP to the south and is known to represent the transcurrent oceanic-continental crust transition with the Algerian Basin that opened during Miocene times (Acosta, Muñoz, Herranz, et al., 2001b; Mauffret et al., 2004b; Camerlenghi et al., 2009b; Driussi, Briais, et al., 2015). In the regional extensional context (ongoing rifting processes in the Valencia and Algerian basins) the BP formed as a result of the compressional deformation associated with the Betic ranges in SE Spain (Ramos-Guerrero et al., 1989; De Galdeano, 1990; Roca, 2001). The Betic thrusts are well expressed onshore both on Ibiza and on Mallorca with the Tramuntana, Central and Llevant Ranges (Figure 5.1) that belong to the External zones of the Betic mountain Ranges (Bourrouilh, 1970; Casas & Sàbat, 1987; FOURCADE et al., 1982; Sàbat et al., 1988; Gelabert et al., 1992, 2004; Sàbat et al., 2011; Etheve et al., 2016). Compression involved Mesozoic and Cenozoic units, along thrusts trending ESE-WNW with variable displacement between NW and SW-directed hanging-wall transport and fold vergence (Figure 5.1) (DURAND, 1980; FOURCADE et al., 1982; Canas & Pujades, 1992; Roca, 1992; Gelabert et al., 1992, 2004; Sàbat et al., 2011). Paleomagnetic studies showed that during the compressional event Mallorca experienced clockwise rotation (Parés et al., 1992; Freeman et al., 1989). Offshore, thrusts are also clearly observed in the lower slope North of Ibiza (Maillard, MAUFFRET, et al., 1992; Roca & Guimerà, 1992b; Etheve et al., 2016). Further North-East, the prolongation and attenuation of this thrust system is still under debate (Gelabert et al., 1992; Maillard, MAUFFRET, et al., 1992; Mauffret et al., 1992; Roca & Guimerà, 1992b; Roca, 2001). The compression has been proposed to have initiated to the south during the Late Oligocene and propagated toward the north during the Burdigalian to Langhian times (Bourrouilh, 1970; Rodriguez Perea, 1984; Sàbat et al., 1988; Gelabert et al., 1992) but could have occurred in a shorter period restricted to 19 to 14Ma bracketed by extension (Moragues et al., 2021). Rifting of the VB that occurred during late Oligocene to lower Miocene also affected the BP. Tilt blocks from this phase are mostly observed in the SW part of the BP. The tilt blocks were then reworked while compression propagated northwestward.

Following the betic compressional phase, the BP underwent another extensional event from Serravallian to Tortonian ages, interpreted as post-orogenic extension by collapse (Roca, 1992,

1992; Benedicto et al., 1993; Cespedes et al., 2001; Booth-Rea et al., 2016; Moragues et al., 2018, 2021). This generated the configuration of basins and ranges onland Mallorca (e.g., the Mallorca Graben), and partly the offshore depressions such as the CMD and the Formentera Basin (Figure 5.1) (Sàbat et al., 1997). The upslope domains of Ibiza and Mallorca margins towards the VB are also structured by recent normal faults postdating the rifting phase and crosscutting the betic thrusts (Maillard, MAUFFRET, et al., 1992; Driussi, Briais, et al., 2015; Etheve et al., 2016, 2018a), probably linked to the same Late Miocene extensional event. The Late Miocene direction of extension was proposed to be perpendicular to the WSW-ENE faults that limit the Mallorca Graben, so globally NW-SE directed (Sabàt et al., 2011). The sub-basins (respectively the Palma, Inca, and Santa Pobra sub-basins; Figure 5.1) located inside the Mallorca Graben have been interpreted as transtensional structures linked to this phase (Giménez, 2003; Giménez & Gelabert, 2002). Local transtensional events occurred at the same time on Ibiza (DURAND, 1980; FOURCADE et al., 1982) and Menorca (Bourrouilh, 1973). These transtensional events are in accordance with recent works that showed kinematic evidence indicating that the WSW-ENE faults were transfer faults showing both dextral and sinistral displacements, related to NE-SW directed extension (Booth-Rea et al., 2016; Moragues et al., 2018; 2021) acting during the Serravallian after the main collapse (subsidence) episode of the sub-basins (Benedicto et al., 1993).

5.2.3 Onland Neogene Geological and Tectonic Record

A complete Neogene record of the evolution of the BP is found onshore Mallorca where two groups of sediments have been distinguished (Pomar et al., 1983; Fornós et al., 1991; Alonso-Zarza, 2003; Sàbat et al., 2011). The lower group comprises pre- and syn-orogenic sediments (lower and middle Miocene; Figure 5.1) that onlap the Paleogene and Mesozoic rocks. The entire record of this group is folded and thrust. The upper group is post-orogenic and Middle Miocene (Serravallian) to Plio-Pleistocene in age (Figure 5.1). It rests uncomfortably on the deformed lower group and/or on the Mesozoic and Paleogene rocks, having undergone tilting and flexure associated with normal and strike-slip faulting during the late Miocene to Middle Pleistocene extensional phase (Figure 5.3) (Pomar et al. 1983; Fornós et al., 1991; Mas et al., 2014; Capó and Garcia, 2019; Moragues et al., 2021). The first post-orogenic sediments consist in continental deposits in the Serravallian that represent lacustrine and alluvial environments

(Manacor and San Verder formations, Figure 5.3), showing extensional and transtensional structures in two orthogonal directions that thin the Early Miocene orogenic nappes (Benedicto et al., 1993; Ramos-Guerrero et al., 2000; Moragues et al., 2018). The extensional/transtensional regime seems to have ceased by the end of the Miocene (Sàbat et al., 2011). Post-Serravallian deposits are up to 1000 m thick and have been divided into five major sedimentary sequences (Fornos & Pomar, 1983; Pomar et al., 1983; Pomar, 1991; Mas Gornals & Fornós, 2013; G. G. Mas, 2015) (Figure 5.3): (i) Lower Tortonian littoral and fan-delta deposits ; (ii) upper Tortonian-Lower Messinian reefal carbonates (Reef Complex); (iii) Late-Messinian Santanyi limestones (TCC sensu Esteban, 1979) including their distal equivalent Gypsum in the Palma bay; (iv) Pliocene-Quaternary marine to eolian/continental deposits (Son Mir Calcisiltites-San Jordi Calcarenites). Some of those sequences record gentle folds that suggest that compression or transpression could have taken place during the Pleistocene. Some post-orogenic extensional structures (e.g. Sencelles Fault; Figure 5.3-A) that developed as normal faults during the Miocene were subsequently reworked as left-lateral strike-slip faults during the Pliocene (Mas et al., 2014). Some authors suggested a change to N-S compression and E-W extension during Pliocene times as supported by some associated compressional deformation during Quaternary times along the Sencelles Fault (Silva et al., 1998, 2001; Giménez & Gelabert, 2002; Giménez, 2003; Mas Gornals et al., 2014).

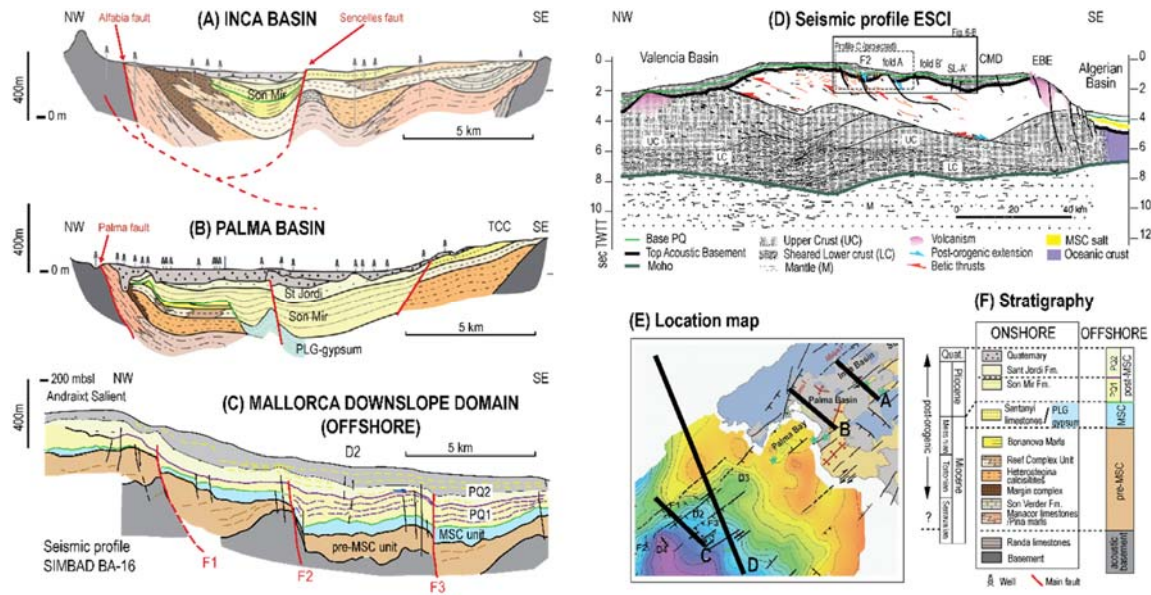


Figure 5.3. Onland-offshore comparison of the geological records (drawn at the same scale) across A-B: the Mallorca Graben (Inca and Palma sub-basins, modified from Capó and Garcia, 2019) and C: the offshore depocenter D2 (drawn from seismic profile Simbad BA-16 (Figure 5.6-A)) located on the downslope domain of Mallorca margin. Deep parts of the Alfabia and Sencelles faults come from figure 16 in Sàbat et al. (2011). Offshore faults can be compared to the faults bounding the Palma and Inca sub-basins. Intra basins faults delineate the same kind of folded structures (along F2, F3 and the Sencelles fault). Infilling units are of comparable thicknesses. D: Correlation of seismic profiles on the large-scale ESCI line (modified from Sàbat et al., 1997), showing deep-seated structures. E: Location of sections and profiles superimposed to the Base Pliocene isobaths map (Figure 5.10). F: Onshore stratigraphy of the study area (modified from Capó and Garcia, 2019) and offshore equivalence.

5.2.4 Present-day Tectonics

Offshore, active tectonic deformation has long been reported locally over the whole BP (Mauffret et al., 1987; Acosta et al., 2003), in accordance with the convergent regional context of the Algero-Balearic domain (Sanz de Galdeano & Alfaro, 2004; Serpelloni et al., 2007). The BP appears to accommodate only a small portion of this convergence as it is characterized by a weak tectonic and seismic activity. Recent post-Messinian deformation (local uplift; normal and strike-slip faulting) is nevertheless well expressed in the western domain of the Promontory, in the Ibiza Channel and on the Alicante shelf, where seismic markers belonging to the Late Miocene’s Messinian Salinity Crisis are deformed up to the seafloor (Alfaro et al., 2002, 2012; Maillard & Mauffret, 2013b; Driussi, Briais, et al., 2015). Between Ibiza and Mallorca gentle folds on the seabed were also interpreted as the result of compressional

deformation (Sàbat et al., 1997). Right lateral NE-SW strike-slip structures are locally evidenced by deformation on the sea-floor, visible particularly both on Mont Ausias Marc and Mont dels Oliva in the CMD (Acosta et al., 2003; 2004a). Acosta et al. (2004a) showed systems of near-vertical normal and/or strike-slip faults affecting Pliocene and Quaternary units, together with numerous pockmarks widespread over the area. On the margins of the BP, the abundance of both volcanic and mass failure structures also suggests active tectonic processes (Acosta et al., 2001b; Acosta, 2003; Acosta et al., 2004a; 2004b; Lastras et al., 2004).

Regarding the present-day tectonics, most of the recorded seismicity is located in the central part of Mallorca Island and offshore in the Mallorca channel (Figure 5.1 and Figure 5.3-D). It is characterized by low to moderate magnitude earthquakes (between 2.6 and 4.3 of magnitude; Figure 5.3-D; Silva et al., 2001) spatially associated with pre-existing Neogene NE–SW faults (Serpelloni et al., 2007; Sanchez-Alzola et al., 2014). On Mallorca Island, geological evidence suggests that the current tectonic regime is characterized by a coeval N-S compression and E-W extension, which varies laterally (Silva et al., 2001; Giménez, 2003). Unfortunately, no focal mechanisms in the islands are available. Based on analysis of strain rates, Sanchez-Alzola et al., (2014) proposed a gradual variation of the regime across the Promontory, with a NW–SE shortening in Menorca and eastern Mallorca, E–W extension in central Mallorca and WNW–ESE extension in Formentera and Ibiza. The present stress regime is consistent with the left-lateral movement on the NE–SW faults bounding the Mallorca Graben (Inca and Campos basins, Figure 5.3; Giménez, 2003; Morey & Mas, 2009; Sàbat et al., 2011; Sanchez-Alzola et al., 2014).

5.3 Dataset and Methodology

5.3.1 Offshore Seismic Dataset

This work relies on the interpretation of a series of 2D seismic profiles available offshore and covering the whole study area (Figure 5.2-A). The datasets consist of both high-resolution (SIMBAD cruise: Maillard & Gaullier, 2013 and CARBMED cruise; Hübscher et al., 2010) and low-resolution profiles (Valsis cruise (Mauffret et al., 1992); SH cruise; MA and FOR profiles provided by the Instituto Geologico y Minero de Espana (IGME); MAP and MED old

oil industry profiles recently re-processed with a standard processing flow until pre-stack time migration and provided by Spectrum and Western Geco Companies).

The seismic lines were interpreted according to the conventional concept of seismic stratigraphy (Mitchum & Vail, 1977) and based on previous works over the area (Maillard et al., 2014; Driussi et al., 2015a, b; Raad et al., 2021). High- and low-resolution lines were interpreted jointly and the main structures were mapped. Seismic horizons were interpreted and picked using the software Petrel® by Schlumberger®. [Bellucci et al. \(2021\)](#) now make the interpreted horizons of the bathymetry, base PQ and the acoustic basement available online with open access as part of a wider dataset in the Western Mediterranean. We constructed maps using the convergent interpolation algorithm provided by Petrel, which is a control point orientated algorithm that converges upon the solution iteratively increasing resolution with each iteration reaching a maximum chosen resolution of 2x2km. In order to quality check the resulting maps, we compared the seismic derived bathymetry map (Figure 5.2-A) with the high-resolution bathymetry shown on figure 1. The Base PQ and Top Basement surfaces (Figure 5.2-B and C, respectively) were compared with the maps published by [Leroux et al. \(2019\)](#).

5.3.2 Backstripping

In order to quantify the amount of post-MSC flexural-isostatic subsidence resulting from sediment load and compaction, we perform pseudo-3D backstripping on a regional scale following the methodology of [Heida et al. \(2021\)](#). The results are shown along the SW-NE section across the CMD shown in Figure 4. This approach allows for the comparison between local Airy isostasy and load subsidence associated with a stronger crust, in order to discuss the potential effect of the considerable post-MSC sediment thickness variations across the CMD, the onshore Balearic Islands and the surrounding Valencia and Algerian basins. The regional scale distribution of the sediment load and depths of horizons used were taken from Heida et al. (2021), then resampled into grids with a resolution of 2.155 by 2.225 km. Time-to-depth conversion of the Miocene-Pliocene boundary follows the exponential time-depth function from [Urgeles et al. \(2011\)](#) derived from well data in the Ebro margin and takes the form shown in Table 3.2 . Densities of the PQ sedimentary load and of the asthenosphere were set at 2100 and 3250 kg/m³ respectively. The values adopted for the effective elastic thickness were between 5 (close to local isostasy) and 15 km, in agreement with the young tectonothermal age

of the region (e.g., Gaspar-Escribano et al., 2004) and with results from spectral analysis of potential fields and topography (Tesauro et al., 2009a; Kaban et al., 2018a). For details about the backstripping methodology and other parameters adopted, see Heida et al. (2021) and references therein. Vertical motions caused by MSC events were not tested here but are addressed in the large-scale study performed in Heida et al., (2021).

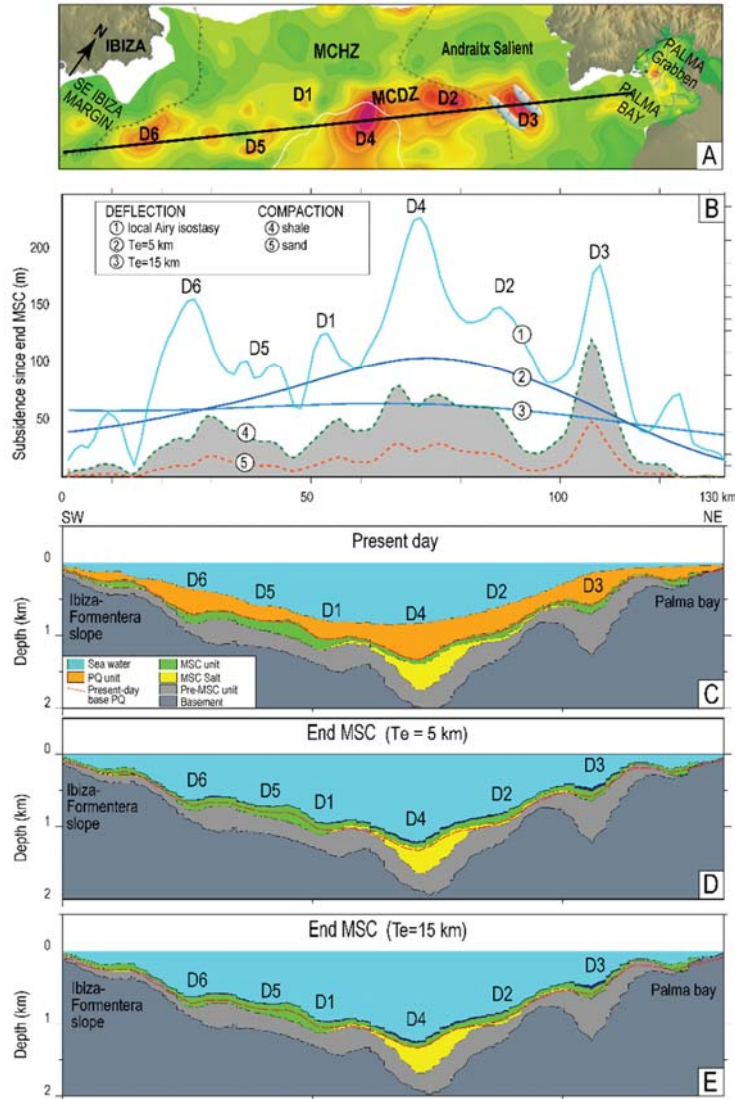


Figure 5.4. Results from the flexural-isostatic reconstruction of the original vertical position of the Plio-Quaternary sediment units along-strike the depocenters D1 to D6. A: Localization of the section on the map displaying the PQ thickness (Figure 5.11-A). B: Sedimentation-induced subsidence contributions of post-MSC (Plio-Quaternary). Stronger TE value leads to a smaller, more uniform subsidence, the narrow shape of the basins means increasing TE values lead to decreasing subsidence values. Sediment compaction values are presented for compaction curves for sand and shale lithologies from [Sclater & Christie, 1980](#). C: Present-day configuration of sediments along profile with depths of key horizons. D: Reconstructed profile for near-local isostasy (TE 5 km) after removal of Plio-Quaternary sediments and decompaction of Pre-MSC sediments. E: same reconstructed profile for TE value of 15 km. See text for comment.

5.4 Results and Interpretation

5.4.1 Offshore Seismic Stratigraphy and Main Units

Figure 5.5 shows the typical seismic stratigraphy in the CMD, that we deduced from the interpretation of high- and low-resolution seismic profiles. Five seismic horizons, bounding four seismic units, were outlined over the study area based on major unconformities and clear changes in seismic facies. The units are described here after from bottom to top:

- **Acoustic basement:** in general, it is characterized by internal chaotic facies with few reflections on both high and low-resolution seismic profiles (Figure 5.5 and Figure 5.6). It can locally present formless internal patterns and can be layered in its upper part (Figure 5.6, Figure 5.7 and Figure 5.12-A). Its top always corresponds with a prominent high-amplitude reflection, sometimes associated with diffracting hyperbolas, attesting to an important lithological contrast with the overlying unit. The top acoustic basement reflection displays an irregular morphology on all seismic lines and reveals a highly tectonized sequence (Figure 5.2-C and Figure 5.7). There is no constraint on the age and lithology of the sediments constituting the basement offshore. Based on the geological context and on the basement rocks outcropping onshore in Mallorca and Ibiza (Figure 5.1), the acoustic basement in the CMD is most probably made of Mesozoic and Neogene sediments belonging to the pre- and syn-orogenic group (Figure 5.3-C and F; Sàbat et al., 2011). This is supported by the presence of some folded-like bedded reflections within the chaotic complex and truncations at its top, suggesting the top acoustic basement boundary to be the post-Betic unconformity (Figure 5.7). Locally, a volcanic origin could also be invoked as part of the acoustic basement (Acosta et al., 2003, 2004b), especially on the EBVM.

Figure 5.8 shows the present-day depth map in s twtt of the Top Acoustic Basement, highlighting the orogenic structures.

- **Pre-Messinian Salinity Crisis unit (pre-MS):** lies unconformably on the acoustic basement (onlaps, Figure 5.5-A and B). Its upper boundary looks conformable with the MSC

unit except locally where it shows toplap terminations (Figure 5.6). This unit is characterized by low internal reflectivity (sometimes reflection-free on low resolution seismic; Figure 5.5) with frequent low amplitude intercalated beddings in some places. Except in the deep CMD, the pre-MSC unit is anisopaquous with several clear “fan-shaped” geometries (Figure 5.6 and Figure 5.7), which suggests deposition in a post-orogenic/syn-extension context, thus probably corresponding the lower part of the second sedimentary group found onshore Mallorca (see section 5.2.3).

- **Messinian Salinity Crisis unit (MSC):** it is generally characterized by a very high reflectivity and horizontal beddings making it clearly distinguishable from the underlying and overlying sedimentary units (Figure 5.2). On high resolution seismic profiles, this unit can be divided into several sub-units that were described in detail by Maillard et al., (2014) and Raad et al., (2021). In the deepest part of the CMD, the MSC unit includes a salt layer (Figure 5.9). The MSC salt layer is characterized by the classic reflection free facies described elsewhere in the Mediterranean (e.g., Lofi et al., 2011; Figure 5.9) and by ductile deformation (salt tectonics, Figure 5.9 and Figure 5.12-B). Salt tectonics is however reduced in the CMD because of the small thickness and limited extension of the layer, and because of the closure of the depression, probably preventing the salt from further gliding and/or spreading.

Figure 5.10 shows the present-day depth map of the Top MSC Surface (base Pliocene). To the north, the top MSC lies at a relatively shallow depth (500 – 900 m deep below sea level) on a high that we call the Mallorca Channel Horst Zone (MCHZ). In the CMD, the top MSC deepens down to 1300 – 1500 m bsl and shallows laterally towards the slopes of the islands. The top MSC surface mimics the present-day bathymetry (Figure 5.2-A and B).

- **Pliocene-Quaternary unit (PQ):** It is bounded below by either the MSC unit, the pre-MSC unit or the substratum (acoustic basement), and above by the sea floor. On the basin scale, the PQ can be divided into 2 sub-units, PQ1 and PQ2, separated by an angular unconformity (intra PQ-unconformity, Figure 5.5). The lower sub-unit PQ1 is characterized by a bedded facies with low reflectivity which is characteristic of the lower Pliocene unit observed elsewhere in the western Mediterranean (transparent Pliocene sensu Lofi et al., 2011). In the CMD, PQ1 drapes the underlying topography represented by the MSC-unit (Figure 5.6 and Figure 5.7). PQ1 is bounded above by the intra-PQ unconformity and overlapped by PQ2. Except in its lower part, PQ2 consists of high reflective continuous beddings on high resolution seismic profiles (Figure 5.5). The internal reflections of PQ2 locally show onlap terminations on the intra-PQ unconformity (Figure 5.6 and Figure 5.7). In the CMD, the stacking pattern of these reflections

shows a progressive filling of the depocenter (Figure 5.9). The topmost part of PQ2 has been sampled on the southern shelf of Mallorca where it is composed of carbonate rich pelagic sediments (Betzler et al., 2011). The lower part of the PQ sequence has been recovered only on the far western part of the BP in two industrial boreholes (Muchamiel and Calpe boreholes on the Alicante shelf; Ochoa et al., 2015, 2018), where it consists of soft silty clays and limestones (Ochoa et al., 2015; their post-evaporitic unit).

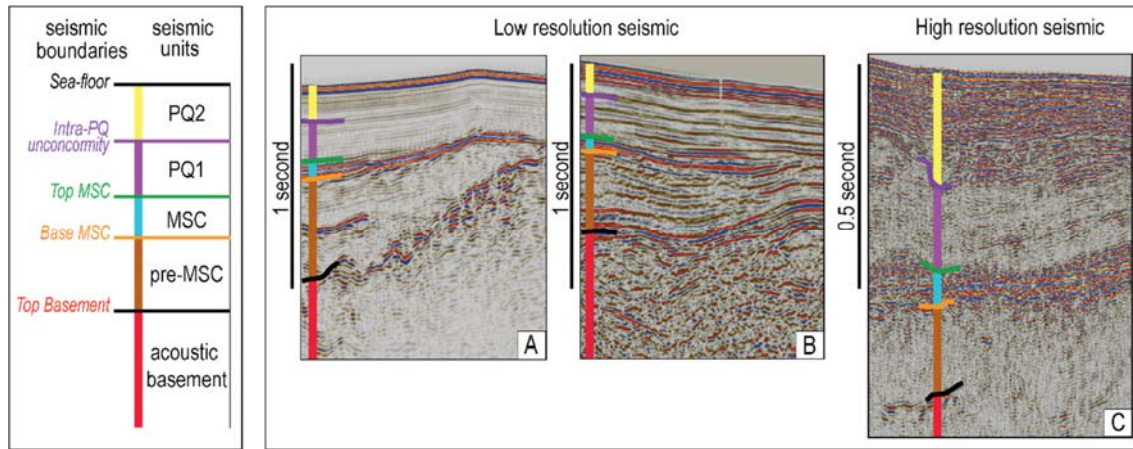


Figure 5.5. Presentation of the interpreted seismic units and their boundaries, on low resolution-deep penetration industrial (A (line MED26) and B (line MAP70)) and academic high-resolution seismic profiles (C (line SIMBAD)). Acoustic basement includes pre- and syn-orogenic units.

5.4.2 Offshore Deformation

5.4.2.1 Post-Messinian Deformation

Several features diagnostic of post-Messinian deformation are observed over the study area. Figure 5.10 presents the distribution of these structures, superimposed on the present-day depth map of the Top MSC (base Pliocene). The post-Messinian deformations appear mainly along the borders of the CMD.

- **Normal faults and associated depocenters:** these faults are evidenced by offset of the reflectors or by the syn-sedimentary deformation of the PQ unit and/or the MSC-unit. We label the normal faults F1 to F4 from NE to SW, respectively (Figure 5.10). In the MCHZ, a set of normal faults, some of which already described by Acosta et al. (2004), are trending N 070°E and are mostly dipping southwards (Figure 5.7 and Figure 5.10). They belong to a system of

two major faults, F1 and F2, that forms a NE-SW structural boundary between the MCHZ topographic high and the CMD low. F1 is the only fault over the study area that can be traced nearly continuously from NE to SE (Figure 5.10). Its footwall includes the MCHZ along strike with the indentation of the Mallorca shelf (Andraitx Salient). Deeper to the south lies F2 with scarps facing North or South alternatively. Both F1 and F2 root in the basement and can be traced down to 2 sec twtt on deep-penetrating seismic profiles (F2 in Figure 5.6, profile Map 70) and are clearly related to crustal tectonics. If these faults were already active before PQ (see section 5.4.2.2), the activity of F1 and F2, as well as other associated faults within that area, persisted during and after the MSC. This is also supported by the following observations:

- Some of these faults are locally reaching the seabed (Figure 5.6 and Figure 5.7).
- Some faults clearly offset the MSC unit by few to 350 m (Figure 5.6-A and Figure 5.7) with local thickening of the MSC unit toward the faults (F2 fault, Figure 5.12-A and B), suggesting that extension along the faults was active during the MSC.
- F1 and F2 are associated with a series of PQ depocenters, labeled D1 to D6, well visible in the PQ unit thickness map (Figure 5.13).

Figure 5.7 illustrates depocenter D1 related to a graben structure bounded to the NNW by F1 and containing a ~350m thick PQ-unit (Figure 5.13). Further NE, depocenter D2 displays a ~500m-thick PQ unit and is bordered by the fault F2 which hanging wall shows a clear tilting of the MSC unit (Figure 5.6). Within the PQ unit, almost only PQ1 is affected by the deformation. PQ1 is thickened in grabens (D1, Figure 5.7) or half-grabens, presenting syn-sedimentary fan-shaped geometries (PQ1 in D2, related to F2, Figure 5.6), which suggests that post-Messinian extension persisted during the deposition of PQ1, up to the intra-PQ unconformity (Figure 5.5). PQ depocenters D1 and D2 are along strike with a third depocenter, D3, located eastward (Figure 5.13). D1, D2 and D3 align with 3 additional depocenters D4, D5, and D6 (Figure 5.4-A) that will be discussed later. They all together form a N070° elongated corridor aligning along the F1 and F2 fault systems and filled with PQ unit up to ~600m thick (Figure 5.13). We call this corridor the Mallorca Channel Depression Zone (MCDZ). Offshore it runs along a 100 km long and 20 km wide line going from the SW Mallorca margin to the Ibiza NE margin, parallel to the Andraitx Salient and the MCHZ (Figure 5.13).

- **Flexure:** D4 belongs both to the MCDZ previously described and to the northern part of the CMD (Figure 5.13). The PQ unit in D4 is up to ~600m thick, thus forming the thickest of the

PQ depocenters. D4 appears not only related to the post-MSC activity of the normal fault F2 but also to a post-MSC flexure involving the MSC unit and the PQ1 unit, both folded isopachously as shown in Figure 5.9. Onlaps of PQ2 onto the intra-PQ unconformity show that the folding occurred at the end or just after the emplacement of PQ1. D4 draws a syncline fold trending NNW/SSE which axis is highlighted by the deformation of the base of the MSC salt. Elsewhere over the study area, the MSC salt is not deformed, except by salt-related gravity-gliding responsible for small halokinetic faults locally observed on the borders of the CMD (Figure 5.9) and with a surficial expression in the bathymetry (Figure 5.1). These faults were active since the salt deposited but are not related to crustal tectonics.

- **Folds and strike-slip faults:** some complex faults systems and associated deformation have been observed from the seismic profiles. On seismic profile Ba 16 (Figure 5.6-A), the fault F2 has a normal offset and dips 75° to 80° southward. On the same seismic profile, fault systems F3 and F4 appear much steeper, almost vertical (Figure 5.14-C). They are located on fold hinges (fold axis Figure 5.13) and could resemble reverse faults. Both F3 and F4 affect the MSC, PQ1 and PQ2 units with little offsets. They occasionally reach the sea floor (Figure 5.6). The MSC and PQ1 units are conformable along the fold associated with F3 suggesting a mainly post PQ1 activity of this individual structure. The next structure toward the south (F4-Fold A) exhibits little thinning of the MSC and PQ1 units at the apex of the fold (Figure 5.6) suggesting some slow development of this structure during that time span.

Furthermore, we outline the existence of a number of folds from both the bathymetric data (Figure 5.1) and the top MSC map (Figure 5.10). They form undulations that run parallel to each other and trend SW-NE (folds A and B-B' in Figure 5.10).

On the SW Mallorca margin, the formation of fold B has been active from PQ1 times up to recent times as demonstrated by onlapping geometries (onlaps of PQ1 on top of the MSC unit and of PQ2 onto the intra PQ unconformity, Figure 5.12-B) and by the deformation of the seafloor, (folds B-B', Figure 5.12-A and B). Fold B was already known from previous studies based on the interpretation of high-resolution sparker data (Acosta et al., 2001a) and multichannel seismic profiles (Sàbat et al., 1995). Other antiform structures are evidenced locally in various locations within the study area (Figure 5.10). A seismic profile running across the Mont Dels Oliva structure clearly images fold C, deforming the MSC unit and crosscut by vertical faults (fold C, Figure 5.12-C). Here, PQ unit reaches 400m in thickness in the lows on each side of the fold, forming the depocenters D5 and D5' located NW of Mont Dels Oliva

(Figure 5.13). Only the PQ1 unit seems deformed by the tectonics associated with the creation of fold C which thus occurred before the deposition of PQ2 deposition. Further south however, fold D, on the SE side of Mont Dels Oliva, is emplaced recently, as attested by the isopachous deformation of the entire PQ unit, and of the presence of associated undulation on the sea floor (fold D, Figure 5.12-D). Folds are mostly observed along the NW-SE trending seismic profiles. The determination of their trends is constrained by the morphology of the Top MSC map and by the bathymetry but remains uncertain due to their low lateral continuity and to the low-density of seismic coverage in this sector (Figure 5.2-A). Vertical faults crosscut fold C and the PQ depocenters D5 and D5'. This complex and highly deformed area represents the SW prolongation of the MCDZ, which terminates with depocenter D6 located further West on the lower Ibiza slope (Figure 5.13).

On the southern Mallorca margin, vertical faults affecting all the units up to the seafloor express active strike-slip motion (SLA and SL-B Figure 5.10 and zooms Figure 5.12). For example, the complex deformation zone presented on Figure 5.12, (SL-A and -A', Figure 5.12-A and B) is a 5-8 km large depression affected by sub-vertical faults deep seated in the acoustic basement and pre-MSC unit, but that also reach the seafloor and involve the MSC and PQ units with normal offset on the borders of the structure (right part of SL-A'). The F2 fault, with normal offset, does not show a typical normal fault dip nor filling geometry, but seems to have been verticalized (Figure 5.6).

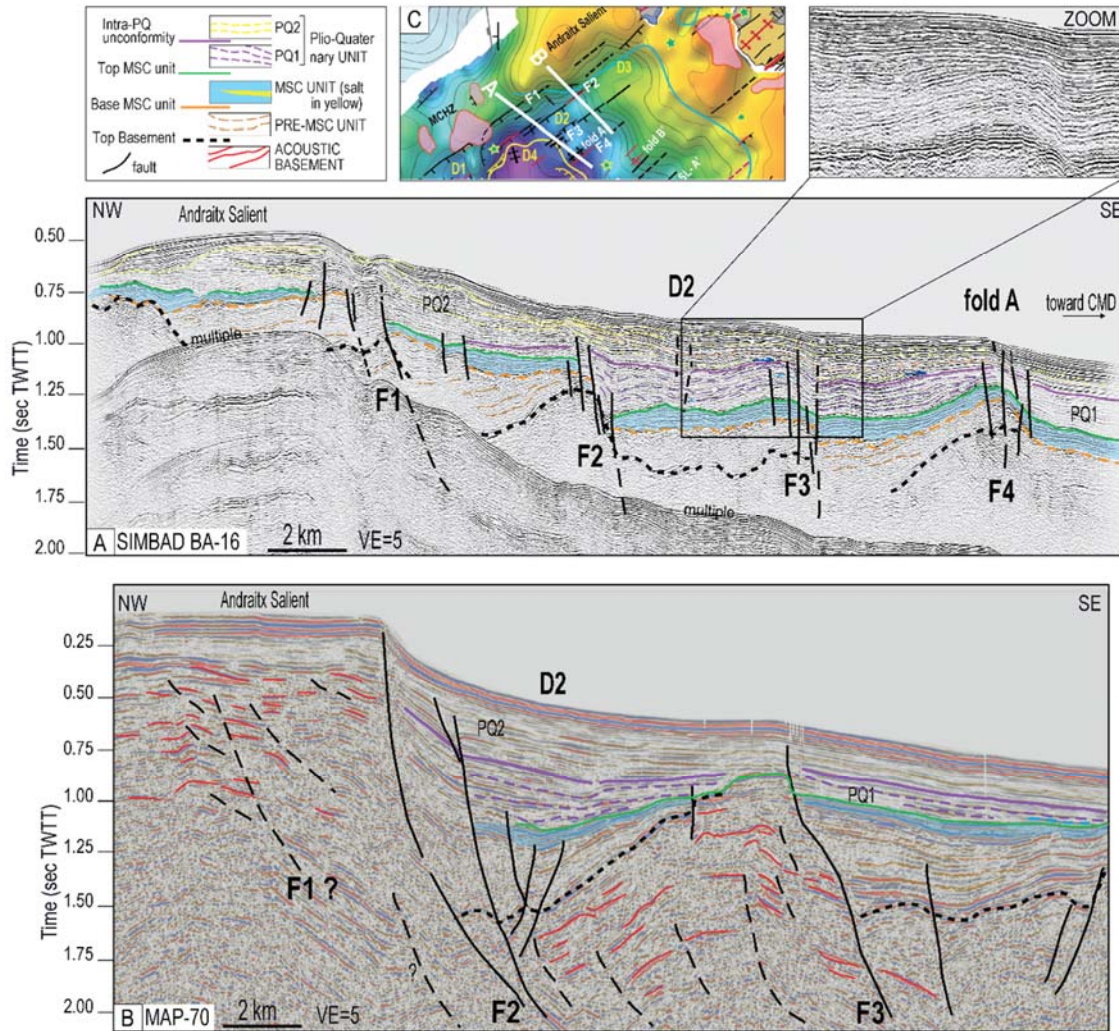


Figure 5.6. A: High-resolution academic seismic profile Simbad BA-16. B: MAP-70 industrial deep penetration seismic profile. Seismic sections crossing depocenter D2 and the complex associated deformation of the area. F1 and F2 faults structure a nice half graben underlain by fan-shaped pre-MSC unit and locally MSC and PQ unit (Map-70). The faults are however particularly vertical and F3 and F4 are associated to folds that reach the seafloor (line BA-16). Remnant of thrusts could be present NW of MAP-70 in the highly deformed acoustic basement. C: Base Pliocene isobaths map (see Figure 5.10) showing the location of the seismic profiles shown in A and B.

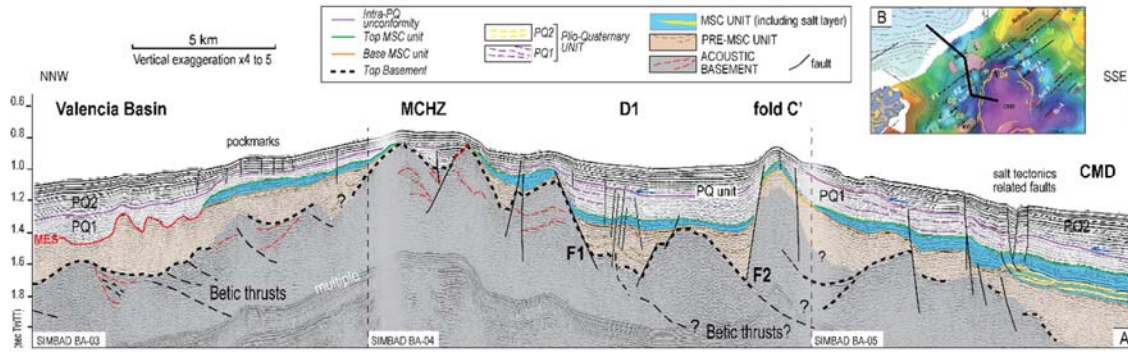


Figure 5.7. A: Seismic profile across the Mallorca Channel, illustrating the MCHZ (Mallorca Channel **H**orst Zone) adjoining the MCDZ (Mallorca Channel **D**epression Zone, here D1 depocenter/mini-basin). Faults clearly offset the MSC unit (in blue) and thicken the PQ unit. Betic orogenic thrusts are observed towards the Valencia Basin and normal faults like F1 could sole at depth into the thrusts, as observed on deep penetration seismic lines. B: Base Pliocene isobaths map (see Figure 5.10) showing the location of the seismic profile shown in A.

5.4.2.2 Chronology of the Deformation

5.4.2.2.1 Remobilization of Former Structures

The post-Messinian deformation is influenced by the Oligo-Miocene tectonic history of the area. Most of the faults offsetting the MSC and PQ units are linked to former structures that influence the latter deformation style.

- **Betic thrusts:** We locate new compressional betic structures on the MCHZ and Andraitx Salient areas (Figure 5.8) that correlate well with deep-seated thrusts identified on the ESCI deep seismic profile (Figure 5.3-D and Figure 5.6) (Gallart, Martínez, et al., 1995; Sàbat et al., 1997a). North of the MCHZ, towards the VB, thrusts are oriented along strike of the downslope domain of Ibiza (NNW of Figure 5.7 and Figure 5.8). Betic thrusts are also observed elsewhere over the study area, for instance near Formentera, where the post-orogenic discontinuity is well imaged thanks to the erosion on top of folds in the acoustic basement (Figure 5.12-D). The thrusts remain poorly observed in the CMD where the thick sequence of sediments possibly prevents their identification. If present, they must have been overprinted by the post-orogenic extension and subsequently by the post-Messinian deformation. This is evidenced by comparing the faults plotted above the acoustic basement and base Pliocene depth maps (Figure 5.8 and

Figure 5.10), which illustrate that the post-Messinian faults and former structures observed deeper in the acoustic basement are superimposed. On the lower slope of the SW Mallorca margin, the sedimentary units are folded from the basement up to the sea floor (fold B and B', Figure 5.12-A and B) where a prominent high seems related to the presence of deep crustal structures. Here, deep reflections dipping SE may be related to Betic deformation, similarly to the thrusts recorded towards the Valencia margin (between fold B and SL-A, Figure 5.12-B). The nearly vertical fault limiting the high to the NW together with the folded MSC and PQ units are indications of a recent (up to Present-day?) remobilization of the structure, probably with a strike-slip motion. The transcurrent zone SL-A -A' also records pre-MSC deformation observed in the acoustic basement, most probably linked to former Betic reverse faults that have been reactivated with a dominant strike-slip motion.

The Betic thrusts on the BP acted during or just after the regional Oligo-Miocene rifting structuration in the surrounding basins. The horsts resulting from this extension (see section 5.2.2) and still largely observed on the BP where post-orogenic extension (almost) did not overprint these former structures (e.g., Ibiza Channel, Formentera margin), are poorly preserved in the study area. However, we cannot disprove that the Betic thrusts observed here are reactivated normal faults linked to the rifting.

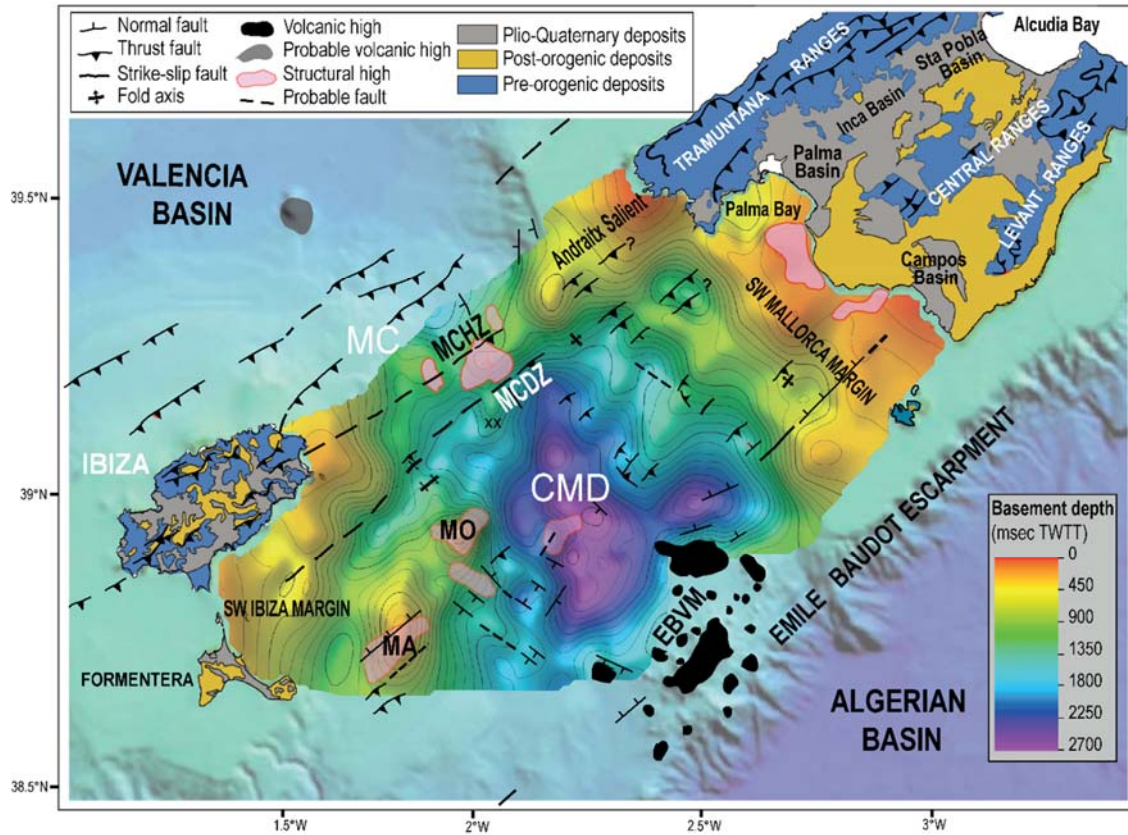


Figure 5.8. Map of the main orogenic structures superimposed on Top Basement depth map (msec TWTT) and onland geology. The thrusts are clearly observed and continuous from Ibiza Island into the Mallorca Channel (MC). They are more difficult to follow from the Tramuntana Ranges to the Andraitx Salient located offshore, but topography prolongates the ranges southwestward. Through the Central Mallorca Depression (CMD), orogenic structures are only observed locally. Onland geology mapping of south Mallorca and North Ibiza is modified from geological map of Spain 1:50000 (IGME). The offshore colored map surrounding the structural map of our study area represent the present-day bathymetry (from Acosta et al., 2003).

- **Normal faults linked to the post orogenic extension:** The pre-MSC deposits are anisopachous with several depocenters (Figure 5.11-B) in which some syn-sedimentary fan-shaped growth strata can be observed in association with the previously mentioned fault systems F1 and F2 (Figure 5.6). These syn-tectonic features in the pre-MSC unit prove that these faults acquired most of their normal offsets prior to MSC times, most probably linked to the post-orogenic extensional phase. At depth, F1 and F2 root in SE-dipping deep reflectors in the acoustic basement that we correlate with thrusts (Figure 5.7 and Figure 5.12-B). On the deep penetration seismic profiles, folds observed in the acoustic basement at the southern border of the MCHZ abut on the vertical faults (Betic thrusts and folds, NW-most fold on F2 in Figure 5.12-B; fold on SE of Mont Dels Oliva

on Figure 5.12-C). These geometries suggest that the compressional structures (thrusts) have been subsequently inversed during the extension phase affecting the pre-MSC unit (D, Figure 5.3). F1 and F2 that are at the origin of the MCDZ were thus structurally controlled by the former thrusts (F2, Figure 5.12-B; Figure 5.3-D), as also proposed by Sàbat et al. (1997), Gallart et al. (1995), and Sàbat et al. (2011). The pre-MSC unit filling grabens or half-grabens (Figure 5.6 and Figure 5.11) also confirm that the CMD already existed before the Messinian times, as proposed by some authors (Roca, 1992; Céspedes et al., 2001; Acosta et al., 2004a; Sàbat et al., 2011). The thickest pre-MSC depocenters (up to 900 m-thick) are located on the southern border of the CMD, as shown by the pre-MSC unit thickness map (Figure 5.11-B). However, we did not identify any major faults controlling the pre-MSC depocenter in this area.

5.4.2.2.2 Plio-Quaternary Deformations

During the Pliocene, the main depocenters shifted northward as shown by the pre-MSC versus PQ units thickness map (Figure 5.11-A). They developed along the MCDZ, bordered by the set of faults F1 and F2 that are characterized by a dominant listric geometry. Some of those steeply dipping faults were previously described and interpreted as triggered by surficial gravitational movements (Acosta et al., 2004). Our results show that they are deep-seated faults that were active during the deposition of the PQ1 unit as evidenced by the syn-sedimentary geometry of its internal reflectors. The unconformity at the top of the PQ1 unit must then correspond to the end of this major extensional episode, although the tectonic activity and subsidence should have carried on with a weaker amplitude until recent times (i.e., PQ2 unit). Accordingly, the existence of PQ depocenters (depressions D1, D2 and D3), present in the NE-SW the MCDZ are related mainly to an extension phase that was active during the PQ1 deposition and later attenuated during the deposition of PQ2.

We also observe very recent strike-slip deformation (Figure 5.10), along similar direction to the main NE-SW trending normal faults that affect the MSC unit. The fact that the normal faults are particularly vertical (Figure 5.6), suggests that some of the major normal faults have been reactivated as strike-slip faults during the deposition of the PQ2 unit. This phase of deformation could still be active today as revealed by some earthquakes epicenters that are localized along the active part of the faults (red faults in Figure 5.15). Transcurrent tectonic

regime is also coherent with the alternations of non-cylindrical highs (related to folds) and lows (related to the depocenters, grey and yellow areas, Figure 5.15). This is supported by the alignment of the PQ depocenters and the folds, both having no lateral extension and forming in small and narrow mini-basins along the NE-SW elongated MCDZ corridor.

We thus observe evidence for two distinct post-MSC tectonic deformation episodes (Figure 5.17-B and C): the first one corresponding to an extension, probably NW-SE trending, coeval with the continuation of the development of grabens and with the deposition of PQ1, and the second one associated with strike-slip tectonics along pre-existing normal fault zones, contemporaneously with the deposition of PQ2 unit, and probably still active at present-day.

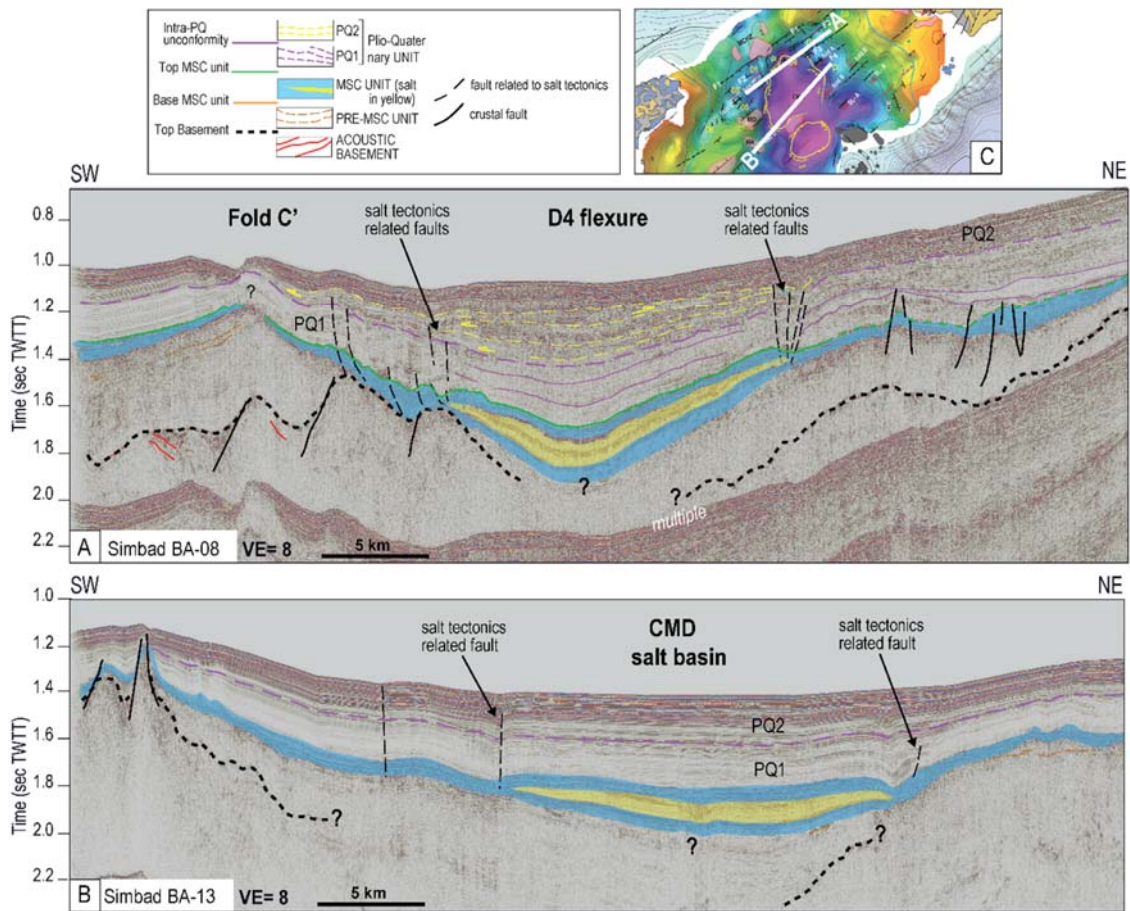


Figure 5.9. A and B: Seismic cross sections along the CMD where MSC salt (in yellow) deposited in between 2 MSC Bedded Units (BU, Raad et al., 2021; in blue). The salt is limited to the deep part of the CMD and usually appears as a flat unit, except due to moderate salt tectonics deformation located at the wedges. High-resolution seismic profile Simbad BA-08 (B) shows a post MSC/syn-PQ flexure (depocenter D4) that must result from crustal tectonics. C: Base Pliocene isobaths map (see Figure 5.10) showing the location of the seismic profiles shown in A and B.

5.4.2.3 Role of Plio-Quaternary charge in the Vertical Movements

The results of the pseudo-3D backstripping performed along strike the mini-basins (Figure 5.4; see section 5.3.2) allow evaluating the contribution of the post-Messinian sediment load, and associated subsidence, on the formation of the PQ depocenters D1 to D6. The reconstructed paleo topography of the top MSC across these depocenters, before deposition of the PQ unit, is shown in Figure 5.4. The results using effective elastic thickness $TE=5$ km (close to local isostasy, Figure 5.4-D) show that the topographic lows were already existing at the end of the MSC, as they remain visible on the backstripped section. The PQ sedimentary cover creates a mean subsidence of approximately 80m, with maximum values in the D4 depocenter reaching 110m (plot 2 in Figure 5.4-B). The PQ sediment load is maximal in D4, which therefore is the most sensitive area to variations of parameters in the backstripping analysis like TE . In D4, the sediment load can significantly amplify the MSC topography. Here a pre-existing low has been enhanced by the syn-PQ2 flexure (Figure 5.9). Results show that for the depocenters D1, D2 and D5, the PQ load only is not enough to significantly deform the top MSC surface. The PQ load may have contributed more significantly to the formation of the depressions D3 and D6, as a result of a thick PQ related to post-MSC shelf progradation (Figure 5.4-A).

Any slight increase in TE value implies a much smaller contribution of PQ sedimentary load-induced subsidence and therefore a more pronounced pre-existing topography in the reconstructed end-MSC surface. With $TE=15$ (regional isostasy, Figure 5.4-E), deflection is thus very small and only reflects the regional large-scale flexure of the CMD. The PQ load is responsible for only 50m of subsidence (Figure 5.4-B). In both models presented above ($TE=5$ and $TE=15$), the restored top MSC surface is relatively similar, both in term of pre-PQ depth and of overall morphology. This is in favour of the development of a mostly rigid deformation resulting from a more efficient regional effect of the surrounding deep basins (Heida et al., 2021). In addition, the morphology of the restored top MSC surface is not very different from the present-day buried one, suggesting that the topographic lows were already present before the PQ load. Because the PQ isostatic load cannot account for the creation of the local depressions, a significant amount of subsidence has to be driven by tectonic deformation, also brought out through our observations.

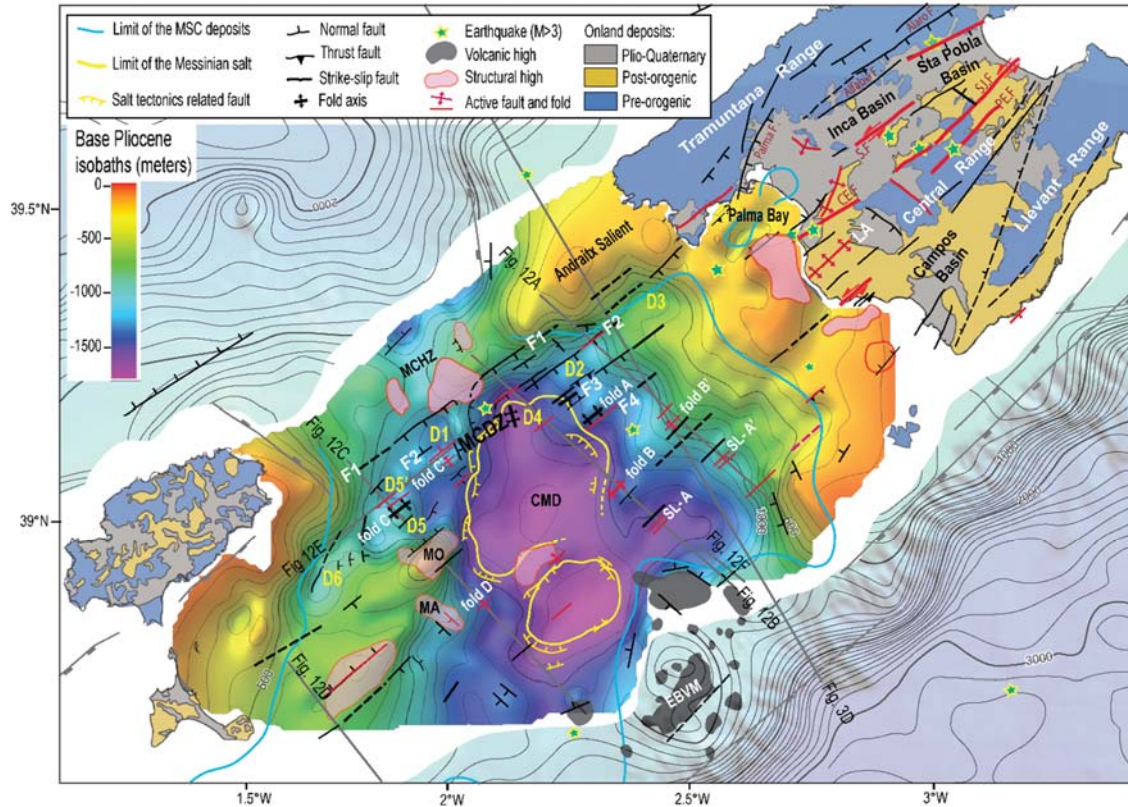


Figure 5.10. Structural map of the post-MSC deformation superimposed on the base Pliocene isobaths map. Onland faults and structures are modified from Silva et al., 2001; Sàbat et al., 2011; Sanchez-Alzola et al., 2014 and Mouragues et al., 2021. Location of earthquakes (from Sanchez-Alzola et al., 2014 and from International Seismological Centre, Bulletin 2020; see Figure 5.1 and Figure 5.2-D for more info) show that they are related to the main faults that bound the Mallorca and Mallorca Channel Depression Zone (MCDZ). The offshore colored map surrounding the structural map of our study area represent the present-day bathymetry (from Acosta et al., 2003). LA = Lluçmajor anticline. CE.F.: Cap Enderrocap Fault; S.F.: Sencelles Fault; SJ.F.: San Joan Fault; PE.F.: Petra Fault.

5.4.3 Land-Sea Correlation and Interpretation

5.4.3.1 Structural Continuity and Comparison

Figure 5.15 shows that the main structures in the Mallorca Channel are along strike with the major structures observed on the Mallorca Island. As attested by the observation of the Betic thrusts in this area, the MCHZ and the Andraitx Salient are the offshore continuation of the Tramuntana Ranges (see section 5.4.2.2; Figure 5.8 and Figure 5.3-D). In the same way, the

Central Ranges may extend offshore via the SW-NE trending topographic/structural high observed on the SW Mallorca margin and extending downslope to the CMD (folds B-B' area where thrusts are observed, Figure 5.8). Between both Ranges, the MCDZ is along strike with the Mallorca Graben. The faults bordering the MCDZ also align with onland structures. The F1 set of faults is at large scale along strike with the Alfabia and Alaro faults (Orient faults system) that limit the Inca and Santa Pobra sub-basins, respectively (Figure 5.15). Figure 5.3 highlights the analogies between the onshore and offshore records. It displays at the same scale two transverse sections across the Inca and Palma depressions onshore (Capó and Garcia et al., 2019) and across the mini-basin related to D2 offshore. These basins are all bordered by faults separating the pre-orogenic basement from the basin fills. The NW fault limiting the Inca sub-basin has been proposed to root on deep Betic thrusts (Sàbat et al., 2011; Figure 5.3-A) and so do the faults F1-F2 bounding the mini-basin related to D2 offshore (see section 5.4.2.2).

The Palma sub-basin is separated to the North from the Tramuntana Ranges by the N15°-N20° trending Palma fault. We do not observe any prolongation of the Palma fault offshore as proposed by Sanchez-Alzola et al. (2014) (Figure 5.15). This structure (former thrust?) may be expressed in the structural high that disconnects the Palma Bay from the mini-basin related to D3 (Figure 5.4-A). Further south, the F3 fault is along strike with the faults limiting the Mallorca Graben from the Central Ranges (CEP fault, Figure 5.10).

The onshore and offshore sections (Figure 5.3) display comparable thicknesses of post-orogenic sediments. Both onland and offshore faults constrain anisopachous pre-MSC units that evidence the post-orogenic extension (Sàbat et al., 2011; Moragues et al., 2021). They remain active during the Plio-Quaternary times as evidenced by the isopach map of the PQ sediments. Indeed Figure 5.13 illustrates a clear alignment of the post-MSC depocenters extending from the Mallorca Graben onshore to the MCDZ offshore. This alignment includes from east to west, the Alcudia Bay, Santa Pobra Basin, Inca Basin, Palma Bay and the mini-basins related to D1 to D6. All of these basins show the same order of dimensions (~6x10 km; Figure 5.3). Their alignment forms a 150km long and continuous NE-SW trending offshore/onshore trough restricted in a narrow (10km) corridor, the MCDZ-Mallorca corridor, or the Northern corridor (Figure 5.15).

Along strike sections show that the depocenters are separated from each other by highs which are unfortunately not clearly imaged due to the quality of the seismic data close to the Palma Bay (Figure 5.4-A and C). For example, the Palma sub-basin onland seems disconnected from

the offshore Palma Bay, which prevents confidently correlating the continuity of the sedimentary units from the CMD to the Palma Bay (Maillard et al., 2014; Raad et al., 2021).

Onland Mallorca, the Sencelles Fault constitutes one of the main post-orogenic extensional structures (Figure 5.16). Its deep structure shows that it roots on the Alfabia fault (Sàbat et al., 2011; Figure 5.3-A). Being initially a normal fault, it reversed during the Pliocene as left-lateral strike-slip fault. Compressive structures affected Neogene and Quaternary materials in the Palma and Inca sub-basins (Giménez, 2003), such as the Son Seguí-Santa Eugènia topographic high (Figure 5.14-A). The Late Messinian limestones associated with this antiform structure are, located in an anomalous position more than 300 m high (Figure 5.14-B), in a fold that affected the Messinian and Pliocene units. Located along the NW extremity of the Sencelles fault, this fold is associated with the transpressive strike-slip motion along the fault (Figure 5.16). Inversely, at the other extremity of the fault, the same deposits are buried in the Llubí area (Figure 5.16; Mas et al., 2014) and the resulting depression is interpreted as a negative flower structure due to a step-over along the Sencelles fault. These structures are interpreted as a push up structure and associated pull apart-like depression respectively along the Sencelles fault (Figure 5.14). Some major detachments resulting from the positive and negative strike-slip structures have been produced (Figure 5.14) (G. Mas & Fornós, 2020), possibly exploiting the clayey plastic sediments belonging to the final MSC stage also known as ‘Lago Mare’ (Andretto, Aloisi, Raad, Heida, Flecker, Agiadi, Lofi, Blondel, Bulian, & Camerlenghi, 2021), but possibly occurring later as slickenlines which are observed in Pliocene calcarenites (Mas, 2015). Offshore, we observe very similar structures on the high-resolution seismic profiles (Figure 5.6). Local non cylindrical folds are indeed of the same order of magnitude as the Son Seguí-Santa-Eugènia antiform in both width and height (200-300m) (Figure 5.14). Changes in footwalls along the offshore faults are also in accordance with strike-slip movements. Other small folds were observed onshore in the Levant and Central Ranges associated with some vertical faults interpreted as positive flower structures (Punta Roja vertical fault, Giménez 2003).

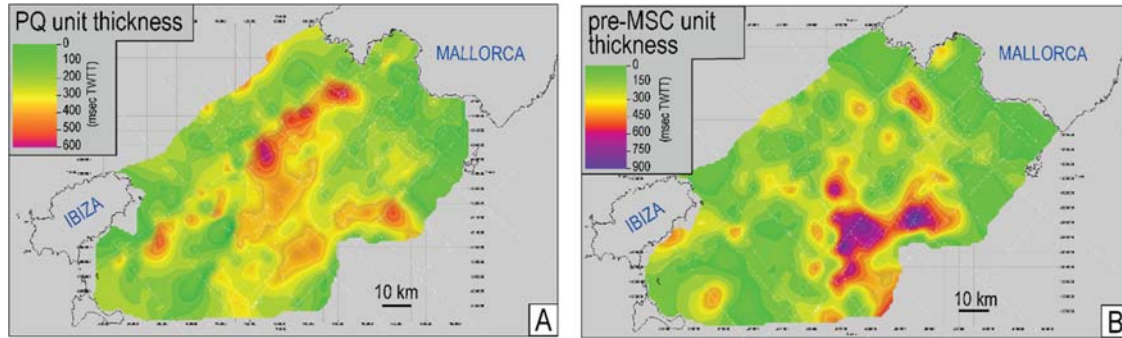


Figure 5.11. Thickness maps, in msec TWTT, of the A: PQ unit (Pliocene-Quaternary sediments) and B: pre-MSC unit (post-orogenic sediments, older than MSC unit). Thin white lines represent the position of the same seismic profiles shown in Figure 5.2-A. Note the evident change of depocenters from Miocene to Pliocene time.

5.4.3.2 Structural Interpretation

We interpret the Son Seguí-Santa Eugènia antiform as the result of recent transcurrent tectonics. This is consistent with the interpretation at larger scale of the tectonics in the entire Mallorca Graben as a strike-slip zone during Pliocene and Quaternary times associated with the sinistral movement of the main NE–SW faults of the island (Giménez and Gelabert, 2002; Giménez, 2003). In accordance with these former works and with our observations, and as the MCDZ is the offshore prolongation of the Mallorca Graben, we interpret the entire MCDZ-Mallorca corridor (Northern corridor) as a transcurrent trough. Therefore, the complex structures forming the MCDZ-Mallorca corridor are interpreted as alternations of transpressional (push up) and transtensional (pull apart) –type like structures respectively, in a large wrench zone allowing the coeval existence of compressional and extensional strains localized along restraining bends and step overs (Figure 5.15 and Figure 5.17-D) (Harding, 1985; Cunningham & Mann, 2007). Location of compressional versus extensional areas are reported in Figure 5.15. The folds that consist of narrow antiforms all cut by vertical faults, resemble positive flower structures that could correspond to restraining bends. This is the case on folds B –B’ where low magnitude earthquakes confirm their activity (Figure 5.10). Remobilization of F2 structure and SL-A-A’ display narrow synform limited by mostly normal separations, that are in that way interpreted as negative flower structures linked to divergent part of a wrench faults area (Huang & Liu, 2017). The D4 flexural depocenter that corresponds to the post-MSC synclinal fold can be linked to local transpression, induced by strike-slip relative movement along the F2 and F3 faults that limit the depocenter to the North (Figure

5.15). Unfortunately, we do not have focal mechanisms of the seism located on the extremity of the F2 fault (Figure 5.15). The MCDZ ends on the SE Ibiza margin, where we observe the curvature of the structure expressed in the area of fold C-C' and the associated offset of the D5, D5' and D6 mini-basins, with faults trending N20° and N15° respectively, associated with surficial deformation in the bathymetry (Acosta et al., 2004). This complex area is likely to be interpreted as the termination of a wrench zone (horsetail like structure?) (Figure 5.15).

Beside the main transcurrent MCDZ-Mallorca (or northern) corridor, some other corridors can be traced from onshore to offshore in the entire study area. On the down slope domain of the SW Mallorca margin, folds B and B' not only display structural highs along strike with the Central Ranges of Mallorca, but also reveal, as suspected by Acosta et al., (2001a), post-Messinian deformation comparable to the recent folds parallel trending (Llucmajor anticline, Figure 5.10; Sanchez-Alzola et al., 2014; Sàbat et al., 2011). The SL-A -A' apparent negative flower structure appears in a depression facing the Campos Basin. These structures are difficult to follow southwestward in the deep CMD domain where the PQ unit is barely deformed, but could be continuous with the Mont dels Oliva and Mont Ausias Marc faults on the other side of the CMD. These 2 mounts indeed show signs of recent faulting (Figure 5.12-C). Mont Ausias seamount shows a NE-SW oriented fault which dissects its flat top with a relief of more than 25 m. This complex fault network has been related with NE-SW transcurrent faulting (Acosta et al., 2003; 2004) with right lateral displacement, not in accordance with the left-lateral movements recorded onland. The deep domain of the CMD is however "split" by a structural high (Figure 5.10) whose nature is unknown but that resembles the B-B' fold. This elongated high could connect the strike slip zone (including faults SL-A-A' and fold B-B') to Mont Ausias fault system in a long transcurrent zone crossing the CMD, that we call the "Southern corridor" (Figure 5.15).

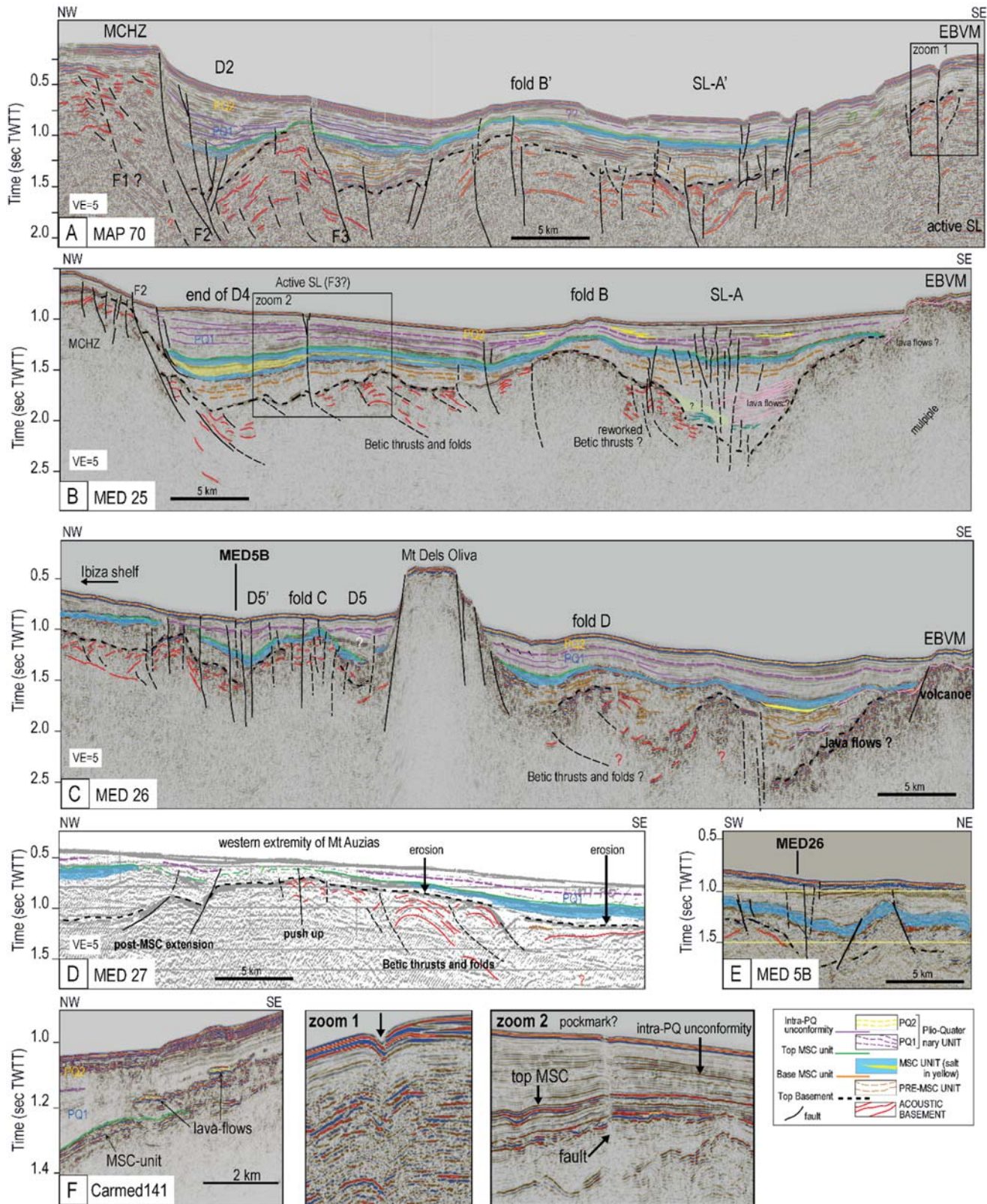


Figure 5.12. Deep penetrating seismic cross lines running from the Mallorca Channel Horst Zone (MCHZ) to the Emile Baudot Volcanic Mounts (EBVM) and illustrating the complex deformation of the study area that reworked Betic thrusts. See text for explanations. Notice the change in facies on the opposite sides of SL-A, could also indicate a strike-slip motion. See Figure 5.10 for locatio

5.4.3.3 Identification of the Units and Dating of Deformation

- **Pre-MSC unit and post orogenic extension phase:** As explained in section 5.4.2.2, the main N070° faults in the study area were active during the post-orogenic extension (middle Miocene times), perpendicular (NW-SE) to the thrusts proposed by Sàbat et al., (2011). They could also be associated with or followed by a NE-SW extension by processes of radial collapse (Moragues et al., 2021) responsible for dextral strike-slips on the N070° faults. The thickness of the post-orogenic sediments (Fuster, 1973) reaches 300-400m in the Palma and Inca sub-basins and includes Plio-Pleistocene sediments with a mean thickness of 100m (Capó and Garcia, 2019), attesting that the subsidence started before the Pliocene. Offshore, depocenters D2 and D3 accumulated around 400m of pre-MSC deposits (Figure 5.11-B) showing that those depressions likewise are pre-Pliocene. They thus display a clear analogy with the Mallorca Graben's depocenters, not only in terms of geometry and width but also in thickness. Based on this analogy, we propose a middle to late Miocene (Serravallian to Messinian pre-MSC) age for the pre-MSC unit offshore, which fan-shaped geometry is in accordance with extension or possible transtension (cf section 5.5.2; Figure 5.17-A). Note that the main depocenter for the pre-MSC units remains in the south of the CMD and are divided into 2 sub-basins (Figure 5.11). One of them is located in the offshore continuation of the Campos basin and could possibly be related to the same type of structuration. The south of the CMD (Southern corridor) was mainly formed during the pre-MSC times, while its northern part underwent tectonic subsidence mostly after the MSC.

- **MSC drawdown:** An important base level fall during the MSC affected the morphology of the area by erosion, as observed on all Mediterranean margins (the MES; Margin Erosion Surface; Lofi et al., 2011; Maillard et al., 2014; Roveri et al., 2014; Mas & Fornós, 2020; Raad et al., 2021). Offshore, this erosion was responsible for the creation of the Palma onshore/offshore valley dug in former grabens that were initiated during the post-orogenic extension (Maillard et al., 2014). Erosion is also observed locally on the slopes of the CMD and on the Mallorca Channel (Raad et al., 2021). In the meantime, MSC-related deposits accumulated in pre-existing depressions both onshore (gypsum sampled by drillings in the Palma sub-basin; see Mas and Fornós, 2020 and references therein) and offshore in the CMD

and on its slopes (Figure 5.9 and Figure 5.10; Maillard et al. 2014; Driussi et al., 2015a; Raad et al., 2021). The MSC event thus affected the study area and generated well identified surfaces and units that are used as a temporal marker (5.97-5.33 Ma). Fan-shaped MSC deposits show that extension persisted during their deposition in the Late Messinian.

-PQ1 unit and Pliocene deformation: The results of Capó and Garcia, (2019), suggested 50 to 150m of subsidence for the onland Palma, Inca and Santa Pobra sub-basins during the Pliocene-Quaternary. Such amplitudes of subsidence rates are in accordance with the PQ load we calculated offshore in the MCDZ (around 50m of subsidence, Figure 5.4-B). Onshore, during the Pliocene, heterogeneous marine sedimentation occurred as attested by the Son Mir Formation in the Mallorca Graben (Capó and Garcia, 2019). In the Palma sub-basin, subsidence is maximal during this period (Figure 5.3) and sediments fill up pre-existing topographic lows. At the scale of the Mallorca Graben, the subsidence rate deduced from accumulation rates decreases from the Lower Pliocene (Son Mir Formation) to the late Pliocene (San Jordi eolian Formation; Capó and Garcia, 2019).

Observations made in the PQ geometries offshore can help understanding the onshore records and vice versa. Based on thickness and geometry analogies, we interpret the PQ1 unit offshore as the equivalent of the Son Mir Formation onshore. The fan-shaped geometry of the PQ1 unit offshore is controlled by nearly vertical faults, while onshore, in the Inca sub-basin, the filling is clearly related to the Sencelles fault (Figure 5.3) which played an important role for creating accommodation space during the Lower Pliocene (Sàbat et al., 2011; Capó and Garcia, 2019). The important activity of the N070° set of faults controlling the depocenters along the MCDZ corridor reveals a localization of the deformation with still NW-SE extensional component with possible progressive change to a strike-slip regime (transtentional) (Figure 5.17-B). Offshore, PQ1 lies directly above the MES or the MSC unit (Fig. 7). Similarly onshore, the Son Mir formation lies unconformably on an erosional surface cutting the top of the Late Messinian Santanyi limestones or of the reef unit (Figure 5.3) which is interpreted as the MES (Mas and Fornós, 2020). The relatively transparent seismic facies of the PQ1 unit suggests homogeneous fine-grained sedimentation, in accordance with the hemipelagic sediments described on the SW Mallorca margin (Acosta et al., 2004a; Lüdmann et al., 2012). It is also in agreement with marlstones facies encountered at the base of the Son Mir formation deposited during high stand see level, in accordance with post-MSC Zanclean refilling.

-PQ2 and late-Pliocene/Quaternary deformation: using borehole data tied to seismic profiles on the BP, Ochoa, (2016) proposed that the top of the transparent PQ unit corresponds to the top of the Zanclean dated at 3.6Ma. Thus, following Ochoa, (2016) we tentatively interpret the change in seismic facies between PQ1 and PQ2 as corresponding to the change in lithology between the Son Mir (Zanclean) and the Sant Jordi (Piacenzian) formations. If so, the distal equivalent of the sandstones forming the Sant Jordi FM tie distally with the more reflective facies observed within PQ2. This facies should then include the Quaternary sediments in its upper part. The PQ2 is less fan-shaped and more isopachous which fits with the diminution of the tectonic subsidence through the Pliocene time onshore, as a result of the decrease in normal faulting activity and the change toward a strike-slip regime. However, there is no evidence onshore for any intra-PQ unconformity, as observed offshore, and the Pliocene succession onshore passes gradually vertically and marginward from deep silty deposits (Son Mir Calcisiltites) into calcarenites (Sant Jordi Calcarenites).

Onland, recent strike-slip movement is attested by late Pliocene/Quaternary tectonic fracturing and brecciation in the Inca sub-basin (Mas et al. 2014), in accordance with evidences for Quaternary seismic activity widespread on the island (Silva et al., 1998, 2001; Giménez & Gelabert, 2002; Giménez, 2003; Fornós et al., 2005). Offshore, normal or transtensive movements seem to decrease during PQ2 deposition, with F1 set of faults becoming non-active. F2 fault and several strike-slip faults southward in the CMD, affecting the sea floor, confirm a recent activity. Folds are particularly active and seem to confirm that transpression could be predominant (Figure 5.17-C), in accordance with reverse movement along the Sencelles fault (Silva et al., 1998; 2001; Giménez and Gelabert, 2002; Giménez, 2003; Mas et al., 2014).

Offshore seismicity (Figure 5.1) is likely to be related to the transcurrent structures, confirming the present-day activity. Significant earthquakes (magnitude > 3) are located offshore on tectonic structures described in this study. One epicenter is located on an active segment of F2, precisely where a transversal fault offsets the MCDZ near the depocenter D4 (Figure 5.15). Another epicenter is located on the fault bordering the Palma Bay to the SE. Some others are in the vicinity of the fold B and correlate with the Southern corridor. The epicenter located precisely on the active strike-slip fault south of the CMD (active SL, zoom 1, Figure 5.12-B) confirm its present-day activity. This corridor appears particularly active when compared with faults system F1 and F2 which could suggest that deformation propagates southwards.

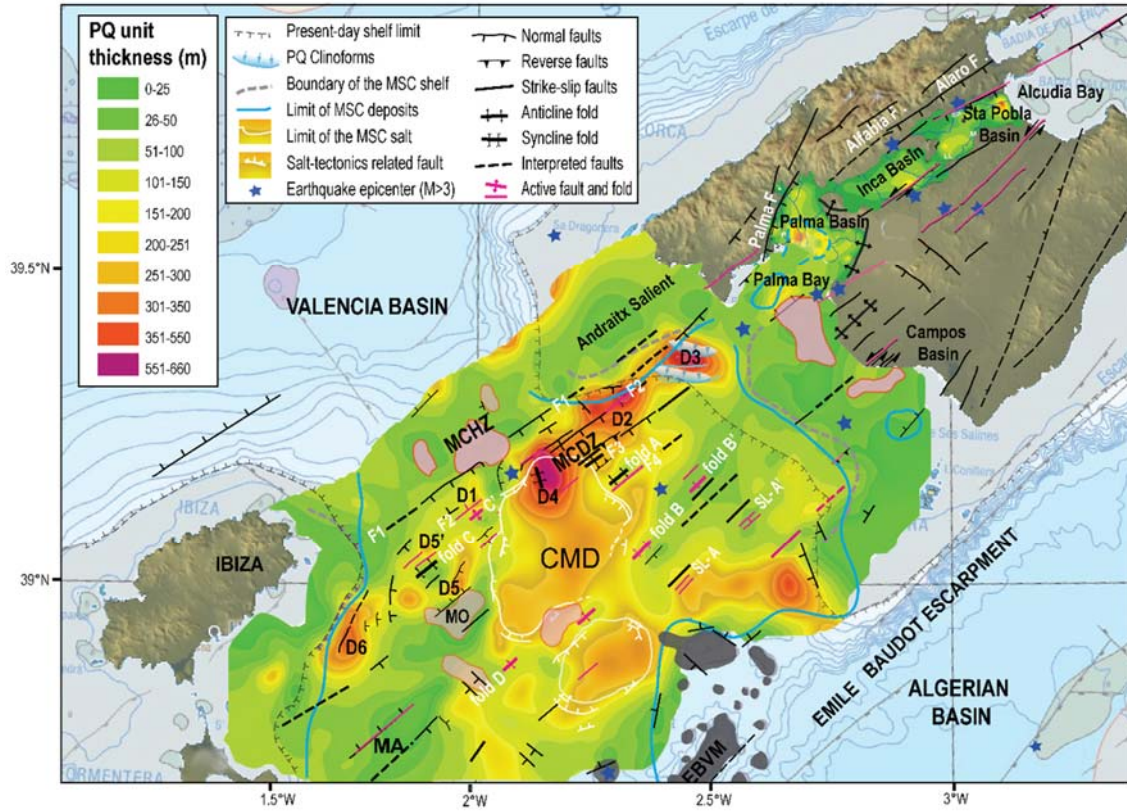


Figure 5.13. Onland-offshore thickness map of the Pliocene-Quaternary (PQ) unit, in meters. It illustrates the relationships between the main post-MSC faults and structures and the PQ depocenters (D1 to D6) in the Mallorca Channel Depression Zone (MCDZ). Land-sea correlation shows the continuity between those depocenters offshore, and the Mallorca Graben onland, with same order of thickness. PQ thickness on Mallorca Island is taken from Capó and Garcia, 2019. Some structures on the South Ibiza margin are modified from Acosta et al., (2004). Surrounding areas are from the geological map of Spain 1:1000000; IGME.

5.5 Discussion

Hereafter, we integrate our study area into the BP and a larger regional scale sketch. How can the tectonic evolution of the CMD from late Miocene to recent fit with the regional tectonic evolution and kinematics? Is it compatible with what is recorded on the other large faults of the area?

5.5.1 Regional Extension of the Corridors

The western termination of the proposed Northern strike-slip corridor is localized offshore, at the SE Ibiza margin where faults are turning toward a N010°-020° direction in the D6 area (Figure 5.10). It may possibly extend further westwards between Ibiza and Formentera Islands as the rough scarp of the Ibiza SW shelf is perfectly aligned with the F1 set of faults and connects westward with a small earthquake swarm along a normal fault (Figure 5.15). Moreover, some important post-Messinian deformation is observed offshore the SW Ibiza margin. It corresponds to a number of active structures such as the Xabia and El Cid Sea Mounts without clear lateral continuity but which are also characterized by a similar N060°-N080° trend (Figure 5.1; Acosta et al., 2001b; Maillard and Mauffret, 2013; Driussi et al., 2015b). Farther to the west, the Ibiza Channel between mainland Spain and Balearic Islands (Figure 5.1) acts as a boundary east of which the main trend of the structural pattern changes slightly from N065-070°E to N080-085°E, becoming roughly parallel to the Mazarron escarpment. The Ibiza Channel could include a NW-SE directed transfer zone extending northward to the western boundary of the Valencia Basin (Nao Fracture Zone that offsets the Betic front, Figure 5.1; Maillard, 1993; Nao FZ, Figure 5.17). Within the Valencia Basin, some other NW-SE transfer zones have been proposed and linked to the Oligo-Miocene rifting episode and associated volcanism (Maillard and Mauffret, 1993; Acosta et al., 2004b; Pellen et al., 2016). One of them, the Ibiza Fracture Zone, was supposed to extend between Ibiza and Mallorca and has been proposed to account for differential rotations between both these Islands during the Betic orogeny (IFZ, Figure 5.17; Parés et al., 1992; Acosta et al., 2001a). In our study area, this transfer zone could be expressed by the NE Ibiza rough escarpment and the NW-SE trending faults east of the Mont Ausias Marc (Figure 5.10). It has been proposed to still be active and responsible for recorded seismic events (Acosta et al., 2001a; Sanchez Alzola et al., 2014). Our results show no evidence for any active NW-SE trending structures, and only some minor NW-SE structures were described from onland Mallorca (Sàbat et al., 2011; Mouragues et al., 2021).

On the other side of the study area, NE of Mallorca, the faults bordering the Santa Pobra sub-basin extend offshore in the Alcudia Bay. There, the activity of these faults and their offshore prolongation is outlined by seismic activity through the location of several earthquakes (Figure 5.15). We do not have enough data coverage to specify how far the faulted corridor extends to the NE on the Mallorca shelf. Further NE, Menorca is separated from the rest of the Promontory

by another major NW-SE trending transfer zone that distinguishes it from the other islands (Central Fracture Zone; Maillard, 1993; Maillard et al., 2020; Pellen et al., 2016; CFZ; Figure 5.17).

South of the study area, the Mont Ausias Marc faults were also interpreted as strike-slip structures by Acosta et al. (2003; 2004a), in accordance with our proposition for a Southern Corridor (Figure 5.15). Moreover, a N060-070°E fault also limits the North of the Formentera Basin (Driussi et al., 2015b; Etheve et al., 2016; Figure 5.1): as poor post-orogenic extension is observed there (Maillard et al., work in progress), it could also accommodate some recent strike-slip deformation, and could therefore correspond to the western prolongation of the Southern corridor.

The strike-slip faults systems outlined from this study are continuous from the east of the Ibiza Channel toward the NE Mallorca shelf and thus reveal a homogeneously deformed Ibiza-Mallorca block during at least the late Miocene to Quaternary times.

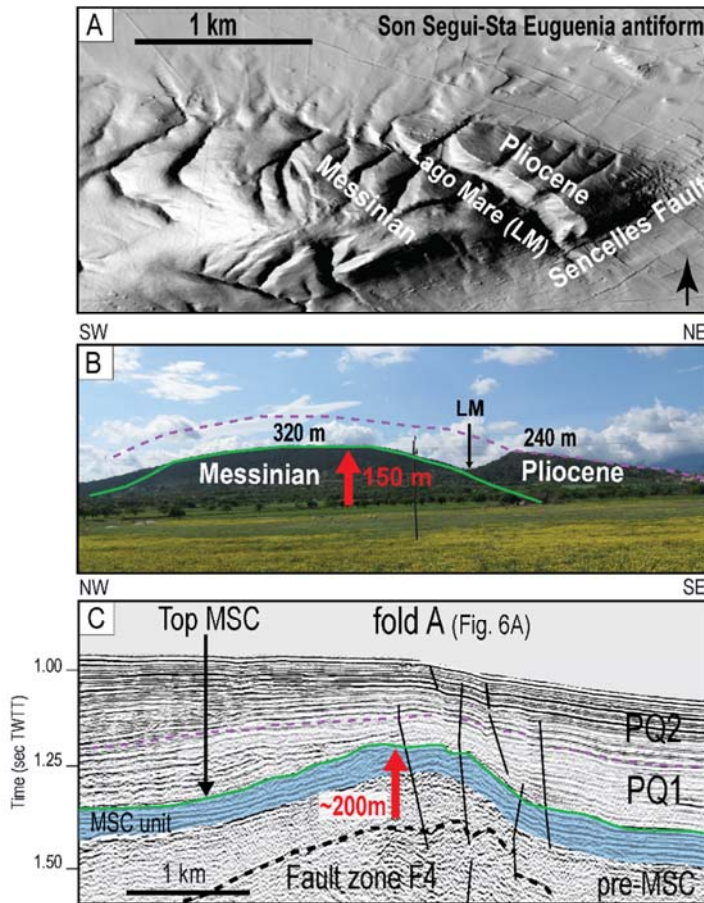


Figure 5.14. Comparison between onshore and offshore positive flower-type structures. A and B: Onshore Son Seguí-Sta Eugènia antiform structure: correspondence between (A) the antiform on a Digital elevation model (DEM; location on Figure 5.16) and (B) the field relief due to the Messinian and Pliocene bending. (DEM data is downloaded from the Spanish Centre for Geographic Information

(<https://www.ign.es/web/ign/portal/qsm-cnig>). C: Offshore, seismic image of fold A on F4 fault zone as visible on profile BA-16 (extract from Figure 5.6-A), at same scale than B (1/1). Both structures are 1-2 km long and 150-200m in height.

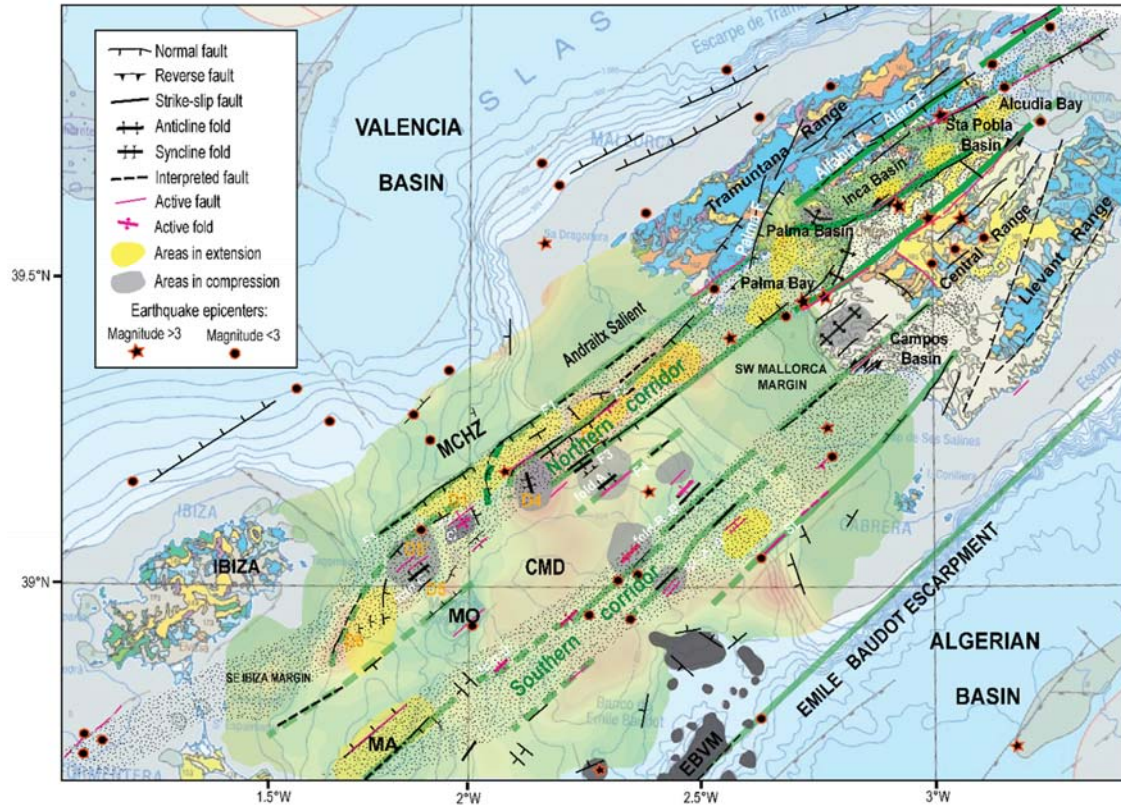


Figure 5.15. Interpretative map of the post-MSC tectonics distributed in long transcurrent onshore-offshore fault zones (in green) resulting in corridors (dotted area) where effects of locally extensional (PQ depocenters) or compressional (folds) environments combine. Surrounding areas showing bathymetry and onland geology are from the geological map of Spain 1:1000000 (legend in Figure 5.1); IGME. Pliocene-Quaternary (PQ) unit thickness map is superimposed displaying the PQ depocenters.

5.5.2 Regional Scheme, Relation with the Emile Baudot Escarpment

We identify several large-scale parallel strike-slip corridors across the entire study area, from both onshore and offshore data (Figure 5.15). Bordering the BP to the south, the EBE is running strictly parallel to these corridors. This major structural lineament must thus be taken into consideration when relocating our observations in a regional tectonics framework.

The EBE is often interpreted as a crustal-scale structure formed by the westward motion of the Alboran block, during the rollback of the slab from the Ligurian Tethys lithospheric slab (Cohen, 1980; Lonergan & White, 1997b; Gutscher et al., 2002; Rosenbaum et al., 2002a;

Mauffret et al., 2004b; MATTAUER, 2006; Gutscher, 2012; Medaouri et al., 2014) presently located under the Gibraltar Arc, as visible in seismic tomographic data (Spakman & Wortel, 2004; Garcia-Castellanos & Villaseñor, 2011b; Vergés & Fernández, 2012). Though the age and even the nature of the Algerian basin are poorly constrained, most authors propose an oceanic accretion phase dated from late Burdigalian or Langhian (19-15Ma) to Tortonian (8Ma), younging westward (Mauffret et al., 2004b; Jolivet et al., 2009; Crespo-Blanc et al., 2016; R. Leprêtre, 2018; Romagny et al., 2020; Haidar et al., 2021). If that right-lateral origin for the EBE is adopted, then it would seem reasonable that the strike-slip corridors of the CMD also originated by the same dextral motion. While we will adopt such interpretation for the following discussion, it must be kept in mind that other regional tectonic models do not involve a large westward rollback at the BP (Garcia-Castellanos & Villaseñor, 2011b; Vergés & Fernández, 2012). In fact, the first post-orogenic deposits on the BP are apparently linked to NW-SE extension rather than to strike-slip tectonics, at least in the central part of the Mallorca Graben (Benedicto et al., 1993; Sàbat et al., 2011). Indeed, the Mallorca Graben faults seem to record normal movement in accordance with the fan-shaped geometry of the pre-MSC units that we observe offshore associated to the structural development of the MCDZ. [Booth-Rea et al. \(2017\)](#) suggested that a WSW-ENE extension on the BP would be expressed by WSW-ENE strike-slip faults acting during late Langhian–Serravallian, as in particular, the dextral-oblique strike-slip system that limits the southern foothills of the Tramuntana ranges (Alfabia/Alaro fault zones). They have related these deformations to the opening of the Algerian Basin coevally with the transfer fault along the EBE. [Etheve et al. \(2016\)](#) proposed to explain the formation of the Formentera basin south of Ibiza by dextral transtensional movement associated to the same episode. Such a movement is coherent with NW-SE trending faults spread all over the BP, not predominant in the CMD but widely observed throughout the South Menorca Block, where they have been related to SW-NE extension ([Driussi et al., 2015](#); Figure 5.17-A). One should however notice that the NW-SE faults from the BP developed over short distances and that they show offsets of the MSC unit. Thus they could alternatively, and preferably, be related to extensional local step-over along the Plio-Quaternary strike-slip faults. [Mouragues et al. \(2021\)](#) recently proposed a collapse during Serravallian associated with low angle normal faults and accompanied by radial extension ranging from SW-NE to NW-SE directions. The NE-SW-directed faults were transfer faults during the first episode of extension, with most of them expressing right-lateral displacement but with a few others showing left-lateral displacements. Such complex displacement pattern is relatively common in transfer fault systems that are related to extension (e.g. [Giaconia et al., 2014](#)). Faults with very similar

orientation have also been observed in the Betics on mainland Spain, and were interpreted in the same way (Figure 5.17) (Martínez-Martínez et al., 2006; Giaconia et al., 2014). These SW-NE trending long faults, as well as the EBE, are usually supporting the kinematic reconstitutions of the Algerian Basin, through a process of slab tearing during upper Miocene times, in accordance with the interpretation of the west Algerian margin as a STEP fault (Medaouri et al., 2014; Leprêtre et al., 2018; Haidar et al., 2021) and the EBE as a transform margin (Mauffret et al., 2004b; Driussi, Briais, et al., 2015). These SW-NE faults in the Betic domain have been suspected to still be active under Plio-Quaternary transpression (e.g. Bousquet, 1979; Giaconia et al., 2012, 2014). Such faults with changing kinematics, with here an early behavior as dextral transtension and followed by later transpression (e.g., Martínez-Martínez et al., 2006; Meijninger & Vissers, 2006; Ferrater et al., 2015), are likely similar to the faulted corridors in the Balearic Promontory. Considering a dextral motion along the main SW-NE faults in eastern mainland Spain and along EBE during the westward drift of the Alboran Block, the faulted corridors described from this study should also record an early dextral movement during Serravalian to Tortonian times (Figure 5.17-A). Our data do not show evidence of right-lateral movement in the pre-MSU unit that would anyway have been overprinted by the following tectonic phases but its fan-shaped geometry could account for transtension. It cannot either be excluded that the initiation of the faults could be older and therefore related to the Oligo-Miocene rifting episode in this region, and if so, they could have recorded also some extensional deformation during the early stages of the post-orogenic collapse (early Serravallian). During Plio-Quaternary times, if a possible left-lateral reactivation of the corridors is compatible with general strain that changed to NS compression (Figure 5.17), its relationship with the EBE is not straightforward, as no clear motion is recorded there. Only very small magnitude earthquakes (magnitude up to 1.9 Mw; Figure 5.2-D) are localized along the EBE, showing little active deformation. Numerous volcanic pinnacles on the EBVM could reveal some relatively recent activity as a Pleistocene age was attributed to a basalt sample recovered from the area (Acosta et al., 2004b). In our seismic data, we recognize some volcanic lava flows interbedded within the PQ unit close to the EBE, which also confirms some recent activity from these volcanoes (seismic profile Carbmed 141, Figure 5.12-F).

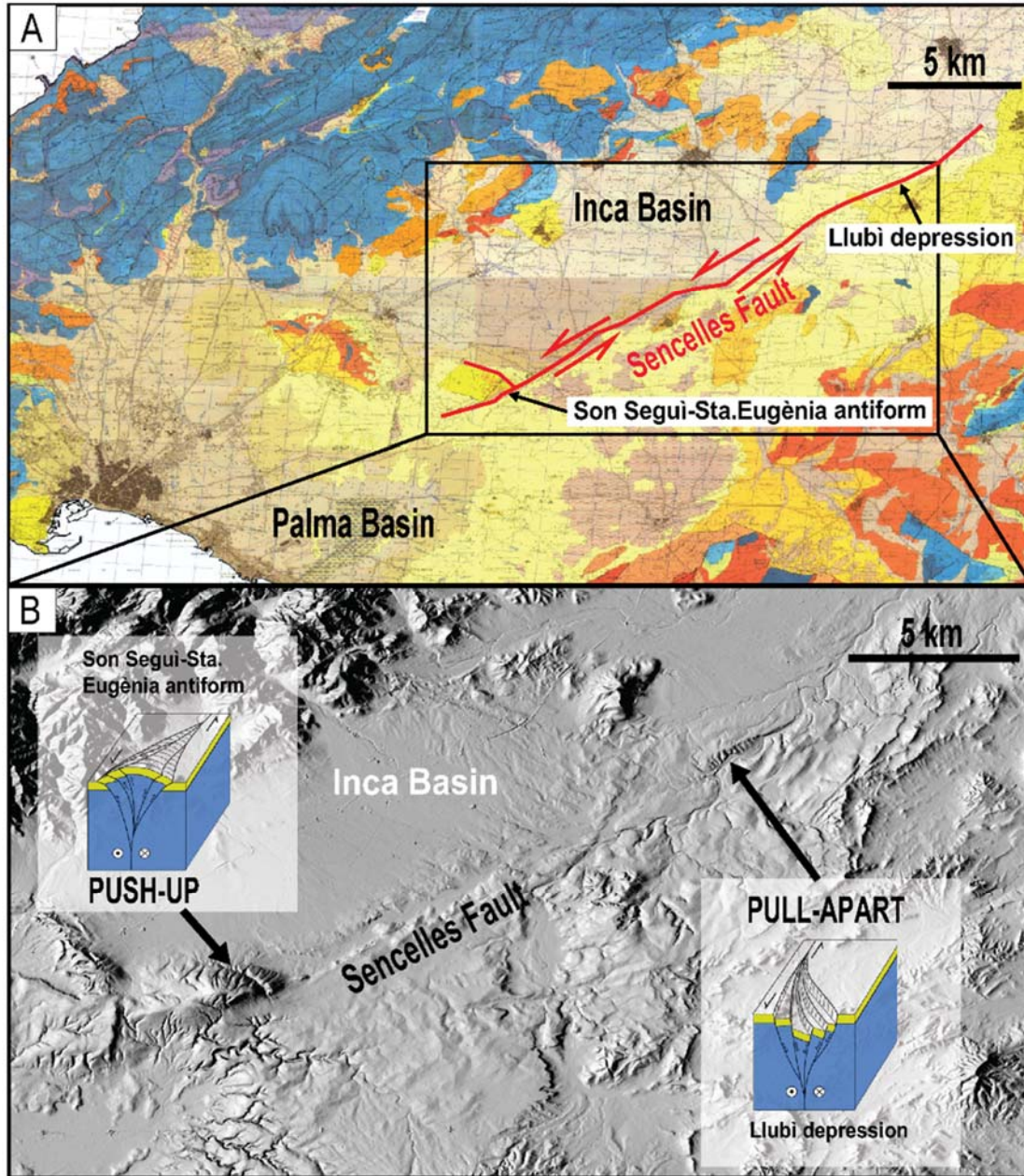


Figure 5.16. A: Geological location of the structures on the Inca sub-basin. B: Digital Elevation Model (DEM) of Inca sub basin illustrating the Sencelles Fault area (DEM data is downloaded from the Spanish Centre for Geographic Information (<https://www.ign.es/web/ign/portal/qsm-cnig>)). Son Seguí-Sta. Eugènia antiform and Llubí depression can be the expression of restraining (push-up positive structure) / releasing (pull-apart negative structure) bends respectively along the Sencelles Fault.

Along the EBE scarp the presence of volcanic material is also suggested by widespread chaotic seismic facies and by magnetic anomalies (Figure 5.1 and [Driussi et al., 2015](#)), attesting for a

period of intense volcanic spreading, which started before the Pliocene. Reflective layers indicative of lava-flows on the seismic profiles are also locally observed in the pre-MSC unit. They may be linked in age to volcanism that grew by local transtension along the EBE, which may have allowed magmatic intrusions along deep fractures (Camerlenghi et al., 2009). The recent magmatism probably initiated during the slab retreat through STEP process along the EBE that then became an active transform zone during the oceanic accretion of the Algerian basin. Volcanism could have continued after EBE became passive. Some transform margins, such as Guinea or Agulhas transform margins, also experienced volcanism during their passive margin stages (Benkhelil et al., 1995; Mercier de Lépinay et al., 2016). Volcanic seamounts can be lined up with transform margins, which could have acted as a lithospheric weakness zone (Deplus et al., 1998; Basile et al., 2013), and inversely, transform margins can be reactivated and can localize deformation (Attoh et al., 2005). Acosta et al. (2001a; 2004b) proposed a genetic link between the recent formation of the volcanic pinnacles with a process of decompression resulting from the extensional deformation. This normal faulting episode consequently led to the subsidence of the CMD. However, as shown by the distribution of the depocenters on the pre-MSC thickness map (Figure 5.11-B), the main subsidence episode already occurred before the Pliocene (Figure 5.10; [Capó & Garcia, 2019](#)). Instead, we prefer to invoke some degree of reactivation of the EBE as a left-lateral fault, triggered by the ongoing convergence between Nubia and Eurasia. However, the occurrence of recent volcanism in the nearby Valencia Basin (e.g., Columbretes Islands and offshore extension, CV., Figure 5.1) may rather require a regional explanation. The alkaline nature of this recent magmatic episode of the Valencia Basin, late Miocene to Quaternary in age (Martí et al., 1992b; J.-P. Réhault et al., 2012), has been related there with recent widespread lithospheric extensional deformation at the European scale (Morocco to North Sea large shear zone, [López-Ruiz et al., 2002](#); [Muñoz et al., 2005](#)). This is not clear for the BP, as the lithospheric thickness is not thin (70 to 80km; [Roca et al., 2004](#); [Carballo et al., 2015](#)) and regional heat flow is as low as in the Valencia Basin (Fernández et al., 1998) and very variable at the western part of the EBE (Poort et al., 2020). Although the recorded high heat flow values are not spatially correlated with the known volcanic intrusions, they could be related to recent volcanism, as observed on the Columbretes Islands where heat flow values reach 120-150 mW/m² (Poort et al., 2020).

The regional setting during the Pliocene is contractional as Africa is currently converging toward Eurasia at a rate of 5 mm/yr in this area (Demets et al., 1990; Nocquet & Calais, 2003; Serpelloni et al., 2007). The deformation associated to this convergence is mainly localized in

the thrust belts of North Africa and in the active Algerian margin, with the major faults showing compressional focal mechanisms (Meghraoui, 1988; Yielding et al., 1989; Déverchère et al., 2003, 2005; Domzig et al., 2006; Yelles, Domzig, Déverchère, Bracène, Lépinay, et al., 2009). Contraction is well expressed on the BP only around the Ibiza Channel where recent folds reshape the Alicante shelf (e.g. Tabarca and Cogedor highs; Figure 5.1 and Figure 5.17-C), as well as numerous recent mass-wasting events on the SW Ibiza margin (Acosta, Muñoz, Herranz, et al., 2001b; Alfaro et al., 2002; Acosta et al., 2003; Acosta, Canals, et al., 2004b; Lastras et al., 2004; Camerlenghi et al., 2009b; Maillard & Mauffret, 2013b). The easiest way to explain left-lateral strike-slip motion during Quaternary along the NE-SW trending corridors of the CMD and of Mallorca is to relate them to the general NS to NNW-SSE contraction, as also proposed by Sàbat et al. (2011). It also explains the compressional deformation recorded on the nearly E-W trending structures of the Alicante shelf, parallel to the Mazarron Escarpment and the strike-slip motion along the Crevillente fault zone where the Llorca earthquake occurred in 2011 (Figure 5.17-C).

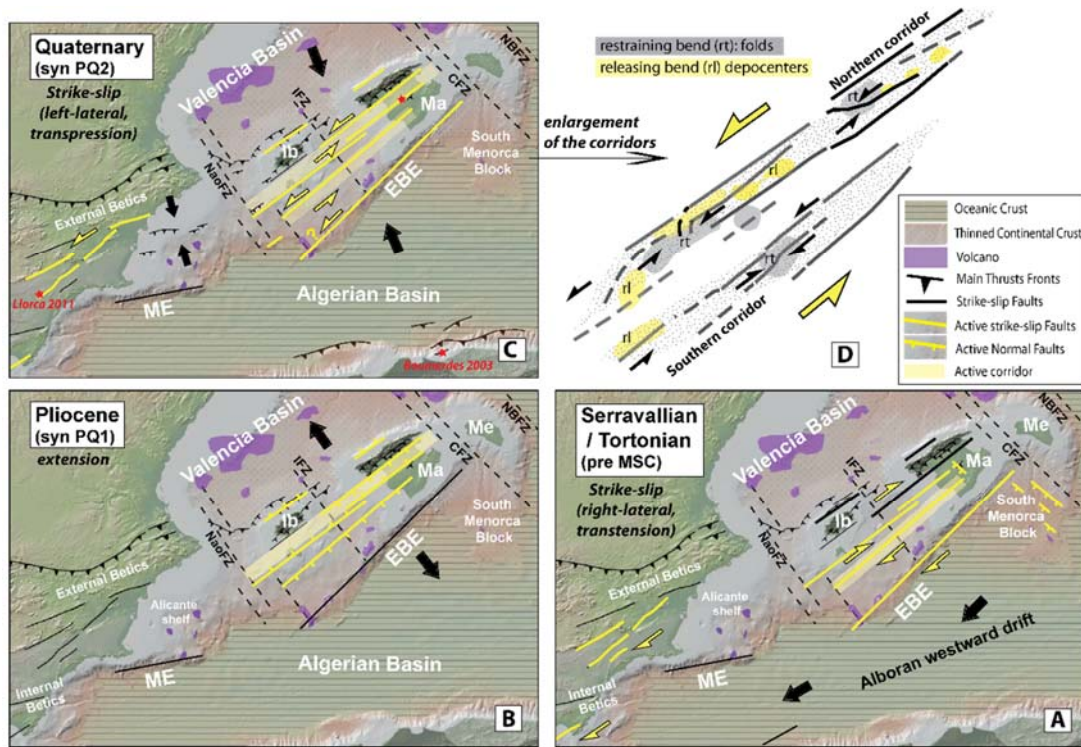


Figure 5.17. Schematic sketch of the evolution of the tectonic regimes proposed in the study area since the Late Miocene. The Ibiza-Mallorca corridors are included in a regional view that does not take into account the kinematics as the blocks are presented in their present-day configuration. In yellow are the active structures. A: During pre-MSC Middle Miocene times, tectonic regime is driven by the Alboran Block southwestward escape and the related accretion in the Algerian Basin; the main depocenters are localized in the Southern Corridor (see Figure 5.11). B: During the Pliocene, extension and/or transtension is responsible for the normal activity of the faults zones that reshape the Ibiza and Mallorca margins and localize the depocenters in the Northern Corridor. C: Quaternary to Present-day convergence accounts for left-lateral reactivation of the Ibiza-Mallorca corridors and the Southeastern Spain faults zones, and the compressional structures on the Alicante shelf. D: zoom of the Quaternary tectonics highlighting the extensional/compressional deformation in strike-slip corridors.

5.6 Conclusion

The results of our investigation on the central part of the Balearic Promontory show moderate but clear post-Messinian tectonics. Our data and analysis, together with onshore-offshore comparisons and correlations, leads us to propose a coherent interpretation for the structures observed offshore in the Pliocene to Quaternary sedimentary units.

In the Central Mallorca depression (CMD), we show that the main recent depocenters, Pliocene to Quaternary in age, display a succession of mini-basins that line up along a large NE-SW corridor, the MCDZ or Northern corridor, along strike with the onshore Mallorca Graben, also

composed of three sub-basins of similar scale. The main fault system bordering the corridor has been correlated with onland faults bordering the Mallorca Graben, which we interpret as reactivated post-orogenic normal faults. Extensional tectonics persists after the Messinian. The combination of onland stratigraphic data and offshore seismic stratigraphy and geometry of the units allows us to date a change of the tectonic regime from extension to strike-slip by the end of the Zanclean stage. Moreover, it led us to specify the correlations between different seismic facies, PQ1 and PQ2, with contrasted lithologies observed onland respectively from the Son Mir (Zanclean) and the Sant Jordi (Late Pliocene) formations with an unconformity in between.

The activity of large strike-slip systems, mainly during the late Pliocene and the Quaternary, can explain the complex and non-cylindrical extensional and compressional structures observed. They consist of narrow open anticlines crossed by vertical faults that resemble positive flower structures in restraining bends, and of small-scale mini-basins corresponding to the depocenters of the Plio-Quaternary series. These mini-basins are therefore interpreted as releasing bends along the strike-slip fault system. We show that some local folds developed offshore along faults that prolongate into the Mallorca Graben. They are equivalent to the one uplifting the Messinian units of 300m onshore along the Sencelles fault in the Inca sub-basin, which confirm the existence of the long offshore/onshore Northern strike-slip corridor. Such recent folds, mini-basins, and associated faults are observed also in the south of the Central Mallorca Depression and can be linked to onshore features such as NE-SW trending folds and sinistral strike-slip faults around the Campos Basin. We thus propose a coherent land-sea tectonic state that includes active strike-slip tectonics responsible for the distribution of earthquake epicenters along the corridors.

At the scale of the Balearic Promontory, we show that the faulted corridors extend east of Mallorca Island to the Alcudia Bay and also westward to the Ibiza Channel, revealing a homogeneously deformed Ibiza-Mallorca block, running parallel to the Emile Baudot Escarpment (EBE) that corresponds to the main morphological feature of the BP, with recent activity expressed by some Pliocene to Quaternary volcanism. Our study shows that, during the late Miocene, the main faults already existed, with syn-extension sedimentation as it can be observed in the post-orogenic grabens onland Mallorca. Thus, our reconstruction through time of successive basin geometries and tectonic pattern illustrates the importance of structural inheritance. Some of the initial Betic thrust systems (pre-Middle Miocene) have been firstly inverted as normal faults during post-orogenic extension in the middle to late Miocene, leading to the development of the Central Mallorca Depression offshore similarly to the Mallorca

Graben onland. The faults could also record some mostly dextral strike-slip displacements during the late Miocene, in accordance with a westward escape of the Alboran Block accommodated by the EBE crustal-scale transform fault between the BP and the surrounding Algerian oceanic basin. Then, most of these deeply-rooted crustal faults have been again reactivated from Pliocene times to Present-day. They localize the PQ depocenters along the MCDZ during the Pliocene while the pre-MSD depocenters were preferentially located to the south of the Central Mallorca Depression. During the Quaternary, the current regional strain characterized by a nearly N-S compression driven by Africa-Eurasia convergence is responsible for reactivation of the faulted corridors of the Central Mallorca Depression with some mostly left-lateral transpressive tectonics.

Chapter 6

Paleo-Topography of the Balearic Promontory: A Regional Flexural Isostatic Restoration

Received: 31 March 2021

Revised: 23 July 2021

Accepted: 12 August 2021

DOI: 10.1111/bre.12610

RESEARCH ARTICLE

Basin
Research

IAG EAGE

WILEY

Flexural-isostatic reconstruction of the Western Mediterranean during the Messinian Salinity Crisis: Implications for water level and basin connectivity

Hanneke Heida¹  | Fadl Raad²  | Daniel Garcia-Castellanos¹ |
Ivone Jiménez- Munt¹ | Agnès Maillard³ | Johanna Lofi²

In the previous chapter, I showed that only moderate post-MSC tectonics affected the central part of the Balearic Promontory. Now to obtain the bathymetry there, the only step needed is to correct for the vertical movements other than tectonics that acted since the late Miocene. To do so, a regional flexural isostatic restoration work at the Western Mediterranean scale was performed in collaboration and by the lead of Hanneke Heida from the SaltGiant project under the supervision of Daniel Garcia-Castellanos.

In the article presented in this chapter, we compile seismic markers from a widespread seismic dataset, to unload the MSC and Plio-Quaternary sedimentary sequences. The article is published in 'Basin Research' journal.

The main take-home message that I would like to give the reader from this chapter is:

- *At the beginning of the MSC evaporites deposition, the Central Mallorca Depression was lying at a maximum depth of ~1500m*
- *Some salt patches of the Balearic Promontory's sub-basins were deposited at depths as shallow as 500m*
- *The obtained paleo-bathymetry in the Central Mallorca Depression is viable and now can be used to model confidently the evaporites deposition, which will be the focus of the next and last result chapter of this thesis.*

Abstract: During the Messinian Salinity Crisis (MSC, 5.97–5.33 Ma), thick evaporites were deposited in the Mediterranean Sea associated with major margin erosion. This has been interpreted by most authors as resulting from water level drop by evaporation but its timing, amplitude and variations between subbasins are poorly constrained due to uncertainty in post-Messinian vertical motions and lack of a clear time- correlation between the marginal basin and offshore records. The Balearic Promontory and surrounding basins exemplify a range of responses to this event, from margin erosion to up to a kilometer-thick Messinian units in the abyssal areas containing the majority of the MSC halite. The Balearic Promontory contains unique patches of halite with thickness up to 325 m at intermediate depths that provide valuable information on water level during the stage of halite deposition. We compile seismic markers potentially indicating ancient shorelines during the drawdown phase: the first is marked by the transition from the MES to UU based on seismic data. The second is the limit between the bottom erosion surface (BES) and abyssal halite deposits. We restore these shorelines to their original depth accounting for flexural isostasy and sediment compaction. The best- fitting scenario involves a water level drop of ca. $1,100 \pm 100$ m for the Upper unit level and $1,500 \pm 100$ m for the BES level. According to our results, halite deposition began in the Central Mallorca Depression at 1,300–1,500 m depth, perched hundreds of meters above the deep basins, which were at 1,500–1,800 m (Valencia Basin) and $>2,900$ m (Algerian Basin). The hypothesis that erosion surfaces were formed subaerially during the drawdown phase is consistent with a model of halite deposition before/during the water level drop of at least 1,000 m, followed by the deposition of the Upper unit until the MSC is terminated by the reinstatement of normal marine conditions.

6.1 Introduction

The Messinian Salinity Crisis (MSC) was a period of rapid and massive environmental changes in the Mediterranean (Hsü et al., 1973a) at the end of the Miocene (5.97-5.33 Ma) (Krijgsman, Hilgen, et al., 1999a; Manzi et al., 2013b) leading to deposition of a layer of evaporitic sediment (mostly halite) thicker than a kilometer in the deep basins and to widespread erosion of the basin margins. Building on the model of Clauzon et al. (1996), a 3-stage model of the crisis has been progressively developed (CIESM, 2008b; Manzi et al., 2013b; Roveri, Flecker, et al., 2014b):

Stage 1 (5.97-5.60 Ma): Onset of MSC with the deposition of ‘Primary Lower Gypsum’ (PLG) in the marginal basins (Lugli et al., 2010) and on open continental shelves and slopes (D. Ochoa et al., 2015a).

Stage 2 (5.60-5.55 Ma): Halite and potash salt deposition in the deep basins and local intermediate basins, e.g. Sicily; (Lugli et al., 1999), synchronous to or followed by erosion and resedimentation of stage 1 PLG.

Stage 3 (5.55-5.33 Ma): deposition of ‘Upper Evaporites’ (UE) consisting of gypsum with marl interbeds with stronger freshwater input and Lago Mare event(s) (Manzi et al., 2009b; Orszag-Sperber, 2006a). This stage is often divided in stage 3.1 (5.55-5.42, Upper Evaporites), and stage 3.2 (5.42-5.33, Lago Mare).

The chronology and environmental conditions during the various depositional and erosional stages are still under debate. For example, some authors suggest that deep-basin halite was formed synchronous to the PLG in stage 1 in a salinity-stratified water column (Meilijson, Hilgen, et al., 2019a; Simon & Meijer, 2017a; Van Ceuvering et al., 1976). Evaporite deposits in the deep basins of the Western Mediterranean have not yet been drilled beyond their topmost layer, and due to the extreme conditions during their deposition they lack biostratigraphic water depth proxies. The main evidence supporting water level variations are erosional surfaces observed in outcrops in marginal basins (Bourillot et al., 2009; Bourillot, Vennin, Rouchy, Blanc-Valleron, et al., 2010; Clauzon et al., 1996a, 2015b; Conesa & Badinot, 1999; Dabrio & Polo Camacho, 1995; Decima & Wezel, 1967; Dela Pierre, Bernardi, Cavagna, Clari, Gennari, Irace, Lozar, Lugli, Manzi, Natalicchio, et al., 2011; Do Couto et al., 2015; Dronkert, 1976; Fortuin et al., 2000; Krijgsman et al., 2001a; Ott d’Estevou & Montenat, 1990; Pagnier, 1976; Riding et al., 1991; J.-M. Rouchy & Saint Martin, 1992; Roveri et al., 2009a; Vai & Lucchi,

1977b) and in the offshore seismic record underlying, intercalated in, and on top of the Messinian deposits, pointing to a kilometric water level drop or (near) desiccation of large parts of the Mediterranean (Ryan, 1976; Ryan & Cita, 1978; Lofi et al., 2005, 2011a, 2011b; Maillard et al., 2006; Raad et al., 2020). The MSC ended abruptly with a geologically-sudden reestablishment of open marine conditions, purportedly due to reflooding through the Strait of Gibraltar causing a deeply eroded channel in the Alboran basin and chaotic deposits associated with the flooding event (P. L. Blanc, 2002; Estrada et al., 2011a; Garcia-Castellanos, D., et al., 2009; Garcia-Castellanos et al., 2020a; Micallef, Camerlenghi, Garcia-Castellanos, Cunarro Otero, et al., 2018). However, some authors have argued for much smaller water level variations (<200 m) and alternative mechanisms for the formation of incised channels (Roveri et al., 2014). The widespread occurrence of brackish lacustrine “Lago Mare” deposits on top of the deep and marginal evaporites has led other authors to suggest that the basins were already connected at high water level before the end of the Messinian (Andreetto, Aloisi, Raad, Heida, Flecker, Agiadi, Lofi, Blondel, Bulian, Camerlenghi, et al., 2021; Andreetto et al., 2020a; Stoica et al., 2016b), which would be at odds with an outburst flood from the Atlantic Ocean.

Messinian erosional surfaces and deposits have been affected by subsidence and possibly phases of rebound since the start of the MSC due to loading by sediment deposition and water level changes (Gargani, 2004; Govers et al., 2009b; Norman & Chase, 1986; W. B. F. Ryan, 1976, 2011). Backstripping (Watts & Ryan, 1976b) is a classical technique used to calculate the isostatic and compaction effects due to sediment loading. Traditionally, this technique has been used to constrain the vertical motions related to tectonic loading by thrusting or extension, provided the availability of precise paleobathymetric measures. However, in areas where tectonic loading is negligible, it can a priori be inverted to constrain paleobathymetry (Amadori et al., 2018). The technique has been applied to constrain the original depth of the Messinian units and erosional surfaces in wells and along sections in the Gulf of Lions (W. B. F. Ryan, 1976), the Tertiary Piedmont Basin (Amadori et al., 2018), the Balearic Promontory (G. Mas et al., 2018), and in the Ebro delta (Urgeles, Camerlenghi, Garcia-Castellanos, De Mol, Garces, et al., 2011). This has led to drawdown estimates in the western Mediterranean of 1300 m of late-Messinian water level drop based on terrace formation in a fluvial erosion network (Urgeles et al., 2011) and a minimum of 800 m drawdown to facilitate faunal colonization of the Balearic Islands (Mas et al., 2018).

Except for (Amadori et al., 2018), the aforementioned studies have been based on either local isostasy or 1D (cross-section) flexural isostasy. While a 2D (planform or pseudo-3D) technique

was used by Govers (2009) and Govers et al. (2009), these studies were not designed to reconstruct the pre-MSC bathymetry nor reconstruct the shoreline positions. For this reason, paleobathymetric reconstructions based on erosional/depositional markers are only locally available in specific areas of the Western Mediterranean and their mutual consistency are difficult to evaluate.

In this paper, we aim at using a 2D (planform, pseudo-3D) flexural backstripping technique supported by an extensive set of seismic data to quantify Messinian and post-Messinian vertical motions, to constrain the paleodepth and the Messinian water level drop at the scale of the Western Mediterranean. To this purpose, we constrain the model with paleoshoreline indicators based on an extensive seismic dataset. The starting hypothesis of our study is therefore that these stratigraphic features were formed near the shore during the MSC. The depth range of the Valencia Basin and Balearic Promontory and their unique distribution of Messinian markers (Figure 6.2) with erosion on the margins (Maillard et al., 2006, 2014; Urgeles et al., 2011; Driussi et al., 2015; Cameselle and Urgeles, 2017), Upper Unit in the Valencia Basin (Maillard et al., 2006a) and a complete MSC trilogy in the deep basin (Figure 6.2-A) (Lofi, Déverchère, et al., 2011; Lofi, Sage, Deverchere, et al., 2011) provide an opportunity to constrain the progression of water level during the MSC in a region that covers the gap between shallow evaporite deposits (primary gypsum) and the deep (abyssal) salt deposits visible in the seismic record. A compilation of key MSC-related features including evaporite deposits and erosional features is presented in Figure 6.1.

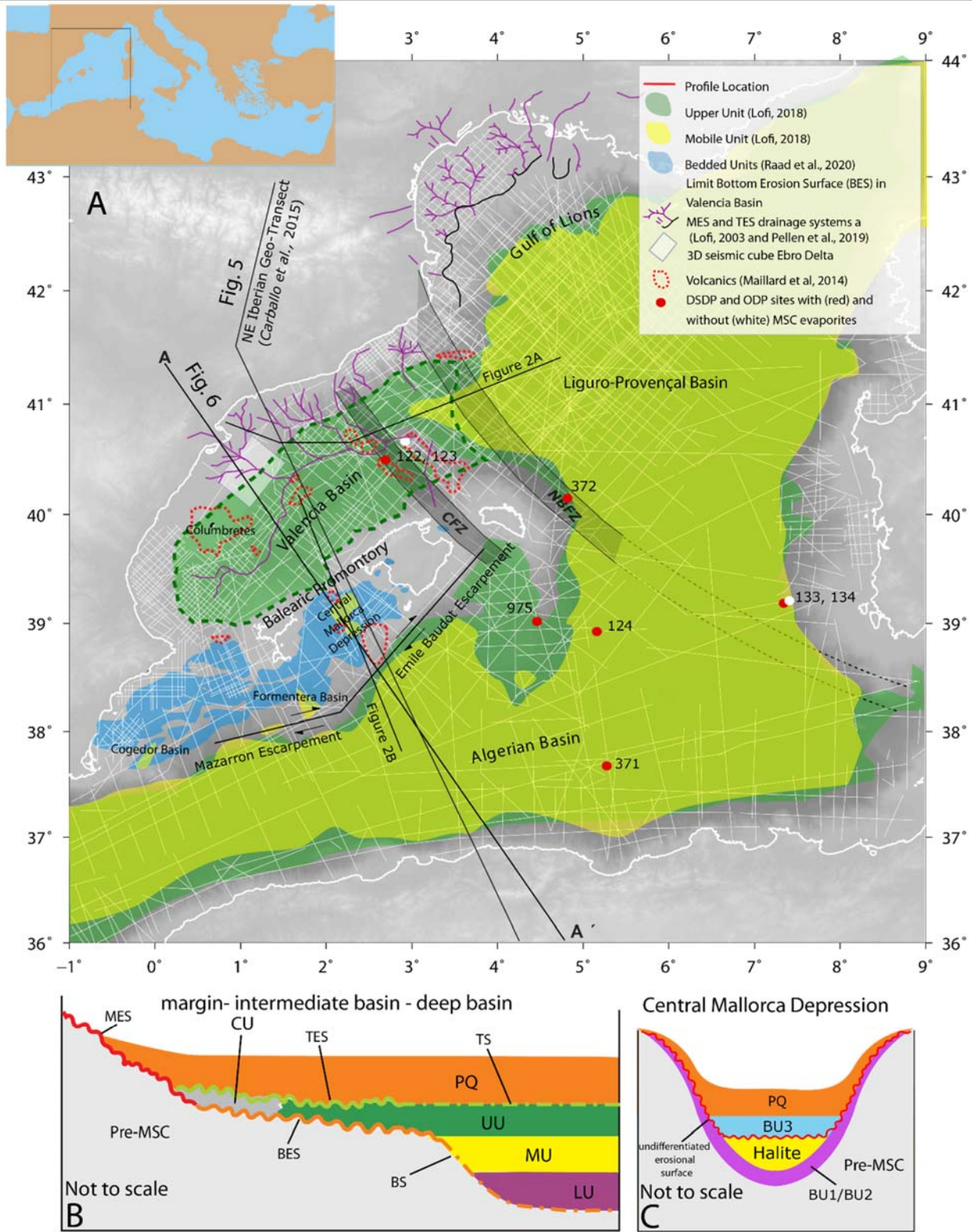


Figure 6.1. A: Topographic map of the Western Mediterranean area with the distribution of the main Messinian deposits and erosional features. It includes the main tectonic structures and locations of DSDP boreholes, seismic data used in this study (thin white lines), and location of the representative seismic profiles (Figure 6.2) used for lithosphere characterization (Figure 6.5) and the backstripping restoration (Figure 6.6). CFZ: Catalan Fracture Zone; NBFZ: North Balearic Fracture Zone. B: Schematic cross section of the Western Mediterranean basin illustrating the present-day distribution of sedimentary units and surfaces after (Lofi, 2018b). C: Schematic cross section of the Central Mallorca Depression (post) Messinian units (BU= Bedded Unit) and surfaces.

6.2 Geodynamic Setting

6.2.1 Tectonic Setting

The Western Mediterranean comprises basins with distinct ages, tectonic styles and crustal nature. They formed as back-arc basins due to slab rollback of the retreating Apennines subduction in a general setting of N-S convergence between the African and Eurasian plates since the Miocene (Faccenna et al., 2004; Gelabert et al., 2002; Gueguen et al., 1998; Jolivet et al., 2006; Malinverno & Ryan, 1986; Martínez-Martínez & Azañón, 1997; Mauffret et al., 1995, 2004; Schettino & Turco, 2006).

The Neogene Valencia Basin is a region of continental crust which was extended between 28 and 10 Ma (Bartrina et al., 1992; Etheve et al., 2018b; Roca & Guimerà, 1992a; Watts & Torné, 1992b), bounded by the Iberian Margin to the northwest and the Balearic Promontory to the southeast. To the east the Valencia Basin is bounded by the North Balearic Fracture Zone (Galdeano and Rossignol, 1977; Rehault et al., 1984; Maillard et al., 2020) which accommodated the anticlockwise rotation of the Corsica-Sardinia-Calabria blocks with the emplacement of the oceanic crust of the Provençal basin between 22 and 16 Ma (Alvarez, 1972; Burrus, 1984; Gueguen et al., 1998b; Speranza et al., 2002b). Contrary to the Provençal Basin, the Valencia Basin extension did not attain the formation of oceanic crust but instead extension jumped to the southern side of the easternmost Betic range to form the Balearic promontory and open the Algerian Basin.

The Algerian Basin opening in the Miocene (16-8 Ma) has long been thought to be the result of the westward migration of the Alboran block due to rollback of the subducting Tethys plate (Lonergan & White, 1997a; Rosenbaum et al., 2002b). However, recent alternative models suggest that it can also be explained by back-arc spreading during the southwards retreat of the neotethyan subducted slabs (Faccenna et al., 2004b; Vergés & Sàbat, 1999), ending before 8 Ma. It is separated from the Balearic Promontory by the Emile Baudot and Mazarron Escarpments, structures that have been proposed to be the remnants of a transfer fault along which the Alboran domain migrated westward (Acosta, Muñoz, Herranz, et al., 2001a; Mauffret et al., 2004a).

With the exception of the Tyrrhenian Basin, all Western Mediterranean basins were mostly formed at the onset of the MSC (W. B. F. Ryan, 1976). The present-day thickness variations of the MSC units are therefore thought to be related to paleo-waterdepth and post-Messinian vertical movements (e.g. Lofi et al. (2011b)). Thin-skinned salt tectonics and subsequent deformation of the salt (diapirism) is another cause for the present-day thickness variation (CIESM, 2008b; Dal Cin et al., 2016). Recent shortening has been reported between Alicante and Ibiza (Maillard & Mauffret, 2013a), and post-MSC tectonics has also been reported in the Mallorca Island and in the CMD, interpreted in relation with strike-slip movements located in WSW-ENE narrow depressions. As these deformation affects the MSC markers only locally, so we do not consider this deformation in our basinwide reconstruction.

6.2.2 Volcanism

Two distinct volcanic phases have been identified in the Western Mediterranean (Maillard, Mauffret, et al., 1992; Martí et al., 1992a). The first, mostly represented by calc-alkaline affinity, has been related to the emplacement of a volcanic arc of the SE-retreating subduction also observed in Sardinia, Corsica and Ligurian domains and is coeval to the Valencia rifting stage (late Oligocene-Early Miocene age), while the second stage is alkaline and represented by the Columbretes and the Southwest Mallorca Field on the Emile Baudot Escarpment (Late Miocene-Recent), and could be linked to regional decompression during extension (Acosta, Ancochea, et al., 2004a; Acosta, Muñoz, Herranz, et al., 2001a; Martí et al., 1992a; J. P. Réhault et al., 2012). This recent volcanism locally deformed the MSC deposits and erosion surface. The large extent of the volcanoes in the Valencia Basin surely affected the thermal history of the basin. Based on well data from the Catalan margin, these volcanic phases have been proposed to have counteracted general subsidence due to relaxation after the end of the main rifting phase at 10 Ma in the Valencia Basin (Watts & Torné 1992).

6.2.3 Messinian Salinity Crisis Stratigraphy

The distribution of the MSC sedimentary sequences is used to define paleoshoreline indicators that constrain our model. They have been identified and widely studied and described mainly

from seismic datasets by several authors (Maillard et al., 2006; Camerlenghi et al., 2009; Lofi et al., 2011b; Urgeles et al., 2011; Driussi et al., 2015; Ochoa et al., 2015; Dal Cin et al., 2016; Cameselle and Urgeles, 2017; Lofi, 2018 and references therein; Pellen et al., 2019; Raad et al., 2020).

The deep basins of the Western Mediterranean (i.e. Provencal and Algerian Basins) contain the full MSC trilogy (e.g. Lofi et al., 2011b see also Figure 6.1-b), identified mainly through seismic reflection profiles with its components listed below:

- Lower unit (LU): age, origin and lithology remain unclear. It has been suggested to be a shale equivalent to Stage 1 PLG (Manzi et al., 2007b, 2018b).
- Mobile unit (MU): here considered representative of “Stage 2” lies conformably above the LU in the deep basins. Towards the limits with the intermediate depths (i.e., Valencia Basin), MU lies above pre-MSC sediment along a bottom erosion surface (BES) or Bottom Surface (BS) where conformable (Figure 6.2-A, C). Its upper boundary is conformable. The MU consist of up to kilometer-thick transparent seismic facies that is thought to contain mainly halite and it is highly deformed by salt tectonics. It pinches out everywhere on the borders of the deep basins (Figure 6.2-A to C, F).
- Upper unit (UU): deposited during “Stage 3” lies conformably above the MU in the deep basins, while towards the intermediate depths beyond the extent of MU it lies above the BS/BES. In the deep basins the upper boundary of the UU is conformable with the overlying PQ unit (TS), whereas in the intermediate Valencia Basin it is cut by a top erosion surface (TES) (Figure 6.2-A, D, E). The uppermost part of the UU has been drilled, and it is made of alternations of gypsum and clastic deposits (ODP initial reports volume 161; Ryan, 2009). Its thickness reaches ~1000m in the deep basins (Figure 6.2-C; Lofi et al., 2011b), where it pinches out towards the slopes (Figure 6.2-B, F). In the Valencia Basin, the UU thins gradually from 500m thickness (Figure 6.2-D, E) pinching out towards the Catalan and Ebro margins. Here the Bottom and Top Erosion Surfaces bounding the UU merge into the polygenic Margin Erosion Surface (MES).

Several interpretations in terms of water level change exist to account for the observed geometries and extent of erosional surfaces. We briefly describe those interpretations and present the scenario we adopt to test in our model. The depositional environment for the Lower Unit is hard to constrain, as its lithology is not known beyond its seismic reflectivity. There are no indications of water level variations during the deposition of this unit, and therefore we do

not consider it as a separate stage in our topographic restoration. It is evident from well data in the Alboran Basin that restriction of the Atlantic-Mediterranean connection started affecting the depositional environment at ~ 7.2 Ma, well before the onset of evaporite deposition (Bulian et al., 2021a).

A water level drop leading to margin erosion occurred after deposition of the PLG in the marginal basins (Krijgsman, Hilgen, et al., 1999a) and the MU precipitated from a brine formed under conditions of restricted, but probable continuous connectivity to the Atlantic. MU deposition possibly started before and surely continued during the stage of water level drop, but without supply of marine waters from the Atlantic cannot have continued throughout a prolonged lowstand. Evidence for a change of deep brine precipitates to playa lake facies inside the halite unit is found in the Realmonte salt mine in Sicily (Lugli et al., 1999a) although this might not be representative for the deep basin deposits. The amplitude of the water level fall is controversial, as it varies between a few hundred meters for some authors (Roveri et al., 2014a and references therein, 2014b) and more than one kilometer for others (Lofi, Sage, Déverchère, et al., 2011). Maillard et al., (2006) believe that it is during this kilometer amplitude water level drawdown that the BES was formed, due to subaerial exposure of the entire Valencia Basin.

Most authors believe that the emplacement of the UU happened during a rise in water level during the final MSC stage, causing its aggrading and onlapping geometry (Lofi et al., 2011a, 2011b). The onlaps of the UU are interpreted as indicators of successive paleoshorelines (Lofi, Gorini, Berné, Clauzon, Tadeu Dos Reis, et al., 2005).

For some authors, the nature of the TES in the Valencia Basin could be a result of dilution during the Lago-Mare phase, and/or subaerial exposure preceding the Zanclean reflooding (Escutia & Maldonado, 1992a; Maillard et al., 2006a). For others, this erosion is minor and can be found only locally due to the dilution during the Lago Mare event (Cameselle & Urgeles, 2017b). A significant water level drop in Valencia Basin with unclear timing and magnitude is agreed upon (Cameselle et al., 2014; Cameselle & Urgeles, 2017b; Maillard et al., 2006a; Urgeles, Camerlenghi, Garcia-Castellanos, De Mol, Garcés, et al., 2011).

In the southwestern Valencia Basin, Cameselle & Urgeles (2017) identified a widespread Complex Unit locally overlain unconformably by a thin UU. The Complex Unit is interpreted here as a mass transport deposit resulting from destabilization of the slope during the first Messinian lowstand exposing the shelf and upper slope. Complex Units with different origin and timing are also present at the downslope mouth of Messinian valleys (Lofi, Gorini, Berné,

Clauzon, Dos Reis, et al., 2005; Maillard et al., 2006a) and especially in the Gulf of Lions (Lofi et al., 2005).

On the Balearic Promontory, recent studies show the presence of widespread bedded units (Bedded Unit) and relatively thin salt patches (Driussi, Maillard, et al., 2015a, 2015a; Maillard et al., 2014a; Raad et al., 2020). These units seem to be discontinuous between the Balearic Promontory and the surrounding deeper basins.

Raad et al. (2020) interpreted the MSC units of the Central Mallorca Depression as an undeformed analog of the Sicilian MSC records. They recognized the equivalent of the PLG, salt and Upper Evaporites (UE). These authors suggest that the CMD was disconnected from the surrounding deep basins during the MSC water level fall. They identify a prominent erosional surface cutting the top of the PLG and of a salt unit in the depocenter (Figure 6.1-C). This surface lies at a present-day depth of ~1550 m below sea level (Figure 6.2-B) and is interpreted as the result of an exposure or dissolution of salt in shallow water.

On Mallorca and Ibiza, the MSC record is mainly expressed by the terminal carbonate complex lying today between 30 and 60 m above sea level (Maillard, Gaullier, et al., 2020b; G. Mas & Fornós, 2011). It is thought that the terminal carbonate complex formed close to sea level, starting from stage 1 of the MSC contemporaneous to the PLG (J. J. Cornée et al., 2004; G. Mas & Fornós, 2013; Roveri et al., 2009a). Onshore drillings in the Palma de Mallorca basin also evidenced the presence of stage 1 PLG (García-Veigas et al., 2018a; Rosell et al., 1998a) lying below the PQ sediment, only a few tens of meters below sea level. Local water level recorded by phreatic overgrowths on speleothems in caves on the SE coast of Mallorca were recently established to have been at 33.3 and 31.8 m above modern just before and during the Stage 1 of the MSC respectively (Dumitru et al., 2021), although these were not corrected for vertical motions induced which the authors point out is necessary to properly interpret these water level results.

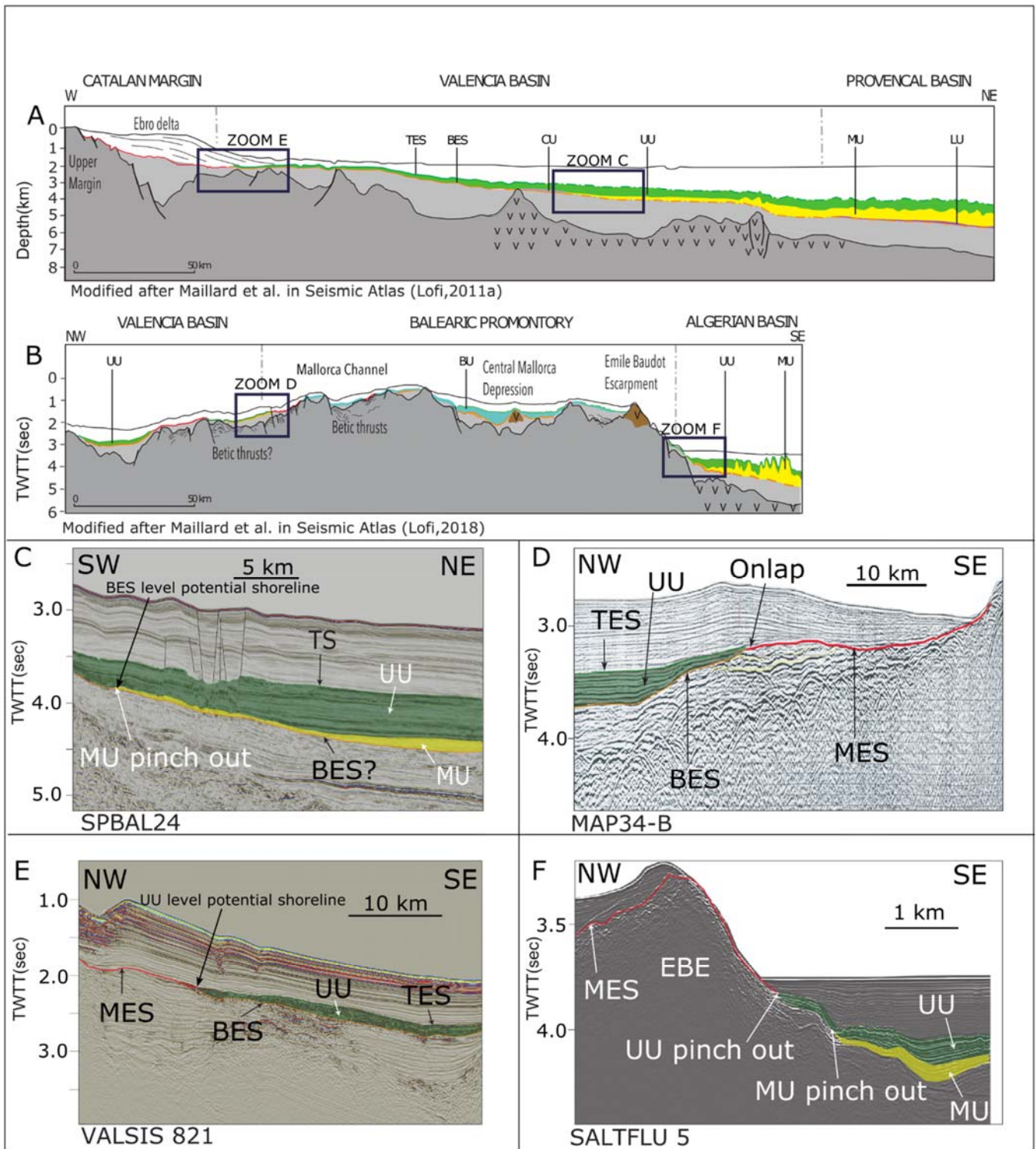


Figure 6.2. A, B: Line drawing composite profiles crossing key structural and sedimentary domains in the Western Mediterranean (from seismic atlases, (Lofi, 2011, 2018b)), position of profiles in Figure 6.1. C-F representative seismic lines with interpreted erosional features and MSC related evaporite units. D: modified after Maillard et al. in (Lofi, 2011). F: modified after Camerlenghi et al. in (Lofi, 2011).

6.3 Data and Methods

6.3.1 Paleo-shoreline Markers and Tested Scenarios

In this study, we constrain vertical motions and bathymetric changes during and after the MSC using pseudo-3D flexural-isostatic backstripping. We consider scenarios with and without a water level fall and investigate their implications for Mediterranean bathymetry, constraining the original depth of the proposed paleo-shoreline markers. The first scenario relies on those by Maillard et al., (2006), Ryan, (2009) and Lofi et al., (2011b) which propose the following MSC seismic markers as potential paleo-shorelines during the MSC:

- The onlap of UU onto the margins is considered the main paleo-shoreline indicator towards the end of the MSC, where the MES splits into a BES and TES bracketing Messinian deposits. The deposition of UU is proposed to occur in shallow waters (Cameselle et al., 2014; Cameselle & Urgeles, 2017b; Lofi, Gorini, Berné, Clauzon, Dos Reis, et al., 2005; Maillard et al., 2006a), before a rapid reflooding (Garcia-Castellanos et al., 2020 and references therein). The onlap of the top of the UU on the MES likely represents the highest water level during its deposition, although the top of the UU shows truncations (TES) that indicate possible variations around this water level. This stage is referred to as the UU level.
- The limit of the BES to MU on the margins is hypothesized to be another indicator of the paleo-shoreline after salt emplacement following an evaporative drawdown (Ryan, 2009). During this lowstand, the Bottom Erosion Surface developed in the Valencia Basin, where almost the entire region was subaerially exposed (Maillard et al., 2006). The elevation of the MU limit is variable due to the extensive erosion/dissolution that affected it after deposition. The shallowest preservation of halite limits the BES and is therefore our reference point. The limit was also affected by halokinetic activity (Badji et al., 2015; Dal Cin et al., 2016). However, the distal limit of the imaged BES offers a constraint on the minimum amount of water level drop required to expose this region, although water level might have been lower, as a constraint on the maximum water level drop is not available. We therefore refer to this shoreline marker as the BES level.

The second tested scenario assumes no significant base level change, maintaining a deep Mediterranean basin throughout the formation of evaporites and erosional surfaces. We present

the bathymetric implications of this scenario during the MSC compared to a scenario with considerable drawdown.

6.3.2 Flexural-Isostatic Backstripping

Pseudo-3D (planform) flexural-isostatic modelling of vertical motions due to surface loading was performed using TISC software (Garcia-Castellanos et al., 2002) allowing for a basin-wide evaluation of the topographic evolution during the MSC. The current basin state with the depth of bounding surfaces and the thickness of the various stratigraphic units is defined in grids of 200x200 resolution spanning an area of 860 by 890 km corresponding to the area in Figure 6.1. We perform backstripping accounting for the subsidence caused by sedimentation and rebound due to the removal of a water load during periods of low water level, as well as compaction of the pre-Messinian sediment unit (Figure 6.3). The flexural calculations adopt an elastic thin plate, assuming that loads are supported only by a strong lithosphere laying on a low-viscosity asthenosphere which behaves like a fluid. This approach does not allow for the evaluation of the initial time-dependent (transient) response to loading, which is rapid (10-30 kyrs) compared to the geological processes we study here, which is why an equilibrium state for the basin is a valid assumption in most circumstances. Figure 6.3 illustrates the workflow and method for matching paleo-shoreline positions to modelling results.

The Effective Elastic Thickness (EET) of the lithosphere controls the magnitude of vertical motions as a response to tectonic and sedimentary loads (Burov & Diament, 1995; Watts, 2001), and is a crucial input parameter for flexural-isostatic modelling. For continental lithosphere, EET values are related to the thermal state (high geothermal gradients due to recent extension causing lower EET) and the state of the crust-mantle interface. *Decoupling*, meaning the existence of a low-strength zone between lower crust and upper mantle, prevents an applied load force from being transferred to and supported by the upper mantle. This reduces the EET value to solely that of the crust. In addition, local curvature of the plate inducing bending stresses can weaken the plate (Burov & Diament, 1995).

We first estimate EET values from the Yield Strength Envelopes of the lithosphere obtained from thermal and structural information (Figure 6.5). Geotherms were calculated for the main domains along the NE Iberian Geo-Transect (Carballo et al., 2015, see Figure 6.1 for location), using MOHO and LAB depth, surface heat flow, average crustal and mantle compositions,

crustal radiogenic heat production and average thermal conductivity. We test for a range of lithospheric strength parameters by using activation energy values from Govers and Wortel, (1995) and Cloetingh and Burov, (1996). Using the tAo code (Garcia-Castellanos et al., 1997b) we calculate the effect of curvature due to sediment loading along a 2-D profile crossing the main crustal blocks (Figure 6.6, see Figure 6.1 for position profile A).

Bathymetry of the target region was derived from the GEBCO_2014 (IOC-IHO) grid. The thickness of the offshore Miocene to Quaternary deposits in the Western Mediterranean (Figure 6.4) was determined from compilations of extensive seismic surveys (Figure 6.1) including partially reinterpreted 2D seismic lines (Acosta, Muñoz, Herranz, et al., 2001a; Gallart, Vidal, et al., 1995; Just et al., 2011; Leroux, Aslanian, & Rabineau, 2019; Maillard et al., 2014a; Maillard, Mauffret, et al., 1992; Maillard & Mauffret, 1993b; Mauffret et al., 1995; Raad et al., 2020; Roca & Guimerà, 1992a; Sàbat et al., 1997b) and a 3D cube in the Ebro delta region (Urgeles, Camerlenghi, Garcia-Castellanos, De Mol, Garcés, et al., 2011). The seismic derived bathymetry, base PQ and the acoustic basement are available online as part of a wider dataset in the Western Mediterranean (Bellucci et al., 2021).

Although some sediments were deposited onshore their limited thickness and lateral distribution make for small effects when considering the regional scale, so we limit our investigation to offshore regions. In the northeastern corner of our region data was not available, so grids were extended manually to be consistent with the deep basin thicknesses and prevent artefact shorelines in the Ligurian and Provençal basins. The reconstruction east of the Gulf of Lions and north of Corsica is therefore not accurate. The thickness of the MU (Figure 6.4-C) is locally higher in the Provençal basin (reaching up to 2 km) due to the presence of diapirs deforming the overlying UU (Figure 6.4-B) and Plio-Quaternary (Figure 6.4-A) units. The volumes of the MU and UU in our study area are 0.11×10^6 and 0.12×10^6 km³ respectively, summing to 0.23×10^6 km³. This is considerably lower than older estimates (0.5×10^6 km³, Ryan, 2008) and still considerably lower than the 0.33×10^6 km³ reported by Haq et al., (2020), but this can be due to the fact that volume from Haq et al. (2020) also includes the Lower Unit evaporites in the Western Mediterranean.

It should be noted that the distribution of the earliest sediment associated by some authors with the MSC (Lower Unit or LU) is not included in this reconstruction. No age control exists for the deep MSC record in the western Mediterranean and some authors question its age and origin (e.g. Raad et al., 2020). Moreover, the passage from pre-MSC sediment to evaporitic facies

marking the onset of the MSC has been proven to be conformable all around the Mediterranean with no evidence of water level drop at this stage (Dela Pierre, Bernardi, Cavagna, Clari, Gennari, Irace, Lozar, Lugli, Manzi, Natalicchio, et al., 2011; Lugli, Manzi, et al., 2010; D. Ochoa et al., 2015a). Therefore, unlike Bache et al., (2009) and Haq et al., (2020) we incorporate the LU in the pre-MSC sediment (Figure 6.4-D).

On the Balearic Islands we estimate the magnitude of post-MSC erosion by distributing the volume of clastic sediment in the Plio-Quaternary deposits on the offshore promontory onto the currently exposed surface area of the Balearic Islands (see Appendix 6-B), assuming the same area of subaerial exposure as in the modern day (the sum of the islands area is 4907 km²) and a range of 30-70% for clastic provenance of sediment as found in the post-Messinian Unit I in ODP borehole 975 (Comas et al., 1996). This rough estimate allows us to describe the changes in surface topography since the MSC as well as the flexural-isostatic effect of this erosion. The onshore PQ sediment in the Palma graben (Capó & Garcia, 2019b) is not considered as this was only transported over short distances, mostly sourced from the northwestern Tramontana range and therefore had a negligible regional isostatic effect.

The full Messinian succession in the deep basin has not been drilled, which means it lacks a definitive constraint on density and other petrophysical characteristics required to convert the travel time of seismic waves to the key horizons to depth and determine the mass of the sediment and evaporite loads. Well data provides constraints for the top of the sequence, and we can assume a degree of similarity with the evaporite record found onshore. For the Pliocene-Quaternary sequence we assume a velocity function proposed by Urgeles et al., (2011) based on calibration from FORNAX-I well data on the Ebro margin. It takes the form :

$$depth[m] = 1135.1 * TWTT[s]^{1.343}$$

The UU is assumed to consist of intercalated gypsum/anhydrite and clays (W. B. F. Ryan, 2009a), similar to the cycles observed in marginal basins which are proposed to have resulted from climate variations by precession cycles (Dronkert, 1985; Manzi et al., 2009b). The MU, similar to the succession found in the Realmonte mine in Sicily is thought to consist of almost pure halite and potash salts (Lugli et al., 1999a; Samperi, Giorgio, Kamaldeen, Alba, Nicolas, Sabrina, Pauselli, et al., 2020), as evidenced by its seismic facies and the widespread halokinetic activity (Gaullier et al., 2008). Velocities and densities used in assessing our load distributions are listed in Table 6.1.

From these densities, we can derive the ratio of a response under *local isostasy* between the load thickness and induced subsidence or rebound for each step (see Appendix 6-A).

For long-wavelength and uniform loads, such as those in the deep Mediterranean basins the response will be close to local isostasy (see Appendix 6-A), but for more variable loads and close to load edges the response will be affected by the load-bearing capacity of the lithosphere. The effect of compaction on the pre-halite bathymetry is determined for compaction following the standard porosity-depth relationship: $\phi_z = \phi_0 * e^{-bz}$.

Where Φ is porosity, z is depth below seafloor (km) and b is the compaction coefficient (km^{-1}), for shale $\Phi_0 = 0.67$, $b = 0.00051$, and for sand $\Phi_0 = 0.49$, $b = 0.00027$ (Sclater & Christie, 1980b). Bessis, (1986) presents a porosity-depth curve based on three wells in the Gulf of Lions which fits a relationship of $\Phi_0 = 0.75$ and $b=0.00115$, suggesting slightly faster compaction than the shale curve from Sclater & Christie (1980). We apply this range of porosity-depth relationships to correct the reconstructed bathymetry for compaction of pre-MSC sediment at each step in our reconstruction.

Water loads for drawdown and reflooding phases have a density of standard seawater in our models (1030 kg m^{-3}), although the real density during the evaporite deposition phases was likely higher due to the formation of more saline waters and brines (1200 kg m^{-3} at halite saturation). This has no significance for the pre-evaporite topographic reconstruction before brine formation at the Mediterranean scale, as the density increase cancels out with the later restoration of open marine conditions during the Zanclean flood.

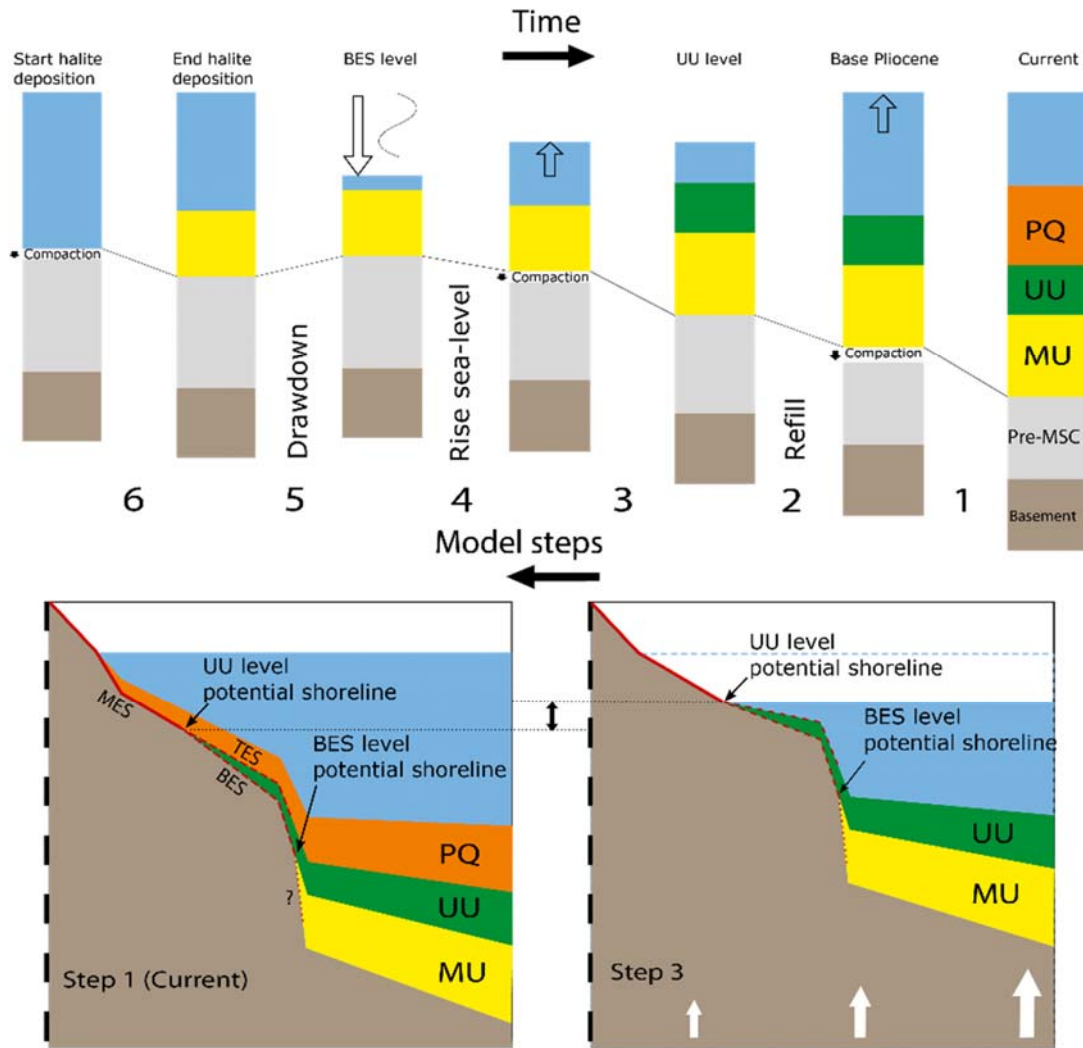


Figure 6.3. Schematic cross section showing step-by-step backstripping of sediment and water to determine flexural-isostatic response and match water level to paleoshorelines. 1: Removal of Plio-Quaternary sediment 2: Restoration of water level to pre-Zanclean flood level (UU lowstand) 3: Removal of UU sediment 4: Lowering of water level to lowest level at “acme” (BES lowstand) 5: Restoration of water level to pre-drawdown level 6: Removal of MU halite, to obtain bathymetry before the onset of stage 2 of the MSC.

Unit	Water	Plio-Quaternary	Upper Unit	Mobile Unit	Pre-halite
Av. Seismic velocity (m/s)	1500	Power law (see text)	3400	4800	2440
Av. Density (kg/m ³)	1030	2100	2500	2170	2700

Table 6.1. Average seismic velocities and densities used for each unit.

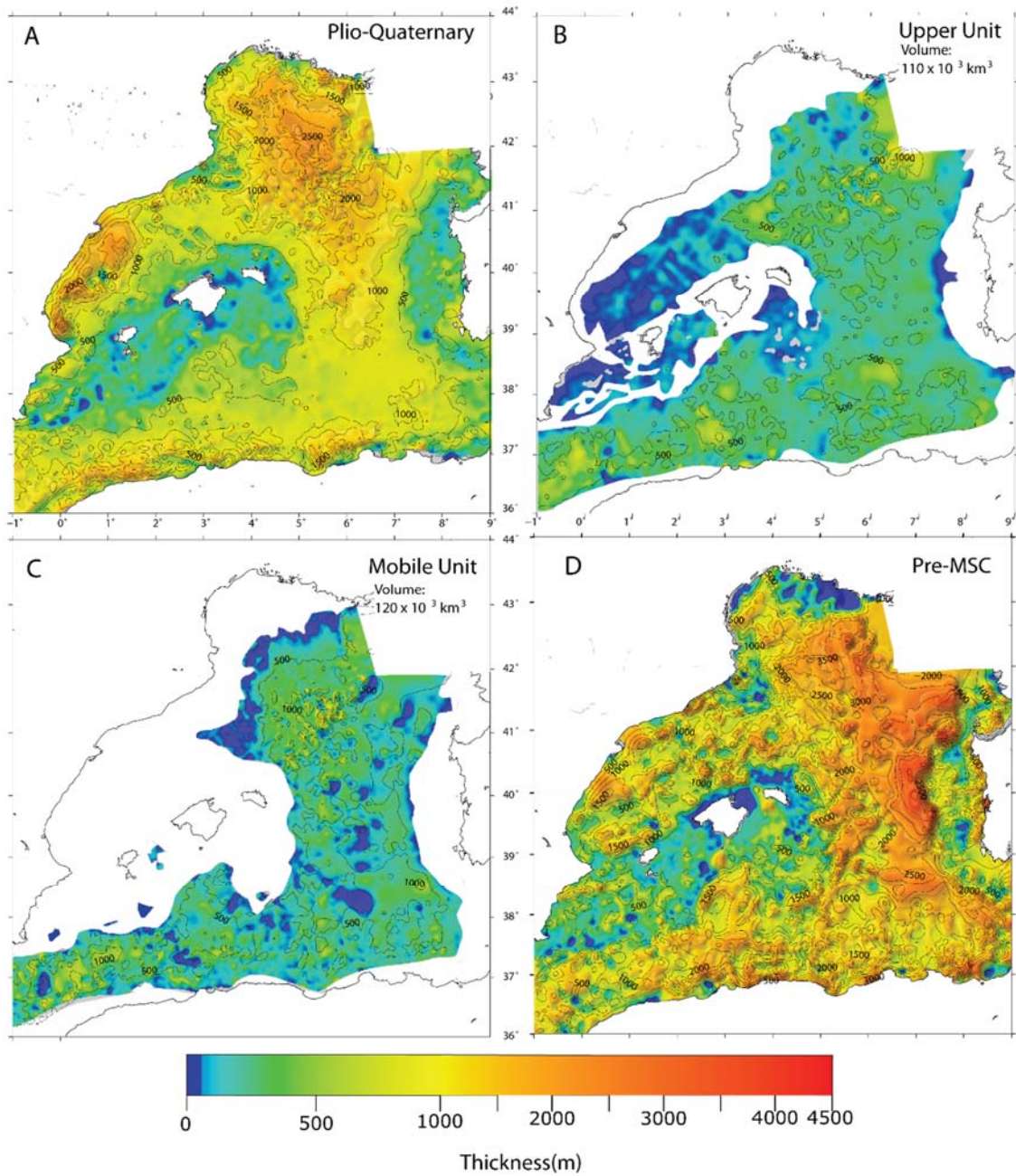


Figure 6.4. Thickness in meters of sedimentary units used in the reconstruction, as interpolated from the seismic dataset compilation in Figure 6.1, using velocities presented in Table 6.1.

6.4 Results

6.4.1 Thermal Subsidence

Fitting the limits of the opening ages of the Algerian (8-16 ma) and Provençal (16-22) basins to the oceanic plate model GDH1 (Stein & Stein, 1992) yields post-Messinian thermal subsidence of 250 to 325 m in the Provençal basin, and 325 to 435 m for the Algerian basin.

The Valencia Basin has been studied extensively regarding its crustal structure and extensional mechanisms (Maillard, Mauffret, et al., 1992; Maillard & Mauffret, 1999; Negredo et al., 1999; Torné et al., 1992b; Watts & Torné, 1992b, 1992a). Best-fit basin histories suggest a finite rifting model with extension between 24 and 10 Ma, and the stretching factor (β) increasing from 1.4 on the basin flanks to 3 in the central basin (Watts & Torné, 1992b). Applying the McKenzie (1978) model yields a post-Messinian component of thermal subsidence in the range of 50-100 m on the flanks and 90-180 m in the center depending on the applied post-rift age. Tectonic subsidence curves show a gradually decaying curve (Watts et al., 1990) meaning part of the thermal relaxation took place during the rifting phase and instantaneous rifting assumed in the McKenzie model does not apply to the Valencia Basin, so true values will fall towards the lower end of this range. Backstripping of wells in the Catalan margin area has yielded tectonic post-Messinian subsidence values ranging from 0 to 300 m (Bartrina et al., 1992; Watts & Torné, 1992b), with this variation in values possibly being related to ongoing activity on normal faults on the margin. Modelling of the basin evolution based on similar geodynamic data yielded maximum post-rift subsidence values of 380 m in the central part of the Valencia Basin since 10 Ma (Negredo et al., 1999). Due to the limitations of such 1D subsidence calculations we do not include the thermal component directly in our platform backstripping, as we are not able to constrain the lateral distribution of subsidence magnitudes accurately. However, we consider these subsidence values in the restored depths per basin presented in Table 6.2. Although thermal subsidence constitutes a considerable part of total vertical motions in the deep basins, because this effect diminishes towards the margins, we consider that it introduces a minor (<100 m) uncertainty in the reconstructed depths of our shorelines.

6.4.2 Effective Elastic Thickness

The results of our EET determination shown in Figure 6.5 yield an EET range of 10 to 45 km in the offshore domain with limited variation, with slightly lower values in the Algerian Basin. On the Emile Baudot Escarpment and the Algerian margin, we see sharp changes in EET values for weaker rheologies, likely due to bending stresses induced by boundaries of the sedimentary load in the deep basin.

European EET has been studied in this region by other authors using two principally different approaches. One is based on analysis of the spectral coherence of gravity anomalies and topography accounting for density variation in sediment, yielding values of 5 to 12 km in the western Mediterranean basins (Kaban et al., 2018b). Alternatively, EET is inferred by integrating the strength of the lithosphere derived from modelling based on thermal and rheological data, yielding values of <30 km for the Western Mediterranean (Tesauro et al., 2009b).

The low strength estimated at the base of the crust along our 2D profile (from 0 MPa in the Iberian and north African margins to a maximum of 150 MPa in the Valencia Basin, see Figure 6.5) suggests a high degree of decoupling between crust and mantle in all regions except the Algerian Basin, which is the only region with true oceanic crust. This decoupling argues in support of using EETs towards the lower end value of our range, close to the 15 km value adopted for the 1D backstripping in Urgelés et al. (2011); and the Cenozoic evolution of the Catalan Coastal Ranges (5 km; Gaspar-Escribano et al., (2004). In addition, the generally low EET values (<20 km, Kaban et al., (2018) in the area derived from recent spectral analysis and the likelihood of decoupling between crust and lithospheric mantle in recently extended continental crust such as the Valencia Basin (Tesauro et al., 2009b) point to values in the lower end of the range presented in Figure 6.5.

6.4.3 Sensitivity of Paleo-Topography to EET

In Figure 6.6 the sensitivity of our reconstructed topography after removing the PQ sediment and a 1 km water column to the end-member EET values is presented along cross section A (see Figure 6.1 for location). The reconstructed topography is strongly dependent on EET value

in the Ebro delta region, where the Plio-Quaternary sediment load is largest. Here the localization of flexural-isostatic subsidence leads to a >700 m difference in post-MSB subsidence, also affecting the slope of the reconstructed bottom shelf which is nearly flat in the 10 km EET scenario but has significant basinward slope for a 45 km EET (Figure 6.6). In the steepest areas of the MES on the Iberian margin where the onlaps of UU are located the sensitivity of topography is still around 500 m, illustrating the importance of the EET parameter when constraining the magnitude of water level changes. Considering the arguments for relatively low EET values in the previous section we adopt an EET value of 15 km for our reference model and vary this parameter between 10 and 20 km to test the uncertainty of reconstructed paleoshoreline depths due to lithospheric strength. Reconstructed shoreline depths vary by +/- 100 m as a result of this variation.

6.4.4 Sensitivity of Paleo-Shoreline Position to Water Level

The magnitude of a drop in water level during the MSC has a two-fold effect on the position of the reconstructed shoreline. First, it controls the magnitude of vertical motions affecting bathymetry, and secondly it determines the depth of the isobath followed by the shoreline. Figure 6.7 presents the sensitivity of the model output shoreline position at different drawdown magnitudes for our reference 15 km EET value, both for the UU level and the BES level. The reconstructed shoreline positions presented in Figure 6.7 are not corrected for thermal subsidence or tectonic deformation since the MSC. This is done due to the lack of lateral constraints on these components discussed in section 6.4.1.

In the Valencia Basin the most notable discrepancies in the paleoshoreline position for the UU level (Figure 6.10-B) are located at the Columbretes volcano, which caused Pliocene-recent deformation of the MES and Valencia Fault, active from Miocene to Pliocene which offsets the MES by about 0.5 seconds TWTT (Maillard & Mauffret, 2013a). Accounting for the max value of 325 m post-MSB thermal subsidence in the Provençal basin (see section 6.4.1) would shift the reconstructed shorelines slightly basinward, as the margin of the basin was in reality shallower than in our reconstruction. In the Valencia Basin this adjustment is not necessary for our UU level reconstruction considering that post-MSB thermal subsidence on its margins was negligible. On the Algerian margin the magnitude of the required adjustment is unclear, as subsidence in this area also carries a potential signal of tectonic origin due to subduction

initiation and southward tilting of the basin (Auzende et al., 1972; A. Leprêtre et al., 2013; Yelles, Domzig, Déverchère, Bracène, Mercier de Lépinay, et al., 2009) affecting the depth of both the MU and UU limits. In the Valencia Basin, the UU limit in the Ebro delta region is likely not accurate, as Urgeles et al. (2011) showed the absence of an UU in their 3D dataset. Rather, they interpret the Messinian “Unit C” as a shallow water detrital fan. A water level of -1300 m is required to expose the Ebro margin in this region. However, water level cannot have been much lower as connectivity must have been maintained between the eastern Valencia Basin and the southwest Valencia Basin where the UU limit is clearly identified and mapped by Cameselle and Urgeles, (2017) varying around a reconstructed depth of -1100 m, although this connection is obscured by post-Messinian volcanic activity in the Columbretes. In the Gulf of Lions, the Upper Unit limit lies considerably deeper, close to the reconstructed shoreline for a -1500 m water level. In the steep Algerian Margin and Emile Baudot Escarpment, the UU limit lies further basinward than even the -2000 m isobath. Tentatively, we suggest this might be related to re-sedimentation of gypsum on steep margins, a process which does not require subaerial exposure (de Lange & Krijgsman, 2010b) combined with tectonic processes mentioned above. As shoreline positions are better defined in the Valencia Basin where data availability is good and we can constrain our water level estimate against that of Urgeles et al. (2010) we consider this the more representative of paleo water level, rather than the deep basin margins where the depth of the UU limit is affected by the aforementioned processes. We therefore choose -1100 +/- 100 m as our reference water level for the UU level.

For the BES level, the limit of the MU fits well with a -1500 m water level in the shallowest MU limit towards the Valencia Basin, which indicated the minimum water level drop required to expose the top of the halite in that region. The depth of the salt limit shows strong variations between -1300 and -2000 m within the Gulf of Lions, while it is consistently deeper than -2000 m along the margins of the deep basins.

The modern salt limit is affected by significant halokinetic activity (Badji et al., 2015; Dal Cin et al., 2016). This, combined with the basin scale tilting of the Algerian Basin mentioned above could explain the discrepancy between our reconstructed shorelines and the limit of both UU and MU in the deep basin margins, but the larger (approximately 2200 m) drawdown required to obtain paleoshorelines in the position of the deep basin evaporite limit would imply a largely exposed sea floor in the Algerian basin (Figure 6.7), with only small local lakes. We choose -1500 m for the BES level value as it allows for complete exposure of the BES in the Valencia Basin but recognize that this constrains a minimum drop in water level which might still have

been considerably lower at moments during the lowstand, as evidenced by the possible continuation of the BES underneath the MU.

Basin		Liguro-Provençal	Algerian	Valencia	Halite CMD	Formentera	Cogedor
Average Bathymetry	Modern	2700	2820	1500	950	1680	620
	UU level (SL -1100)	2300-2755	2120-2610	1110-1420	775-920	1302-1442	206-311
	UU level (no SL drop)	2650-3105	2470-2970	1460-1770	980-1125	1618-1767	455-560
	BES level (SL -1500)	2270-2690	2120-2575	1085-1395	825-970	1292-1432	127-232
	BES level (no SL drop)	2750-3170	2595-3055	1435-1745	1030-1175	1687-1827	422-527
	Pre-halite (drawdown)	3020-3325	2915-3255	1485-1795	1280-1425	1832-1972	543-648
	Pre-halite (no drawdown)	2800-3105	2695-3045	1435-1745	1235-1380	1687-1827	443-548
Average Sediment thickness	Plio-Quaternary	1325	818	920	295	220	190
	Upper Unit	545	480	50	95	160	55
	Mobile Unit	665	505	-	215	70	75
	Total	2535	1803	970	605	450	320
Average Subsidence of Base MU	Plio-Quaternary	640	390	500	60	75	150
	Refilling	350	350	300	205	325	250
	Upper Unit	350	300	25	45	100	90
	Rise sea-level	130	125	50	0	70	45
	Mobile Unit	340	235	-	10	70	100
	Drawdown	-700	-695	-400	-250	-540	-395
	Compaction pre-MSC	550-780	340-570	150-410	45-190	55-195	30-135
	Thermal	250-325	325-435	50-100	0	?	?
	Total	1910-2215	1370-1710	675-985	115-260	155-295	292-397

Table 6.2. Bathymetry of Western Mediterranean sub-basins in modern day and at key moments during MSC, sediment thicknesses and vertical motion components. Average values are presented, but strong variations in sediment thicknesses and depths occur throughout the basins. In the CMD values correspond the average in the area of current halite occurrence. Paleodepth is determined by modern bathymetry - thickness sediment + decompaction pre-Messinian sediment + flexural-isostatic and thermal subsidence.

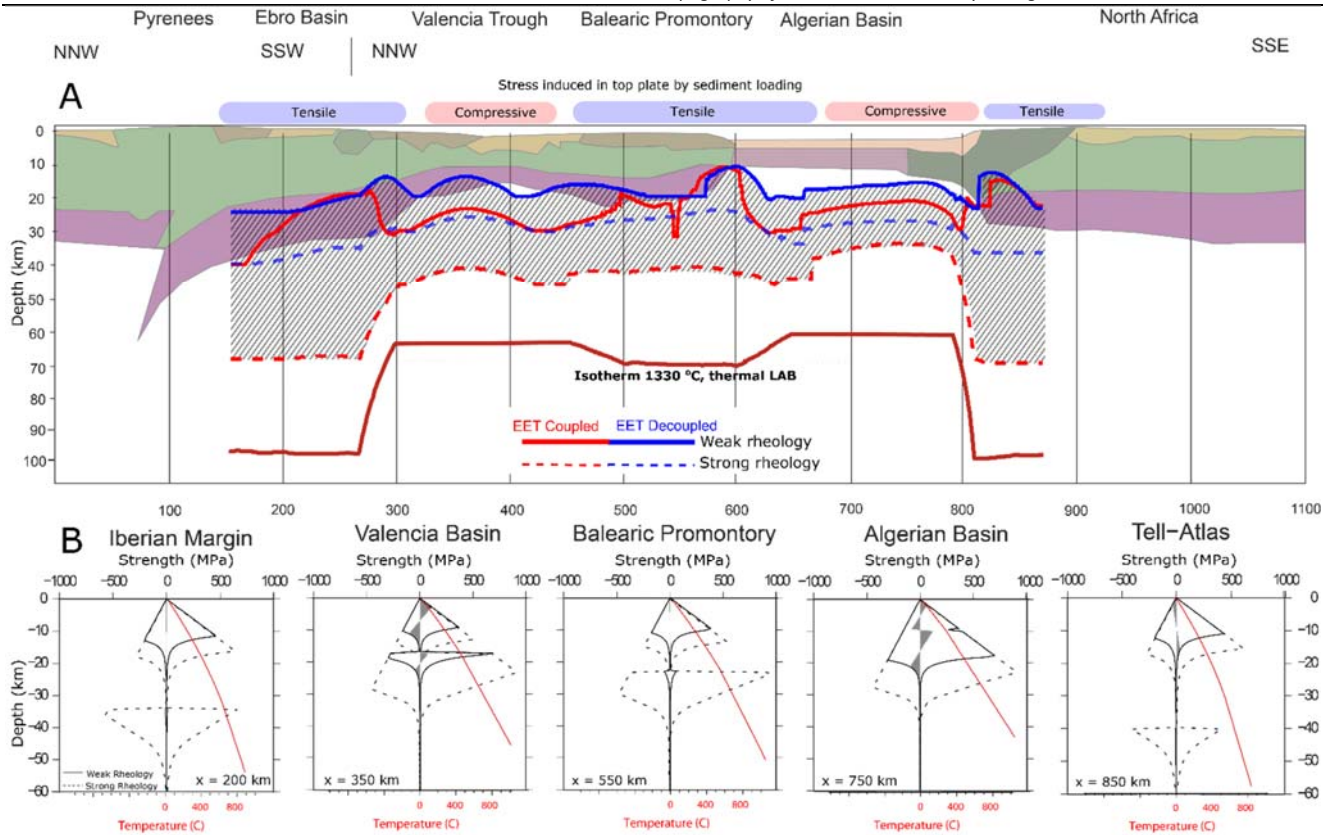


Figure 6.5. A: Effective Elastic Thickness variation from tAo model along a NE Iberia Geo-Transect (see Figure 6.1 for location). Crustal units with different density, heat production and thermal conductivity used for constructing geotherms derived from a compilation of crustal structural data (colour filled bodies) and thermal lithosphere asthenosphere boundary (LAB, red-dark line) from Carballo et al., (2015). EET values determined for weak and strong rheological parameters for lower crust and upper mantle from Govers and Wortel, (1995) and Cloetingh and Burov, (1996) and for coupled vs decoupled crust and mantle. EET values are determined using tAo code by constructing Yield Strength Envelopes along transect based on rheology, geotherms and induced bending stresses by sediment loading since onset MSC. Range of plausible EET values hashed. Also shown is the stress regime induced on top of the plate by bending due to loading of sediment since onset MSC. B: Yield Strength Envelopes constructed per region for weak and strong rheological parameters for lower crust and upper mantle from (Govers & Wortel, 1995) and (Cloetingh & Burov, 1996), showing decoupling in all regions but the Algerian Basin. Included are used geotherms and stresses (shaded grey area) at reference points along section.

6.4.5 Reference Model

Based on the results presented above, our reference model assumes a 15 km EET and water levels of -1100 +/-100 m for UU level, which is the shallowest value for UU deposition found in places with a well constrained UU limit, although it should be noted that the UU is absent in some areas with a deeper reconstructed bathymetry, i.e., the Ebro Margin.

The BES level in our reference model lies at -1500 +/-100 m, which is the minimum water level drop needed to subaerially expose the BES to salt limit in the Valencia Basin, with the salt limit substantially deeper in other areas. In the Gulf of Lions our BES level shoreline along the 'Christiane' profile presented by Ryan (1976) is located at -2050 +/- 100 m, which fits well with their result of -1900 depth for the Late Messinian, even though we do not account for the isostatic effects of erosion in this region.

In the no-drawdown scenario our potential shorelines are positioned approximately 200 m deeper than when the flexural effect of removal of the water column is considered.

Each panel in Figure 6.8 represents a single step in our reconstruction and can be interpreted as the flexural-isostatic effect on the Base MU surface of the applied load. The drop in water level at step 5 (Figure 6.8-E) results in a large rebound of up to 700 m in the deep basins, causing basin-wide shallowing even significantly affecting the margins and Balearic Promontory. The change in water level between BES and UU levels (Figure 6.8-D) and UU deposition (Figure 6.8-C) are not able to undo the entirety of this rebound, and the basins remain at their shallowest point throughout these steps. This strongly affects the bathymetry and depth of paleoshoreline markers formed during the BES and UU levels. The reflooding (Figure 6.8-B) and subsequent sedimentation (Figure 6.8-A) restore the basins to close to their pre-drawdown depth. The flexural-isostatic subsidence by sediment loading (Figure 6.9-A) was accompanied by compaction of the pre-halite sediment underlying the MSC units (Figure 6.9-B), and the total vertical motion on the Base MU surface since the onset of MU deposition is presented in Figure 6.9-C.

The final resulting topography and shoreline positions, accounting for compaction and flexural-isostatic motions are presented in Figure 6.10. These maps exclude the thermal subsidence, which lateral variations are not accurately constrained. This explains the differences in reconstructed depths between Figure 6.10 and Table 6.2, where Table 6.2 represents the more

accurate reconstructed depths. For the BES and UU levels the topography including (Figure 6.10-B, D) and excluding (Figure 6.10-C, E) water level drop are presented.

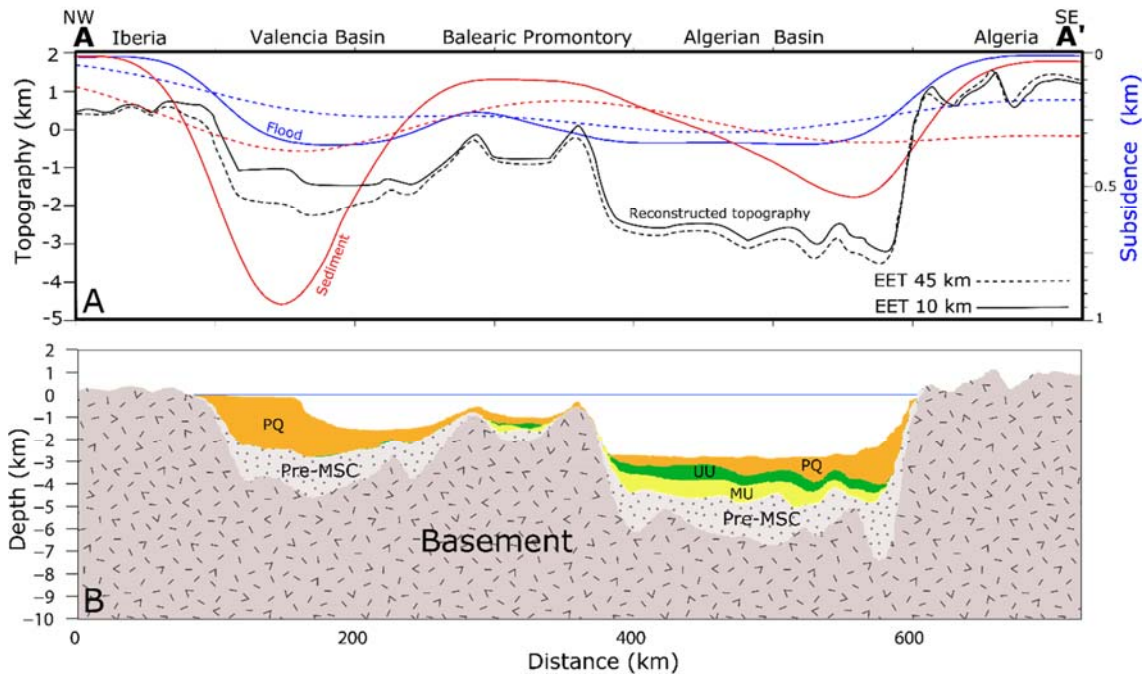


Figure 6.6. A: Schematic overview of results of backstripped profile A (see Figure 6.1 for location) for 10 and 45 km EET. Black: Reconstructed topography at end MSC, before deposition PQ sediment and water level at -1000 m. Blue: vertical motions caused by 1 km change in water level (subsidence due to flooding). Orange: vertical motion due to sedimentation of Plio-Quaternary sediment (post-MSC subsidence). B: Bathymetry and thicknesses of stratigraphic units used in backstripping along profile A. Orange: Plio-Quaternary sediment, Green: in deep basin: Upper Unit, on Balearic Promontory: Bedded Unit3, Yellow: Mobile Unit, Light Grey: Pre-MSC sediment, Dark Grey: Basement.

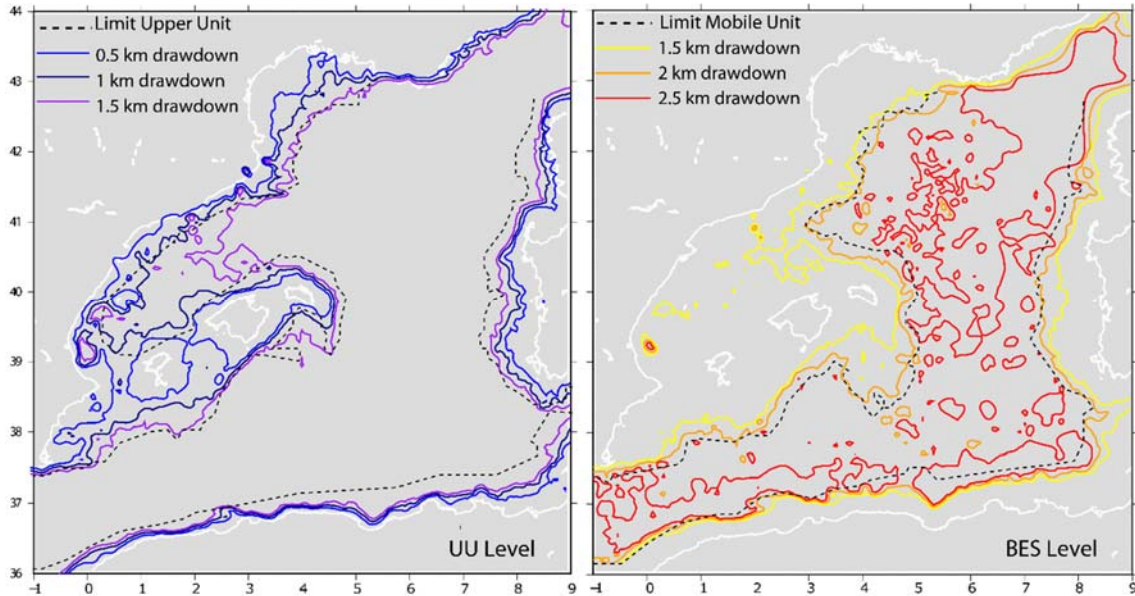


Figure 6.7. Sensitivity of the calculated paleo-shoreline to the magnitude of water level fall (EET=15 km). Dashed black lines: position of paleo-shoreline markers (see Figure 6.1). Solid lines: reconstructed isobaths for various water levels. Left: UU level, Right: BES level.

6.5 Discussion

A key outstanding question around the MSC concerns the spatial distribution of evaporites and its link to paleo water depths. We describe the evolution of the Western Mediterranean basins from the perspective of our flexural-isostatic reconstruction for each sub-basin starting from the pre-Messinian bathymetry, and the implications for the paleoenvironmental changes during the MSC.

Assuming the paleoshoreline-based constraints on water level during the MSC are correct, our flexural-isostatic reconstruction shows that bathymetry of the intermediate basins before the onset of halite deposition (Figure 6.10-B) was slightly deeper than today, having since undergone subsidence by compaction, isostatic compensation and thermal cooling that combined was smaller than the sediment fill. The Valencia Basin reached 1500-1800 m depending on the chosen compaction curve (Table 6.2, Figure 6.9-B), and underwent a maximum of 1100 m of subsidence since the MSC (Figure 6.9-C). Because the UU in the Valencia Basin is relatively thin and MU is absent, its depth in our reconstruction during the MSC is controlled primarily by water level and the PQ load. The pre-halite depths of the

Algerian and Provençal basins reached about 3 km depth on average (Figure 6.10-B, Table 6.2), which is similar to the present-day bathymetry. They underwent between 1200 and 2000 m of subsidence since the MSC (Figure 6.9-C) which is close to the sediment thickness accumulated in that same period. The significantly greater depth of the Provençal and Algerian basins compared to the intermediate basins can explain the much larger salt thickness, as they were not as extensively exposed during the drawdown stage. In addition, any exposed and dissolved salt would be trapped, in contrast to the Valencia Basin, from which it could be transported to the deep basins.

The water column above the top halite surface at the end of the MU deposition in the deep basins was approximately 2700-3300 m if halite was deposited in high water (Manzi et al., 2005a), and 700-1200 m if the drawdown to BES level (of 1500 m) occurred. At the halite limit in the Valencia Basin this water column pre-drawdown was still 2 km, reducing to 0 after the drawdown.

In our reference model the uplift induced by the water level drop (Figure 6.8-E), yields basins shallower than today during the UU deposition. If our best-fit water level of -1100 m at the UU level is correct (in accordance with proposed values by [Maillard et al., 2006] and [Cameselle et al., 2014], slightly higher than previous estimates by [Urgeles et al., 2011] and [Mas et al., 2018]) this implies a maximum water depth of approximately 400 m at the transition from the Valencia Basin to the deep basin (Figure 6.10-E) at the end of UU deposition, and shallower (300-350 m) if we correct for thermal subsidence. At the same time, water depth in the deep basins reached 1000-1600 (average) to 2000 (max) m (Figure 6.10-E), which might suggest a different sedimentary environment and consequently a change in the nature of the UU between the Provençal Basin and the Valencia Basin. Without this drawdown isostatic effect, topography of the basins is 300 m deeper in the basin centers and water depths are therefore up to 3400 m (Figure 6.10-F).

In the no-drawdown scenario (Figure 6.10-E, F) we see that halite preservation occurs from laterally variable depths, from 1500 m (western Gulf of Lions) to 2500 m in the Valencia Basin and 3000-3500 m in the deep basins (Figure 6.10-E). These discrepancies could be explained by halokinetic activity, but the absence of halite in the Valencia Basin cannot be explained by such a mechanism alone, so either precipitation in that region must be prevented by a so-far unidentified mechanism, or halite must have been removed by submarine dissolution/erosion up to a very considerable depth (at least 2500 m) which we consider unlikely. The onlap depth of the UU in this scenario is also very variable, from 500-1000 m in the Valencia Basin to 2500

m in the deep basins, and considerable thickness of the UU is only reached at depths >2500 m. Considering the clastic nature of the UU, it is hard to explain these trends in a high water level scenario considering that the Valencia Basin and shallower margins would have had the biggest sediment supply. We therefore do not favor this scenario.

The main sources of uncertainty are the poor constraints on the EET and compaction of pre-halite sediment, as well as the magnitude of erosion in the exposed parts of the basin during the drawdown. We observe a disconnection between the UU and Bedded Unit3 lying on the Balearic Promontory (map in Figure 6.11), onlapping on both sides of a topographic high situated between the CMD and Valencia Basin. Assuming this sill was exposed and considering the depth of this high when compensating for post-Messinian sedimentation, this indicates that the water level was at some point at least 600 to 750 m below modern sea level. Moreover, the onlaps of Bedded Unit3 in the CMD are positioned at a reconstructed depth of 750-900 m at the UU level, which is shallower than those of the UU on the southwest margin of the Valencia Basin (>1000 m). This supports the interpretation that stage 3 MSC deposits in the CMD (Bedded Unit3) were accumulated in isolated basins perched above the Valencia Basin water level. It implies deposition in an independent hydrological environment from the deep basin controlled by erosion and resedimentation on the Balearic Promontory.

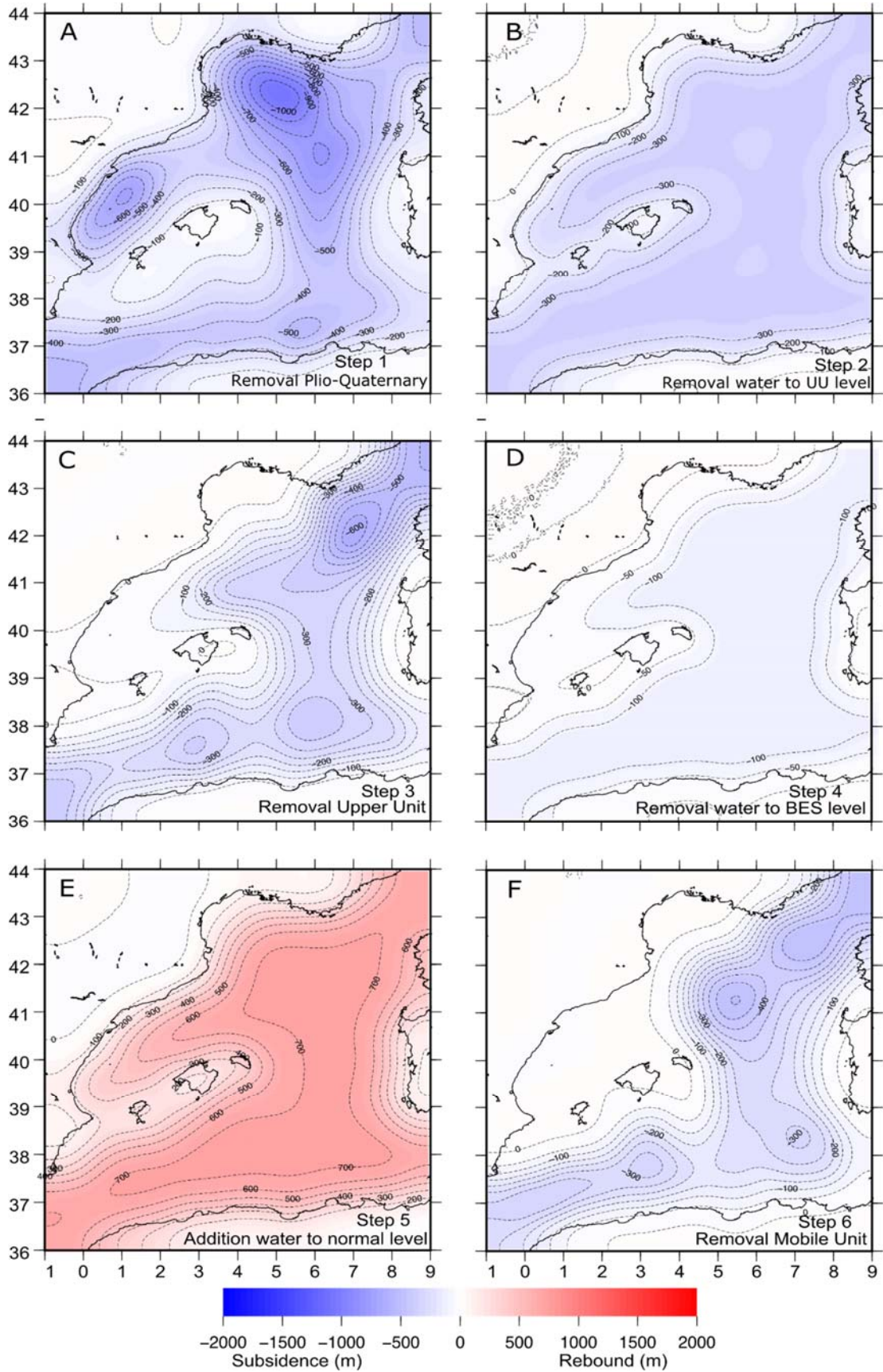


Figure 6.8. Flexural-isostatic vertical motions in m corresponding to each step of our reference model scenario. Sedimentation and floodings caused subsidence represented by negative values (blue), while water level drop caused rebound represented by positive values (red). Not included are effects of onshore erosion/sedimentation.

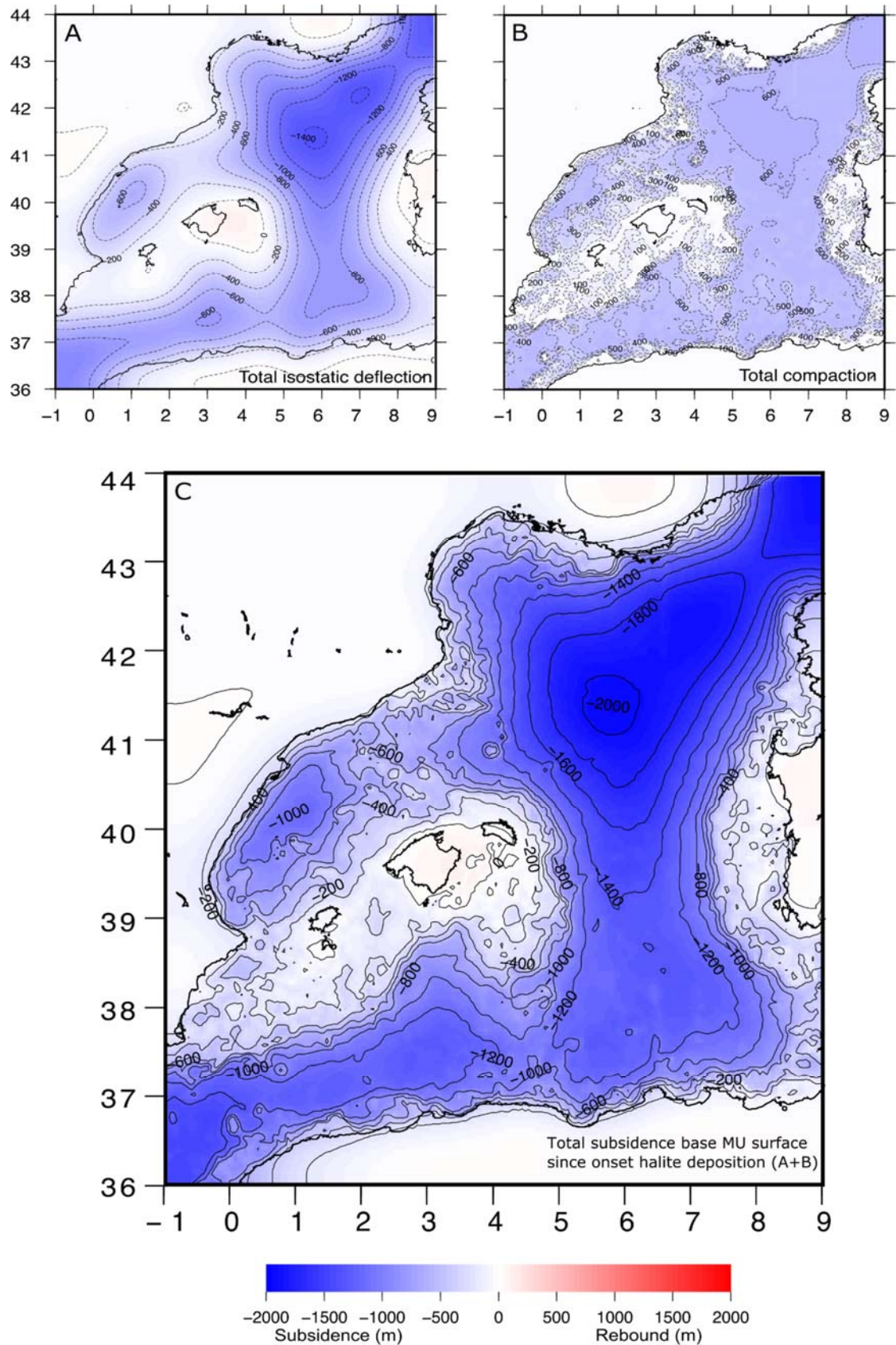


Figure 6.9. A: Sum of flexural-isostatic vertical motions in m since the onset of halite deposition, for the reference setup. B: total compaction of pre-halite sediment. C: Total subsidence of the base of Messinian sediment and MES since the onset of MU deposition (A+B). All values for reference model scenario. Not included are effects of onshore erosion/sedimentation and thermal subsidence.

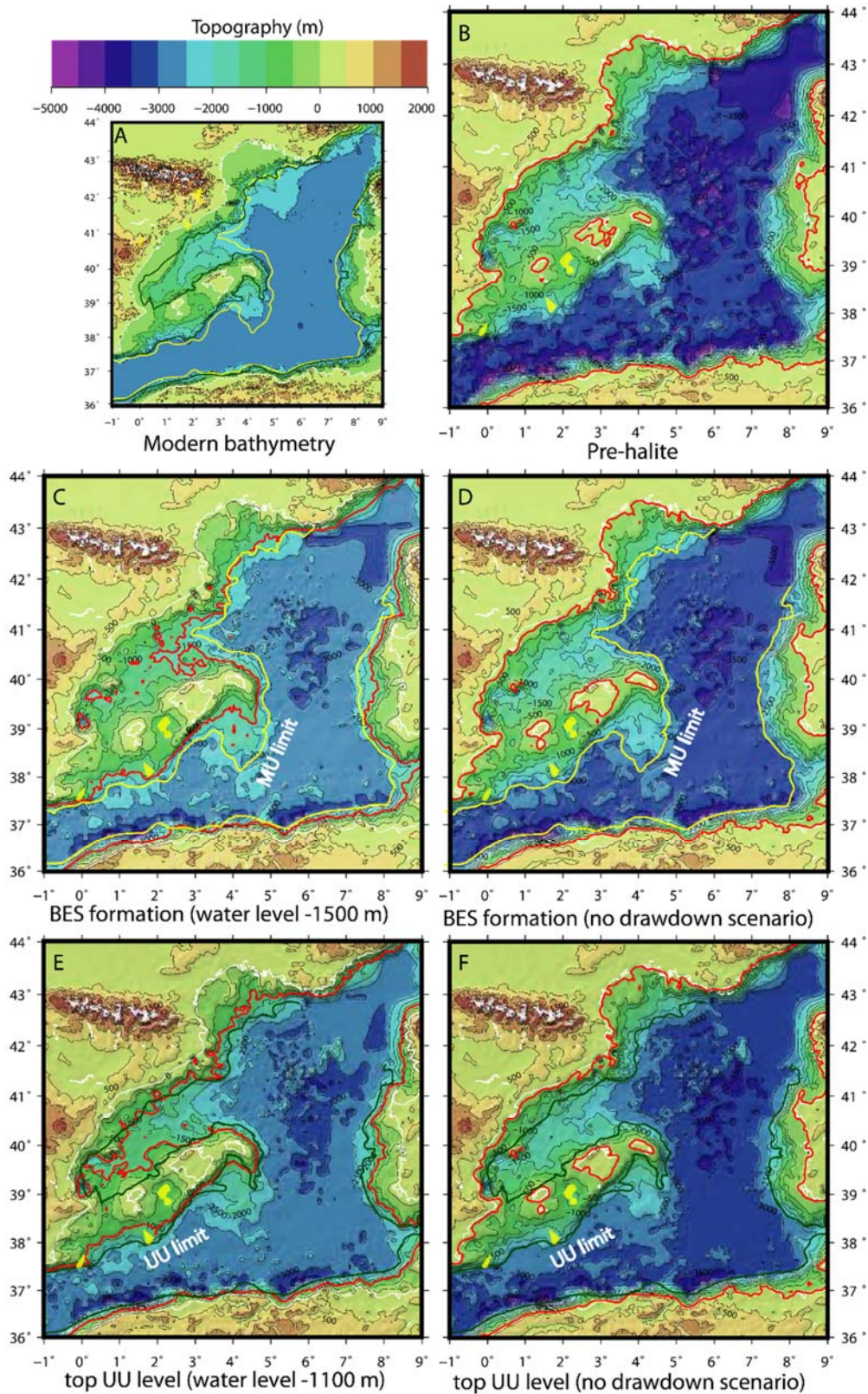


Figure 6.10. Modern topography (A) and reconstructed paleobathymetry results for our reference setup. These maps are not compensated for the thermal subsidence effect, overestimating the depth of the deep basins. B: pre-halite deposition. C: BES level (top MU) with water level at -1500 D: alternative BES level (top MU) for no-drawdown scenario. E: UU level (top UU) with water level at -1100. F: alternative UU level (top UU) with for no-drawdown scenario. Yellow line in B, C: limit MU, green line in D,E: limit UU). Solid red line: reconstructed shoreline. Yellow: halite isolated halite patches in CMD, Formentera and Cogedor basins. Note the discrepancy in required water level at the BES and UU levels of approximately 400 m in the drawdown scenarios (C vs. E).

On the Balearic Promontory, the halite patches (Figure 6.1 and Figure 6.11) occur at a wide range of present-day depths. Halite precipitation in the CMD depocenter started at a depth of 1280-1425 m, depending on the decompaction curve applied for the pre-halite sediment (see Table 6.2). Halite also deposited in basins with a restored depth as shallow as 550-660 m (Cogedor) which pre-halite depth could be as shallow as 450 m if we assume no drawdown ever occurred, as this close to the margin the remnant uplift of the -1500 m change in water level in our reference model affects the pre-halite bathymetry. However, here we do not account for post-Messinian tectonics. Constraining these in this area is difficult due to the complex way the Balearic Promontory deformed, with large variations along its structure. Its western part (near Alicante shelf) was deformed by compression (Maillard & Mauffret, 2013a) the vertical component of which would not have been more than 200-300 m. The true paleodepth might thus have been deeper, up to 960 m but the true magnitude of this effect is not well constrained. The aforementioned effect of residual shallowing due to the -1500 m drawdown also affects the Formentera Basin, which has a reconstructed depth of 1830-1970 m pre-halite, but could be 150 m shallower if no drawdown occurred.

A striking feature in these patches is the absence of any halite thickness vs. paleodepth relationship (Figure 6.11-D). The deepest pre-MSC basin (Figure 6.11-C, Formentera) has a much thinner halite unit than the CMD (Figure 6.11-A), which was lying up to 500 m shallower at the onset of the MU deposition (see Table 6.2 for depths and thicknesses). This could suggest that halite thickness in these patches was controlled by the local geometry of the basins and possibly the depths of their outlets. The open nature of the Cogedor and Formentera basins (Figure 6.10), with respect to the completely silled-off CMD might have made them more susceptible to dissolution of the halite during the lowstand. Dissolved salt in Cogedor and Formentera would escape to the deep basin while in the CMD it is trapped inside the depression. This has been hypothesized by Raad et al. (2020) for the CMD, and a similar scenario has been proposed for the outcropping Sicilian halite (García-Veigas et al., 2018a). It should be noted that especially on the western Balearic Promontory and potentially in the CMD, the effect of tectonic deformation since the MSC should be accounted for in order to achieve a higher accuracy in the paleodepth restoration. This is beyond the scope of this paper but will shed more light on the role of the sills related to the halite patches during their formation.

Halite is conspicuously absent in the Valencia Basin, which had a pre-halite depth reaching at least 1500 m (Table 6.2). This can tentatively be explained as follows: it has been proposed by

several authors that halite deposition occurred in deep water, in a strongly stratified water column (Simon & Meijer, 2017a; Yoshimura et al., 2016). Any brine formed in the Valencia Basin may have sunk towards the deep Provençal Basin, as there was no topographic sill in between, although we could reasonably expect some salt trapping in the westernmost part of the Valencia Basin where volcanic edifices and structural highs were already present and depth variations allowed for the deposition of the MSC-related Complex Unit related to the lowstand (Cameselle & Urgeles, 2017b). Alternatively, halite was deposited on the floor of the Valencia Basin but was later dissolved/eroded during the BES lowstand (-1500 m) when the basin floor was subaerially exposed. A combination of both processes is not excluded. These contrasting models are presented in Figure 6.12. Our results do not allow us to distinguish between these models, but the reconstructed depths of the basins do evidence the importance of explaining the observed halite distribution.

The flexural-isostatic effect of the deep-basin isostatic loads on Mallorca Island suggest a close to zero effect (Figure 6.9-C) of vertical motion by MSC events, as rebound due to the drawdown (Figure 6.8-E) was reversed by flooding and Plio-Quaternary sedimentation (Figure 6.8-A, B). Based on the volume of post-Messinian sediment lying on the Balearic Promontory platform offshore (see Appendix 6-B), we estimate the isostatic erosional rebound assuming it was eroded from the current onshore Balearic Islands (effect not included in Figure 6.8 Figure 6.9 Figure 6.10 due to their relative magnitudes). Using the constraints outlined in section 6.3.2, the eroded mass onshore is equivalent to a uniform load of 130-310 m. It should be noted that this height does not account for porosity changes from consolidated rock to sediment, so their true height would be smaller, but the mass removed from the islands is not affected by this simplification. We also do not account for the onshore post-MSC sedimentation in the Palma graben (see Capó and Garcia [2019] for thickness maps onshore), which suggest that the central part of Mallorca island was not exposed to erosion until recently. This implies the rebound due to erosion would be more concentrated on the NW and SE regions of the island than shown in our results (see). The erosion magnitude yields an average erosion rate of 0.03 to 0.04 mm/yr over the Pliocene and Quaternary, which is on the same order of magnitude as measured rates of seacliff erosion (Balaguer & Fornós, 2003). The rebound on the Balearic Islands due to erosion affects the pre-Messinian reefs on the eastern coast of Mallorca by up to 60 m since the MSC. We tentatively suggest that this explains the present-day elevation of the terminal carbonate complex on Mallorca island, originally formed near sea-level (G. Mas & Fornós, 2013), and that a higher eustatic sea-level before the MSC is not required to explain the

elevation of phreatic overgrowths on speleothems as proposed by Dumitru et al. (2021). Previous estimates of long-term deformation on the eastern shore of Mallorca based on six Pliocene sea-level indicators yielded a median value of 0.002 mm/yr (Dumitru et al., 2019), which would yield a total post-MSC uplift of approximately 10 m, which is significantly below our estimate.

Another important outcome of our results on the Balearic Promontory and the margins of the deep basins is the potentially large differential rebound and subsidence resulting from sudden drawdown and refilling events (see Figure 6.8-B, D, E). While the subsidence and rebound induced by sedimentation and erosion develop gradually, the water level changes associated with the MSC are thought to have happened over very short time lapses (a few thousand years for the drawdown [Meijer and Krijgsman, 2005; Garcia-Castellanos and Villaseñor, 2011] and a few years for the reflooding [Garcia-Castellanos et al., 2009]), implying geologically-instantaneous changes in the surface isostatic loading. Thus, the isostatic time response is limited by the viscosity of the asthenosphere and forced to be also very rapid (stress relaxation in the asthenosphere takes place in time periods of about 20 kyr [Watts, 2001; Watts et al., 2013]). Since the density contrast between water, air and asthenosphere lead to a 0.3 to 0.4 ratio of the flexural response relative to the water level change, the kilometeric drawdown imposed vertical motions in excess of several hundred meters in the aforementioned time scales. Because the uplift due to water level drop was reversed during subsequent stages, lasting effects on the deep basins is hard to distinguish in the modern basin, although it has been linked to a basin-wide magmatic pulse (Sternai et al., 2017). On the margins, these events caused differential motions of up to 700 m over a distance of about 100 km (Figure 6.8), which could result in (re)activation of fault systems. Evidence for a tectonic response to this rebound would be very distinct from general normal fault activity, as it could be expressed as a phase of tectonic inversion. Although so far such evidence has not been described, it could independently strengthen the water level fall hypothesis for the MSC.

Our water level estimate implies a disconnection between the western and eastern Mediterranean at the platform between Sicily and Tunisia throughout a large part of MSC stage 3. The current depth of the Sicily Sill is 430 m, although its paleodepth during the crisis is not well constrained (P. L. Blanc, 2006a). A recent study shows that the isostatic subsidence caused on the Malta platform due to sediment accumulation in the Ionian Sea during the PQ is very minor (Micallef, Camerlenghi, Garcia-Castellanos, Cunarro Otero, et al., 2018). Assuming the sill was there during the MSC, this means that water levels in the Eastern and Western basins

were decoupled and dependent on local hydrological budgets, and that during the reflooding of the basin water level would have remained stagnant at the level of the Sicily Sill until water levels in the Eastern Basin reached that of the sill, as previously suggested by (P. L. Blanc, 2006a; Garcia-Castellanos & Villaseñor, 2011a; Lofi, Gorini, Berné, Clauzon, Dos Reis, et al., 2005; P. Meijer & Krijgsman, 2005b) and supported by terrace formation at various depths in different parts of the Mediterranean (Just et al., 2011; Micallef, Camerlenghi, Garcia-Castellanos, Cunarro Otero, et al., 2018) and references therein).

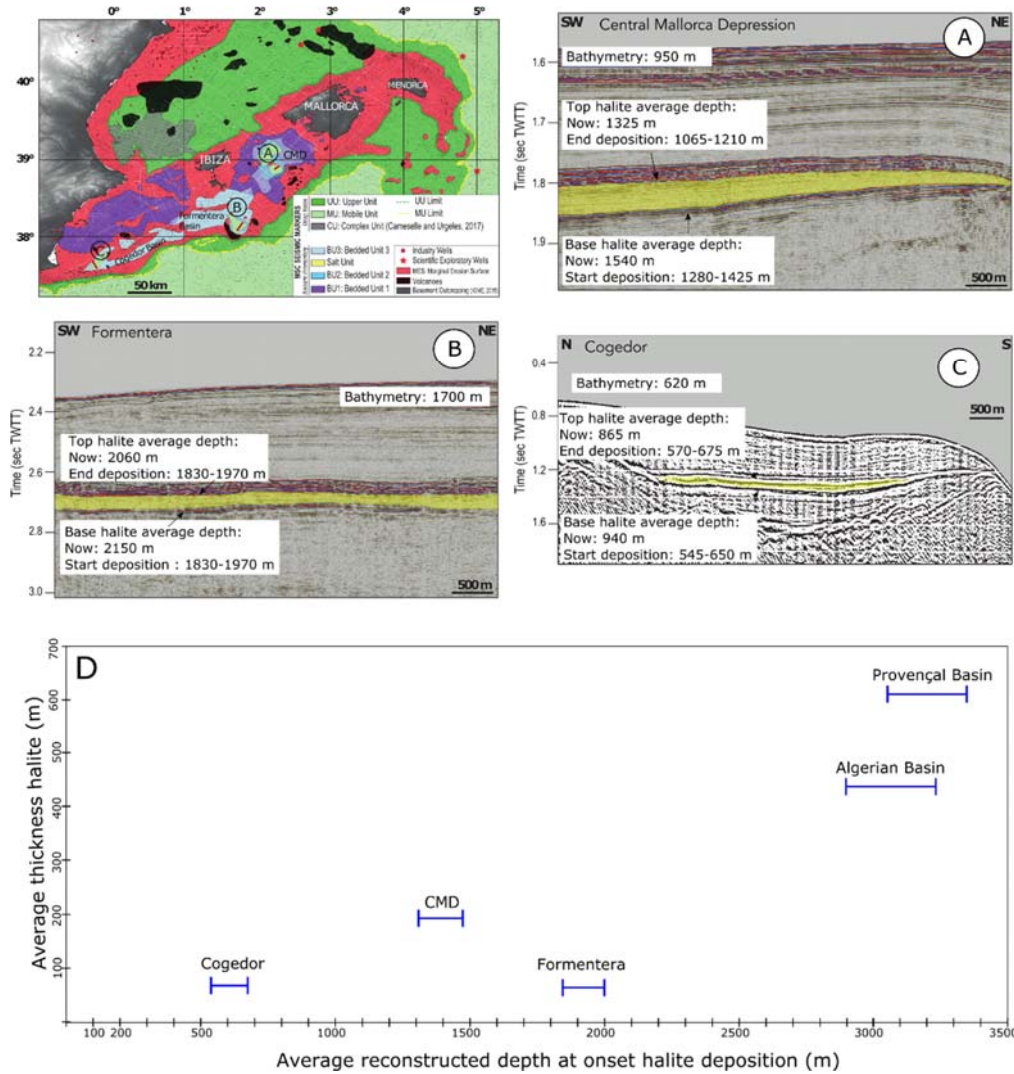


Figure 6.11. Seismic images of halite patches in CMD (A), Cogedor (B) and Formentera (C) basins showing current top and base depth of the halite (yellow) in TWTT (ms). Included are the reconstructed paleo-depths of both horizons not including the effect of water unloading. Map from Raad et al., 2020. D: Relationship of halite thickness to average reconstructed depth. Although the maximum thickness is reached in the deep basins, the smaller halite patches show no thickness-depth relationship.

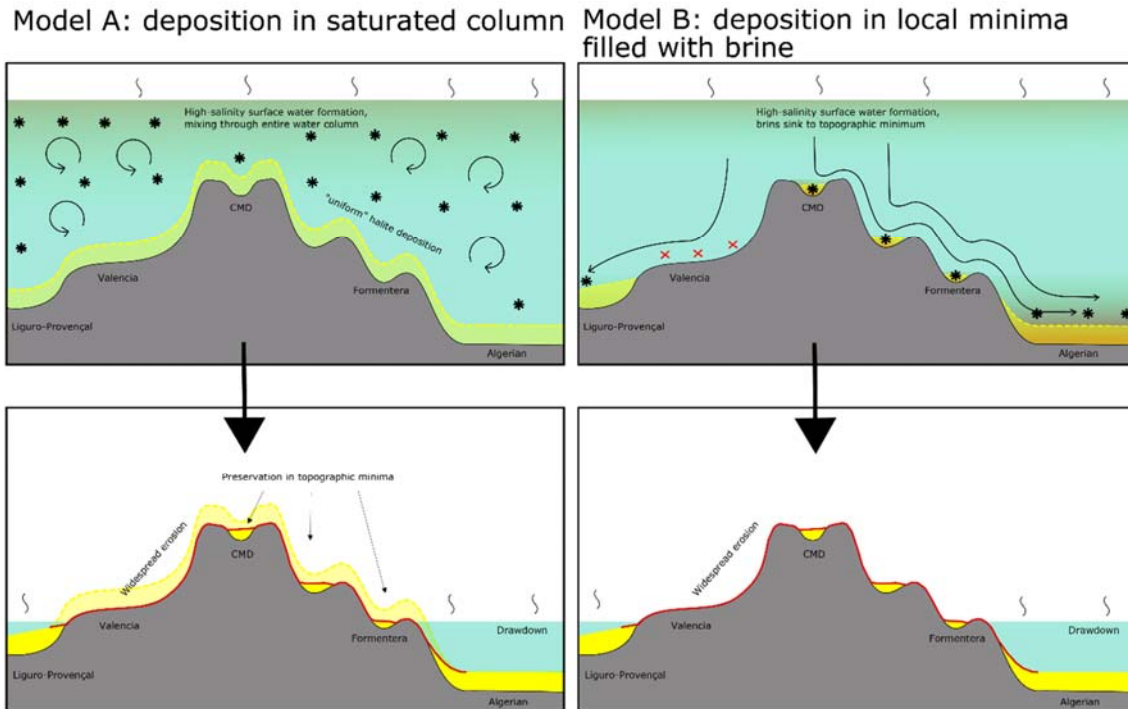


Figure 6.12. Contrasting models of halite deposition explaining the current depth-thickness distribution of halite. A: Halite is deposited throughout/in the top of the water column over the entire region, and subsequent drawdown exposes the intermediate basins removing all halite. In topographic minima some halite is preserved, as well as in the seep basins. B: Halite is deposited in local minima where dense brine can accumulate, while the Valencia Basin which is deeper than the CMD does not see halite accumulation because the dense brine sinks towards the deep basin. In this scenario the thickness of deposited halite in local minima depends on the geometry of the depressions.

6.6 Conclusions

We present a reconstruction of Messinian paleo-topography in the Western Mediterranean accounting for the flexural-isostatic response to sedimentation and water level variations since the onset of the Messinian Salinity Crisis. We test a scenario in which a main drawdown phase follows the emplacement of the MU (salt), and where the overlying UU emplaced in shallow waters, contrasted with a model without drawdown. Combining a thermo-mechanically constrained flexural-isostatic modelling we arrive at the following conclusions:

1. If the BES surface was formed by subaerial erosional processes, then the level of the western Mediterranean water surface was at least as low as -1500 ± 100 m prior to UU deposition.

2. If the extent of the UU deposits mark the coeval paleo-shoreline, then the water level was no higher than -1100 +/-100 m at the end of the UU deposition.
3. The 1500-m-drawdown scenario would imply a 700-m rebound of the deep basins causing the basins to be significantly shallower during the final stage of the MSC compared to times preceding and following the MSC lowstand.
4. The isostatic subsidence, compaction and thermal subsidence since the Messinian largely compensate the accumulation of sediment, implying that the bathymetry of the various basins at the onset of MU deposition was similar to the modern day.

There exists no thickness-paleodepth relationship for halite in the perched CMD, Formentera and Cogedor basins. We interpret this lack of a trend, together with the absence of halite in the deeper Valencia Basin, as the result of halite being deposited or preserved only in local bathymetric minima, with the halite thickness being controlled by the depth of such depressions and their outlets (e.g., spillways of brine to deeper regions).

Appendix 6-A

Local Isostasy Calculations

Deflection sediment units:

$$(1) \quad (h_s - w) * \rho_w + d * \rho_m = h_s * \rho_s$$

$$(2) \quad w * \rho_m - d * \rho_w = h_s * \rho_s - h_s * \rho_w$$

$$(3) \quad w * (\rho_m - \rho_w) = h_s * (\rho_s - \rho_w)$$

$$(4) \quad w = h_s * \frac{(\rho_s - \rho_w)}{(\rho_m - \rho_w)}$$

Deflection flood:

$$(1) \quad h_f * \rho_w = w * \rho_m + (h_f - w) * \rho_{air}$$

$$(2) \quad w = h_f * \frac{\rho_w}{\rho_m}$$

Deflection Sea-level drop:

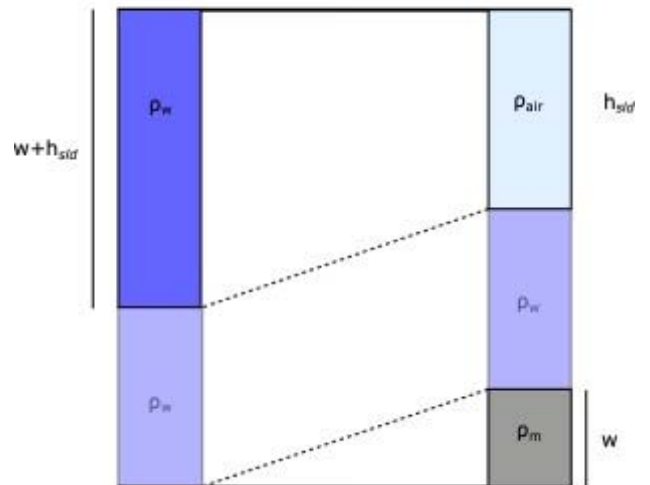
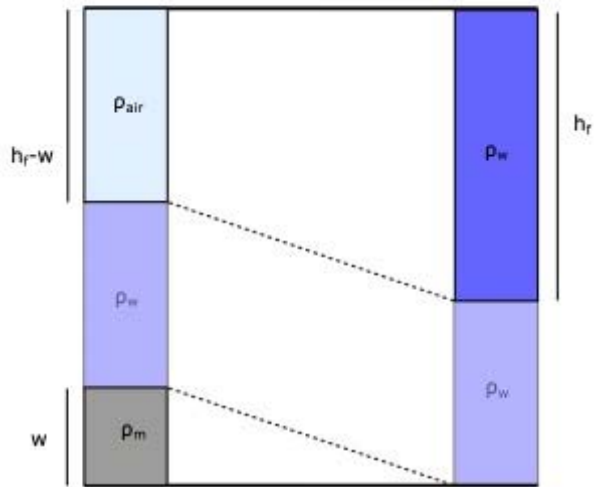
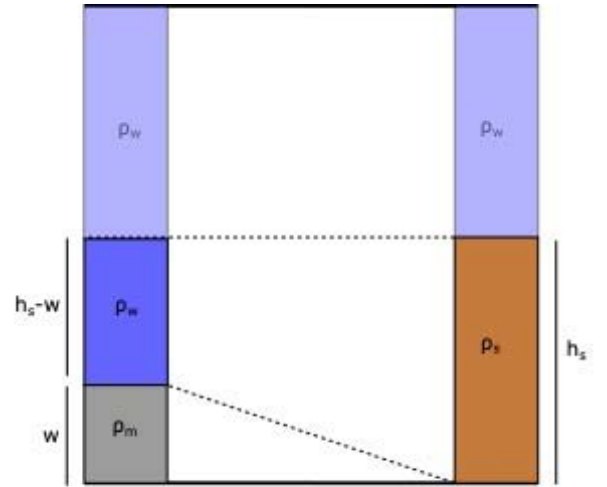
$$(1) \quad h_{sld} * \rho_w + d * \rho_w = h_{sld} * \rho_{air} + w * \rho_m$$

$$(2) \quad w * (\rho_a - \rho_w) = h_{sld} * \rho_w$$

$$(3) \quad w = h_{sld} * \frac{\rho_w}{(\rho_m - \rho_w)}$$

Where:

w is the magnitude of deflection



ρ_w = water density (1030 kg/m³)

ρ_m = mantle density (3250 kg/m³)

ρ_{air} = air density (0 kg/m³)

ρ_s = sediment density (see Table 1)

h_s = sediment thickness

h_{slid} is the magnitude of water level drop

h_f is the magnitude of change in water level during flooding

Load vs. deflection ratio for each modelling step under local isostasy

<i>Unit</i>	<i>Equation</i>	<i>ratio w/h</i>
<i>MU</i>	$w = h_s * \frac{\rho_s - \rho_w}{\rho_a - \rho_w}$	0.51
<i>UU</i>	$w = h_s * \frac{\rho_s - \rho_w}{\rho_a - \rho_w}$	0.66
<i>PQ</i>	$w = h_s * \frac{\rho_s - \rho_w}{\rho_a - \rho_w}$	0.48
<i>Flooding</i>	$w = h_f * \frac{\rho_w}{\rho_a}$	0.317
<i>Sea-level drop</i>	$w = h_{slid} * \frac{\rho_w}{\rho_a - \rho_w}$	0.46

Table 6.3. Relationship between load thickness (*h*) and deflection (*w*) for each step of the backstripping. For sedimentation steps, we assume sediments are replacing water. Variable names same as above.

Appendix 6-B

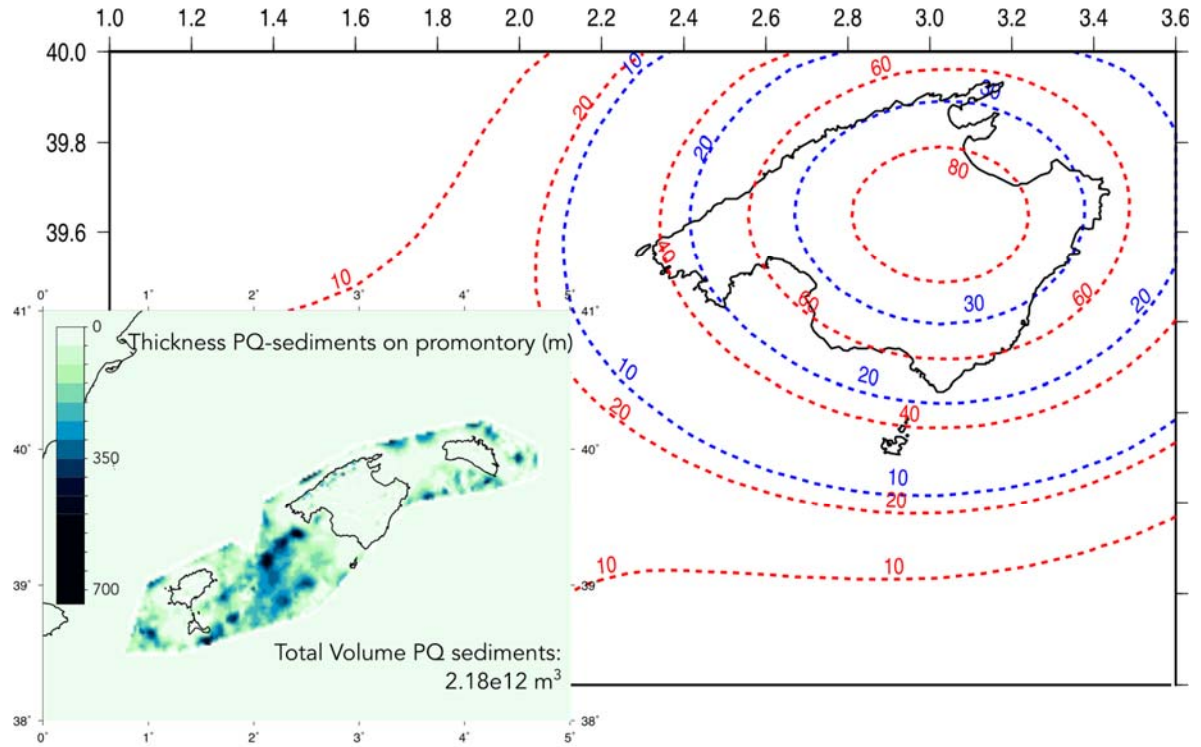


Figure 6.13. Thickness map of PQ sediments on the Balearic promontory and isolines for flexural-isostatic rebound effect in m for range of post-Messinian erosion values based on 30-70% clastic provenance sediments on Balearic Promontory. Blue: minimum volume clastics ($0.65e12 m^3$, corresponding to the 30% clastic component limit and implying an average 133 m of erosion onland) Red: maximum volume clastics ($1.52e12 m^3$, corresponding to the 70% clastic component limit and implying an average 310 m of erosion onland). Rebound calculated for EET value of 15 km .

Appendix 6-C

Results of the 2D backstripping of seismic profile MED25

The main goal of this approach is to obtain a pre-MSC paleo-bathymetry along a profile that takes into account the syn- and post-MSC tectonic deformation, which was not considered in the 3D planform regional backstripping presented earlier in this chapter. In chapter 5, all the tectonic phases affecting the Central Mallorca Depression since the beginning of the MSC were described. Those phases can be shortly resumed as follows: (1) a syn-MSC post-orogenic extensional/transensional phase which initiated already earlier in the Serravallian and became (2) pure strike-slip at a later stage, during the Pliocene-Quaternary. The main fault activity in those tectonic phases took place along the re-activated orogenic thrusts inherited from the Betic orogeny that formed the mountain ranges surrounding the area (see section 5.2.2). Thus, the main present-day active faults are rooting deep in the crust. On the seismic profile MED25, it is clear that the faults are rooting deeply in the acoustic basement (Figure 6.14-A) along thrust faults becoming low-angle in depth. What is not clear, due to the loss of the seismic signal in depth, is how deep they are rooting and what their relationship is with the main structural feature in the whole area, i.e., the Emile Baudot Escarpment (Figure 6.14). A choice on how to root and connect the faults in depth had to be done prior to the restoration of the movement along the faults. The adapted model chosen, and only existing model so far, is the one proposed by Sàbat et al., (1997), based on the deep ESCI seismic profile (Figure 5.3-D).

The result of the fault movement restoration is shown in Figure 6.14-C. After restoring the MSC and PQ sedimentary units to their initial geometrical position at the time of deposition, a very low extension rate was obtained, which is barely visible on the southeastern end of the restored profile in Figure 6.14-C, because of the very limited obtained horizontal movement. The obtained extension rate is in the order of 0.1 mm/yr, which is the same rate proposed by Sàbat et al. (2011).

The results of the isostatic deflection caused by mass movement along the faults is shown in Figure 6.15. In the CMD, it varies between 100 to 150 m of uplift (Figure 6.15-A). Adding up the deflection caused by the MSC and PQ sediment load in the CMD, which by their turn give an effect in the order of -100 to 150m (i.e., subsidence), it becomes evident that both effects cancel each other.

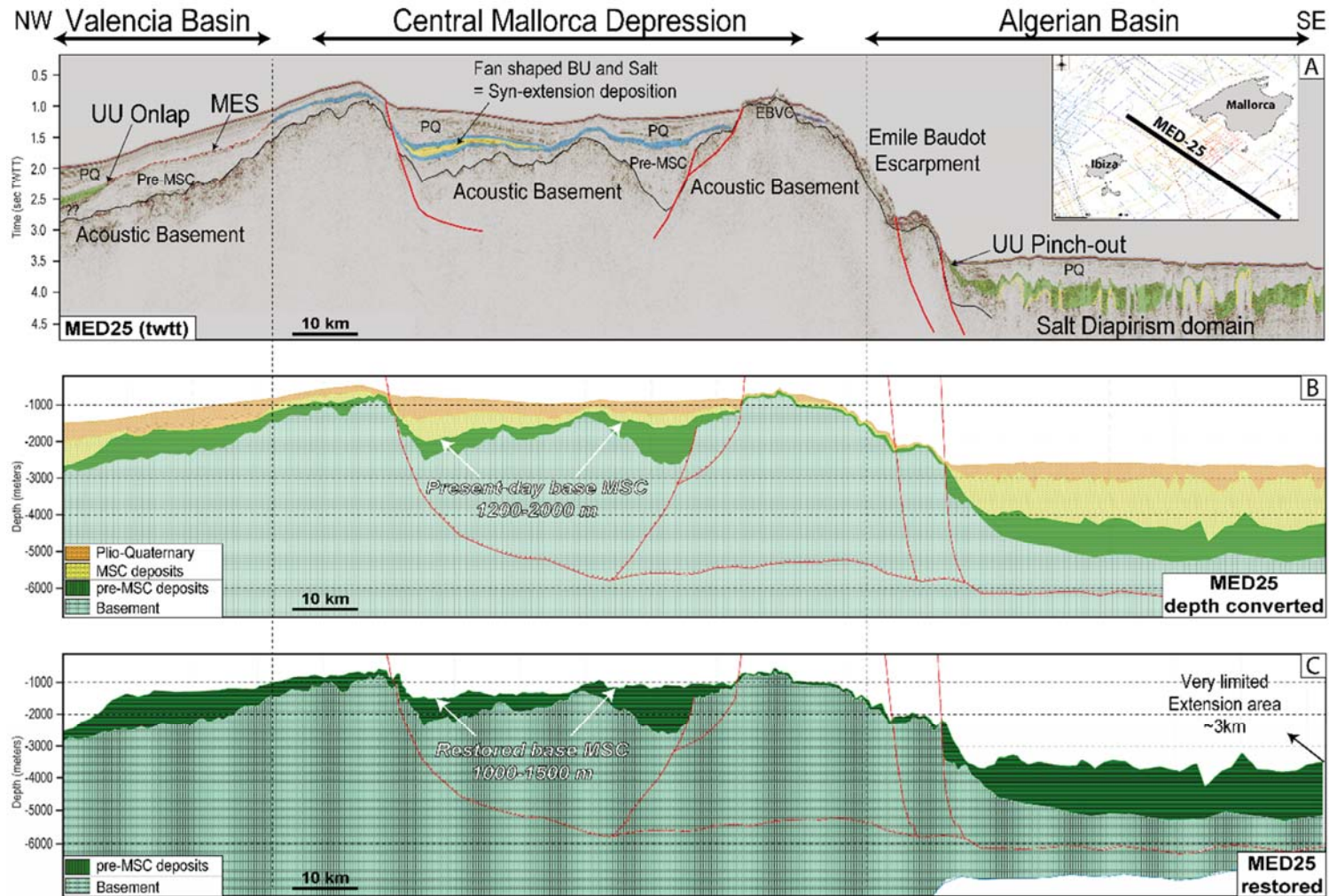


Figure 6.14. A: Interpreted seismic profile MED25 in twtt used for the 2D backstripping. B: Depth converted profile MED25 showing the present-day depth of the main horizons across the Central Mallorca Depression. The rooting in depth of the faults is adapted following the crustal model of Sabat et al. (1997). C: Restored profile after the move on fault procedure described in section 3.2.2.1. Note how the obtained horizontal movement and the corresponding extension rate is very low. Indeed, the extension rate obtained is as small as 0.1mm/yr, which is in accordance to the rates proposed by Sabat et al. (2011). The rooting of the faults in the CMD at around 5km is compatible with the interpretations of Sabat et al. (2011) and Etheve et al. (2016). Note that, however, the continuation of the faults in depth towards the Algerian Basin is not geologically realistic and was drawn only for technical issues related to the limitation of the used software (MOVE; see section 3.2.2.1.1 in chapter 3).

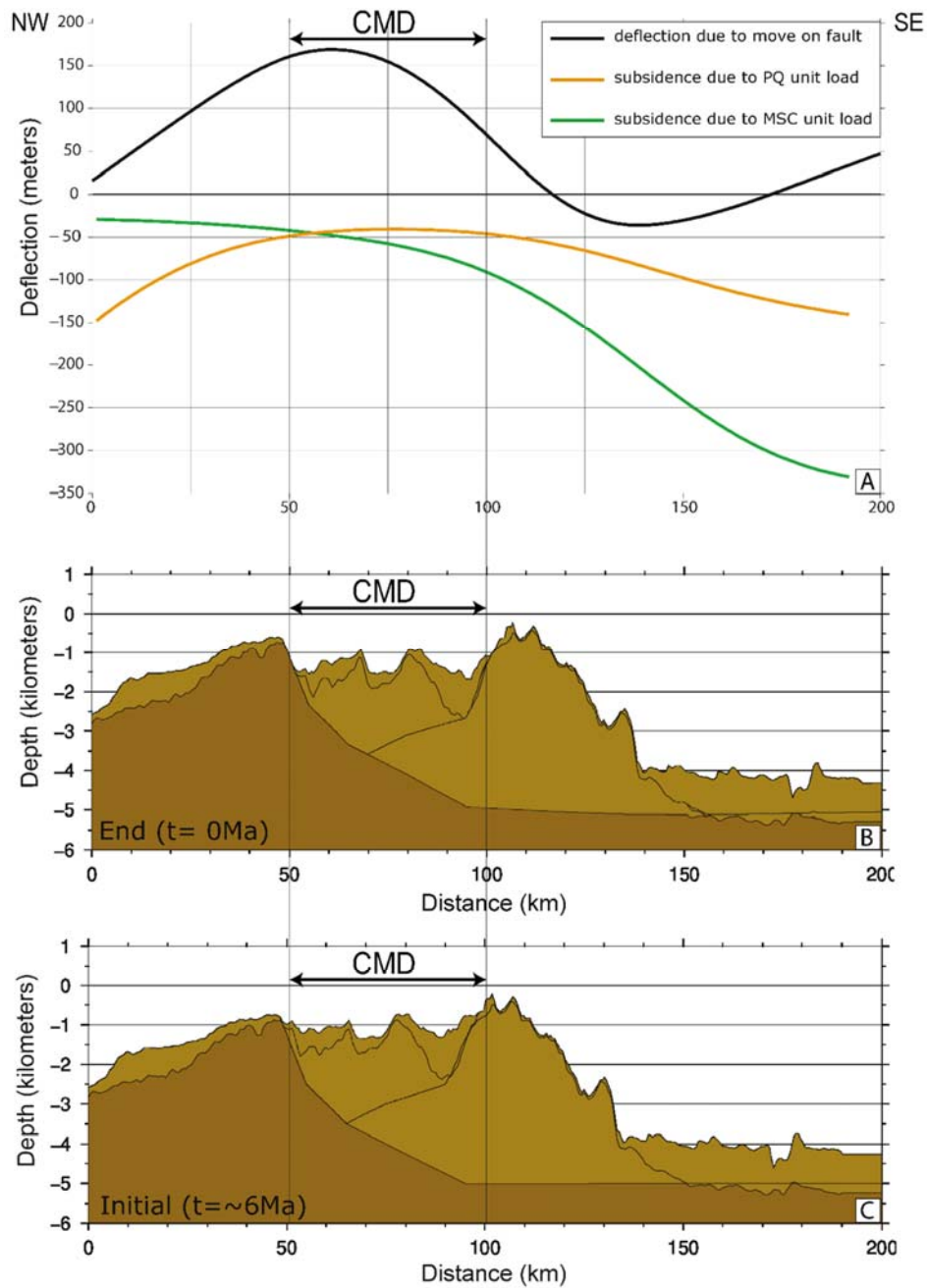


Figure 6.15. A: Results of the calculated isostatic deflection along the MED25 profile, obtained from both the mass movement along the faults and the sediments loads of the MSC and PQ deposits. Included in the calculation is also the effect of the decompaction of the pre-MSC sediments (see section 3.2.2.1). B and C: drawing of the restored profile shown in figure 6.14-C before (C) and after (B) the mass movement along the faults. Note from the graphs in panel A that the deflection caused by mass movement on fault in the CMD (~ +100 to 150m) compensates for the effect of the deflection caused by the MSC and PQ sediment load summed up together (~ -100 to 150 m).

Chapter 7

Modelling of the evaporites deposition in the Central Mallorca Depression

A song of volumes, surfaces and fluxes – The case study of the Central Mallorca Depression (Balearic Promontory) during the Messinian Salinity Crisis

Fadl Raad¹, Ronja Ebner*², Hanneke Heida³, Paul Meijer², Johanna Lofi¹, Agnès Maillard⁴, Daniel Garcia-Castellanos³

* Corresponding author: r.m.ebner@uu.nl

Having obtained the paleo-bathymetry, now I proceeded to model the conditions (salinity and water fluxes) under which the evaporites in the CMD deposited. To do so I applied physics-based numerical modelling in collaboration with Ronja Ebner a colleague from SaltGiant project, under the supervision of Paul Meijer. The theory behind the models I used as well as the coding were written and developed by Ronja and Paul.

Me and Ronja wrote a scientific article on this work, which is presented below in this chapter. The article was submitted to Basin Research journal and got minor revisions which are being worked on.

Here I'm not going to give the take-home message because it's the final step of this PhD thesis and the results and conclusions of this chapter are immediately presented in the conclusion section of the chapter, and in the final chapter (conclusions and perspectives) of the thesis.

Abstract: The Central Mallorca Depression (CMD) located in the Balearic Promontory (Western Mediterranean), contains a well-preserved evaporitic sequence belonging to the Messinian Salinity Crisis (MSC) salt giant, densely covered by high- and low-resolution seismic reflection data. It has been proposed recently that the MSC evaporitic sequence in the CMD could be a non-deformed analogue of the key MSC area represented by the Caltanissetta Basin in Sicily. This presumed similarity makes the CMD an interesting system to better understand the MSC events.

Physics-based box models of the water mixing between sub-basins, built on conservation of mass of water and salt, help constrain the hydrological conditions under which evaporites formed during the MSC. Those models have been widely used in the literature of the MSC in the past two decades. They have been mostly applied to the Mediterranean Sea as a whole focusing on the Mediterranean-Atlantic connection, or focusing on the influence of the Sicily Sill connecting the Western and Eastern Mediterranean Sea. In this study, we apply a downscaled version of such modeling technique to the CMD.

First, we quantify the present-day volumes of the MSC units. We then use a reconstructed pre-MSC paleo-bathymetry to model salinity changes as a function of flux exchanges between the CMD and the Mediterranean. We show that a persistent connection between the CMD and the Mediterranean brine near gypsum saturation can explain volume of Primary Lower Gypsum under a sea level similar to the present. For the halite, on the contrary, we show that the observed halite volume cannot be deposited from a connected CMD-Mediterranean scenario, suggesting a drawdown of at least 850 m (sill depth) is necessary. Comparison between the deep basin halite volume and that of the CMD shows that it is possible to obtain the observed halite volume in both basins from a disconnected Mediterranean basin undergoing drawdown, although determining the average salinity of the Western Mediterranean basin at the onset of drawdown requires further investigation.

7.1 Introduction

The reduction of water exchange between the Atlantic and Mediterranean caused by the tectonic uplift of the Gibraltar arc during the Late Miocene Messinian Salinity Crisis (MSC; 5.97-5.33 Ma) led to the deposition of a large evaporitic body, also known as the Mediterranean Salt Giant, in a relatively short geological time interval of ~640 kyr (Hsü, 1973; W. B. F. Ryan, 1973; Krijgsman et al., 1999; CIESM, 2008). It has been suggested that deposition of the Mediterranean MSC salt giant has greatly affected the global oceans, by sequestering up to ~6-10 % of their salt content into the Mediterranean Sea (Garcia-Castellanos & Villaseñor, 2011; Haq et al., 2020). The mechanisms and time spans for the deposition of the MSC evaporites are still not clear and highly debated despite the numerous studies in the last half century, although a generally accepted chronostratigraphic model that divides the MSC events into 3 stages has been proposed (CIESM, 2008; Roveri, Flecker, et al., 2014). According to this model, the onset of the MSC is marked, at least in marginal basins (<200 m paleo-depth), by up to 16 precessionally driven cycles of gypsum intercalated with marls/carbonates, also called the Primary Lower Gypsum (PLG). The deposition of the PLG took place during the first stage of the MSC (stage 1; 5.971-5.60 Ma; Krijgsman et al., 1999; Lugli et al., 2010). It was followed by stage 2 (5.60-5.55 Ma) in which part of the PLG was removed (by erosion and/or as mass transport deposit) and resedimented as Resedimented Lower Gypsum (RLG) (Roveri et al., 2006; Clauzon et al., 2015; Manzi et al., 2021), and a halite unit was deposited in intermediate (~200 to 1000m paleo-depth; e.g. Caltanissetta Basin and Central Mallorca Depression; Lugli et al., 1999; Raad et al., 2021) to deep basins (>1000m paleo-depth; e.g. Provencal and Levant basins; Lofi et al., 2011). During this stage, margins and slopes underwent intense erosion of subaerial origin according to some authors (e.g., Clauzon, 1978; Lofi et al., 2005) or of submarine origin according to others (e.g., Roveri, Manzi, et al., 2014). The third and last MSC stage is divided in 2 substages, substage 3.1 (5.55-5.42 Ma) in which the Upper Evaporites (UE) deposited in hypersaline conditions (Manzi et al., 2009), and substage 3.2 (5.42-5.33 Ma) which witnessed more hyposaline conditions, also known as the Lago Mare phase (Andretto et al., 2021).

Several aspects and implications of the consensus model remain ambiguous and continuously questioned. For example, whether the halite deposition took place synchronously and exclusively during stage 2 (Roveri, Flecker, et al., 2014; Manzi et al., 2018; Manzi, Gennari,

et al., 2021) or started already during stage 1 (Meilijson et al., 2018, 2022). Another controversy is whether the isolated conditions persisted during the whole stage 3 or the Atlantic-Mediterranean connection was restored at the beginning of that stage (Andreetto et al., 2021), with a Mediterranean probably supplied also by Paratethyan brackish water (Marzocchi et al., 2016). Many more aspects continue to puzzle regarding the MSC: the amplitude and duration of the main water level drawdown, the reason for the absence of evaporites on most of the shelves and slopes of the open deep basins, the cause of lack of a clear paleodepth distribution of halite (e.g. deep halite-free Valencia Basin versus shallower Balearic Promontory containing halite; Heida et al., 2021).

The Balearic Promontory (BP), a prominent high in the Western Mediterranean (Figure 7.1), presents a unique opportunity place to investigate the formation of the MSC evaporites, thanks to the well-preserved evaporitic units deposited since the beginning of the crisis (Maillard et al., 2014; Ochoa et al., 2015b; Driussi, Maillard, et al., 2015; Raad et al., 2021). Lying between Mallorca and Ibiza, the Central Mallorca Depression (CMD), contains the most complete and least tectonically deformed evaporitic sequence in the BP, including halite (Raad et al., 2021; Maillard et al., 2022). This sequence has been studied and accurately mapped recently by several authors (Figure 7.1) (Maillard et al., 2014; Driussi, Maillard, et al., 2015; Raad et al., 2021). Most recently, Raad et al. (2021) showed that the MSC evaporitic sequence in the CMD could be an undeformed analogue of the intermediate-depth Caltanissetta Basin in Sicily, a rare example of onshore record holding MSC halite, which makes the CMD an interesting place to study for furthering our understanding of the MSC.

Physics-based models help in examining some hydrological factors under which the MSC evaporites formed. Those models have been widely used in MSC research in the past two decades (Blanc, 2000; Meijer & Krijgsman, 2005; Blanc, 2006; Meijer, 2006; Krijgsman & Meijer, 2008; Topper et al., 2011; P. T. Meijer, 2012; Topper & Meijer, 2013; Simon et al., 2017). All those studies worked on a Mediterranean scale aimed at the Atlantic-Western Mediterranean and Western-Eastern Mediterranean connections through the Gibraltar and Sicily straits, respectively. In this study, we scale down as we apply models based on conservation of mass of water and salt and a simplified representation of strait dynamics, on a single sub-basin within the Western Mediterranean, the CMD (Figure 7.1). A similar approach has been applied recently in the Sorbas Basin using those models by Modestou et al. (2017). In the CMD, the presence of a good, high- and low-resolution seismic reflection data coverage,

allows the determination of the thicknesses and respective volumes of the evaporites (Figure 7.2-A). In addition, the availability of a restored pre-MSC paleo-bathymetry, published recently by Heida et al. (2021), allows the establishment of the hypsometry of the basin during the MSC. The main objectives of this study are to: (1) establish the hydrological conditions (salinity and fluxes) and mechanisms under which the evaporites (gypsum and halite) in the CMD formed during MSC stages 1 and 2, and (2) examine the amplitude of a potential water level drawdown in the CMD needed to explain the required hydrological conditions.

To reach these objectives, we use the calculated volumes of the MSC evaporites and the restored pre-MSC bathymetry to (1) make water budget calculations of the CMD and compare those with the observed evaporitic volumes, (2) test the factors (fresh water budget and fluxes) controlling the salinity of the CMD as an isolated basin, (3) calculate the fastest evolution possible of the CMD and Valencia Basin in terms of salinity and time to deposit the observed evaporites, and (4) discuss our results and observations in the frame of the whole Mediterranean Salt Giant complex and compare them to the consensus model.

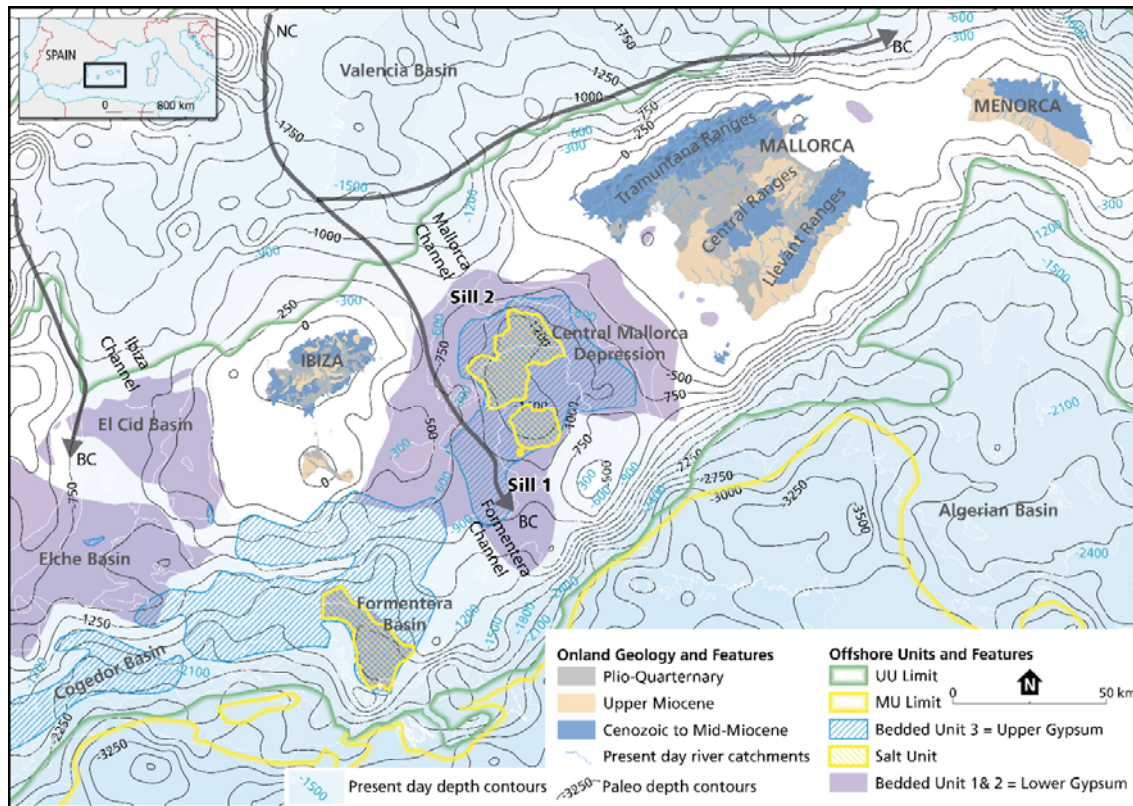


Figure 7.1. Map of the MSC units over the Balearic Promontory (BP), Valencia Basin and Algerian Basin. Our study area focusses on the Central Mallorca Depression (CMD) located between the islands of Mallorca and Ibiza, which contains several Bedded Units (BUs) and a Halite unit geometrically/attitudinally separated from the deep basin's Mobile Unit (MU) and Upper Unit (UU). MSC units of the BP are modified from Raad et al. (2021). Onland geology of the Balearic Islands is modified from geological map of Spain 1:50000 (IGME). Thin white lines in the background represent the present-day Bathymetry taken from the European Marine Observation and Data network (EMODnet) database available online (www.emodnet-bathymetry.eu). Thin black lines represent the paleo-bathymetry at the start of the MSC, modified after Heida et al. (2021). Arrows indicate the present day currents (from Pinot et al. (2002) and Lüdmann et al. (2012)). NC=Northern Current. BC=Balearic Current.

7.2 Geological Background

The present-day BP is characterized by a series of sub-basins lying at a wide range of depths (Figure 7.1; e.g. -650 m Elche Basin and -1700m Formentera Basin). They show different levels of inter-basinal connection and all contain MSC sediments up to ~500m thick (Figure 7.1 and Figure 7.2; Driussi et al., 2015a; Ochoa et al., 2015; Raad et al., 2021). The MSC sediments of the BP have been mainly studied through seismic reflection data due to the absence of exploratory scientific boreholes. They consist of Bedded Units covering most of the BP area

(BU sensu Lofi et al., 2011; Lofi, 2018; divided subsequently into BU1, BU2 and BU3 by Raad et al., 2021; Table 7.1) as well as salt patches present in some sub-basins depocenters (Figure 7.1) (Mauffret, 1977; Acosta et al., 2004; Maillard et al., 2014; Driussi, Maillard, et al., 2015; Raad et al., 2021; Heida et al., 2021) Figure 7.1. The sub-basins are believed to have inherited their structure from the pre-Messinian tectonic evolution of the promontory, and thus to have been preexisting topographic lows during the MSC allowing the accumulation of evaporites (Sàbat et al., 2011; Driussi, Briais, et al., 2015).

In this work, we focus mainly on the CMD, an intermediate-depth (sensu Roveri et al., 2014) sub-basin containing a well-preserved MSC sequence.

7.2.1 The Central Mallorca Depression: Present-day vs paleo-topography

Today, the maximum water depth of the CMD reaches -1050 m (Figure 7.1; Acosta et al., 2004). The CMD is surrounded by the gently dipping slopes of Mallorca and Ibiza to the NNE and WSW respectively. It is connected northward to Valencia Basin through the ~730 m deep, ~20km wide Mallorca Channel (Pinot et al., 2002), and southward to the Algerian Basin through the ~1000 m deep, ~30 km wide channel that we call the Formentera Channel (Figure 7.1). The CMD underwent limited post-MSC tectonics with some local deformation caused by extension and strike-slip motions (Acosta et al., 2004; Sàbat et al., 2011), which guaranteed a good preservation of the MSC deposits. Other sources of vertical motions, such as isostatic subsidence, compaction and thermal subsidence, did not strongly affect the CMD due to the nature of the lithosphere below the BP and the limited extent and thickness of the sediments (Heida et al., 2021 and references therein). Heida et al. (2021) applied a pseudo-3D backstripping restoration of the Messinian paleotopography of a large area in the Western Mediterranean, including the BP. They obtained pre-MSC paleo-depths of the BP sub-basins ranging from ~550 m (e.g. Cogedor Basin) to ~1800 m (e.g. Formentera Basin). The CMD was at ~1500 m in its deepest part (Figure 7.1, Figure 7.3 and Table 7.3; Heida et al., 2021) whereas the Mallorca and Formentera channels were at 750 m and 850 m (± 50 m; Heida et al., 2021) respectively (Sill 02 and sill 01, respectively, in Figure 7.1 and Figure 7.3).

7.2.2 Present-day Hydrography and Water Masses in the Central Mallorca Depression

Generally, four water masses can be distinguished in the Western Mediterranean: the Modified Atlantic Surface Water; the Levantine Intermediate Water; the Western Mediterranean Deep Water; and the Bottom Water (La Violette, 1994; Pinot et al., 2002; Lüdmann et al., 2012). The Mallorca and Ibiza channels play a main role in the regional water exchange and circulation of those water masses. In particular, the Northern Current carrying northern waters from the Gulf of Lions southward along the continental slope of the Valencia Basin, is in part blocked by the Balearic Islands and consequently bifurcates north of Ibiza. One branch, called the Balearic Current, passes through the Ibiza and Mallorca channels into the Algerian Basin (Figure 7.1). Several studies surveyed and quantified the present-day oceanographic parameters of these currents (water exchanges, fluxes, salinities) across the Mallorca Channel (Pinot et al., 2002; Barceló-Llull et al., 2019; Vargas-Yáñez et al., 2020).

The fresh water from river runoff reaching the CMD is very limited ($\ll 10 \text{ m}^3 \text{ s}^{-1}$; Table 7.3) with minor river catchments draining from the Tramuntana and Central ranges onshore Mallorca, and the central part of Ibiza Island (Figure 7.1; Garcia et al., 2017 and references therein). Most of the catchments are draining mainly Mesozoic carbonates (Figure 7.1).

7.2.3 Messinian Salinity Crisis in the Central Mallorca Depression

So far, only two studies were dedicated to the MSC deposits in the CMD. Maillard et al. (2014) were the first to study and map the BUs and to image the salt offshore at an intermediate depth. The authors present all possible scenarios for the deposition of the MSC sediments based on the observed features and markers (see their figure 12). In the most recent study dedicated to the MSC deposits in the BP, Raad et al. (2021) made a step forward by dividing the BUs into 3 sub-units (Table 1) based on their seismic-stratigraphic position and seismic facies. Including the salt unit, they performed a unit-by-unit comparison to the MSC evaporites outcropping in the Sicilian Caltanissetta Basin. Following their division and comparison, Raad et al. (2021) interpreted the MSC units of the CMD and proposed a depositional model as follows (see their figure 10 and discussion for a detailed description and interpretation of each unit):

- BU1: equivalent to the PLG and deposited during stage 1 of the MSC (Table 1). It is the only drilled MSC unit of the BP and is made of a succession of precession-driven cycles of selenitic gypsum and marls (Ochoa et al., 2015). This unit is topped by a clear erosional surface everywhere on the BP (Maillard et al., 2014; Ochoa et al., 2015; Raad et al., 2021). In the CMD, BU1 reaches a maximum thickness of ~180m in the proximal domain (Figure 7.2-B) when it is preserved. It thins towards the distal domain (~40m), and/or where it is eroded by paleo-incisions (Figure 7.2-B; Raad et al., 2021).

- BU2: possible time equivalent of BU1 (i.e. MSC stage 1), it would represent its distal facies equivalent. According to Raad et al. (2021), this unit likely consists mainly of cumulate gypsum, alternated with non-evaporitic sediments. The cumulate gypsum is commonly known to form in a supersaturated water column in which gypsum crystals nucleate at the top or within water column and then precipitate and settle on the seafloor as laminar gypsum (Hardie & Lowenstein, 2004; Babel & Schreiber, 2014; Natalicchio et al., 2021). No erosional features mark the top or the base of this unit. Both BU1 and BU2 were deposited during a high stand, and were then followed by an important base level drawdown, during which only BU1 was exposed.

- Salt unit: it consists mainly of halite and might include more soluble salts (K- and Mg-salts), similar to the salts observed in Caltanissetta Basin (Lugli et al., 1999; Manzi et al., 2012). The salt unit in the CMD is truncated at its upper limit by an erosional surface, probably due to exposure and/or dissolution in relatively shallow water when the maximum base level drawdown was reached. It reaches a maximum thickness of ~280m in the deepest depocenter (Figure 7.2-C).

- BU3: this unit is interpreted as the equivalent of the Upper Evaporites of the Caltanissetta Basin, and consisting of alternating terrigenous and gypsum beds deposited during stage 3 of the MSC (Table 7.1). It lies unconformably above the BU1 and the salt. It lies conformably below the lowermost Pliocene pelagic sediments. BU3 reaches thicknesses up to ~170 m (Figure 7.2-D). It shows no physical relationship or continuation with the deep basin's MSC evaporites. For this reason Raad et al. (2021) and Heida et al. (2021) concluded that the CMD was disconnected from all the surrounding basins during the final stage of the MSC, before getting reconnected during the Zanclean reflooding with the rest of the Mediterranean at the end of the crisis (Garcia-Castellanos et al., 2009). In this scenario, the sulfate ions needed for

gypsum precipitation are exclusively derived from dissolution of stage 1 PLG (W. B. F. Ryan, 2009; Andretto et al., 2021).

MSC unit	Interpreted lithology	MSC stage and duration	Velocity for TWTT to depth conversion	Evaporites/clastic ratio	Total volume (m ³)	Evaporitic volume (m ³)	Thickness (meters)	Bounding surfaces
BU1 = LE (PLG)	Selenitic gypsum intercalated with marls	Stage 1 (5.97-5.60 Ma)	4500 m/s (Ochoa et al., 2015)	80%	3.73E+11	2.99E+11	40-180m	Base: Conformable Top: TES
BU2 = LE	pelagic gypsum intercalated with marls	Stage 1 (5.97-5.60 Ma)	4500 m/s	80%	3.73E+11	2.99E+11	40-180m	Base: Conformable Top: Conformable
Salt unit	halite	Stage 2 (5.60-5.55 Ma)	4780 m/s (Samperi et al., 2020)	100%	9.63E+10	9.63E+10	280m	Base: Conformable Top: IES
BU3 = UE + LM?	Alternations of gypsum and clastics	Stage 3 (5.55-5.33 Ma)	3500 m/s	50%	1.63E+11	8.14E+10	150m	Base: IES Top: Conformable

Table 7.1. Characteristics and parameters of the MSC units present in the CMD. BU=Bedded Unit; LE=Lower Evaporites; PLG=Primary Lower Gypsum; UE=Upper Evaporites; LM=Lago Mare; TES= Top Erosion Surface; IES= Intermediate Erosion Surface.

7.3 Data and Methods

7.3.1 Seismic dataset and volume calculations

We use widespread high- and low-resolution seismic reflection profiles to calculate the volumes of the MSC units in the CMD (Figure 7.2-A). This dataset has been interpreted, described and used in several previous studies (e.g. (Maillard et al., 2014; Bellucci et al., 2021; Raad et al., 2021)). Following the interpretation of the MSC units on the seismic profiles, a thickness map for each unit was created (Figure 7.2) using the internal velocities shown in Table 7.1 for the time to depth conversion.

For the volume calculations we consider 80% of the total volume of BU1 (=PLG) and BU2 as gypsum, since elsewhere around the Mediterranean the PLG cycles contain only thin non-evaporitic intercalations and much thicker gypsum beds (Table 7.1; e.g., Lugli et al., 2010;

Ochoa et al., 2015 for the BP offshore area; García-Veigas et al., 2018; Mas & Fornós, 2020). For the BU3 (=UE) we consider only 50% of its volume as gypsum since the gypsum/non-evaporitic deposit ratio of the UE is lower than the PLG (Table 7.1; e.g., Manzi et al., 2009 for Sicily; Manzi et al., 2016 for Cyprus; Lugli et al., 2015 for the Upper Unit in offshore DSDP and ODP sites). No such assumptions are made for the halite volume as we consider the entire salt unit as made of halite with negligible amount of clastics (Lugli et al., 1999; Manzi et al., 2012; Samperi et al., 2020).

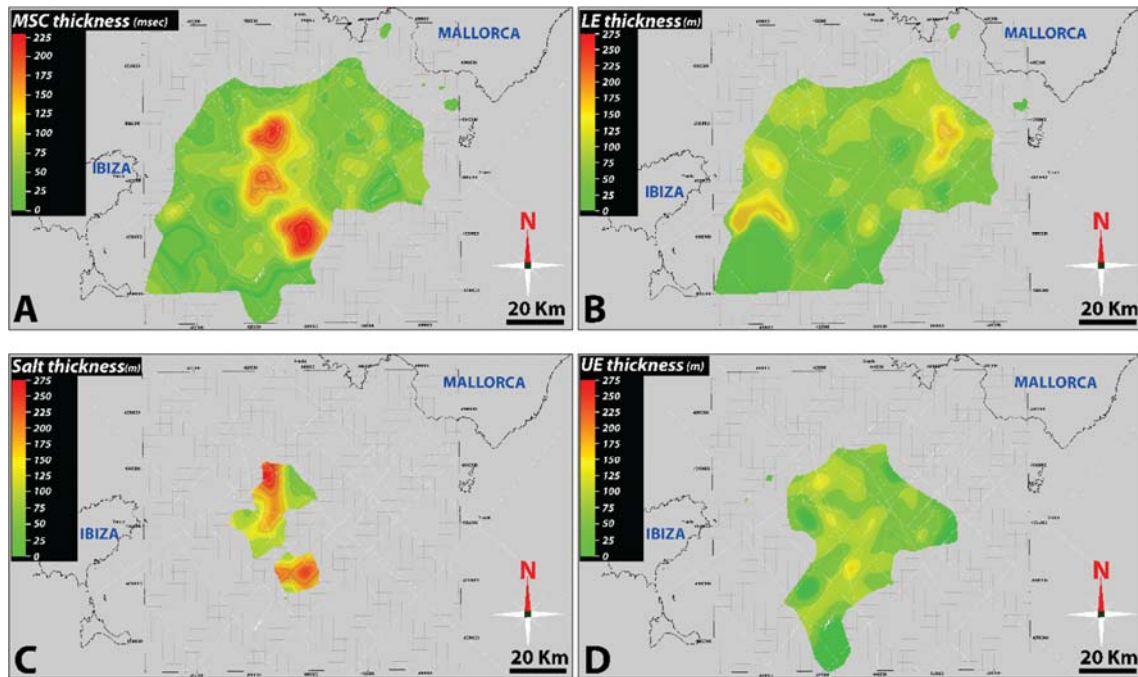


Figure 7.2. Thickness maps of the MSC units of the CMD. A: Thickness map in TWTT of the whole MSC units, including all BUs and Halite in TWTT. B: Thickness map in meters of BU1 + BU2 interpreted as stage 1 MSC Lower Evaporites (LE), with gypsum content ranging between of about 80% (see text and Table 7.1 for explanation). C: Thickness map in meters of the halite unit. D: Thickness map in meters of BU3 interpreted as MSC stage 3 Upper Evaporites (UE). The white thin lines mark the locations of seismic profiles used to map the deposits.

7.3.2 Theoretical model

Investigating the possible scenarios that could have led to the Messinian deposits of the CMD requires that we consider the salinity of the basin itself as well as the salinity of the surrounding waters. In this study, we define salinity (S) as dissolved mass of salts (m) per volume of water (V), ($S = \frac{m}{V} [kg m^{-3}]$).

We treat salinity as a sum of concentrations and differentiate between the salts of interest, i.e., gypsum and halite:

$$S = \frac{\sum m_{salts}}{V} = \sum [salt] = c[CaSO_4] + c[NaCl] + c[other\ salts] \quad (1)$$

Since the exact composition of seawater during the MSC is not known, we use a composition that has been used in previous studies (e.g., Gladstone et al., 2007; Krijgsman & Meijer, 2008; Topper & Meijer, 2013; Simon et al., 2017) and assume a proportional increase of the partial concentrations with increasing salinity, until saturation is reached. Saturation is defined as the salinity at which the water body cannot hold any extra ions of the salt in question. Adding the concentration of the three ion groups (Table 7.2) to eq. (1), we define our reference salinity to be $S_{reference} = 35.05 \text{ kg m}^{-3} = 1.27 \text{ kg m}^{-3} + 27.21 \text{ kg m}^{-3} + 6.57 \text{ kg m}^{-3}$ (Leeder, 2009). Assuming seawater is saturated in gypsum at 145 kg m^{-3} (McCaffrey et al., 1987; De Lange et al., 1990) and in halite at 350 kg m^{-3} (McCaffrey et al., 1987; Babel & Schreiber, 2014), we can then calculate the saturation concentration for gypsum, $c[CaSO_4]^{sat} = 5.25 \text{ kg m}^{-3}$ and halite $c[NaCl]^{sat} = 272.1 \text{ kg m}^{-3}$ (Krijgsman & Meijer, 2008; R. Topper & Meijer, 2013). A direct application of these values is to quantify the volume of water, at saturation concentration, that would be needed to form an observed volume of deposit. Since a lower concentration would require a bigger volume of water to precipitate the deposit, this water volume at saturation will be called V_{min} :

$$V_{min} = \frac{m_{salt}}{c[salt]^{sat}} = \frac{V_{deposit} * \rho_{deposit}}{c[salt]^{sat}} \quad (2)$$

In which m_{salt} is the salt mass that forms the deposit that can be derived from the volume of the deposit, $V_{deposit}$ in $[m^3]$ and its density, $\rho_{deposit}$ $[kg m^{-3}]$ (Table 7.2).

	Gypsum	Halite	Reference
Density (kg/m ³)	2300	2200	Leeder, 1999
Fraction of longroup (-)	1.27/ 35	27.21/ 35	Leeder, 1999 Topper & Meijer (2013)
Saturation Concentration (kg/m ³)	5.25	271.1	Leeder, 1999 Topper & Meijer (2013)
Area covered by deposit (m ²)	5.33E+9	6.65E+8	This work
Volume in CMD (m ³)	3.80E+11	9.63E+10	This work
Erosion rate (mm/a)	From 0.20 ^a up to 3.16 ^b	0.5–0.75 ^c (for 50mm/a precipitation) -- 20 ^d (for 100mm/a rainfall)	^a Sanna et al., (2015) ^b Calaforra and Forti (1993) ^c Frumkin (1994) ^d Mottershead et al. (2005)
Precipitation rate (mm/a)	1 ^a –100 ^b	100 ^c . ^d –150 ^e	^a Orti et al., (1985) ^b Schreiber & Hsu, (1980) ^c Lensky et al., (2005) ^d Sirota et al., (2018) ^e Manzi et al., (2012)

Table 7.2. Table showing the parameters used in our modelling for Halite and Gypsum with the corresponding references. Erosion rates are not used in the modelling but are used for considerations in the discussion.

The water volume of the CMD is defined by the physical limits of the basin as retrieved from the pre-Messinian paleo-bathymetry of the CMD (Figure 7.3) (Heida et al., 2021). From the same reconstruction, we draw cross sections through the southern and the northern connection between the CMD and the adjacent Mediterranean Sea. With a width of 70-80 km at sea level and a depth of up to 850 m, these connections are larger than the Strait of Gibraltar (12 km wide, 300 m deep; Lacombe & Richez, 1982). They are best described as wide openings with a sill that is elevated well above the seafloor north and south of the CMD but still located at significant water depth (Figure 7.3). The openings would form a narrow strait and/or shallow sill only when the water level is significantly lower than today. From modern measurements (Pinot et al., 2002; Barceló-Llull et al., 2019) it is known that there are both fluxes into and out of the basin through each of the two connections (see section 7.2.2).

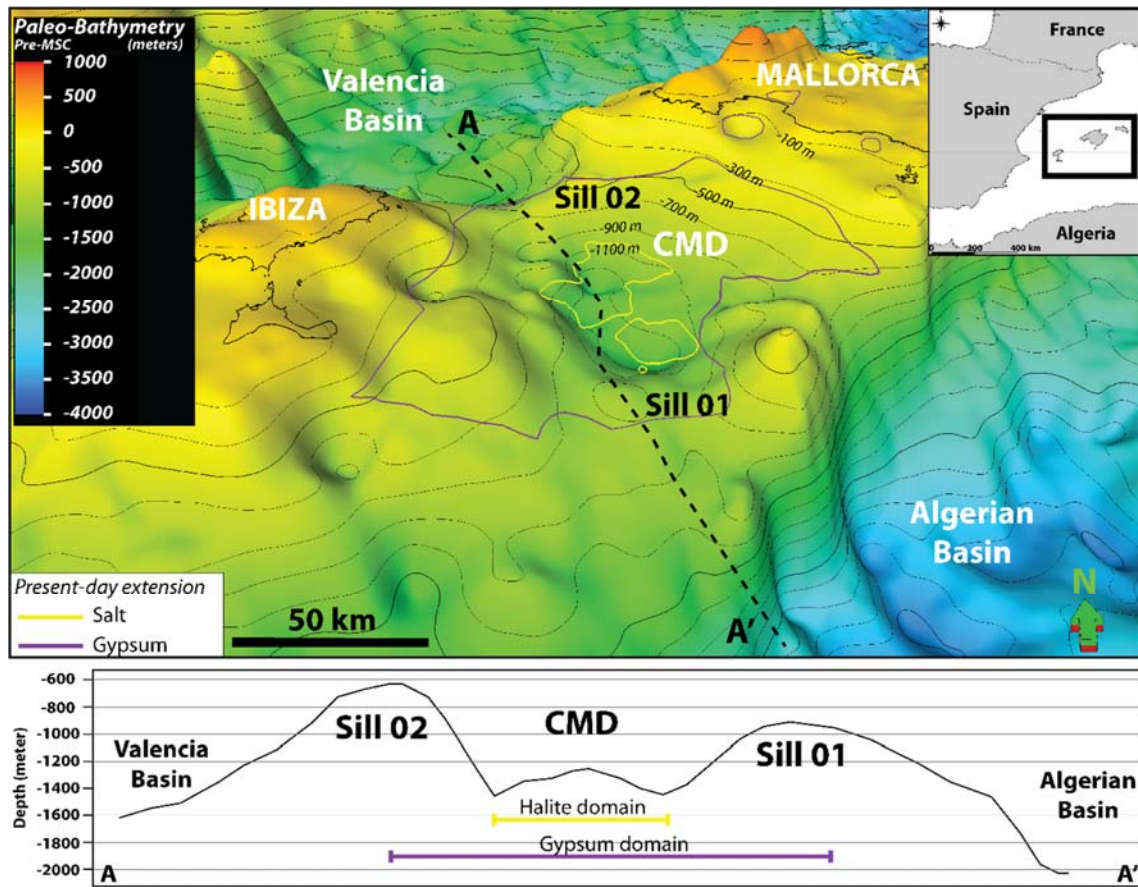


Figure 7.3. 3D paleo-bathymetry of the CMD at the beginning of the MSC. The CMD is connected to the deep basin through two silled channels/connections. Sill 01 is deeper and is the one that is used in the modelling as a connection between the CMD and the open Mediterranean. A-A' is a 2D profile highlighting the geometry of the CMD and the sills. The violet and yellow polygons represent the present-day extension of the gypsum and halite, respectively. They are 2D polygons projected above the 3D paleo-bathymetry.

It is possible to apply basic principles that allow us to learn about the CMD and its fluxes as a system while making as little assumptions as possible. One of these principles is the conservation of water volume for a system that is in balance. This means that the volume of water in the basin does not change when the sum of fluxes into the basin is of the same size as the sum of outward fluxes. In contrast, when there is a net outflux, the volume of water inside the basin will decrease over time, with a rate defined by the absolute difference between the in- and outflux. This is for example the case for a disconnected basin with a negative freshwater budget. This loss of fresh water is described by a volume flux [m^3s^{-1}] (positive when the basin loses water) and named freshwater budget (*fwb*).

$$fwb = (E - P) * A - R \quad (3)$$

In which E is the rate of evaporation [$m s^{-1}$], P the rate of precipitation [$m s^{-1}$], A the surface area of the basin [m^2] and R the inflow of river water [$m^3 s^{-1}$]. In this scenario the basin experiences a drawdown due to the loss of water volume to the atmosphere until the surface area A is so small that the net evaporative loss is of the same size as the river inflow R . When the water volume decreases, the salinity increases until an equilibrium is reached, since neither net evaporation nor river inflow transport ions. In this case, the evolution of salinity S with time t is given by,

$$S(t) = \frac{m_{salt}}{V_0 - fwb * t} \quad (4)$$

Where m_{salt} is the mass of salt [kg] contained in the basin at the start of drawdown (i.e., upon disconnection) and V_0 the initial volume of the basin [m^3].

	CMD	Valencia Basin	Reference
Present-day area (m2)	11.83E+9	57.60E+9	This work
Maximum paleo-depth (m)	1500	1800	Heida et al., 2021
Sills paleo-depth (m)	Sill02 = 700 Sill01 = 850	No sill (open basin)	This work
River inflow (m3/s)	$\leq 10^a$ Present-day	500 ^b Paleo	^a Garcia et al., (2017) ^b Urgeles et al., (2011)
Evaporation rate (m/a) ^b (for the model)**	0.25 – 1.5 ^a 1.04 ^b	0.25-1.5 ^a	^a Estrani et al., (2011) ^b Simon & Meijer, (2017)
Strait parameter g ($m^3/s/\sqrt{kg/m^3}$)	10 ^{^5} Present-day	-	Barcelo-Llull et al., (2019)

Table 7.3. Table showing the morphometric parameters of the study area used as input for our modelling. **Evaporation rates are present-day values (Estrany et al., 2011; Simon & Meijer, 2017b) assumed to be similar to those during the MSC.

During at least part of its MSC evolution, the CMD is likely to also have been subject to saline water fluxes through its connections. This means that the concentration of ions would have

changed while the water volume stayed the same. For a basin with a negative freshwater budget that is fully balanced by a saline inflow (Figure 7.4-B), the concentration of dissolved ions, and hence the salinity, increases over time. If either gypsum or halite reaches its saturation concentration in the process, the mass that exceeds this threshold concentration is taken to be precipitated as a uniform layer without getting re-dissolved. In the following we use $\Gamma = \frac{m_{prec}}{t}$ [$kg\ s^{-1}$] to describe the rate at which mass is precipitated. It is important to note that salinity can increase past the point at which precipitation begins since the ion group of the other salts can continue to concentrate (equation 1). In that scenario the evolution of salinity S with time t is dependent on the magnitude of the influx Q_{in} and its salinity S_{in}

$$S(t) = S_0 + \frac{Q_{in} * S_{in} - \Gamma}{V_0} * t \quad (5)$$

For a basin like the CMD, it is likely that the exchange through the two sections is more complex than only inflow to balance the freshwater budget. By assuming that the salinity of the inflow through the northern connection is the same or close to the salinity of the inflow through the southern connection, we can simplify the system by combining these two fluxes to one inwards flux. The same applies to the fluxes leaving the basin through the two connections (Figure 7.4-C). In this scenario the salinity of the basin, S_{out} , is dependent on the properties of these combined in- and outflows respectively.

$$S(t) = S_0 + \frac{Q_{in} * S_{in} - Q_{out} * S_{out} - \Gamma}{V_0} * t \quad (6)$$

A special case to consider is the situation where neither salinity nor water volume of the basin change in a system of this kind. These two conditions can be described as $\frac{dV(t)}{dt} = 0$ and $\frac{dS(t)}{dt} = 0$ and lead to two expressions

$$Q_{in} = Q_{out} + fwb \quad (7a)$$

$$Q_{in} * S_{in} = Q_{out} * S_{out} + \Gamma \quad (7b)$$

For the special case without precipitation ($\Gamma = 0$), these two can be combined in a way that allows us to calculate the fluxes that would be needed to attain a certain salinity ratio (Knudsen, 1900),

$$Q_{out} = \frac{fwb}{\frac{S_{out}}{S_{in}} - 1} \text{ and } Q_{in} = \frac{fwb}{1 - \frac{S_{in}}{S_{out}}} \quad (8)$$

If the basin has already reached saturation, Γ will become non-zero and must be considered. There are scenarios for which we can calculate values for Γ as a function of other parameters of the system. The simplest case is a scenario in which both the in- and the outflow are saturated in a salt, either gypsum or halite. While the salinity can increase, the concentration of the salt in question cannot, leading to the precipitation of the excessive mass. Applying eq. (7) to only the concentration of a single salt for a system in balance gives an expression for the precipitation rate in that special case. We thus have,

$$c[salt]_{in} = c[salt]^{sat} \text{ and } c[salt]_{out} = c[salt]^{sat}$$

with which eq. (7b) yields,

$$\Gamma_{salt} = (Q_{in} - Q_{out}) * c[salt]^{sat}$$

Combined with eq. (7a) we find,

$$\Gamma_{salt} = fwb * c[salt]^{sat} \quad (9)$$

For a more realistic scenario, where the inflow is below saturation while the basin has reached that threshold, the number of unknowns increases, and the precipitation becomes dependent on the magnitude of the outflux and the concentration of the influx. The conditions for the concentrations can now be written as

$$c_{in} < c[salt]^{sat} \text{ and } c[salt]_{out} = c[salt]^{sat}$$

Inserting those conditions into eq. (7b) and substituting Q_{in} again with eq. (7a) gives

$$\Gamma_{salt} = Q_{out}c_{in} + fwb * c_{in} - Q_{out} * c[salt]^{sat}$$

Which can be rewritten in a way to express it in dependence of the ratio between the concentrations of the in- and outflow

$$\Gamma_{salt} = c[salt]_{in} * \left(Q_{out} * \left(1 - \frac{c[salt]^{sat}}{c[salt]_{in}} \right) + fwb \right) \quad (10)$$

With eq. (10) it is now possible to explore the rate of precipitation for a set of scenarios that are not only defined by their fwb but also by Q_{out} and c_{in} . To compare the results of eqs. (9) and (10) to literature values they need to be expressed as rate of sedimentation (i.e., thickness of deposit per unit of time rather than mass). For this we need the density of the deposit, $\rho_{deposit}$ (Table 7.2), and the area, $A_{deposit}$, covered by the deposit of interest. It is then also possible to calculate the duration of the period of deposition for each Γ , from an observed volume of the deposit,

$$T_{prec} = \frac{V_{deposit} * \rho_{deposit}}{\Gamma_{salt}} \quad (11)$$

Applying eq. (11) to the total volume of the deposit gives the total timespan during which this salt would need to precipitate at a given rate to form the observed deposit. To get the average duration of precipitation per precessional cycle (23 kyr) the volume needs to be divided by the number of total cycles during which it formed.

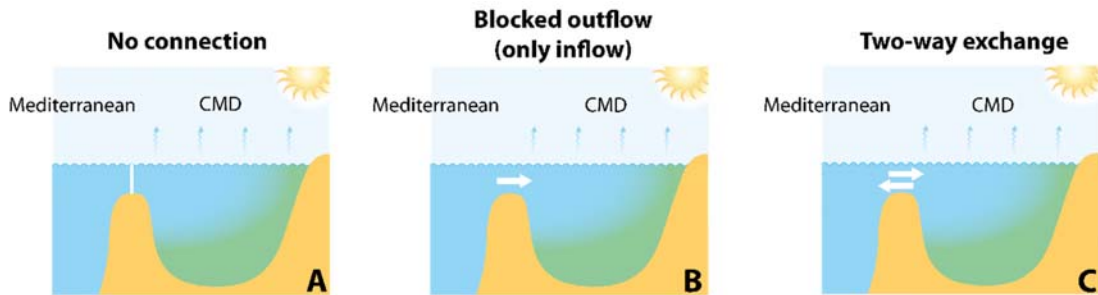


Figure 7.4. Different ways to approach the connection between the CMD and the open Mediterranean. A: No connection between the CMD and the Mediterranean and thus both influx and outflux are cut. B: The basin is connected to the open Mediterranean in a way that inflow compensates the loss of freshwater due to evaporation. C: There is a two-way exchange over the sill. The inflow now compensates the freshwater budget as well as the saline outflow. Those three ‘approaches’ should not be conflated with the ‘scenarios’ that we present and discuss in the text, as they are strictly theoretical.

It is worth noting that the depositional process used in our modelling is pure evaporative and does not take into consideration more complex bio-geochemical processes that might have played a role in the PLG formation, at least locally where low salinity values were obtained from water inclusions in PLG gypsum crystals (e.g. Piedmont Basin, Italy; Natalicchio et al., 2014; Calabria, Italy; Costanzo et al., 2019), although the reliability of the salinities obtained

from fluid inclusions measurements was recently questioned (Bigi et al., 2022). With the modelling approach presented here, we also do not take the influence of erosion into account.

7.4 Results

In this section we apply the theory as described in section 7.3.2 to the data that was presented in section 7.3.1 to identify the key processes that are needed to explain the MSC deposits in the CMD. We find that a saline flow into as well as from the CMD is needed to form the gypsum deposit, while the halite deposit could have formed from a disconnected CMD filled with saturated brine undergoing a water level drop.

7.4.1 Water and evaporites volume considerations

As a first step, we calculate the volumes of water required to precipitate the observed volume of evaporites, V_G for gypsum and V_H for halite, and compare these to the (reconstructed) volume of the CMD. This will allow us to judge whether the evaporites could have formed by concentration of the water contained within the CMD or whether an additional influx of water and salt must be invoked.

For a range of water volumes (m^3) representing the CMD at a given water level, we calculate the concentration ($kg\ m^{-3}$) the water would attain if the mass of the observed evaporite (in kg) was dissolved in it. If the calculated concentration is lower than the concentration at which the water is saturated in the salts ($CaSO_4$, gypsum; $NaCl$, halite), then the water volume is big enough to hold the volume of the evaporite in a dissolved state. The minimal volume of water needed is determined as the volume at which the calculated concentration equals halite or gypsum saturation and was defined by eq. (1) and can be calculated with data as listed in Table 7.2.

The results, depicted in Figure 7.5, show that for the halite deposit this minimal water volume

$$V_{min} = \frac{9.633 \cdot 10^{10} m^3 \cdot 2200 kg\ m^{-3}}{272.1 kg\ m^{-3}} \approx 780 km^3$$

which is about equal to the capacity of the CMD below the level of the sill lying at -850 m (sill 01 in Figure 7.3). If instead we take the observed

mass of halite and assume this to be dissolved in the volume of water comprised by the CMD below each horizontal level (i.e., water level below 0; Figure 7.5), we find the basin water to attain saturation values once the level is lowered to the depth of the sills (orange line in Figure 7.5). This is of course consistent with the V_{min} calculation and confirms its result.

In a similar type of calculation, we take the volume of water comprised by the basin at sill depth (Table 7.3) and assume saturation concentration of gypsum and halite respectively. This way we compute the maximum volume of gypsum or halite that can be precipitated from a disconnected basin. These calculations show that only a fraction of the observed gypsum volume (0.9%) of the BU1/2 (Table 7.1) could precipitate from the water volume available below sill depth, while more than 100% of the observed halite volume could be stored in the basin volume below the sill.

The results indicate that the gypsum deposit is too massive to originate from a disconnected basin, even if it was saturated in gypsum, while the halite deposit could have precipitated from a disconnected basin saturated in halite (Table 7.4). The calculation does not inform us about the timespan over which the halite deposit was formed. This can be determined by the time it would take until a disconnected CMD would reach a new equilibrium between river inflow and net evaporation, which is addressed in the next section (section 7.4.2).

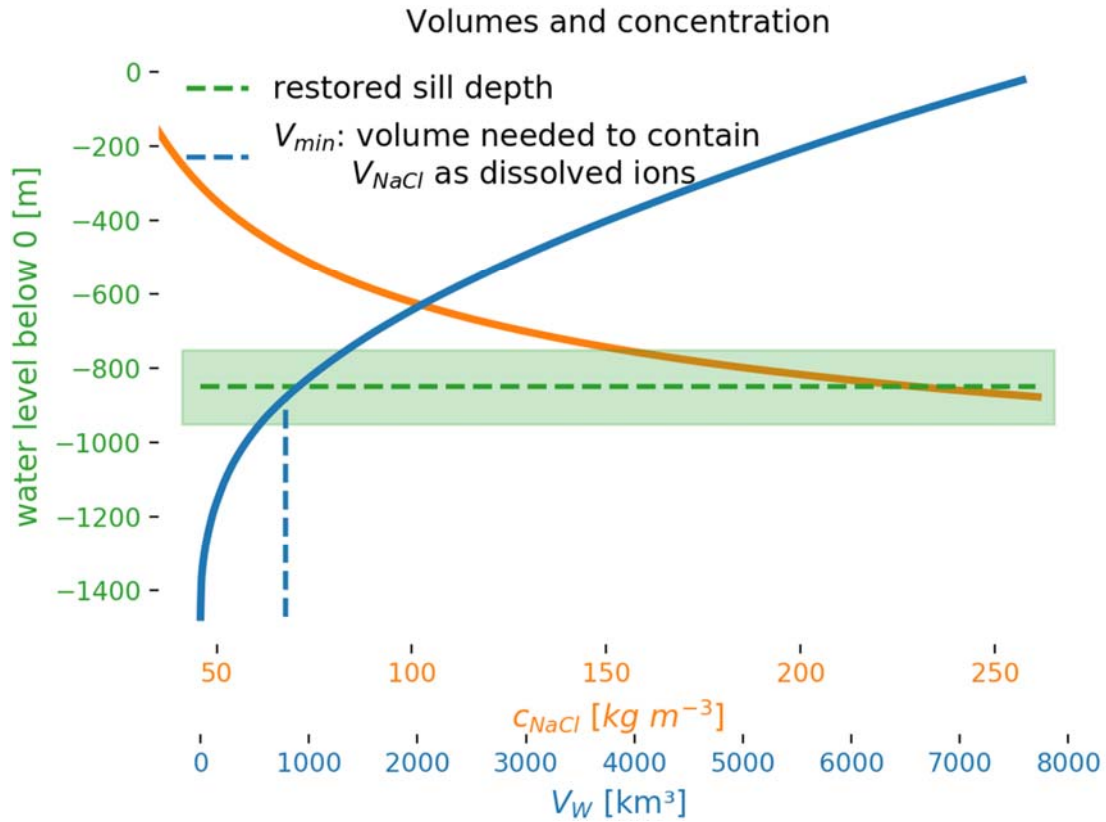


Figure 7.5. With water level on the vertical axis, the solid blue line gives the water volume of the pre-Messinian CMD below each level (see blue horizontal axis). The dashed green line depicts the level of the sills, with an uncertainty of ± 50 m (green area). The water volume of the CMD below sill depth (i.e., at the crossing between the solid blue and dashed green lines) is about equal to the volume of halite-saturated water required to form the observed halite deposit (V_{min}) which is indicated with the vertical blue dashed line. Also shown as a function of water level is the concentration that the basin waters would attain if the observed mass of halite were dissolved in it (solid orange line and orange horizontal axis). Since the volume of water decreases with a lower water level, the resulting concentration increases until it reaches $c[\text{NaCl}]^{\text{sat}} = 271 \text{ kg m}^{-3}$ at a depth of -879m , which corresponds to a water volume of $V_{min} = 780 \text{ km}^3$ (see text for details).

Unit	Percentage of observed volume that can be precipitated from a CMD filled to the sill (-850m) with water at saturation
BU1/2	0.9 % (1.1 %)
BU3	2.2 % (2.8 %)
BU1/2+BU3	0.6 % (0.7 %)
Halite	141 % (170 %)

Table 7.4. The maximal volumes of gypsum and halite that can be precipitated from the CMD as a disconnected basin. The calculations use the available water volume below sill depth at -850m and -800m according to pre-MSD hypsometry and saturation concentration for Gypsum (145 kg/m³) and Halite (350kg/m³). For each deposit or combinations of deposits, the volume of water in the basin is adjusted to account for the preexisting deposits that occupies accommodation space.

7.4.2 Desiccation of an isolated basin

The only realistic process that could isolate the CMD is a water level drop in the Mediterranean Sea that lowers the level of the surrounding waters below the level of the sills. Bringing the level below that sill would cancel the exchange of saline water through the connections and the later evolution of the CMD would be independent of the rest of the sea. In this section we investigate such a scenario (Figure 7.4-A).

For such an isolated basin the new balance is described by the f_{wb} , as defined in eq. (3) and thus dependent on the river influx R and loss of water to the atmosphere $(E - P) * A$. As long as more water is lost than added, the CMD experiences a drawdown that is not depending on the drawdown of the Mediterranean Sea. This process changes the surface area that is available for net evaporation and continues until a new stable state is reached where the flux to the atmosphere is of the same size as the river inflow, which may, to first approximation, be considered constant. These two fluxes thus determine the water level in the new steady state that is defined by $f_{wb}=0$ (eq. 3), as well as the time needed to reach it. The results are depicted in Figure 6, which shows that the timespan on which the process takes place is less than 1 kyr. The fastest change occurs in an extreme scenario without any river input at all (solid lines). In that case the steady state of a completely desiccated basin is reached after less than 900 yr. A river input of $R = 1 \text{ m}^3 \text{ s}^{-1}$ is close to the present-day situation (Garcia et al., 2017) and would

lead to a stable state after less than 1000 yr (dashed lines). In contrast to the first scenario, the basin would not completely desiccate, and the remaining water would have a depth of 8 m. A ten times higher river input of $R = 10 \text{ m}^3\text{s}^{-1}$, leads to a larger remaining volume and a remaining water depth of 140 m. In theory there is also a corresponding river influx R for each net-evaporation $(E - P) * A$, and vice versa, that would prevent a drawdown for the disconnected basin, i.e., $fwb = 0$ for a basin with its surface at sill depth. To achieve this, a net evaporation of 0.75 m yr^{-1} would have to be balanced by an unrealistically high influx of $340 \text{ m}^3\text{s}^{-1}$, while inversely, the more realistic influx of $1 \text{ m}^3\text{s}^{-1}$ (Table 7.3; Garcia et al., 2017) would require a net-evaporation as low as 0.002 m yr^{-1} . Both combinations are unrealistic, which implies that a disconnected CMD would experience a drawdown, until the surface area is small enough for the river inflow to balance the net-evaporation. The loss of freshwater during that time would lead to an increase in salinity because the dissolved ions stay in the system.

In the previous section (section 7.4.1), simply looking at volumes, it was argued that the halite deposit could have formed from a situation where the CMD was already at, or close to, halite saturation at the moment of disconnection. In that case, the water within the CMD would become oversaturated during a drawdown leading to the precipitation of the surplus ions (eq. 4). However, it follows from the reasoning in the current section that the resulting halite deposit will be smaller in mass and volume than the observed one, since the inflow from rivers prevents a complete desiccation. For a scenario with a high river inflow of $R = 10 \text{ m}^3\text{s}^{-1}$ only 2.3% percent of the initial water volume remains in the basin and since a disconnected CMD at halite saturation could precipitate 144 % of the observed halite volume, this effect is small enough to be ignored.

The question yet to be answered is if and how the CMD could reach halite saturation before it was disconnected.

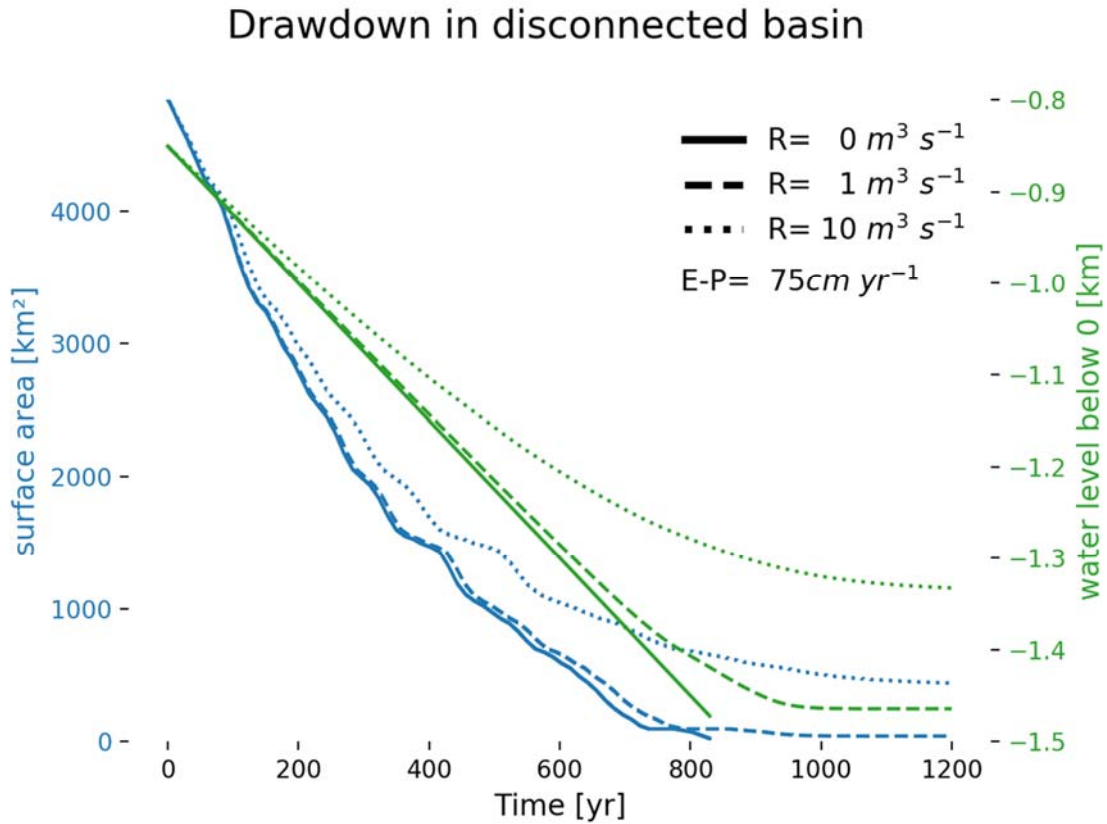


Figure 7.6. Desiccation of the CMD. This figure shows the change over time in water level (green) and surface area (blue) for three different strengths of river inflow, R [$\text{m}^3 \text{s}^{-1}$] for a disconnected basin at a given net-evaporation, $E-P$ [cm/yr]. As soon as the CMD is disconnected from the surrounding waters, the negative freshwater budget causes the water level to fall further below the sill depth (850 m). The basin only desiccates completely if there is no inflow from rivers (solid lines), for non-zero values of R (dashed, dotted) the system will reach a balance where it loses as much through evaporation as it gains by river input.

7.4.3 Full basin, inflow only

To understand if it is possible that the CMD reached halite saturation before the end of Stage 1 (i.e., the end of gypsum deposition) we consider the fastest change in concentration possible for a basin with constant volume (eq. 5). The same is applied to the Valencia Basin, which allows us to compare the behavior of the two basins.

For this scenario, we will not assume a drawdown but keep the water level steady at 0 m. To preserve volume, all water lost to the atmosphere is replaced by saline water that is flowing into the basins from the open Mediterranean (Figure 7.4-B). This process adds ions to the water volume of the basins which can only be removed by precipitation, since there is no saline

outflux. Unless $fwb = (E - P) * A - R < 0$, the salinity will increase (Figure 7.7). The rate of this increase is dependent on the fwb , the water volume of the basin as well as the salinity S_0 of the inflow. Since S_0 is the same for the CMD and the VB, the difference in the rate of change between the CMD and VB is dependent on the ratio between their volume and the corresponding fwb . The latter is also dependent on the surface area of the basin in question (Table 7.3). We find that for the VB the net-evaporation needed to balance a realistic river inflow is 0.27 m yr^{-1} , which is 100 times higher than for the CMD. The much larger volume of the VB explains why this basin experiences a different rate of salinity increase for the same net-evaporation rate E-P even when, for the CMD, a very high river input ($10 \text{ m}^3 \text{ s}^{-1}$ instead of $\sim 1 \text{ m}^3 \text{ s}^{-1}$ taken from Garcia et al., 2017; Table 7.3) is chosen (Figure 7.7). The slow salinification of the VB in comparison to the CMD even for higher values of E-P might be an indicator that the salinity of the VB was lower than the one of the CMD.

Focusing on the CMD, it follows from Figure 7.7 (see also Table 7.5) that the time needed to form the observed halite deposit, $T[NaCl]_{vol}$, is short enough for this to have happened during Stage 2 ($\sim 50 \text{ kyr}$). The same applies to the time needed to reach halite saturation, $T[NaCl]_{sat}$. With $T[NaCl]_{sat} = 21 \text{ kyr}$ for the slowest scenario tested, this time span is shorter than the duration of Stage 1, meaning that the basin would have reached halite saturation even before the beginning of Stage 2. However, $T[NaCl]_{sat}$ is much shorter than the time needed to precipitate the gypsum of BU1/2, i.e., duration $T[CaSO_4]_{vol}$. This means that in this scenario the basin would reach halite saturation before the observed volume of the gypsum deposit could be precipitated, which indicates that the inflow-only scenario is incompatible with the observed presence of gypsum and halite.

To find out whether there is a set-up where halite saturation is reached only after the full volume of the BU1/2 has been deposited, $T[NaCl]_{sat}$ as described in eq. (5) must be equal to $T[CaSO_4]_{vol}$ which can be derived from eq. (10). This leaves us with an expression which is not dependent of the fwb and shows that for an inflow salinity of $S_0 = 35.05 \text{ kg m}^{-3}$ the volume of the CMD would have to be 8.3 times larger than its volume at normal sea level. This again indicates that the gypsum and halite cannot have formed by the same mechanism (i.e., blocked outflow). It is likely that the formation of the gypsum deposit requires a more complex mechanism than the one considered here. A saline outflow would not only keep the salinity

from quickly rising to halite saturation values but would also be more realistic for a basin with two wide connections to surrounding waters.

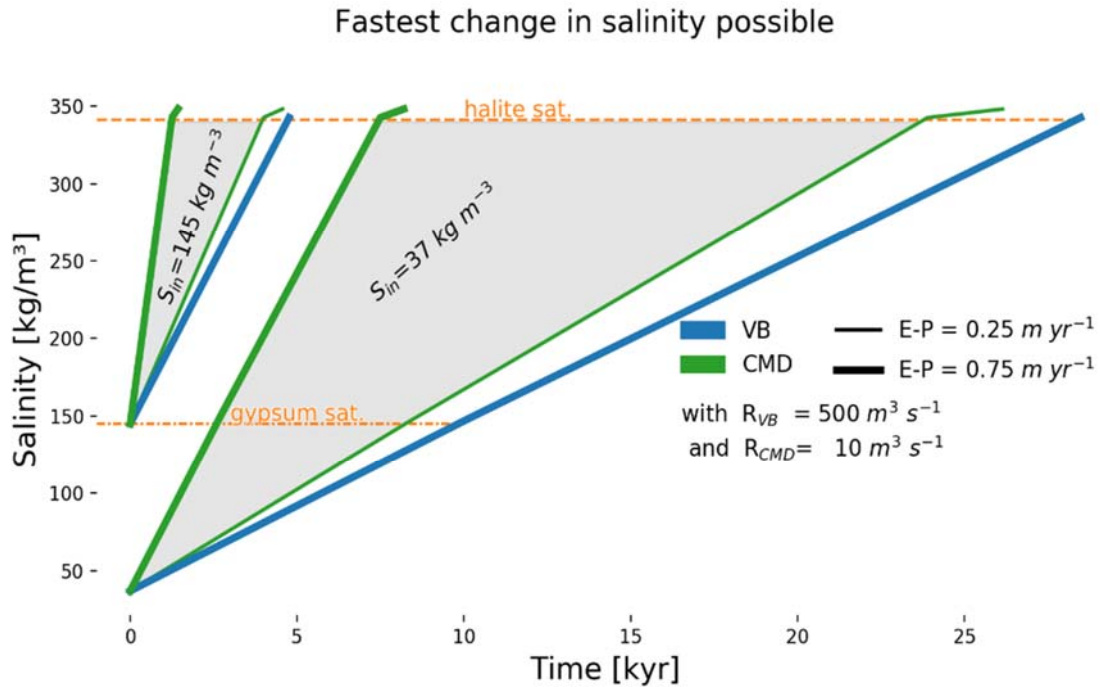


Figure 7.7. Fastest change in salinity possible for CMD and Valencia Basin (VB). All fresh water that is removed from the system due to $fwb > 0$ is replaced by saline water representing an inflow. No saline outflow is applied. The increase in salinity is shown for the CMD (green lines) and VB (blue lines) for two different inflow salinities ($S_{in}=37 \text{ kg m}^{-3}$; $S_{in}=145 \text{ kg m}^{-3}$) as well as for two different net-evaporation rates ($E-P=0.25 \text{ m yr}^{-1}$, thin lines; $E-P=0.75 \text{ m yr}^{-1}$, thick lines). The grey swaths filling the space between the thick and the thin green line resemble the family of functions with the same S_{in} but varying fwb .

S_{in} [kg m^{-3}]	E-P [m/yr]	$T[\text{CaSO}_4]_{vol}$ [kyrs]	$T[\text{NaCl}]_{sat}$ [kyrs]	$T[\text{NaCl}]_{vol}$ [kyrs]
37	25	182	21	0.62
145	75	15	1	0.16

Table 7.5. Comparison of the time the CMD would need to deposit the gypsum deposit ($T[\text{CaSO}_4]_{vol}$) or halite deposit ($T[\text{NaCl}]_{vol}$) compared to the time it would reach halite saturation ($T[\text{NaCl}]_{sat}$) for the same conditions and the scenario as described in Figure 7.7 and shown in Figure 7.4-B.

7.4.4 Two-way exchange

The presence of an outflow from the CMD to the surrounding western Mediterranean would have allowed the CMD to maintain a salinity in the range of gypsum saturation for a longer period of time than in a blocked outflow scenario. To explore this new scenario, we now quantify the size of the volume flux of water out of the basin for the case that the basin stabilizes just below gypsum saturation, while maintaining constant volume. Let us consider the two extremes of the mathematical solution, a non-existent and an infinite outflow. The first, a non-existent outflow, would lead to the situation described in Figure 7.7, with ever-increasing salinity. In the second extreme, the salinity of the basin would be the same as that of the inflow. In between these two extremes there exists an outflow strength for every inflow salinity such that the basin maintains gypsum saturation. If the outflow is larger than the calculated value, gypsum saturation will not be reached. We thus compute the maximal outflux that would still allow for gypsum saturation. The absolute value of this maximal outflux as given by (eq. 8) is dependent on the salinity of the inflow as well as the fwb of the basin. The latter is defined by a given $E - P$, the surface area as well as a river inflow which is set to $R = 2 \text{ m}^3\text{s}^{-1}$.

The results of this calculation are shown in Figure 8 as a function of the inflow salinity and the level of the water surface. The three swaths represent families of curves that describe a range of $E - P$ and are defined by a given outflow strength. Swaths corresponding to a relatively large outflow sit at higher inflow salinity, since with relatively large exchange the basin salinity is close to that of the adjacent water. If the basin is to attain gypsum saturation, the salinity of the inflow must already be close to that.

For a given value of the outflow, i.e., within a given swath in Figure 8, the curves shift towards higher inflow salinity for lower $E - P$, with the lowest $E - P$ defining the right-hand border of the swath. When $E - P$ is small, fwb is small, the inflow thus exceeds the outflow by a smaller amount (equation 7a) and its salinity must be higher to still achieve saturation. The slope of the curves towards the right in Figure 7.8, i.e., the shift to higher inflow salinity for lower water level, is explained by the same mechanism. The change in fwb is in that case caused by the decrease in surface area for lower water levels. Thus, a given $E - P$ then corresponds to a smaller fwb and less net input of salt to the basin. Comparing the fwb for a water level at sea level to a water level at the depth of the sills (-850 m) shows a decrease of about 50%, (e.g. $E - P =$

0.25 m yr^{-1} , $R = 10 \text{ m}^3 \text{ s}^{-1}$, decrease= 53%). The influence of drawdown is thus smaller than one order of magnitude.

For low inflow salinities, the fluxes needed for the basin to reach gypsum saturation ($S_{in} < 80 \text{ kg m}^{-3}$) are several orders of magnitude smaller than the ones that are measured today ($\sim 0.1 \text{ Sv}$; Barcelló-Lull, 2019). This means that in a situation where the inflow salinity is less than 140 kg m^{-3} the fluxes to and from the basin would need to decrease several orders of magnitude for the basin to stay at gypsum saturation, independently of drawdown and net evaporation. Without any external factors that decrease the magnitude of the fluxes, like a strong slow-down of the circulation, the only way for the CMD to reach gypsum saturation is when the salinity of the surface to intermediate layer of the Western Mediterranean Sea is already very close to saturation. The same applies to reaching halite saturation in the basin.

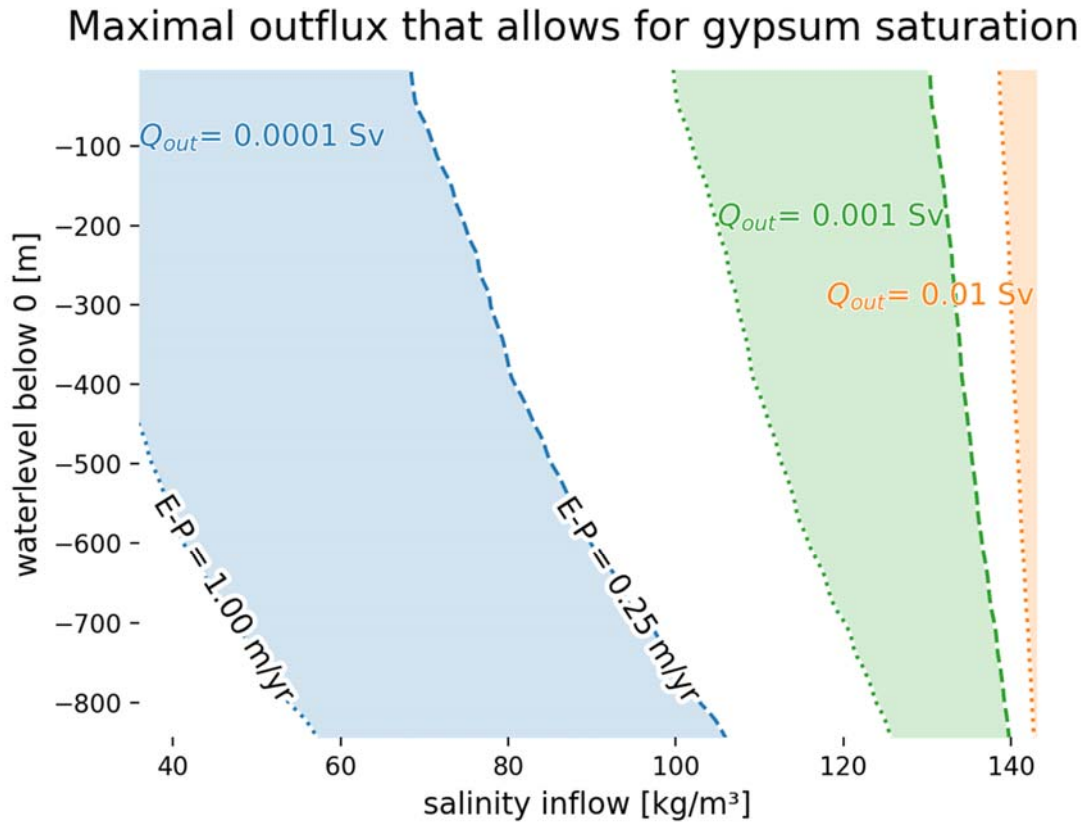


Figure 7.8. Model estimation of the precipitation of gypsum in the CMD as a function of water level and salinity in the Mediterranean, and the magnitude of the water flow into the CMD. With two-way flow across the sills that connect it to the western Mediterranean, the CMD will reach a constant salinity. This graph illustrates the conditions under which the CMD stabilizes exactly at gypsum saturation (calculated with equation 8). Each colored swath corresponds to a certain magnitude of the outflow and comprises the curves obtained for a range of values of E-P, as indicated. The swaths are plotted as a function of inflow salinity on the horizontal axis. The vertical axis gives the level of the water surface: since the area subject to evaporation becomes less upon drawdown, the water level together with E-P determines fwb. The path for $Q_{out} = 0.1 \text{ Sv}$ is too thin to be properly displayed in this figure and would be located in a narrow band close to an inflow salinity of 145 kg m^{-3} .

7.4.5 Precipitation of gypsum

In the previous section (section 7.4.4) we focused on the situation right before precipitation and the fluxes which would be needed to maintain this. We now calculate precipitation rates resulting from specific combinations of outflow, fwb and salinity of the inflow (eq. 9). To reduce the number of unknowns we now look at a full basin and consider a single value for E-P. This is allowed since it is already known from previous calculations that a drawdown only has a minimal effect on the system (see section 7.4.2). Net evaporation also has an influence,

but just like drawdown, this influence is minor and does not change the overall behavior of the system.

Based on equations 9 and 10 we can calculate first the precipitation rate (Γ) and then the duration of precipitation that follows from this precipitation rate as being required to explain the observed volume of gypsum. The lower the precipitation rate, the longer it would take to precipitate the observed volume and for the mathematically correct but unrealistic solution this time span would tend to infinity. To avoid this type of solution the results are filtered to be within geologically realistic limits. From previous studies it is known that a realistic margin for the precipitation rate of gypsum ranges from 1 m kyr^{-1} (Orti Cabo et al., 1984) to 100 m kyr^{-1}

(Schreiber & Hsü, 1980), while the duration of precipitation per precessional cycle cannot be longer than the length of the cycle itself (assumed to be 23 kyr).

The results are shown in Figure 7.9 (compare with section 7.4.4; Figure 7.8). The grey line indicates the minimum inflow salinity that would lead to gypsum saturation for a given outflux strength. The higher the magnitude of the outflow, the higher the salinity of the inflow needs to be for the basin to reach gypsum saturation. Precipitation starts when this salinity (145 kg m^{-3}) is exceeded and the duration of precipitation itself ranges between 0.8 and 5 kyr per cycle and thus lasts between 5% to 20% of a precessional cycle. For lower magnitudes of outflow, for example, it becomes clear that the higher the inflow salinity is, the shorter the duration of precipitation per cycle. This can be explained by the increasing amount of excess ions that are transported into the basin for higher salinities. The same observation is valid for halite (Figure 7.10) and will be discussed in section 7.5.2.

Another interesting aspect is that, the stronger the outflow through the connections is, the smaller the range of possible salinities that would lead to a realistic precipitation rate becomes. This means that knowing the actual strength of the fluxes would not only provide us with a range of inflow salinities and thus salinity of the upper layer of the Mediterranean Sea at that time, but also that the higher those fluxes are, the smaller the range of possible salinities is. While for an outflux of $Q_{out} = 10 \text{ m}^3 \text{ s}^{-1}$ an inflow salinity of $[40 \text{ kg m}^{-3}, 145 \text{ kg m}^{-3}]$ could lead to the observed BU1/2, this range would be limited to $[144 \text{ kg m}^{-3}, 145 \text{ kg m}^{-3}]$ for $Q_{out} = 10^5 \text{ m}^3 \text{ s}^{-1}$. The latter is close to the strength that is measured today (Barcelló-Llull et al., 2019).

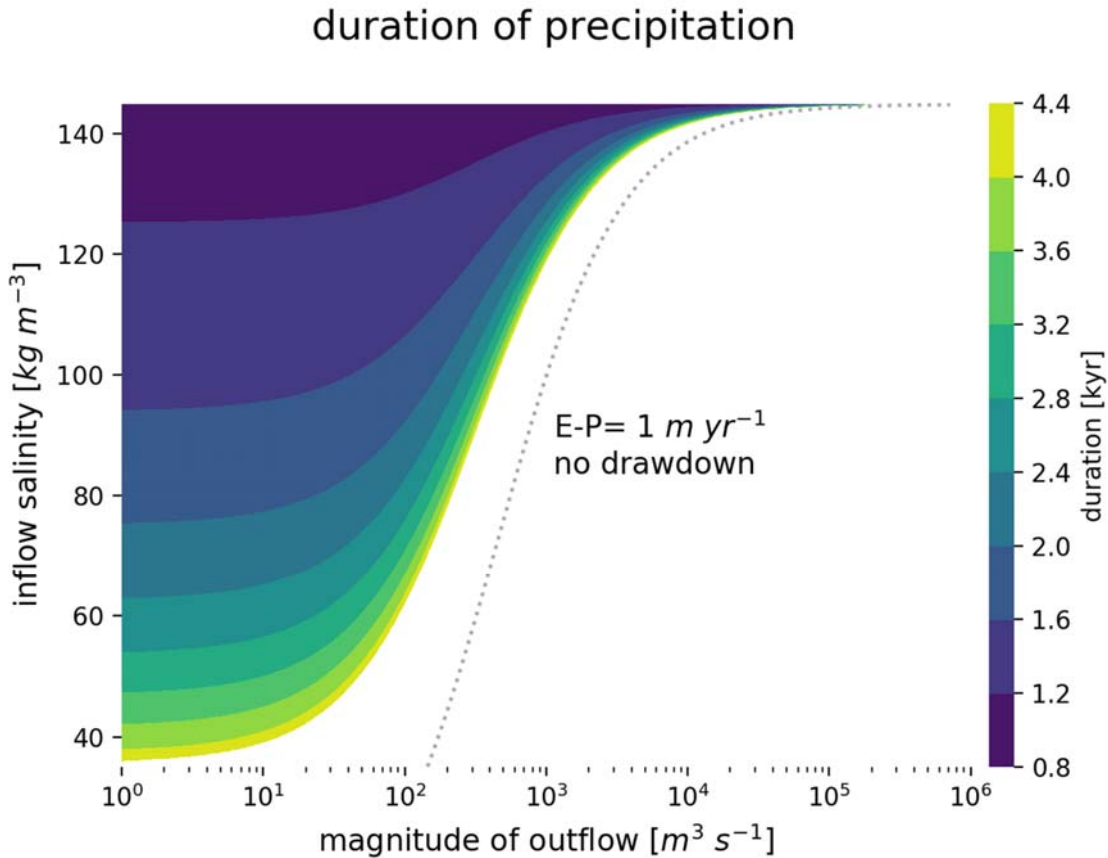


Figure 7.9. Duration of the period required to precipitate the observed volume of gypsum in the CMD, for different values of the outflow and the salinity of the inflow, when no drawdown is applied and $E-P = 1 \text{ m yr}^{-1}$. The grey dotted line indicates the minimum inflow salinity that is needed for the CMD to reach gypsum saturation for a given outflow magnitude. For each pair of outflow strength (x-axis, logarithmic) and inflow salinity (y-axis, linear) the timespan per cycle that is needed to precipitate the observed gypsum volume of the BU1/2 is calculated. The results are clipped by limiting the rate of precipitation rate to be between $1 \text{ m kyr}^{-1} < \Gamma < 100 \text{ m kyr}^{-1}$.

7.5 Discussion

In this section, we discuss the significance of our results on the MSC events in the CMD and in the Western Mediterranean. Sub-section 7.5.1 focuses on the first stage of the MSC, known also as the PLG stage (5.97-5.60 Ma). The main outcome from sub-section 5.1 is that during stage 1 of the MSC, the salinity of the upper water layer of the Western Mediterranean reached gypsum saturation for relatively ‘brief’ periods of precessional cycles, and provided the CMD

with the necessary Ca^{2+} and SO_4^{2-} ions to deposit the observed gypsum volume through a two-way exchange of fluxes.

Sub-section 7.5.2 focuses on stage 2 of the MSC (5.60-5.55 Ma). The main crucial conclusion in this sub-section is that the only way possible to deposit the observed halite volume in the CMD during this stage is a scenario in which it is disconnected from the open Mediterranean. This requires a high amplitude base-level drawdown of at least ~ 850 m, in which halite saturation is reached both in the CMD and in the Western Mediterranean only when the water level was significantly lowered (Figure 7.11).

7.5.1 The pre-halite lower gypsum in the CMD: Stage 1 of the MSC

The pre-Halite MSC units of the CMD (BU1 and BU2) are interpreted as Lower Gypsum belonging to stage 1 of the MSC (Table 7.1; see section 7.2.3 and Raad et al., 2021). The estimated volume of the evaporitic gypsum content of both units is $\sim 3 \times 10^{11}$ m³. Due to estimation uncertainties, related mainly to the limited seismic coverage in some parts of the CMD (Figure 7.2) and assumptions on the internal lithology of BU1 and BU2, there is a chance that this volume has been slightly underestimated, but this would not change the following line of reasoning which is based on qualitative results. Even an underestimation of 30% of the gypsum volume would only have a noticeable influence on the duration of precipitation, changing the interval from 5% - 20% to 6.5%-20%.

Our results show that the volume of pre-halite gypsum observed in the CMD (Table 7.1) is too high to precipitate from a disconnected basin scenario. A CMD filled with water at gypsum saturation concentration (145 kg m^{-3}) up to the sill depth would produce a volume of gypsum that is far too small with respect to the observed volume (0.9%; Table 7.4). This implies that if the CMD was ever disconnected from the surrounding waters, gypsum should have started deposition before the disconnection happened, i.e. when the CMD was still supplied with an input of Ca^{2+} and SO_4^{2-} ions. In this case, two possible scenarios can be considered: (1) A basin with only an influx from the surrounding Mediterranean waters into the CMD without an outflux; (2) A CMD with 2-way fluxes from and into the surrounding Mediterranean waters. For the first case (1), our results presented in Figure 7.7 show that even in the slowest possible scenario ($E-P=0.25 \text{ m yr}^{-1}$), the salinity of the CMD would increase very rapidly jumping to gypsum saturation in about 7 kyr and continuing to halite saturation concentration in 21 kyr,

thus not allowing enough time for the observed gypsum volume to precipitate ($T[CaSO_4]_{vol}=182$ kyr; Table 7.5). In the second case (2), a saline outflux would slow down the rapid salinity increase in the CMD giving longer timespans for the gypsum to precipitate. Figure 7.8 shows that in this scenario, for the CMD to stabilize at gypsum saturation, the saline influx should be very close to if not exactly at gypsum saturation concentration (between 140 and 145 $kg\ m^{-3}$; Figure 7.8) for an outflux which is equal to or one order of magnitude less than the one measured today across the silled channels (0.1 and 0.01 Sv, respectively; Figure 7.8). This is mainly due to the small volume of the CMD compared to its large connection to the surrounding waters (Figure 7.3) through the wide and deep channels, which maintains the salinity of the CMD equal to the salinity of the upper layer of the Mediterranean waters. Unless a drastic decrease in the fluxes caused by a more sluggish circulation (e.g., slowdown of the currents due to a base-level drop) of the Mediterranean currents took place, the CMD will have had almost the same salinity as the upper Mediterranean water layer, as is true for the present-day situation (Barcello Llull et al., 2019). To our knowledge, until present, no studies showed or quantified such a decrease in the Mediterranean currents and its consequences during the MSC. Our calculations also show that gypsum precipitation could not have persisted for the whole duration of a precessional cycle. Instead, the duration of gypsum deposition is restricted to 5% to 20% (i.e., 0.8-4.4 kyr/23 kyr) of a precessional cycle (Figure 7.9).

Our inferences have several important implications for what might have happened in the Mediterranean during stage 1 of the MSC. One important implication is that the saturation concentration of gypsum must have been reached in the upper layers of the open Western Mediterranean (Figure 7.12), at least during the dry periods of precessional cycles (i.e., insolation minima). Several studies showed that, due to the negative fresh water budget that characterizes the Mediterranean Basin, a reduction of the strait efficiency in the proximity of Gibraltar would lead to a drastic increase of the salinity of the Mediterranean waters (Meijer and Krijgsman, 2005; Blanc, 2006; Topper and Meijer, 2013; Meijer, 2021). The drop in diversity until the complete disappearance of planktic foraminifera in the Mediterranean during summer insolation minima, is, for example, one indication that surface waters reached salinities above the maximum tolerance of these organisms (F. J. Sierro et al., 1999; Blanc-Valleron et al., 2002; F. Sierro et al., 2003; Bulian et al., 2021). One might argue that the salinity tolerance of planktic foraminifera generally does not exceed 50 $kg\ m^{-3}$ (Bijma et al., 1990), meaning that salinities in the Mediterranean water column did not necessarily reach gypsum saturation. This might be true for most of the duration of each precessional cycle of stage 1, but salinity

probably peaked reaching gypsum saturation during relatively short timespans (Figure 7.9). Indeed, Topper & Meijer, (2015) showed that the salinity of the open Mediterranean waters could rise to gypsum saturation, following a restriction with the Atlantic Ocean, in timespans that are as fast as 3 kyr.

Our result, thus, contradicts what has been proposed by Lugli et al. (2010) who suggested that gypsum saturation concentration was reached only in silled marginal basins whose salinity increase and the subsequent gypsum deposition was due to circulation restrictions imposed by the presence of the sill itself. This observation has been indeed also supported by Meijer, (2021) who showed that in the case of a Mediterranean-marginal basin connection through sills, a strait efficiency as small as $10^3 \text{ m}^3 \text{ s}^{-1}$ should occur in order for the marginal basins to reach gypsum saturation with a Mediterranean at normal salinity. This extremely low strait efficiency value is ‘unrealistic’ as it is in the order of magnitude of a large river flowing to the Mediterranean at present. Also De Lange & Krijgsman, (2010) suggested that gypsum saturation and precipitation took place at all shallow-water depths when the upper Mediterranean waters were at gypsum saturation. In our opinion, the example of the CMD is an evidence that there is no need for a ‘shallow’ structural sill for gypsum to deposit. Most of the basins from which the shallow sill control idea comes from are basins now lying onshore and that underwent complex post-MSW tectonic evolution since the formation of the evaporites. Restoring their structural setting, including sill depths, at the MSC time is not straightforward and needs sophisticated tectonic reconstructions. Moreover, the few places in the offshore Western Mediterranean area where PLG was recovered in boreholes, are open shelves not or partially surrounded by sills (e.g., Alicante shelf and Valencia Basin; Soria et al., 2008; del Olmo, 2011; Ochoa et al., 2015; and offshore Western Algeria in the Arzew borehole; Buroillet et al., 1978).

It follows that PLG could have been deposited almost everywhere in the Mediterranean Basin during stage 1, including open shelves (Krijgsman & Meijer, 2008; De Lange & Krijgsman, 2010), with probably selenitic gypsum dominating in the shallow oxygenated water layer and cumulatic gypsum below a certain water depth limited by the depth of anoxia level (Figure 7.12) (De Lange & Krijgsman, 2010; Dela Pierre et al., 2011; Natalicchio et al., 2021). In the CMD this facies change could be marked by the passage from the MSC seismic unit BU1 to BU2 (Raad et al., 2021; see section 7.2.3). In the deep basin, the so-called Lower Unit (LU) (Montadert et al., 1978; Bache et al., 2009; Lofi et al., 2011) could thus be the sediment resulting from this phase constituting of gypsum cumulates, clastic gypsum and dolostones (Figure 7.12). Local conditions such as high river inflow might have prevented gypsum

formation by locally reducing the salinity (e.g., Ebro delta in the VB; Figure 7.7). Other local geo-chemical and geo-biological factors might have also prevented the formation of gypsum locally in deep basin context (e.g., reduced supply of gypsum from the water column and higher rates of bacterial sulfate reduction, deriving from permanent seafloor anoxia and larger availability of organic matter; Natalicchio et al., 2021; Guibourdenche et al., 2022). In shallow water where freshwater dilution did not play a role, the absence of PLG must mean that it has been removed after deposition. This removal of PLG could be due to two different causes. (1) It might have been redeposited into deeper settings due to gravitational instability (De Lange & Krijgsman, 2010). Such a process combined with local tectonic activity, might be at the origin of the Resedimented Lower Gypsum (RLG) observed in some basins (Roveri et al., 2006; Manzi, Roveri, et al., 2021), but could have happened in any moment after the gypsum's deposition and not necessarily during stage 2 of the MSC (Figure 7.12), as also supported by observations from the MSC PLG in Cyprus by Artiaga et al. (2021); (2) It could have been the result of subaerial erosion during the main MSC water level drawdown which amplitude has been recently revised to 1.5 km in the Western Mediterranean (Heida et al., 2021). Indeed, present-day denudation rates measured in gypsum (by denudation), including MSC gypsum from the Sorbas Basin (Calaforra et al., 1993; Sanna et al., 2015; Table 2), vary from low (0.20 mm yr^{-1}) to high (3.16 mm yr^{-1}). Such rates make it realistic to assume that even hundreds of meters of Gypsum could have been eroded during stages 2 and 3 of the MSC (total duration of $\sim 270 \text{ kyr}$), during which the water level was lowered, and the shelves underwent intense erosion as attested by the Messinian Erosion Surface (Lofi et al., 2005, 2011; Urgeles et al., 2011). It remains unclear, however, why PLG is preserved only locally. Subaerial erosion and/or slope instability may have been more efficient on some margins compared to others. Interpretation of stratigraphic and/or borehole data from onshore (Caltanissetta Basin, Manzi et al., 2021; Piedmont Basin, Dela Pierre et al., 2011) and offshore (Levant Basin, Manzi et al., 2018) 'intermediate to deep basins' contradicts the presence of gypsum in the distal domain of such basins, where the distal equivalent of stage 1 'marginal' PLG is represented by organic shales (Foraminifer Barren Interval, FBI; Manzi et al., 2018). This interpretation has been recently modified, at least for the Piedmont Basin, where Natalicchio et al. (2021) inferred the presence of Gypsiferous Mudstones in the distal domain of the basin. Regarding the deep Levant Basin, Meilijson et al. (2018) have already opposed such interpretation by putting the halite as stage 1 distal equivalent of the PLG. In addition, very recent XRD data from the deep Levant Basin's halite shows important inclusions of calcium sulfates within the halite (Aloisi et al., in prep - personal communication).

The duration of gypsum sedimentation within a precessional cycle is also of relevance. Lugli et al. (2010) suggested that time spans for gypsum formation within a precessional cycle could have been restricted to the peak of the aridity phase of the cycle (i.e., few thousands of years), which is in accordance with our calculations. Indeed, the relatively high deposition rates of gypsum (Table 7.2), compared to the low sedimentation rates of the terrigenous intercalations between consecutive gypsum beds (Lugli et al., 2010) makes it realistic that the sedimentation of the latter occupies most of the precessional cycles.

7.5.2 Halite in the CMD: Stage 2 of the MSC

The salt unit of the CMD is interpreted as halite belonging to stage 2 of the MSC (Table 7.1; see section 7.2.3 and Raad et al., 2021) and it has an estimated volume of $\sim 9.63 \times 10^{10} \text{ m}^3$. The seismic data coverage imaging the halite in the CMD is sufficient to assume that the volume estimation is reliable, and any error in the volume estimation would not exceed $\pm 5\%$ of our observed volume (Figure 7.2).

Contrary to the gypsum volume, our calculations show that the observed halite volume in the CMD can be deposited in a disconnected basin scenario. A CMD filled up to sill depth with water at halite saturation concentration (350 kg m^{-3}) would produce a volume of halite that is even bigger than observed (140%; Table 7.4). Three possible scenarios can reproduce our observations: (1) A CMD that undergoes evaporation and progressive drawdown with the consequent increase in salinity, reaching halite saturation concentration when the sea surface reaches the level of the sill ($\sim 850 \text{ m}$; sill 01 in Figure 7.3) and the basin disconnects from the Mediterranean; (2) A full CMD at normal sea level having a stratified water column with depth-increasing salinities, where halite saturation is reached only at depths comparable to the depth of the deeper sill (sill 01 in Figure 7.3); (3) The volume of the halite deposit is not correlated to the volume of water at halite saturation and only appears to be by chance.

In the first scenario (1), our results show that blocking the outflow of ions from the CMD toward the Mediterranean (Figure 7.7) is enough to reach the halite saturation rapidly in the basin. Knowing that by the end of stage 1 the inflow salinity from the Mediterranean waters must have been very close to or even at gypsum saturation (see previous section 7.5.1), the time to reach halite saturation can be as short as 1 kyr (Figure 7.7 and Table 7.5). This process of salinity increase must have been accompanied by a drawdown that reached at least the depth of the deep sill ($\sim 850 \text{ m}$; sill 01 in Figure 7.3) and disconnected the CMD from the

Mediterranean. Once the halite saturation is reached and the CMD is disconnected from the Mediterranean, the CMD starts precipitating the halite. The drawdown in the CMD now proceeds independently from the drawdown of the rest of the surrounding Mediterranean. Figure 7.6 shows that a quasi-desiccation in the CMD, and the subsequent halite deposition, would take place rapidly (~ 1.2 kyr in the slowest case scenario) and that even the highest possible fresh water input by river would have a negligible effect on the amount of halite deposited.

In the second scenario (2), the basin is filled with water at halite saturation up to the sill depth and overlaid with a ~ 800 m thick column of relatively fresher water ($< 350 \text{ kg m}^{-3}$), sealing the brine off against atmospheric influence (i.e., evaporation). The brine, hence, is not affected by a sink of freshwater and needs a source of ions to surpass halite saturation and precipitate halite (see mechanism in Simon & Meijer, 2017). Such a source of ions would need an area at the surface where water is so dense, that it is transported to the depth. This means that the stratification that characterizes this scenario would have to be broken at least locally and at least intermittently. Given the limited horizontal dimensions of the basin and the resulting salinity gradient in this case (due to its connection to the open Mediterranean), such a scenario is unlikely to take place in the CMD. This also applies to the double diffusion as a process (Arnon et al., 2016; Ouillon et al., 2019), for which the vertical salinity difference needs to be so small that the effect of temperature on density and saturation point cannot be ignored anymore (see mechanism in Arnon et al., 2016). In this case, in fact, the CMD would have to be inversely stratified with slightly higher salinity in the (warm) surface layer at least part of the year. Furthermore, the volume of the deposited halite would not depend on the water volume of the deep layer, but on the transports of ions into said volume. The more ions are imported to the volume, the more halite will be deposited. Such mechanisms observed in present-day evaporative basins (e.g., Dead Sea; Lensky et al., 2005; Sirota et al., 2018), are associated to high deposition rate of halite that can reach 0.15 m yr^{-1} (Table 7.2). Consequently, in such a scenario, the time needed to deposit the whole observed halite volume in the CMD is less than 2 kyr in the slowest case scenario, which is only 4% of the duration of stage 2 (~ 50 kyr). Therefore, even if this mechanism is stopped (by drawdown and disconnection), an excess volume of halite would be produced, which is not observed in the present-day halite volume.

Scenario 3 (3) is similar, with the only difference being that the whole basin is assumed to be at halite saturation and long enough to precipitate the observed halite deposit. In this scenario, the inflow salinity has either to be very close to halite saturation or the fluxes from the

Mediterranean to be small enough to increase the salinity locally in the CMD. Figure 7.10-A shows that the magnitude of the fluxes from the CMD to the Mediterranean (Eq. 7a) has to be $10^2 \text{ m}^3 \text{ s}^{-1}$ or smaller to reach halite saturation in the CMD when the Mediterranean inflow is still at gypsum saturation. With the cross sections of the connections between the CMD and the rest of the Mediterranean through the channels, this would require extremely slow horizontal velocities in the order of $v \approx 10^{-6} \text{ m}^3 \text{ v}^{-1}$ and smaller (Figure 7.10-B), which is the same order of magnitude as vertical velocities of the present-day global ocean (Liang et al., 2017). Horizontal velocities, however, tend to be much larger (e.g. River flows: $v_{river} \approx 10^0 \text{ m s}^{-1}$, Schulze et al., 2005; horizontal ocean currents: $v_{current} \approx 10^1 \text{ m s}^{-1}$, Lumpkin & Johnson, 2013; wind induced surface currents of the Dead Sea: $V_{DeadSea} \approx 10^{-2} - 10^{-1} \text{ m s}^{-1}$, Padon & Ashkenazy, 2018). There is no reason to assume that the horizontal currents in the Western Mediterranean became slower than the sinking speed that is observed in the present-day global circulation. It is thus reasonable to assume that the inflow salinity in this scenario was at halite saturation. Again, given the short period of time needed to precipitate the halite deposit (Figure 7.10-A), this high salinity inflow only needs to be reached for 150 yrs -1500 yrs to deposit the observed volume. The longer the connection lasts, the larger the deposited halite volume, which is something that we do not observe in the present-day halite volumes, hinting again that the CMD has to disconnect from the Mediterranean.

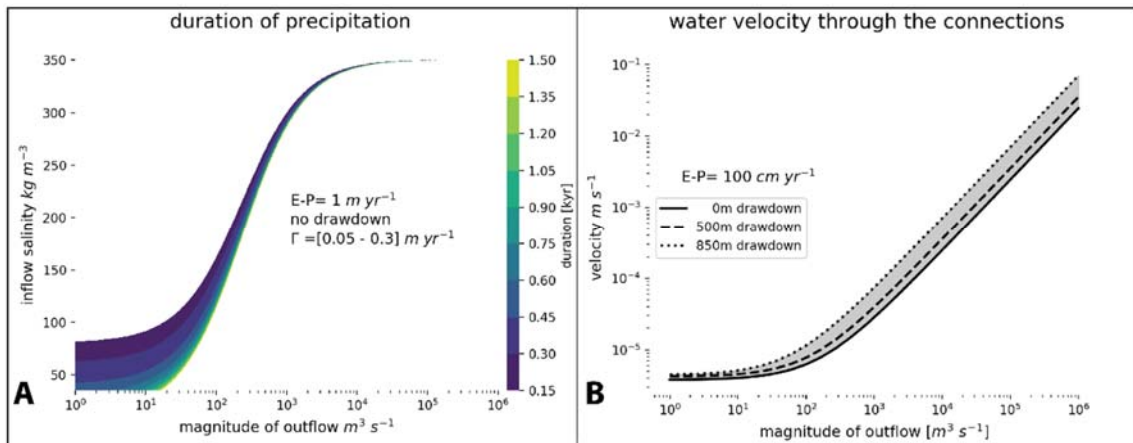


Figure 7.10. A: Duration of precipitation for the halite deposit in analogy to Figure 7.9. The boundaries for the precipitation rate are oriented at those of the Dead Sea (Table 7.2), with ± 2 order of magnitude to cover broader boundaries. B: velocity of water fluxes through the connection in dependence of drawdown and magnitude of outflow.

Our results supporting a quasi-desiccation of the CMD seem consistent with previously reported observations. Starting locally from the CMD itself, Raad et al. (2021) evidenced the presence of an erosional event truncating within the top of the halite unit in the depocenter of the CMD. The authors interpreted this erosion as due to subaerial exposure and/or dissolution of halite in relatively shallow water. Since our calculations show that no complete desiccation is possible due to river input (Figure 7.6), the subaqueous but shallow origin should be preferred. However, we cannot exclude that the salt was subaerially exposed on the flanks of the depocenter while a residual water body was present in its deeper part.

A similar observation from another intermediate-depth basin, the Caltanissetta Basin of Sicily, also supports an important sea level drawdown during the halite stage, where an erosional surface with desiccation cracks is cutting the top of a K- and Mg- salt rich level (Decima & Wezel, 1973; Garcia-Veigas et al., 1995; Lugli et al., 1999; Rouchy & Caruso, 2006). Some authors associated this erosional surface to the local desiccation of the Caltanissetta Basin (Roveri et al., 2008; Manzi et al., 2012) during stage 2. This is consistent with our interpretation and we propose that the Sicilian salt may have deposited during stage 2 in the Caltanissetta basin in a similar way to the one described above for the CMD (scenario 1), as both basins are classified as intermediate-depth and their MSC record share many similarities (Raad et al., 2021).

	Western Mediterranean	Eastern Mediterranean	Reference
Area covered by Halite (m ²)	5.38E+11	2.80E+11	Lofi, (2018)
FWB (m ³ /a)	-2.5*(10E+15)E-3		Simon et al., (2017)
Volume of MSC evaporites (m ³) *	977E+12		Haq et al., (2020)

Table 7.6. Table showing the area and volume of the halite in the Mediterranean area. FWB = Fresh water budget (calculated for both Western and Eastern Mediterranean).

* The volume of evaporites from Haq et al. (2020) includes pre-halite, halite and post-halite MSC units.

As long as the CMD is connected to the main Mediterranean basin, its water level will follow that of the Mediterranean. Studies showed evidences of a drawdown of even higher amplitudes than the depth of 850m of our sill, varying from ~1500 m (Urgeles et al., 2011; Heida et al., 2021) up to quasi-desiccation of the deep basins (W. B. Ryan, 1978; Pellen et al., 2019). This

means that the drawdown might have continued further in the Mediterranean, whereas the CMD had its own base level evolution as explained in section 7.4.2 and shown in Figure 7.6. With the aim of evaluating the present-day observed halite volume in the frame of the consensus model (CIESM, 2008; Roveri, Flecker, et al., 2014), we performed a simple calculation, similar to the one done for the CMD but on the scale of the whole Mediterranean, using the parameters shown in Table 7.6 and the mechanism in Figure 7.4-B. We keep a restricted Mediterranean-Atlantic connection, allowing for an Atlantic inflow with a salinity of 35 kg m^{-3} replacing the net-freshwater loss (i.e., no drawdown; Meijer, 2012) for the whole MSC stage 2 duration (~ 50 kyr as assumed in Roveri et al., 2014) where the Mediterranean waters are at halite saturation. Results of our calculations show that we would precipitate $\times 1.5$ times the observed deep basin evaporite volume ($977 \times 10^{12} \text{ m}^3$, Table 7.6) calculated by Haq et al. (2020). This is not a contradiction to the results of Krijgsman & Meijer (2008), who used the same approach but estimated the volume of halite by combining the areal extent of halite as indicated by the distribution map of Rouchy and Caruso (2006), a thickness of 1000 m in the western basin and 3500 m in the eastern basin (after Lofi et al., 2005). Their calculated volume was close to the estimated one. Note that the volume given by Haq et al. (2020) includes the pre- and post-halite MSC units and it is thus an overestimation of the deep basin halite volume. Thus, we would expect to accumulate a volume of halite that could be at least two-times bigger than the observed one. However, the volume estimation by Haq et al. (2020) is more reliable and thus our calculation could be considered an improvement to Krijgsman & Meijer (2008). As for the CMD, our calculation suggests that the open Mediterranean could not have remained connected to the Atlantic during the whole duration of stage 2. Consequently, a drawdown must have occurred upon the Mediterranean's disconnection from the Atlantic because of the negative water budget that characterizes the Mediterranean (e.g., Meijer, 2006; Krijgsman & Meijer, 2008) and desiccation and refilling of the Mediterranean could have taken place very rapidly (within one precessional cycle; Meijer & Krijgsman, 2005). Of course, this calculation is very simplistic since it overlooks some factors such as the sill effect between the Eastern and Western Mediterranean (Blanc 2000, 2006; Topper & Meijer, 2013), and the fact that the salt in the deep basin might have started deposition already during stage 1, at least in the eastern basin (Meilijson et al., 2019, 2022). Although, in their modelling of the MSC halite stage, Topper and Meijer (2013) tested the efficiency of the Siculo-Tunisian sill between the eastern and western Mediterranean basins and arrived to the same conclusion that a high amplitude drawdown (~ 1500 m) must have happened at the end of halite deposition in the deep basin (see their figure 10).

Another step to place the results obtained in the CMD in the wider context of the wider MSC events in the Western Mediterranean Basin, is comparing the obtained halite volumes formed during water level drop in the CMD, to those in the deep basin of the Western Mediterranean. The deep basin halite volume in the Western Mediterranean has been estimated at around $120 \times 10^3 \text{ km}^3$ (Heida et al., 2021), which is considerably smaller than previous estimates (Haq et al., 2020). Using the reconstructed hypsometry of the western basin at the beginning of halite deposition derived from the paleo-bathymetry published in Heida et al. (2021), we can calculate the volume of halite that would result for different average starting salinities for the Western Mediterranean (Figure 7.11) for a disconnected basin that experiences drawdown (as in figure 4A). For a low starting salinity model ($190\text{-}210 \text{ kg m}^{-3}$) and halite saturation reached after a drawdown of $\sim 850\text{m}$, a large drop in water level ($>3000\text{m}$) is required to obtain $>85\%$ of the halite volume. A fully desiccated basin, which is physically impossible since the system would reach an equilibrium before (comparable to figure 6), would also not lead to the total volume. This volume is only reached for a water column that starts precipitating after a drawdown of $\sim 700 \text{ m}$ or sooner which implies an average Salinity of 232 kg m^{-3} or higher (Figure 7.11). For a salinity of 350 kg m^{-3} , i.e. halite saturation, the drawdown needed to form the western Mediterranean MU halite is even reduced to 1600 m . This type of calculation simplifies a complex basin to one uniform water column and thus ignores effects like horizontal salinity differences, dynamic changes during the drawdown, like a continuous (even though reduced) supply of ions from the Atlantic to the deep Western Mediterranean Basin. This however, as well as our calculations on the CMD itself, strongly indicate that halite did not start depositing before the beginning of the drawdown.

Halite precipitation in the Western Med. using a reconstructed hypsometry

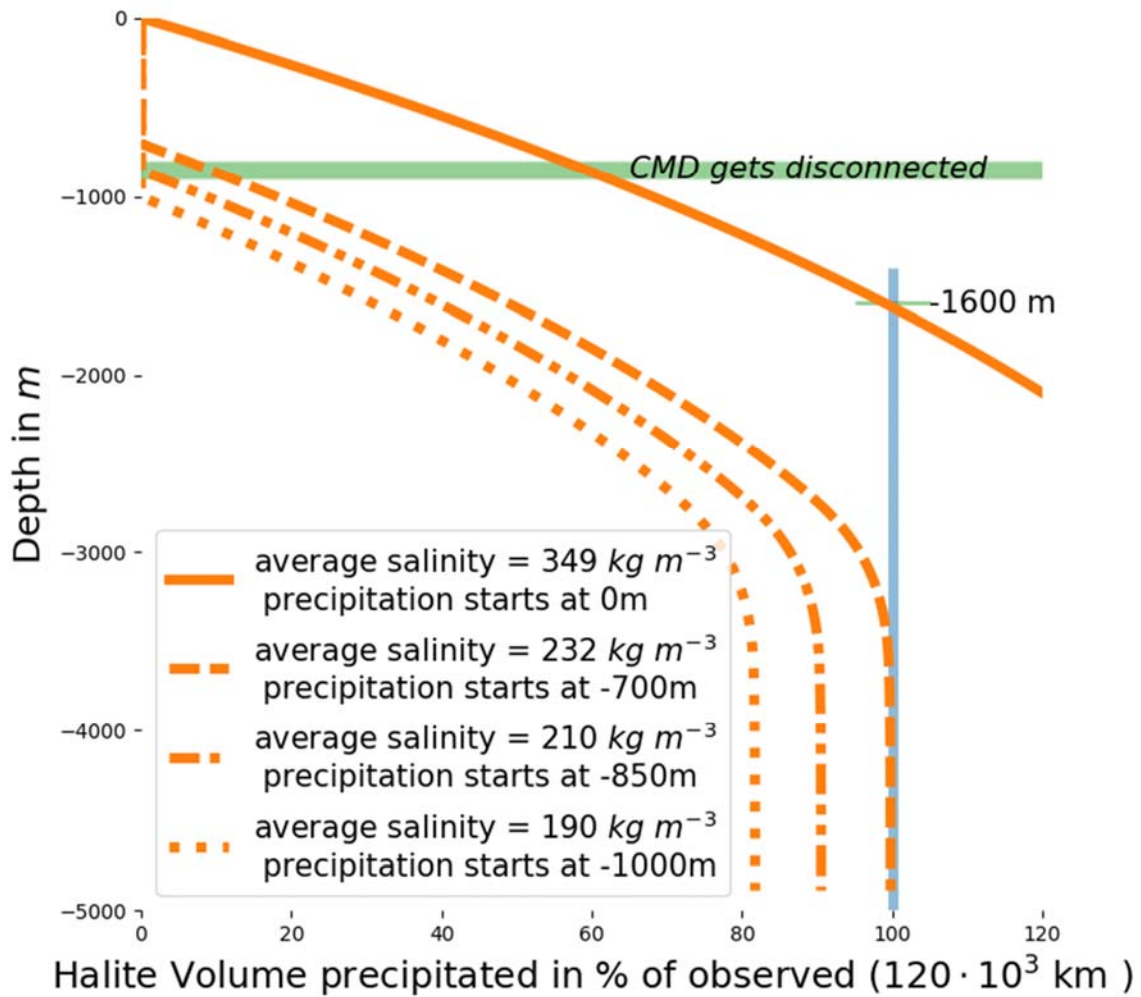


Figure 7.11. Halite volume that would form from a drawdown in the Western Mediterranean. The orange lines show the precipitated volume of halite in function of the amplitude of the drawdown. The shape of the curves is determined by the hypsometry of the basin and the average salinities of the water column before drawdown. Once the drawdown is progressed, the water volume of the basin is decreased enough so that it reaches halite saturation and precipitation begins. The green bar indicates the depth at which the CMD would have become disconnected, and the thin green line marks the depth at which the full deposit would have formed from a full water column at halite saturation.

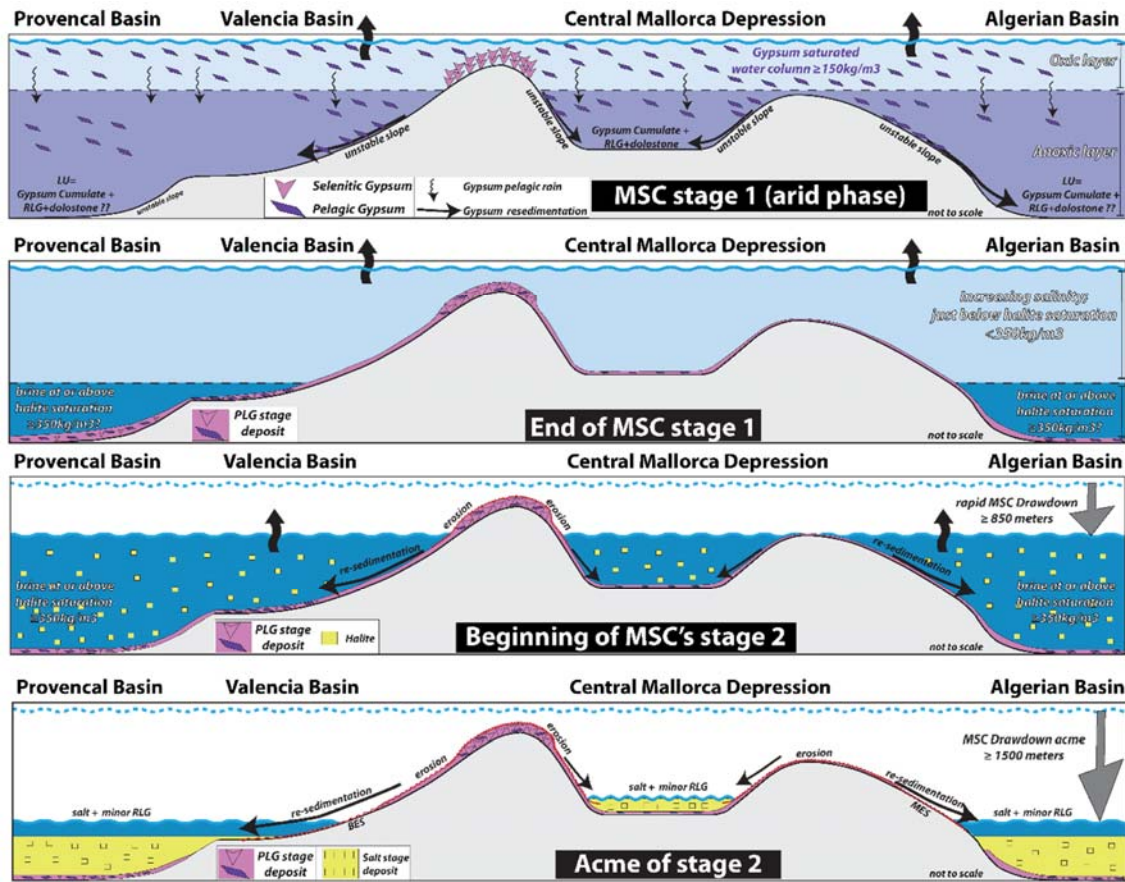


Figure 7.12. Schematic representation of the depositional conditions in the Western Mediterranean during stages 1 and 2 of the MSC according to our modelling results. The non-silled Valencia Basin does not feature the presence of Halite on seismic dataset in its present-day setting (Maillard et al., 2006). Erosion rates measured in exposed halite can be as high as 20 mm yr^{-1} (Frumkin, 1994; Mottershead et al., 2005) suggesting that halite was subsequently removed towards the deeper Provençal Basin following the acme of the drawdown (Heida et al., 2021).

7.6 Conclusions

We carried out numerical modelling of the Messinian Salinity Crisis (MSC) evaporites accumulation in the Central Mallorca Depression (CMD) using physics-based models built on conservation of mass of water and salt and a simplified model for the flow in sea straits. The interpretation of a widespread seismic dataset covering the CMD allowed the estimation of the

volumes of the MSC evaporites that are used to constrain both our isostatic and evaporite precipitation models. According to the results and observations, we conclude the following:

- During stage 1 of the MSC (5.97-5.60 Ma), the upper water layer of the Mediterranean had to be at gypsum saturation salinity to supply the CMD with Ca^{2+} and SO_4^{2-} ions needed to deposit the observed volume of PLG. Gypsum deposition likely occurred only during part of precessional cycles (maximum duration of ~4.5 kyrs).
- The need of shallow topographic sills in the deposition of PLG appears not to be a pre-requirement, and PLG deposition was not necessarily limited to 200m water depth but was rather constrained by the depth at which anoxia starts.
- Our results suggest that during stage 1, gypsum possibly deposited almost everywhere in the Mediterranean, including on open shelves. PLG may have successively been removed at any time by subaerial erosion or slopes instabilities, and re-sedimented in deeper contexts.
- The deep basin's Lower Unit, traditionally associated to the MSC could thus at least partly be made of cumulatic and resedimented gypsum.
- Following the gypsum deposition, a phase of rapid base level drawdown commenced (beginning of stage 2; 5.60-5.55 Ma) accompanied with increasing salinities. The outflow of ions from the CMD toward the Mediterranean is blocked allowing halite saturation to be reached rapidly in the basin. After a period as short as ~1.5 kyr, the drawdown reached the depth of the basin sill lying at ~850 mbsl, leading to the complete disconnection of the CMD, and to halite precipitation.
- The base level in the CMD successively evolved separately from rest of the western Mediterranean Sea, still ongoing a drawdown. A quasi-desiccation in the CMD has likely been reached, and halite locally subaerially exposed while a residual water body was present in the deepest part.
- In the deep western Mediterranean basins, halite saturation was likely reached earlier than in the CMD in a basin strongly stratified before the beginning of the drawdown. Salt deposition however, probably started after the beginning of the base-level drawdown, implying that salt deposition started in a relatively deep water context and ended when the acme of the drawdown was reached. Halite emplacement in the deep basin could have been completed before the end of stage 2.

On a larger basin scale, during stage 1 of the MSC, a normal, even though restricted, connection

between the Atlantic and Mediterranean must have persisted, with no significant base level drop. This connection must have been further restricted until total interruption during stage 2, leading to the important base-level drop and the deposition of halite. Such drawdown must have led to the disconnection between the Western and Eastern Mediterranean basins during this stage, but halite deposition is not necessarily synchronous in both basins due to the further restriction imposed to the eastern basin by the Siculo-Tunisian sill as attested by several studies.

Even though many observations from the Balearic Promontory and the Western Mediterranean are coherent with the 3-step MSC consensus model, our results also highlight that some aspects of such model (e.g., limiting the PLG deposition to shallow >200 m silled basins; and the synchronous onset of the RLG and halite) may need to be reconsidered in future studies.

Chapter 8

Conclusions and Perspectives

In this chapter, I arrange my conclusions from the works introduced in the previous chapters. I provide answers to the research questions that I postulated in the introduction of the dissertation and discuss the implications of my results in the Balearic Promontory with regard to the MSC in a broader context. Finally, I propose future perspectives that I believe necessary to improve our understanding of the Messinian Salinity Crisis.

8.1 Conclusions

This PhD thesis was carried out in the framework of the SaltGiant ETN, which was created with the objective of better understanding the origin and evolution of the Messinian Salinity Crisis (MSC) event that led to the deposition of the Mediterranean Salt Giant. I carried out my work as part of Work Package 1 (WP1) of the project, which has as objective creating a unified model for the MSC. In collaboration with other researchers from the project, I used different geological and geophysical approaches to answer some important questions (see below) that could contribute significantly to the development of a new unified model of the MSC.

The study area I investigated throughout the thesis is the Balearic Promontory (BP). The BP is a prominent high in the Western Mediterranean that contains MSC evaporites (including salt) distributed in a series of perched sub-basins scattered from shallow to intermediate depths. The relevance of the BP is that it underwent minor post-deposition deformation, unlike most of the Mediterranean MSC basins from which the present sedimentary and or/chronostratigraphic models (including the consensus model) derive from. For this reason, the BP is a unique area to evaluate the existing models and refine our understanding of the MSC event.

In this concluding chapter, I highlight the main conclusions linked to the research questions that I targeted in my PhD work. Those conclusions benefit from numerous discussions with most of the members of the SaltGiant project and in particular those from WP1.

1- What is the nature of the evaporites of the BP and what is their relationship (spatial, geometric and temporal) with other Mediterranean marginal to deep MSC deposits?

The interpretation of the available seismic dataset allowed the mapping of 4 different seismic units belonging to the MSC, based on their seismic facies and on their geometrical and seismostratigraphic relationships. Those seismic units include 3 Bedded Units (BUs) and one transparent salt unit. From the oldest to the most recent, the units were labeled BU1/BU2, Salt Unit and BU3. BU1 and BU2 are widespread all over the BP's sub-basins, covering most of the marginal and distal domains at paleo-depths spanning from 0 to 1500m. The salt unit is limited to the depocenters of perched and semi-perched sub-basins, namely Cogedor Basin (650m deep at the beginning of halite deposition), Central Mallorca Depression (1400m deep

at the beginning of halite deposition) and Formentera Basin (1900m deep at the beginning of halite deposition). BU3 is also limited to the topographic lows of some sub-basins where it overlies the salt unit in the depocenter, and it drapes the lower slopes (beyond the pinch-out of the salt) where it onlaps the underlying BU1/BU2 at a paleo-depths that vary from 600 to 800 meters. Those units are best expressed in the Central Mallorca Depression (CMD), where the density of high-resolution seismic profiles is also the greatest.

In the absence of drillings, the possible nature of the units was deduced by applying an indirect approach consisting in a unit-by-unit comparison between the MSC records of the CMD and those from the Sicilian Caltanissetta Basin (CB). The records in both basins show a high resemblance in terms of geometries, facies, thickness and distribution and the CMD is now thought to be an undeformed analogue of the Sicilian basin. Based on this comparison, and taking into consideration other observations, the seismic units were interpreted as follows:

- BU1 is the equivalent of stage 1 Primary Lower Gypsum (PLG) and is the only MSC unit that has been drilled on the BP on the Alicante shelf. It is made of a succession of precession-driven cycles of selenitic gypsum and marls,
- BU2 is interpreted as the lateral time equivalent of BU1, extending basinward below the salt of the CMD. It is proposed to be made of primary pelagic gypsum cumulates mixed with clastic sediments,
- the salt unit is interpreted as consisting mainly of halite, probably including more soluble K and Mg- salts. The unit shows evidences of erosion at the top, either due to subaerial exposure or dissolution in shallow waters,
- BU3 is interpreted as the equivalent of stage 3 Upper Evaporites, consisting of alternating terrigenous and gypsum beds. It might include the Lago Mare-stage deposits in its topmost part.

Thus, the evaporites filling the sub-basins of the BP are comparable with the “classical” MSC records contained in some marginal and intermediate-depth basins such as the Sorbas (SE Spain) or the Caltanissetta (Sicily) basins. The particular analogy shown between the CMD and CB is of important relevance as the latter is a key basin on which most of the proposed MSC models are built.

2- Under what paleo-environmental conditions (water level and salinity) did the MSC evaporites emplace in the BP?

The investigation of the post-MSC deformation acting in the CMD, the key sub-basin of the BP, followed by a regional pseudo-3D backstripping restoration allowed obtaining a confident paleo-bathymetry at the beginning of the MSC. At the onset of the MSC, the depocenter of the CMD was lying at a maximum depth of ~1500 m and was bounded by two silled channels (750 and 850 m deep) restricting it from the Mediterranean's Valencia and Algerian basins. This paleo-bathymetry was successively used as an input to model the conditions under which the evaporites in the CMD deposited. Results and implications are schematically presented in Figure 8.1 and summarized hereafter:

PLG phase: the gypsum of PLG (BU1) in the BP deposited during the arid phases of the precessional cycles of stage 1 of the MSC. During this phase, the duration of gypsum sedimentation was relatively short (< 4.5 kyrs) and the upper water layer of the Mediterranean was at gypsum saturation, supplying the BP's sub-basins with the calcium and sulfate ions that are necessary for gypsum growth. No major base level drawdown took place during the PLG stage and any eventual sea level oscillations did not exceed the tens of meters, as also inferred from onshore observations in marginal basins containing PLG.

Based on the restored paleo-bathymetry, the PLG deposition took place at depths that are clearly exceeding 200 m, extending down to ~800 to 900m of water depth. Beyond this depth and towards >1000m depths, a change in facies from BU1 to BU2, clearly observed on the high-resolution seismic profile, possibly indicates a passage from primary bottom growth selenitic facies to primary pelagic gypsum cumulates, possibly mixed with resedimented clastic gypsum. This facies transition is tentatively interpreted as marking the passage from the oxygenized to the anoxic water layer, and could thus be used in future studies as an indicator for the depth at which anoxia starts during the PLG stage (Figure 8.1 – PLG phase). In addition, since the CMD was surrounded by deep silled channels (> 800m water depth) at the beginning of the MSC, the presence of PLG in this basin contradicts the critical need for shallow water topographic sills in the deposition of PLG.

PLG gypsum are thus expected to have been deposited on most of the shelves and slopes of the Mediterranean basin, and to have been subsequently eroded and resedimented in deeper water

settings as suggested by the widespread erosion surface observed on the seismic profiles. It remains unclear, however, why it is preserved only locally. Subaerial erosion and/or slopes instability may have been more efficient on other margins, as a result of several factors including steeper slopes, larger river drainage basins, and local geo-chemical and geo-biological conditions. The main factor on the BP seems to be the presence of perched /closed sub-basins.

The so-called Resedimented Lower Gypsum (RLG) could be also associated to this stage of the MSC and not restricted to stage 2 as figured in the consensus model. By definition, the origin of the RLG is strictly related to active syn-MSC tectonics combined with the sea level drawdown. The evaporites, however, are likely to have undergone gravitational gliding and resedimentation due to slope instability at any time after their deposition (Figure 8.1 – PLG phase).

Salt phase:

Following the PLG phase, a rapid increase in salinity accompanied by a base level drawdown that reached at least the depth of the 850m deep silled channel of the CMD took place. This led to the disconnection of the CMD from the rest of the Mediterranean basin. Upon disconnection, halite saturation was reached in the CMD and consequently halite was emplaced (Figure 8.1 – salt phase). The CMD then evolved separately from the rest of the Mediterranean until the connection was reestablished. A similar scenario can have happened in the other sub-basins of the BP containing halite (i.e., Cogedor and Formentera basins). This would explain the lack of relationship between halite thickness and the depth of the perched CMD, Formentera and Cogedor basins, as the volume of deposited halite in each of them would depend on the volume of the residual brine upon their disconnection from the Mediterranean.

As the drawdown proceeded, the halite in the perched basins of the BP was subject to erosion and/or dissolution in shallow water context, as evidenced by the truncation of internal reflectors observed on the top of the salt unit in the CMD. The geometry of these truncations further indicates that the extension of the salt unit in the CMD was originally presenting a wider extent than today. It was possibly initially covering part of the slopes bordering the depression, and was successively eroded and resedimented in the depocenter. Halite possibly also accumulated widely in the surrounding basin of Valencia, not only in its eastern part as observed today, but having no sills separating it from the deep Provençal basin, it was successively completely

washed away eastward towards the deep basin (Figure 8.1 – salt phase). Subsidence analysis presented in this thesis indicates that if the origin of the Bottom Erosion Surface (BES) in the Valencia basin is subaerial, then the level of the western Mediterranean water surface was at least as low as -1500 +/-100 m at the end of halite deposition in the deep basin.

UE phase:

The upper evaporites phase is the most ambiguous of all the phases, in terms of basin connectivity and base level. Except for its nature, geometry and extension, the BU3-UE was not particularly investigated in the modelling applied in this work. Its presence in the BP is limited to the distal domains of the sub-basins, showing locally aggradation geometries and clear onlaps towards the higher slopes suggesting that its deposition took place, at least partly, during a lowstand when the BP sub-basins were still disconnected from the Mediterranean. Modelling results in the CMD shows that when disconnected from the Mediterranean, the lake-level in the CMD would stabilize at a maximum of 150m above the bottom of the paleo-seafloor. This level is lower than the onlap of top BU3-UE which is between ~800 and 600 m above the paleo-seafloor (600-800m below the paleo-zero level). However, adding the thickness of the underlying deposits from the PLG and salt stages (~400 meters) and the thickness of BU3-UE itself, the onlap depth happens to be at the same depth as the observed one. Three possible scenarios can be proposed during this phase:

- 1- The CMD was connected, continuously or periodically (cyclic spillovers?), to the Mediterranean through its deepest sill (~850m) that surprisingly has a depth which is close to the depth of onlap of BU3-UE. Such connection would generate a channel system in the sill area, which is not observed on the available seismic data.
- 2- The CMD was connected normally to the Mediterranean and the BU3-UE deposited only at certain depth in a salinity-stratified water column condition.
- 3- The CMD disconnected, continuously or periodically, from the Mediterranean. In this scenario the source of calcium and sulfate ions necessary to form the BU3-UE deposit would result from the erosion of the previous gypsum deposits of the PLG stage.

The BU3-UE of the BP shows no geometrical continuity with the deeper basin's Upper Unit (UU) present in the surrounding basins (Algerian, Provençal and Valencia basins). In addition,

the onlap depth of BU3-UE is much shallower than the one of the UU (~1100m below the paleo-zero level in the Valencia Basin, and much deeper in the oceanic Provençal and Algerian basins; Figure 8.1 – upper evaporites phase). Numerical modelling results from this work show that the salinity of the CMD cannot differentiate by much from the salinity of the Mediterranean if the two are connected. It follows that a salinity-stratified water column scenario during the UE phase is very unlikely, otherwise one would expect that the top BU3 onlap/pinch-out to be at the same level of the onlap of the UU. This reasoning again points towards a lowstand, at least periodically during this stage. A lowstand scenario during this phase in the Western Mediterranean is also supported by the erosional features preserved offshore on both the continental shelves and lower-middle slope domain down to the pinch-out of the evaporites. Subsidence analysis presented in this thesis indicates that if this erosion is of subaerial origin then the BU3 in the CMD and the UU in the deep basin constrain the water level in the Western Mediterranean basin between -1100 and -600 +/-100 m during the final lowstand at the end of this phase.

3- Is the chronostratigraphic ‘consensus model’ applicable/compatible with the observations from the MSC record of the BP?

Observations from the BP evidenced throughout the work of this thesis, pointed out that many results are coherent with a 3-step model as the one presented by the consensus model. This is evidenced mainly by the tripartite character (3-stages) of the MSC units extending all over the promontory.

However, the results also highlight that some aspects of the consensus model may need to be reconsidered in future studies, among which:

- PLG gypsum is not limited to silled marginal basins, and may have deposited as deep as 800 m in water depth;
- The time equivalent of the PLG, at least in the Western Mediterranean basins, could be primary cumulatic and resedimented gypsum instead of the ‘evaporite-free Foraminifer Barren Interval’;
- RLG is not necessarily restricted to the halite phase (stage 2 of the consensus model), but could have deposited already in the PLG phase (stage 1) and continued throughout stage 3;

- Halite deposition did not initiate contemporaneously everywhere as evidenced by the modelling presented in this work. A diachronous deposition is inferred at least between the various sub-basins of the Western Mediterranean, but also possibly between the Western and Eastern Mediterranean.

A high amplitude sea-level drawdown ($>850\text{m}$) accompanied by halite deposition first in the deep and later in the intermediate basins is inferred from the observations.

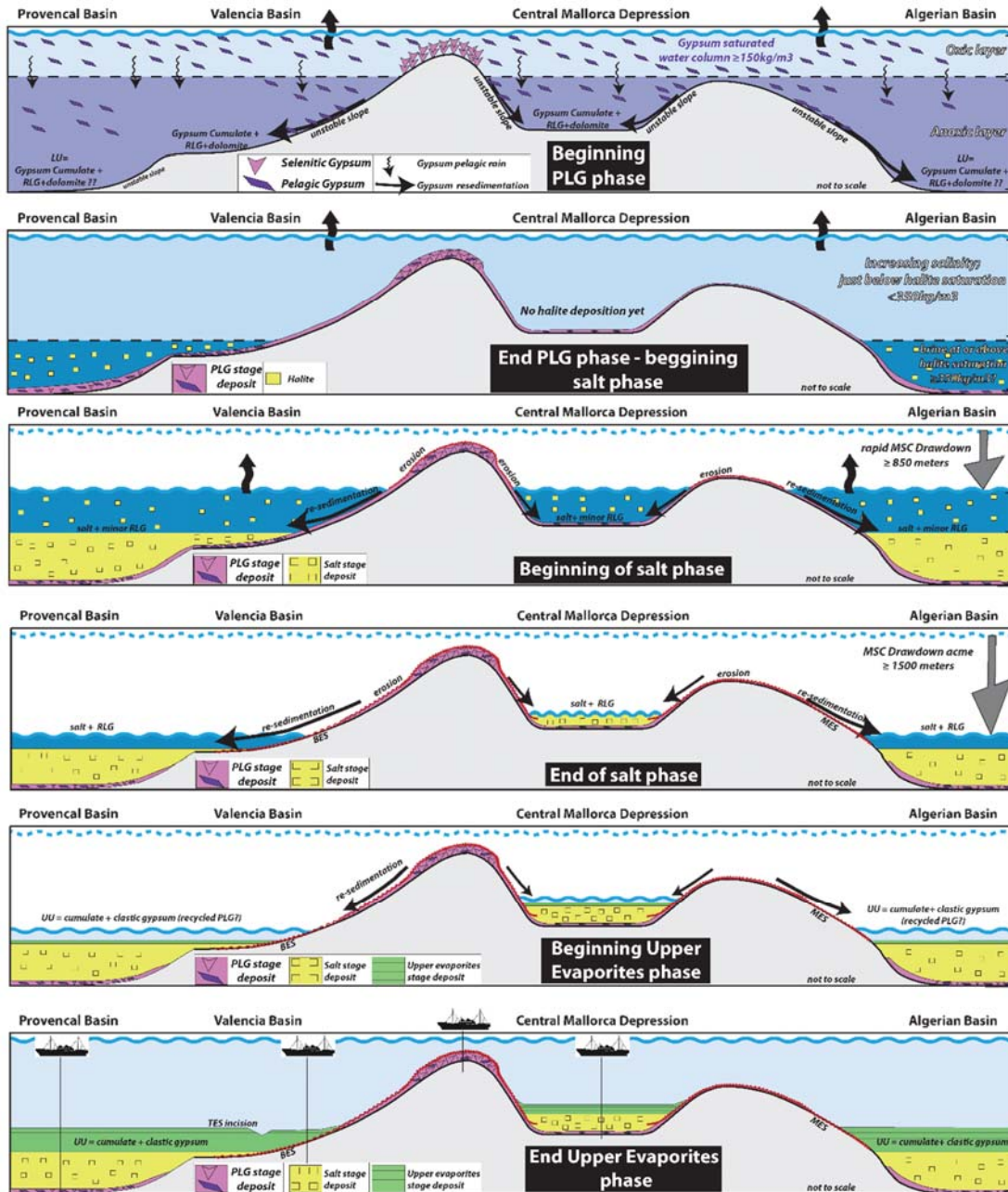


Figure 8.1. Schematic representation of the proposed scenario of the depositional conditions in the Western Mediterranean during the different stages of the MSC following the results and observations obtained in this work.

8.2 Perspectives

A future focus on the offshore domain, which hosts more than 90% of the Mediterranean salt giant, is necessary to reveal what is buried there and give answers to many of the speculations and long-living questions. Any information about the MSC evaporites from the offshore domain of the Western Mediterranean is valuable due to the lack of data from this area even after more than 50 years of the discovery of the Mediterranean Salt Giant. As the reader might have understood by now reading this dissertation, the Balearic Promontory provides a unique opportunity to exploit and focus on in future offshore studies, thanks to its strategic position and the excellent preservation of its evaporites. The results and conclusions that I extracted in my study in the BP mostly derive from observations through ‘indirect’ methods. To evaluate and emphasize the importance of the implications of my results, a direct access to the MSC evaporites through boreholes is absolutely needed in the area. A series of drillings covering a marginal-intermediate-deep transect would be ideal and would provide a complete temporal and spatial correlation between the deposits from the three domains thus providing many answers to some of the puzzling questions about the MSC. In Figure 8.1 (upper evaporites phase, showing all the MSC-related deposits in place) I suggest a drilling transect from the BP to the Provencal Basin that covers all the depositional domains from marginal to deep basins. Recovered samples from such drillings would provide a load of benefits for the MSC problematic among which:

- Reveal the nature of the lithology of the whole offshore MSC succession, especially the ‘MSC trilogy’ for the first time;
- Resolve the temporal and spatial connectivity between the MSC evaporites from different depth domain;
- Allow performing direct petrographic, paleontological and geochemical analysis that would provide answers on the paleo-environmental conditions at each step of the MSC.

There was an initiative in the past years to launch IODP (International Ocean Drilling Program) drillings in several areas in the Western and Eastern Mediterranean, including the Balearic Promontory, led by experts from the MSC community. The initiative went under the acronym of DREAM (Deep Sea Record of Mediterranean Messinian Events; see Camerlenghi & Aloisi, 2020). These proposals at the scale of the Mediterranean are nevertheless difficult to realize both for their cost and their practical implementation and other older requests have not been successful. The continuous mobilization of the scientific community towards the realization of

such projects will help to see them succeed one day. For the moment, a smaller alternative project could be done, limited to the Balearic Promontory: a single borehole on the Mallorca slope could reach the 3 Bedded Units and the salt unit (Figure 8.1). A seismic reflection survey necessary prior to the drilling has already been refused by the Spanish authorities due to environmental laws in action. A request to use 'light' Sparker source seismic imaging, having proved its worth as regards the Messinian problem, could possibly be proposed.

In the meantime, a proposal, led by Giovanni Aloisi the SaltGiant project coordinator, to sample some of the MSC evaporites outcropping on the seafloor of the Mediterranean using submarine Autonomous Underwater Vehicle (ROV, AUV) or manned submersible nautilic has been submitted. I am largely involved in this proposal as I investigated and proposed several potential sites where MSC evaporites from different MSC stages are potentially outcropping.

Conclusions

Cette thèse de doctorat a été réalisée dans le cadre du projet 'ETN SaltGiant', qui a été créé dans le but de mieux comprendre l'origine et l'évolution d'un événement environnemental extrême : la Crise de Salinité messiniennne (CSM) responsable du dépôt du Géant Salifère méditerranéen. J'ai réalisé mon travail dans le cadre du Work Package 1 (WP1), qui a pour objectif de créer un modèle consensuel cohérent pour la CSM. En collaboration avec d'autres chercheurs du projet, j'ai utilisé différentes approches géologiques et géophysiques pour tenter de répondre à certaines questions importantes (voir ci-dessous) dont la résolution pourrait contribuer de manière significative à l'élaboration d'un nouveau modèle unique et cohérent de la CSM.

La zone d'étude que j'ai étudiée tout au long de la thèse est le Promontoire Baléares (BP). Le BP est un haut structural englobant les îles Baléares situé au cœur de la Méditerranée occidentale. Il est en grande partie recouvert de séries évaporitiques liées à la crise (y compris du sel) distribuées dans une série de sous-bassins perchés qui, pendant le Messinien, se trouvaient à des profondeurs étagées de faibles à intermédiaires. L'intérêt du BP est qu'il a subi une déformation post-CSM mineure, contrairement à la plupart des bassins marginaux méditerranéens dont sont issus les modèles sédimentaires et/ou chronostratigraphiques actuels (y compris le modèle consensuel), situés dans des zones tectoniquement actives. Pour cette raison, le BP est une zone unique, de par sa position, pour imager le lien entre les dépôts marginaux et les dépôts profonds et donc pour évaluer les modèles existants et affiner notre compréhension de l'événement CSM. Dans ce chapitre final, je souligne les principales conclusions liées aux questions fondamentales que j'ai ciblées dans mon travail de doctorat. Ces conclusions ont bénéficié également de nombreuses et fructueuses discussions avec la plupart des membres du projet SaltGiant et en particulier ceux associés au WP1.

I- Quelle est la nature des évaporites du BP et quelle est leur relation (spatiale, temporelle et géométrique) avec les autres dépôts (émergés, peu profonds et profonds) de la crise?

L'interprétation des données sismiques disponibles a permis de cartographier 4 unités sismiques différentes appartenant à la CSM, en fonction de leur faciès sismique et de leurs relations géométriques et sismo-stratigraphiques. Ces unités sismiques comprennent 3 unités litées ('Bedded Units', BUs) et une unité transparente interprétée comme le sel massif et mobile. De la plus ancienne à la plus récente, les unités ont été étiquetées BU1/BU2, Salt Unit,

et BU3. Ces unités sont très bien imagées dans la Dépression Centrale de Majorque (CMD) située entre les îles d'Ibiza et de Majorque, là où la densité de profils sismiques haute résolution est également la plus grande.

En l'absence de forages, la nature possible des unités a été postulée par une approche indirecte consistant en une comparaison, unité par unité, entre les enregistrements dans la Dépression Centrale de Majorque et ceux dans le bassin sicilien de Caltanissetta (CB). Les enregistrements dans les deux bassins montrent une grande ressemblance en termes de géométries, de faciès, d'épaisseur et de distribution : la Dépression Centrale de Majorque est maintenant considérée comme un analogue non déformé du bassin messinien sicilien. Sur la base de cette comparaison et en tenant compte d'autres observations, les unités sismiques ont été interprétées comme suit:

- BU1 est l'équivalent du stade 1 du gypse inférieur primaire ('Primary Lower Gypsum' PLG) et est la seule unité de la crise qui a été forcée sur le BP, sur la plateforme d'Alicante. Elle est constituée d'une succession de cycles de gypse séléniteux et de marnes régis par la précession,
- L'unité BU2 est interprétée comme l'équivalent temporel latéral de l'unité BU1, s'étendant vers le bassin en partie distale sous le sel de la dépression centrale. Il est proposé qu'elle soit constituée de cumulats de gypse pélagique primaire mélangés à des sédiments clastiques,
- l'unité 'Salt unit' est interprétée comme étant constituée principalement de halite, incluant probablement des sels de K et de Mg plus solubles. L'unité présente des signes d'érosion à son sommet, soit par exposition subaérienne, soit par dissolution dans des eaux peu profondes,
- L'unité BU3 est interprétée comme l'équivalent du stade 3 des évaporites supérieures, consistant en une alternance de lits terrigènes et gypseux. Elle pourrait inclure les dépôts du stade Lago Mare dans sa partie supérieure.

Ainsi, les évaporites qui remplissent les sous-bassins du BP sont comparables aux enregistrements de la CSM "classiques" contenus dans certains bassins marginaux et de profondeur intermédiaire tels que les bassins de Sorbas (sud-est de l'Espagne) ou de Caltanissetta (Sicile). L'analogie particulière montrée entre la Dépression Centrale de Majorque et le bassin de Caltanissetta est d'une importance capitale car ce dernier est un bassin clé sur lequel la plupart des modèles proposés se sont construits.

2- *Dans quelles conditions paléo-environnementales (niveau d'eau et salinité) les évaporites messiniennes se sont-elles mises en place dans le Promontoire Baléares ?*

Dans la Dépression Centrale de Majorque, sous-bassin clé du BP, l'impact de la déformation post-MSB ayant été pris en compte et une restauration régionale par pseudo-3D backstripping ayant été réalisée, une paléo-bathymétrie fiable a pu être obtenue pour le début de la crise. Ainsi, le dépo-centre de la dépression se trouvait à une profondeur maximale de ~1500 m et était connecté aux bassins adjacents de Valence et d'Algérie par deux seuils de 750 et 850 m de profondeur respectivement. Cette paléo-bathymétrie a été ensuite utilisée comme entrée pour modéliser les conditions dans lesquelles les évaporites se sont déposées dans la Dépression Centrale. Les résultats et les implications sont résumés ci-après :

Phase PLG : le gypse PLG (BU1) dans le BP s'est déposé pendant les phases arides des cycles précessionnels du stade 1 de la CSM. Pendant cette phase, la durée de sédimentation du gypse était relativement courte (< 4,5 kyrs) et la couche d'eau supérieure de la Méditerranée était à la saturation du gypse, fournissant aux sous-bassins du BP les ions calcium et sulfate nécessaires à la croissance du gypse. Aucune baisse majeure du niveau de base n'a eu lieu pendant la phase PLG et les éventuelles oscillations du niveau de la mer n'ont pas dépassé quelques dizaines de mètres, comme le suggèrent également les observations à terre dans les bassins marginaux contenant du PLG.

Au vu de la paléo-bathymétrie restaurée, le dépôt de PLG a eu lieu à des profondeurs qui dépassent clairement 200 m, s'étendant jusqu'à ~800 à 900 m de profondeur d'eau. Au-delà de cette profondeur et vers des profondeurs >1000m, un changement de faciès de BU1 à BU2, clairement observé sur les profils de sismique haute résolution, indique probablement le passage d'un faciès sélénitique de croissance primaire de fond à des cumulats de gypse pélagique primaire, probablement mélangés à du gypse clastique resédimenté. Cette transition de faciès est provisoirement interprétée comme marquant le passage de la couche d'eau oxygénée à la couche d'eau anoxique, et pourrait donc être utilisée dans des études futures comme indicateur de la profondeur à laquelle l'anoxie commence pendant le stade PLG. De plus, étant donné que la Dépression Centrale était entourée de seuils profonds (> 800m de

profondeur d'eau) au début de la crise, la présence de PLG dans ce bassin contredit le besoin seuils topographiques peu profonds pour le dépôt des PLG.

Suite à ce résultat, on s'attend donc à ce que le gypse PLG ait été déposé sur la plupart des plateaux et des pentes du bassin méditerranéen, et qu'il ait ensuite été érodé et resédimenté dans des eaux plus profondes, comme le suggère la surface d'érosion majeure (MES) observée partout sur les profils sismiques. La raison pour laquelle elle est préservée localement, sur les pentes de Majorque et d'Ibiza notamment, n'est cependant pas claire. L'érosion subaérienne et/ou l'instabilité des pentes peuvent avoir été plus efficaces sur certaines marges, en raison de plusieurs facteurs, des pentes plus raides, des bassins de drainage fluviaux plus importants, et des conditions géochimiques et géobiologiques locales particulières. Mais notons que les PLG sur le BP se trouvent dans et sur les pentes de bassins fermés et perchés, ce qui semble le facteur dominant conditionnant leur présence. (RQ : 1- où y a-t-il des plg décrites ailleurs qu'à terre ds les bassins marginaux ? ! 2- je rajouterais aussi qu'on n'a pas cherché des PLG partout avec de la sismique appropriée !!)

Le gypse inférieur resédimenté (RLG) pourrait également être associé à ce stade de la crise et ne pas être limité au stade 2 comme indiqué dans le modèle de la CIESM. Par définition, l'origine du RLG est liée à une tectonique active syn-messinienne combinée à la baisse du niveau de la mer. Les séries évaporitiques peuvent donc subir du glissement gravitaire et une redistribution dès leur dépôt.

Phase saline :

Après la phase PLG, une augmentation rapide de la salinité accompagnée d'une baisse du niveau de base d'au moins 850m, profondeur du seuil de la Dépression Centrale du BP, a eu lieu. Ceci a provoqué la déconnexion de ce sub-bassin du reste du bassin méditerranéen. Lors de la déconnexion, la saturation en halite a été atteinte et, par conséquent, la couche de sel, 'Salt unit', a été mise en place. La Dépression Centrale a ensuite évolué séparément du reste de la Méditerranée jusqu'à ce que la connexion soit rétablie. Un scénario similaire peut s'être produit dans les autres sous-bassins du BP contenant aussi de la halite (les bassins de Cogedor et de Formentera). Cela expliquerait l'absence de proportionnalité entre l'épaisseur de sel précipité et la profondeur des bassins perchés du BP, car le volume d'halite déposé dans chacun d'eux dépendrait du volume initial de la saumure résiduelle lors de leur déconnexion de la Méditerranée.

Au fur et à mesure de la chute du niveau marin, la couche de halite des bassins perchés du BP a été soumise à l'érosion et/ou à la dissolution en contexte d'eaux peu profondes, comme en témoigne la troncature des réflecteurs internes observés au sommet de l'unité de sel dans la Dépression Centrale. La géométrie de ces troncatures indique en outre que cette couche présentait à l'origine une plus grande étendue qu'aujourd'hui. Elle recouvrait peut-être initialement une partie des pentes bordant la dépression, et a pu être successivement érodée et resédimentée dans le dépo-centre. Il est possible que la halite se soit également accumulée partout dans le bassin adjacent de Valence, et non seulement dans sa partie profonde à l'est comme observé actuellement : en l'absence de seuil le séparant du bassin profond provençal, elle a pu être ultérieurement complètement redéposée vers ce dernier. L'analyse de subsidence présentée dans cette thèse indique que si l'origine de la surface d'érosion basale (BES) dans le bassin de Valence est subaérienne, alors le niveau de la surface de l'eau de la Méditerranée occidentale était au moins aussi bas que -1500 ± 100 m à la fin du dépôt d'halite dans le bassin profond.

La phase UE :

La phase des évaporites supérieures est la plus ambiguë de toutes les phases, en termes de connectivité des bassins et de niveau de base. A l'exception de sa nature, de sa géométrie et de son extension, l'unité BU3 (UE) n'a pas été particulièrement étudiée dans la modélisation réalisée au cours de ce travail. Sa présence dans le BP est limitée aux domaines distaux des sous-bassins, montrant localement des géométries d'aggradation et de clairs onlaps sur les pentes. Ceci suggère que son dépôt a eu lieu, au moins partiellement, en bas niveau lorsque les sous-bassins du BP étaient encore déconnectés de la Méditerranée. Les résultats de la modélisation dans la Dépression Centrale montrent qu'une fois déconnecté de la Méditerranée, le niveau du lac résiduel dans le fond de la cuvette se stabiliserait à un maximum de 150m au-dessus du paléo-fond bathymétrique. Ce niveau est inférieur à l'onlap de BU3 qui se situe entre ~ 800 et 600 m au-dessus du paléo-fond ($600-800$ m en dessous du niveau paléo-zéro). Cependant, si l'on ajoute l'épaisseur des dépôts sous-jacents des stades PLG et salin (~ 400 mètres) et l'épaisseur du BU3-UE lui-même, la profondeur du onlap se trouve être à la même profondeur que celle observée. Trois scénarios possibles peuvent alors être proposés durant cette phase :

1- La Dépression Centrale était connectée, de façon continue ou périodique (déversements cycliques ?), à la Méditerranée par son seuil le plus profond (~850m) qui, étonnamment, a une profondeur proche de la profondeur de l'onlap de BU3 sur les pentes. Une telle connexion générerait un système de chenaux dans la zone du seuil, ce qui n'est pas observé sur les données sismiques disponibles.

2- Le Dépression Centrale était connectée normalement à la Méditerranée et la BU3 ne s'est déposée qu'à une certaine profondeur sous une colonne d'eau stratifiée par la salinité.

3- Le Dépression Centrale était déconnectée, de façon continue ou périodique, de la Méditerranée. Dans ce scénario, la source d'ions calcium et sulfate nécessaire à la formation du dépôt BU3-UE résulterait de l'érosion des précédents dépôts de gypse de l'étage PLG.

L'unité BU3 (UE) du BP ne montre aucune continuité géométrique avec les Evaporites Supérieures (Upper Unit, UU) des bassins profonds qui l'entourent (les bassins algériens, de Valence et provençal). En outre, la profondeur de l'onlap de BU3 est beaucoup plus faible que celle de l'UU (~1100m en dessous du niveau paléo-zéro dans le bassin de Valence et bien plus profond dans les bassins océaniques algérien et provençal). Les résultats de la modélisation montrent que la salinité de la Dépression Centrale ne peut pas différer de beaucoup de la salinité de la Méditerranée si les deux sont connectées. Il s'ensuit qu'un scénario de colonne d'eau stratifiée par la salinité pendant la phase UE est très peu probable, car alors on s'attendrait à ce que l'onlap de la BU3 soit au même niveau que celui de l'UU. Ce raisonnement pointe à nouveau vers un étiage, au moins périodique pendant cette phase. Un scénario de bas niveau pendant cette phase en Méditerranée occidentale est également soutenu par les évidences d'érosion intense à la fois sur les plateaux continentaux et dans le domaine de la pente continentale des bassins profonds, jusqu'à l'onlap des évaporites supérieures. L'analyse de la subsidence présentée dans cette thèse indique que si cette érosion est d'origine subaérienne, alors la BU3 dans le CMD contraint le niveau d'eau dans le bassin de la Méditerranée occidentale entre -1100 et -600 +/-100 m pendant les bas-stands de cette phase.

3- *Le 'modèle consensuel' chronostratigraphique est-il applicable/compatible avec les enregistrements de la crise observés sur le BP ?*

Les observations sur le BP mises en évidence tout au long du travail de cette thèse ont montré que de nombreux résultats sont cohérents avec un modèle en 3 étapes comme celui présenté par le modèle consensuel. Ceci est principalement mis en évidence par le caractère tripartite (3 étapes) des unités CSM s'étendant sur tout le promontoire.

Cependant, les résultats soulignent également que certains aspects du modèle consensuel doivent être reconsidérés dans les études futures, parmi lesquels :

- Le gypse PLG n'est pas limité aux bassins marginaux fermés par des seuils, et peut s'être déposé jusqu'à 800 m de profondeur d'eau.
- L'équivalent temporel du PLG, au moins dans les bassins de la Méditerranée occidentale, pourrait être du gypse primaire cumulatif et resédimenté au lieu de l'intervalle 'evaporite-free Foraminifer Barren Interval'.
- Le RLG n'est pas nécessairement limité à la phase halite (stade 2 du modèle consensuel), mais pourrait s'être déposé déjà dans la phase PLG (stade 1) et avoir continué tout au long du stade 3.
- Le dépôt de la halite n'a pas commencé partout de façon synchrone comme le montre la modélisation présentée dans ce travail. Un dépôt diachrone est possible au moins entre les différents sous-bassins de la Méditerranée occidentale, mais aussi entre la Méditerranée occidentale et orientale.
- Une baisse du niveau marin de grande amplitude (>850m) est déduite des observations, avec un dépôt de sel d'abord dans les bassins profonds et ensuite dans les bassins intermédiaires.

Perspectives

C'est sur le domaine offshore, qui abrite plus de 90% du géant de sel méditerranéen, qu'il sera encore nécessaire de se concentrer à l'avenir pour accéder ce qui y est enfoui et apporter des réponses à de nombreuses spéculations et questions persistantes. Toute information sur les évaporites MSC du domaine offshore de la Méditerranée occidentale est précieuse en raison du manque 'abyssal' de données sur cette zone, même plus de 50 ans après la découverte du Géant salifère.

Comme le lecteur a pu le comprendre à la lecture de ce mémoire, le Promontoire des Baléares offre une opportunité unique à exploiter et à privilégier dans les futures études offshore, grâce

à sa position stratégique et à l'excellente préservation de ses évaporites. Les résultats et les conclusions de mon étude sur ce promontoire proviennent principalement d'observations réalisées par des méthodes " indirectes ". Pour prouver certaines suppositions déduites de ces observations indirectes et ainsi renforcer l'importance des implications de mes résultats, un accès direct aux évaporites messiniennes par des forages est absolument nécessaire dans la région. Une série de forages couvrant un transect marginal-intermédiaire-profond serait idéale et permettrait d'établir une corrélation temporelle et spatiale complète entre les dépôts des trois domaines, apportant ainsi les réponses à certaines des nombreuses questions encore posées par la crise MSC. Dans la figure 8.1 (phase des évaporites supérieures montrant l'ensemble des dépôts messiniens en place), je suggère un transect 'Balearo-Provençal' de forages qui couvre idéalement tous les domaines de dépôt, des bassins marginaux aux bassins profonds. Les échantillons récupérés à partir de ces forages fourniraient une foule d'avantages pour la problématique du MSC, parmi lesquels :

- Révéler la nature de la lithologie de l'ensemble de la succession MSC offshore, en particulier la "trilogie MSC" pour la première fois ;
- Résoudre la connectivité temporelle et spatiale entre les évaporites provenant de différents domaines de profondeur.
- Permettre de réaliser des analyses pétrographiques, paléontologiques et géochimiques directes qui fourniraient des réponses sur les conditions paléo-environnementales à chaque étape du MSC.

Ces dernières années, une initiative a été proposée pour lancer des forages IODP (International Ocean Drilling Program) dans plusieurs zones de la Méditerranée occidentale et orientale, y compris le Promontoire des Baléares, sous la direction d'experts de la communauté MSC. L'initiative a été baptisée DREAM (Deep Sea Record of Mediterranean Messinian Events ; voir Camerlenghi & Aloisi, 2020).

Entre-temps, une proposition, dirigée par Giovanni Aloisi, coordinateur du projet SaltGiant, visant à échantillonner certaines des évaporites MSC affleurant sur le plancher océanique de la Méditerranée à l'aide des robots sous-marins autonomes (ROV, AUV) ou habités (le Nautille) a été soumise. Je suis largement impliqué dans cette proposition pour laquelle j'ai étudié et proposé plusieurs sites potentiels où affleurent des évaporites de MSC de différents stades.

Ces propositions à l'échelle géographique de la Méditerranée sont néanmoins difficile à réaliser tant pour leur coût que leur mise en place pratique et d'autres demandes plus anciennes n'ont pas abouti. La mobilisation de la communauté scientifique autour de tels projets aidera à les voir aboutir un jour. En attendant, un projet alternatif de moindre ampleur pourrait se faire, limité au Promontoire Baléare: 1 seul forage sur la pente de Majorque pourrait atteindre les 3 unités BU3/UU, le sel et les unités BU1/PLG (figure 8.1). Un complément de sismique réflexion nécessaire à un forage ayant déjà été refusé par les autorités espagnoles suivant lois environnementales en action, un projet de demande par imagerie ' légère' style Sparker, ayant fait ses preuves quant à la problématique messinienne, pourrait éventuellement être proposé.

References

- Abdel-Fattah, M. (2014). Petrophysical characteristics of the Messinian Abu Madi Formation in the Baltim East and North fields, Offshore Nile Delta, Egypt. *Journal of Petroleum Geology*, 37. <https://doi.org/10.1111/jpg.12577>
- Acosta, J., Ancochea, E., Canals, M., Huertas, M. J., & Uchupi, E. (2004a). Early Pleistocene volcanism in the Emile Baudot Seamount, Balearic Promontory (western Mediterranean Sea). *Marine Geology*, 207(1–4), 247–257. <https://doi.org/10.1016/j.margeo.2004.04.003>
- Acosta, J., Ancochea, E., Canals, M., Huertas, M. J., & Uchupi, E. (2004b). Early Pleistocene volcanism in the Emile Baudot Seamount, Balearic Promontory (western Mediterranean Sea). *Marine Geology*, 207. <https://doi.org/10.1016/j.margeo.2004.04.003>
- Acosta, J., Canals, M., Carbó, A., Muñoz, A., Urgeles, R., Muñoz-Martín, A., & Uchupi, E. (2004a). Sea floor morphology and Plio-Quaternary sedimentary cover of the Mallorca Channel, Balearic Islands, western Mediterranean. *Marine Geology*, 206(1–4), 165–179. <https://doi.org/10.1016/j.margeo.2004.02.008>
- Acosta, J., Canals, M., Carbó, A., Muñoz, A., Urgeles, R., Muñoz-Martín, A., & Uchupi, E. (2004b). Sea floor morphology and Plio-Quaternary sedimentary cover of the Mallorca Channel, Balearic Islands, western Mediterranean. *Marine Geology*, 206(1–4), 165–179. <https://doi.org/10.1016/j.margeo.2004.02.008>
- Acosta, J., Canals, M., López-Martínez, J., Muñoz, A., Herranz, P., Urgeles, R., Palomo, C., & Casamor, J. L. (2003). The Balearic Promontory geomorphology (western Mediterranean): Morphostructure and active processes. *Geomorphology*, 49(3–4), 177–204. [https://doi.org/10.1016/S0169-555X\(02\)00168-X](https://doi.org/10.1016/S0169-555X(02)00168-X)
- Acosta, J., Fontán, A., Muñoz, A., Muñoz-Martín, A., Rivera, J., & Uchupi, E. (2013). The morpho-tectonic setting of the Southeast margin of Iberia and the adjacent oceanic Algero-Balearic Basin. *Marine and Petroleum Geology*, 45, 17–41. <https://doi.org/10.1016/j.marpetgeo.2013.04.005>

- Acosta, J., Muñoz, A., Herranz, P., Palomo, C., Ballesteros, M., Vaquero, M., & Uchupi, E. (2001a). Geodynamics of the Emile Baudot Escarpment and the Balearic Promontory, western Mediterranean. *Marine and Petroleum Geology*, *18*, 00003–00004.
- Acosta, J., Muñoz, A., Herranz, P., Palomo, C., Ballesteros, M., Vaquero, M., & Uchupi, E. (2001b). Geodynamics of the Emile Baudot Escarpment and the Balearic Promontory, western Mediterranean. *Marine and Petroleum Geology*, *18*(3), 349–369. [https://doi.org/10.1016/S0264-8172\(01\)00003-4](https://doi.org/10.1016/S0264-8172(01)00003-4)
- Acosta, J., Muñoz, A., P., H., C., P., Ballesteros, M., M., V., & E., U. (2001). Pockmarks in the Ibiza Channel and Western end of the Balearic Promontory (Western Mediterranean) revealed by multibeam mapping. *Geo-Marine Letters*, *21*, 123–130. <https://doi.org/10.1007/s003670100074>
- Albanese, C., & Sulli, A. (2012). Backthrusts and passive roof duplexes in fold-and-thrust belts: The case of Central-Western Sicily based on seismic reflection data. *Tectonophysics*, *s 514–517*, 180–198. <https://doi.org/10.1016/j.tecto.2011.11.002>
- Alfaro, P., Delgado, J., Estévez, A., Soria, J. M., & Yébenes, A. (2002). Onshore and offshore compressional tectonics in the eastern Betic Cordillera (SE Spain). *Marine Geology - MAR GEOLOGY*, *186*, 337–349. [https://doi.org/10.1016/S0025-3227\(02\)00336-5](https://doi.org/10.1016/S0025-3227(02)00336-5)
- Alfaro, P., DELGADO, J., Garcia-Tortosa, F., Lenti, L., J.A., L., López-Casado, C., & Martino, S. (2012). Widespread landslides induced by the Mw 5.1 earthquake of 11 May 2011 in Lorca, SE Spain. *Engineering Geology*, *s 137–138*, 40–52. <https://doi.org/10.1016/j.enggeo.2012.04.002>
- Alonso-Zarza, A. M. (2003). Palaeoenvironmental significance of palustrine carbonates and calcretes in the geological record. *Earth-Science Reviews*, *60*(3), 261–298. [https://doi.org/10.1016/S0012-8252\(02\)00106-X](https://doi.org/10.1016/S0012-8252(02)00106-X)
- Alvarez, W. (1972). Rotation of the Corsica–Sardinia Microplate. *Nature Physical Science*, *235*(58), 103–105. <https://doi.org/10.1038/physci235103a0>
- Amadori, C., Garcia-Castellanos, D., Toscani, G., Sternai, P., Fantoni, R., Ghielmi, M., & Giulio, A. D. (2018). Restored topography of the Po Plain-Northern Adriatic region during the Messinian base-level drop—Implications for the physiography and

compartmentalization of the palaeo-Mediterranean basin. *Basin Research*, 30(6), 1247–1263. <https://doi.org/10.1111/bre.12302>

- Andreetto, F., Aloisi, G., Raad, F., Heida, H., Flecker, R., Agiadi, K., Lofi, J., Blondel, S., Bulian, F., & Camerlenghi, A. (2021). Freshening of the Mediterranean Salt Giant: Controversies and certainties around the terminal (Upper Gypsum and Lago-Mare) phases of the Messinian Salinity Crisis. *Earth-Science Reviews*, 103577.
- Andreetto, F., Aloisi, G., Raad, F., Heida, H., Flecker, R., Agiadi, K., Lofi, J., Blondel, S., Bulian, F., Camerlenghi, A., Caruso, A., Ebner, R., Garcia-Castellanos, D., Gaullier, V., Guibourdenche, L., Gvirtzman, Z., Hoyle, T. M., Meijer, P. T., Moneron, J., ... Krijgsman, W. (2021). Freshening of the Mediterranean Salt Giant: Controversies and certainties around the terminal (Upper Gypsum and Lago-Mare) phases of the Messinian Salinity Crisis. *Earth-Science Reviews*, 216, 103577. <https://doi.org/10.1016/j.earscirev.2021.103577>
- Andreetto, F., Matsubara, K., Beets, C. J., Fortuin, A. R., Flecker, R., & Krijgsman, W. (2020a). High Mediterranean water-level during the Lago-Mare phase of the Messinian Salinity Crisis: Insights from the Sr isotope records of Spanish marginal basins (SE Spain). *Palaeogeography, Palaeoclimatology, Palaeoecology*, 562, 110139. <https://doi.org/10.1016/j.palaeo.2020.110139>
- Andreetto, F., Matsubara, K., Beets, C. J., Fortuin, A. R., Flecker, R., & Krijgsman, W. (2020b). High Mediterranean water-level during the Lago-Mare phase of the Messinian Salinity Crisis: Insights from the Sr isotope records of Spanish marginal basins (SE Spain). *Palaeogeography, Palaeoclimatology, Palaeoecology*, 110139. <https://doi.org/10.1016/j.palaeo.2020.110139>
- Arenas, C., & Pomar, L. (2010). Microbial deposits in upper Miocene carbonates, Mallorca, Spain. *Palaeogeography, Palaeoclimatology, Palaeoecology*, 297(2), 465–485. <https://doi.org/10.1016/j.palaeo.2010.08.030>
- Arnon, A., Selker, J. S., & Lensky, N. G. (2016). Thermohaline stratification and double diffusion diapycnal fluxes in the hypersaline Dead Sea. *Limnology and Oceanography*, 61(4), 1214–1231. <https://doi.org/10.1002/lno.10285>
- Artiaga, D., García-Veigas, J., Cendón, D. I., Atalar, C., & Gibert, L. (2021). The Messinian evaporites of the Mesaoria basin (North Cyprus): A discrepancy with the current

chronostratigraphic understanding. *Palaeogeography, Palaeoclimatology, Palaeoecology*, 584, 110681. <https://doi.org/10.1016/j.palaeo.2021.110681>

- Attoh, K., Brown, L., & Haenlein, J. (2005). The role of Pan-African structures in intraplate seismicity near the termination of the Romanche fracture zone, West Africa. *Journal of African Earth Sciences*, 43(5), 549–555. <https://doi.org/10.1016/j.jafrearsci.2005.09.006>
- Auzende, J. M., Olivet, J. L., & Bonnin, J. (1972). Une structure compressive au nord de l'Algérie? *Deep Sea Research and Oceanographic Abstracts*, 19(2), 149–155. [https://doi.org/10.1016/0011-7471\(72\)90047-2](https://doi.org/10.1016/0011-7471(72)90047-2)
- Babel, M. (2007). *Depositional environments of a salina-type evaporite basin recorded in the Badenian gypsum facies in the northern Carpathian Foredeep*. <https://doi.org/10.1144/SP285.7>
- Babel, M., & Schreiber, B. (2014). Geochemistry of Evaporites and Evolution of Seawater. In *Treatise on Geochemistry: Second Edition* (Vol. 9, pp. 483–560). <https://doi.org/10.1016/B978-0-08-095975-7.00718-X>
- Bache, F., Gargani, J., Suc, J.-P., Gorini, C., Rabineau, M., Popescu, S.-M., Leroux, E., Couto, D. D., Jouannic, G., Rubino, J.-L., Olivet, J.-L., Clauzon, G., Dos Reis, A. T., & Aslanian, D. (2015). Messinian evaporite deposition during sea level rise in the Gulf of Lions (Western Mediterranean). *Marine and Petroleum Geology*, 66, Part 1, 262–277. <https://doi.org/10.1016/j.marpetgeo.2014.12.013>
- Bache, F., Olivet, J. L., Gorini, C., Rabineau, M., Baztan, J., Aslanian, D., & Suc, J. P. (2009a). Messinian erosional and salinity crises: View from the Provence Basin (Gulf of Lions, Western Mediterranean). *Earth and Planetary Science Letters*, 286(1–2), 139–157. <https://doi.org/10.1016/j.epsl.2009.06.021>
- Bache, F., Olivet, J. L., Gorini, C., Rabineau, M., Baztan, J., Aslanian, D., & Suc, J.-P. (2009b). Messinian erosional and salinity crises: View from the Provence Basin (Gulf of Lions, Western Mediterranean). *Earth and Planetary Science Letters*, 286(1–2), 139–157. <https://doi.org/10.1016/j.epsl.2009.06.021>
- Bache, F., Popescu, S.-M., Rabineau, M., Gorini, C., Suc, J.-P., Clauzon, G., Olivet, J.-L., Rubino, J.-L., Melinte-Dobrinescu, M. C., & Estrada, F. (2012). A two-step process for the

reflooding of the Mediterranean after the Messinian Salinity Crisis. *Basin Research*, 24(2), 125–153.

- Badji, R., Charvis, P., Bracene, R., Galve, A., Badsì, M., Ribodetti, A., Benaissa, Z., Klingelhofer, F., Medaouri, M., & Beslier, M.-O. (2015). Geophysical evidence for a transform margin offshore Western Algeria: A witness of a subduction-transform edge propagator? *Geophysical Journal International*, 200(2), 1029–1045. <https://doi.org/10.1093/gji/ggu454>
- Bailey, J. V., Orphan, V. J., Joye, S. B., & Corsetti, F. A. (2009). Chemotrophic microbial mats and their potential for preservation in the rock record. *Astrobiology*, 9(9), 843–859. <https://doi.org/10.1089/ast.2008.0314>
- Bakker, P. (2002). *Image structure analysis for seismic interpretation*. Citeseer.
- Balaguer, P., & Fornós, J. J. (2003). Erosive processes at Eastern Mallorca seacliffs (Illes Balears, western Mediterranean): Evaluation of erosion rates by granular disgregation, Preliminary data. *Bolleti de La Societat d'Historia Natural de Les Balears*, 46.
- Bannikov, A. F., Werner, S., & Carnevale, G. (2018). Neogene Paratethyan croakers (Teleostei, Sciaenidae). *Rivista Italiana Di Paleontologia e Stratigrafia*, 124(3), 535–571.
- Barceló-Llull, B., Pascual, A., Ruiz, S., Escudier, R., Torner, M., & Tintoré, J. (2019). Temporal and Spatial Hydrodynamic Variability in the Mallorca Channel (Western Mediterranean Sea) From 8 Years of Underwater Glider Data. *Journal of Geophysical Research: Oceans*, 124(4), 2769–2786. <https://doi.org/10.1029/2018JC014636>
- Baron, A., & Gonzalez, C. (1985). Correlation and geometry of the Messinian facies on the oriental edge of the Palma plain (Island of Mallorca). *6th European Regional Meeting Lleida (5 Pp., April)*.
- Bartrina, M. T., Cabrera, L., Jurado, M. J., Guimerà, J., & Roca, E. (1992). Evolution of the central Catalan margin of the Valencia trough (western Mediterranean). *Tectonophysics*, 203(1–4), 219–247. [https://doi.org/10.1016/0040-1951\(92\)90225-U](https://doi.org/10.1016/0040-1951(92)90225-U)
- Basile, C., Maillard, A., Patriat, M., Gaullier, V., Loncke, L., Roest, W., Mercier de Lépinay, M., & Pattier, F. (2013). Structure and evolution of the Demerara Plateau, offshore French Guiana: Rifting, tectonic inversion and post-rift tilting at transform–

- divergent margins intersection. *Tectonophysics*, 591, 16–29. <https://doi.org/10.1016/j.tecto.2012.01.010>
- Bellucci, M., Pellen, R., Leroux, E., Bache, F., Garcia, M., Do Couto, D., Raad, F., Blondel, S., Rabineau, M., Gorini, C., Moulin, M., Maillard, A., Lofi, J., Del Ben, A., Camerlenghi, A., Poort, J., & Aslanian, D. (2021a). *A comprehensive and updated compilation of the seismic stratigraphy markers in the Western Mediterranean Sea* [Data set]. SEANO. <https://doi.org/10.17882/80128>
 - Bellucci, M., Pellen, R., Leroux, E., Bache, F., Garcia, M., Do Couto, D., Raad, F., Blondel, S., Rabineau, M., Gorini, C., Moulin, M., Maillard, A., Lofi, J., Del Ben, A., Camerlenghi, A., Poort, J., & Aslanian, D. (2021b). *A comprehensive and updated compilation of the seismic stratigraphy markers in the Western Mediterranean Sea* [Data set]. SEANO. <https://doi.org/10.17882/80128>
 - Benedicto, A., Guerrero, E. R., Ponsatí, A. C., Montserrat, F. S., & Périz, A. B. (1993). Evolución tectonosedimentaria de la cubeta neógena de Inca (Mallorca). *Revista de la Sociedad Geológica de España*, 6(1–2), 167–176.
 - Benkhelil, J., Mascle, J., & Tricart, P. (1995). The Guinea continental margin: An example of a structurally complex transform margin. *Tectonophysics*, 248(1), 117–137. [https://doi.org/10.1016/0040-1951\(94\)00246-6](https://doi.org/10.1016/0040-1951(94)00246-6)
 - Bertoni, C., & Cartwright, J. A. (2005). 3D seismic analysis of circular evaporite dissolution structures, Eastern Mediterranean. *Journal of the Geological Society*, 162(6), 909–926. <https://doi.org/10.1144/0016-764904-126>
 - Bertoni, C., & Cartwright, J. A. (2006). Controls on the basinwide architecture of late Miocene (Messinian) evaporites on the Levant margin (Eastern Mediterranean). *Sedimentary Geology*, 188–189, 93–114. <https://doi.org/10.1016/j.sedgeo.2006.03.019>
 - Bertoni, C., & Cartwright, J. A. (2007). Major erosion at the end of the Messinian Salinity Crisis: Evidence from the Levant Basin, Eastern Mediterranean. *Basin Research*, 19(1), 1–18. <https://doi.org/10.1111/j.1365-2117.2006.00309.x>
 - Bessis, F. (1986a). Some remarks on the study of subsidence of sedimentary basins Application to the Gulf of Lions margin (Western Mediterranean). *Marine and Petroleum Geology*, 3(1), 37–63. [https://doi.org/10.1016/0264-8172\(86\)90055-3](https://doi.org/10.1016/0264-8172(86)90055-3)

- Bessis, F. (1986b). Some remarks on the study of subsidence of sedimentary basins Application to the Gulf of Lions margin (Western Mediterranean). *Marine and Petroleum Geology*, 3(1), 37–63. [https://doi.org/10.1016/0264-8172\(86\)90055-3](https://doi.org/10.1016/0264-8172(86)90055-3)
- Betzler, C., Braga, J. C., Jaramillo-Vogel, D., Römer, M., Hübscher, C., Schmiedl, G., & Lindhorst, S. (2011). Late Pleistocene and Holocene cool-water carbonates of the Western Mediterranean Sea. *Sedimentology*, 58(3), 643–669. <https://doi.org/10.1111/j.1365-3091.2010.01177.x>
- Bigi, D., Lugli, S., Manzi, V., & Roveri, M. (2022). Are fluid inclusions in gypsum reliable paleoenvironmental indicators? An assessment of the evidence from the Messinian evaporites. *Geology*. <https://doi.org/10.1130/G49475.1>
- Blanc, P. L. (2000). Of sills and straits: A quantitative assessment of the Messinian Salinity Crisis. *Deep-Sea Research Part I: Oceanographic Research Papers*, 47(8), 1429–1460. [https://doi.org/10.1016/S0967-0637\(99\)00113-2](https://doi.org/10.1016/S0967-0637(99)00113-2)
- Blanc, P. L. (2002). The opening of the plio-quadernary gibraltar strait: Assessing the size of a cataclysm. *Geodinamica Acta*, 15(5–6), 303–317. <https://doi.org/10.1080/09853111.2002.10510763>
- Blanc, P. L. (2006a). Improved modelling of the Messinian Salinity Crisis and conceptual implications. *Palaeogeography, Palaeoclimatology, Palaeoecology*, 238(1–4), 349–372. <https://doi.org/10.1016/j.palaeo.2006.03.033>
- Blanc, P. L. (2006b). Improved modelling of the Messinian Salinity Crisis and conceptual implications. *Palaeogeography, Palaeoclimatology, Palaeoecology*, 238(1–4), 349–372. <https://doi.org/10.1016/j.palaeo.2006.03.033>
- Blanc, P.-L. (2002). The opening of the Plio-Quaternary Gibraltar Strait: Assessing the size of a cataclysm. *Geodinamica Acta*, 15.
- Blanc-Valleron, M.-M., Pierre, C., Caulet, J. P., Caruso, A., Rouchy, J.-M., Cespuglio, G., Sprovieri, R., Pestrea, S., & Di Stefano, E. (2002). Sedimentary, stable isotope and micropaleontological records of paleoceanographic change in the Messinian Tripoli Formation (Sicily, Italy). *Palaeogeography, Palaeoclimatology, Palaeoecology*, 185(3), 255–286. [https://doi.org/10.1016/S0031-0182\(02\)00302-4](https://doi.org/10.1016/S0031-0182(02)00302-4)

- Blondel, S., Camerlenghi, A., Ben, A., Raad, F., & Lofi, J. (2020, May 3). *Improved imaging of Late Miocene (Messinian) to Plio-Quaternary units in the Algero-Balearic basin*. European Geosciences Union (EGU) general assembly. <https://doi.org/10.5194/egusphere-egu2020-13769>
- Bonaduce, G., & Sgarrella, F. (1999). Paleocological interpretation of the latest Messinian sediments from southern Sicily (Italy). *Memorie Della Società Geologica Italiana*, 54, 83–91.
- Bonanni, D. M. (2018). *The Messinian Salinity Crisis. The Mystery Of Vanished Sea—Special Volume*. Calameo.Com. <https://www.calameo.com/books/005189853f97dfded4cba>
- Booth-Rea, G., Hernández, J. M. A., García, F. J. R., Moragues, L., Peña, J. V. P., & Ruiz, R. M. M. (2016). WSW-ENE extension in Mallorca, key for integrating the Balearic Promontory in the Miocene tectonic evolution of the western Mediterranean. *Geotemas (Madrid)*, 16, 81–84.
- Booth-Rea, G., Moragues, L., Azañón, J. M., Roldán, F. J., & Pérez-Peña, J. V. (2017). *SW-NE extensional low-angle faults in Mallorca, key for integrating the Balearic Promontory in the Miocene tectonic evolution of the western Mediterranean*. 12817.
- Bouillin, J.-P., Durand-delga, M., & Olivier, Ph. (1986). Betic-Rifian and Tyrrhenian Arcs: Distinctive Features, Genesis and Development Stages. In F.-C. Wezel (Ed.), *Developments in Geotectonics* (Vol. 21, pp. 281–304). Elsevier. <https://doi.org/10.1016/B978-0-444-42688-8.50017-5>
- Bourillot, R., Vennin, E., Rouchy, J. M., Blanc-Valleron, M. M., Caruso, A., & Durllet, C. (2010). The end of the Messinian Salinity Crisis in the western Mediterranean: Insights from the carbonate platforms of south-eastern Spain. *Sedimentary Geology*, 229(4), 224–253. <https://doi.org/10.1016/j.sedgeo.2010.06.010>
- Bourillot, R., Vennin, E., Rouchy, J. M., Durllet, C., Rommevaux, V., Kolodka, C., & Knap, F. (2009). Structure and evolution of a Messinian mixed carbonate-siliciclastic platform: The role of evaporites (Sorbas Basin, South-east Spain). *Sedimentology*, 57(2), 477–512. <https://doi.org/10.1111/j.1365-3091.2009.01092.x>

- Bourillot, R., Vennin, E., Rouchy, J.-M., Durllet, C., Rommevaux, V., Kolodka, C., & Knap, F. (2010). Structure and evolution of a Messinian mixed carbonate-siliciclastic platform: The role of evaporites (Sorbas Basin, South-east Spain). *Sedimentology*, 57(2), 477–512.
- Bourrouilh, R. (1970). Le probleme de Minorque et des Sierras de Levante de Majorque. *Extr. ANN. SOCo GEOL. DU NORD*, 90, 363–380.
- Bourrouilh, R. (1973). *Stratigraphie, sédimentologie et tectonique de l'île de Minorque et du Nord-Est de Majorque (Baléares. La terminaison nord-orientale des Corfillères bétiques en Méditerranée occidentale)*. Université de Paris.
- Bourrouilh, R. (1983). *Estratigrafia, sedimentologia y tectonica de la isla de Menorca y del noreste de Mallorca (Baleares): La terminacion nororiental de las cordilleras beticas en el mediterraneo occidental*. IGME.
- Bousquet, J.-C. (1979). Quaternary strike-slip faults in southeastern Spain. *Tectonophysics*, 52(1), 277–286. [https://doi.org/10.1016/0040-1951\(79\)90232-4](https://doi.org/10.1016/0040-1951(79)90232-4)
- BOUTET, C., Y, R., P, R., H, V., & M, D. D. (1982). DECOUVERTE D'UNE MICROFLORE D'AGE NORIEN DANS LA SIERRA NORTE DE MAJORQUE (BALEARES, ESPAGNE). *DECOUVERTE D'UNE MICROFLORE D'AGE NORIEN DANS LA SIERRA NORTE DE MAJORQUE (BALEARES, ESPAGNE)*.
- Bove, C., Sàbat, F., Roca, E., Muñoz, J., Vergés, J., Sans, M. R., Masana, E., Santanach, P., & Estévez, A. (1994). Role of extension and compression in the evolution of the eastern margin of Iberia: The ESCI-Valencia Trough seismic profile. *Sàbat, F.; Roca, E.; Muñoz, J.A.; Vergés, J.; Sans, M.; Masana, E.; Santanach, P.; Estévez, A. and Santisteban, C. Role of Extension and Compression in the Evolution of the Eastern Margin of Iberia: The ESCI-València Trough Seismic Profile. En Revista de La Sociedad Geológica de España, Vol. 8 (4) 1994., 8.*
- Bowman, S. A. (2012). A comprehensive review of the MSC facies and their origins in the offshore Sirt Basin, Libya. *Petroleum Geoscience*, 18(4), 457–469. <https://doi.org/10.1144/petgeo2011-070>
- Bulian, F., Sierro, F. J., Ledesma, S., Jiménez-Espejo, F. J., & Bassetti, M.-A. (2021a). Messinian West Alboran Sea record in the proximity of Gibraltar: Early signs of Atlantic-

- Mediterranean gateway restriction. *Marine Geology*, 434, 106430. <https://doi.org/10.1016/j.margeo.2021.106430>
- Bulian, F., Sierro, F. J., Ledesma, S., Jiménez-Espejo, F. J., & Bassetti, M.-A. (2021b). Messinian West Alboran Sea record in the proximity of Gibraltar: Early signs of Atlantic-Mediterranean gateway restriction. *Marine Geology*, 434, 106430. <https://doi.org/10.1016/j.margeo.2021.106430>
 - Burgess, P. M., Winefield, P., Minzoni, M., & Elders, C. (2013). Methods for identification of isolated carbonate buildups from seismic reflection data. *AAPG Bulletin*, 97(7), 1071–1098. <https://doi.org/10.1306/12051212011>
 - Burollet, P. F., Said, A., & Trouve, P. (1978). Slim holes drilled on the Algerian shelf. *Initial Reports of Deep Sea Drilling Project, Government Press*(D. A. Ross and Y. P. Neprocnov), 1181–1184.
 - Burov, E. B., & Diament, M. (1992). Flexure of the continental lithosphere with multilayered rheology. *Geophysical Journal International*, 109(2), 449–468. <https://doi.org/10.1111/j.1365-246X.1992.tb00107.x>
 - Burov, E. B., & Diament, M. (1995). The effective elastic thickness (T_e) of continental lithosphere: What does it really mean? *Journal of Geophysical Research*. <https://doi.org/10.1029/94JB02770>
 - Burrus, J. (1984). Contribution to a geodynamic synthesis of the Provençal Basin (North-Western Mediterranean). *Marine Geology*, 55, 247–269.
 - Butler, R. W. H., & LICKORISH, W. (1997). Using high-resolution stratigraphy to date fold and thrust activity: Examples from the Neogene of south-central Sicily. *Journal of The Geological Society - J GEOL SOC*, 154, 633–643. <https://doi.org/10.1144/gsjgs.154.4.0633>
 - Butler, R. W. H., Lickorish, W. H., Grasso, M., Pedley, H. M., & Ramberti, L. (1995). Tectonics and sequence stratigraphy in Messinian basins, Sicily: Constraints on the initiation and termination of the Mediterranean salinity crisis. *GSA Bulletin*, 107(4), 425–439. [https://doi.org/10.1130/0016-7606\(1995\)107<0425:TASSIM>2.3.CO;2](https://doi.org/10.1130/0016-7606(1995)107<0425:TASSIM>2.3.CO;2)
 - Butler, R. W. H., McClelland, E., & Jones, R. E. (1999). Calibrating the duration and timing of the Messinian salinity crisis in the Mediterranean: Linked tectonoclimatic signals in

thrust-top basins of Sicily. *Journal of the Geological Society*, 156. <https://doi.org/10.1144/gsjgs.156.4.0827>

- Calaforra, J. M., dell’Aglia, A., & Forti, P. (1993). Preliminary data on the chemical corrosion in gypsum karst: 1-The Sorbas region (Spain). *XI International Congress of Speleology*, 77–99.
- Camerlenghi, A., Accettella, D., Costa, S., Lastras, G., Acosta, J., Canals, M., & Wardell, N. (2009a). Morphogenesis of the SW Balearic continental slope and adjacent abyssal plain, Western Mediterranean Sea. *International Journal of Earth Sciences*, 98(4), 735–750. <https://doi.org/10.1007/s00531-008-0354-8>
- Camerlenghi, A., Accettella, D., Costa, S., Lastras, G., Acosta, J., Canals, M., & Wardell, N. (2009b). Morphogenesis of the SW Balearic continental slope and adjacent abyssal plain, Western Mediterranean Sea. *International Journal of Earth Sciences*, 98(4), 735–750. <https://doi.org/10.1007/s00531-008-0354-8>
- Camerlenghi, A., & Aloisi, V. (2020). Uncovering the Mediterranean Salt Giant (MEDSALT)—Scientific Networking as Incubator of Cross-disciplinary Research in Earth Sciences. *European Review*, 28(1), 40–61.
- Camerlenghi, A., Ben, A. D., Hübscher, C., Forlin, E., Geletti, R., Brancatelli, G., Micallef, A., Saule, M., & Facchin, L. (2019, August 22). *Seismic markers of the Messinian salinity crisis in the deep Ionian Basin*. Basin Research. <https://doi.org/10.1111/bre.12392>
- Cameselle, A. L. (2015). *Sedimentary processes and resulting continental margin configuration during large-scale sea-level drawdown: The Messinian Salinity Crisis in the Western Mediterranean Sea* (Issue November).
- Cameselle, A. L., & Urgeles, R. (2017a). Large-scale margin collapse during Messinian early sea-level drawdown: The SW Valencia trough, NW Mediterranean. *Basin Research*, 29(S1), 576–595. <https://doi.org/10.1111/bre.12170>
- Cameselle, A. L., & Urgeles, R. (2017b). Large-scale margin collapse during Messinian early sea-level drawdown: The SW Valencia trough, NW Mediterranean. *Basin Research*, 29, 576–595. <https://doi.org/10.1111/bre.12170>
- Cameselle, A. L., Urgeles, R., De Mol, B., Camerlenghi, A., & Canning, J. C. (2014). Late Miocene sedimentary architecture of the Ebro Continental Margin (Western

Mediterranean): Implications to the Messinian Salinity Crisis. *International Journal of Earth Sciences*, 103(2), 423–440. <https://doi.org/10.1007/s00531-013-0966-5>

- Canas, J. A., & Pujades, L. G. (1992). The Valencia trough: Coda-Q. *Tectonophysics*, 203(1), 125–132. [https://doi.org/10.1016/0040-1951\(92\)90219-V](https://doi.org/10.1016/0040-1951(92)90219-V)
- Capó, A., & Garcia, C. (2019a). Basin filling evolution of the central basins of Mallorca since the Pliocene. *Basin Research*, 31(5), 948–966. <https://doi.org/10.1111/bre.12352>
- Capó, A., & Garcia, C. (2019b). Basin filling evolution of the central basins of Mallorca since the Pliocene. *Basin Research*, 31(5), 948–966. <https://doi.org/10.1111/bre.12352>
- Carballo, A., Fernandez, M., Jiménez-Munt, I., Torne, M., Vergés, J., Melchiorre, M., Pedreira, D., Afonso, J. C., Garcia-Castellanos, D., Díaz, J., Villaseñor, A., Pulgar, J. A., & Quintana, L. (2015). From the North-Iberian Margin to the Alboran Basin: A lithosphere geo-transect across the Iberian Plate. *Tectonophysics*, 663, 399–418. <https://doi.org/10.1016/j.tecto.2015.07.009>
- Carballo, A., Fernandez, M., Torne, M., Jiménez-Munt, I., & Villaseñor, A. (2015). Thermal and petrophysical characterization of the lithospheric mantle along the northeastern Iberia geo-transect. *Gondwana Research*, 27(4), 1430–1445. <https://doi.org/10.1016/j.gr.2013.12.012>
- Carminati, E., Lustrino, M., & Doglioni, C. (2012). Geodynamic evolution of the central and western Mediterranean: Tectonics vs. Igneous petrology constraints. *Tectonophysics*, 579, 173–192. <https://doi.org/10.1016/j.tecto.2012.01.026>
- Carminati, E., Wortel, M. J. R., Meijer, P. T., & Sabadini, R. (1998). The two-stage opening of the western-central Mediterranean basins: A forward modeling test to a new evolutionary model. *Earth and Planetary Science Letters*, 160(3–4), 667–679. [https://doi.org/10.1016/S0012-821X\(98\)00119-8](https://doi.org/10.1016/S0012-821X(98)00119-8)
- Caruso, A., Blanc-Valleron, M.-M., Da Prato, S., Pierre, C., & Rouchy, J. M. (2020). The late Messinian “Lago-Mare” event and the Zanclean Reflooding in the Mediterranean Sea: New insights from the Cuevas del Almanzora section (Vera Basin, South-Eastern Spain). *Earth-Science Reviews*, 200, 102993. <https://doi.org/10.1016/j.earscirev.2019.102993>
- Caruso, A., Pierre, C., Blanc-Valleron, M.-M., & Rouchy, J. M. (2015). Carbonate deposition and diagenesis in evaporitic environments: The evaporative and sulphur-bearing

limestones during the settlement of the Messinian Salinity Crisis in Sicily and Calabria. *Palaeogeography, Palaeoclimatology, Palaeoecology*, 429, 136–162. <https://doi.org/10.1016/j.palaeo.2015.03.035>

- Caruso, A., & Rouchy, J.-M. (2006). The Upper Gypsum unit. In: In: Roveri, M. (Ed.), Post-Congress FieldTrip of the RCMNS Interim Colloquium. *Acta Naturalia de "L'Ateneo Parmense*, 42, 157–168.
- Casas, J. M., & Sàbat, F. (1987). An example of three-dimensional analysis of thrust-related tectonites. *Journal of Structural Geology*, 9, 647–657. [https://doi.org/10.1016/0191-8141\(87\)90149-0](https://doi.org/10.1016/0191-8141(87)90149-0)
- Catalano, R., & D'argenio, B. (1982). Guida alla geologia della Sicilia occidentale. *Società Geologica Italiana*, 0–155.
- Catalano, R., Di Stefano, P., Sulli, A., & Vitale, F. P. (1996). Paleogeography and structure of the central Mediterranean: Sicily and its offshore area. *Tectonophysics*, 260, 291–323. [https://doi.org/10.1016/0040-1951\(95\)00196-4](https://doi.org/10.1016/0040-1951(95)00196-4)
- Catalano, R., Valenti, V., Albanese, C., Accaino, F., Sulli, A., Tinivella, U., Gasparo Morticelli, M., Zanolla, C., & Giustiniani, M. (2012). Sicily's fold-thrust belt and slab roll-back: The SI.RI.PRO. seismic crustal transect. *Journal of the Geological Society*, 170. <https://doi.org/10.1144/jgs2012-099>
- Cavazza, W., Roure, F., & Ziegler, P. A. (2004). The Mediterranean Area and the Surrounding Regions: Active Processes, Remnants of Former Tethyan Oceans and Related Thrust Belts. In W. Cavazza, F. Roure, W. Spakman, G. M. Stampfli, & P. A. Ziegler (Eds.), *The TRANSMED Atlas. The Mediterranean Region from Crust to Mantle: Geological and Geophysical Framework of the Mediterranean and the Surrounding Areas* (pp. 1–29). Springer. https://doi.org/10.1007/978-3-642-18919-7_1
- Cespedes, A., Giménez, J., & Sàbat, F. (2001). Caracterización del campo de esfuerzos neógenos en Majorca mediante el análisis de poblaciones de fallas. *Geogaceta*, 30, 199–202.
- CHUMAKOV, I. (1973). PLIOCENE AND PLEISTOCENE DEPOSITS OF THE NILE VALLEY IN NUBIA AND UPPER EGYPT. *PLIOCENE AND PLEISTOCENE DEPOSITS OF THE NILE VALLEY IN NUBIA AND UPPER EGYPT*.

- CIESM. (2008a). The Messinian salinity crisis from mega-deposits to microbiology. *Briand, F. (Ed.), A Consensus Report, in 33ème CIESM Workshop Monographs, 33., CIESM, 16, bd de Suisse, MC-98000, Monaco, 1–168.*
- CIESM. (2008b). The Messinian Salinity Crisis from mega-deposits to microbiology—A consensus report. In *CIESM Workshop Monographs* (CIESM Workshop Monographs, pp. 168–168).
- Cipollari, P., Cosentino, D., Radeff, G., Schildgen, T. F., Faranda, C., Grossi, F., Gliozzi, E., Smedile, A., Gennari, R., Darbas, G., Dudas, F. O., Gurbuz, K., Nazik, A., & Echtler, H. (2012). Easternmost Mediterranean evidence of the Zanclean flooding event and subsequent surface uplift: Adana Basin, southern Turkey. *Geological Society, London, Special Publications, 372, 473–494.* <https://doi.org/10.1144/sp372.5>
- Cita, M. B. (1973). Mediterranean evaporite; paleontological arguments for a deep-basin desiccation model. *Pages, 206228.* <https://eurekamag.com/research/018/284/018284469.php>
- Cita, M. B., Santambrogio, S., Melillo, B., & Rogate, F. (1990). 14. Messinian paleoenvironments: New evidence from the Tyrrhenian sea (ODP LEG 107). *Proc Ocean Drill Program, Sci Results, 107, 211–227.*
- CITA, M., & COLOMBO, L. (2006). Sedimentation in the latest Messinian at Capo Rosselo (Sicily). *Sedimentology, 26, 497–522.* <https://doi.org/10.1111/j.1365-3091.1979.tb00926.x>
- CITA, M., RC, W., WBF, R., & A, L. (1978). MESSINIAN PALEOENVIRONMENTS. *MESSINIAN PALEOENVIRONMENTS.*
- Clauzon, G. (1978). The Messinian Var canyon (Provence, southern France)—Paleogeographic implications. *Marine Geology, 27(3), 231–246.* [https://doi.org/10.1016/0025-3227\(78\)90033-6](https://doi.org/10.1016/0025-3227(78)90033-6)
- Clauzon, G., Suc, J. P., Couto, D. D., Jouannic, G., Melinte-Dobrinescu, M. C., Jolivet, L., Quillévéré, F., Leuret, N., Mocochain, L., Popescu, S. M., Martinell, J., Doménech, R., Rubino, J. L., Gumiaux, C., Warny, S., Bellas, S. M., Gorini, C., Bache, F., Rabineau, M., & Estrada, F. (2015a). New insights on the Sorbas Basin (SE Spain): The onshore reference

- of the Messinian Salinity Crisis. *Marine and Petroleum Geology*, 66, 71–100. <https://doi.org/10.1016/j.marpetgeo.2015.02.016>
- Clauzon, G., Suc, J. P., Couto, D. D., Jouannic, G., Melinte-Dobrinescu, M. C., Jolivet, L., Quillévéré, F., Lebret, N., Mocochain, L., Popescu, S. M., Martinell, J., Doménech, R., Rubino, J. L., Gumiaux, C., Warny, S., Bellas, S. M., Gorini, C., Bache, F., Rabineau, M., & Estrada, F. (2015b). New insights on the Sorbas Basin (SE Spain): The onshore reference of the Messinian Salinity Crisis. *Marine and Petroleum Geology*, 66, 71–100. <https://doi.org/10.1016/j.marpetgeo.2015.02.016>
 - Clauzon, G., Suc, J. P., Gautier, F., Berger, A., & Loutre, M. F. (1996a). Alternate interpretation of the Messinian salinity crisis: Controversy resolved? *Geology*, 24(4), 363–366. [https://doi.org/10.1130/0091-7613\(1996\)024<0363:AIOTMS>2.3.CO;2](https://doi.org/10.1130/0091-7613(1996)024<0363:AIOTMS>2.3.CO;2)
 - Clauzon, G., Suc, J.-P., Gautier, F., Berger, A., & Loutre, M.-F. (1996b). Alternate interpretation of the Messinian salinity crisis: Controversy resolved? *Geology*, 24(4), 363–366.
 - Clauzon, G., Suc, J.-P., Popescu, S.-M., Marunteanu, M., Rubino, J., Marinescu, F., & Melinte-Dobrinescu, M. (2005). Influence of Mediterranean sea-level changes on the Dacic Basin (Eastern Paratethys) during the late Neogene: The Mediterranean Lago Mare facies deciphered. *Basin Research*, 17, 437–462. <https://doi.org/10.1111/j.1365-2117.2005.00269.x>
 - Clavell, E., & Berastegui, X. (1991). Petroleum geology of the Gulf of Valencia. *Generation, Accumulation and Production of Europe's Hydrocarbons*, 7, 355–368.
 - Cloetingh, S., & Burov, E. B. (1996). Thermomechanical structure of European continental lithosphere: Constraints from rheological profiles and EET estimates. *Geophysical Journal International*, 124(3), 695–723. <https://doi.org/10.1111/j.1365-246X.1996.tb05633.x>
 - Cohen, C. R. (1980). Plate tectonic model for the oligo-miocene evolution of the western Mediterranean. *Tectonophysics*, 68(3), 283–311. [https://doi.org/10.1016/0040-1951\(80\)90180-8](https://doi.org/10.1016/0040-1951(80)90180-8)
 - Colom, G. (1980). Sobre la posible extensión del Aquitaniense marino a lo largo de las sierras de Levante de Mallorca. *Bolletí de La Societat d'Història Natural de Les Balears*, 7–14.

- Comas, M. C., Zahn, R., Klaus, A., Mascle, J., Lohmann, G. P., & Clift, P. D. (1996). Proceedings of the Ocean Drilling Program, Initial Reports. In *Proceedings of the Ocean Drilling Program, Initial Reports* (Vol. 161). Ocean Drilling Program. <https://doi.org/10.2973/odp.proc.ir.159.1996>
- Conesa, G., & Badinot, J. F. (1999). Early Messinian carbonate platforms from Sorbas Basin (SE Spain): Sedimentary setting, microfaunas and palaeoenvironments. *Revue de Micropaléontologie*, 42, 255–267.
- Cornée, J. J., Saint Martin, J. P., Conesa, G., Münch, P., André, J. P., Saint Martin, S., & Roger, S. (2004). Correlations and sequence stratigraphic model for Messinian carbonate platforms of the western and central Mediterranean. *International Journal of Earth Sciences*, 93(4), 621–633. <https://doi.org/10.1007/s00531-004-0400-0>
- Cornée, J.-J., Münch, P., Achalhi, M., Merzeraud, G., Azdimousa, A., Quillévéré, F., Melinte-Dobrinescu, M., Chaix, C., Moussa, A. B., Lofi, J., Séranne, M., & Moissette, P. (2016). The Messinian erosional surface and early Pliocene reflooding in the Alboran Sea: New insights from the Boudinar basin, Morocco. *Sedimentary Geology*, 333(Supplement C), 115–129. <https://doi.org/10.1016/j.sedgeo.2015.12.014>
- Cornée, J.-J., Saint Martin, J.-P., Conesa, G., Münch, P., André, J.-P., Saint Martin, S., & Roger, S. (2004). Correlations and sequence stratigraphic model for Messinian carbonate platforms of the western and central Mediterranean. *International Journal of Earth Sciences*, 93(4), 621–633. <https://doi.org/10.1007/s00531-004-0400-0>
- Cosentino, D., Buchwaldt, R., Sampalmieri, G., Iadanza, A., Cipollari, P., Schildgen, T. F., Hinnov, L. A., Ramezani, J., & Bowring, S. A. (2013). Refining the Mediterranean “Messinian gap” with high-precision U-Pb zircon geochronology, central and northern Italy. *Geology*, 41(3), 323–326. <https://doi.org/10.1130/G33820.1>
- Costanzo, A., Cipriani, M., Feely, M., Cianflone, G., & Dominici, R. (2019). Messinian twinned selenite from the Catanzaro Trough, Calabria, Southern Italy: Field, petrographic and fluid inclusion perspectives. *Carbonates and Evaporites*, 34(3), 743–756. <https://doi.org/10.1007/s13146-019-00516-0>
- Cravatte, J., Dufaure, P., Prim, M., & Rouaix, S. (1974). Les sondages du Golfe du Lion: Stratigraphie et sédimentologie. *Notes et Mémoires de La Compagnie Française Des Pétroles*.

- Crespo-Blanc, A., Comas, M., & Balanyá, J. (2016). Clues for a Tortonian reconstruction of the Gibraltar Arc: Structural pattern, deformation diachronism and block rotations. *Tectonophysics*, 683. <https://doi.org/10.1016/j.tecto.2016.05.045>
- Cuevas, F. (1958). Informe geológico y minero de los yacimientos de cobre de Banyalbufar y Valldemossa. *Mallorca. Informe Técnico, Inédito*.
- Cunningham, W. D., & Mann, P. (2007). *Tectonics of strike-slip restraining and releasing bends* | Geological Society, London, *Special Publications* (Special Publications, 290(1)). Geological Society, London. <https://sp.lyellcollection.org/content/290/1/1>
- Curzi, P., Fornos, J., ROSSI, P., SABAT, F., & MAUFFRET, A. (1985). The South-Balearic Margin (Menorca Rise): Objectives and preliminary results of the cruise Bal-84. *Rendiconti Della Società Geologica Italiana*, 8, 91–96.
- Dabrio, C. J., & Polo Camacho, M. D. (1995). Oscilaciones eustáticas de alta frecuencia en el Neógeno superior de Sorbas (Almería, sureste de España). *GeoActa*, 18, 75–78.
- Dal Cin, M., Del Ben, A., Mocnik, A., Accaino, F., Geletti, R., Wardell, N., Zgur, F., & Camerlenghi, A. (2016). Seismic imaging of Late Miocene (Messinian) evaporites from Western Mediterranean back-arc basins. *Petroleum Geoscience*, 22(4), 297–308. <https://doi.org/10.1144/petgeo2015-096>
- De Galdeano, C. S. (1990). Geologic evolution of the Betic Cordilleras in the Western Mediterranean, Miocene to the present. *Tectonophysics*, 172(1), 107–119. [https://doi.org/10.1016/0040-1951\(90\)90062-D](https://doi.org/10.1016/0040-1951(90)90062-D)
- De Lange, G. J., Boelrijk, N. A. I. M., Catalano, G., Corselli, C., Klinkhammer, G. P., Middelburg, J. J., Müller, D. W., Ullman, W. J., Van Gaans, P., & Woittiez, J. R. W. (1990). Sulphate-related equilibria in the hypersaline brines of the Tyro and Bannock Basins, eastern Mediterranean. *Marine Chemistry*, 31(1), 89–112. [https://doi.org/10.1016/0304-4203\(90\)90032-8](https://doi.org/10.1016/0304-4203(90)90032-8)
- de Lange, G. J., & Krijgsman, W. (2010a). Messinian salinity crisis: A novel unifying shallow gypsum/deep dolomite formation mechanism. *Marine Geology*, 275(1–4), 273–277.

- de Lange, G. J., & Krijgsman, W. (2010b). Messinian salinity crisis: A novel unifying shallow gypsum/deep dolomite formation mechanism. *Marine Geology*, 275(1–4), 273–277. <https://doi.org/10.1016/j.margeo.2010.05.003>
- de Neira, J. A. D., & Gil, J. (2009). Unidades litoestratigráficas del Cretácico de Ibiza (Islas Baleares, España). *Boletín de La Real Sociedad Española de Historia Natural (Sección Geológica)*, 103, 5–21.
- Decima, A. (1976). *INITIAL DATA ON THE BROMINE DISTRIBUTION IN THE MIOCENE SALT FORMATION OF SOUTHERN SICILY*. <http://pascal-francis.inist.fr/vibad/index.php?action=getRecordDetail&idt=PASCALGEODEBRGM7920049707>
- Decima, A., McKenzie, J. A., & Schreiber, B. C. (1988). The origin of “evaporitive” limestones; an example from the Messinian of Sicily (Italy). *Journal of Sedimentary Research*, 58(2), 256–272. <https://doi.org/10.1306/212F8D6E-2B24-11D7-8648000102C1865D>
- Decima, A., & Wezel, F. (1973a). *Late Miocene Evaporites of the Central Sicilian Basin, Italy*. <https://doi.org/10.2973/DSDP.PROC.13.144-1.1973>
- Decima, A., & Wezel, F. C. (1967). Late Miocene Evaporites of the Central Sicilian Basin, Italy. In *Deep Sea Drilling Project Initial Reports Volume 13* (pp. 1234–1256).
- Decima, A., & Wezel, F. C. (1971). Osservazioni sulle evaporiti messiniane della Sicilia centro-meridionale. *Rivista Mineraria Siciliana 130–134*, 172–187.
- Decima, A., & Wezel, F. C. (1973b). LATE MIOCENE EVAPORITES OF THE CENTRAL SICILIAN BASIN, ITALY. *LATE MIOCENE EVAPORITES OF THE CENTRAL SICILIAN BASIN, ITALY*.
- del Olmo, W. M. (2011a). The Messinian in the Gulf of Valencia and Alboran Sea (Spain): Paleogeography and paleoceanography implications. *Revista de la Sociedad Geológica de España*, 24, 22.
- del Olmo, W. M. (2011b). The Messinian reef of the core Torre Vieja Marino C-1 from the seismic lines (Mediterranean Sea, SE. of Spain). *Revista de la Sociedad Geológica de España*, 24 (3-4), 14.

- Dela Pierre, F., Bernardi, E., Cavagna, S., Clari, P., Gennari, R., Irace, A., Lozar, F., Lugli, S., Manzi, V., & Natalicchio, M. (2011). The record of the Messinian salinity crisis in the Tertiary Piedmont Basin (NW Italy): The Alba section revisited. *Palaeogeography, Palaeoclimatology, Palaeoecology*, 310(3–4), 238–255.
- Dela Pierre, F., Bernardi, E., Cavagna, S., Clari, P., Gennari, R., Irace, A., Lozar, F., Lugli, S., Manzi, V., Natalicchio, M., Roveri, M., & Violanti, D. (2011). The record of the Messinian salinity crisis in the Tertiary Piedmont Basin (NW Italy): The Alba section revisited. *Palaeogeography, Palaeoclimatology, Palaeoecology*, 310(3–4), 238–255. <https://doi.org/10.1016/j.palaeo.2011.07.017>
- Dela Pierre, F., Natalicchio, M., Ferrando, S., Giustetto, R., Birgel, D., Carnevale, G., Gier, S., Lozar, F., Marabello, D., & Peckmann, J. (2015). Are the large filamentous microfossils preserved in Messinian gypsum colorless sulfide-oxidizing bacteria? *Geology*, 43(10), 855–858. <https://doi.org/10.1130/G37018.1>
- Demets, C., Gordon, R., Argus, D., & Stein, S. (1990). Current Plate Motions. *Geophysical Journal International*, 101, 425–478. <https://doi.org/10.1111/j.1365-246X.1990.tb06579.x>
- Deplus, C., Diament, M., Hébert, H., Bertrand, G., Dominguez, S., Dubois, J., Malod, J., Patriat, P., Pontoise, B., & Sibilla, J.-J. (1998). Direct evidence of active deformation in the eastern Indian oceanic plate. *Geology*, 26(2), 131–134. [https://doi.org/10.1130/0091-7613\(1998\)026<0131:DEOADI>2.3.CO;2](https://doi.org/10.1130/0091-7613(1998)026<0131:DEOADI>2.3.CO;2)
- Déverchère, J., Yelles, K., Calais, E., Domzig, A., Gaullier, V., Kherroubi, A., de Lépinay, B., Roy, P., Pauc, H., & Savoye, B. (2003). *Active deformation along the Algerian margin (MARADJA cruise): Framework of the May 21, 2003, Mw-6-8 Boumerdes earthquake.*
- Déverchère, J., Yelles, K., Domzig, A., Mercier de Lépinay, B., Bouillin, J.-P., Gaullier, V., Bracène, R., Calais, E., Savoye, B., Kherroubi, A., Le Roy, P., Pauc, H., & Dan, G. (2005). Active thrust faulting offshore Boumerdes, Algeria, and its relations to the 2003 Mw 6.9 earthquake. *Geophysical Research Letters*, 32(4). <https://doi.org/10.1029/2004GL021646>
- Dewey, J. F., Helman, M. L., Knott, S. D., Turco, E., & Hutton, D. H. W. (1989). Kinematics of the western Mediterranean. *Geological Society, London, Special Publications*, 45(1), 265–283. <https://doi.org/10.1144/GSL.SP.1989.045.01.15>

- Díaz de Neira, J. A., & Gil-Gil, J. (2013). Ascription of the island of Ibiza to the Prebetic of Alicante (Betic Range, Spain) after correlation of Lower Cretaceous sedimentary successions. *Cretaceous Research*, 41, 194–209. <https://doi.org/10.1016/j.cretres.2012.12.007>
- Do Couto, D., Gumiaux, C., Jolivet, L., Augier, R., Le Bret, N., Folcher, N., Jouannic, G., Suc, J. P., & Gorini, C. (2015). 3D modelling of the Sorbas Basin (Spain): New constraints on the Messinian Erosional Surface morphology. *Marine and Petroleum Geology*, 66. <https://doi.org/10.1016/j.marpetgeo.2014.12.011>
- Doglioni, C., Gueguen, E., Sàbat, F., & Fernandez, M. (1997). The Western Mediterranean extensional basins and the Alpine orogen. *Terra Nova*, 9(3), 109–112. <https://doi.org/10.1046/j.1365-3121.1997.d01-18.x>
- Domzig, A., Yelles, K., Le Roy, C., Déverchère, J., Bouillin, J.-P., Bracène, R., Mercier de Lépinay, B., Le Roy, P., Calais, E., Kherroubi, A., Gaullier, V., Savoye, B., & Pauc, H. (2006). Searching for the Africa–Eurasia Miocene boundary offshore western Algeria (MARADJA’03 cruise). *Comptes Rendus Geoscience*, 338(1), 80–91. <https://doi.org/10.1016/j.crte.2005.11.009>
- dos Reis, A. T., Gorini, C., & Mauffret, A. (2005). Implications of salt–sediment interactions on the architecture of the Gulf of Lions deep-water sedimentary systems—Western Mediterranean Sea. *Marine and Petroleum Geology*, 22(6–7), 713–746. <https://doi.org/10.1016/j.marpetgeo.2005.03.006>
- Driussi, O. (2014). *Evolution de la région Baléares (Méditerranée occidentale) du Néogène à l’ Actuel: Aspects géodynamiques et paléo-environnementaux*.
- Driussi, O., Briaïs, A., & Maillard, A. (2015). Evidence for transform motion along the South Balearic margin and implications for the kinematics of opening of the Algerian basin. *Bulletin de La Société Géologique de France*, 186(4–5), 353–370. <https://doi.org/10.2113/gssgfbull.186.4-5.353>
- Driussi, O., Maillard, A., Ochoa, D., Lofi, J., Chanier, F., Gaullier, V., Briaïs, A., Sage, F., Sierro, F., & Garcia, M. (2015a). Messinian Salinity Crisis deposits widespread over the Balearic Promontory: Insights from new high-resolution seismic data. *Marine and Petroleum Geology*, 66, 41–54. <https://doi.org/10.1016/j.marpetgeo.2014.09.008>

- Driussi, O., Maillard, A., Ochoa, D., Lofi, J., Chanier, F., Gaullier, V., Briais, A., Sage, F., Sierro, F., & Garcia, M. (2015b). Messinian Salinity Crisis deposits widespread over the Balearic Promontory: Insights from new high-resolution seismic data. *Marine and Petroleum Geology*, *66, Part 1*, 41–54. <https://doi.org/10.1016/j.marpetgeo.2014.09.008>
- Dronkert, H. (1976). Late miocene evaporites in the Sorbas Basin and adjoining areas. *Mem.Soc.Geol. It.*, *16*, 341–361.
- Dronkert, H. (1985). *Evaporite Models and Sedimentology of Messinian and Recent Evaporites*.
- Drooger, C. w. (1976). Messinian Events in the Mediterranean. In *Geodynamics: Progress and Prospects* (pp. 29–31). American Geophysical Union (AGU). <https://doi.org/10.1029/SP005p0029>
- Duggen, S., Hoernle, K., Bogaard, P. van den, & Harris, C. (2004). Magmatic evolution of the Alboran region: The role of subduction in forming the western Mediterranean and causing the Messinian Salinity Crisis. *Earth and Planetary Science Letters*, *1–2(218)*, 91–108. [https://doi.org/10.1016/S0012-821X\(03\)00632-0](https://doi.org/10.1016/S0012-821X(03)00632-0)
- DUGGEN, S., Hoernle, K., & Van den Bogaard, P. (2005). Post-Collisional Transition from Subduction to Intraplate-type Magmatism in the Westernmost Mediterranean: Evidence for Continental-Edge Delamination of Subcontinental Lithosphere. *Journal of Petrology - J PETROL*, *46*, 1155–1201. <https://doi.org/10.1093/petrology/egi013>
- Duggen, S., Hoernle, K., Van den Bogaard, P., Rüpke, L., & Morgan, J. P. (2003). Deep roots of the Messinian salinity crisis. *Nature*, *422(6932)*, 602–606.
- Dumitru, O. A., Austermann, J., Polyak, V. J., Fornós, J. J., Asmerom, Y., Ginés, J., Ginés, A., & Onac, B. P. (2019). Constraints on global mean sea level during Pliocene warmth. *Nature*, *574(7777)*, 233–236. <https://doi.org/10.1038/s41586-019-1543-2>
- Dumitru, O. A., Austermann, J., Polyak, V. J., Fornós, J. J., Asmerom, Y., Ginés, J., Ginés, A., & Onac, B. P. (2021). Sea-level stands from the Western Mediterranean over the past 6.5 million years. *Scientific Reports*, 1–10. <https://doi.org/10.1038/s41598-020-80025-6>
- DURAND, D. (1980). LA MEDITERRANEE OCCIDENTALE: ETAPE DE SA GENESE ET PROBLEMES STRUCTURAUX LIES A CELLE-CI. *LA MEDITERRANEE*

OCCIDENTALE: ETAPE DE SA GENESE ET PROBLEMES STRUCTURAUX LIES A CELLE-CI.

- Durand-Delga, M., Freneix, S., Magne, J., Meon, H., & Rangheard, Y. (1993). La série saumâtre et continentale d'âge Miocène moyen et supérieur d'Eivissa (ex-Ibiza, Baléares). *Acta Geologica Hispanica*, 33–46.
- Durand-Delga, M., & Rangheard, Y. (2013). Structure de l'île d'Eivissa (Ibiza) et sa place dans le cadre baléaire. *Bolletí de La Societat d'Història Natural de Les Balears*, 56, 25–50.
- El-Sharkawy, A., Meier, T., Lebedev, S., Behrmann, J. H., Hamada, M., Cristiano, L., Weidle, C., & Köhn, D. (2020). The Slab Puzzle of the Alpine-Mediterranean Region: Insights From a New, High-Resolution, Shear Wave Velocity Model of the Upper Mantle. *Geochemistry, Geophysics, Geosystems*, 21(8), e2020GC008993. <https://doi.org/10.1029/2020GC008993>
- EMEIS, K., ROBERTSON, A., & Richter, C. (1996). *Proceedings of the Ocean Drilling Program: Initial report* (Vol. 160). The Program.
- Escutia, C., & Maldonado, A. (1992a). Palaeogeographic implications of the Messinian surface in the Valencia trough, northwestern Mediterranean Sea. *Tectonophysics*, 203(1–4), 263–284. [https://doi.org/10.1016/0040-1951\(92\)90227-W](https://doi.org/10.1016/0040-1951(92)90227-W)
- Escutia, C., & Maldonado, A. (1992b). Palaeogeographic implications of the Messinian surface in the Valencia trough, northwestern Mediterranean Sea. *Tectonophysics*, 203, 263–284. [https://doi.org/10.1016/0040-1951\(92\)90227-W](https://doi.org/10.1016/0040-1951(92)90227-W)
- Esteban, M. (1979). Significance of the upper miocene coral reefs of the Western Mediterranean. *Palaeogeography, Palaeoclimatology, Palaeoecology*, 29, 169–188. [https://doi.org/10.1016/0031-0182\(79\)90080-4](https://doi.org/10.1016/0031-0182(79)90080-4)
- Estrada, F., Ercilla, G., Gorini, C., Alonso, B., Vázquez, J. T., García-Castellanos, D., Juan, C., Maldonado, A., Ammar, A., & Elabbassi, M. (2011a). Impact of pulsed Atlantic water inflow into the Alboran Basin at the time of the Zanclean flooding. *Geo-Marine Letters*, 31(5–6), 361–376. <https://doi.org/10.1007/s00367-011-0249-8>
- Estrada, F., Ercilla, G., Gorini, C., Alonso, B., Vázquez, J. T., García-Castellanos, D., Juan, C., Maldonado, A., Ammar, A., & Elabbassi, M. (2011b). Impact of pulsed Atlantic water

- inflow into the Alboran Basin at the time of the Zanclean flooding. *Geo-Marine Letters*, 31(5–6), 361–376. <https://doi.org/10.1007/s00367-011-0249-8>
- Estrany, J., Garcia, C., Walling, D., & Ferrer, L. (2011). Fluxes and storage of fine-grained sediment and associated contaminants in the Na Borges River (Mallorca, Spain). *Catena*, 87, 291–305. <https://doi.org/10.1016/j.catena.2011.06.009>
 - Etheve, N., Frizon de Lamotte, D., Mohn, G., Martos, R., Roca, E., & Blanpied, C. (2016). Extensional vs contractional Cenozoic deformation in Ibiza (Balearic Promontory, Spain): Integration in the West Mediterranean back-arc setting. *Tectonophysics*, 682, 35–55. <https://doi.org/10.1016/j.tecto.2016.05.037>
 - Etheve, N., Mohn, G., Frizon de Lamotte, D., Roca, E., Tugend, J., & Gómez-Romeu, J. (2018a). Extreme Mesozoic Crustal Thinning in the Eastern Iberia Margin: The Example of the Columbrets Basin (Valencia Trough). *Tectonics*, 37(2), 636–662. <https://doi.org/10.1002/2017TC004613>
 - Etheve, N., Mohn, G., Frizon de Lamotte, D., Roca, E., Tugend, J., & Gómez-Romeu, J. (2018b). Extreme Mesozoic Crustal Thinning in the Eastern Iberia Margin: The Example of the Columbrets Basin (Valencia Trough). *Tectonics*, 37(2), 636–662. <https://doi.org/10.1002/2017TC004613>
 - Faccenna, C., Piromallo, C., Crespo-Blanc, A., Jolivet, L., & Rossetti, F. (2004a). Lateral slab deformation and the origin of the western Mediterranean arcs. *Tectonics*, 23(1). <https://doi.org/10.1029/2002TC001488>
 - Faccenna, C., Piromallo, C., Crespo-Blanc, A., Jolivet, L., & Rossetti, F. (2004b). Lateral slab deformation and the origin of the western Mediterranean arcs. *Tectonics*, 23(1). <https://doi.org/10.1029/2002TC001488>
 - Faranda, C., Gliozzi, E., Cipollari, P., Grossi, F., Darbas, G., Gürbüz, K., Nazik, A., Gennari, R., & Cosentino, D. (2013). Turkish Journal of Earth Sciences Messinian paleoenvironmental changes in the easternmost Mediterranean Basin: Adana Basin, southern Turkey. *TURKISH JOURNAL OF EARTH SCIENCES*, 22, 839–863. <https://doi.org/10.3906/yer-1205-11>
 - Farran, M. (2008). IMAGE2SEGY: Una aplicación informática para la conversión de imágenes de perfiles sísmicos a ficheros en formato SEG Y. *Geo-Temas* 10, 1215–1218.

- Feng, Y. E., Yankelzon, A., Steinberg, J., & Reshef, M. (2016). Lithology and characteristics of the Messinian evaporite sequence of the deep Levant Basin, eastern Mediterranean. *Marine Geology*, 376, 118–131. <https://doi.org/10.1016/j.margeo.2016.04.004>
- Fernández, M., Marzán, I., Correia, A., & Ramalho, E. (1998). Heat flow, heat production, and lithospheric thermal regime in the Iberian Peninsula. *Tectonophysics*, 291(1), 29–53. [https://doi.org/10.1016/S0040-1951\(98\)00029-8](https://doi.org/10.1016/S0040-1951(98)00029-8)
- Ferrater, M., Booth-Rea, G., Pérez-Peña, J. V., Azañón, J. M., Giaconia, F., & Masana, E. (2015). From extension to transpression: Quaternary reorganization of an extensional-related drainage network by the Alhama de Murcia strike-slip fault (eastern Betics). *Tectonophysics*, 663, 33–47. <https://doi.org/10.1016/j.tecto.2015.06.011>
- Flecker, R., Krijgsman, W., Capella, W., de Castro Martins, C., Dmitrieva, E., Mayser, J. P., Marzocchi, A., Modestou, S., Ochoa, D., Simon, D., Tulbure, M., van den Berg, B., van der Schee, M., de Lange, G., Ellam, R., Govers, R., Gutjahr, M., Hilgen, F., Kouwenhoven, T., ... Yousfi, M. Z. (2015). Evolution of the Late Miocene Mediterranean–Atlantic gateways and their impact on regional and global environmental change. *Earth-Science Reviews*, 150, 365–392. <https://doi.org/10.1016/j.earscirev.2015.08.007>
- Fontboté, J., Guimerà, J., Roca, E., Sàbat, F., Santanach, P., & Ortigosa, J. F. (1990). The Cenozoic geodynamic evolution of the Valencia Trough (Western Mediterranean). *Revista de La Sociedad Geológica de España*, 3, 7–18.
- Fornós, J. J., Balaguer, P., Gelabert, B., & Gómez-Pujol, L. (2005). Pleistocene formation, evolution and retreat rates of a carbonate coastal cliff (Mallorca Island, Western Mediterranean). *Journal of Coastal Research*, 15–21.
- Fornós, J. J., Marzo, M., Pomar, L., Ramos-Guerrero, E., & Rodríguez-Perea, A. (1991). Evolución tectono-sedimentaria y análisis estratigráfico del Terciario de la Isla de Mallorca. *Guía de Campo. I Congreso Del Grupo Espa-Ol Del Terciario*.
- Fornos, J. J., & Pomar, L. (1983). *Mioceno superior de Mallorca: Unidad calizas de Santanyi*, «Complejo Terminal». 177–206. <http://pascal-francis.inist.fr/vibad/index.php?action=getRecordDetail&idt=8881378>

- Fortuin, A. R., Kelling, J. M. D., & Roep, T. B. (1995). The enigmatic Messinian-Pliocene section of Cuevas del Almanzora (Vera Basin, SE Spain) revisited-erosional features and strontium isotope ages. *Sedimentary Geology*, 97(3–4), 177–201. [https://doi.org/10.1016/0037-0738\(95\)00009-W](https://doi.org/10.1016/0037-0738(95)00009-W)
- Fortuin, A. R., & Krijgsman, W. (2003). The Messinian of the Nijar Basin (SE Spain): Sedimentation, depositional environments and paleogeographic evolution. *Sedimentary Geology*, 160(1), 213–242. [https://doi.org/10.1016/S0037-0738\(02\)00377-9](https://doi.org/10.1016/S0037-0738(02)00377-9)
- Fortuin, A. R., Krijgsman, W., Hilgen, F. J., & Sierro, F. J. (2000). Late Miocene Mediterranean desiccation: Topography and significance of the ‘Salinity Crisis’ erosion surface on-land in southeast Spain: Comment. *Sedimentary Geology*, 133(3–4), 167–174. [https://doi.org/10.1016/S0037-0738\(00\)00040-3](https://doi.org/10.1016/S0037-0738(00)00040-3)
- Fossen, H. (2016). *Structural Geology*. Cambridge University Press.
- FOURCADE, E., P, C., & G, C. (1982). STRATIGRAPHIE ET TECTONIQUE DE L’ILE D’IBIZA, TEMOIN DU PROLONGEMENT DE LA NAPPE SUBBETIQUE AUX BALEARES (ESPAGNE). *STRATIGRAPHIE ET TECTONIQUE DE L’ILE D’IBIZA, TEMOIN DU PROLONGEMENT DE LA NAPPE SUBBETIQUE AUX BALEARES (ESPAGNE)*.
- Freeman, R., Sàbat, F., Lowrie, W., & Fontboté, J.-M. (1989). Paleomagnetic results from Mallorca (Balearic Islands, Spain). *Tectonics*, 8(3), 591–608. <https://doi.org/10.1029/TC008i003p00591>
- Frey-Martinez, J., Cartwright, J. A., Burgess, P. M., & Bravo, J. V. (2004). 3D Seismic Interpretation of the Messinian Unconformity in the Valencia Basin, Spain. *Geological Society, London, Memoirs*, 29(1), 91–100. <https://doi.org/10.1144/GSL.MEM.2004.029.01.10>
- Frizon de Lamotte, D., Raulin, C., Mouchot, N., Wrobel-Daveau, J.-C., Blanpied, C., & Ringenbach, J.-C. (2011). The southernmost margin of the Tethys realm during the Mesozoic and Cenozoic: Initial geometry and timing of the inversion processes. *Tectonics*, 30(3), n/a-n/a. <https://doi.org/10.1029/2010TC002691>
- Frumkin, A. (1994). Hydrology and denudation rates of halite karst. *Journal of Hydrology*, 162(1), 171–189. [https://doi.org/10.1016/0022-1694\(94\)90010-8](https://doi.org/10.1016/0022-1694(94)90010-8)

- Fuster, J. (1973). *Estudio de las reservas hidráulicas totales de Baleares. Informe de síntesis general*. Ministerio de Obras Públicas, Industria y Agricultura.
- Galdeano, A., & Rossignol, J. C. (1977). Contribution de l'aeromagnetisme a l'étude du golfe de Valence (Mediterranee occidentale). *Earth and Planetary Science Letters*, 34(1), 85–99. [https://doi.org/10.1016/0012-821X\(77\)90109-1](https://doi.org/10.1016/0012-821X(77)90109-1)
- Gallart, J., Martínez, N. V., Rubio, A. E., Pous, J., Monserrat, F. S., Bové, C. de S., & Suriñach, E. (1995). The ESCI-Valencia Trough vertical reflection experiment: A seismic image of the crust from the NE Iberian Peninsula to the Western Mediterranean. *Revista de la Sociedad Geológica de España*, 8(4), 401–415.
- Gallart, J., Vidal, N., Estévez, A., Pous, J., Sàbat, F., Santisteban, C., Surinach, E., & Group, E. V. T. (1995). The ESCI-València Troug Vertical reflection Experiment: A Seismic Image of the Crust from the NE Iberian Peninsula to the Western Mediterranean. *Revista de La Sociedad Geologica de Espana*, 8 (4), 401–415.
- Garcia, C., Amengual, A., Homar, V., & Zamora, A. (2017). Losing water in temporary streams on a Mediterranean island: Effects of climate and land-cover changes. *Global and Planetary Change*, 148, 139–152. <https://doi.org/10.1016/j.gloplacha.2016.11.010>
- Garcia-Castellanos, D. (2002). Interplay between lithospheric flexure and river transport in foreland basins: Lithospheric flexure and fluvial transport. *Basin Research*, 14(2), 89–104. <https://doi.org/10.1046/j.1365-2117.2002.00174.x>
- Garcia-Castellanos, D., Estrada, F., Jiménez-Munt, I., Gorini, C., Fernandez, M., Vergés, J., Vicente, D., & R. (2009). Catastrophic flood of the Mediterranean after the Messinian salinity crisis. *Nature*, 462, 778–782.
- Garcia-Castellanos, D., Estrada, F., Jiménez-Munt, I., Gorini, C., Fernández, M., Vergés, J., & De Vicente, R. (2009). Catastrophic flood of the Mediterranean after the Messinian salinity crisis. *Nature*, 462(7274), 778–781.
- Garcia-Castellanos, D., Fernández, M., & Torne, M. (1997a). Numerical modeling of foreland basin formation: A program relating thrusting, flexure, sediment geometry and lithosphere rheology. *Computers and Geosciences*, 23(9), 993–1003. [https://doi.org/10.1016/S0098-3004\(97\)00057-5](https://doi.org/10.1016/S0098-3004(97)00057-5)

- Garcia-Castellanos, D., Fernández, M., & Torne, M. (1997b). Numerical modeling of foreland basin formation: A program relating thrusting, flexure, sediment geometry and lithosphere rheology. *Computers and Geosciences*, 23(9), 993–1003. [https://doi.org/10.1016/S0098-3004\(97\)00057-5](https://doi.org/10.1016/S0098-3004(97)00057-5)
- Garcia-Castellanos, D., Fernández, M., & Torne, M. (2002). Modeling the evolution of the Guadalquivir foreland basin (southern Spain). *Tectonics*, 21(3). <https://doi.org/10.1029/2001TC001339>
- Garcia-Castellanos, D., Micallef, A., Estrada, F., Camerlenghi, A., Ercilla, G., Periáñez, R., & Abril, J. M. (2020a). The Zanclean megaflood of the Mediterranean – Searching for independent evidence. *Earth-Science Reviews*, 201(December 2019), 103061–103061. <https://doi.org/10.1016/j.earscirev.2019.103061>
- Garcia-Castellanos, D., Micallef, A., Estrada, F., Camerlenghi, A., Ercilla, G., Periáñez, R., & Abril, J. M. (2020b). The Zanclean megaflood of the Mediterranean – Searching for independent evidence. *Earth-Science Reviews*, 201, 103061. <https://doi.org/10.1016/j.earscirev.2019.103061>
- Garcia-Castellanos, D., & Villaseñor, A. (2011a). Messinian salinity crisis regulated by competing tectonics and erosion at the Gibraltar arc. *Nature*, 480(7377), 359–363. <https://doi.org/10.1038/nature10651>
- Garcia-Castellanos, D., & Villaseñor, A. (2011b). Messinian salinity crisis regulated by competing tectonics and erosion at the Gibraltar arc. *Nature*, 480(7377), 359–363. <https://doi.org/10.1038/nature10651>
- Garcia-Veigas, F. J., Ortí, F., Rosell, L., Ayora, C., Rouchy, J. M., & Lugli, S. (1995). The Messinian salt of the Mediterranean: Geochemical study of the salt from the Central Sicily Basin and comparison with the Lorca Basin (Spain). *Bulletin de La Societe Geologique de France*, 166, 699–710.
- García-Veigas, J., Cendón, D. I., Gibert, L., Lowenstein, T. K., & Artiaga, D. (2018a). Geochemical indicators in Western Mediterranean Messinian evaporites: Implications for the salinity crisis. *Marine Geology*, 403, 197–214. <https://doi.org/10.1016/j.margeo.2018.06.005>

- García-Veigas, J., Cendón, D. I., Gibert, L., Lowenstein, T. K., & Artiaga, D. (2018b). Geochemical indicators in Western Mediterranean Messinian evaporites: Implications for the salinity crisis. *Marine Geology*, 403, 197–214. <https://doi.org/10.1016/j.margeo.2018.06.005>
- García-Yagüe, A., & Muntaner, A. (1968). Estudio hidrogeológico del llano de Palma. *Madrid, SGOP*, 2.
- Gargani, J. (2004). Modelling of the erosion in the Rhone valley during the Messinian crisis (France). *Quaternary International*, 121(1), 13–22. <https://doi.org/10.1016/j.quaint.2004.01.020>
- Gaspar-Escribano, J. M., Garcia-Castellanos, D., Roca, E., & Cloetingh, S. (2004a). Cenozoic vertical motions of the Catalan Coastal Ranges (NE Spain): The role of tectonics, isostasy, and surface transport. *Tectonics*, 23(1). <https://doi.org/10.1029/2003TC001511>
- Gaspar-Escribano, J. M., Garcia-Castellanos, D., Roca, E., & Cloetingh, S. (2004b). Cenozoic vertical motions of the Catalan Coastal Ranges (NE Spain): The role of tectonics, isostasy, and surface transport: VERTICAL MOTIONS CCR (NE SPAIN). *Tectonics*, 23(1), n/a-n/a. <https://doi.org/10.1029/2003TC001511>
- Gass, I. G. (1960). The geology and mineral resources of the Dhali area. *Authority of the Government of Cyprus*.
- GAULLIER, V., & BELLAICHE, G. (1996). Diapirisme liguro-provençal: Les effets d'une topographie résiduelle sous le sel messinien. Apports de la modélisation analogique. *Diapirisme Liguro-Provençal: Les Effets d'une Topographie Résiduelle Sous Le Sel Messinien. Apports de La Modélisation Analogique*, 322(3), 213–220.
- Gaullier, V., Loncke, L., Vendeville, B. C., Deverchere, J., Droz, L., Obone Zeu Obame, E. M., & Mascle, J. (2008). Salt Tectonics in the deep Mediterranean: Indirect clues for understanding the Messinian Salinity Crisis. In: *The Messinian Salinity Crisis from mega-deposits to microbiology—A consensus report*.
- Gaullier, V., Vendeville, B., Huguen, H., Déverchère, J., Droz, L., Domzig, A., Obame, E., & Yelles, K. (2006). Role of thick-skinned tectonics on thin-skinned salt tectonics in the western Mediterranean: A comparison between the Algerian and North-Balearic basins. *Geophysical Research Abstracts*, 8, 1029–7006.

- Gautier, F., Clauzon, G., Suc, J.-P., Cravatte, J., & Violanti, D. (1994). Age et durée de la crise de salinité messinienne. *Comptes Rendus de l'Académie Des Sciences. Série 2. Sciences de La Terre et Des Planètes*, 318(8), 1103–1109.
- Gelabert, B., Sàbat, F., Hardy, S., & Rodríguez-Perea, A. (2004). Significance of Inherited Normal Faults during Inversion Tectonics: An example from the Tramuntana Range, Mallorca. *Geodinamica Acta*, 17(6), 363–373. <https://doi.org/10.3166/ga.17.363-373>
- Gelabert, B., Sabat, F., & Rodríguez-Perea, A. (1992). A structural outline of the Serra de Tramuntana of Mallorca (Balearic Islands). *Tectonophysics*, 203(1), 167–183. [https://doi.org/10.1016/0040-1951\(92\)90222-R](https://doi.org/10.1016/0040-1951(92)90222-R)
- Gelabert, B., Sàbat, F., & Rodríguez-Perea, A. (2002a). A new proposal for the late Cenozoic geodynamic evolution of the western Mediterranean. *Terra Nova*, 14(2), 93–100. <https://doi.org/10.1046/j.1365-3121.2002.00392.x>
- Gelabert, B., Sàbat, F., & Rodríguez-Perea, A. (2002b). A new proposal for the late Cenozoic geodynamic evolution of the Western Mediterranean. *Terra Nova*, 14, 93–100. <https://doi.org/10.1046/j.1365-3121.2002.00392.x>
- Ghielmi, M., Minervini, M., Nini, C., Rogledi, S., & Rossi, M. (2013). Late Miocene–Middle Pleistocene sequences in the Po Plain – Northern Adriatic Sea (Italy): The stratigraphic record of modification phases affecting a complex foreland basin. *Marine and Petroleum Geology*, 42, 50–81. <https://doi.org/10.1016/j.marpetgeo.2012.11.007>
- Giaconia, F., Booth-Rea, G., Martínez-Martínez, J. M., Azañón, J. M., & Pérez-Peña, J. V. (2012). Geomorphic analysis of the Sierra Cabrera, an active pop-up in the constrictional domain of conjugate strike-slip faults: The Palomares and Polopos fault zones (eastern Betics, SE Spain). *Tectonophysics*, 580, 27–42. <https://doi.org/10.1016/j.tecto.2012.08.028>
- Giaconia, F., Booth-Rea, G., Martínez-Martínez, J. M., Azañón, J. M., Storti, F., & Artoni, A. (2014). Heterogeneous extension and the role of transfer faults in the development of the southeastern Betic basins (SE Spain). *Tectonics*, 33(12), 2467–2489. <https://doi.org/10.1002/2014TC003681>
- Giménez, J. (2003). Nuevos datos sobre la actividad post-Neógena en la Isla de Mallorca. *Geogaceta*, 33, 91–96.

- Giménez, J., & Gelabert, B. (2002). *Recent Tectonic Activity Analysis of Mallorca Island*. 27.
- Gladstone, R., Flecker, R., Valdes, P., Lunt, D., & Markwick, P. (2007). The Mediterranean hydrologic budget from a Late Miocene global climate simulation. *Palaeogeography, Palaeoclimatology, Palaeoecology*, 251(2), 254–267. <https://doi.org/10.1016/j.palaeo.2007.03.050>
- Gliozzi, E., Ceci, M., Grossi, F., & Ligios, S. (2007). Paratethyan Ostracod immigrants in Italy during the Late Miocene. *Geobios - GEOBIOS-LYON*, 40, 325–337. <https://doi.org/10.1016/j.geobios.2006.10.004>
- Govers, R. (2009a). Choking the Mediterranean to dehydration: The Messinian salinity crisis. *Geology*, 37(2), 167–170. <https://doi.org/10.1130/G25141A.1>
- Govers, R. (2009b). Choking the Mediterranean to dehydration: The Messinian salinity crisis. *Geology*, 37(2), 167–170. <https://doi.org/10.1130/G25141A.1>
- Govers, R., Meijer, P., & Krijgsman, W. (2009a). Regional isostatic response to Messinian Salinity Crisis events. *Tectonophysics*, 463(1–4), 109–129. <https://doi.org/10.1016/j.tecto.2008.09.026>
- Govers, R., Meijer, P., & Krijgsman, W. (2009b). Regional isostatic response to Messinian Salinity Crisis events. *Tectonophysics*, 463(1–4), 109–129. <https://doi.org/10.1016/j.tecto.2008.09.026>
- Govers, R., & Wortel, M. J. R. (1995). Extension of stable continental lithosphere and the initiation of lithospheric scale faults. *Tectonics*, 14(4), 1041–1055. <https://doi.org/10.1029/95TC00500>
- Grasso, M., & Butler, R. W. H. (1991). Tectonic controls on the deposition of late Tortonian sediments in the Caltanissetta basin of Central Sicily. *Memorie Della Societa Geologica Italiana*, 47, 313–324.
- Griffin, D. L. (2002). Aridity and humidity: Two aspects of the late Miocene climate of North Africa and the Mediterranean. *Palaeogeography, Palaeoclimatology, Palaeoecology*, 182(1), 65–91. [https://doi.org/10.1016/S0031-0182\(01\)00453-9](https://doi.org/10.1016/S0031-0182(01)00453-9)
- Grossi, F., Gliozzi, E., Castorina, F., Voltaggio, M., & AnadÃ³n, P. (2015). Is *Cyprideis agrigentina* Decima a good paleosalinometer for the Messinian Salinity Crisis?

Morphometrical and geochemical analyses from the Eraclea Minoa section (Sicily). *Palaeogeography, Palaeoclimatology, Palaeoecology*.
<http://dx.doi.org/10.1016/j.palaeo.2014.09.024>

- Gueguen, E., Doglioni, C., & Fernandez, M. (1998a). On the post-25 Ma geodynamic evolution of the western Mediterranean. *Tectonophysics*, 298(1–3), 259–269. [https://doi.org/10.1016/S0040-1951\(98\)00189-9](https://doi.org/10.1016/S0040-1951(98)00189-9)
- Gueguen, E., Doglioni, C., & Fernandez, M. (1998b). On the post-25 Ma geodynamic evolution of the western Mediterranean. *Tectonophysics*, 298(1–3), 259–269. [https://doi.org/10.1016/S0040-1951\(98\)00189-9](https://doi.org/10.1016/S0040-1951(98)00189-9)
- GUENNOG, P., GORINI, C., & MAUFFRET, A. (2000). Histoire géologique du golfe du Lion et cartographie du rift oligo-aquitainien et de la surface messinienne. *Histoire Géologique Du Golfe Du Lion et Cartographie Du Rift Oligo-Aquitainien et de La Surface Messinienne*, 3, 67–97.
- Gutscher, M.-A. (2012). Subduction beneath Gibraltar? Recent studies provide answers. *Eos, Transactions American Geophysical Union*, 93(13), 133–134. <https://doi.org/10.1029/2012EO130001>
- Gutscher, M.-A., Malod, J., Rehault, J.-P., Contrucci, I., Klingelhoefer, F., Mendes-Victor, L., & Spakman, W. (2002). Evidence for active subduction beneath Gibraltar. *Geology*, 30(12), 1071–1074. [https://doi.org/10.1130/0091-7613\(2002\)030<1071:EFASBG>2.0.CO;2](https://doi.org/10.1130/0091-7613(2002)030<1071:EFASBG>2.0.CO;2)
- Gvirtzman, Z., Manzi, V., Calvo, R., Gavrieli, I., Gennari, R., Lugli, S., Reghizzi, M., & Roveri, M. (2017). Intra-Messinian truncation surface in the Levant Basin explained by subaqueous dissolution. *Geology*, 45(10), 915–918. <https://doi.org/10.1130/G39113.1>
- Gvirtzman, Z., Reshef, M., Buch-Leviatan, O., & Ben-Avraham, Z. (2013). Intense salt deformation in the Levant Basin in the middle of the Messinian Salinity Crisis. *Earth and Planetary Science Letters*, 379, 108–119. <https://doi.org/10.1016/j.epsl.2013.07.018>
- Haidar, S., Déverchère, J., Graindorge, D., Arab, M., Medaouri, M., & Klingelhoefer, F. (2021, March 5). *Back-arc dynamics controlled by slab rollback and tearing: A reappraisal of seafloor spreading and kinematic evolution of the Eastern Algerian basin (western Mediterranean) in Middle-Late Miocene (world)* [Preprint]. Earth and Space Science Open

Archive; Earth and Space Science Open Archive.
<http://www.essoar.org/doi/10.1002/essoar.10506942.1>

- Haq, B., Gorini, C., Baur, J., Moneron, J., & Rubino, J. L. (2020a). Deep Mediterranean's Messinian evaporite giant: How much salt? *Global and Planetary Change*, 184(October 2019), 103052–103052. <https://doi.org/10.1016/j.gloplacha.2019.103052>
- Haq, B., Gorini, C., Baur, J., Moneron, J., & Rubino, J.-L. (2020b). Deep Mediterranean's Messinian evaporite giant: How much salt? *Global and Planetary Change*, 184, 103052. <https://doi.org/10.1016/j.gloplacha.2019.103052>
- Hardie, L. A., & Lowenstein, T. K. (2004). Did the Mediterranean Sea Dry Out During the Miocene? A Reassessment of the Evaporite Evidence from DSDP Legs 13 and 42A Cores. *Journal of Sedimentary Research*, 74(4), 453–461. <https://doi.org/10.1306/112003740453>
- Harding, T. P. (1985). Seismic Characteristics and Identification of Negative Flower Structures, Positive Flower Structures, and Positive Structural Inversion1. *AAPG Bulletin*, 69(4), 582–600. <https://doi.org/10.1306/AD462538-16F7-11D7-8645000102C1865D>
- Hayford, J. F. (1909). *Geodesy: The Figure of the Earth and Isostasy from Measurements in the United States*. Government Printing Office.
- Heida, H., Raad, F., Garcia-Castellanos, D., Jiménez-Munt, I., Maillard, A., & Lofi, J. (2021). Flexural-isostatic reconstruction of the Western Mediterranean during the Messinian Salinity Crisis: Implications for water level and basin connectivity. *Basin Research*, bre.12610. <https://doi.org/10.1111/bre.12610>
- Henriquet, M., Dominguez, S., Barreca, G., Malavieille, J., & Monaco, C. (2020). Structural and tectono-stratigraphic review of the Sicilian orogen and new insights from analogue modeling. *Earth-Science Reviews*, 208, 103257. <https://doi.org/10.1016/j.earscirev.2020.103257>
- Hersey, J. B. (1965). Sedimentary basins of the Mediterranean Sea. In *Submarine geology and geophysics* (Vol. 17, pp. 75–91). Butterworths London.
- Hilgen, F., Bissoli, L., Iaccarino, S., Krijgsman, W., Meijer, R., Negri, A., & Villa, G. (2000). Integrated stratigraphy and astrochronology of the Messinian GSSP at Oued Akrech (Atlantic Morocco). *Earth and Planetary Science Letters*, 182, 237–251. [https://doi.org/10.1016/S0012-821X\(00\)00247-8](https://doi.org/10.1016/S0012-821X(00)00247-8)

- Hilgen, F. J., Krijgsman, W., Langereis, C. G., Lourens, L. J., Santarelli, A., & Zachariasse, W. J. (1995). Extending the astronomical (polarity) time scale into the Miocene. *Earth and Planetary Science Letters*, 136(3), 495–510. [https://doi.org/10.1016/0012-821X\(95\)00207-S](https://doi.org/10.1016/0012-821X(95)00207-S)
- Hilgen, F., Kuiper, K. F., Krijgsman, W., Snel, E., & Laan, E. (2007). Astronomical tuning as the basis for high resolution chronostratigraphy: The intricate history of the Messinian Salinity Crisis. *Stratigraphy*, 4.
- Hilgen & Krijgsman. (1999). Cyclostratigraphy and astrochronology of the Tripoli diatomite formation (pre-evaporite Messinian, Sicily, Italy). *Terra Nova*, 11(1), 16–22. <https://doi.org/10.1046/j.1365-3121.1999.00221.x>
- Hovland, M. (2008). *Deep-Water Coral Reefs. Unique Biodiversity Hot-Spots*. <https://doi.org/10.1007/978-1-4020-8460-7>
- Hsü, K. J. (1972). Origin of saline giants: A critical review after the discovery of the Mediterranean Evaporite. *Earth-Science Reviews*, 8(4), 371–396. [https://doi.org/10.1016/0012-8252\(72\)90062-1](https://doi.org/10.1016/0012-8252(72)90062-1)
- Hsü, K. J. (1973). The desiccated deep-basin model for the Messinian events. *Drooger, C.W. (Ed.), Messinian Events in the Mediterranean. North-Holland Publ. Co., Amsterdam*, 60–67.
- Hsü, K. J., Ryan, W. B. F., & Cita, M. B. (1973a). Late Miocene dessication of the Mediterranean. *Nature*, 242(5395), 240–244.
- Hsü, K. J., Ryan, W. B. F., & Cita, M. B. (1973b). Late Miocene Desiccation of the Mediterranean. *Nature*, 242(5395), 240–244. <https://doi.org/10.1038/242240a0>
- Hsu, K., Montadert, L., & et al. (1978). *Initial Reports of the Deep Sea Drilling Project, 42 Pt. 1: Vol. 42 Pt. 1*. U.S. Government Printing Office. <https://doi.org/10.2973/dsdp.proc.42-1.1978>
- Huang, L., & Liu, C. (2017). Three Types of Flower Structures in a Divergent-Wrench Fault Zone. *Journal of Geophysical Research: Solid Earth*, 122(12), 10,478-10,497. <https://doi.org/10.1002/2017JB014675>

- Hübscher, C., Betzler, C., & Grevemeyer, I. (2010). Sedimentology, rift-processes and neotectonic in the western Mediterranean, Cruise No. 69, August 08-September 20, 2006. *Meteor-Berichte*, 10–11.
- Huebscher, C., Tahchi, E., Klauke, I., Maillard, A., & Sahling, H. (2009). Salt tectonics and mud volcanism in the Latakia and Cyprus Basins, eastern Mediterranean. *Tectonophysics*, 470, 173–182. <https://doi.org/10.1016/j.tecto.2008.08.019>
- Iaccarino, S., & Bossio, A. (1999). PALEOENVIRONMENT OF UPPERMOST MESSINIAN SEQUENCES IN THE WESTERN MEDITERRANEAN (Sites 974, 975, and 978). *Proceedings of the Ocean Drilling Program, Scientific Results*, 161, 529–541.
- Jolivet, L., Augier, R., Robin, C., Suc, J. P., & Rouchy, J. M. (2006a). Lithospheric-scale geodynamic context of the Messinian salinity crisis. *Sedimentary Geology*, 188–189, 9–33. <https://doi.org/10.1016/j.sedgeo.2006.02.004>
- Jolivet, L., Augier, R., Robin, C., Suc, J.-P., & Rouchy, J. M. (2006b). Lithospheric-scale geodynamic context of the Messinian salinity crisis. *Sedimentary Geology*, 188–189, 9–33. <https://doi.org/10.1016/j.sedgeo.2006.02.004>
- Jolivet, L., & Faccenna, C. (2000). Mediterranean extension and the Africa-Eurasia collision. *Tectonics*, 19(6), 1095–1106. <https://doi.org/10.1029/2000TC900018>
- Jolivet, L., Faccenna, C., & Piromallo, C. (2009). From mantle to crust: Stretching the Mediterranean. *Earth and Planetary Science Letters*, 285(1), 198–209. <https://doi.org/10.1016/j.epsl.2009.06.017>
- Jolivet, L., Gorini, C., Smit, J., & Leroy, S. (2015). Continental breakup and the dynamics of rifting in back-arc basins: The Gulf of Lion margin. *Tectonics*, 34(4), 662–679. <https://doi.org/10.1002/2014TC003570>
- Just, J., Hübscher, C., Betzler, C., Lüdmann, T., & Reicherter, K. (2011). Erosion of continental margins in the Western Mediterranean due to sea-level stagnancy during the Messinian Salinity Crisis. *Geo-Marine Letters*, 31(1), 51–64. <https://doi.org/10.1007/s00367-010-0213-z>
- Kaban, M. K., Chen, B., Tesauro, M., Petrunin, A. G., El Khrepy, S., & Al-Arifi, N. (2018a). Reconsidering Effective Elastic Thickness Estimates by Incorporating the Effect

- of Sediments: A Case Study for Europe. *Geophysical Research Letters*, 45(18), 9523–9532. <https://doi.org/10.1029/2018GL079732>
- Kaban, M. K., Chen, B., Tesauro, M., Petrunin, A. G., El Khrepy, S., & Al-Arifi, N. (2018b). Reconsidering Effective Elastic Thickness Estimates by Incorporating the Effect of Sediments: A Case Study for Europe. *Geophysical Research Letters*, 45(18), 9523–9532. <https://doi.org/10.1029/2018GL079732>
 - Kastens, K. A., & Mascle, J. (Eds.). (1990). *Proceedings of the Ocean Drilling Program, 107 Scientific Results* (Vol. 107). Ocean Drilling Program. <https://doi.org/10.2973/odp.proc.sr.107.1990>
 - KASTENS, K., MASCLE, J., AUROUX, C., BONATTI, E., BROGLIA, C., CHANNELL, J., CURZI, P., EMEIS, K.-C., GLAÇON, G., HASEGAWA, S., HIEKE, W., MASCLE, G., McCOY, F., MCKENZIE, J., MENDELSON, J., MÜLLER, C., RÉHAULT, J.-P., ROBERTSON, A., SARTORI, R., ... TORII, M. (1988). ODP Leg 107 in the Tyrrhenian Sea: Insights into passive margin and back-arc basin evolution. *GSA Bulletin*, 100(7), 1140–1156. [https://doi.org/10.1130/0016-7606\(1988\)100<1140:OLITTS>2.3.CO;2](https://doi.org/10.1130/0016-7606(1988)100<1140:OLITTS>2.3.CO;2)
 - Kearey, P., Brooks, M., & Hill, I. (2002). *An Introduction to Geophysical Exploration*. John Wiley & Sons.
 - Kirkham, C., Bertoni, C., Cartwright, J., Lensky, N. G., Sirota, I., Rodriguez, K., & Hodgson, N. (2019). The demise of a ‘salt giant’ driven by uplift and thermal dissolution. *Earth and Planetary Science Letters*, 115933. <https://doi.org/10.1016/j.epsl.2019.115933>
 - Knudsen, M. (1900). Ein hydrographischer lehrsatz. *Annalen Der Hydrographie Und Maritimen Meteorologie*, 28(7), 316–320.
 - Krijgsman, W., Capella, W., Simon, D., Hilgen, F. J., Kouwenhoven, T. J., Meijer, P. Th., Sierro, F. J., Tulbure, M. A., van den Berg, B. C. J., van der Schee, M., & Flecker, R. (2018). The Gibraltar Corridor: Watergate of the Messinian Salinity Crisis. *Marine Geology*, 403, 238–246. <https://doi.org/10.1016/j.margeo.2018.06.008>
 - Krijgsman, W., Fortuin, A. R., Hilgen, F. J., & Sierro, F. J. (2001a). Astrochronology for the Messinian Sorbas basin (SE Spain) and orbital (precessional) forcing for evaporite cyclicity. *Sedimentary Geology*, 140(1–2), 43–60. [https://doi.org/10.1016/S0037-0738\(00\)00171-8](https://doi.org/10.1016/S0037-0738(00)00171-8)

- Krijgsman, W., Fortuin, A. R., Hilgen, F. J., & Sierro, F. J. (2001b). Astrochronology for the Messinian Sorbas basin (SE Spain) and orbital (precessional) forcing for evaporite cyclicity. *Sedimentary Geology*, 140(1), 43–60. [https://doi.org/10.1016/S0037-0738\(00\)00171-8](https://doi.org/10.1016/S0037-0738(00)00171-8)
- Krijgsman, W., Hilgen, F. J., Raffi, I., Sierro, F. J., & Wilson, D. S. (1999a). Chronology, causes and progression of the Messinian salinity crisis. *Nature*, 400(August), 652–655.
- Krijgsman, W., Hilgen, F. J., Raffi, I., Sierro, F. J., & Wilson, D. S. (1999b). Chronology, causes and progression of the Messinian salinity crisis. *Nature*, 400(6745), 652–655.
- Krijgsman, W., HILGEN, F., Marabini, S., & Vai, G. B. (1999). New paleomagnetic and cyclostratigraphic age constraints on the Messinian of the Northern Apennines (Vena del Gesso Basin, Italy). *Mem. Soc. Geol. It*, 54, 25–33.
- Krijgsman, W., & Meijer, P. T. (2008). Depositional environments of the Mediterranean “Lower Evaporites” of the Messinian salinity crisis: Constraints from quantitative analyses. *Marine Geology*, 253. <https://doi.org/10.1016/j.margeo.2008.04.010>
- La Violette, P. E. (1994). *Seasonal and Interannual Variability of the Western Mediterranean Sea*. American Geophysical Union.
- Lacombe, H., & Richez, C. (1982). The Regime of the Strait of Gibraltar. In J. C. J. Nihoul (Ed.), *Elsevier Oceanography Series* (Vol. 34, pp. 13–73). Elsevier. [https://doi.org/10.1016/S0422-9894\(08\)71237-6](https://doi.org/10.1016/S0422-9894(08)71237-6)
- Lanaja, J. M. (1987). *Contribución de la exploración petrolífera al conocimiento de la geología de España*. IGME.
- Lastras, G., Canals, M., Urgeles, R., Hughes-Clarke, J. E., & Acosta, J. (2004). Shallow slides and pockmark swarms in the Eivissa Channel, western Mediterranean Sea. *Sedimentology*, 51(4), 837–850. <https://doi.org/10.1111/j.1365-3091.2004.00654.x>
- Leeder, M. R. (2009). *Sedimentology and Sedimentary Basins: From Turbulence to Tectonics*. John Wiley & Sons.
- Lensky, N. G., Dvorkin, Y., Lyakhovsky, V., Gertman, I., & Gavrieli, I. (2005). Water, salt, and energy balances of the Dead Sea. *Water Resources Research*, 41(12). <https://doi.org/10.1029/2005WR004084>

- Leprêtre, A., Klingelhoefer, F., Graindorge, D., Schnurle, P., Beslier, M. O., Yelles, K., Déverchère, J., & Bracene, R. (2013). Multiphased tectonic evolution of the Central Algerian margin from combined wide-angle and reflection seismic data off Tipaza, Algeria. *Journal of Geophysical Research: Solid Earth*, 118(8), 3899–3916. <https://doi.org/10.1002/jgrb.50318>
- Leprêtre, R. (2018). The Tell-Rif orogenic system (Morocco, Algeria, Tunisia) and the structural heritage of the southern Tethys margin. *Bulletin de La Société Géologique de France*, 189(2). <https://doi.org/10.1051/bsgf/2018009>
- Leroux, E., Aslanian, D., & Rabineau, M. (2019). *Atlas of the stratigraphic markers in the Western Mediterranean with focus on the Messinian, Pliocene and Pleistocene of the Gulf of Lion*. Commission de la carte géologique du monde.
- Leroux, E., Aslanian, D., Rabineau, M., Gorini, C., Rubino, J.-L., Poort, J., Suc, J.-P., Bache, F., & Blanpied, C. (2019). *ATLAS OF THE STRATIGRAPHIC MARKERS IN THE WESTERN MEDITERRANEAN WITH FOCUS ON THE MESSINIAN, PLIOCENE AND PLEISTOCENE OF THE GULF OF LION*. CCGM-CGMW. <https://doi.org/10.14682/2019GULFLIONATL>
- Lezin, C., Maillard, A., Odonne, F., Colinet, G., Chanier, F., & Gaullier, V. (2017). Tectono-sedimentary evolution of the Miocene-Pliocene series of Ibiza: New onshore evidence of the Messinian Salinity Crisis. *IAS Octobre 2017 Toulouse*.
- Liang, X., Spall, M., & Wunsch, C. (2017). Global Ocean Vertical Velocity From a Dynamically Consistent Ocean State Estimate. *Journal of Geophysical Research: Oceans*, 122(10), 8208–8224. <https://doi.org/10.1002/2017JC012985>
- Lickorish, W. H., Grasso, M., Butler, R. W. H., Argnani, A., & Maniscalco, R. (1999). Structural styles and regional tectonic setting of the “Gela Nappe” and frontal part of the Maghrebian thrust belt in Sicily. *Tectonics*, 18(4), 655–668. <https://doi.org/10.1029/1999TC900013>
- Linol, B., Bercovici, A., Bourquin, S., Diez, J. B., López-Gómez, J., Broutin, J., Durand, M., & Villanueva-Amadoz, U. (2009). Late Permian to Middle Triassic correlations and palaeogeographical reconstructions in south-western European basins: New sedimentological data from Minorca (Balearic Islands, Spain). *Sedimentary Geology*, 220(1–2), 77–94. <https://doi.org/10.1016/j.sedgeo.2009.06.003>

- Lofi, J. (2011). *Seismic Atlas of the Messinian Salinity Crisis markers in the Mediterranean and Black Seas—Volume 1* (Vol. 1). Société Géologique de France. <https://ccgm.org/en/home/148-seismic-atlas-of-the-messinian-salinity-crisis-markers-2853630978.html>
- Lofi, J. (2018a). *Seismic Atlas of the Messinian Salinity Crisis markers in the Mediterranean Sea—Volume 2* (Vol. 2). CGMW and Mémoires de la Société Géologie de France. http://commons.wikimedia.org/wiki/Category:Messinian_salinity_crisis.
- Lofi, J. (2018b). *Seismic Atlas of the Messinian Salinity Crisis markers in the Mediterranean Sea—Volume 2: Vol. t.181* (C. for the G. M. of the World, Ed.). Société Géologique de France. <https://hal.archives-ouvertes.fr/hal-01975763>
- Lofi, J., & Berné, S. (2008). Evidence for pre-Messinian submarine canyons on the Gulf of Lions slope (Western Mediterranean). *Marine and Petroleum Geology*, 25(8), 804–817. <https://doi.org/10.1016/j.marpetgeo.2008.04.006>
- Lofi, J., Déverchère, J., Gaullier, V., Gillet, H., Gorini, C., Guennoc, P., Loncke, L., Maillard, A., Sage, F., Thinon, I., & World, C. for the G. M. of the. (2011). Seismic Atlas of the Messinian Salinity Crisis markers in the Mediterranean and Black Seas. In *Memoires de la Société Géologique de France* (Vol. 179, p. p72). http://ccgm.free.fr/Atlas_Messinien_gb.html
- Lofi, J., Gorini, C., Berné, S., Clauzon, G., Dos Reis, A. T., Ryan, W. B. F., & Steckler, M. S. (2005). Erosional processes and paleo-environmental changes in the Western Gulf of Lions (SW France) during the Messinian Salinity Crisis. *Marine Geology*, 217(1–2), 1–30. <https://doi.org/10.1016/j.margeo.2005.02.014>
- Lofi, J., Gorini, C., Berné, S., Clauzon, G., Tadeu Dos Reis, A., Ryan, W. B. F., & Steckler, M. S. (2005). Erosional processes and paleo-environmental changes in the Western Gulf of Lions (SW France) during the Messinian Salinity Crisis. *Marine Geology*, 217(1–2), 1–30. <https://doi.org/10.1016/j.margeo.2005.02.014>
- Lofi, J., Sage, F., Deverchere, J., Loncke, L., Maillard, A., Gaullier, V., Thinon, I., Gillet, H., Guennoc, P., & Gorini, C. (2011). Refining our knowledge of the Messinian salinity crisis records in the offshore domain through multi-site seismic analysis. *Bulletin de La Societe Geologique de France*, 182(2), 163–180. <https://doi.org/10.2113/gssgfbull.182.2.163>

- Lofi, J., Sage, F., Déverchère, J., Loncke, L., Maillard, A., Gaullier, V., Thion, I., Herve, G., & Guennoc, P. (2011). Refining our knowledge of the Messinian Salinity Crisis records in the offshore domain through Multi-site seismic analysis. *Bulletin de La Société Géologique de France*, 182. <https://doi.org/10.2113/gssgfbull.182.2.163>
- Loget, N., & Van Den Driessche, J. (2006). On the origin of the Strait of Gibraltar. *Sedimentary Geology*, 188–189, 341–356. <https://doi.org/10.1016/j.sedgeo.2006.03.012>
- Loncke, L., Gaullier, V., Mascle, J., Vendeville, B., & Camera, L. (2006). The Nile deep-sea fan: An example of interacting sedimentation, salt tectonics, and inherited subsalt paleotopographic features. *Marine and Petroleum Geology*, 23(3), 297–315. <https://doi.org/10.1016/j.marpetgeo.2006.01.001>
- Londeix, L., Benzakour, M., Anne, de V., Jean Louis, T., & Suc, J.-P. (1999). *Late Neogene dinoflagellate cyst assemblages from the Strait of Sicily, Central Mediterranean Sea: Paleoecological and biostratigraphical implications*. (pp. 65–91).
- Londeix, L., Benzakour, M., Suc, J.-P., & Jean Louis, T. (2007). Messinian palaeoenvironments and hydrology in Sicily (Italy): The dinoflagellate cyst record. *Geobios*, 40, 233–250. <https://doi.org/10.1016/j.geobios.2006.12.001>
- Lonergan, L., & White, N. (1997a). Origin of the Betic-Rif mountain belt. *Tectonics*, 16(3), 504–522. <https://doi.org/10.1029/96TC03937>
- Lonergan, L., & White, N. (1997b). Origin of the Betic-Rif Mountain Belt. *Tectonics*, 16, 504–522. <https://doi.org/10.1029/96TC03937>
- López-Ruiz, J., Cebriá, J. M., & Doblas, M. (2002). *Cenozoic volcanism I: The Iberian peninsula*. <https://doi.org/10.1144/GOSPP.17>
- Lowenstein, T. K., & Hardie, L. A. (1985). Criteria for the recognition of salt-pan evaporites. *Sedimentology*, 32(5), 627–644. <https://doi.org/10.1111/j.1365-3091.1985.tb00478.x>
- Lüdmann, T., Wiggershaus, S., Betzler, C., & Hübscher, C. (2012). Southwest Mallorca Island: A cool-water carbonate margin dominated by drift deposition associated with giant mass wasting. *Marine Geology, Complete*(307–310), 73–87. <https://doi.org/10.1016/j.margeo.2011.09.008>

- Lugli, S., Gennari, R., Gvirtzman, Z., Manzi, V., Roveri, M., & Schreiber, B. (2013). Evidence of Clastic Evaporites In the Canyons of the Levant Basin (Israel): Implications For the Messinian Salinity Crisis. *Journal Of Sedimentary Research*, 83. <https://doi.org/10.2110/jsr.2013.72>
- Lugli, S., Manzi, V., Roveri, M., & Schreiber, B. C. (2015). The deep record of the Messinian salinity crisis: Evidence of a non-desiccated Mediterranean Sea. *Palaeogeography, Palaeoclimatology, Palaeoecology*, 433, 201–218. <https://doi.org/10.1016/j.palaeo.2015.05.017>
- Lugli, S., Manzi, V., Roveri, M., & Schreiber, C. B. (2010). The Primary Lower Gypsum in the Mediterranean: A new facies interpretation for the first stage of the Messinian salinity crisis. *Palaeogeography, Palaeoclimatology, Palaeoecology*, 297(1), 83–99. <https://doi.org/10.1016/j.palaeo.2010.07.017>
- Lugli, S., Schreiber, B. C., & Triberti, B. (1999a). Giant polygons in the Realmonte Mine (Agrigento, Sicily); evidence for the desiccation of a Messinian halite basin. *Journal of Sedimentary Research*, 69(3), 764–771. <https://doi.org/10.2110/jsr.69.764>
- Lugli, S., Schreiber, B., & Triberti, B. (1999b). Giant polygons in the Realmonte Mine (Agrigento, Sicily); evidence for the desiccation of a Messinian halite basin. *Journal of Sedimentary Research*, 69, 764–771. <https://doi.org/10.2110/jsr.69.764>
- Lugli, S., Vinicio, M., Marco, R., & Charlotte, S. B. (2010). The Primary Lower Gypsum in the Mediterranean: A new facies interpretation for the first stage of the Messinian salinity crisis. *Palaeogeography, Palaeoclimatology, Palaeoecology*, 297(1), 83–99.
- Lumpkin, R., & Johnson, G. C. (2013). Global ocean surface velocities from drifters: Mean, variance, El Niño–Southern Oscillation response, and seasonal cycle. *Journal of Geophysical Research: Oceans*, 118(6), 2992–3006. <https://doi.org/10.1002/jgrc.20210>
- Madof, A. S., Bertoni, C., & Lofi, J. (2019). Discovery of vast fluvial deposits provides evidence for drawdown during the late Miocene Messinian salinity crisis. *Geology*, 47(2), 171–174. <https://doi.org/10.1130/G45873.1>
- Maillard, A. (1993). *Structure et riftogenese de Golfe de Valence (Mediterranee Nord-Occidentale)* [Doctoral dissertation].

- Maillard, A., Driussi, O., Lofi, J., Briais, A., Chanier, F., Hübscher, C., & Gaullier, V. (2014a). Record of the Messinian Salinity Crisis in the SW Mallorca area (Balearic Promontory, Spain). *Marine Geology*, 357, 304–320. <https://doi.org/10.1016/j.margeo.2014.10.001>
- Maillard, A., Driussi, O., Lofi, J., Briais, A., Chanier, F., Hübscher, C., & Gaullier, V. (2014b). Record of the Messinian Salinity Crisis in the SW Mallorca area (Balearic Promontory, Spain). *Marine Geology*, 357, 304–320. <https://doi.org/10.1016/j.margeo.2014.10.001>
- Maillard, A., & Gaullier, V. (2013). *SIMBAD cruise, Téthys II R/V*. <https://doi.org/10.17600/13450010>
- Maillard, A., Gaullier, V., Lézin, C., Chanier, F., Odonne, F., & Lofi, J. (2020a). New onshore/offshore evidence of the Messinian Erosion Surface from key areas: The Ibiza-Balearic Promontory and the Orosei-Eastern Sardinian margin. *BSGF - Earth Sciences Bulletin*, 191, 9. <https://doi.org/10.1051/bsgf/2020007>
- Maillard, A., Gaullier, V., Lézin, C., Chanier, F., Odonne, F., & Lofi, J. (2020b). New onshore/offshore evidence of the Messinian Erosion Surface from key areas: The Ibiza-Balearic Promontory and the Orosei-Eastern Sardinian margin. *BSGF - Earth Sciences Bulletin*, 191, 9–9. <https://doi.org/10.1051/bsgf/2020007>
- Maillard, A., Gorini, C., Mauffret, A., Sage, F., Lofi, J., & Gaullier, V. (2006a). Offshore evidence of polyphase erosion in the Valencia Basin (Northwestern Mediterranean): Scenario for the Messinian Salinity Crisis. *Sedimentary Geology*, 188–189, 69–91. <https://doi.org/10.1016/j.sedgeo.2006.02.006>
- Maillard, A., Gorini, C., Mauffret, A., Sage, F., Lofi, J., & Gaullier, V. (2006b). Offshore evidence of polyphase erosion in the Valencia Basin (Northwestern Mediterranean): Scenario for the Messinian Salinity Crisis. *Sedimentary Geology*, 188–189, 69–91. <https://doi.org/10.1016/j.sedgeo.2006.02.006>
- Maillard, A., Hübscher, C., Benkhelil, J., & Tahchi, E. (2011). Deformed Messinian markers in the Cyprus Arc: Tectonic and/or Messinian Salinity Crisis indicators?: Deformed Messinian markers in the Cyprus Arc. *Basin Research*, 23(2), 146–170. <https://doi.org/10.1111/j.1365-2117.2010.00464.x>

- Maillard, A., Jolivet, L., Lofi, J., Thinon, I., Couëffé, R., Canva, A., & Dofal, A. (2020). Transfer zones and associated volcanic province in the eastern Valencia Basin: Evidence for a hot rifted margin? *Marine and Petroleum Geology*, 119(July 2019), 104419–104419. <https://doi.org/10.1016/j.marpetgeo.2020.104419>
- Maillard, A., & Mauffret, A. (1993a). Structure et volcanisme de la fosse de Valence (Mediterranee nord-occidentale). *Bulletin de La Société Géologique de France*, 164(3), 365–383.
- Maillard, A., & Mauffret, A. (1993b). Structure et volcanisme de la fosse de Valence (Méditerranée nord-occidentale). *Bull. La Société Géologique Fr.*, 164(3), 365–383.
- Maillard, A., & Mauffret, A. (1999). Crustal structure and riftogenesis of the Valencia Trough (north-western Mediterranean Sea). *Basin Research*, 11(4), 357–379. <https://doi.org/10.1046/j.1365-2117.1999.00105.x>
- Maillard, A., & Mauffret, A. (2006). Relationship between erosion surfaces and Late Miocene Salinity Crisis deposits in the Valencia Basin (northwestern Mediterranean): Evidence for an early sea-level fall. *Terra Nova*, 18(5), 321–329. <https://doi.org/10.1111/j.1365-3121.2006.00696.x>
- Maillard, A., & Mauffret, A. (2013a). Structure and present-day compression in the offshore area between Alicante and Ibiza Island (eastern Iberian margin). *Tectonophysics*, 591, 116–130. <https://doi.org/10.1016/j.tecto.2011.07.007>
- Maillard, A., & Mauffret, A. (2013b). Structure and present-day compression in the offshore area between Alicante and Ibiza Island (Eastern Iberian Margin). *Tectonophysics*, 591. <https://doi.org/10.1016/j.tecto.2011.07.007>
- Maillard, A., Mauffret, A., Watts, A. B., Torné, M., Pascal, G., Buhl, P., & Pinet, B. (1992). Tertiary sedimentary history and structure of the Valencia trough (western Mediterranean). *Tectonophysics*, 203(1–4), 57–75. [https://doi.org/10.1016/0040-1951\(92\)90215-R](https://doi.org/10.1016/0040-1951(92)90215-R)
- Maillard, A., MAUFFRET, A., Watts, A., Torne, M., PASCAL, G., BUHL, P., & PINET, B. (1992). Tertiary sedimentary history and structure of the Valencia Trough Western Mediterranean), In *Geology and Geophysics of the Valencia Trough, Western*

Mediterranean. *Tectonophysics*, 203, 57–75. [https://doi.org/10.1016/0040-1951\(92\)90215-R](https://doi.org/10.1016/0040-1951(92)90215-R)

- Malinverno, A., & Ryan, W. B. F. (1986a). Extension in the Tyrrhenian Sea and shortening in the Apennines as result of arc migration driven by sinking of the lithosphere. *Tectonics*, 5(2), 227–245.
- Malinverno, A., & Ryan, W. B. F. (1986b). Extension in the Tyrrhenian Sea and shortening in the Apennines as result of arc migration driven by sinking of the lithosphere. *Tectonics*, 5(2), 227–245. <https://doi.org/10.1029/TC005i002p00227>
- Manzi, V., Gennari, R., Hilgen, F., Krijgsman, W., Lugli, S., Roveri, M., & Sierro, F. J. (2013a). Age refinement of the Messinian salinity crisis onset in the Mediterranean. *Terra Nova*, 25(4), 315–322.
- Manzi, V., Gennari, R., Hilgen, F., Krijgsman, W., Lugli, S., Roveri, M., & Sierro, F. J. (2013b). Age refinement of the Messinian salinity crisis onset in the Mediterranean. *Terra Nova*, 25(4), 315–322. <https://doi.org/10.1111/ter.12038>
- Manzi, V., Gennari, R., Lugli, S., Minelli, N., Reghizzi, M., Roveri, M., & Schreiber, B. C. (2016). Comment on “Carbonate deposition and diagenesis in evaporitic environments: The evaporative and sulphur-bearing limestones during the settlement of the Messinian Salinity Crisis in Sicily and Calabria” by Caruso et al., 2015. *Palaeo3*, 429, 136–162. *Palaeogeography, Palaeoclimatology, Palaeoecology*, C(459), 585–596. <https://doi.org/10.1016/j.palaeo.2016.01.037>
- Manzi, V., Gennari, R., Lugli, S., Persico, D., Reghizzi, M., Roveri, M., Schreiber, B. C., Calvo, R., Gavrieli, I., & Gvirtzman, Z. (2018a). The onset of the Messinian salinity crisis in the deep Eastern Mediterranean basin. *Terra Nova*, 30(3), 189–198.
- Manzi, V., Gennari, R., Lugli, S., Persico, D., Reghizzi, M., Roveri, M., Schreiber, B. C., Calvo, R., Gavrieli, I., & Gvirtzman, Z. (2018b). The onset of the Messinian salinity crisis in the deep Eastern Mediterranean basin. *Terra Nova*, 30(3), 189–198. <https://doi.org/10.1111/ter.12325>
- Manzi, V., Gennari, R., Lugli, S., Persico, D., Roveri, M., Gavrieli, I., & Gvirtzman, Z. (2021). Synchronous onset of the Messinian salinity crisis and diachronous evaporite deposition: New evidences from the deep Eastern Mediterranean basin. *Palaeogeography,*

Palaeoclimatology, Palaeoecology, 584, 110685.
<https://doi.org/10.1016/j.palaeo.2021.110685>

- Manzi, V., Gennari, R., Lugli, S., ROVERI, M., Scafetta, N., & Schreiber, B. C. (2012). High-Frequency Cyclicity In the Mediterranean Messinian Evaporites: Evidence For Solar–Lunar Climate Forcing. *Journal of Sedimentary Research*, 82(12), 991–1005. <https://doi.org/10.2110/jsr.2012.81>
- Manzi, V., Lugli, S., Lucchi, F. R., & Roveri, M. (2005a). Deep-water clastic evaporites deposition in the Messinian Adriatic foredeep (northern Apennines, Italy): Did the Mediterranean ever dry out? *Sedimentology*, 52(4), 875–902. <https://doi.org/10.1111/j.1365-3091.2005.00722.x>
- Manzi, V., Lugli, S., Lucchi, F. R., & Roveri, M. (2005b). Deep-water clastic evaporites deposition in the Messinian Adriatic foredeep (northern Apennines, Italy): Did the Mediterranean ever dry out? *Sedimentology*, 52(4), 875–902. <https://doi.org/10.1111/j.1365-3091.2005.00722.x>
- Manzi, V., Lugli, S., Roveri, M., & Charlotte Schreiber, B. (2009a). A new facies model for the Upper Gypsum of Sicily (Italy): Chronological and palaeoenvironmental constraints for the Messinian salinity crisis in the Mediterranean. *Sedimentology*, 56(7), 1937–1960.
- Manzi, V., Lugli, S., Roveri, M., & Charlotte Schreiber, B. (2009b). A new facies model for the Upper Gypsum of Sicily (Italy): Chronological and palaeoenvironmental constraints for the Messinian salinity crisis in the Mediterranean. *Sedimentology*, 56(7), 1937–1960. <https://doi.org/10.1111/j.1365-3091.2009.01063.x>
- Manzi, V., Lugli, S., Roveri, M., Dela Pierre, F., Gennari, R., Lozar, F., Natalicchio, M., Schreiber, B. C., Taviani, M., & Turco, E. (2016). The Messinian salinity crisis in Cyprus: A further step towards a new stratigraphic framework for Eastern Mediterranean. *Basin Research*, 28(2), 207–236. <https://doi.org/10.1111/bre.12107>
- Manzi, V., Lugli, S., Roveri, M., Schreiber, B., & Gennari, R. (2011). The Messinian “Calcare di Base” (Sicily, Italy) revisited. *Geological Society of America Bulletin*, 123, 347–370. <https://doi.org/10.1130/B30262.1>
- Manzi, V., Roveri, M., Argnani, A., Cowan, D., & Lugli, S. (2021). Large-scale mass-transport deposits recording the collapse of an evaporitic platform during the Messinian

- salinity crisis (Caltanissetta basin, Sicily). *Sedimentary Geology*, 424, 106003. <https://doi.org/10.1016/j.sedgeo.2021.106003>
- Manzi, V., Roveri, M., Gennari, R., Bertini, A., Biffi, U., Giunta, S., Iaccarino, S., Lanci, L., Lugli, S., Negri, A., Riva, A., Rossi, M., & Taviani, M. (2007a). The deep-water counterpart of the Messinian Lower Evaporites in the Apennine foredeep: The Fanantello section (Northern Apennines, Italy). *Palaeogeography Palaeoclimatology Palaeoecology*, 251, 470–499. <https://doi.org/10.1016/j.palaeo.2007.04.012>
 - Manzi, V., Roveri, M., Gennari, R., Bertini, A., Biffi, U., Giunta, S., Iaccarino, S. M., Lanci, L., Lugli, S., Negri, A., Riva, A., Rossi, M. E., & Taviani, M. (2007b). The deep-water counterpart of the Messinian Lower Evaporites in the Apennine foredeep: The Fanantello section (Northern Apennines, Italy). *Palaeogeography, Palaeoclimatology, Palaeoecology*, 251(3–4), 470–499. <https://doi.org/10.1016/j.palaeo.2007.04.012>
 - Martí, J., Mitjavila, J., Roca, E., & Aparicio, A. (1992a). Cenozoic Magmatism of the Valencia trough (western Mediterranean): Relationships between structural evolution and volcanism. *Tectonophysics*, 203, 145–165.
 - Martí, J., Mitjavila, J., Roca, E., & Aparicio, A. (1992b). Cenozoic magmatism of the valencia trough (western mediterranean): Relationship between structural evolution and volcanism*. *Tectonophysics*, 203(1), 145–165. [https://doi.org/10.1016/0040-1951\(92\)90221-Q](https://doi.org/10.1016/0040-1951(92)90221-Q)
 - Martín, JoséM., & Braga, J. C. (1994). Messinian events in the Sorbas Basin in southeastern Spain and their implications in the recent history of the Mediterranean. *Sedimentary Geology*, 90(3–4), 257–268. [https://doi.org/10.1016/0037-0738\(94\)90042-6](https://doi.org/10.1016/0037-0738(94)90042-6)
 - Martín-Closas, C., & Guerrero, E. R. (2005). Palaeogene Charophytes of the Balearic Islands (Spain). *Geologica Acta*, 3(1), 39–58.
 - Martínez-Martínez, J. M., & Azañón, J. M. (1997). Mode of extensional tectonics in the southeastern Betics (SE Spain): Implications for the tectonic evolution of the peri-Alborán orogenic system. *Tectonics*, 16(2), 205–225. <https://doi.org/10.1029/97TC00157>
 - Martínez-Martínez, J. M., Booth-Rea, G., Azañón, J. M., & Torcal, F. (2006). Active transfer fault zone linking a segmented extensional system (Betics, southern Spain): Insight

into heterogeneous extension driven by edge delamination. *Tectonophysics*, 422(1), 159–173. <https://doi.org/10.1016/j.tecto.2006.06.001>

- Marzocchi, A., Flecker, R., Baak, C. G. C. van, Lunt, D. J., & Krijgsman, W. (2016). Mediterranean outflow pump: An alternative mechanism for the Lago-mare and the end of the Messinian Salinity Crisis. *Geology*, 44(7), 523–526. <https://doi.org/10.1130/G37646.1>
- Mas, G., & Fornós, J. J. (2011). *The Messinian Salinity Crisis Record in the Palma Basin (Mallorca, Balearic Islands, Western Mediterranean)*.
- Mas, G., & Fornós, J. J. (2013). *Late Messinian Lago-Mare deposits of the island of Mallorca (Western Mediterranean). Implications on the MSC events*.
- Mas, G., & Fornós, J. J. (2020). The Messinian Salinity Crisis in Mallorca: New insights for a Western Mediterranean stratigraphic scenario. *Marine and Petroleum Geology*, 122, 104656. <https://doi.org/10.1016/j.marpetgeo.2020.104656>
- Mas, G. G. (2015). *EL REGISTRE ESTRATIGRÀFIC DEL MESSINIÀ TERMINAL I DEL PLIOCÈ A L'ILLA DE MALLORCA. RELACIONS AMB LA CRISI DE SALINITAT DE LA MEDITERRÀNIA*. Universitat des Iles Baléares.
- Mas, G., Maillard, A., Alcover, J. A., Fornós, J. J., Bover, P., & Torres-Roig, E. (2018). Terrestrial colonization of the Balearic Islands: New evidence for the Mediterranean sea-level drawdown during the Messinian Salinity Crisis. *Geology*, 46(6), 527–530. <https://doi.org/10.1130/G40260.1>
- Mas Gornals, G., Bisconti, M., Torres-Roig, E., Juárez Ruiz, J., & Sacarès, J. (2018). *THE LAST WHALE OF THE MESSINIAN. FIRST RECORD OF A MYSTICETE CETACEAN FROM THE MEDITERRANEAN MESSINIAN SALINITY CRISIS*.
- Mas Gornals, G., & Fornós, J. (2012). The Messinian Salinity Crisis Record in the Palma basin (Mallorca, Balearic Islands). *Geogaceta*, 52, 57–60.
- Mas Gornals, G., & Fornós, J. (2013). *Late Messinian Lago-Mare deposits of the island of Mallorca (Western Mediterranean). Implications on the MSC events*.
- Mas Gornals, G., Gelabert, B., & Fornós, J. (2014). *Evidencias de desplazamiento direccional de la falla de Sencelles (Mallorca, Islas Baleares). Evidence of strike-slip displacement of the Sencelles fault (Mallorca, Balearic Islands)*.

- Mascle, G., & Mascle, J. (2019). The Messinian salinity legacy: 50 years later. *Mediterranean Geoscience Reviews*, *1*(1), 5–15. <https://doi.org/10.1007/s42990-019-0002-5>
- Mascle, J., & Réhault, J. (1990). *A Revised Seismic Stratigraphy of the Tyrrhenian Sea: Implications for the Basin Evolution*. <https://doi.org/10.2973/ODP.PROC.SR.107.181.1990>
- MATAILLET, R., & J, P. (1978). *ETUDE GEOLOGIQUE DE L'EXTREMITÉ OCCIDENTALE DE LA SIERRA NORD DE MAJORQUE (BALEARES, ESPAGNE)*.
- MATTAUER, M. (2006). Comment est née la méditerranée? Hypothèses sur les rôles respectifs du rift oligocène ouest-européen et des grands courants asthénosphériques mio-pliocènes. *Bulletin de La Société d'histoire Naturelle de Toulouse*, *142*, 5–8.
- Mauffret, A. (1969). Les dômes et les structures “anticlinales” de la Méditerranée occidentale au Nord-Est des baléares. *Inst. Francais Petrole Rev.*, *24*(7–8), 953–960.
- Mauffret, A. (1977). *Etude géodynamique de la marge des îles Baléares*.
- Mauffret, A., El-Robrini, M., & Genesseeux, M. (1987). Indice de la compression recente en mer Mediterranee; un bassin losangique sur la marge nord-algerienne. *Bulletin de La Société Géologique de France*, *III*(6), 1195–1206. <https://doi.org/10.2113/gssgfbull.III.6.1195>
- Mauffret, A., Frizon de Lamotte, D., Lallemand, S., Gorini, C., & Maillard, A. (2004a). E-W opening of the Algerian Basin (Western Mediterranean). *Terra Nova*, *16*(5), 257–264. <https://doi.org/10.1111/j.1365-3121.2004.00559.x>
- Mauffret, A., Frizon de Lamotte, D., Lallemand, S., Gorini, C., & Maillard, A. (2004b). E-W opening of the Algerian Basin (Western Mediterranean). *Terra Nova*, *16*, 257–264. <https://doi.org/10.1111/j.1365-3121.2004.00559.x>
- Mauffret, A., Maillard, A., Torné, M., Pascal, G., Buhl, P., & Pinet, B. (1992). *Long-listening multichannel seismic profiles in the Valencia trough (Valsis 2) and the Gulf of Lions (ECORS): A comparison*. <https://doi.org/10.13039/100000001>
- Mauffret, A., Pascal, G., Maillard, A., & Gorini, C. (1995). Tectonics and deep structure of the north-western Mediterranean Basin. *Marine and Petroleum Geology*, *12*(6), 645–666. [https://doi.org/10.1016/0264-8172\(95\)98090-R](https://doi.org/10.1016/0264-8172(95)98090-R)

- McCaffrey, M. A., Lazar, B., & Holland, H. D. (1987). The evaporation path of seawater and the coprecipitation of Br (super -) and K (super +) with halite. *Journal of Sedimentary Research*, 57(5), 928–937. <https://doi.org/10.1306/212F8CAB-2B24-11D7-8648000102C1865D>
- McKenzie, D. (1978). Some remarks on the development of sedimentary basins. *Earth and Planetary Science Letters*, 40(1), 25–32. [https://doi.org/10.1016/0012-821X\(78\)90071-7](https://doi.org/10.1016/0012-821X(78)90071-7)
- Medaouri, M., Déverchère, J., Graindorge, D., Bracene, R., Badji, R., Ouabadi, A., Yelles-Chaouche, K., & Bendiab, F. (2014). The transition from Alboran to Algerian basins (Western Mediterranean Sea): Chronostratigraphy, deep crustal structure and tectonic evolution at the rear of a narrow slab rollback system. *Journal of Geodynamics*, 77, 186–205. <https://doi.org/10.1016/j.jog.2014.01.003>
- Meghraoui, M. (1988). *Géologie des zones sismiques du Nord de l'Algérie: Paléosismologie, tectonique active et synthèse sismotectonique* [These de doctorat, Paris 11]. <https://www.theses.fr/1988PA112220>
- Meijer, P. (2006). A box model of the blocked-outflow scenario for the Messinian Salinity Crisis. *Earth and Planetary Science Letters*, 248(1–2), 486–494. <https://doi.org/10.1016/j.epsl.2006.06.013>
- Meijer, P., & Krijgsman, W. (2005a). A quantitative analysis of the desiccation and re-filling of the Mediterranean during the Messinian Salinity Crisis. *Earth and Planetary Science Letters*, 240(2), 510–520. <https://doi.org/10.1016/j.epsl.2005.09.029>
- Meijer, P., & Krijgsman, W. (2005b). A quantitative analysis of the desiccation and re-filling of the Mediterranean during the Messinian Salinity Crisis. *Earth and Planetary Science Letters*, 240(2), 510–520. <https://doi.org/10.1016/j.epsl.2005.09.029>
- Meijer, P. T. (2012). Hydraulic theory of sea straits applied to the onset of the Messinian Salinity Crisis. *Marine Geology*, 326–328, 131–139. <https://doi.org/10.1016/j.margeo.2012.09.001>
- Meijninger, B. M. L., & Vissers, R. L. M. (2006). Miocene extensional basin development in the Betic Cordillera, SE Spain revealed through analysis of the Alhama de Murcia and Crevillente Faults. *Basin Research*, 18(4), 547–571. <https://doi.org/10.1111/j.1365-2117.2006.00308.x>

- Meilijson, A., Hilgen, F., Sepúlveda, J., Steinberg, J., Fairbank, V., Flecker, R., Waldmann, N. D., Spaulding, S. A., Bialik, O. M., Boudinot, F. G., Illner, P., & Makovsky, Y. (2019a). Chronology with a pinch of salt: Integrated stratigraphy of Messinian evaporites in the deep Eastern Mediterranean reveals long-lasting halite deposition during Atlantic connectivity. *Earth-Science Reviews*, 194(May), 374–398. <https://doi.org/10.1016/j.earscirev.2019.05.011>
- Meilijson, A., Hilgen, F., Sepúlveda, J., Steinberg, J., Fairbank, V., Flecker, R., Waldmann, N., Spaulding, S., Bialik, O., Boudinot, F. G., Illner, P., & Makovsky, Y. (2019b). Chronology with a pinch of salt: Integrated stratigraphy of Messinian evaporites in the deep Eastern Mediterranean reveals long-lasting halite deposition during Atlantic connectivity. *Earth-Science Reviews*. <https://doi.org/10.1016/J.EARSCIREV.2019.05.011>
- Meilijson, A., Liu, J., & Makovsky, Y. (2022). *In and Out of the Salt: How to Overcome Stratigraphic Uncertainty in Evaporitic Systems? A Case Study from the MSC in the Deep Levant Basin* (pp. 213–216). https://doi.org/10.1007/978-3-030-72547-1_47
- Meilijson, A., Makovsky, Y., Steinberg, J., Bialik, O., Spaulding, S. A., Hilgen, F., Waldmann, N., Flecker, R., Boudinot, F. G., Fairbank, V., & Sepúlveda, J. (2019). *Data for: Chronology with a pinch of salt: integrated stratigraphy of Messinian evaporites in the deep Eastern Mediterranean reveals long lasting halite deposition during Atlantic connectivity. 1*. <https://doi.org/10.17632/ngjtc2hzk9.1>
- Meilijson, A., Steinberg, J., Hilgen, F., Bialik, O. M., Waldmann, N. D., & Makovsky, Y. (2018). Deep-basin evidence resolves a 50-year-old debate and demonstrates synchronous onset of Messinian evaporite deposition in a non-desiccated Mediterranean. *Geology*, 46(3), 243–246. <https://doi.org/10.1130/G39868.1>
- Mercier de Lépinay, M., Loncke, L., Basile, C., Roest, W. R., Patriat, M., Maillard, A., & De Clarens, P. (2016). Transform continental margins – Part 2: A worldwide review. *Tectonophysics*, 693, 96–115. <https://doi.org/10.1016/j.tecto.2016.05.038>
- Micallef, A., Camerlenghi, A., Garcia-Castellanos, D., Cunarro Otero, D., Gutscher, M. A., Barreca, G., Spatola, D., Facchin, L., Geletti, R., Krastel, S., Gross, F., & Urlaub, M. (2018). Evidence of the Zanclean megaflood in the eastern Mediterranean Basin. *Scientific Reports*, 8(1), 1–8. <https://doi.org/10.1038/s41598-018-19446-3>

- Micallef, A., Camerlenghi, A., Garcia-Castellanos, D., Otero, D. C., Gutscher, M.-A., Barreca, G., Spatola, D., Facchin, L., Geletti, R., Krastel, S., Gross, F., & Urlaub, M. (2018). Evidence of the Zanclean megaflood in the eastern Mediterranean Basin. *Scientific Reports*, 8(1), 1078. <https://doi.org/10.1038/s41598-018-19446-3>
- Micallef, A., Camerlenghi, A., Georgiopoulou, A., Garcia-Castellanos, D., Gutscher, M.-A., Lo Iacono, C., Huvenne, V. A. I., Mountjoy, J. J., Paull, C. K., Le Bas, T., Spatola, D., Facchin, L., & Accettella, D. (2019). Geomorphic evolution of the Malta Escarpment and implications for the Messinian evaporative drawdown in the eastern Mediterranean Sea. *Geomorphology*, 327, 264–283. <https://doi.org/10.1016/j.geomorph.2018.11.012>
- Mitchum, R. M., & Vail, P. R. (1977). *Seismic Stratigraphy and Global Changes of Sea Level, Part 7: Seismic Stratigraphic Interpretation Procedure*. <https://doi.org/10.1306/M26490C9>
- MONTADERT, L., J, S., JP, F., J, D., & E, W. (1970). *DE L'AGE TERTIAIRE DE LA SERIE SALIFERE RESPONSABLE DES STRUCTURES DIAPIRIQUES EN MEDITERRANEE OCCIDENTALE (NORD-EST DES BALEARES)*.
- MONTENAT, C., OTT D'ESTEVOU, P., & COPPIER, G. (1990). Les bassins néogènes entre Alicante et Cartagena. *Les Bassins Néogènes Entre Alicante et Cartagena*, 12–13, 313–368.
- Moragues, L., Booth-Rea, G., Ruano, P., Azañón, J. M., Gaidi, S., & Pérez-Peña, J. V. (2018). Middle Miocene extensional tectonics in Southeast Mallorca Island (Western Mediterranean). *Revista de La Sociedad Geológica de España*, 31(2), 101–110.
- Moragues, L., Ruano, P., Azañón, J., Garrido, C. J., Hidas, K., & Booth-Rea, G. (2021). *Two Cenozoic extensional phases in Mallorca and their implications in the geodynamic evolution of the western Mediterranean*. <https://doi.org/10.1002/essoar.10506816.1>
- Morey, B., & Mas, G. (2009). Aproximació al Neogen de Santa Eugènia (Mallorca, Illes Balears, Mediterrània occidental). *Bolletí de la Societat d'Història Natural de les Balears*, 99–122.
- Mottershead, D. N., DUANE, W., Inkpen, R., & J.S.Wright. (2005). *Subaerial karstic erosion of small scale saltrock terrains, Cardona, Spain*.

- Muñoz, A., Lastras, G., Ballesteros, M., Canals, M., Acosta, J., & Uchupi, E. (2005). Sea floor morphology of the Ebro Shelf in the region of the Columbretes Islands, Western Mediterranean. *Geomorphology*, 72(1–4), 1–18.
- Natalicchio, M., Birgel, D., Dela Pierre, F., Martire, L., Clari, P., Spötl, C., & Peckmann, J. (2012). Polyphasic carbonate precipitation in the shallow subsurface: Insights from microbially-formed authigenic carbonate beds in upper Miocene sediments of the Tertiary Piedmont Basin (NW Italy). *Palaeogeography Palaeoclimatology Palaeoecology*. <https://doi.org/10.1016/j.palaeo.2012.02.026>
- Natalicchio, M., Dela Pierre, F., Lugli, S., Lowenstein, T. K., Feiner, S. J., Ferrando, S., Manzi, V., Roveri, M., & Clari, P. (2014). Did late miocene (Messinian) gypsum precipitate from evaporated marine brines? Insights from the piedmont basin (Italy). *Geology*, 42(3), 179–182. <https://doi.org/10.1130/G34986.1>
- Natalicchio, M., Pellegrino, L., Clari, P., Pastero, L., & Dela Pierre, F. (2021). Gypsum lithofacies and stratigraphic architecture of a Messinian marginal basin (Piedmont Basin, NW Italy). *Sedimentary Geology*, 425, 106009. <https://doi.org/10.1016/j.sedgeo.2021.106009>
- Negrodo, A., Fernández, M., Torné, M., & Doglioni, C. (1999). Numerical modeling of simultaneous extension and compression: The Valencia trough (western Mediterranean). *Tectonics*, 18(2), 361–374. <https://doi.org/10.1029/1998TC900026>
- Nely, G. (1994). *Evaporite Sequences in Petroleum Exploration: Geophysical Methods* (Technip Editions, 1994, Vol. 2).
- Nesteroff, W. D. (1973). Un modèle pour les évaporites messiniennes en Méditerranée: Des bassins peu profonds avec dépôts d'évaporites lagunaires. In *Messinian events in the Mediterranean* (Vol. 7, pp. 68–81). North-Holland Amsterdam.
- Nocquet, J.-M., & Calais, E. (2003). Crustal velocity field of western Europe from permanent GPS array solutions, 1996–2001. *Geophysical Journal International*, 154(1), 72–88. <https://doi.org/10.1046/j.1365-246X.2003.01935.x>
- Norman, S. E., & Chase, C. G. (1986). Uplift of the shores of the western mediterranean due to messinian desiccation and flexural isostasy. *Nature*, 322(6078), 450–451. <https://doi.org/10.1038/322450a0>

- Obone-Zue-Obame, E. M., Gaullier, V., Sage, F., Maillard, A., Lofi, J., Vendeville, B., Thinon, I., Rehault, J.-P., & the Mauresc Shipboard scientific party. (2011). The sedimentary markers of the Messinian salinity crisis and their relation with salt tectonics on the Provençal margin (western Mediterranean): Results from the “MAURESC” cruise. *Bulletin de La Société Géologique de France*, 182(2), 181–196. <https://doi.org/10.2113/gssgfbull.182.2.181>
- Ochoa, D. L. (2016). *Astrobiochronological Constraints on Margin to deep basin correlations across the Balearic Promontory and the Valencia basin* [Http://purl.org/dc/dcmitype/Text, Universidad de Salamanca]. <https://dialnet.unirioja.es/servlet/tesis?codigo=155521>
- Ochoa, D., Sierro, F., Hilgen, F., Cortina, A., Lofi, J., Kouwenhoven, T., & Flores, J. (2018). Origin and implications of orbital-induced sedimentary cyclicity in Pliocene well-logs of the Western Mediterranean. *Marine Geology*, 403. <https://doi.org/10.1016/j.margeo.2018.05.009>
- Ochoa, D., Sierro, F. J., Lofi, J., Maillard, A., Flores, J. A., & Suárez, M. (2015a). Synchronous onset of the Messinian evaporite precipitation: First Mediterranean offshore evidence. *Earth and Planetary Science Letters*, 427, 112–124. <https://doi.org/10.1016/j.epsl.2015.06.059>
- Ochoa, D., Sierro, F. J., Lofi, J., Maillard, A., Flores, J. A., & Suárez, M. (2015b). Synchronous onset of the Messinian evaporite precipitation: First Mediterranean offshore evidence. *Earth and Planetary Science Letters*, 427, 112–124. <https://doi.org/10.1016/j.epsl.2015.06.059>
- Ochoa, D., Sierro, F. J., Lofi, J., Maillard, A., Flores, J.-A., & Suárez, M. (2015c). Synchronous onset of the Messinian evaporite precipitation: First Mediterranean offshore evidence. *Earth and Planetary Science Letters*, 427, 112–124. <https://doi.org/10.1016/j.epsl.2015.06.059>
- Odonne, F., Maillard, A., Lézin, C., Chanier, F., Gaullier, V., & Guillaume, D. (2019). Large-scale boudinage of late Miocene platform series triggered by margin collapse during the messinian salinity crisis (Ibiza island, Spain). *Marine and Petroleum Geology*, 109, 852–867. <https://doi.org/10.1016/j.marpetgeo.2019.06.058>

- Ogniben, L. (1957). *Petrografia della serie solfifera siciliana e considerazioni geologiche relative*. <https://fr.maremagnum.com/libri-antichi/petrografia-della-serie-solfifera-siciliana-e-considerazioni/131340543>
- Olivet, J. (1996). La cinématique de la plaque Ibérique. *Bulletin Des Centres de Recherches Exploration-Production Elf-Aquitaine*, 20, 131–195.
- Orszag-Sperber, F. (2006a). Changing perspectives in the concept of “Lago-Mare” in Mediterranean Late Miocene evolution. *Sedimentary Geology*, 188–189, 259–277. <https://doi.org/10.1016/j.sedgeo.2006.03.008>
- Orszag-Sperber, F. (2006b). Changing perspectives in the concept of “Lago-Mare” in Mediterranean Late Miocene evolution. *Sedimentary Geology*, 188–189, 259–277. <https://doi.org/10.1016/j.sedgeo.2006.03.008>
- Orszag-Sperber, F., Caruso, A., Blanc-Valleron, M.-M., Merle, D., & Rouchy, J. M. (2009). The onset of the Messinian salinity crisis: Insights from Cyprus sections. *Sedimentary Geology*, 217(1–4), 52–64.
- Orti Cabo, F., Pueyo Mur, J. J., Geisler-Cussey, D., & Dulau, N. (1984). *Evaporitic sedimentation in the coastal salinas of Santa Pola, Alicante, Spain*.
- Ott d’Estevou, P., & Montenat, C. (1990). Le bassin de Sorbas-Tabernas. In *Les bassins Neogenes du domaine Betique Oriental (Espagne)* (pp. 101–128).
- Ouillon, R., Lensky, N. G., Lyakhovsky, V., Arnon, A., & Meiburg, E. (2019). Halite precipitation from double-diffusive salt fingers in the Dead Sea: Numerical simulations. *Water Resources Research*, May, 2019WR024818-2019WR024818. <https://doi.org/10.1029/2019WR024818>
- Padon, O., & Ashkenazy, Y. (2018). Non-hydrostatic effects in the Dead Sea. *Journal of Marine Systems*, 187, 36–51. <https://doi.org/10.1016/j.jmarsys.2018.06.007>
- Pagnier, H. (1976). Depth of deposition of Messinian selenitic gypsum in the Basin of Sorbas (SE Spain). *Mem. Soc. Geol. It.* 16, 363-367., 16, 363–367.
- Panieri, G., Lugli, S., Manzi, V., Roveri, M., Schreiber, B., & Palinska, K. (2010). Ribosomal RNA gene fragments from fossilized cyanobacteria identified in primary gypsum from the late Miocene, Italy. *Geobiology*, 8, 101–111. <https://doi.org/10.1111/j.1472-4669.2009.00230.x>

- Parés, J., Freeman, R., & Roca, E. (1992). *Neogene structural development in the Valencia trough margins from palaeomagnetic data*. [https://doi.org/10.1016/0040-1951\(92\)90218-U](https://doi.org/10.1016/0040-1951(92)90218-U)
- Pascal, G., Torné, M., Buhl, P., Watts, A. B., & Mauffret, A. (1992). Crustal and velocity structure of the Valencia Trough (Western Mediterranean) Part II: detailed interpretation of 5 expanded spread profiles. *Tectonophysics*, 203, 21–35.
- Pautot, G., Auzende, J.-M., & Le Pichon, X. (1970). Continuous Deep Sea Salt Layer along North Atlantic Margins related to Early Phase of Rifting. *Nature*, 227(5256), 351–354. <https://doi.org/10.1038/227351a0>
- PEDLEY, M., & MANISCALCO, R. (1999). Lithofacies and faunal succession (faunal phase analysis) as a tool in unravelling climatic and tectonic signals in marginal basins; Messinian (Miocene), Sicily. *Journal of the Geological Society*, 156(4), 855–863. <https://doi.org/10.1144/gsjgs.156.4.0855>
- Pellegrino, L., Natalicchio, M., Abe, K., Jordan, R. W., Longo, S. E. F., Ferrando, S., Carnevale, G., & Pierre, F. D. (2021). Tiny, glassy, and rapidly trapped: The nano-sized planktic diatoms in Messinian (late Miocene) gypsum. *Geology*, 49(11), 1369–1374. <https://doi.org/10.1130/G49342.1>
- Pellen, R., Aslanian, D., Rabineau, M., Leroux, E., Gorini, C., Silenziario, C., Blanpied, C., & Rubino, J.-L. (2016). The Minorca Basin: A buffer zone between the Valencia and Liguro-Provençal Basins (NW Mediterranean Sea). *Terra Nova*, 28(4), 245–256. <https://doi.org/10.1111/ter.12215>
- Pellen, R., Aslanian, D., Rabineau, M., Suc, J. P., Gorini, C., Leroux, E., Blanpied, C., Silenziario, C., Popescu, S. M., & Rubino, J. L. (2019a). The Messinian Ebro River incision. *Global and Planetary Change*, 181(July), 102988–102988. <https://doi.org/10.1016/j.gloplacha.2019.102988>
- Pellen, R., Aslanian, D., Rabineau, M., Suc, J. P., Gorini, C., Leroux, E., Blanpied, C., Silenziario, C., Popescu, S. M., & Rubino, J. L. (2019b). The Messinian Ebro River incision. *Global and Planetary Change*, 181, 102988. <https://doi.org/10.1016/j.gloplacha.2019.102988>

- Perri, E., Gindre-Chanu, L., Caruso, A., Cefala, M., Scopelliti, G., & Tucker, M. (2017). Microbial-mediated pre-salt carbonate deposition during the Messinian salinity crisis (Calcare di Base fm., Southern Italy). *Marine and Petroleum Geology*, 88. <https://doi.org/10.1016/j.marpetgeo.2017.08.028>
- Pierre, C., Caruso, A., Blanc-Valleron, M.-M., Rouchy, J. M., & Orzsag-Sperber, F. (2006). Reconstruction of the paleoenvironmental changes around the Miocene–Pliocene boundary along a West–East transect across the Mediterranean. *Sedimentary Geology*, 188–189, 319–340. <https://doi.org/10.1016/j.sedgeo.2006.03.011>
- Pigott, J. D., & Abdel-Fattah, M. I. (2014). Seismic stratigraphy of the Messinian Nile Delta coastal plain: Recognition of the fluvial Regressive Systems Tract and its potential for hydrocarbon exploration. *Journal of African Earth Sciences*, 95, 9–21. <https://doi.org/10.1016/j.jafrearsci.2014.02.003>
- Piñol, F. C., Astó, J. J. F., Marzo, M., Gomà, L. P., Guerrero, E. R., & Perea, A. R. (1991). *Evolución tectono-sedimentaria y análisis estratigráfico del terciario de la isla de Mallorca: I Congreso Español del Terciario*. F. Colombo. <https://dialnet.unirioja.es/servlet/libro?codigo=784303>
- Pinot, J.-M., López-Jurado, J. L., & Riera, M. (2002). The CANALES experiment (1996–1998). Interannual, seasonal, and mesoscale variability of the circulation in the Balearic Channels. *Progress in Oceanography*, 55(3), 335–370. [https://doi.org/10.1016/S0079-6611\(02\)00139-8](https://doi.org/10.1016/S0079-6611(02)00139-8)
- Pomar, L. (1991). Reef geometries, erosion surfaces and high-frequency sea-level changes, upper Miocene Reef Complex, Mallorca, Spain. *Sedimentology*, 38, 243–269. <https://doi.org/10.1111/j.1365-3091.1991.tb01259.x>
- Pomar, L. (2001). Ecological control of sedimentary accommodation: Evolution from a carbonate ramp to rimmed shelf, Upper Miocene, Balearic Islands. *Palaeogeography, Palaeoclimatology, Palaeoecology*, 175(1–4), 249–272. [https://doi.org/10.1016/S0031-0182\(01\)00375-3](https://doi.org/10.1016/S0031-0182(01)00375-3)
- Pomar, L., Marzo, M., & Baron, A. (1983). *El Terciario de Mallorca*. 21–44. <http://pascal-francis.inist.fr/vibad/index.php?action=getRecordDetail&idt=8881371>

- Pomar, L., WARD, W., & Green, D. (1996). Upper Miocene reef complex of the Lluçmajor area, Mallorca, Spain. In *Models for carbonate stratigraphy from Miocene reef complexes of Mediterranean regions* (pp. 191–225). <https://doi.org/10.2110/csp.96.01.0191>
- Poort, J., Lucazeau, F., Le Gal, V., Dal Cin, M., Leroux, E., Bouzid, A., Rabineau, M., Palomino, D., Battani, A., Akhmanov, G. G., Ferrante, G. M., Gafurova, D. R., Si Bachir, R., Koptev, A., Tremblin, M., Bellucci, M., Pellen, R., Camerlenghi, A., Migeon, S., ... Khlystov, O. M. (2020). Heat flow in the Western Mediterranean: Thermal anomalies on the margins, the seafloor and the transfer zones. *Marine Geology*, *419*, 106064. <https://doi.org/10.1016/j.margeo.2019.106064>
- Raad, F., Lofi, J., Maillard, A., Tzevahirtzian, A., & Caruso, A. (2020). The Messinian Salinity Crisis deposits in the Balearic Promontory: An undeformed analog of the MSC Sicilian basins?? *Marine and Petroleum Geology*, *124*, 104777. <https://doi.org/10.1016/j.marpetgeo.2020.104777>
- Raad, F., Lofi, J., Maillard, A., Tzevahirtzian, A., & Caruso, A. (2021). The Messinian Salinity Crisis deposits in the Balearic Promontory: An undeformed analog of the MSC Sicilian basins?? *Marine and Petroleum Geology*, *124*, 104777.
- Ramos-Guerrero, E., Berrio, I., Fornós, J. J., & Moragues, L. (2000). *The Middle Miocene Son Verdera Lacustrine-Palustrine System (Santa Margalida Basin, Mallorca)*. <https://doi.org/10.1306/St46706C40>
- Ramos-Guerrero, E., Rodríguez-Perea, A., Sabat, F., & Serra-Kiel, J. (1989). Cenozoic tectosedimentary evolution of Mallorca island. *Geodinamica Acta*, *3*(1), 53–72. <https://doi.org/10.1080/09853111.1989.11105174>
- Rangheard, Y., Müller, C., & Durand-Delga, M. (2011). Apport de la micropaléontologie, spécialement du nannoplancton, à la connaissance de l'évolution géologique au Miocène de l'île d'Eivissa (Ibiza, Baléares, Espagne). *Comptes Rendus Palevol*, *10*(7), 537–549. <https://doi.org/10.1016/j.crpv.2011.06.004>
- Réhault, J. P., Honthaas, C., Guennoc, P., Bellon, H., Ruffet, G., Cotten, J., Sosson, M., & Maury, R. C. (2012). Offshore Oligo-Miocene volcanic fields within the Corsica-Liguria Basin: Magmatic diversity and slab evolution in the western Mediterranean Sea. *Journal of Geodynamics*, *58*, 73–95. <https://doi.org/10.1016/j.jog.2012.02.003>

- Rehault, J. P., Mascle, J., & Boillot, G. (1984a). Evolution geodynamique de la Méditerranée depuis l'Oligocène. *Memorie Della Società Geologica Italiana*, 27, 85–96.
- Rehault, J. P., Mascle, J., & Boillot, G. (1984b). Evolution geodynamique de la Méditerranée depuis l'Oligocène. *Memorie Della Società Geologica Italiana*, 27, 85–96.
- Réhault, J.-P., Honthaas, C., Guennoc, P., Bellon, H., Ruffet, G., Cotten, J., Sosson, M., & Maury, R. C. (2012). Offshore Oligo-Miocène volcanic fields within the Corsica-Liguria Basin: Magmatic diversity and slab evolution in the western Mediterranean Sea. *Journal of Geodynamics*, 58, 73–95. <https://doi.org/10.1016/j.jog.2012.02.003>
- Riding, R., Braga, J. C., & Martin, J. M. (1991). Oolite stromatolites and thrombolites, Miocène, Espagne: Analogues of Recent giant Bahamian examples. *Sedimentary Geology*, 71(3–4), 121–127. [https://doi.org/10.1016/0037-0738\(91\)90096-V](https://doi.org/10.1016/0037-0738(91)90096-V)
- Riding, R., Braga, J., Martín, J., & Sánchez-Almazo, I. (1998). *Mediterranean Messinian Salinity Crisis: Constraints from a coeval marginal basin, Sorbas, southeastern Spain*. [https://doi.org/10.1016/S0025-3227\(97\)00136-9](https://doi.org/10.1016/S0025-3227(97)00136-9)
- Roca, E. (1992). “L'estructura de la Conca Catalano-balear: Paper de la compressió i de la distensió en la seva gènesi” - PDF Free Download [PhD Thesis, Universitat de Barcelona]. <https://docplayer.es/58709808-L-estructura-de-la-conca-catalano-balear-paper-de-la-compressio-i-de-la-distensio-en-la-seva-genesi.html>
- Roca, E. (2001). The northwest Mediterranean Basin (Valencia Trough, Gulf of Lions and Liguro-Provençal basins): Structure and geodynamic evolution. *Undefined*. [https://www.semanticscholar.org/paper/The-northwest-Mediterranean-Basin-\(Valencia-Trough%2C-Roca/ccb35a41e5a1d0f5a695719ae15e6fa710c8b62d](https://www.semanticscholar.org/paper/The-northwest-Mediterranean-Basin-(Valencia-Trough%2C-Roca/ccb35a41e5a1d0f5a695719ae15e6fa710c8b62d)
- Roca, E., Frizon de Lamotte, D., Mauffret, A., Bracène, R., Vergés, J., Benaouali, N., Fernandez, M., Muñoz, J. A., & Zeyen, H. (2004). *TRANSMED Transect II: Aquitaine Basin - Pyrenees - Ebro Basin - Catalan Coastal Ranges - Valencia Trough - Balearic Promontory - Algerian Basin - Kabylies - Atlas - Saharan Domain*. <https://digital.csic.es/handle/10261/240849>
- Roca, E., & Guimerà, J. (1992a). The Neogene structure of the eastern Iberian margin: Structural constraints on the crustal evolution of the Valencia trough (western

- Mediterranean). *Tectonophysics*, 203(1–4), 203–218. [https://doi.org/10.1016/0040-1951\(92\)90224-T](https://doi.org/10.1016/0040-1951(92)90224-T)
- Roca, E., & Guimerà, J. (1992b). The Neogene structure of the eastern Iberian margin: Structural constraints on the crustal evolution of the Valencia trough (western Mediterranean). *Tectonophysics*, 203(1), 203–218. [https://doi.org/10.1016/0040-1951\(92\)90224-T](https://doi.org/10.1016/0040-1951(92)90224-T)
 - Rodríguez Perea, A. (1984). *El Mioceno de la Serra Nord de Mallorca. Estratigrafia, Sedimentologia e implicaciones estructurales*. <http://dspace.uib.es/xmlui/handle/11201/2491>
 - Roksandić, M. M. (1978). Seismic Facies Analysis Concepts *. *Geophysical Prospecting*, 26(2), 383–398. <https://doi.org/10.1111/j.1365-2478.1978.tb01600.x>
 - Romagny, A., Jolivet, L., Menant, A., Bessiere, E., Maillard, A., Canva, A., Gorini, C., & Augier, R. (2020). Detailed tectonic reconstructions of the Western Mediterranean region for the last 35 Ma, insights on driving mechanisms. *BSGF - Earth Sciences Bulletin*, 191. <https://doi.org/10.1051/bsgf/2020040>
 - Rosell, L., Orti, F., Kasprzyk, A., Playa, E., & Peryt, T. M. (1998a). Strontium geochemistry of Miocene primary gypsum; Messinian of southeastern Spain and Sicily and Badenian of Poland. *Journal of Sedimentary Research*, 68(1), 63–79. <https://doi.org/10.2110/jsr.68.63>
 - Rosell, L., Orti, F., Kasprzyk, A., Playa, E., & Peryt, T. M. (1998b). Strontium geochemistry of Miocene primary gypsum; Messinian of southeastern Spain and Sicily and Badenian of Poland. *Journal of Sedimentary Research*, 68(1), 63–79. <https://doi.org/10.2110/jsr.68.63>
 - Rosenbaum, G., Lister, G., & Duboz, C. (2002a). Reconstruction of the tectonic evolution of the Western Mediterranean since the Oligocene. *Journal of the Virtual Explorer*, 8, 107–130. <https://doi.org/10.3809/jvirtex.2002.00053>
 - Rosenbaum, G., Lister, G. S., & Duboz, C. (2002b). Reconstruction of the tectonic evolution of the western Mediterranean since the Oligocene. *Journal of the Virtual Explorer*, 8(January). <https://doi.org/10.3809/jvirtex.2002.00053>

- ROUCHY, J. (1976). MISE EN EVIDENCE DE NANNOPLANCTON CALCAIRE DANS CERTAINS TYPES DE GYPSE FINEMENT LITE (BALATINO) DU MIOCENE TERMINAL DE SICILE ET CONSEQUENCES SUR LA GENESE DES EVAPORITES MEDITERRANEENNES DE CET AGE. *MISE EN EVIDENCE DE NANNOPLANCTON CALCAIRE DANS CERTAINS TYPES DE GYPSE FINEMENT LITE (BALATINO) DU MIOCENE TERMINAL DE SICILE ET CONSEQUENCES SUR LA GENESE DES EVAPORITES MEDITERRANEENNES DE CET AGE.*
- ROUCHY, J. (1982). LA CRISE EVAPORITIQUE MESSINIENNE DE MEDITERRANEE: NOUVELLES PROPOSITIONS POUR UNE INTERPRETATION GENETIQUE. *LA CRISE EVAPORITIQUE MESSINIENNE DE MEDITERRANEE: NOUVELLES PROPOSITIONS POUR UNE INTERPRETATION GENETIQUE.*
- Rouchy, J. M., & Caruso, A. (2006). The Messinian salinity crisis in the Mediterranean basin: A reassessment of the data and an integrated scenario. *Sedimentary Geology*, 188, 35–67.
- Rouchy, J. M., Orszag-Sperber, F., Blanc-Valleron, M.-M., Pierre, C., Rivière, M., Combourieu-Nebout, N., & Panayides, I. (2001). Paleoenvironmental changes at the Messinian Pliocene boundary in the eastern Mediterranean (southern Cyprus basins): Significance of the Messinian Lago-Mare. *Sedimentary Geology*, 145, 93–117. [https://doi.org/10.1016/S0037-0738\(01\)00126-9](https://doi.org/10.1016/S0037-0738(01)00126-9)
- Rouchy, J., & Saint Martin, J.-P. (1992). Late Miocene events in the Mediterranean as recorded by carbonate-evaporite relations. *Geology*, 20, 629–632. [https://doi.org/10.1130/0091-7613\(1992\)020<0629:LMEITM>2.3.CO;2](https://doi.org/10.1130/0091-7613(1992)020<0629:LMEITM>2.3.CO;2)
- Rouchy, J.-M., & Saint Martin, J.-P. (1992). Late Miocene events in the Mediterranean as recorded by carbonate-evaporite relations. *Geology*, 20, 629–632. [https://doi.org/10.1130/0091-7613\(1992\)](https://doi.org/10.1130/0091-7613(1992)020<0629:LMEITM>2.3.CO;2)
- Roveri, M., Bassetti, M. A., & Ricci Lucchi, F. (2001). The Mediterranean Messinian salinity crisis: An Apennine foredeep perspective. *Sedimentary Geology*, 140(3–4), 201–214. [https://doi.org/10.1016/S0037-0738\(00\)00183-4](https://doi.org/10.1016/S0037-0738(00)00183-4)
- Roveri, M., Flecker, R., Krijgsman, W., Lofi, J., Lugli, S., Manzi, V., Sierro, F. J., Bertini, A., Camerlenghi, A., & De Lange, G. (2014a). The Messinian Salinity Crisis: Past and future of a great challenge for marine sciences. *Marine Geology*, 352, 25–58.

- Roveri, M., Flecker, R., Krijgsman, W., Lofi, J., Lugli, S., Manzi, V., Sierro, F. J., Bertini, A., Camerlenghi, A., De Lange, G., Govers, R., Hilgen, F. J., Hübscher, C., Meijer, P. T., & Stoica, M. (2014b). The Messinian Salinity Crisis: Past and future of a great challenge for marine sciences. *Marine Geology*, 352, 25–58. <https://doi.org/10.1016/j.margeo.2014.02.002>
- Roveri, M., Gennari, R., Ligi, M., Lugli, S., Manzi, V., & Reghizzi, M. (2019). The synthetic seismic expression of the Messinian salinity crisis from onshore records: Implications for shallow- to deep-water correlations. *Basin Research*, bre.12361. <https://doi.org/10.1111/bre.12361>
- Roveri, M., Gennari, R., Lugli, S., & Manzi, V. (2009a). The Terminal Carbonate Complex: The record of sea-level changes during the Messinian salinity crisis. *GeoActa*, 8(April 2015), 63–77.
- Roveri, M., Gennari, R., Lugli, S., & Manzi, V. (2009b). The Terminal Carbonate Complex: The record of sea- level changes during the Messinian salinity crisis. *GeoActa*, 8, 63–77.
- Roveri, M., Gennari, R., Lugli, S., Manzi, V., Minelli, N., Reghizzi, M., Riva, A., Rossi, M., & Schreiber, B. (2016). The Messinian salinity crisis: Open problems and possible implications for Mediterranean petroleum systems. *Petroleum Geoscience*, 22, petgeo2015-089. <https://doi.org/10.1144/petgeo2015-089>
- Roveri, M., Lugli, S., Manzi, V., Gennari, R., & Schreiber, B. C. (2014). High-resolution strontium isotope stratigraphy of the Messinian deep Mediterranean basins: Implications for marginal to central basins correlation. *Marine Geology*, 349, 113–125. <https://doi.org/10.1016/j.margeo.2014.01.002>
- Roveri, M., Lugli, S., Manzi, V., Reghizzi, M., & Rossi, F. P. (2020). Stratigraphic relationships between shallow-water carbonates and primary gypsum: Insights from the Messinian succession of the Sorbas Basin (Betic Cordillera, Southern Spain). *Sedimentary Geology*, 404, 105678. <https://doi.org/10.1016/j.sedgeo.2020.105678>
- Roveri, M., Lugli, S., Manzi, V., & Schreiber, B. C. (2008a). The Messinian salinity crisis: A sequence-stratigraphic approach. *GeoActa*, 1, 169–190.

- Roveri, M., Lugli, S., Manzi, V., & Schreiber, B. C. (2008b). The Messinian Sicilian stratigraphy revisited: New insights for the Messinian salinity crisis. *Terra Nova*, 20(6), 483–488.
- Roveri, M., Manzi, V., Bergamasco, A., Falcieri, F. M., Gennari, R., Lugli, S., & Schreiber, B. C. (2014). Dense shelf water cascading and messinian canyons: A new scenario for the mediterranean salinity crisis. *American Journal of Science*, 314(3), 751–784. <https://doi.org/10.2475/05.2014.03>
- Roveri, M., Manzi, V., Bergamasco, A., Falcieri, F. M., Gennari, R., Lugli, S., & Schreiber, B. C. (2014). Dense shelf water cascading and Messinian Canyons: A new scenario for the Mediterranean salinity crisis. *American Journal of Science*, 314(3), 751–784. <https://doi.org/10.2475/05.2014.03>
- Roveri, M., Manzi, V., Lucchi, F. R., & Rogledi, S. (2003). Sedimentary and tectonic evolution of the Vena del Gesso basin (Northern Apennines, Italy): Implications for the onset of the Messinian salinity crisis. *Geological Society of America Bulletin*, 115(4), 387–405.
- Roveri, M., Manzi, V., Lugli, S., Schreiber, B., Caruso, A., Rouchy, J.-M., Iaccarino, S., Gennari, R., Vitale, F., & Lucchi, F. (2006). Clastic vs. Primary precipitated evaporites in the Messinian Sicilian basins. *L'Ateneo Parmense. Acta Naturalia: Organo Della Società Di Medicina e Scienze Naturali Di Parma*, 42, 125–199.
- Royden, L. H. (1993). Evolution of retreating subduction boundaries formed during continental collision. *Tectonics*, 12(3), 629–638. <https://doi.org/10.1029/92TC02641>
- Ruf, A., Simo, T., Hughes, T., & Steffen, K. (2008). *Insights on the Evolution of Oligocene-miocene Carbonate Buildups from 3D Seismic Data, East Java Basin, Indonesia (Best of AAPG)*. <https://doi.org/10.3997/2214-4609.20147548>
- Ruggieri, G. (1967). *THE MIOCENE AND LATER EVOLUTION OF THE MEDITERRANEAN SEA*.
- Ryan, W. B. (1978). Messinian badlands on the southeastern margin of the Mediterranean Sea. *Marine Geology*, 27(3), 349–363.
- Ryan, W. B. F. (1971). *The Tectonics and Geology of the Mediterranean Sea*. John Wiley & Sons.

- Ryan, W. B. F. (1973). Geodynamic implications of the Messinian crisis of salinity—Google Scholar. *Messinian Events in the Mediterranean*. https://scholar.google.com/scholar?hl=en&as_sdt=0%2C5&q=Geodynamic+implications+of+the+Messinian+crisis+of+salinity&btnG=
- Ryan, W. B. f. (1976). Quantitative evaluation of the depth of the western Mediterranean before, during and after the Late Miocene salinity crisis. *Sedimentology*, 23(6), 791–813. <https://doi.org/10.1111/j.1365-3091.1976.tb00109.x>
- Ryan, W. B. F. (1976). Quantitative evaluation of the depth of the western Mediterranean before, during and after the Late Miocene salinity crisis. *Sedimentology*, 23(6), 791–813. <https://doi.org/10.1111/j.1365-3091.1976.tb00109.x>
- Ryan, W. B. F. (2008). Modeling the magnitude and timing of evaporative drawdown during the Messinian salinity crisis. *Stratigraphy*, 5(3), 227–243.
- Ryan, W. B. F. (2009a). Decoding the mediterranean salinity crisis. *Sedimentology*, 56(1), 95–136. <https://doi.org/10.1111/j.1365-3091.2008.01031.x>
- Ryan, W. B. F. (2009b). Decoding the Mediterranean salinity crisis. *Sedimentology*, 56(1), 95–136. <https://doi.org/10.1111/j.1365-3091.2008.01031.x>
- Ryan, W. B. F. (2011). Geodynamic responses to a two-step model of the Messinian salinity crisis. *Bulletin de La Societe Geologique de France*, 182(2), 73–78. <https://doi.org/10.2113/gssgfbull.182.2.73>
- Ryan, W. B. F., & Cita, M. B. (1978). The nature and distribution of Messinian erosional surfaces—Indicators of a several-kilometer-deep Mediterranean in the Miocene. *Marine Geology*, 27(3–4), 193–230. [https://doi.org/10.1016/0025-3227\(78\)90032-4](https://doi.org/10.1016/0025-3227(78)90032-4)
- Ryan, W. B. F., & Hsü, K. J. (1973). *Initial Reports of the Deep Sea Drilling Project, 13* (Vol. 13). U.S. Government Printing Office. http://deepseadrilling.org/13/dsdp_toc.htm
- Sàbat, F., Gelabert, B., & Perea, A. R. (2018). Minorca, an exotic Balearic island (western Mediterranean). *Geologica Acta*, 411–426.
- Sàbat, F., Gelabert, B., Rodríguez-Perea, A., & Giménez, J. (2011). Geological structure and evolution of Majorca: Implications for the origin of the Western Mediterranean. *Tectonophysics*, 510(1), 217–238. <https://doi.org/10.1016/j.tecto.2011.07.005>

- Sabat, F., Muñoz, J. A., & Santanach, P. (1988). Transversal and oblique structures at the Serres de Llevant thrust belt (Mallorca Island). *Geologische Rundschau*, 77(2), 529–538. <https://doi.org/10.1007/BF01832396>
- Sàbat, F., Roca, E., Muñoz, J. A., Vergés, J., Santanach, P., Sans, M., Massana, E., Estévez, A., & Santisteban, C. (1997a). Role of extension and compression in the evolution of the eastern margin of Iberia: The ESCI-Valencia Trough seismic profile. *Revista de La Sociedad Geológica de España*, 8(4), 431–448.
- Sàbat, F., Roca, E., Muñoz, J. A., Vergés, J., Santanach, P., Sans, M., Massana, E., Estévez, A., & Santisteban, C. (1997b). Role of extension and compression in the evolution of the eastern margin of Iberia: The ESCI-Valencia Trough seismic profile. *Revista de La Sociedad Geológica de España*, 8(4), 431–448.
- Sàbat, F., Roca, E., Munoz, J. A., Verges, J., Santanach, P., & Sans, M. R. (1995). Margin of Iberia: The ESCI-València Trough seismic profile. *Rev. Soc. Geol. España*, 8(4).
- Sage, F., Gronefeld, G. V., Déverchère, J., Gaullier, V., Maillard, A., & Gorini, C. (2005). Seismic evidence for Messinian detrital deposits at the western Sardinia margin, northwestern Mediterranean. *Marine and Petroleum Geology*, 22(6–7), 757–773. <https://doi.org/10.1016/j.marpetgeo.2005.03.007>
- Samperi, L., Giorgio, M., Kamaldeen, O. O., Alba, Z., Nicolas, W., Sabrina, N., Cristina, P., & Francesco, B. (2020). Estimation of the physical, petrophysical and mineralogical properties of Messinian salt rocks, Sicily: Implications for multidisciplinary applications. *Marine and Petroleum Geology*, 112, 104032. <https://doi.org/10.1016/j.marpetgeo.2019.104032>
- Samperi, L., Giorgio, M., Kamaldeen, O. O., Alba, Z., Nicolas, W., Sabrina, N., Pauselli, C., & Francesco, B. (2020). Estimation of the physical, petrophysical and mineralogical properties of Messinian salt rocks, Sicily: Implications for multidisciplinary applications. *Marine and Petroleum Geology*, 112(September 2019), 104032–104032. <https://doi.org/10.1016/j.marpetgeo.2019.104032>
- Sanchez-Alzola, A., Sánchez, C., Giménez, J., Alfaro, P., Gelabert, B., Borque, M., & Gil, A. J. (2014). Crustal velocity and strain rate fields in the Balearic Islands based on continuous GPS time series from the XGAIB network (2010-2013). *Journal of Geodynamics*, 82. <https://doi.org/10.1016/j.jog.2014.05.005>

- Sanna, L., De Waele, J., Calaforra, J. M., & Forti, P. (2015). Long-term erosion rate measurements in gypsum caves of Sorbas (SE Spain) by the Micro-Erosion Meter method. *Geomorphology*, 228, 213–225. <https://doi.org/10.1016/j.geomorph.2014.09.009>
- Sansò, F., & Sideris, M. G. (2013). *Geoid Determination: Theory and Methods*. Springer Science & Business Media.
- Sanz de Galdeano, C., & Alfaro, P. (2004). Tectonic significance of the present relief of the Betic Cordillera. *Geomorphology*, 63(3), 175–190. <https://doi.org/10.1016/j.geomorph.2004.04.002>
- Schettino, A., & Turco, E. (2006a). Plate kinematics of the Western Mediterranean region during the Oligocene and Early Miocene. *Geophysical Journal International*, 166(3), 1398–1423. <https://doi.org/10.1111/j.1365-246X.2006.02997.x>
- Schettino, A., & Turco, E. (2006b). Plate kinematics of the Western Mediterranean region during the Oligocene and Early Miocene. *Geophysical Journal International*, 166(3), 1398–1423. <https://doi.org/10.1111/j.1365-246X.2006.02997.x>
- Schmalz, R. F. (1969). Deep-Water Evaporite Deposition: A Genetic Model. *AAPG Bulletin*, 53(4), 798–823. <https://doi.org/10.1306/5D25C7FD-16C1-11D7-8645000102C1865D>
- Schreiber, B. C. (1978). Environments of Subaqueous Gypsum Deposition. *Dean, E., Schreiber, B.C. (Eds.), Marine Evaporites. SEPM Short Course*, 4, 43–73.
- Schreiber, B. C., & Hsü, K. J. (1980). Evaporites. *Developments in Petroleum Geology*, 87–138.
- Schreiber, B., FRIEDMAN, G., DECIMA, A., & SCHREIBER, E. (2006). Depositional environments of Upper Miocene (Messinian) evaporite deposits of the Sicilian Basin*. *Sedimentology*, 23, 729–760. <https://doi.org/10.1111/j.1365-3091.1976.tb00107.x>
- Schulze, K., Hunger, M., & Döll, P. (2005). Simulating river flow velocity on global scale. *Advances in Geosciences*, 5, 133–136.
- Schwarzhans, W., Agiadi, K., & Carnevale, G. (2020). LATE MIOCENE–EARLY Pliocene evolution of Mediterranean gobies and their environmental and biogeographic significance. *Rivista Italiana Di Paleontologia e Stratigrafia*, 126(3), 657–724.

- Sciuto, F., Baldanza, A., Temani, R., & Privitera, G. (2018). New reports of Paratethyan ostracods affinity from the Mediterranean Basin (Sicily, Italy). *Palaeontologia Electronica*, 1–19. <https://doi.org/10.26879/800>
- Sclater, J. G., & Christie, P. a. F. (1980a). Continental stretching: An explanation of the Post-Mid-Cretaceous subsidence of the central North Sea Basin. *Journal of Geophysical Research: Solid Earth*, 85(B7), 3711–3739. <https://doi.org/10.1029/JB085iB07p03711>
- Sclater, J. G., & Christie, P. A. F. (1980b). Continental stretching: An explanation of the post-mid-cretaceous subsidence of the central north sea basin. *Journal of Geophysical Research*, 85(80), 3711–3739.
- Selli, R. (1954). *Il bacino del Metauro: Descrizione geologica, risorse minerarie, idrogeologia*. Museo geologico Giovanni Cappellini.
- Selli, R. (1960). Il Messiniano Mayer-Eymar 1867: Proposta di un neostatotipo. *Giornale di geologia.*, 28.
- Selli, R. (1973). An outline of the Italian Messinian. In *Messinian Events in the Mediterranean* (Vol. 7, pp. 150–171). North-Holland Amsterdam.
- Serpelloni, E., Vannucci, G., Pondrelli, S., Argnani, A., Casula, G., Anzidei, M., Baldi, P., & Gasperini, P. (2007). Kinematics of the Western Africa-Eurasia plate boundary from focal mechanisms and GPS data. *Geophysical Journal International*, 169(3), 1180–1200. <https://doi.org/10.1111/j.1365-246X.2007.03367.x>
- Sgarrella, F., SPROVIERI, R., STEFANO, E., & Caruso, A. (1997). Paleoceanographic conditions at the base of the Pliocene in the Southern Mediterranean Basin. *Rivista Italiana Di Paleontologia e Stratigrafia*, 103. <https://doi.org/10.13130/2039-4942/5291>
- Sierro, F., Flores, J. A., Francés, G., Vazquez, A., Utrilla, R., Zamarreño, I., Erlenkeuser, H., & Bárcena, M. Á. (2003). Orbitally-controlled oscillations in planktic communities and cyclic changes in western Mediterranean hydrography during the Messinian. *Palaeogeography, Palaeoclimatology, Palaeoecology*, 190, 289–316. [https://doi.org/10.1016/S0031-0182\(02\)00611-9](https://doi.org/10.1016/S0031-0182(02)00611-9)
- Sierro, F. J., Flores, J. A., Zamarreño, I., Vázquez, A., Utrilla, R., Francés, G., Hilgen, F. J., & Krijgsman, W. (1999). Messinian pre-evaporite sapropels and precession-induced

oscillations in western Mediterranean climate. *Marine Geology*, 153(1), 137–146. [https://doi.org/10.1016/S0025-3227\(98\)00085-1](https://doi.org/10.1016/S0025-3227(98)00085-1)

- Silva, P. G., Carrasco, P., Hernández, F. M., Goy, J. L., Zazo, C., Luque, L., Santos, G., Delgado, M., & Poza, L. J. (2002). Prospección geofísica de la Falla de Sencelles (Mallorca, España): Una metodología preliminar para la realización de trincheras de falla. *Geotemas*, 1, 359–363.
- Silva, P. G., Goy, J. L., & Zazo, C. (1998). Origen y desmantelamiento del Antiforme Plio-Cuaternario de Marratxí (Mallorca, España). *Geogaceta*, 23, 143–146.
- Silva, P. G., Hernández, F., Goy, J., Zazo, C., & Carrasco, P. (2001). Paleo and historical seismicity in Mallorca (Balears, Spain): A preliminary approach. *Undefined*. <https://www.semanticscholar.org/paper/Paleo-and-historical-seismicity-in-Mallorca-Spain%3A-Silva-Hern%C3%A1ndez/48250d6a879605c11e771bc75f1e8cf1b324795e>
- Simo, J. (1982). *El mioceno terminal de Ibiza y Formentera*. Universidad de Barcelona.
- Simon, D., Marzocchi, A., Flecker, R., Lunt, D. J., Hilgen, F. J., & Meijer, P. T. (2017). Quantifying the Mediterranean freshwater budget throughout the late Miocene: New implications for sapropel formation and the Messinian Salinity Crisis. *Earth and Planetary Science Letters*, 472. <https://doi.org/10.1016/j.epsl.2017.05.013>
- Simon, D., & Meijer, P. (2015). Dimensions of the Atlantic–Mediterranean connection that caused the Messinian Salinity Crisis. *Marine Geology*, 364, 53–64. <https://doi.org/10.1016/j.margeo.2015.02.004>
- Simon, D., & Meijer, P. T. (2017a). Salinity stratification of the Mediterranean Sea during the Messinian crisis: A first model analysis. *Earth and Planetary Science Letters*, 479. <https://doi.org/10.1016/j.epsl.2017.09.045>
- Simon, D., & Meijer, P. T. (2017b). Salinity stratification of the Mediterranean Sea during the Messinian crisis: A first model analysis. *Earth and Planetary Science Letters*, 479. <https://doi.org/10.1016/j.epsl.2017.09.045>
- Sirota, I., Enzel, Y., & Lensky, N. G. (2018). Halite focusing and amplification of salt layer thickness: From the Dead Sea to deep hypersaline basins. *Geology*, 46(10), 851–854. <https://doi.org/10.1130/G45339.1>

- Soria, J. M., Martín, J., Corbí, H., Dinarès-Turell, J., Lancis, C., Tent-Manclús, J., & Yébenes, A. (2007). Estratigrafía y biomagnetoestratigrafía del Messiniense en la sección del Garruchal (Cuenca del Bajo Segura). Implicaciones para la crisis de salinidad del Mediterráneo. *Geogaceta*, *41*, 215–218.
- Soria, J. M., Martín, J., Corbí, H., Dinarès-Turell, J., Lancis, C., Tent-Manclús, J., & Yébenes, A. (2008). The Bajo Segura Basin (SE Spain): Implications for the Messinian Salinity Crisis in the Mediterranean margins. *Stratigraphy*, *5*, 259–265.
- Spakman, W., & Wortel, R. (2004). A Tomographic View on Western Mediterranean Geodynamics. In W. Cavazza, F. Roure, W. Spakman, G. M. Stampfli, & P. A. Ziegler (Eds.), *The TRANSMED Atlas. The Mediterranean Region from Crust to Mantle* (pp. 31–52). Springer Berlin Heidelberg. https://doi.org/10.1007/978-3-642-18919-7_2
- Speranza, F., Villa, I. M., Sagnotti, L., Florindo, F., Cosentino, D., Cipollari, P., & Mattei, M. (2002a). Age of the Corsica-Sardinia rotation and Liguro-Provençal Basin spreading: New paleomagnetic and Ar/Ar evidence. *Tectonophysics*, *347*(4), 231–251. [https://doi.org/10.1016/S0040-1951\(02\)00031-8](https://doi.org/10.1016/S0040-1951(02)00031-8)
- Speranza, F., Villa, I. M., Sagnotti, L., Florindo, F., Cosentino, D., Cipollari, P., & Mattei, M. (2002b). Age of the Corsica-Sardinia rotation and Liguro-Provençal Basin spreading: New paleomagnetic and Ar/Ar evidence. *Tectonophysics*, *347*(4), 231–251. [https://doi.org/10.1016/S0040-1951\(02\)00031-8](https://doi.org/10.1016/S0040-1951(02)00031-8)
- Stampfli, G. M., & Höcker, C. F. W. (1989). Messinian palaeorelief from a 3-D seismic survey in the Tarraco concession area (Spanish Mediterranean Sea). *Geologie En Mijnbouw*, *68*, 201–210.
- Stein, C. A., & Stein, S. (1992). A model for the global variation in oceanic depth and heat flow with lithospheric age. *Nature*, *359*(6391), 123–129. <https://doi.org/10.1038/359123a0>
- Sternai, P., Caricchi, L., Garcia-Castellanos, D., Jolivet, L., Sheldrake, T. E., & Castelltort, S. (2017). Magmatic pulse driven by sea-level changes associated with the Messinian salinity crisis. *Nature Geoscience*, *10*(10), 783–787. <https://doi.org/10.1038/ngeo3032>
- Stich, D., Ammon, C. J., & Morales, J. (2003). Moment tensor solutions for small and moderate earthquakes in the Ibero-Maghreb region. *Journal of Geophysical Research: Solid Earth*, *108*(B3). <https://doi.org/10.1029/2002JB002057>

- Stoica, M., Krijgsman, W., Fortuin, A., & Gliozzi, E. (2015). Paratethyan ostracods in the Spanish Lago-Mare: More evidence for interbasinal exchange at high Mediterranean sea level. *Palaeogeography, Palaeoclimatology, Palaeoecology*, 441. <https://doi.org/10.1016/j.palaeo.2015.10.034>
- Stoica, M., Krijgsman, W., Fortuin, A., & Gliozzi, E. (2016a). Paratethyan ostracods in the Spanish Lago-Mare: More evidence for interbasinal exchange at high Mediterranean sea level. *Palaeogeography, Palaeoclimatology, Palaeoecology*, 441, 854–870. <https://doi.org/10.1016/j.palaeo.2015.10.034>
- Stoica, M., Krijgsman, W., Fortuin, A., & Gliozzi, E. (2016b). Paratethyan ostracods in the Spanish Lago-Mare: More evidence for interbasinal exchange at high Mediterranean sea level. *Palaeogeography, Palaeoclimatology, Palaeoecology*, 441, 854–870. <https://doi.org/10.1016/j.palaeo.2015.10.034>
- Storchak, D. A., Harris, J., Brown, L., Lieser, K., Shumba, B., & Di Giacomo, D. (2020). Rebuild of the Bulletin of the International Seismological Centre (ISC)—part 2: 1980–2010. *Geoscience Letters*, 7(1), 18. <https://doi.org/10.1186/s40562-020-00164-6>
- Storchak, D. A., Harris, J., Brown, L., Lieser, K., Shumba, B., Verney, R., Di Giacomo, D., & Korger, E. I. M. (2017). Rebuild of the Bulletin of the International Seismological Centre (ISC), part 1: 1964–1979. *Geoscience Letters*, 4(1), 32. <https://doi.org/10.1186/s40562-017-0098-z>
- Suarez-Gonzalez, P., Arenas, C., Benito, M. I., & Pomar, L. (2019). Interplay between biotic and environmental conditions in pre-salt Messinian microbialites of the western Mediterranean (Upper Miocene, Mallorca, Spain). *Palaeogeography, Palaeoclimatology, Palaeoecology*, 533, 109242. <https://doi.org/10.1016/j.palaeo.2019.109242>
- Suc, J.-P., Violanti, D., Londeix, L., Poumot, C., Robert, C., Clauzon, G., Gautier, F., Jean Louis, T., Ferrier, J., Chikhi, H., & Cambon, G. (1995). Evolution of the Messinian Mediterranean environments: The Tripoli Formation at Capodarso (Sicily, Italy). *Review of Palaeobotany and Palynology - REV PALAEOBOT PALYNOL*, 87, 51–79. [https://doi.org/10.1016/0034-6667\(94\)00144-9](https://doi.org/10.1016/0034-6667(94)00144-9)
- Tesauro, M., Kaban, M. K., & Cloetingh, S. A. P. L. (2009a). A new thermal and rheological model of the European lithosphere. *Tectonophysics*, 476(3–4), 478–495. <https://doi.org/10.1016/j.tecto.2009.07.022>

- Tesauro, M., Kaban, M. K., & Cloetingh, S. A. P. L. (2009b). How rigid is Europe's lithosphere? *Geophysical Research Letters*, 36(16), 2–7. <https://doi.org/10.1029/2009GL039229>
- Thinon, I., Guennoc, P., Rehault, J.-P., & Ferrandini, J. (2004). Reconstitution of the Messinian events on the eastern Corsican margin in the Corsica Basin. *4th International Congress "Environment and Identity in the Mediterranean": The Messinian Salinity Crisis Revisited, Corte, Corsica (France)*, 19–25.
- Thinon, I., Guennoc, P., Serrano, O., Maillard, A., Lasseur, E., & Réhault, J. P. (2016). Seismic markers of the Messinian Salinity Crisis in an intermediate-depth basin: Data for understanding the Neogene evolution of the Corsica Basin (northern Tyrrhenian Sea). *Marine and Petroleum Geology*, 77(Supplement C), 1274–1296. <https://doi.org/10.1016/j.marpetgeo.2016.02.017>
- Topper, R., Flecker, R., Meijer, P., & Wortel, M. (2011). A box model of the Late Miocene Mediterranean Sea: Implications from combined Sr-87/Sr-86 and salinity data. *Paleoceanography*, 26. <https://doi.org/10.1029/2010PA002063>
- Topper, R., & Meijer, P. (2013). A modeling perspective on spatial and temporal variations in Messinian evaporite deposits. *Marine Geology*, 336, 44–60. <https://doi.org/10.1016/j.margeo.2012.11.009>
- Torné, M., Pascal, G., Buhl, P., Watts, A. B., & Mauffret, A. (1992a). Crustal and velocity structure of the Valencia trough (western Mediterranean), Part I. A combined refraction/wide-angle reflection and near-vertical reflection study. *Tectonophysics*, 203(1–4), 1–20. [https://doi.org/10.1016/0040-1951\(92\)90212-O](https://doi.org/10.1016/0040-1951(92)90212-O)
- Torné, M., Pascal, G., Buhl, P., Watts, A. B., & Mauffret, A. (1992b). Crustal and velocity structure of the Valencia trough (western Mediterranean), Part I. A combined refraction/wide-angle reflection and near-vertical reflection study. *Tectonophysics*, 203(1–4), 1–20. [https://doi.org/10.1016/0040-1951\(92\)90212-O](https://doi.org/10.1016/0040-1951(92)90212-O)
- Urgeles, R., Camerlenghi, A., Garcia-Castellanos, D., De Mol, B., Garcés, M., Vergés, J., Haslam, I., & Hardman, M. (2011). New constraints on the Messinian sealevel drawdown from 3D seismic data of the Ebro Margin, western Mediterranean. *Basin Research*, 23(2), 123–145. <https://doi.org/10.1111/j.1365-2117.2010.00477.x>

- Urgeles, R., Camerlenghi, A., Garcia-Castellanos, D., De Mol, B., Garces, M., Verges, J., Haslam, I., & Hardman, M. (2011). New constraints on the Messinian sealevel drawdown from 3D seismic data of the Ebro Margin, western Mediterranean. *BASIN RESEARCH*, 23(2), 123–145. <https://doi.org/10.1111/j.1365-2117.2010.00477.x>
- Vai, G. B. (1997). Cyclostratigraphic estimate of the Messinian Stage duration. *Miocene Stratigraphy: An Integrated Approach. Developments in Paleontology and Stratigraphy*, 15, 463–476.
- Vai, G. B., & Lucchi, F. R. (1977a). Algal crusts, autochthonous and clastic gypsum in a cannibalistic evaporite basin: A case history from the Messinian of Northern Apennines. *Sedimentology*, 24(2), 211–244. <https://doi.org/10.1111/j.1365-3091.1977.tb00255.x>
- Vai, G. B., & Lucchi, F. R. (1977b). Algal crusts, autochthonous and clastic gypsum in a cannibalistic evaporite basin: A case history from the Messinian of Northern Apennines. *Sedimentology*, 24(2), 211–244. <https://doi.org/10.1111/j.1365-3091.1977.tb00255.x>
- Van Ceuvering, J. A., Berggren, W. A., Drake, R. E., Aguirre, E., & Curtis, G. H. (1976). The terminal Miocene event. *Marine Micropaleontology*, 1, 263–286.
- Van Couvering, J., Castradori, D., Cita, M., Hilgen, F., & Rio, D. (2000). The base of the Zanclean Stage and of the Pliocene Series. *Episodes*, 23. <https://doi.org/10.18814/epiiugs/2000/v23i3/005>
- van der Laan, E., Snel, E., de Kaenel, E., Hilgen, F. J., & Krijgsman, W. (2006). No major deglaciation across the Miocene-Pliocene boundary: Integrated stratigraphy and astronomical tuning of the Loulja sections (Bou Regreg area, NW Morocco). *Paleoceanography*, 21(3). <https://doi.org/10.1029/2005PA001193>
- Van Hinsbergen, D. J. J., Vissers, R. L. M., & Spakman, W. (2014). Origin and consequences of western Mediterranean subduction, rollback, and slab segmentation. *Tectonics*, 33(4), 393–419. <https://doi.org/10.1002/2013TC003349>
- Vargas-Yáñez, M., Juza, M., Balbín, R., Velez-Belchí, P., García-Martínez, M. C., Moya, F., & Hernández-Guerra, A. (2020). Climatological Hydrographic Properties and Water Mass Transports in the Balearic Channels From Repeated Observations Over 1996–2019. *Frontiers in Marine Science*, 7. <https://www.frontiersin.org/article/10.3389/fmars.2020.568602>

- Vergés, J., & Fernández, M. (2012). *Tethys–Atlantic interaction along the Iberia–Africa plate boundary: The Betic–Rif orogenic system*. 29.
- Vergés, J., & Sàbat, F. (1999). Constraints on the Neogene Mediterranean kinematic evolution along a 1000 km transect from Iberia to Africa. *Geological Society, London, Special Publications*, 156(1), 63–80. <https://doi.org/10.1144/GSL.SP.1999.156.01.05>
- Vigliotti, L., & Langenheim, V. E. (1995). When did Sardinia stop rotating? New palaeomagnetic results. *Terra Nova*, 7(4), 424–435. <https://doi.org/10.1111/j.1365-3121.1995.tb00538.x>
- Villasenor, A., Spakman, W., & Engdahl, E. (2003). Influence of Regional Travel Times in Global Tomographic Models. *Geophys. Res. Abstr.*
- W. Martínez del Olmo, & D. Martín. (2016). The Messinian record of Spanish onshore and offshore data (Atlantic Ocean and Western Mediterranean Sea). *Petroleum Geoscience*, 22(4), 291–296.
- Warren, J. K. (2010). Evaporites through time: Tectonic, climatic and eustatic controls in marine and nonmarine deposits. *Earth-Science Reviews*, 98(3), 217–268. <https://doi.org/10.1016/j.earscirev.2009.11.004>
- Warren, J. K. (2016). *Evaporites: A Geological Compendium*. Springer.
- Watts, A. B. (2001). *Isostasy and Flexure of the Lithosphere* (p. 458). Cambridge University Press.
- Watts, A. B., & Ryan, W. B. F. (1976a). Flexure of the Lithosphere and Continental Margin Basins* *Lamont-Doherty Contribution No. 2395. In M. H. P. Bott (Ed.), *Developments in Geotectonics* (Vol. 12, pp. 25–44). Elsevier. <https://doi.org/10.1016/B978-0-444-41549-3.50006-2>
- Watts, A. B., & Ryan, W. B. F. (1976b). Flexure of the Lithosphere and Continental Margin Basins. *Tectonophysics*, 36, 25–44.
- Watts, A. B., & Torné, M. (1992a). Crustal structure and the mechanical properties of extended continental lithosphere in the Valencia trough (western Mediterranean). *Journal of the Geological Society*, 149(5), 813–827. <https://doi.org/10.1144/gsjgs.149.5.0813>

- Watts, A. B., & Torné, M. (1992b). Subsidence history, crustal structure, and thermal evolution of the Valencia Trough: A young extensional basin in the western Mediterranean. *Journal of Geophysical Research*, 97(B13), 20021–20021. <https://doi.org/10.1029/92JB00583>
- Watts, A. B., Torné, M., Buhl, P., Mauffret, A., Pascal, G., & Pinet, B. (1990). Evidence for reflectors in the lower continental crust before rifting in the Valencia trough. *Nature*, 348(6302), 631–635. <https://doi.org/10.1038/348631a0>
- Watts, A. B., Zhong, S. J., & Hunter, J. (2013). The Behavior of the Lithosphere on Seismic to Geologic Timescales. *Annual Review of Earth and Planetary Sciences*, 41(1), 443–468. <https://doi.org/10.1146/annurev-earth-042711-105457>
- Wortel, M. J. R., & Spakman, W. (2000). Subduction and slab detachment in the Mediterranean-Carpathian region. *Science*, 290(5498), 1910–1917. <https://doi.org/10.1126/science.290.5498.1910>
- Yelles, A., Domzig, A., Déverchère, J., Bracène, R., Lépinay, B. M. de, Strzeczynski, P., Bertrand, G., Boudiaf, A., Winter, T., Kherroubi, A., Roy, P. L., & Djellit, H. (2009). Plio-Quaternary reactivation of the Neogene margin off NW Algiers, Algeria: The Khayr al Din bank. *Tectonophysics*, 475(1), 98. <https://doi.org/10.1016/j.tecto.2008.11.030>
- Yelles, A., Domzig, A., Déverchère, J., Bracène, R., Mercier de Lépinay, B., Strzeczynski, P., Bertrand, G., Boudiaf, A., Winter, T., Kherroubi, A., Le Roy, P., & Djellit, H. (2009). Plio-Quaternary reactivation of the Neogene margin off NW Algiers, Algeria: The Khayr al Din bank. *Tectonophysics*, 475(1), 98–116. <https://doi.org/10.1016/j.tecto.2008.11.030>
- Yielding, G., Ouyed, M., King, G. C. P., & Hatzfeld, D. (1989). Active tectonics of the Algerian Atlas Mountains—Evidence from aftershocks of the 1980 El Asnam earthquake. *Geophysical Journal International*, 99(3), 761–788. <https://doi.org/10.1111/j.1365-246X.1989.tb02057.x>
- Yoshimura, T., Kuroda, J., Lugli, S., Tamenori, Y., Ogawa, N. O., Jiménez-Espejo, F. J., Isaji, Y., Roveri, M., Manzi, V., Kawahata, H., & Ohkouchi, N. (2016). An X-ray spectroscopic perspective on Messinian evaporite from Sicily: Sedimentary fabrics, element distributions, and chemical environments of S and Mg. *Geochemistry, Geophysics, Geosystems*, 17(4), 1383–1400. <https://doi.org/10.1002/2015GC006233>

- Zecchin, M., Civile, D., Caffau, M., Muto, F., Di Stefano, A., Maniscalco, R., & Critelli, S. (2013). The Messinian succession of the Croton Basin (southern Italy) I: Stratigraphic architecture reconstructed by seismic and well data. *Marine and Petroleum Geology*, 48, 455–473. <https://doi.org/10.1016/j.marpetgeo.2013.08.014>
- Ziegenbalg, S. B., Brunner, B., Rouchy, J. M., Birgel, D., Pierre, C., Böttcher, M. E., Caruso, A., Immenhauser, A., & Peckmann, J. (2010). Formation of secondary carbonates and native sulphur in sulphate-rich Messinian strata, Sicily. *Sedimentary Geology*, 227(1), 37–50. <https://doi.org/10.1016/j.sedgeo.2010.03.007>

Annex A

This Annex is a review of the terminal stage of the Messinian Salinity Crisis (Upper Evaporites and Lago Mare phases) that I actively participated in. It was inspired and led by the colleague from SaltGiant Federico Andreetto (ESR5 in the SaltGiant project), with the objective of putting some order to the bibliography of one of the most intriguing and complex phases of the MSC events. My contribution to the review was mainly the focus on the deposits of this stage in the offshore domain (chapter 4 of the review paper), mostly studied by seismic dataset, but also recovered in some of the boreholes from the DSDP and ODP drillings. I also actively contributed together with Federico to the discussion where the controversial issues of the MSC terminal stage are presented and discussed (chapter 7 of the review).



Freshening of the Mediterranean Salt Giant: controversies and certainties around the terminal (Upper Gypsum and Lago-Mare) phases of the Messinian Salinity Crisis

F. Andreetto^{a,*}, G. Aloisi^b, F. Raad^c, H. Heida^d, R. Flecker^e, K. Agiadi^f, J. Lofi^c, S. Blondel^g, F. Bulian^h, A. Camerlenghi^g, A. Carusoⁱ, R. Ebner^j, D. Garcia-Castellanos^d, V. Gaullier^k, L. Guibourdenche^b, Z. Gvirtzman^{l,m}, T.M. Hoyle^{a,n}, P.T. Meijer^j, J. Moneron^{l,m}, F.J. Sierro^h, G. Travan^k, A. Tzevahirtzianⁱ, I. Vasiliev^o, W. Krijgsman^a

^a Paleomagnetic Laboratory "Fort Hoofddijk", Dept. of Earth Sciences, Utrecht University, Budapestlaan 17, 3584 CD Utrecht, The Netherlands

^b Université de Paris, Institut de physique du globe de Paris, CNRS, F-75005 Paris, France

^c Géosciences Montpellier, CNRS, Université de Montpellier, Montpellier, France

^d Geosciences Barcelona, GEO3BCN, CSIC, Solé i Sabaris s/n, Barcelona, Spain

^e BRIDGE, School of Geographical Sciences and Cabot Institute, University of Bristol, University Road, Bristol BS8 1SS, United Kingdom

^f Department of Palaeontology, University of Vienna, Althanstraße 14 (UZA II), 1090 Vienna, Austria

^g Istituto Nazionale di Oceanografia e di Geofisica Sperimentale (OGS), Trieste, Italy

^h Department of Geology, University of Salamanca, Salamanca, Spain

ⁱ Dipartimento di Scienze della Terra e del Mare, Università degli studi di Palermo, via Archirafi 20-22, 90123 Palermo, Italy

^j Department of Earth Sciences, Utrecht University, Utrecht, The Netherlands

^k Univ. Lille, CNRS, Univ. Littoral Côte d'Opale, UMR 8187, LOG, Laboratoire d'Océanologie et de Géosciences, F 59000, Lille, France

^l Geological Survey of Israel, Jerusalem 95501, Israel

^m Institute of Earth Sciences, The Hebrew University of Jerusalem, Israel

ⁿ CASP, West Building, Madingley Rise, Madingley Road, Cambridge CB3 0UD, United Kingdom

^o Senckenberg Research Biodiversity and Climate Research Centre, Senckenberganlage 25, 60325 Frankfurt am Main, Germany

ARTICLE INFO

Keywords:

Messinian Salinity Crisis
Mediterranean stratigraphy
Connectivity proxies
Paleogeography
Paratethys
Lago-Mare

ABSTRACT

The late Miocene evolution of the Mediterranean Basin is characterized by major changes in connectivity, climate and tectonic activity resulting in unprecedented environmental and ecological disruptions. During the Messinian Salinity Crisis (MSC, 5.97-5.33 Ma) this culminated in most scenarios first in the precipitation of gypsum around the Mediterranean margins (Stage 1, 5.97-5.60 Ma) and subsequently > 2 km of halite on the basin floor, which formed the so-called Mediterranean Salt Giant (Stage 2, 5.60-5.55 Ma). The final MSC Stage 3, however, was characterized by a "low-salinity crisis", when a second calcium-sulfate unit (Upper Gypsum; substage 3.1, 5.55-5.42 Ma) showing (bio)geochemical evidence of substantial brine dilution and brackish biota-bearing terrigenous sediments (substage 3.2 or Lago-Mare phase, 5.42-5.33 Ma) deposited in a Mediterranean that received relatively large amounts of riverine and Paratethys-derived low-salinity waters. The transition from hypersaline evaporitic (halite) to brackish facies implies a major change in the Mediterranean's hydrological regime. However, even after nearly 50 years of research, causes and modalities are poorly understood and the original scientific debate between a largely isolated and (partly) desiccated Mediterranean or a fully connected and filled basin is still vibrant. Here we present a comprehensive overview that brings together (chrono)stratigraphic, sedimentological, paleontological, geochemical and seismic data from all over the Mediterranean. We summarize the paleo-environmental, paleohydrological and paleoconnectivity scenarios that arose from this cross-disciplinary dataset and we discuss arguments in favour of and against each scenario.

* Corresponding author.

E-mail address: f.andreetto@uu.nl (F. Andreetto).

<https://doi.org/10.1016/j.earscirev.2021.103577>

Received 1 November 2020; Received in revised form 4 February 2021; Accepted 25 February 2021

Available online 3 March 2021

0012-8252/© 2021 The Author(s). Published by Elsevier B.V. This is an open access article under the CC BY license (<http://creativecommons.org/licenses/by/4.0/>).

1. Introduction

At the end of the Miocene, orbital and tectonic drivers combined to alter the amount of water delivered to the Mediterranean Basin by the Atlantic Ocean from the west, the brackish Eastern Paratethys (i.e. Euxinic-Caspian Basin system) from the east and the major peri-Mediterranean freshwater drainage systems (e.g. African rivers and Rhône; Griffin, 2002; Gladstone et al., 2007; Van der Laan et al., 2006; Hilgen et al., 2007; Ryan, 2009; Flecker et al., 2015; Marzocchi et al., 2015, 2016, 2019; Simon et al., 2017; Krijgsman et al., 2018; Capella et al., 2020). The changes in extra and intrabasinal connectivity resulted in unprecedented paleoceanographic and paleohydrological budget changes that led to a relatively short-lived environmental and ecological crisis (approx. 660 kyr; 5.97-5.33 Ma), for which the term Messinian Salinity Crisis (MSC) was coined (Selli, 1954, 1960). Most conspicuous was the rapid accumulation of several kilometers of halite (i.e. ~1 million km³) on the Mediterranean abyssal plains (e.g. Hsü, 1972; Ryan, 1973; Montadert et al., 1978; Haq et al., 2020). This happened within 50 kyr, from 5.60-5.55 Ma, according to Roveri et al. (2014a) and Manzi et al. (2018), or in >300 kyr, when starting at 5.97 Ma, as put forward by Meilijson et al. (2018, 2019). During the ~200 kyr lapse (i.e. MSC Stage 3 following Roveri et al., 2014a; Fig. 1a) between the end of salt precipitation (5.55 Ma) and the restoration of the still enduring marine conditions (5.33 Ma), the Mediterranean underwent a sequence of paleohydrological and base-level changes that are the topic of intense and long-standing debates. The initial and still widely endorsed hypothesis was that the Mediterranean Sea, following the major drawdown event that led to halite deposition (i.e. Stage 2), maintained the isolated, deeply-desiccated geography containing a series of hypersaline (substage 3.1; 5.55-5.42 Ma) and

hyposaline (substage 3.2; 5.42-5.33 Ma) ponds which only received water from local streams and were colonized by Black Sea organisms carried by aquatic migratory birds (Fig. 1b; e.g. Ruggieri, 1967; Decima and Sprovieri, 1973; Decima and Wezel, 1971, 1973; Cita et al., 1978; Müller et al., 1990; Benson and Rakic-El Bied, 1991; Benson et al., 1991; Müller and Mueller, 1991; Butler et al., 1995; Orszag-Sperber et al., 2000; Rouchy et al., 2001; Kartveit et al., 2019; Madof et al., 2019; Camerlenghi et al., 2019; Caruso et al., 2020; Raad et al., 2021). As morphological and seismic reflection studies at the Strait of Gibraltar documented a ~400 km long erosional trough connecting the Gulf of Cadiz (Atlantic Ocean) to the Mediterranean Sea, this scenario of a lowered Mediterranean Sea was promptly linked to the termination of the MSC (McKenzie, 1999; Blanc, 2002; Garcia-Castellanos et al., 2009, 2020). This conclusion has recently been reinforced by the discovery of vast chaotic deposits sitting at the claimed Miocene/Pliocene transition in the area of the Malta Escarpment-Ionian Abyssal Plain (Micallef et al., 2018, 2019; Spatola et al., 2020). In more recent years, the desiccated basin model was challenged by the observation of deposits that are uniform in terms of sedimentology and stratigraphic architecture (Roveri et al., 2008a), ostracod content (Glozzi et al., 2007; Stoica et al., 2016) and geochemistry (McCulloch and De Deckker, 1989; Garcia-Veigas et al., 2018; Andreetto et al., 2021) throughout the Mediterranean marginal belt and of $\delta D_{n-alkanes}$ and $\delta D_{alkenones}$ sharing similarities with the coeval Atlantic Ocean and Black Sea, respectively (Vasiliev et al., 2017). A model of a (relatively) full Mediterranean Sea developed (Fig. 1c), where the debate mainly concerns the provenance of the hydrological fluxes and the resultant hydrochemical composition of the water mass. In this scenario, the Mediterranean was first, during substage 3.1, transformed into a new gypsum-precipitating basin filled with marine and continent-derived

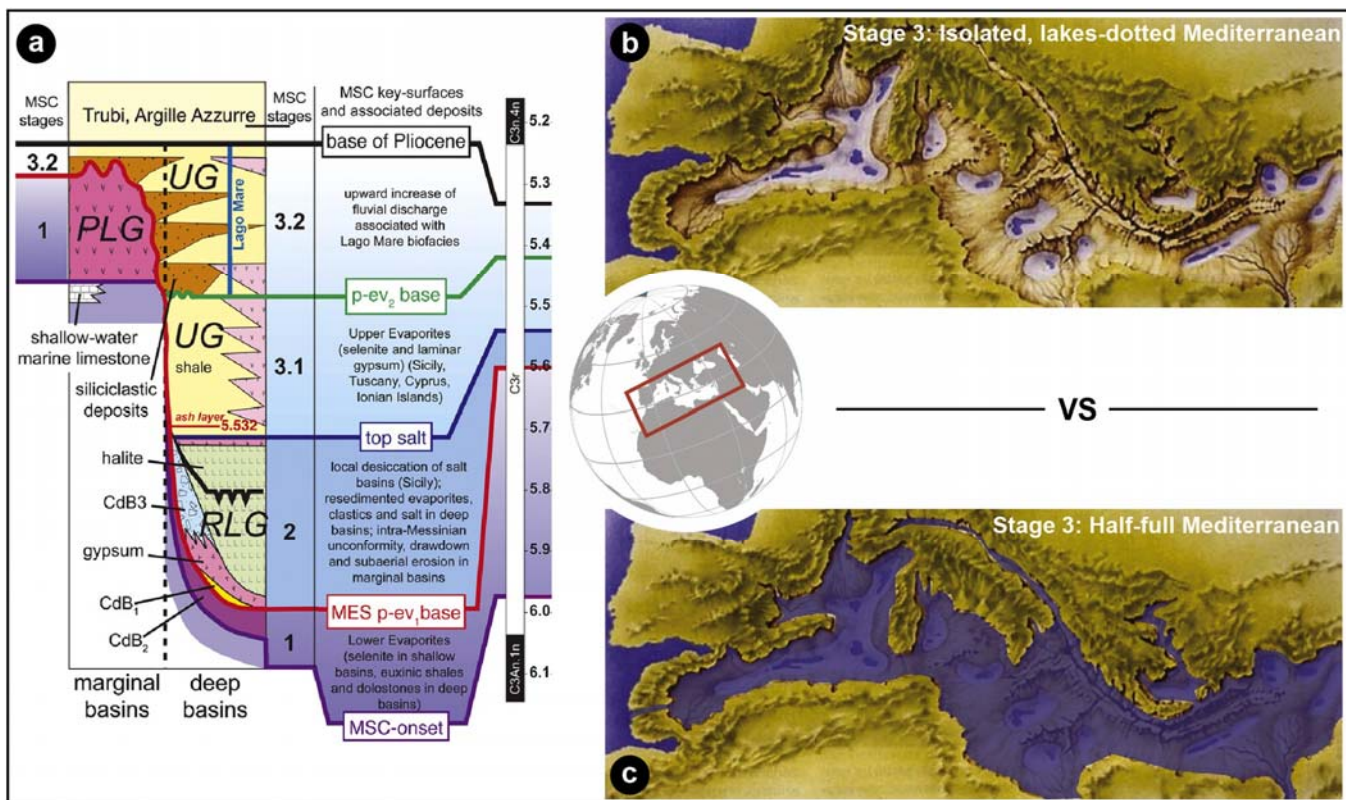


Fig. 1. (a) Consensus chronostratigraphic model for the MSC events (Roveri et al., 2014a). Stage 3, here of interest, spans between 5.55 Ma and 5.332 Ma, the astronomical ages of the base of the Upper Gypsum Unit (following Manzi et al., 2009) and Trubi Formation (Van Couvering et al., 2000) in the Sicilian Eraclea Minoa section, respectively. CdB: Calcare di Base; PLG: Primary Lower Gypsum; RLG: Resedimented Lower Gypsum; UG: Upper Gypsum. (b), (c) Map of the Mediterranean region showing the two extreme and mutually exclusive paleoenvironmental scenarios proposed to have featured the Mediterranean during Stage 3 (see discussion in Chapter 7; modified after Krijgsman et al., 2018).

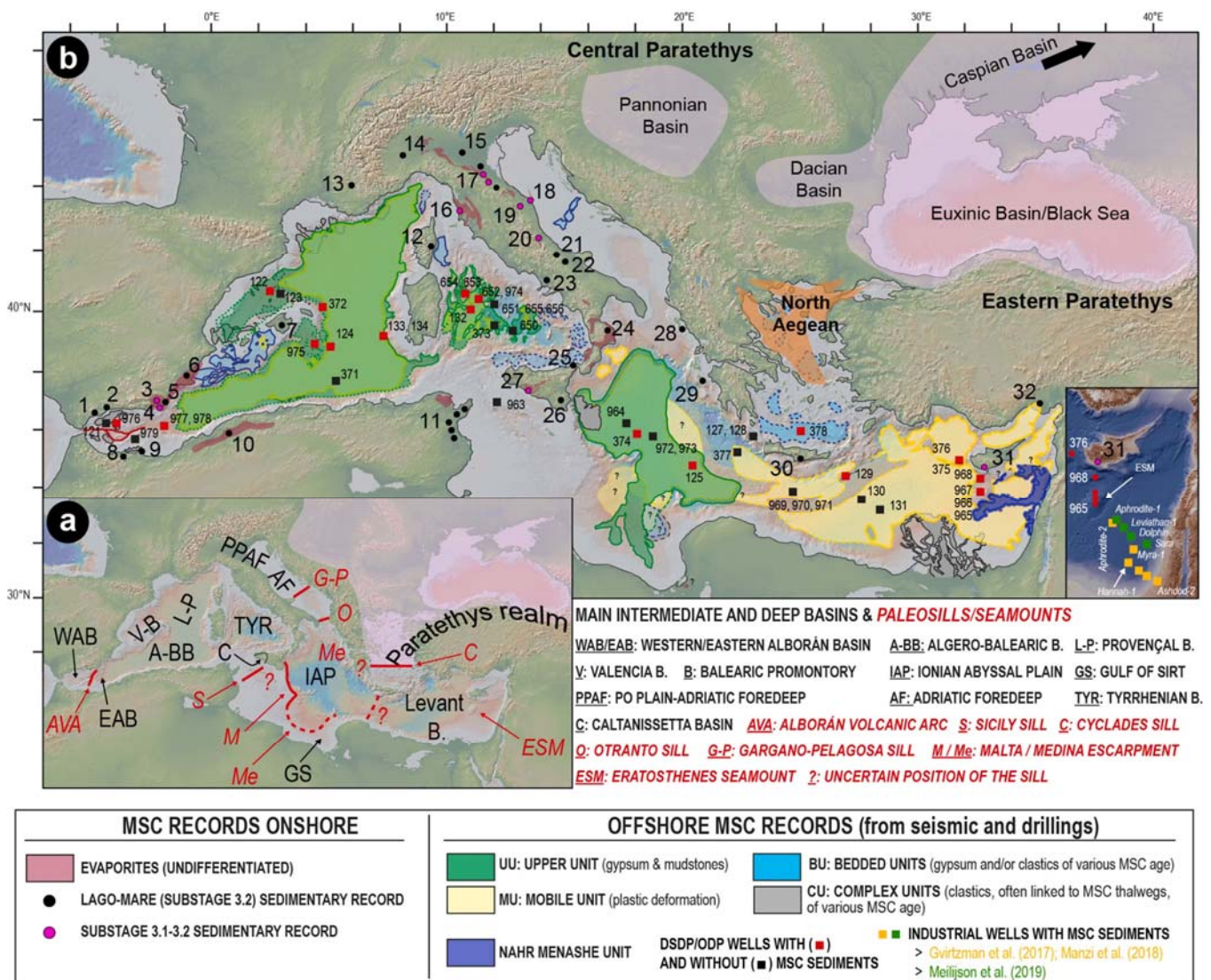


Fig. 2. Map of the Mediterranean Basin (modified from Lofi, 2018) showing: a) the location of the key intermediate and deep basins as well as physical thresholds that influenced the connectivity history of the Mediterranean; b) the onshore (i.e. basins and/or sections) and offshore (DSDP/ODP/Industrial drill sites) localities where deposits attributed to MSC Stage 3 have been studied. Mixed assemblages of Paratethyan-like ostracods and foraminifera are known from all mentioned onshore localities and some offshore locations (see text). The present-day spatial extent of the MSC seismic units, except for the Lower Unit, is also shown. The paleogeography of the (Eastern and Central) Paratethys and of the North Aegean domain is contoured after Van Baak et al. (2017) and Krijgsman et al. (2020a), respectively. W-E onshore localities: 1-6 Betic Cordillera (SE Spain): 1-Marbella and 2-Malaga basins (Guerra-Merchán et al., 2010); 3-Sorbas Basin (Roveri et al., 2009, 2019a); 4-Nijar Basin (Fortuin and Krijgsman, 2003); 5-Vera Basin (Fortuin et al., 1995); 6-Bajo Segura Basin (Soria et al., 2005, 2008a, 2008b); 7-Mallorca (Mas and Fornós, 2020); 8-Melilla Basin (Rouchy et al., 2003); 9-Boudinar Basin (Merzeraud et al., 2019); 10-Chelif Basin (Rouchy et al., 2007); 11-Sahel area (Frigui et al., 2016); 12-Aléria Basin and 13-Rhône Valley (Carbonnel, 1978); 14-Piedmont Basin (Dela Pierre et al., 2011, 2016); 15-Po Plain (Ghielmi et al., 2010, 2013; Amadori et al., 2018); 16-Fine Basin (Cava Serredi section; Carnevale et al., 2006a, 2008). 17-21 Apennine system: Romagna sections (17, Roveri et al., 1998), Trave section (18, Iaccarino et al., 2008), Maccarone section (19, Bertini, 2006, Grossi et al., 2008; Sampalmieri et al., 2010; Pellen et al., 2017), Colle di Votta (20)-Fontedei Pulcini (21)-Stingeti (22) sections (Cosentino et al., 2005, 2012, 2013, 2018), Mondragone 1 well (23, Cosentino et al., 2006), Crotona Basin (24, Roveri et al., 2008a); 25-27 Sicily: Villafranca Tirrena (25) and Licodia Eubea (26) sections (Sciuto et al., 2018), Caltanissetta Basin (27, Manzi et al., 2009); 28-Corfu (Pierre et al., 2006); 29-Zakinthos (Karakitsios et al., 2017b); 30-Crete (Cosentino et al., 2007); 31-Cyprus (Rouchy et al., 2001; Manzi et al., 2016a); 32-Adana Basin (Radeffet et al., 2016).

waters (e.g. Manzi et al., 2009; Roveri et al., 2014c; Flecker et al., 2015; Vasiliev et al., 2017; García-Veigas et al., 2018; Grothe et al., 2020). Then, during substage 3.2, it became a brackish lake-sea comparable to the present-day Black Sea or Caspian Sea (Roveri et al., 2008a; Stoica et al., 2016; Andreetto et al., 2021), depending on whether a marine connection with the Atlantic was active (Manzi et al., 2009; Roveri et al., 2014b, 2014c; Flecker et al., 2015; Marzocchi et al., 2016; Vasiliev et al., 2017; García-Veigas et al., 2018) or not (e.g. McCulloch and De Deckker, 1989; Roveri et al., 2008a), and with a base-level fluctuating by hundreds of meters with precessional periodicity (Fortuin and Krijgsman, 2003; Ben Moshe et al., 2020; Andreetto et al., 2021). In the relatively full scenario, the revival of marine conditions is ascribed to either connectivity changes (Marzocchi et al., 2016) or to a moderate sea-level rise (Andreetto et al., 2021). In contrast, Carnevale et al. (2006a, 2006b, 2008, 2018) and Grunert et al. (2016), based on the recovery of fish remains ascribed to marine species, proposed that fully marine conditions were in force in the Mediterranean already at the end of substage 3.1.

After nearly 50 years of research on both onshore and offshore localities (Fig. 2), the observations backing up the competing desiccated and full-basin Mediterranean models remain extremely difficult to reconcile. Uncertainties regarding the chronostratigraphic framework of Stage 3 deposits, the origin and migration of its characteristic biota, the meaning of the data derived from the applied geochemical techniques and the relationship between the Mediterranean and its surrounding water bodies (i.e. Atlantic Ocean, Indian Ocean and Paratethys) all inhibit a clear understanding of the Mediterranean base-level and its hydrochemical structure.

In this paper we attempt to summarize all the existing, but heavily scattered, data resulting from ~50 years of cross-disciplinary studies with the aim of providing a comprehensive overview of the stratigraphic arrangement of Stage 3 onshore and offshore deposits, as well as of their sedimentological, paleontological, geochemical and seismic properties. Subsequently, we assemble the observations favoring both end-member scenarios of a relatively desiccated and relatively full Mediterranean. Finally, we focus on novel future analytical techniques and approaches that have the potential to constrain Mediterranean base-level during MSC Stage 3 as well as the changing hydrological fluxes and connectivity phases between the intra-Mediterranean basins and the neighboring Atlantic Ocean and Paratethyan domains as a mean of reconstructing the state of the art of the complex history of this enigmatic period of the Mediterranean history once and for all.

2. The terminal Stag 3 of the MSC

2.1 Historic overview of nomenclature and concepts

The final phase of the MSC (i.e. substage 3.2), also known as “Lago-Mare”, finds its sedimentary expression in cyclically-arranged terrigenous and evaporitic sediments hosting unique faunal assemblages of ostracods, mollusks and dinoflagellate cysts (dinocysts). They are related, at species level, to those inhabiting, during the Miocene, the brackish basins of the Paratethys realm (e.g. Gliozzi et al., 2007; Stoica et al., 2016). But what exactly is the “Lago-Mare”? This widely employed expression in the MSC literature encompasses a variety of meanings that make its application doubtful and misleading. The root of the wording “Lago-Mare” is to be found in the Russian scientific literature of the late 1800s. Nikolai Andrusov (1890) used the corresponding Russian term with a geographical and chronological connotation in reference to the series of central-eastern European basins that during the Miocene turned from marine settings to desalinated semi-isolated lakes with an endemic fresh-brackish water biota association (e.g. Popov et al., 2006 and references therein). The original monograph of Andrusov (1890) was not widely available outside Russia, but his attendance of international conferences allowed his research to spread outside the Russian borders. From the publications of the French

geologists Suzette Gillet (Gillet, 1932, 1933) and Maurice Gignoux (Gignoux, 1936a) we can state with relative certainty that the original meaning of the word “Lago-Mare” (here reported with the French counterpart “Lac-Mer”) had its provenance in the Russian literature:

“[...] An isolation of the basin, that became a brackish, isolated basin. Then, a uniform fauna populated this immense lac-mer which was divided [...] into Pannonian basin, [...] Dacique Basin, and Euxin and Caspian basin [...]” (Gillet, 1932).

“[...] During the Volhynien (Sarmatique inferior) there was a lac-mer of uniform fauna that extended through all the eastern Europe. [...] and the fauna of the eastern regions of that huge lac-mer was completely differentiated [sic] from the one in the western regions. [...]” (Gillet, 1933). “[...] The Pontien fauna is not anymore a fauna characteristic of an internal saline sea, as in the Sarmantien, but is a fauna of a “desalinated lagoon”, a lac-mer, as the Russian geologists named it. [...]” (Gignoux, 1936b).

In the late 19th (Capellini, 1880) and 20th century (Ogniben, 1955; Ruggieri, 1962, 1967; Decima, 1964), late Messinian ostracod- and mollusk-bearing deposits in the Mediterranean were described at several Italian localities. Initially, the expressions “Congeria beds” (Capellini, 1880) and “Melanopsis beds” (Ruggieri, 1962) were used. Later on, Ruggieri (1967) pointed out the affinity of these faunal elements with those of the Pontian of the Paratethys. Consequently, he speculated on a feasible Paratethys-like paleoenvironmental configuration for the Mediterranean in the latest Messinian and he coined the Italian translation (i.

e. “Lago-Mare”) from the French “Lac-Mer” in reference to the shallow-water lakes claimed to be widely distributed across the Mediterranean. Progress in the 1970s in onshore and offshore exploration highlighted the temporally well-constrained distribution of the Paratethyan organisms in the Mediterranean (Carbonnel, 1978). On this premise, Hsü et al. (1978a) proposed to use “Lago-Mare” to “designate the latest Messinian oligohaline environment, postdating evaporite deposition and predating Pliocene marine sedimentation [...] in order to distinguish it from “lac mer” which, strictly speaking, was a Paratethyan environment”. Notwithstanding the new definition, in various parts of the text they used “Lago-Mare” to refer to the Paratethyan lakes (pp. 1071-1072: “[...] The upper Messinian Mediterranean was flooded by a series of desert basins, some with salt lakes, prior to inundation by the Lago-Mare.”), thus giving rise to the confusion on how to use the term properly.

In the most recent stratigraphic overview of the MSC (Fig. 1a; Roveri et al., 2014a), the terminal MSC stage is called Stage 3, which is in turn subdivided into substages 3.1 and 3.2 (also termed Lago-Mare). Beside such a chronostratigraphic definition, the term “Lago-Mare” has also been used for a typical biofacies of the late Messinian Mediterranean (e.g. Fortuin et al., 1995; Gliozzi, 1999; Gliozzi and Grossi, 2008; Sciuto et al., 2018), for the pelitic beds encasing the Paratethyan-related fauna (i.e. a lithofacies; e.g. Fortuin and Krijgsman, 2003; Sciuto et al., 2018), as the name of an informal lithostratigraphic unit (usually distinguished by its fossil content) sandwiched between the Sicilian Upper Gypsum and the Arenazzolo Fm. (Fig. 4b; Clauzon et al., 2005; Londeix et al., 2007; Popescu et al., 2009; Bache et al., 2012) and to denote multiple (3 to 4) spilling events of the Paratethys into the Mediterranean (Clauzon et al., 2005, 2015; Popescu et al., 2007, 2009, 2015; Suc et al., 2011; Bache et al., 2012; Do Couto et al., 2014; Frigui et al., 2016; Mas and Fornós, 2020).

This being a review, we use the widely employed definition of the model of Roveri et al., 2014a) (Fig. 1a) and regard the Lago-Mare as a “phase of massive biota migration from the Paratethys realm, cyclostratigraphically constrained between 5.42 Ma and 5.332 Ma (Roveri et al., 2008a; Grossi et al., 2011), during which the Mediterranean sedimentary environments underwent an impressive freshening”. Nevertheless, we call for caution in the use of this definition of “Lago-Mare” in future studies, since 5.42 Ma as the (astronomical) age of the first entrance of Paratethyan organisms into the Mediterranean is likely

to be incorrect (see subsection 5.1) and evidence of ‘impressive freshening’ are already present much earlier (e.g. at Eraclea Minoa; [Vasiliev et al., 2017](#); [García-Veigas et al., 2018](#)).

2.2 Development of a chronostratigraphic framework

Issues of the timing and duration of the MSC only began to be tackled in the 1990s, in parallel with discussion concerning the nature of its extreme paleoenvironments ([Schmalz, 1969](#); [Hsü et al., 1973a, 1973b, 1973c](#), [Hsü et al., 1978a, 1978b](#); [Nesteroff, 1973](#); [De Benedetti, 1982](#)). While published models ([Butler et al., 1995](#); [Clauzon et al., 1996](#); [Krijgsman et al., 1999a](#); [Rouchy and Caruso, 2006](#)) mostly converged on the (astronomical) age of the marine replenishment at the beginning of the Pliocene (5.332 Ma; [Van Couvering et al., 2000](#)), there were disagreements about the age of the onset of the MSC (synchronous vs diachronous) and of specific events within it (see discussion in [Roveri et al., 2014a](#)). Among these, the work of [Krijgsman et al. \(1999a\)](#) has obtained wide consensus. Their cyclostratigraphic tuning and correlation of continuous and biomagnetostratigraphically constrained pre- evaporitic sections in Spain (Sorbas), Sicily (Giblicemi/Falconara) and Greece (Metochia) resulted in a synchronous age of 5.96 ± 0.02 Ma for the MSC onset (later refined to 5.97 Ma by [Manzi et al., 2013](#)). The astronomical ages for the onset ([Krijgsman et al., 1999a](#)) and termination ([Van Couvering et al., 2000](#)) of the MSC are not contentious since the characteristic sedimentary cyclicity and sediments’ properties (e.g. color of the lithologies and biota content) of the pre- and post-MSC successions fit robustly with the insolation curve (see also [Van der Laan et al., 2006](#) and [Topper and Meijer, 2015](#)).

The cyclic arrangement of the MSC sediments ([Fig. 3a](#)) led scientists to interpret that the same cyclostratigraphic approach could be used to

gain precise dates for events within the MSC (e.g. [Hilgen et al., 1995](#); [Vai, 1997](#); [Krijgsman et al., 1999b, 2001](#)), bypassing the challenge posed by the unsuitability of the classic biomagnetostratigraphic tools for the MSC successions. Characteristic interference patterns of eccentricity and precession have been tentatively recognized in the Sicilian Eraclea Minoa section (see subsection 3.8; [Van der Laan et al., 2006](#)). However, clear orbital signals are typically poorly expressed in MSC records and, when they are present, like in Sicily, they are not (vertically) repeated with sufficient frequency to establish clear phase relations with the astronomical cyclicity. For this reason, the simple counting of cycles with no analysis of cyclostratigraphic pattern in proxy records has mostly been employed as a correlation method ([Roveri et al., 2008a](#); [Manzi et al., 2009](#); [Manzi et al., 2016a](#); [Cosentino et al., 2013](#)).

The age of the base of Stage 3 is largely determined by correlating the sedimentary cycles of the Upper Gypsum unit (UG) at Eraclea Minoa (Sicily) with the astronomical curve La2004 ([Laskar et al., 2004](#)). The UG sedimentary cyclicity consists of alternating gypsum and mudstone beds of variable thickness ([Figs. 5g-i](#); see subsection 3.8). Precessional variation of the Mediterranean freshwater budget tied tightly to the African monsoon and Atlantic storms are the drivers interpreted to lie behind the gypsum-mudstone cycles (e.g. [Marzocchi et al., 2015, 2019](#); [Simon et al., 2017](#)). Variations of the freshwater discharge cause the pycnocline to shift vertically, resulting in brine concentration and gypsum precipitation during the arid/dry phases of the precession cycles (precession maximum-insolation minima) and brine dilution and mudstone deposition during the humid/wet phases (precession minimum-insolation maxima) ([Van der Laan et al., 2006](#); [Manzi et al., 2009](#)). Two different tuning options exist in literature ([Van der Laan et al., 2006](#) versus [Manzi et al., 2009](#); [Fig. 3a](#)):

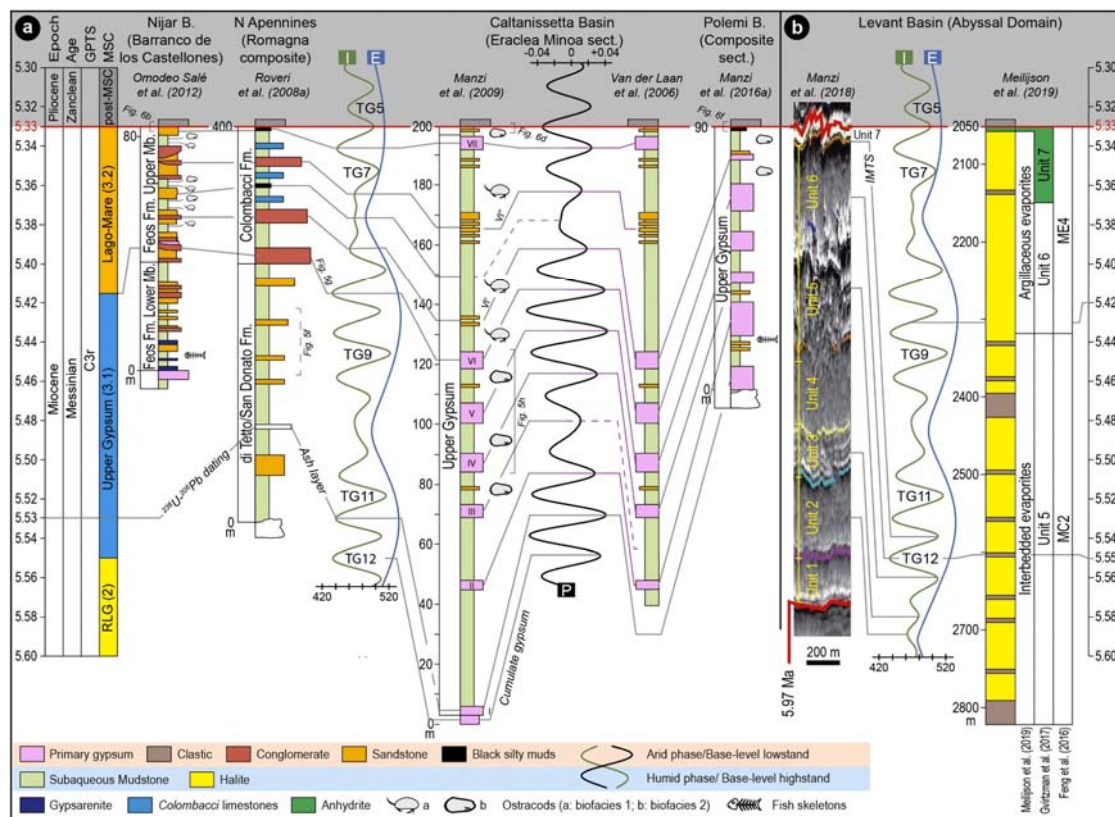


Fig. 3. (a), (b) Available astronomical tunings to astronomic curves of climatic precession (P), 100 kyr eccentricity (E) and 65°N insolation curve (I) of [Laskar et al. \(2004\)](#) of the lithological cyclicity of onshore Stage 3 sections (a) and of the seismic cycles and/or well logs (gamma ray and resistivity) of the MU in the Levant Basin (b). Tunings of onshore sections in (a) are carried out downward from the M/P boundary (conformable in all sections). Astronomically-tuned glacial (even numbers) and interglacial (odd numbers) stages (i.e. TG) as defined by [Hodell et al. \(1994\)](#) are also indicated.

1. Van der Laan et al. (2006) tentatively recognized sedimentary patterns that they correlated with the astronomical curves by using the same phase relationships between the sedimentary cycles and the astronomical cycles as are seen in Plio-Pleistocene sapropel-bearing marine successions of the Mediterranean (Hilgen, 1991). The four closely spaced gypsum beds III to VI were regarded as a cluster, i.e. the sedimentary expression of a 100 kyr eccentricity maximum (Hilgen, 1991; Strasser et al., 2006), whereas the preceding and following evaporite-free marly interval were attributed to a phase of low-amplitude precession oscillations caused by a 100 kyr eccentricity minimum (Fig. 3a). Tuning downward from the conformable Miocene/Pliocene boundary (Fig. 6d) and arguing that the precession peak at ~5.38 Ma, which has an extremely low amplitude, is not expressed in the sedimentary record, Van der Laan et al. (2006) correlated gypsums III to VI with the four successive precession/insolation peaks of the 100 kyr eccentricity maximum dated around 5.44 Ma and the overlying and underlying gypsum-free marly interval fell within 100 kyr eccentricity minimum cycles (Fig. 3a, right log). This tuning resulted in an astronomical age of ~5.51 Ma for the first gypsum bed in their log (i.e. gypsum II in the log of Manzi et al., 2009), and an approximate duration of 175 kyr for Stage 3 as whole.
2. An alternative tuning by Manzi et al., 2009; Fig. 3a, left log) argued that every precessional/insolation peak must have an expression in the rock record. Manzi et al. (2009) agreed with the solution of Van der Laan et al. (2006) on the sedimentary inexpressiveness of the (barely visible) insolation minima peak at ~5.38 Ma. However, these authors considered the insolation minima peaks immediately above and below of too low amplitude to promote the conditions required for gypsum precipitation, but also too high not to have some sedimentary expression. They therefore identified sandstone horizons VI' and VI'' as the sedimentary response to these weak insolation/precession signals. The addition of two precessional cycles (i.e. a total of 9) resulted in an astronomical solution that was adjusted one precessional cycle lower than that of Van der Laan et al. (2006), translating into an age of 5.53 Ma for the base of the UG and a total duration of ~200 kyr for Stage 3. But the more conspicuous difference between the two astronomical solutions discussed lies in the timing at which gypsum precipitation occurred, restricted to the 100 kyr eccentricity maxima according to Van der Laan et al. (2006), extended to the 100 kyr eccentricity minima by Manzi et al. (2009).

An age of 5.53 Ma for the first gypsum bed was also obtained by the astronomical tuning of the Upper Gypsum in Cyprus (Manzi et al., 2016a), but there the tuning is performed just by following the recognition, from the base up, of 6 gypsum beds just like in Sicily and therefore arguing for a bed-to-bed correlation with the Sicilian gypsums I-VI. In the consensus model of Roveri et al. (2014a) the base of Stage 3 coincides with the base of the Sicilian UG, placed by Manzi et al. (2009) at 5.55 Ma (Fig. 1A). However, in the model of Manzi et al. (2009) this age is attributed to a cumulate gypsum horizon interpreted as laterally equivalent of the Halite (i.e. Stage 2), and therefore implying the kickoff of Stage 3 at 5.53 Ma (Fig. 3a). The post-evaporitic successions of the Romagna (Cusercoli and Sapigno sections; Roveri et al., 1998) and Marche (e.g. Trave and Maccarone sections; Iaccarino et al., 2008; Cosentino et al., 2013) areas provided evidence that led to the splitting of Stage 3 into substage 3.1 and 3.2. In the resulting composite section (Roveri et al., 2008a), a shift in the sedimentary facies and stacking pattern is observed (see description in subsection 3.7). Correlation of the sedimentary cyclicity in Romagna was from the (conformable) base of the Pliocene downwards (or from an U-Pb-dated ash layer upward; Cosentino et al., 2013) and linked three fluvial conglomerates and two black mudstone layers of unknown sedimentological significance to the arid phases of the precession cycles (Fig. 3a; Roveri et al., 2008a). The greater thickness of the oldest conglomerate was possibly assumed to be evocative of an oscillation of the amplitude of the corresponding precession minima peak

rather than the amplitude of the peaks responsible for the formation of the other facies. This approach resulted in an age of 5.42 Ma for the first conglomerate (i.e. the substage 3.1/3.2 transition; Fig. 5g) and an approximate duration of 90 kyr for substage 3.2 (the Lago-Mare phase). The same astronomical age is obtained by tuning the Upper Member of the Feos Formation in the Nijar Basin (Omodeo-Salé et al., 2012), where four pelite-conglomerate cycles plus one sandstone capped by the Miocene/Pliocene boundary mark the interval attributed to Stage 3.2 (Fortuin and Krijgsman, 2003).

Although the substage 3.1/3.2 transition is linked to a major Mediterranean-scale hydrological re-organization possibly coinciding with the migration of the Paratethyan biota (Roveri et al., 2008a; Grossi et al., 2011), the facies change used for its definition is hardly recognizable elsewhere (see Chapter 3). As such, other tools have been used to equip fragmentary and/or lithological cyclicity-lacking sections with an age model: the (highly controversial) ostracod biozonation (see subsection 5.1; e.g. Stoica et al., 2016; Karakitsios et al., 2017a; Cosentino et al., 2018; Caruso et al., 2020) and the astronomical tuning of magnetic susceptibility records (e.g. Fonte dei Pulcini section, Central Apennines; Cosentino et al., 2012). Comparison of Atlantic oxygen isotope records (Van der Laan et al., 2005, 2006) and the chronostratigraphy of Roveri et al. (2014a) revealed that Stage 3 sedimentation started during a prominent global eustatic lowstand associated with oxygen isotope (glacial) stage TG12, followed by a latest Messinian deglacial interval which comprised multiple obliquity- and possibly precession-forced global eustatic phases. As documented by Hodell et al. (2001) (later revised by Drury et al., 2018), Van der Laan et al. (2006) and Roveri et al. (2014a), the marine replenishment of the Mediterranean did not coincide with any major deglaciation, so non-eustatic causes of the Zanclean megaflood hypothesis are required.

3. Onshore domain: Key sections, sedimentary expression and faunal content

3.1 The Alborán region

The westernmost outcrops of Stage 3 deposits in the Mediterranean are located in the Alborán region, close to the present-day Strait of Gibraltar (Fig. 2b). MSC deposits on the margins of this region are poorly developed, possibly because of a late Tortonian uplift that raised the margins above the Mediterranean water level (López-Garrido and Sanz de Galdeano, 1999). Near Malaga, however, two facies associations consisting of m-thick conglomerate-sandstone beds alternating with laminated pelites are documented in the Rio Mendelín section (informally referred to as "LM unit"; Guerra-Merchán et al., 2010) and attributed to (part of) the Lago-Mare phase (Fig. 4a) based on their paleontological content. These sediments are squeezed between the Paleozoic basement units, with an erosive contact and associated angular unconformity, and the Pliocene, from which they are separated by another erosional surface draped by conglomeratic accumulations (Fig. 6a). A well-preserved and diverse *in situ* Paratethyan-type ostracod and molluscan fauna (i.e. *Lymnocardiinae* and *Dreissenidae*) typical of shallow waterbodies (up to 100 m deep; Grossi et al., 2008; Gliozzi and Grossi, 2008) with low salinities (5-18‰) is reported from the pelitic units (Guerra-Merchán et al., 2010). The overlying Pliocene in the deeper depocenters starts with 30 m-thick littoral conglomerates with marine mollusks passing progressively upwards into deeper water facies, while fan deltas developed at the basin margins (López-Garrido and Sanz de Galdeano, 1999; Guerra-Merchán et al., 2010, 2014). Notably, the overall thickness of the Pliocene deposits reaches 600 m. The detailed regional studies by López-Garrido and Sanz de Galdeano (1999) and Guerra-Merchán et al. (2014) concluded that accommodation space was created during (Zanclean) sedimentation by local fault-driven subsidence, and that movement on these faults only reversed at the end of the Zanclean causing uplift.

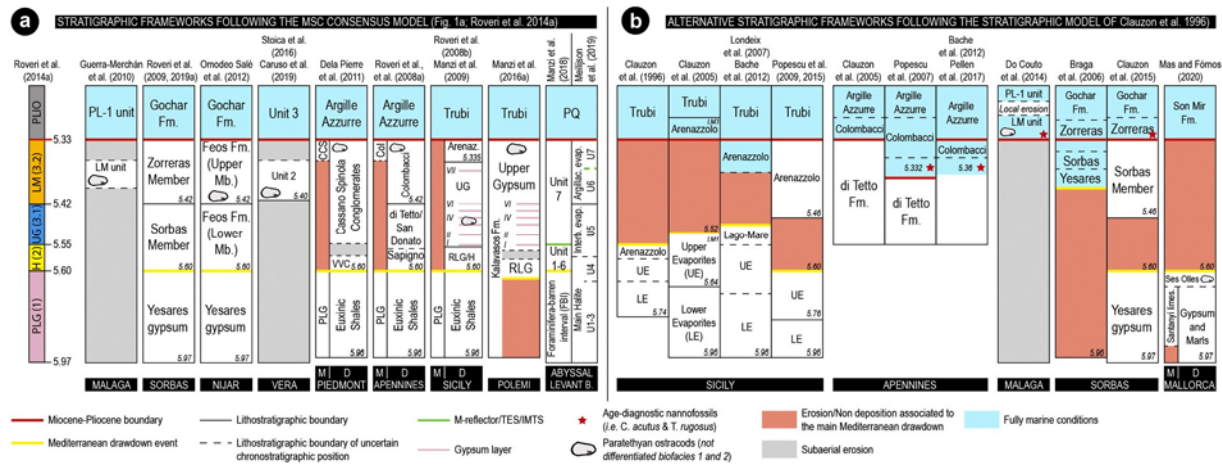


Fig. 4. Schematic overview of different chronostratigraphic models for some of the Messinian successions presented in Chapter 3. Note the large controversies in timing, duration and chronostratigraphic position of the main erosion phase between models in (a) and (b). Models in (a) follow the recently established MSC chronostratigraphic model of Roveri et al. (2014a), according to which the Mediterranean base-level dropped and halite deposited on sea floor during Stage 2 and the Upper Gypsum/Upper Evaporites-Lago-Mare sequence followed. Models in (b) were proposed following the alternative scenario of Clauzon et al. (1996, 2005), which envisaged two Lago-Mare episodes (LM1 and LM3) that occurred before and after the main Mediterranean drawdown event, during which LM2 was deposited in the deep desiccated basins (Do Couto et al., 2014; Popescu et al., 2015; see Roveri et al., 2008c and Grothe et al., 2018 for further explanations). Note, in (b), the shifting of the position of the main erosional phase in Sicily through time as well as the time of the marine replenishment in the Apennines.

An alternative scenario, based on the finding of (a few) specimens of the nannofossil *Ceratolithus acutus*, ascribed the LM unit of Guerra-Merchán et al. (2010) to the earliest Zanclean (Fig. 4b; Do Couto et al., 2014).

On the southern Alborán margin in Morocco, latest Messinian deposits are reported from the Boudinar and Melilla basins (Fig. 2b). Up to 100 m-thick chaotic deposits containing selenite gypsum fragments, azoic conglomerates, sandstones yielding planktic foraminifera and nannofossils and lacustrine limestones are capped by early Pliocene marine marls (Rouchy et al., 2003; Azdimousa et al., 2006; Cornée et al., 2016; Merzeraud et al., 2019). Due to their stratigraphic position, these continental to lacustrine deposits are interpreted as the local expression of the Lago-Mare phase (Cornée et al., 2016) or alternatively as Zanclean successions (Azdimousa et al., 2006).

3.2 Algeria

The Chelif Basin in Algeria (Fig. 2b) displays the typical marginal Messinian succession comprising Tortonian to lower Messinian blue marls, diatomite-bearing sediments (Tripoli unit), cyclically-arranged primary evaporites (13 couplets), ostracod-rich post-evaporitic deposits and Zanclean foraminiferal marls (Rouchy et al., 2007). The post-evaporitic sediments show a great lateral variability in both thickness (from few meters up to 125 m) and facies. They are mainly dominated by terrigenous clastic lithologies, associated in the marginal areas with sandy carbonates and stromatolitic limestones. A mixed faunal assemblage of non-marine (Paratethyan-like ostracods) and marine (benthic and planktic foraminifera) organisms is present, showing an increase in ostracod species diversity from the bottom to the top (Rouchy et al., 2007).

3.3 Neogene basins of the Eastern Betics (Spain)

The external Neogene basins (Sorbas, Nijar, Vera and Bajo Segura) of the eastern Betic Cordillera (SE Spain; Fig. 2b) represent an important laboratory for understanding Messinian events. In particular, the Sorbas and Nijar basins preserve two allegedly continuous successions spanning the entire MSC (e.g. Roveri et al., 2009; Omodeo-Salé et al., 2012). The two basins are similar in many respects. Their stratigraphic organization, for example, suggests they were connected for much of the late

Miocene up until MSC Stage 1 (Fortuin and Krijgsman, 2003), which is represented by the gypsiferous Yesares Member (e.g. Lu, 2006). However, facies differences are prominent in the Stage 3 formations according to the chronostratigraphic frameworks of Roveri et al. (2009) for the Sorbas Basin and Omodeo-Salé et al. (2012) for the Nijar Basin (Fig. 4a). Lithostratigraphically, two members are discerned between the Yesares Member and the basal Zanclean: the Sorbas and Zorreras members in the Sorbas Basin (Figs. 4a, 5a) and the lower and upper members of the Feos Fm. in Nijar (Figs. 3a, 4a; Roep et al., 1998; Krijgsman et al., 2001; Fortuin and Krijgsman, 2003; Braga et al., 2006; Roveri et al., 2009, 2019a; Omodeo-Salé et al., 2012).

The Sorbas Member (see Roep et al., 1998 and Aufgebauer and McCann, 2010 for a more detailed sedimentological description) consists of three overlapping coarsening-upward depositional sequences made of offshore clays and marls passing upward into shelf muds and coastal sandstone bodies. Still unclear is the chemistry of the subaqueous environment during the formation of the Sorbas Member and the provenance of the water fluxes. These shallow-water deposits are conformably replaced upward by the Zorreras Member that comprises alternations of reddish siltstones and sandstones (Fig. 5a) organized in five (or eight) lithological cycles expressing continental environments (Martín-Suárez et al., 2000; Aufgebauer and McCann, 2010). Up to four lenticular white limestone beds bearing brackish Paratethyan-like ostracods (*Cyprideis*, *Loxocorniculina djafarovi* and freshwater species of the family Limnocytheridae, bivalves and *Chara* oogonia (Roep and Harten, 1979; Aufgebauer and McCann, 2010) are found interrupting the fluvial sequence (Fig. 5a) and are linked to either episodic flooding by local rivers (Braga et al., 2006; Aufgebauer and McCann, 2010) or episodic Mediterranean incursions (Fortuin and Krijgsman, 2003; Andreetto et al., 2021). A correct interpretation of the paleo-depositional environment of these limestone beds is crucial for the discussion concerning the Mediterranean base-level position during the Lago-Mare phase. In fact, if the Sorbas Basin was relatively shallow during Zorreras deposition (50-100 m; Roveri et al., 2019a, 2020), repeated and sudden Mediterranean incursions would indicate that the Mediterranean Basin was relatively full and that its base level was oscillating, possibly with precessional periodicity (Andreetto et al., 2021). The contact between the Zorreras Mb. and the overlying near-

shore Pliocene (<50 m depositional paleodepth; Roveri et al., 2019a) in the Sorbas Basin is conformable and expressed differently around the

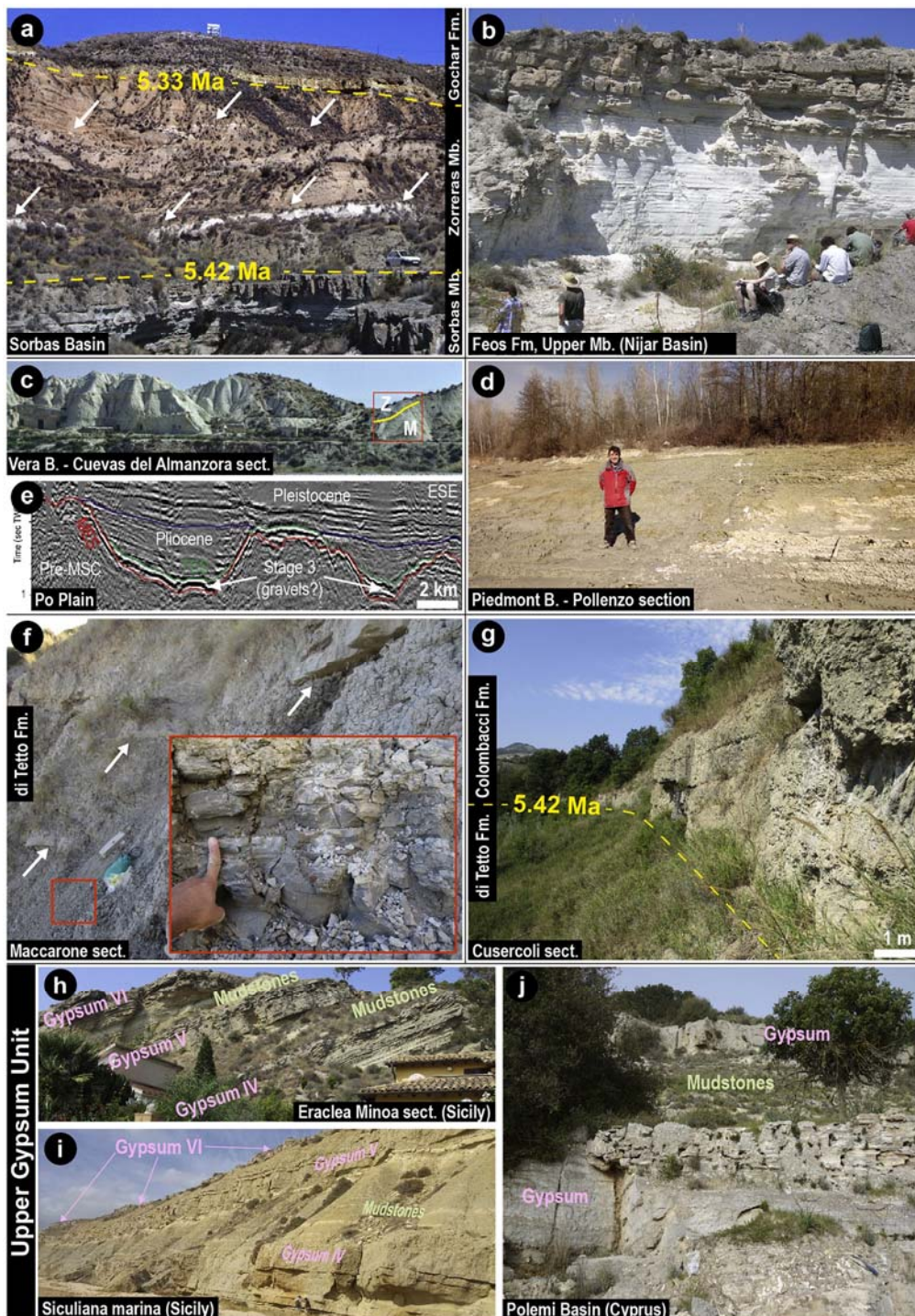


Fig. 5. Sedimentary expression of Stage 3 from selected onshore Mediterranean localities. (a) Photograph from the Sorbas Basin showing the red continental sediments of the Zorreras member with intercalated white limestones (white arrows; from Andreetto et al., 2021). The conformable resting of the Zorreras Mb. above the Sorbas Mb. and underneath the Gochar Fm. of Pliocene age is also appreciable. Car for scale. (b) One typical lithological (and precessional) cycle of the Upper Mb. of the Feos Fm. in the Nijar Basin, here constituted by an ostracod-bearing, white and laminated mudstone bed overlain by an azoic fluvial sandstone (courtesy of Anne Fortuin). (c) Panoramic view of the Cuevas del Almanzora section (from Andreetto et al., 2021). Red rectangle indicates the position of the section straddling the Messinian (M)/Zanclean (Z) transition and studied by Fortuin et al. (1995), Stoica et al. (2016), Caruso et al. (2020) and Andreetto et al. (2021). Buildings for scale. (d) The sub-unit a of the Piedmont Basin composed of azoic grey mudstones grading into yellowish, mammal-rich overbank deposits. (e) WNW-ESE seismic profile in the Po Plain showing incised valleys filled during Stage 3 by suggested clastic deposits and sealed by deep-water turbidites in the Zanclean (modified from Amadori et al., 2018). (f) Typical aspect of the di Tetto/San Donato Formation in the Northern Apennines composed by grey mudstones (detail in the inset) with interbedded sandstone bodies (white arrows). The picture is taken from the Maccarone section. (g) The di Tetto Fm.-Colombacci Fm. transition in the Cusercoli area (Eastern Romagna, Fig. 2b), defined by the facies change underlined by the appearance of a fluvial conglomerate. This lithostratigraphic boundary also corresponds to substage 3.1/3.2 boundary of Roveri et al. (2014a). (h), (i), (l) Lithological cycles of the Upper Gypsum Unit in Eraclea Minoa (h), Siciliana Marina (i) and Polemi (l) sections. Cycles are several m-thick and primarily composed by beds of primary gypsum alternating with mudstones bearing Paratethyan ostracods (at least in Eraclea Minoa).

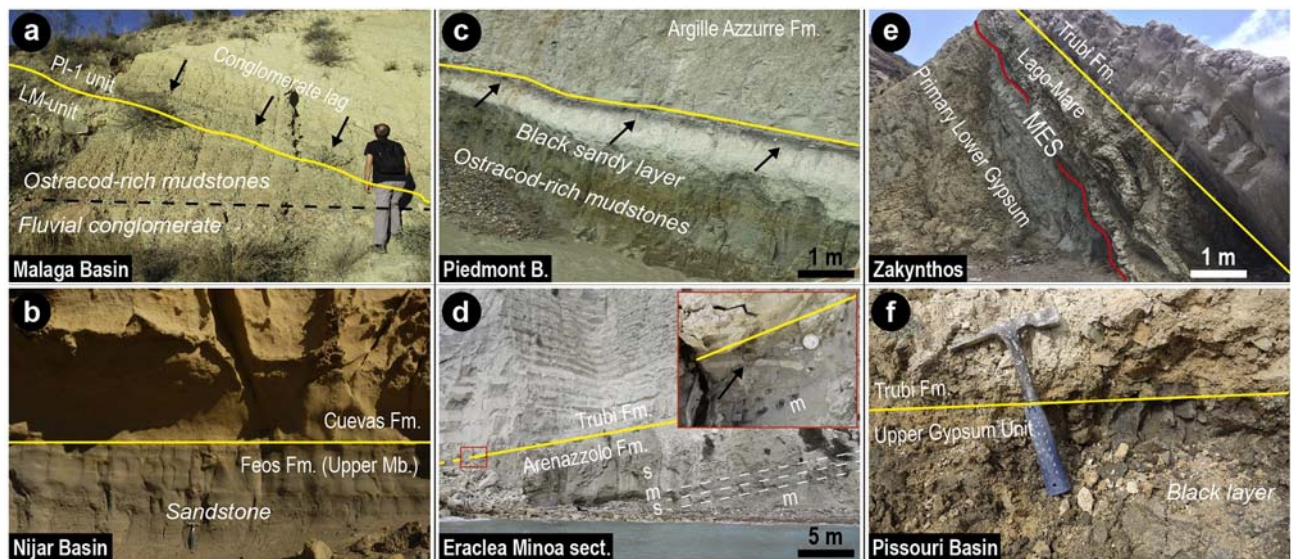


Fig. 6. Photographs of the Miocene/Pliocene boundary (yellow lines) from selected onshore Mediterranean localities. (a) Erosive M/P transition in the Mendelín section (Malaga Basin). Note the conglomeratic lag draping the erosional surface and sharply overlain by foraminifera-rich marls. (b) Conformable stratigraphic contact between the uppermost Messinian sandstone of the Feos Fm. and the Zanclean biocalcarenes of the Cuevas Fm. in the Barranco de los Castellones section, Nijar Basin (hammer for scale; modified from Andreetto et al., 2021). (c) The Messinian/Zanclean boundary in the Pollenzo section (Piedmont Basin) marked by a characteristic black layer interbedded between Paratethyan ostracods-rich mudstones and marine foraminifera-rich marls (modified from Dela Pierre et al., 2016). (d) Uppermost segment of the Eraclea Minoa section (Caltanissetta Basin, Sicily) displaying the (non erosive) contact between the Pliocene Trubi Formation above and the sandy Arenazzolo Formation below. The inset is a close view of the transition, which occurs above a ~50 cm-thick burrowed mudstone horizon rich in Paratethyan ostracods and marine foraminifera. (e) Lago-Mare sediments in the Kalamaki section (Zakynthos) unconformable, through an erosional surface (i.e. the Messinian Erosional Surface, MES), over the PLG unit and also unconformable beneath the Trubi Fm. (modified from Karakitsios et al., 2017b). (f) Close view of the M/P boundary in the Pissouri Basin, where the foraminifera-rich Trubi marls lie above a black layer (paleosol according to Rouchy et al., 2001).

basin, ranging from a bivalves-rich bed overlain by a yellow, fossiliferous calcarenite floored by a gravelly lag deposit (Mather et al., 2001) to a grey marl horizon with marine foraminifera assemblages followed by a second shell-rich bed (Roveri et al., 2019a). Similar to the situation in Malaga, the rare identification of *Ceratolithus acutus* in sediments of the continental Zorreras Mb. led Clauzon et al. (2015) to put forward an alternative chronostratigraphic and paleoenvironmental interpretation for the Sorbas MSC succession, shifting the Zorreras Mb. into the Pliocene (Fig. 4b) and thus associating the presence of brackish Paratethyan-like ostracods with exchanges between the Mediterranean and Paratethys following the Mediterranean re-filling, at high sea level.

In the Nijar Basin (Fig. 2b), the latest Messinian Feos Formation is bracketed at the base and top by an erosional surface along the basin margins and its correlative conformity in the deeper parts (Fig. 3a; Fortuin and Krijgsman, 2003; Aguirre and Sánchez-Almazo, 2004; Omodeo-Salé et al., 2012). The Lower Feos Member consists of azoic, graded and locally slumped siliciclastic-carbonate beds alternating with gypsarenites and gypsiltites and including a laterally continuous Mn-rich bed (Fortuin and Krijgsman, 2003; Omodeo-Salé et al., 2012). In the basin center (e.g. Barranco de los Castellones section; Fig. 3a) the Upper Feos member comprises four complete lithological cycles of m-thick conglomerate to sandstone beds alternating with laminated pelites (Fig. 5b), and one incomplete cycle, which only consists of a sandstone horizon conformably capped by the Pliocene Cuevas Fm. (Fig. 6b; Fortuin and Krijgsman, 2003). A rich fauna of mixed brackish ostracods and marine foraminifera is found in all four pelitic beds (Bassetti et al., 2006). Its origin is questionable. These ostracods were regarded as endemic to the Mediterranean and inhabiting endorheic lakes by Bassetti et al. (2006). However, later they were shown to have been misidentified and were instead considered Paratethys-derived by Stoica et al. (2016; see subsection 5.1). Planktonic and deep-water benthic foraminifera are widely considered reworked by Fortuin and Krijgsman

(2003), Bassetti et al. (2006) and Omodeo-Salé et al. (2012), in place by Aguirre and Sánchez-Almazo (2004).

In the Vera Basin (Fig. 2b), in situ gypsum deposits are missing because of widespread erosion or non-deposition and MSC deposits are only represented by ~12 m of laminated varicolored marly clays (Unit 2 Fig. 4a), which are best exposed in the Cuevas del Almanzora section (Fortuin et al., 1995; Fig. 5c). These clays contain a well-preserved and diversified *in situ* fauna of Paratethyan-like ostracod and shallow-water, benthic foraminifera mixed with physically reworked (mostly from the lower Messinian Abad marls) planktic and deep-water benthic foraminifera (Fortuin et al., 1995; Stoica et al., 2016; Caruso et al., 2020). The marly clays are assigned by Stoica et al. (2016) and Caruso et al. (2020) to (roughly) the whole late Messinian Lago-Mare phase (Fig. 4a) based on the ostracod biozonation of Grossi et al. (2011) and are considered to represent either sedimentation in an isolated lake subject to base-level and salinity fluctuations (Caruso et al., 2020) or deposition in a coastal lagoon that was connected to the water mass filling the open Mediterranean (Stoica et al., 2016; Andreetto et al., 2021). Similar to Malaga, these sediments are topped by an erosive surface draped by a conglomeratic accumulation which is overlain by the open marine fauna-rich sediments of the basal Zanclean (Fortuin et al., 1995; Caruso et al., 2020). This erosion feature likely indicates that the Miocene/Pliocene transition followed a base-level lowstand in the Vera Basin. Stage 3 deposits (Garrucha Fm.) in the easternmost basin of the Betic Cordillera, the Bajo Segura Basin (Fig. 2b), are bounded below and above by two erosional surfaces related to lowered Mediterranean base-levels and discontinuously present due to the widespread fluvial erosion that occurred at the Miocene/Pliocene boundary (Soria et al., 2005, 2008a, 2008b). The Garrucha Fm. shows a maximum thickness of 100 m in its type section (Soria et al., 2007, 2008b). It consists of 20-50 cm thick sandstone bodies interrupting a dominantly marly succession deposited in a subaqueous environment inhabited by *Cyprideis* sp. and

euryhaline, shallow-water benthic foraminifera (*Ammonia beccarii*, *Elphidium granosum*, *Elphidium macellum*, *Haynesina germanica* and *Quinqueloculina laevigata*). Planktic foraminifera are also observed and for a long time were considered to be physically reworked (Soria et al., 2005, 2008b). However, some stratigraphic levels contain dwarf tests of long-ranging taxa such as *Globoturborotalita decoraperta*, *Globigerina bulloides*, and *Neogloboquadrina spp.* which recently have been interpreted as being *in-situ* mostly due to the absence of notable signs of reworking (Corbí and Soria, 2016). Among these dwarf taxa is *Neo-globoquadrina acostaensis* (dextral; Corbí and Soria, 2016). Since this group is mainly dextral in the latest Messinian Atlantic successions (e.g. Sierro et al., 1993; Bassetti et al., 2006), this may indicate that Atlantic inflow to the Mediterranean occurred during the late Messinian and the base level of the Mediterranean was high enough to reach the marginal Bajo Segura Basin. The Miocene/Pliocene boundary is, once again, marked by an erosional surface which outlines up to 200 m deep paleovalleys engraved down into the pre-MSC sediments and filled with conglomerates and sandstones of claimed coastal and shallow marine environments (Soria et al., 2005, 2008b; García-García et al., 2011; Corbí et al., 2016).

3.4 Mallorca

Mallorca, which constitutes an emerged segment of the Balearic Promontory (Fig. 2), does not expose the classical MSC evaporite sequence. Instead, two main MSC-related units are found above late Tortonian-Messinian reefal carbonates (Reef Complex Unit) and beneath the Pliocene: the Santanyí limestones and the Ses Olles Formation (Mas and Fornós, 2020 and references therein). The Santanyí limestones are microbialites and oolite-dominated sediments in which a baleen whale neurocranium has been found (Mas et al., 2018a). This unit was interpreted either as a Terminal Carbonate Complex (TCC) laterally equivalent to the Primary Lower Gypsum (PLG) which has been drilled in the deeper parts of the bay of Palma (Mas and Fornós, 2020) or as time-equivalent to the Reef Complex Unit (e.g. Arenas and Pomar, 2010; Suárez-González et al., 2019). The Ses Olles Formation consists of marls, sandy-marls and marly-calcareous lacustrine deposits rich in *in-situ* freshwater *Chara spp.*, brackish water Paratethyan-like mollusks and ostracods and littoral benthic foraminifera (*Elphidium sp.*, *Ammonia sp.*).

The upper contact of the Ses Olles Formation with the Pliocene corresponds to an erosional ravinement surface draped by a transgressive lag of coastal deposits usually containing coquinas and/or conglomerates (Mas, 2013, 2015; Mas and Fornós, 2020). The lower contact of the Ses Olles Formation with the Santanyí limestones is sporadically marked by a well-developed reddish paleosol (Mas, 2013, 2015; Mas and Fornós, 2020), which indicates that a (unquantified) period of subaerial exposure occurred before the emplacement of the Ses Olles Fm. However, in their more recent study, Mas and Fornós (2020) surprisingly conclude that the Ses Olles Formation has a conformable contact with the Santanyí limestones, ascribed to part of Stage 1. This led Mas and Fornós (2020) to conclude that the emplacement of the Ses Olles Fm. pre-dated the MSC peak and that the erosional surface marking the Miocene/Pliocene boundary is associated with a 270 kyr hiatus linked to the main MSC base-level drawdown (Fig. 4b). This conclusion is, however, in disagreement with the unconformity at the base of the Ses Olles Fm., which instead points to the deposition of the Ses Olles Fm. (and therefore to the arrival of the Paratethyan fauna in Mallorca) at some point during Stage 3 of Roveri et al. (2014a).

3.5 Piedmont Basin

The Piedmont Basin (NW Italy) contains the northernmost record of the MSC (Fig. 2b). The terminal MSC sediments (i.e. the Cassano Spinola Conglomerates Fm.) overlay pre-MSC units, the PLG deposits (Gesso Solifera Fm.) or reworked evaporites (Valle Versa chaotic complex, VVC) and underly the Zanclean marls of the Argille Azzurre Fm. (Dela

Pierre et al., 2011).

The Cassano Spinola Conglomerates is splitted in two sub-units by Dela Pierre et al. (2016). Sub-unit *a* consists of azoic grey mudstones turning to yellowish silty mudstones (Fig. 5d) typified by *in situ* root traces, paleosols and mud cracks and including three/four intercalated lens-shaped, cross-bedded conglomeratic layers (Ghibaudo et al., 1985; Dela Pierre et al., 2011, 2016). Abundant land plant leaves and a diverse terrestrial vertebrate fauna are found in the yellowish siltstones, which have been interpreted as overbank deposits (Harzhauser et al., 2015; Colombero et al., 2017 and references therein). In this continental interval, a low-diversity fish fauna consisting of otoliths of marine and Paratethyan species is found (Grunert et al., 2016; Carnevale et al., 2018; Schwarzshans et al., 2020). These otoliths were Sr-dated to the early-middle Miocene (Grunert et al., 2016). Nevertheless, they were concluded not to be physically reworked, but rather to have been transported by large marine predators, therefore implying a Piedmont Basin-(marine) Mediterranean connection was in force (Grunert et al., 2016; see subsection 5.6). Sub-unit *b* (i.e. Strati a Congeria *sensu* Sturani, 1973) is made of grey mudstones bearing a mixture of *in-situ* brackish water mollusks (Sturani, 1973; Esu, 2007) and ostracods (Trenkwalder et al., 2008) of Paratethyan affinity along with physically reworked foraminifera and calcareous nannofossils (Trenkwalder et al., 2008; Violanti et al., 2009). The transition to the Pliocene Argille Azzurre Fm. is sharp above a characteristic black and azoic sandy layer (Fig. 6c) rich in terrigenous and intrabasinal (i.e., glaucony and phosphates) grains and disarticulated valves of both brackish-water and continental bi-valves, but barren of *in-situ* fossils (Trenkwalder et al., 2008). The occurrence, at its top and directly below the Argille Azzurre Fm., of abundant *Thalassinoides* trace fossils filled with Pliocene sediments led Trenkwalder et al. (2008) and Dela Pierre et al. (2016) to interpret the top surface of this layer as an omission surface. This surface indicates a period of basin starvation (and therefore a hiatus) due to a sudden increase in water-depth, ascribed by Trenkwalder et al. (2008) to the Zanclean reflooding. This hiatus may have lasted for only part of the late Messinian (Violanti et al., 2009; Dela Pierre et al., 2016) or may have endured into the Pliocene (Trenkwalder et al., 2008).

3.6 Po Plain

To the east, the Messinian sediments in the Piedmont Basin disappear beneath the km-thick Plio-Quaternary succession of the Po Plain- Adriatic Foredeep (PPAF; Fig. 2a). By definition of Ghielmi et al. (2010) and Amadori et al. (2018), the PPAF includes two main elongated depocenters enclosed within the northern Apennines to the South and the Southern Alps to the North: the easternmost portion of the Po Plain and the whole present-day northern Adriatic Sea. Here, for simplicity, we include in the definition of PPAF also its westernmost depocenters of the Western Po Plain Foredeep. The Messinian-Pleistocene sedimentary sequence, studied through the integration of seismic and borehole observations, is mostly represented by thick sequences of turbidite deposits in the foreland depo-center passing, towards the margins, to fluvial and deltaic systems related to the proximity of the marginal thrust-fold-belts (Cipollari et al., 1999; Ghielmi et al., 2010, 2013; Rossi et al., 2015a; Rossi, 2017). During MSC Stage 1, primary evaporites and dolomicrites were deposited in some shallow-water settings, while evaporitic deposition was inhibited in the deep-water settings, where it was replaced by deposition of anoxic mudstones (Ghielmi et al., 2010). Instead, the post-evaporitic deposits consist of large thicknesses (up to 1 km) and volumes of coarse-grained clastics (LM1 and LM2 of Rossi and Rogledi, 1988; ME3 or Fusignano Fm. of Ghielmi et al., 2010; ME4 of Ghielmi et al., 2013; ME3b and possibly ME3a of Rossi et al., 2015a). Several authors (Ghielmi et al., 2010, 2013; Rossi et al., 2015a; Amadori et al., 2018; Cazzini et al., 2020) showed that these post-evaporitic sediments are the infilling of ca. N-S and NW-SE trending, V-shaped valleys (Fig. 5e). These valleys were carved at least as far as 50 km into the Alps, to a

depth up to 1 km into the pre- and syn-evaporitic Messinian deposits and nicely shape the present-day river network of the southern Alps (Amadori et al., 2018).

Different mechanisms for the incision have been proposed, with major implications for the desiccated vs full Mediterranean controversy (Figs. 1b-c). Ghielmi et al. (2010, 2013), Rossi et al. (2015a), Amadori et al. (2018) and Cazzini et al. (2020) ascribed the valley incision along the PPAF northern margin to fluvial erosion, whose basinward shifting was triggered by the Stage 2 Mediterranean drawdown, estimated to have been around 800-900 m (Ghielmi et al., 2013; Amadori et al., 2018). In this case, Stage 3 deposition in the PPAF occurred in endorheic lakes fed by the Alpine rivers and kept isolated until the Zanclean, when the sudden sea-level rise following the Zanclean reflooding was enough to bypass morphological highs (e.g. Gargano-Pelagosa and/or Otranto paleosills) located in the southern Adriatic foredeep (Fig. 2a; see Pellenet et al., 2017; Amadori et al., 2018; Manzi et al., 2020). Conversely, Winterberg et al. (2020) suggested that the over-deepened valleys on the southern slope of the Alps are related to Pleistocene glacial erosion. Although Winterberg et al. (2020) do not address the paleoenvironment during the Messinian, this interpretation does not rule out the possibility that (at least part of) Stage 3 sedimentation occurred in a PPAF connected to the Mediterranean water mass and that no catastrophic reflooding occurred at the Miocene/Pliocene boundary. The conclusion of a non-catastrophic refilling was also drawn by Pellen et al. (2017) on the basis of the onshore Adriatic record (see subsection 3.7).

3.7 Apennine system

The Messinian deposits resurface to the south of the PPAF sector and extensive sections are found in several basins on both the foreland domain (Adriatic side of the partially uplifted Apennine chain), subjected to compressional tectonics during the late Messinian, and the back-arc domain (Tyrrhenian side), contemporaneously affected by extension (Fig. 2b; Cipollari et al., 1999; Schildgen et al., 2014; Cosentino et al., 2018). Overall, the MSC record of the Apennines is subdivided into an evaporitic and post-evaporitic interval squeezed in between two marine units (Messinian Euxinic Shales Fm. at the base and Zanclean Argille Azzurre Fm. atop; Fig. 4a). Different vertical motions related to ongoing Apenninic tectonics resulted in the deposition of Stage 3 sediments with highly variable sedimentary expression and stratigraphic resolution from basin to basin. The post-evaporitic deposits are alternatively found resting unconformably, with an erosional contact associated to an angular unconformity, above the alternations of the Gessoso Solifera Fm./PLG, or conformably above evaporitic-free cycles lateralequivalent of the marginal PLG (Fig. 4a; e.g. Roveri et al., 1998, 2008a). This led to the conclusion that both shallow and deep-water successions are present in the Apennine foredeep system (Roveri et al., 2001).

The physical-stratigraphic model developed for the post-evaporitic interval in the Romagna area (i.e. Northern Apennines) and applied to the whole Apennine domain was subdivided into two allunits (named p-ev₁ and p-ev₂) based on a basin-wide shift in facies, overall stacking patterns and depositional trends (i.e. progradational and retrogradational, respectively; Roveri et al., 1998, 2001, 2005, 2008a; Manzi et al., 2005, 2007, 2020). Allunit p-ev₁ only accumulated in deep-water settings (e.g. Cusercoli, Sapigno, Maccarone and Trave sections; Roveri et al., 1998; Iaccarino et al., 2008; Cosentino et al., 2013) during the subaerial exposure of the basin margins (e.g. Vena del Gesso Basin, Monticino quarry, Pellen et al., 2017). It starts with resedimented clastic evaporites (i.e. Sapigno Fm.) followed by a coarsening- and shallowing-upward succession (i.e. di Tetto or San Donato Fm.) of mudstones with intercalated turbiditic sandstones (Fig. 5f) and a volcanoclastic marker bed dated initially by ⁴⁰Ar-³⁹Ar at ~5.5 Ma (Odin et al., 1997) and later by ²³⁸U-²⁰⁶Pb at 5.5320±0.0046/0.0074 Ma (Cosentino et al., 2013; Fig. 3a). Allunit p-ev₂ (i.e. Colombacci Fm.) occurs in the deeper depocenters in 4/5 sedimentary cycles consisting of three > 5 m-thick coarse-grained bodies (conglomerates and sandstones) and two black-

colored mudstone beds alternating with fine-grained mudstones/clays with intercalated three micritic limestones (known in literature as *Colombacci* limestones; Figs. 3a, 5g; Bassetti et al., 2004). By contrast, an incomplete Colombacci Fm. deposited in the shallower thrust-top basins (e.g. Vena del Gesso Basin and Molise sections; Pellen et al., 2017; Cosentino et al., 2018). The p-ev₂ cycles have been interpreted as reflecting the alternation of wet (mudstones and Colombacci limestones in Eastern Romagna) and dry (coarse-grained facies and Colombacci limestones in the Maccarone section) phases controlled by Milankovitch-driven climatic factors (Fig. 3a; Roveri et al., 2008a; Cosentino et al., 2013) and, as such, they have been used for the astronomical tuning of the Colombacci Fm. to the Lago-Mare phase (Figs. 3a, 4a; see subsection 2.2). By contrast, Clauzon et al. (2005) and Popescu et al. (2007) moved the Colombacci Fm. into the Pliocene (Fig. 4b). However, this conclusion has been proven to rely on wrong stratigraphic and paleontological arguments (see Roveri et al., 2008c, Grothe et al., 2018 and subsection 5.5). Substage 3.2 records in the Apennines do not always contain the three prominent conglomeratic facies as in Romagna, but only laminated to massive clays with sandy intercalations equivalent to the ones typifying substage 3.1 records (e.g. Maccarone section; Sampalmieri et al., 2010; Cosentino et al., 2013; Fig. 5f). The absence of a lithological cyclicity that clearly mimics an orbital signal largely hampered the astronomical tuning of these clay-dominated sections, although an attempt has been made with the Maccarone section (Cosentino et al., 2013). The only exception is represented by the Fonte dei Pulcini section, which has been equipped with an age framework by astronomical tuning of the magnetic susceptibility record (Cosentino et al., 2012). Despite the lack of outstanding lithological changes these sections are often provided with a lithostratigraphic subdivision using the same nomenclature as in the Romagna area. When applied, the di Tetto Fm.-Colombacci Fm. boundary is placed high in the sections, i.e. few tens of meters underneath the Miocene/Pliocene boundary, resulting in a much different thickness of the formations compared to the Romagna area.

Stage 3 sediments are poorly exposed on the Tyrrhenian Sea onshore of Italy (Fig. 2b). The best known succession crops out in the Cava Serredi quarry in the Fine Basin (Tuscany; Bossio et al., 1978, 1993; Carnevale et al., 2006b, 2008). Here the MSC has a thickness of ~150 m, of which only the uppermost ~100 m are attributed, without clear arguments, to Stage 3 by Carnevale et al. (2006b). The lowermost ~40 m of the Stage 3 unit consists of mudstone with alternating sandstone bodies which have been attributed to Roveri et al. (1998)'s p-ev₁ allunit, while the uppermost ~60 m form the p-ev₂ allunit and include two prominent conglomerate bodies alternating with mudstones interbedded with sandstone horizons and black, organic-rich layers (Carnevale et al., 2006b). A few and more fragmented sections are also described on the Tyrrhenian Sea side of Italy by Cipollari et al. (1999). The

Miocene/Pliocene boundary is variably expressed through the Apennine system: unconformable above the ostracod-bearing clays and highlighted by erosional surfaces draped by conglomeratic accumulations (e.g. Stingeti section in Molise; Cosentino et al., 2018), conformable above 0.5-1 m-thick black mudstones similar to how it is observed in Piedmont area and Maccarone section; Roveri et al., 1998; Gennari et al., 2008) or conformable above the ostracod-rich mudstones (e.g. Maccarone and Fonte dei Pulcini sections; Cosentino et al., 2005, 2012, 2013; Sampalmieri et al., 2010).

All p-ev₁ deposits studied are almost devoid of in-situ biota, except for fish otoliths and three fish skeletons found in the upper substage 3.1 part of Cava Serredi (Carnevale et al., 2006b). The p-ev₂/Colombacci deposits, instead, host typical Paratethyan assemblages of brackish-water mollusks, ostracods, dinocysts and fish (Bassetti et al., 2003; Bertini, 2006; Popescu et al., 2007; Grossi et al., 2008; Iaccarino et al., 2008; Cosentino et al., 2012, 2018; Schwarzhan et al., 2020). A diverse array of marine fossils (benthic and planktic foraminifera, calcareous nannofossils, dinocysts and fish otoliths and skeletons) has also been

reported from the horizons containing these Paratethyan taxa (Bertini, 2006; Carnevale et al., 2006a; Popescu et al., 2007; Pellen et al., 2017). While the autochthony of ostracods, when considered, is unquestioned, the allochthonous vs autochthonous character of the other mentioned fossils is disputed and still unclear (see Chapter 5).

3.8 Sicily

The MSC record is widely exposed on Sicily, mainly in the Caltanissetta Basin and in scattered locations on the Hyblean Plateau (i.e. Ragusa-Siracusa area) and the Messina area (Fig. 2b; Butler et al., 1995; Manzi et al., 2009; Sciuto et al., 2018). Like the Northern Apennines, it shows a complex distribution and variable stratigraphy that mirrors the structuring of Sicily into basins with different characters, geometries and depocenters which subsided at different times and rates (Butler et al., 1995; Catalano et al., 2013). This structural setting permitted the simultaneous deposition of shallow and intermediate-water sediments (Roveri et al., 2008b). Mostly found in the Caltanissetta Basin, these intermediate-water successions have for decades been considered the onshore counterpart of the offshore evaporitic trilogy seen in seismic data from the Western Mediterranean Basin (Decima and Wezel, 1973). More recently, Raad et al. (2021) attempted a similar onshore-offshore correlation but with the intermediate Central Mallorca Depression. The currently endorsed stratigraphic model (Fig. 4a), refined over the years by Decima and Wezel (1971, 1973), Decima et al. (1988), Butler et al. (1995), García-Veigas et al. (1995), Rouchy and Caruso (2006), Roveri et al. (2008b) and Manzi et al. (2009), envisages two 'evaporitic cycles'. The 'First cycle', overlying both alluvial and deep-water sediments (Tripoli Fm., Licata Fm. and Terravecchia Fm.; see Maniscalco et al., 2019 and references therein), comprises the disputed Calcare di Base (Manzi et al., 2011, 2016b vs Caruso et al., 2015), PLG or Gessi di Cattolica Fm. (Decima and Wezel, 1973; Lugli et al., 2010) and the Halite Unit (Lugli et al., 1999). The 'Second cycle' comprises the Upper Gypsum (UG) or Gessi di Pasquasia Fm., which is only present in depocenters of the Caltanissetta Basin (see Manzi et al., 2009 for a detailed overview), sporadically overlain by the siliciclastic Arenazzolo Fm. (Decima and Wezel, 1973; Cita and Colombo, 1979). The whole succession is sealed by the Pliocene marine Trubi Fm. (Fig. 4a). The two evaporite cycles are separated by an erosional surface (MES) associated with an angular discordance broadly linked to the main Mediterranean drawdown event (e.g. Butler et al., 1995; Roveri et al., 2008b). Clauzonet al. (1996), however, placed the MES at the Arenazzolo Fm.-Trubi Fm. transition, implying that the entire evaporitic deposition in the Caltanissetta Basin pre-dated the offshore one, but they do not provide evidence of erosion at that level. In more recent publications from the same research group, the MES is shifted towards the base of the Arenazzolo Fm. (e.g. Bache et al., 2012), again without evidence of major erosion, and different ages are assigned (see Fig. 4b and Grothe et al., 2018 for details). The Upper Gypsum successions are commonly incomplete in many of the Caltanissetta Basin sections (Pasquasia-Capodarso, Casteltermini, Alimena, Nicosia, Siculiana-Marina; Decima and Sprovieri, 1973; Rouchy and Caruso, 2006; Manzi et al., 2009; Fig. 5i). In the most complete section, Eraclea Minoa (Fig. 3a), the Upper Gypsum Unit consists of 6 (Van der Laan et al., 2006) to 7 (Manzi et al., 2009) primary gypsum beds with a repetitive internal organization of facies (see Schreiber, 1997 and Manzi et al., 2009 for facies description) interbedded with marls and lenticular terrigenous sandstone bodies, gypsarenites and gypsrudites (Fig. 5h). Two of the terrigenous sandstone bodies are highlighted by Manzi et al. (2009) in the thick (~60 m), *Cyprideis agrigentina*-rich (Grossi et al., 2015), marly interval dividing gypsum VI and VII for its alleged astronomical significance (Fig. 3a; see subsection 2.2). A mixed (physically reworked) marine (foraminifera and dino-cysts) and (*in-situ*) brackish biota (ostracods and dinocysts) of Paratethyan origin characterizes the marly interbeds from at least gypsum III upwards (following the investigations carried on the Eraclea Minoa

section; Bonaduce and Sgarrella, 1999; Rouchy and Caruso, 2006; Londeix et al., 2007; Grossi et al., 2015; Fig. 3a). Calcareous nannofossils have been found along with the above organisms in a more northerly location by Maniscalco et al. (2019) and considered reworked. Above the last gypsum, the ~6-7 m-thick Arenazzolo Fm. is found, represented by reddish arkosic cross-laminated and poorly consolidated sand (Bonaduce and Sgarrella, 1999; Roveri et al., 2008b) and interpreted as the expression of a shallow-water delta, albeit without a sedimentological investigation (e.g. Decima and Wezel, 1973; Cita and Colombo, 1979). The whole Stage 3 sequence is conformably overlain by the Zanclean marine Trubi Fm. in the basin center (e.g. at Eraclea Minoa and Capo Rossello; Fig. 6d; Broolsma, 1975; Cita and Colombo, 1979; Van Couvering et al., 2000; Rouchy and Caruso, 2006; Manzi et al., 2009; Fig. 6d) and unconformably in the shallower, marginal areas (Manzi et al., 2009; Roveri et al., 2019b). Only Decima and Wezel (1973) and Raad et al. (2021) report the Miocene/Pliocene transition in the key, intermediate water-representative section of Eraclea Minoa as erosive. However, they do not provide evidence (e.g. photographic documentation) for the presence of an erosional unconformity and, moreover, Raad et al. (2021) erroneously refer to Cita and Colombo (1979), where no erosion is mentioned at the M/P boundary in Eraclea Minoa.

The bathymetric jump between the <100 m of water depth during the late Messinian and the >200 m at the base of the Trubi Fm. is often regarded as a key onshore evidence of the sudden and catastrophic Mediterranean-Atlantic re-connection at the Miocene/Pliocene boundary (e.g. Caruso et al., 2020). However, the real depth of the base of the Trubi is all but obvious. In fact, variable estimates have been proposed based on the observed benthic foraminifera and/or psychrospheric ostracods at Capo Rossello and Eraclea Minoa: 200-500 m (Decima and Wezel, 1973), 600-800 m (Sgarrella et al., 1997, 1999; Barra et al., 1998), 1400-2400 m (Cita and Colombo, 1979).

3.9 Greece

Several MSC localities are reported from the Greek Ionian Islands (Corfu, Cephalonia and Zakynthos) and from Crete (Fig. 2b).

On the NW coast of Corfu (Aghios Stefanos section), the PLG unit is missing and only a 32 m-thick cyclically-arranged terrigenous succession is present comprising three m-thick conglomerate beds alternating with fine-grained deposits rich in unspecified species of brackish water ostracods (Pierre et al., 2006).

In the southern part of Zakynthos, an evaporitic succession composed of eight gypsum cycles (Kalamaki section) occurs above marine marly deposits (Karakitsios et al., 2017b). These gypsum beds were initially ascribed to the UG unit (Pierre et al., 2006) and later to the PLG (Karakitsios et al., 2017b). The gypsum unit is overlain by approximately ~13 m of siltstones and marls with scattered, cm-thick beds of sandstones, conglomerates and carbonates with nodular texture (Pierre et al., 2006; Karakitsios et al., 2017b). Although no ostracods are reported from this interval, due to its stratigraphic position the post-evaporitic unit is correlated to the Lago-Mare phase (Karakitsios et al., 2017b). Except for the rare presence of marine nannofossils (*Ceratolithus acutus* together with *Reticulofenestra zancleana*) just below the Miocene/Pliocene boundary, only reworked marine fauna has been reported from the post-evaporitic package (Karakitsios et al., 2017b). This dominantly terrigenous succession is unconformably overlain by the Zanclean Trubi Formation (Fig. 6e; Karakitsios et al., 2017b).

MSC deposits on Crete (e.g. Meulenkamp et al., 1979; Delrieu et al., 1993; Cosentino et al., 2007; Roveri et al., 2008a; Zachariasse et al., 2008, 2011) were deposited in Miocene extensional, fault-bound basins driven by tectonic subsidence that ceased in the late Pliocene and Pleistocene (Van Hinsbergen and Meulenkamp, 2006). Because of the strong tectonic and eustatic sea-level-related fragmentation of the stratigraphic record, reconstructing the late Miocene stratigraphy of Crete has not been straightforward (Zachariasse et al., 2008, 2011). Several primary and clastic gypsum facies are recognized, but their

correlation with the MSC stratigraphy is disputed (see Cosentino et al., 2007; Roveri et al., 2008a, 2014a; Zachariasse et al., 2008). Coarse-grained, mammal-bearing terrigenous facies irregularly alternating with marls are in places found unconformably overlying the gypsum and separated from the Pliocene facies by an erosion surface (see Meulenkamp et al., 1979; Delrieu et al., 1993; Cosentino et al., 2007). In two localities on the Messarà Plain, Cosentino et al. (2007) described a highly diversified ostracod fauna with Paratethyan affinity in some marly intervals.

Messinian evaporites and/or Lago-Mare deposits are also reported from the North Aegean region onshore in the Strymon Basin (Snel et al., 2006; Suc et al., 2015; Karakitsios et al., 2017a) and Dardanelles region (Melinte-Dobrinescu et al., 2009) and offshore (Prinos-Nestos Basin; Karakitsios et al., 2017a), but recent integrated studies suggested that the sections studied by the above listed authors are older than the MSC (see Krijgsman et al., 2020a, 2020b). In particular, Krijgsman et al. (2020a) proposed that for most, if not all, of the MSC the North Aegean was a brackish water, mostly Paratethyan-fed basin restricted by the Cyclades sill to the south (Fig. 2a) and forming a passageway for Paratethyan overspill waters towards the Mediterranean.

3.10 Cyprus

MSC deposits on Cyprus outcrop in the Pissouri, Psematismenos, Mesaoria and Polemi basins on the southerly fringe of the Troodos massif (Fig. 2b; Rouchy et al., 2001; Manzi et al., 2016a). According to Rouchy et al. (2001) and Orszag-Sperber et al. (2009), sediments belonging to all MSC stages of Roveri et al. (2014a) are preserved in the Cypriot basins. By contrast, Robertson et al. (1995) and Manzi et al. (2016a) considered that PLG evaporites on Cyprus are only present as fragments reworked within a chaotic unit (the Lower Gypsum and Intermediate breccia units of Orszag-Sperber et al., 2009) and that the only *in situ* evaporites belong to the overlying Upper Gypsum Unit, which encompasses the whole of Stage 3 (Figs. 3a, 4a). A continuous, Eraclea Minoa-like section is not known in Cyprus (Manzi et al., 2016a). The best exposure of the lower 60 m of this unit is found in the Polemi Basin (Manzi et al., 2016a). It comprises up to six gypsum beds (the lower three of which are mainly selenitic, while the upper three are predominantly laminated; Fig. 3a). Gypsum beds range in thickness from 1 to 6

m and are separated by laminated marls (Fig. 5j) occasionally interbedded with conglomerates and sandstones (e.g. between the 5th and 6th gypsum layers; Rouchy, 1982; Rouchy et al., 2001; Manzi et al., 2016a). The sixth gypsum bed is reported by Rouchy et al. (2001) to be hollowed in the upper part with the cavities filled with overlying sediments. The similarity of the cyclicity and facies association of this Cyprus succession with the substage 3.1 interval of the Sicilian UG led Manzi et al. (2016a) to propose a bed-to-bed correlation and to recognize the substage 3.1/3.2 boundary at the top of the last gypsum bed (Fig. 3a). According to Orszag-Sperber et al. (2000) and Rouchy et al. (2001), this chronostratigraphic boundary coincides with a Mediterranean-scale sea-level drop, a conclusion that arises from the interpretation of the cavities in the uppermost gypsum as the product of karstic dissolution following a prolonged period of subaerial exposure.

The sedimentary sequence overlying the last gypsum bed and assigned by Manzi et al. (2016a) to the Lago-Mare phase lacks a clear and rhythmic sedimentary cyclicity. In the Pissouri Basin this interval (up to 25–30 m-thick) mostly consists of conglomerates, sandstones, limestones, paleosols (which appear as dm to m-thick dark marly horizons, in one case with pulmonated gastropods) and subordinated clay-marly horizons (Rouchy et al., 2001). By contrast, in the Polemi sections the clay-marly facies dominates this interval (Rouchy et al., 2001). *In situ* fresh-brackish water species of articulated mollusks (*Limnocardiidae*, *Melanopsis*), Paratethyan (*Loxocorniculina djafarovi*, *Euxynocythere praeabaquana*) and Mediterranean (*Cyprideis agrigentina*) ostracods and foraminifera (*Ammonia beccarii*), *Characeae*, abundant fragments of the marine euryhaline fish *Clupeidae* and a fish skeleton of

the euryhaline *Aphanius crassicaudus* are described from some of the substage 3.1 and 3.2 fine-grained facies and within the terrigenous laminae of some *balatino* gypsum (Orszag-Sperber et al., 2000; Rouchy et al., 2001; Orszag-Sperber, 2006; Manzi et al., 2016a). The upward change in diversity of the ostracod fauna seen elsewhere (e.g. Malaga, Nijar, Vera, Apennines and Eraclea Minoa) is not reported in Cyprus but this may be because no detailed study of ostracod assemblages in Stage 3 sediments has been published. The Miocene/Pliocene boundary, near Polemi village is described by Manzi et al. (2016a) as a sharp contact above a dark, organic-rich layer (Fig. 6f). It appears to be similar to the boundary reported from Piedmont (Fig. 6c; Trenkwalder et al., 2008; Dela Pierre et al., 2016) and Northern Apennines (Gennari et al., 2008; Grossi et al., 2008), if not for the presence, in Cyprus, of (possibly) *in situ* *Cyprideis agrigentina* (Manzi et al., 2016a). A layer with the same field appearance, thickness (~1 m) and stratigraphic position is reported in Pissouri by Rouchy et al. (2001), which they interpreted as a paleosol based on mottling, oxidized roots, carbonate concretions and plant fragments.

3.11 Southern Turkey

The tectonically active, during the Miocene, thrust-top basin of Adana in southern Turkey (Radeff et al., 2017) retains the most complete and better exposed easternmost successions of the MSC (Fig. 2b), whose deposits were attributed to the Handere Fm. (Cosentino et al., 2010; Radeff et al., 2016).

MSC Stage 3 finds expression in a >1 km thick continental unit unconformable, through an erosional surface, above the pre-evaporitic, Stage 1 anhydrite-shale alternations (Radeff et al., 2016) and resedimented gypsum-bearing Stage 2 deposits (Cosentino et al., 2010; Cipollari et al., 2013). This unit mainly consists of fluvial coarse- and fine-grained deposits representing channel fill and overbank deposits. Sporadically, some fine-grained intercalations are found containing a mixed brackish (ostracod) and marine (foraminifera and calcareous nannofossils) fauna. The ostracod fauna has affinity with the Paratethyan fauna but, unlike to many other Mediterranean onshore localities, is poorly diversified, with monospecific assemblages of *Cyprideis agrigentina* (Avadan section and T-191 borehole; Cipollari et al., 2013) or with *Cyprideis agrigentina* accompanied by rare to abundant specimens of *Loxoconcha muelleri*, *Euxinocythere (Maeotocythere) praeabaquana*, and *Loxoconcha* sp. (Adana section; Faranda et al., 2013). Ostracods are often associated with *Ammonia beccarii* and rare *Elphidium* and *Cribrorhynchium*, which are the only foraminifera considered as autochthonous. Conversely, the entire nannoflora is interpreted as physically reworked (Cipollari et al., 2013; Faranda et al., 2013).

The Handere Fm. is followed by early Zanclean marine sediments (Avadan Fm.) deposited, according to the paleoecology of the benthic foraminifera species recognized, at bathymetries ranging from 200 to 500 m (Cipollari et al., 2013). The lithological nature of the Miocene/Pliocene boundary in the Adana Basin is not clear, but it occurs either above the continental or subaqueous, ostracod-bearing facies.

A similar stratigraphic sequence is present in the subsurface. Here, however, chaotic gypsum-bearing deposits are not found and two halite bodies ~20 and ~170 m-thick are present, separated and followed by fluvial gravels, sands and silts (Cipollari et al., 2013).

3.12 Summary of the onshore Stage 3 record

Most of the onshore Stage 3 records formed in shallow marginal Mediterranean basins, which underwent substantial uplift from the Messinian till nowadays and are assumed to have had their depocenter at ~200 to 50 m below the Atlantic level during the late Messinian (Roveri et al., 2014a, 2019a; Radeff et al., 2016, 2017). The Caltanissetta Basin (Sicily), some basins along the Apennines and (possibly) Cyprus represent, instead, possible onshore representative of intermediate basins. The nature and duration of these records is quite variable,

and there are only six sections that may record an entire Stage 3 sequence (i.e. Sorbas, Nijar, Northern Apennines, Eraclea Minoa and Cyprus; Fig. 3a). Reasons for the fragmentary nature of the Stage 3 sedimentary record include different durations of subaerial exposure following the Stage 2 drawdown, local tectonics and associated syn-depositional erosion and deposition. One of the consequences of this is that any sedimentary cyclicity that resulted from orbital fluctuations is typically either less well developed or poorly preserved, making the chronology of Stage 3 rather uncertain or controversial in places.

Despite this variability, several fairly consistent characteristics are widely expressed. These are:

- 1) Stage 3 sedimentation follows a period of intensive tectonic and/or eustatic-driven erosion of the margins, as demonstrated by the frequent presence of erosional unconformities and/or chaotic Stage 2 deposits (RLG unit);
- 2) Stage 3 lithologies are mostly terrigenous (conglomerates, sandstones and mudstones) and deposited in a variety of continental (fan delta, fluvial channels and alluvial plains) and shallow water environments (endorheic lakes or water bodies connected with the Mediterranean water mass is the riddle). Carbonate intercalations are sometimes present (e.g. Sorbas Basin and *Colombacci* limestones in the Apennines). Stage 3 gypsum is only found in deeper-water intermediate basins of Caltanissetta in Sicily and Cyprus.
- 3) A diversified fossil assemblage with Paratethyan affiliation (ostracods, dinocysts, mollusks) is commonly found in the shallow-water sediments of Lago-Mare successions. Only in the intermediate Caltanissetta Basin (Sicily) do these diversified Paratethyan forms (only ostracods) occur earlier, in the sediments from substage 3.1. Where these have been studied in detail, these assemblages typically show an increase in diversity with time (possibly every wet phase of the precession cycles). Some of these sediments also contain marine fossils and there is controversy over whether these are *in situ* and contemporaneous or reworked.
- 4) In outcrop, the Miocene/Pliocene boundary has four main sedimentary expressions: erosive and followed by a conglomeratic lag (e.g. Malaga, Vera, Mallorca; Fig. 6a); conformable above continental facies (e.g. Nijar Basin; Fig. 6b); conformable above ostracod-rich mudstones (e.g. Eraclea Minoa; Fig. 6d); sharp contact above a black layer of still largely unknown paleoenvironmental significance (Piedmont, Apennines and Cyprus; Fig. 6c, f).

For a better understanding of how Stage 3 developed across the Mediterranean these marginal records now need to be considered alongside the evidence from intermediate to deep offshore settings.

We note that alternative chronostratigraphic frameworks have been proposed for several onshore (Malaga, Sorbas, Mallorca, Apennines, Sicily) and offshore (Sites 134B, 976B, 978A) locations (see Fig. 4b for references), but we have omitted them as they are shown to rely on incorrect (bio)stratigraphic arguments (see Roveri et al., 2008c, Grothe et al., 2018 and subsection 5.5).

4. Offshore domain

The offshore Mediterranean is a complex array of variable-depth and morphologically complex subbasins framed by morphological highs or sills. Traditionally it is divided into two main domains (Fig. 2a), the Western and Eastern Mediterranean, with the intervening divide (or Sicily sill) situated in the Sicily channel at present with a maximum depth of 316 m. The Alborán Basin, the depressions on the Balearic Promontory, the Corsica, Valencia, Algero-Balearic, Liguro (or Sardo)-Provençal and Tyrrhenian basins belong to the "Western Mediterranean" (Fig. 2a). The Adriatic foredeep, the Ionian, Sirte, Aegean and Levant basins belong in the "Eastern Mediterranean" (Fig. 2a). Smaller-sized depressions, again surrounded by sills of variable depth, are identified and labelled within each of these subbasins.

Although the exact topography and hypsometry of the Messinian Mediterranean is difficult to reconstruct, this present-day geography is generally assumed to have been in place, with five main differences: (1) the Alborán Basin was split into a Western (WAB) and Eastern Alborán (EAB) by a volcanic arc (Booth-Rea et al., 2018); (2) the Tyrrhenian Basin was only partly opened (Lymer et al., 2018); (3) the precise depth and width of the ancient Sicily Sill are difficult to estimate, but may have been much deeper than today (~300 m; Meijer and Krijgsman, 2005; Jolivet et al., 2006). Paleodepth estimations for the Messinian configuration range from 380 m (Just et al., 2011) to 430 m (García-Castellanos et al., 2009); (4) one or two sills were present at the southern termination of the Adriatic foredeep (Pellen et al., 2017; Amadori et al., 2018; Manzi et al., 2020); (5) the North Aegean was partially isolated from the Mediterranean by the Cyclades Sill and with high Paratethys affinity (Krijgsman et al., 2020a). Following the schematic classification of the Messinian sub-basins by Roveri et al. (2014a), all these subbasins are regarded as either intermediate (i.e. relatively deep-water,

200–1000 m) or deep (water depth > 1000 m).

Compared with the onshore domain, the offshore basins hold a far greater percentage of the total volume of MSC sediments (Ryan, 1973; Haq et al., 2020). The architecture, geometry and main lithologies of the MSC and younger deposits are well known thanks to the high density of seismic data and the fact that evaporites (halite particularly) are easily identified on seismic profiles due to their unusual seismic properties, especially compared to those of terrigenous and carbonate sediments (see Lofi et al., 2011a, 2011b; Lofi, 2018; Haq et al., 2020). However, the detailed lithological, sedimentological, paleontological and geochemical nature and their chronostratigraphy are still poorly constrained offshore because these cannot be univocally defined on the basis of seismic data alone (Roveri et al., 2019b) and direct information about these deep MSC successions is limited to a small number of cores (16) drilled during the DSDP (Ryan et al., 1973; Hsü et al., 1978b) and ODP (Kastens et al., 1987; Comas et al., 1996; Emeis et al., 1996) drilling campaigns that penetrated exclusively the uppermost tens of meters of the deep MSC suite in very scattered localities (Fig. 2b). Only recently, access to industrial boreholes crossing the base of the halite in the deep Levant Basin has been granted, providing a rare glimpse of the deep MSC deposits in the easternmost part of the Mediterranean (Gvirtzman et al., 2017; Manzi et al., 2018; Meilijson et al., 2018, 2019).

The MSC is commonly described as tripartite ('Messinian trilogy' after Montadert et al., 1978) in the Western Mediterranean (Lower-Mobile-Upper units: LU-MU-UU, respectively). However, in the Ionian Basin is described as bipartite (MU-UU) by Camerlenghi et al. (2019) while according to Lofi et al. (2011a), Gvirtzman et al. (2013, 2017), Lofi (2018) and Camerlenghi et al. (2019), the Levant Basin consists of the MU and the UU is only present locally and possibly represented by evaporite-free terrigenous accumulations (Kartveit et al., 2019; Madof et al., 2019). The lack of many age constraints within the offshore MSC successions hampers unambiguous correlation with onshore sequences (Fig. 1a; Roveri et al., 2014a). Nevertheless, different authors have proposed onshore-offshore correlation of specific events (e.g. onset, Ochoa et al., 2015; and termination of the MSC, Biscaye et al., 1972,

Iaccarino et al., 1999) and stratigraphic schemes (Decima and Wezel, 1971; Raad et al., 2021) based on and biostratigraphic evidence (Cosentino et al., 2006), $^{87}\text{Sr}/^{86}\text{Sr}$ isotope ratios (Roveri et al., 2014b; Gvirtzman et al., 2017; Manzi et al., 2018) and astronomical tuning of the deep seismic record (Ochoa et al., 2015, 2018; Manzi et al., 2018; Meilijson et al., 2018, 2019). Here we focus on the seismic and

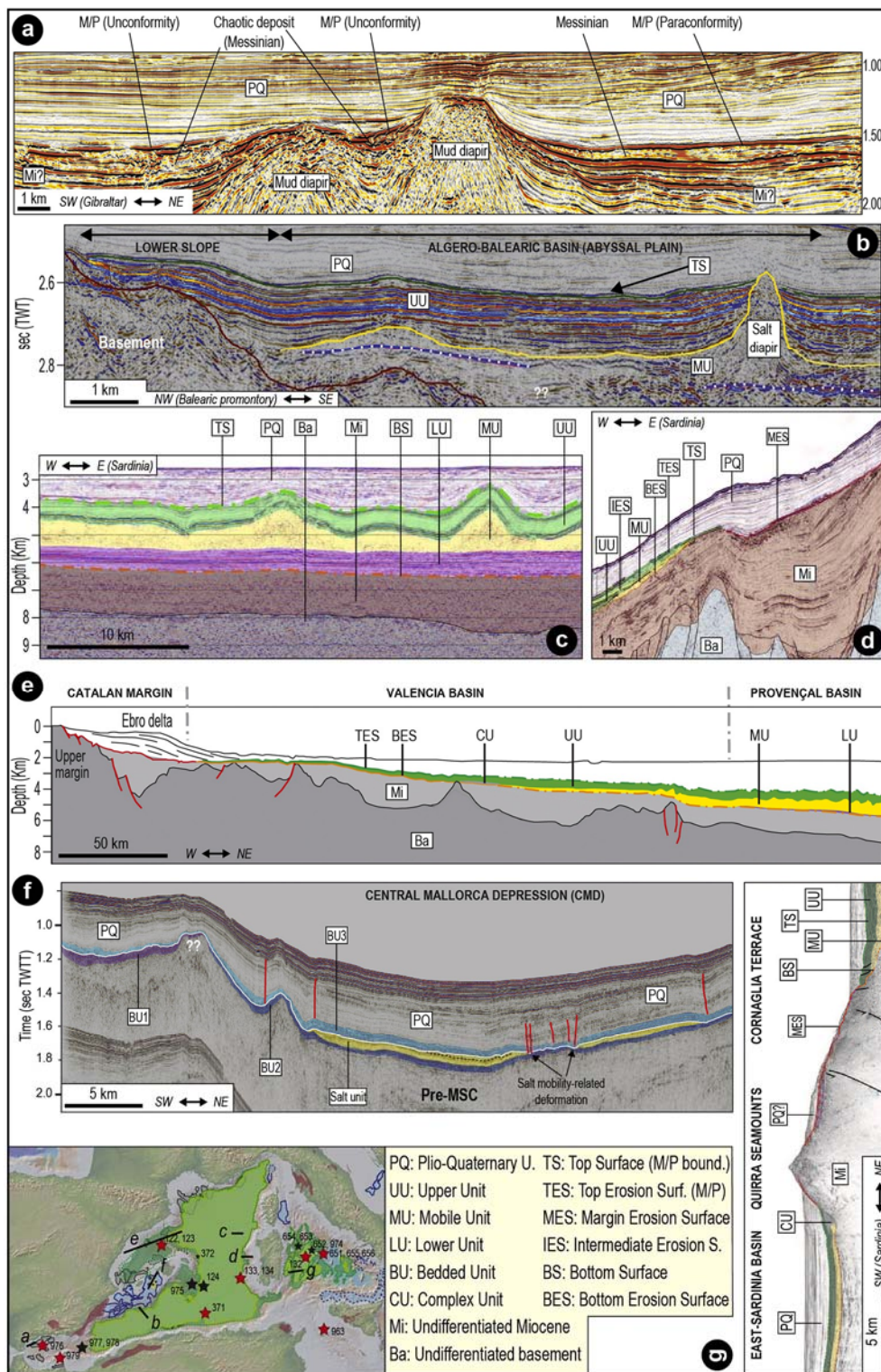


Fig. 7. Seismic profiles from intermediate-deep Western Mediterranean basins containing MSC markers/units. (a) Seismic reflection line CAB01-104 from the WAB (modified from Booth-Rea et al., 2018). The line shows the variable geometry of the inferred M/P boundary, erosive in proximity of mud diapirs, (para)conformable in tectonically undisturbed sectors. Chaotic reflectors are occasionally imaged below the inferred M/P boundary. (b) Seismic profile SF12-09 imaging the lower slope of the south Algero-Balearic margin and part of the Algero-Balearic abyssal plain (modified from Mocnik et al., 2014). Here a high reflecting and horizontally stratified UU covers a thin layer of MU evidenced by salt diapirism. Note the concordant deformation of the UU and MU. (c) Line MS-39 from the abyssal plain of the Liguro-Provençal Basin showing the Messinian trilogy and non-erosive bottom and top surfaces (BS and TS; Dal Cin et al., 2016). Halokinesis of MU gives rise to domes that deform the UU and PQ units. (d) Interpreted seismic profile from the lower-middle slope of the west Sardinian margin (modified from Dal Cin et al., 2016). Thin MU and UU are present on the lower slope, while on the middle slope (and upper slope here not shown) they converge in the margin erosion surface MES. (e) Line drawing of seismic line imaging from the Catalan margin (or Ebro Basin) to the abyss of the Liguro-Provençal basin (modified from Maillard et al., 2011b). Note the pinch out of the MU in the Valencia Basin and of the UU in the Ebro Basin, which is MSC free. (f) Interpreted seismic profile Simbad 15 crossing the depocenter of the CMD showing all the MSC units and erosional surfaces (modified from Raad et al., 2021). (g) Interpreted seismic profile MYS40 illustrating the MU-UU-PQ units in the East-Sardinia Basin and Cornaglia Terrace, separated by the MSC deposits-free Quirra Seamounts (modified from Lymer et al., 2018).

geological (core-derived)¹ properties of the Upper Unit (and laterally grading/interfingering sediments when present), stratigraphically below the Plio-Quaternary deposits (PQ) suggesting that it belongs to (at least part of) Stage 3.

4.1 Western Alborán Basin and westernmost East Alborán Basin

The Alborán Basin has received particular attention because of its proximity to the Gibraltar Corridor (Estrada et al., 2011; Popescu et al., 2015 and references therein). Evaporites only occur on the eastern side of the EAB (which is treated in subsection 4.2; Fig. 2a). To the west of the volcanic archipelago (Booth-Rea et al., 2018, i.e. the WAB) and immediately to the east on the western side of the EAB only terrigenous sediments occur in the MSC interval (Booth-Rea et al., 2018; de la Peña et al., 2020). Sediments at the Miocene/Pliocene boundary appear in the seismic reflection data as parallel reflectors with increasing reflectivity (Comas et al., 1996, 1999; Booth-Rea et al., 2018). Locally, just below the M discontinuity, some of the reflectors suggest a chaotic seismic facies (Fig. 7a; Booth-Rea et al., 2018; Bulian et al., 2021). Miocene sediments with a maximum thickness of 100 m have been recovered from two out of nine holes drilled in the region (ODP 976B, 978A; Comas et al., 1996, 1999). These sediments mostly consist of claystones, siltstones and sandstones with *Chondrites* and *Zoophycos* ichnofacies at site 976B and include a conglomerate close to the Miocene/Pliocene boundary at Site 978A. The lack of age-diagnostic fossils hampers their correlation with the Geologic Time Scale (GTS). However, the presence, high in the Miocene section, of an oligotypic association of ostracods (*Candona* sp., *Loxococoncha muelleri*, and *Cyprideis* sp.) with different stages of growth (Site 978A; Iaccarino and Bossio, 1999) and Paratethyan dinocysts (including *Galeacysta etrusca*; see subsection 5.2; Popescu et al., 2015) indicates a latest Messinian (substage 3.2) age and brackish paleodepositional conditions. Foraminifera and nanofossils are also present, but all species recognized are of no help in narrowing down the paleoenvironmental interpretation because they are considered either definitely or likely to be reworked (Iaccarino and Bossio, 1999). By contrast, Popescu et al. (2015) interpreted some species of calcareous nanofossils (*Reticulofenestra pseudumbilicus*, *Discoaster quinqueramus*, *Ceratolithus acutus*, *Triquetrorhabdulus rugosus*, *Amaurolithus primus*) and marine dinocysts as autochthonous.

The nature of the Miocene/Pliocene boundary is also uncertain. According to some authors, the “M” discontinuity is a high-amplitude reflector with evidence of erosion attributed to subaerial processes (Estrada et al., 2011; Urgeles et al., 2011) and locally (e.g. close to Site 121; Ryan et al., 1973) associated with an angular unconformity that abruptly truncates the upper Miocene deposits and morphological highs (Comas et al., 1999; Estrada et al., 2011; Garcia-Castellanos et al., 2020). Although the M-reflector was drilled at Sites 976B, 977A and 978A, a lithological contact was only recovered at Site 976B coinciding with a major erosional surface between the early Messinian and the base of the Pliocene (Bulian et al., 2021). Only at Site 978A (and possibly 977A) was a few meters of what may be the contact interval recovered (Comas et al., 1996). This comprises a 25 m-thick cemented succession containing pebbles of volcanic and sedimentary rocks likely to derive from the Alborán substrate (46R, 620.9-630.67 mbsf, between the Pliocene-bearing core 45R and the Messinian-bearing core 47R; Comas et al., 1996). In contrast, Booth-Rea et al. (2018) concluded that the M-reflector is an unconformity only close to the mud diapirs and owes its erosive shape and angular discordance to the activity of these structures

¹ Lithostratigraphic and biostratigraphic information from DSDP and ODP cores are primarily extracted from the Scientific Shipboard Party documents, accessible from <https://www.marum.de/en/Research/Cores-at-BCR.html>. These documents are referenced in the text as follows: Ryan et al. (1973): DSDP 120-134; Hsü et al. (1978b): DSDP 371-378; Kastens et al. (1987): ODP 650-656; Comas et al. (1996): ODP 974-979; Emeis et al. (1996): ODP 963-973.

(Fig. 7a). In more undisturbed sectors these authors argue that the boundary is a paraconformity with no evidence of erosion (Fig. 7a). The lack of Messinian erosion in the shallow regions of the WAB margins has prompted the hypothesis that this area did not desiccate during the MSC (Booth-Rea et al., 2018; de la Peña et al., 2020). This contradicts much of the interpretation made of the DSDP and ODP cores of this interval in the Alborán Sea. The succession recovered by drilling from beneath the Pliocene comprises gravels that contain a mixed Miocene fauna. These sediments and their faunal content are thought to have been reworked from older sediments exposed as Alborán substrate with no evidence of an extensive wet Lago Mare interval immediately before the Zanclean (Comas et al., 1996).

Two W-E-aligned erosional channels straddling the Strait of Gibraltar and stretching for 390 km from the easternmost Gulf of Cádiz (Atlantic Ocean) into the Alborán Basin are clearly observed in seismic profiles (Garcia-Castellanos et al., 2009; Estrada et al., 2011). There is disagreement, however, concerning the timing and nature of their formation. These incisions are classically considered to occur at the very top of the MSC suite (when present) and to be the consequence of the Zanclean megaflood (Garcia-Castellanos et al., 2009, 2020; Estrada et al., 2011 among others). More recently, Krijgsman et al. (2018) highlighted that an accurate age determination for these channel incisions is lacking and that they might have been formed earlier during the MSC as a result of the Mediterranean-Atlantic gateway currents. Interpretation of E-W seismic profiles across the Alborán Basin combined with mammal records in Africa and Iberia led Booth-Rea et al. (2018) to suggest the existence of an emergent volcanic archipelago that temporarily connected southeastern Iberia with northern Africa, separating an open marine, Atlantic-influenced West Alborán Basin realm from a restricted, hydrologically complex Mediterranean realm to the east.

4.2 Eastern Alborán, Algero-Balearic and Liguro-Provençal basins

From the eastern margin of the EAB as far east as the Tyrrhenian coast of Italy, the Messinian (evaporites-bearing) trilogy LU-MU-UU is found and sealed by the PQ. The MU and UU are interpreted to fill the deepest depocenters (Algero-Balearic, Valencia and Liguro-Provençal basins; with minor interruptions due to seamounts) and the lower slope domain, where they comprise ~500 to ~800 m of UU and ~1000 m of MU/halite (Figs. 7b-d; Camerlenghi et al., 2009; Lofi et al., 2011a, 2011b; Geletti et al., 2014; Mocnik et al., 2014; Dal Cin et al., 2016; Lofi et al., 2018). Upslope, a thinner, possibly incomplete UU is locally described on the middle-upper continental slopes of Western Corsica (Guennoc et al., 2011) and Sardinia (Mocnik et al., 2014; Dal Cin et al., 2016) and the northern (Maillard et al., 2006) and southern (Maillard and Mauffret, 2013; Mocnik et al., 2014; Dal Cin et al., 2016) flanks of the Balearic Promontory, even though the structural settings of these locations are mostly dominated by erosion (Fig. 7d). MSC evaporites are absent on the continental shelves bordering the deep Algero-Balearic and Liguro-Provençal basins, where the PQ directly overlies the MES which, in turn, cuts through the middle Miocene deposits (Gorini et al., 2005; Lofi et al., 2005). The only late Messinian sediments are present as Complex Units (Gulf of Lion, Bessis, 1986; Gorini et al., 2005; Lofi et al., 2005; Algerian Basin, Medaouri et al., 2014; Arab et al., 2016; Fig. 7e). CUs can have

various origin (Lofi et al., 2011a, 2011b), but when identified as the outlet of drainage systems, they are commonly interpreted as Messinian clastics supplied by rivers (Lofi et al., 2005). In the Gulf of Lion, the MES is a high angle unconformity with substantial erosion along highly rugged relief thought to have been generated by fluvial incision (Lofiet et al., 2005). In contrast, Roveri et al. (2014c) suggested that the drainage networks visible on the seismic could be of subaqueous origin. When not involved in MU-related deformation processes, the UU appears as a highly reflective series of flat reflectors alternating with less reflective, but concordant, reflectors (Figs. 7b-c; Lofi et al., 2011a, 2011b) aggrading in the basin center and onlapping the margins

4.3 Valencia Basin

(Fig. 7b; Camerlenghi et al., 2009; Lofi et al., 2011a, 2011b; Gelettiet al., 2014; Mocnik et al., 2014; Dal Cin et al., 2016). The aggrading nature, shelf-ward thinning and the onlap terminations of the UU are interpreted as evidence of sedimentation in a lake with fluctuating base level (e.g. Lofi et al., 2005; Lofi et al., 2011a). In the abyssal plains (Figs. 2a, 7c), nine to ten cycles have been interpreted on high resolution seismic profiles as corresponding to gypsum-marl alternations (Geletti et al., 2014; Mocnik et al., 2014). At Sites 124 and 372, ~40-50 m of the UU have been drilled at the feet of the east Menorca continental rise and the northern Menorca slope, where 3-4 gypsum-marl cycles are recognized (Fig. 2b; Ryan et al., 1973; Hsü et al., 1978a). Primary gypsum facies are widely overprinted by post-depositional diagenetic processes, but the still recognizable laminated and clastic primary textures indicate precipitation at the water-air interface and emplacement by gravity flows, respectively (Lugli et al., 2015). The marl interbeds are made from stiff to firm dolomitic mud containing substantial quantities of detrital material intercalated with current-bedded sandstones and, at Site 124, with diatoms (Ryan et al., 1973). *Cyprideis* sp. specimens are reported from some mudstone interbeds at Site 372, while dwarf planktonic foraminifera are present just below the Miocene/Pliocene boundary at Site 124 (Ryan et al., 1973).

The Miocene/Pliocene boundary coincides with the top of the UU where present (labelled TES when erosional and TS when conformable; Lofi et al., 2011a, 2011b). In the abyssal plain-lower slope domain it appears to be undulating, although this geometry is related to the deformation of the underlying salt (Figs. 7b-c), and it actually corresponds to a sharp surface lacking signs of erosion (Lofi et al., 2011a, 2011b; Geletti et al., 2014; Mocnik et al., 2014). By contrast, the UU-PQ boundary commonly appears strongly erosional in the middle-upper slope and shelf domain, where it coincides with the MES (Fig. 7d; Lofi et al., 2005; Maillard et al., 2006; Geletti et al., 2014; Mocnik et al., 2014). Among the six DSDP-ODP Sites drilled in this region (Fig. 2b), only Hole 975B recovered the Miocene/Pliocene boundary (Iaccarino and Bossio, 1999; Marsaglia and Tribble, 1999). Here the Messinian is a few centimeters thick and consists of banded micritic silty clays with minor calcareous siltstones to sandstones typified by a diverse faunal assemblage consisting of dwarf planktonic foraminifera, *Ammonia tepida* tests and brackish Paratethyan ostracods (*Loxocorniculina djafarovi*, *Euxinocythere praeabaquana*, *Ammicythere idonea*, *Leptocythere limbata*, *Candona* sp., and *Cyprideis* sp.; Iaccarino and Bossio, 1999).

Halite is present at the bottom of Hole 134 drilled within the UU (Ryan et al., 1973; Sage et al., 2005; Lugli et al., 2015). High-resolution seismic profiles from both the Algero-Balearic and Ligurian-Provençal basins confirm the presence of a halite layer high in the UU sequence (Geletti et al., 2014; Mocnik et al., 2014). This layer is up to 50 m thick (Dal Cin et al., 2016) and is correlated with an erosional surface (called IES: Intermediate Erosional Surface by Lofi et al., 2011a, 2011b) associated with an angular unconformity which is better developed on the lower slope (Fig. 7d). Geletti et al. (2014) and Mocnik et al. (2014) interpreted this layer as autochthonous and indicative of at least one important sea level drop during UU deposition. However, this intra UU halite layer is always described from areas strongly affected by salt diapirism (just like in the Ionian Abyssal Plain; see subsection 4.6.1) and is never found in adjacent, undisturbed areas (see Camerlenghi et al., 2009; Geletti et al., 2014; Mocnik et al., 2014; Dal Cin et al., 2016), two features that may suggest it has an allochthonous origin. Site 134 shows evidence of a “desiccation crack” cutting through a sandy silt layer interbedded with unaffected laminated halite (Hsü et al., 1973c). Unfortunately, the core photograph of this crack has been published in two different orientations (Hsü et al., 1973a, 1973b), leading both Hardie and Lowenstein (2004) and Lugli et al. (2015) to question the evidence for subaerial desiccation. Because of these ambiguities, we suggest to dismiss this example from the book of evidence.

The Valencia Basin (VB; Fig. 2a) is an aborted rift formed during the late Oligocene-early Miocene opening of the back-arc Liguro-Provençal Basin (e.g. Jolivet et al., 2006). It is located between the Spanish Ebro Margin to the west and the Balearic Promontory to the east, while it grades into the Liguro-Provençal Basin to the E/NE (Fig. 7e; Maillard and Mauffret, 2006; Maillard et al., 2006).

Numerous exploratory boreholes exist on the western Ebro margin. These boreholes, tied to seismic data, confirm that MSC-related sedimentations on the northwestern shelf are missing (Fig. 7e; Urgeles et al., 2011; Pellen et al., 2019). The only MSC feature present is a prominent erosional surface (the MES) incising Serravallian-early Messinian sedimentations (Urgeles et al., 2011). By contrast, on the southwestern and southern part of the margin, well data show the presence of evaporitic sediments (e.g. Delta L and Golfo de Valencia D1 boreholes; Del Olmo, 2011; Del Olmo and Martín, 2016; Lozano, 2016). Del Olmo and Martín (2016) described these evaporites as primary selenites and ascribed them to MSC Stage 1 (their unit M7). Lozano (2016) described the same evaporitic deposits in the same boreholes as ‘white anhydrites’, leaving open the question as to whether the anhydrite is primary (sabhka’s) or secondary at the expense of a primary gypsum facies. On the eastern margin of the VB boreholes and seismic studies suggest there are no MSC units with only a prominent MES cutting pre-MSC sedimentations (Driussiet al., 2015; Raad et al., 2021). All authors conclude that the shelves of VB were exposed to subaerial erosion during and following the main drawdown. MSC deposits are also absent along the slopes and, where present,

consist of coarse- and fine-grained terrigenous facies filling valleys largely related to fluvial incision (Fig. 7e; Stampfli and Höcker, 1989). A

different situation features in the depocenter. Despite its present-day depth of > 2000 m, no MU is observed in the depocenter, as the salt pinches-out at the edge of the deeper Provençal Basin (Fig. 7e). Only the seismic properties of UU suggest that it is roughly continuous from the Provençal Basin into the VB (Fig. 7e; see subsection 4.2), although it thins from ~1000 m to < 500 m. The UU is characterized by aggrading and onlapping geometries towards the slopes, where it also thins out until it disappears along the middle-upper slope (Fig. 7e; Maillard et al., 2006; Cameselle and Urgeles, 2017). Maillard et al. (2006), Urgeles et al. (2011), Cameselle et al. (2014) and Cameselle and Urgeles (2017) all stated that the UU formed during an important Mediterranean-level lowstand (~1000 m). Several Complex Units (CU), with different origin, have been observed and described as belonging to the MSC (Cameselle and Urgeles, 2017).

DSDP Site 122, drilled at the mouth of a valley incision, recovered a few meters of sand-gravels made of well-rounded basalt, marine limestone nodules of crystalline gypsum and mollusk fragments in a clay-silty matrix rich in deep-water benthonic foraminifera and early Pliocene nannofossils, all interpreted as erosional products of the VB seabed (Ryan et al., 1973). The uppermost Messinian in two industrial wells (Ibiza Marino and Cabriel boreholes; see Lozano, 2016) is represented by intercalations of clastic gypsum/anhydrite and marls (unit M8-P1 of Del Olmo and Martín, 2016). These are interpreted as turbidites sourced from the shelf and/or slope during a lowstand phase of the Mediterranean base level (Del Olmo, 2011; Del Olmo and Martín, 2016; Cameselle and Urgeles, 2017).

In seismic profiles, the UU/PQ transition (M-reflector or TES) is locally both sharp and smooth (in more distal settings) and erosional (in more proximal settings; Fig. 7e). Maillard and Mauffret (2006) indicate that the smooth parts have been caused by increasing fresh water influx during the Lago-Mare phase, leading to dissolution of the evaporites, and the rough erosional segments are of subaerial origin. For Cameselle and Urgeles (2017), the top of the UU is a smooth and conformable downlap surface, representing the rapid inundation of the basin with only local minor erosional features.

4.4 Balearic Promontory

Sticking out from the surrounding deep-water locations, the Balearic Promontory (BP; Fig. 2a) is a continental high that has undergone tectonic extension since the late Serravallian (Roca and Guimera, 1992; Sabat et al., 2011). During the Messinian, it comprised in topographic lows/subbasins at different water depths and separated by structural highs/sills (Maillard et al., 2014; Driussi et al., 2015; Roveri et al., 2019b; Raad et al., 2021). The area has been the subject of multiple studies (Maillard et al., 2014; Driussi et al., 2015; Ochoa et al., 2015; Roveri et al., 2019b; Raad et al., 2021) and several controversies arose after the publication of Roveri et al. (2019b).

The first controversy concerns the Messinian paleodepth of the BP's subbasins. According to Roveri et al. (2019b) the subbasins were shallow during the Messinian and acquired today's paleodepths following a strong post-MSD subsidence; Maillard and Mauffret (2011), Maillard et al. (2014) and Raad et al. (2021), instead, consider the tectonic movements in the BP to have been minor since the late Miocene (Messinian) and the region to have been already structured as it is today during the MSC. Well-to-seismic ties in the shallower basins closer to the Spanish coast (i.e. Bajo Segura, San Pedro and Elche basins) comprise up to 14 Stage 1 primary gypsum-marl cycles similar to the onshore PLG unit (Lugli et al., 2010) truncated at the top by the MES (Soria et al., 2008a, 2008b; Ochoa et al., 2015). At first, Ochoa et al. (2015) concluded that all sediments overlying the MES are Pliocene in age. A later re-appraisal of the same downhole logging data and cuttings led Ochoa et al. (2018) to attribute the first ~13 m-thick micritic and evaporite-free sediments to the late Messinian (stage 2 or 3 of the MSC according to the authors). The MSC stratigraphy of the shallowest offshore basins of the BP closely resembles that described from cores and outcrops onshore Mallorca (see subsection 3.4; Roveri et al., 2019b).

High resolution seismic reflection data in the Central Mallorca Depression (CMD) highlighted up to 500 m of MSC deposits made of a Bedded Unit (BU) and a thin salt layer (Maillard et al., 2014; Driussi et al., 2015). This BU has never been drilled and, therefore, lacks lithological and chronostratigraphic constraints. Two contrasting chronostratigraphic and lithological interpretations are proposed: Roveri et al. (2019b) ascribed these sediments to Stage 2 and 3 and suggested that only reworked evaporites and halite are present. By contrast, following the seismostratigraphic description of Maillard et al. (2014), Ochoa et al. (2015) and Raad et al. (2021) inferred the presence of Stage 1 gypsum also in the CMD.

Raad et al. (2021) made a step forward by disclosing a possible tri-partition of the BU unit (Fig. 7f). In their seismostratigraphic framework, Raad et al. (2021) noticed that the uppermost evaporite-bearing unit (called BU3), ~120 m-thick in the CMD, has geometric, stratigraphic and facies analogies with the astronomically-tuned UG unit of the Caltanissetta Basin (Fig. 3a) that endorse its attribution to Stage 3. Similar to the UU in the deepest basins (see subsection 4.2), BU3 consists of up to 9 low- and medium-amplitude reflectors that are interpreted as alternating terrigenous and gypsum beds (Maillard et al., 2014; Raad et al., 2021). Reflectors are parallel and continuous in the more distal areas, while they appear more chaotic in the more proximal sectors (Raad et al., 2021). The base of BU3 coincides with the erosional top of the salt, interpreted as created by salt exposure, dissolution and locally salt gliding towards the depocenter (Fig. 7f; Raad et al., 2021). By contrast, the top of BU3, which corresponds to the Miocene/Pliocene boundary, is largely flat without signs of erosion (Fig. 7f; Maillard et al., 2014; Raad et al., 2021). An irregular geometry is sometimes visible, but is likely to be related to deformation of the underlying salt (Fig. 7f; Raad et al., 2021).

4.5 Tyrrhenian Basin

The Tyrrhenian Basin to the east of Sardinia is a back-arc basin that opened by continental rifting and oceanic spreading related to the

eastward migration of the Apennine subduction system from middle Miocene to Pliocene times (Gaullier et al., 2014; Lymer et al., 2018; Loreto et al., 2020 and references therein). Three main domains are traditionally identified (Lymer et al., 2018 and references therein): 1) the East Sardinia Basin, with present-day water depths between 200-2000 m consisting of a system of seamounts and depressions that do not contain MSC sediments (Lymer et al., 2018); 2) the Cornaglia Terrace (2000-3000 m deep), a wide, flat area with dispersed structural highs; 3) the Tyrrhenian Basin *s.s.*, with water depths varying from 3000-3600 m. Whether the Tyrrhenian Basin acquired the present-day topography and hypsometry before the MSC (Lymer et al., 2018) or at least part of it (e.g. Eastern Sardinia margin, where Site 654 is located, and Northern Tyrrhenian) was much shallower (possibly comparable to the Caltanissetta Basin; Roveri et al., 2014b) and underwent extension and subsidence during the Messinian-Pliocene (e.g. Kastens and Mascle, 1990; Loreto et al., 2020) is still unresolved.

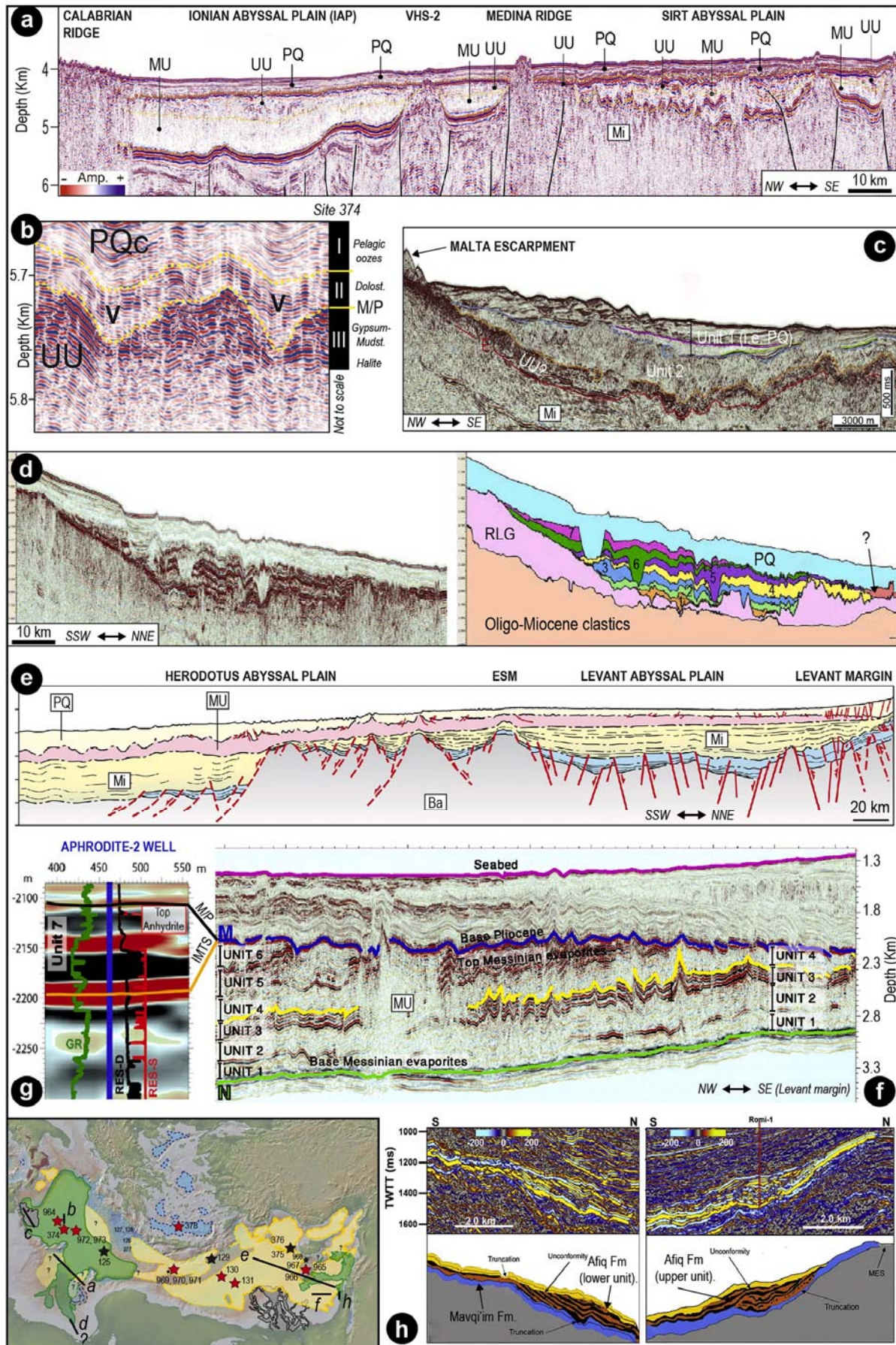
The MSC units in seismic profiles from the Tyrrhenian Basin (Fig. 7g) are very similar to the ones described in the Algero-Balearic and Liguro-Provençal basins (Fig. 7b-c; Gaullier et al., 2014; Lymer et al., 2018). ODP Sites 652, 653 and 654 confirmed the seismic-inferred lithological nature of UU as consisting of gypsum-mudstone alternations (8 are counted at Site 654; Kastens et al., 1987; Borsetti et al., 1990; Roveri et al., 2014b). Intercalations of ripple-cross-laminated, fine-grained, azoic sandstones occur within the mudstone intervals in places (Cita et al., 1990; Iaccarino and Bossio, 1999). In some mudstone samples, the ostracod *Cyprideis* sp. (Site 654) and *Candona* sp. (DSDP Hole 974B) and the foraminifera *Ammonia beccarii* and *Ammonia tepida* have been found, indicating a shallow-water (< 50 m) brackish environment (see subsections 5.1 and 5.4; Cita et al., 1990; Iaccarino and Bossio, 1999). $^{87}\text{Sr}/^{86}\text{Sr}$ isotope ratios of UU gypsum and planktic foraminifera of the overlying Pliocene (Unit 1 at Site 654) show values much lower (from 0.708627 to 0.708745) and roughly equivalent (from 0.708935 to 0.709112) to coeval ocean water (~0.709020-30; McArthur et al., 2012), respectively (Müller et al., 1990; Müller and Mueller, 1991). Similar $^{87}\text{Sr}/^{86}\text{Sr}$ values were obtained from the gypsum cored at Site 652 (0.708626-0.708773; Müller and Mueller, 1991).

The Miocene/Pliocene boundary at DSDP Site 132 is placed above a cross-bedded sand rich in quartz, mica, pyrite, rounded fragments of gypsum and specimens of *Ammonia beccarii* and *Elphidium macellus* (Ryan et al., 1973). In the adjacent ODP Site 653 a similar sandstone is found slightly below the biostratigraphically-defined Messinian/Pliocene boundary and ~70 cm of grey mudstones with foraminifera and nannofossils of undiscovered provenance are squeezed in between (Cita et al., 1990). These mudstones also contain rare dwarf planktic foraminifera (*Globorotalia acostaensis*, *Orbulina universa*, and *Globigerina bulbosa*; Cita et al., 1990).

Overall, the uppermost Messinian sediments of the Tyrrhenian Basin are interpreted as having been deposited in lakes with periodic episodes of increased salinity and dilution under the strong influence of high energy rivers and, perhaps occasionally, of the Atlantic (Cita et al., 1990; Müller et al., 1990; Müller and Mueller, 1991).

4.6 Ionian Basin

The deepest basin in the Mediterranean today is the Ionian Basin, with its lowest point at 5,267 meters. The so-called Ionian Abyssal Plain (IAP) is bounded on all sides by pre-MSD structural highs (Fig. 2a; Camerlenghi et al., 2019): the Malta Escarpment to the west; the Medina Escarpment to the south separating it from the Gulf of Sirt (Fig. 8a); the Gargano-Pelagosa and/or Otranto sill to the north dividing it from the Adriatic Foreland and, finally, an unnamed sill to the east, separating the IAP from the Levant Basin. Evidence from recent high-resolution seismic studies across the region have been used to support Stage 3 desiccation models (e.g. Hsü et al., 1978a, 1978b; Bowman, 2012; Micallef et al., 2018, 2019; Camerlenghi et al., 2019; Spatola et al., 2020).



(caption on next page)

Fig. 8. Seismic profiles from intermediate-deep Eastern Mediterranean basins containing MSC markers/units (see Fig. 7 for abbreviations). (a) High-resolution seismic line MS27 imaging the PQ and the uppermost MSC's UU and MU in the Ionian Abyssal Plain and Gulf of Sirt (modified from Camerlenghi et al., 2019). Note how the MSC units are thinner, more difficult to distinguish and more deformed in the Sirt Abyssal Plain than in the IAP. PQ, UU and MU all onlap the structural highs of the Medina Ridge and VHS-2 sill. (b) High-resolution imaging of the lower part of the Plio-Quaternary (PQc unit) and upper part of the Messinian (UU) in the IAP (Camerlenghi et al., 2019). The MSC-PQ boundary is a highly irregular surface, describing apparent V-shaped incisions (symbol V) of controversial origin (see subsection 4.6.1 for insights). Note the coherent deformation of PQc with the underlying MSC sequence and the absence of fluvial facies within the incisions (Unit II is made of lower Pliocene dolomitic marls recovered in Site 374 drilled nearby the seismic line; see text). (c) Multichannel seismic reflection profile MEM-07-203 running approximately parallel to the Malta Escarpment and showing the relationship between Unit 2 of Micallef et al. (2018) with the overlying and underlying Zanclean and Messinian sediments, respectively (modified from Spatola et al., 2020). (d) Uninterpreted (left) and interpreted (right) seismic profiles showing the cyclic and channelized nature of the uppermost Messinian observed in the offshore Sirt Basin (modified from Bowman, 2012). (e) Interpreted 2D regional WNW–ESE seismic profile crossing the continental shelf and offshore Levant Basin and the Herodotus Abyssal Plain (Jagger et al., 2020). Note the lateral continuity of the Messinian MU. (f) Seismic profile from the Levant Basin showing the 6 sub-units distinguished inside the MU as well as its lower (N-reflector) and upper (M-reflector) boundaries (modified from Gvirtzman et al., 2013). (g) High-resolution seismic reflection image with wireline logs from Aphrodite-2 well illustrating that M-reflector previously considered as top evaporitic sequence and M/P boundary here consists of a ~100-m-thick unit (i.e. Unit 7 of Gvirtzman et al., 2017) in which different layers are distinguished (modified from Gvirtzman et al., 2017). (h) Interpreted and uninterpreted seismic profiles imaging the Mavqi'im and Afiq formations described in the canyons on the Levant continental margin (modified from Ben Moshe et al., 2020).

4.6.1 Ionian Abyssal Plain

The typical “trilogy” of seismic units representing the MSC deposition in the Western Mediterranean is recognized also in the IAP by Gallais et al. (2018) and Mocnik et al. (2018). However, Camerlenghi et al. (2019) states the MSC sequence in the IAP is ~1,300 m-thick and composed of only two units (Fig. 8a). The lowermost 150–700 m-thick Mobile Unit (MU) is seismically transparent without discernible bedding and with diapiric structures, all features diagnostic of halite. By contrast, the 350–1,000 m-thick Upper Unit (UU) alternates highly reflective with acoustically transparent reflectors (Figs. 8a–b), similar to those described of the UU sequences of the Western Mediterranean (Figs. 7b–c). These are therefore assumed to represent gypsum-mudstone cycles (Camerlenghi et al., 2019). The uppermost 80 m of UU has been recovered from DSDP Site 374 (Hsü et al., 1978b), confirming the presence of gypsum (both primary cumulate and clastic; Lugli et al., 2015) alternating with mudstones (Unit III; Hsü et al., 1978b). These mudstones are largely barren of *in situ* fossils. However, the presence of some foraminifera and siliceous microfossils led Cita et al. (1978) and Hsü et al. (1978a) to suggest that sporadic marine incursions, possibly from the Indian Ocean, took place during Stage 3. Similar to Site 372, the basal part of Hole 374 intercepted one thin (~3.5 m) halite layer within the UU (Hsü et al., 1978b).

The UU and the overlying Zanclean (subunit PQc of Camerlenghi et al., 2019) reflectors are conformably folded throughout most of the abyssal plain, locally showing chaotic internal structure, irregular folding mimicking V-shaped incisions and truncations (Fig. 8b; Camerlenghi et al., 2019). These features are interpreted by Camerlenghi et al. (2019) as fluvial valleys carved in subaerially exposed evaporites by the Eso-Sahabi fluvial system, the closest fluvial drainage network to the area (see Micallef et al., 2018) that drained Libya in the late Miocene (Griffin, 2002) and has been traced across the Gulf of Sirt offshore (Sabato Ceraldi et al., 2010; Bowman, 2012). Several arguments counteract this interpretation: 1) the coherent deformation, mostly of post-Messinian age, of both the UU and the lower Zanclean; 2) the absence of fluvial facies above the bottom of the “valleys”, which instead correspond to a mudstone interval that underwent post-depositional dolomitization (Unit II; see below; Fig. 8b); 3) the unlikelihood that the Eso-Sahabi fluvial system managed to bypass the Medina Ridge divide (Fig. 8a). Alternatively, the apparent incisions at the M/P boundary in the IAP may represent post-sedimentary folds resulting from post-Messinian tectonic and/or salt movements-driven deformation (e.g. Mocnik et al., 2018). At Site 374 the Miocene/Pliocene boundary has been recovered (Unit II), but its primary nature (likely a mudstone) is obscured by diagenesis (cementation by dolomite; Hsü et al., 1978b). A lithified dolostone at the (seismic) predicted depth of the M-Horizon is a characteristic of several sites. Sometimes this interval has been recovered (e.g. Sites 125 and 374; Ryan et al., 1973; Hsü et al., 1978b; Comas et al., 1996); at others the hard lithology is inferred by the torqueing of the drill string (resistance to turning) accompanied by

bouncing of the drill bit at the (e.g. Sites 122, 124, 125, 132, 133 and 134; Ryan et al., 1973). Dolomitization was (Hsü et al., 1973a, 1973b; Ryan et al., 1973) and still is (e.g. Ryan, 2009) largely considered a “diagnostic feature of tidal (sabkha) sediments” (Friedman, 1973, pp. 705). Its occurrence at locations with present-day water depth exceeding 2000 m was therefore considered strong evidence that the Mediterranean floor was subaerially exposed prior to the Zanclean marine replenishment (e.g. Ryan et al., 1973). It is, however, now widely accepted that dolomite precipitation is not exclusive of sabkha environments, but rather is a common process also in bottom sediments under a relatively deep water column (see Dela Pierre et al., 2012, 2014 and references therein). In the specific case of the offshore Mediterranean’s M/P boundary on the Ionian Abyssal Plain, already in the ‘70s dolomitization was thought to have occurred after burial (Hsü et al., 1978b), a conclusion recently reinforced by McKenzie et al. (2017).

4.6.2 Malta Escarpment

At the foot of the Malta Escarpment, Micallef et al. (2018, 2019) and Spatola et al. (2020) amalgamated the MU and UU into one seismic unit, Unit 3, which is separated from the Plio-Quaternary marine sediments (Unit 1) by Unit 2, a chaotic transparent seismic package (Fig. 8c). Unit 2 has a maximum thickness of 760–860 m, a volume of 1430–1620 km³ and a wedge-shaped geometry that thins eastwards, disappearing before reaching the IAP (Micallef et al., 2018). Micallef et al. (2018) and Spatola et al. (2020) proposed a lithological/sedimentological interpretation of this chaotic body, suggesting it is composed of well-sorted sediments of the Pelagian Platform to the west of the Malta Escarpment, with coarser material at the mouth grading into more distal finer sediments. This chaotic body has recently been attributed to the Zanclean megaflood during its passage from the western to the eastern Mediterranean via a gateway located in south-eastern Sicily (Micallef et al., 2018, 2019; Spatola et al., 2020). Given the rapidity of the reflooding (≥ years, Garcia-Castellanos et al., 2009, 2020), this interpretation implies rapid mass deposition. Other interpretations of this Unit 2 include being the result of extensive marine mass movement (Polonia et al., 2011), being folded UU (Butler et al., 2015) or being a complex unit built during lower sea level phases (Lofi et al., 2011a, 2011b).

4.6.3 Gulf of Sirt

The Gulf of Sirt (or Sirt embayment; Figs. 2a, 8a), the offshore extension of the Sirt Basin onshore Libya (Griffin, 2002 and references therein), is cross-cut by high-density seismic and well datasets as a result of oil potential of the region (Fiduk, 2009). However, only few studies have tackled the MSC (e.g. Hallett, 2002; Fiduk, 2009; Bowman, 2012). In the Sirt embayment the MSC unit(s) is unevenly distributed in sub-basins controlled by a pre-existing topography, there is little distinction between the MU and UU, the overall thickness of the MSC unit(s) is slower and the degree of deformation is higher than in the adjacent IAP (Fig. 8a; Camerlenghi et al., 2019). The presence of halite in the Sirt

embayment is debated, but most authors think it is absent (see [Fiduk, 2009](#); [Sabato Ceraldi et al., 2010](#); [Lofi, 2018](#); [Jagger et al., 2020](#); [Fig. 2b](#)). [Bowman \(2012\)](#) distinguishes seven seismic units within the MSC-related sequence ([Fig. 8d](#)). On the basis of high-resolution 3D and 2D data, each seismic unit has been interpreted consisting of clastics filling erosional channels cutting up to 100 m deep and wide ([Fig. 8d](#)) and evaporites (gypsum and anhydrite) alternating with precessional cyclicity ([Bowman, 2012](#)). The presence of anhydrite in the topmost part of the sequence is confirmed by the B1 NC 35A well ([Hallett, 2002](#)). [Sabato Ceraldi et al. \(2010\)](#) and [Bowman \(2012\)](#) envisaged a three-step evolution of each unit: 1) evaporitic deposition during precession maxima in a dried out Sirt embayment; 2) erosion of the valleys during the arid-wet transition fed by the Eso-Sahabi paleofluvial system; 3) filling of the valleys with the fluvial sediments during the wet phase. Based on this chronostratigraphic interpretation, the evaporite cycles should be time equivalent to most of Stage 3, with the upper four seismic units reflecting the Lago-Mare phase ([Fig. 1a](#)).

4.7 Levant Basin

4.7.1 Abyssal plain

Old seismic data in the Levant Basin show an up to 2 km-thick, high velocity, acoustically transparent sequence bounded by the N-reflector at the base and the M-reflector at the top ([Figs. 8e-f](#); [Ryan, 1978](#); [Net- zeband et al., 2006](#)). This sequence thickens and extends for tens of kilometers towards WNW and thins eastward along the continental margin ([Fig. 8e](#)), where the N and M-reflectors converge forming the condensed MSC section of the Mavqim and Afq formations (described in subsection 4.7.2; [Gvirtzman et al., 2017](#); [Manzi et al., 2018](#)). High resolution 2D and 3D industrial seismic and well data from the southern Levant Basin revealed that this transparent sequence is largely made of pure halite with internal stratification picked out by diatomite, clay- and clastic-rich layers that allowed the division of the sequence into six sub-units, basinward-tilted and truncated at the top by the flat TES ([Fig. 8f](#); [Gvirtzman et al., 2013, 2015, 2017](#); [Feng et al., 2016, 2017](#); [Manzi et al., 2018](#); [Meilijson et al., 2018, 2019](#)). Clastic beds ~3 to 20 m-thick are abundant in the highly reflective and chaotic Unit 5 (i.e. Interbedded evaporites of [Meilijson et al., 2019](#); MC2 unit of [Feng et al., 2016](#); [Figs. 3b, 4a](#)), where they are interbedded with evaporites (probably halite with minor occurrences of anhydrite) varying in thickness from ~6 to 30 m ([Manzi et al., 2018](#); [Meilijson et al., 2019](#)). Paleontological analyses of cuttings probably belonging to one of the clastic beds revealed the presence of a few mollusk fragments, ostracods, echinoid spines and a relatively rich assemblage of benthic and planktic foraminifera which [Meilijson et al. \(2019\)](#) concluded to be reworked. Based on seismic and well-log data, clastic intercalations (probably of clays, silts and sands) within a halite-dominated sequence are thought to persist in the overlying Unit 6, although they diminish in thickness and frequency ([Gvirtzman et al., 2013](#); [Feng et al., 2016](#); [Meilijson et al., 2019](#)). The expression of the end of the MSC is highly controversial. Until recently, the M-reflector of [Ryan \(1978\)](#) (later renamed as the Top Erosion Surface, TES; [Lofi et al., 2011a, 2011b](#)) bounding Unit 6 at the top was considered to be the Miocene/Pliocene boundary ([Fig. 8f](#); [Ryan, 1978](#); [Gvirtzman et al., 2013](#); [Feng et al., 2016](#)). Instead, [Gvirtzman et al. \(2017\)](#) showed that in higher resolution seismic data the M-reflector/ TES is a bundle of reflectors forming a distinct layer (Unit 7) overlying a truncation surface (i.e. Unit 6/7 boundary) that they re-labelled intra-Messinian truncation surface (IMTS; [Fig. 8g](#)) and ascribed to subaqueous dissolution rather than subaerial incision (e.g. [Bertoni and Cartwright, 2007](#); [Lofi et al., 2011a, 2011b](#); [Kartveit et al., 2019](#); [Madof et al., 2019](#)). This conclusion was recently corroborated by the independent study of [Kirkham et al. \(2020\)](#). Analysis of gamma-ray and resistivity logs in three deep basin wells (Aphrodite-2, Myra-1, Sara-1; [Fig. 2b](#)) and correlation with the Or-South-1 well (located between the deep basin and the shelf) showed that Unit 7 maintains a constant thickness of ~100 m-thick and consists of clastic-rich anhydrite of undisclosed provenance.

[Meilijson et al. \(2019\)](#)'s lithological interpretation of industrial bore- holes slightly farther to the NE ([Fig. 2b](#)) give Unit 7 a significantly smaller thickness (5 m; [Fig. 3b](#)). Independent studies offshore Lebanon and Syria ([Kartveit et al., 2019](#); [Madof et al., 2019](#)) describe a unit (Nahr Menashe complex) interpreted as a thicker (up to 300 m; [Madof et al., 2019](#)), but lateral equivalent of [Gvirtzman et al. \(2017\)](#)'s Unit 7. Based on its channelized morphology identified upslope near the Lebanese coast, [Kartveit et al. \(2019\)](#) and [Madof et al. \(2019\)](#) interpreted the Nahr Menashe Unit and the IMTS underneath as fluvial in origin, deposited/ formed on a subaerially exposed floor of the Levant Basin. Six ([Madof et al., 2019](#)) to eight ([Madof and Connell, 2018](#)) lobes were identified and are proposed to have stacked with precessional frequency. The Nahr Menashe sequence has been correlated by the same authors with the AbuMadi Fm. located within the Messinian canyons offshore Egypt ([AbdelAal et al., 2000](#); [Loncke et al., 2006](#); [Abdel-Fattah, 2014](#)), the Handere Formation offshore Turkey ([Radeff et al., 2017](#)) and with the Eosahabi deposits offshore Libya ([Bowman, 2012](#)). This interpretation implies a low base-level during the final stage of the MSC.

[Manzi et al. \(2018\)](#) and [Meilijson et al. \(2018, 2019\)](#) attempted astronomical dating of the abyssal MSC succession of the Levant Basin by integrating biostratigraphy on the pre-MU succession, reflector counting within the MU (only [Meilijson et al., 2019](#)) and well-log data ([Fig. 3b](#)). They achieved two contrasting results that gave rise to an outstanding controversy ([Figs. 3b, 4a](#)). [Manzi et al. \(2018\)](#) proposed that Stage 1 in the deep Levant is represented by a foraminifera-barren, evaporite-free shales interval labelled FBI (foraminifer barren interval) observed in the deep Aprodite-2 well and in the more proximal Myra-1 well. In this interpretation Unit 7 comprises the whole of Stage 3 (with the IMTS corresponding to the Stage 2/3 transition) and all halite deposition took place in ~50 kyr estimated during Stage 2 of the MSC ([Fig. 1a](#); [Roveriet et al., 2014a](#)). By contrast, the FBI is not present in the Dolphin well targeted by [Meilijson et al. \(2019\)](#), which is located in an intermediate position between the Aprodite-2 and Myra-1 wells studied by [Manzi et al., 2018](#); [Fig. 2b](#)). Instead, in the Dolphin well a relatively open-marine, foraminifera-rich sequence extends below the (conformable) base of the MU, placed in correspondence to a ~2 to 5.5 m-thick anhydrite/shale (Unit 0; [Manzi et al., 2018](#) and [Meilijson et al., 2018](#), respectively). Astronomical tuning of the ~33 cycles counted in the MU in the Dolphin well, which are assumed to be precessional, results in the Main Halite body (i.e. Unit 0-4 of [Gvirtzman et al., 2013](#) and [Manzi et al., 2018](#)) spanning MSC Stage 1 and 2, the Interbedded Evaporites/ Unit 5 covering substage 3.1 and the Argillaceous Evaporites/ Unit 6-7 to encompass the Lago-Mare phase ([Figs. 3b, 4a](#)). In this interpretation from [Meilijson et al. \(2019\)](#), halite deposition in the Levant Basin started in Stage 1 and persisted throughout the entire MSC, including Stage 3, during which more allochthonous material was delivered to the basin ([Fig. 3b](#)). [Madof and Connell \(2018\)](#) and [Madof et al. \(2019\)](#) also attempted an astronomical tuning of the Nahr Menashe Unit, concluding that it spans throughout substage 3.2 and part of substage 3.1. [Feng et al. \(2016\)](#) claim, however, that the impressive thickness of clastics found in the Levantine MU is more indicative of distinct short-term events (shorter than the precession cycle) associated with transport of extraordinary power and magnitude. Late Messinian sediments have also been recovered at several DSDP (129, 375, 376; [Ryan et al., 1973](#); [Hsü et al., 1978b](#)) and ODP Sites (965, 967, 968; [Emeis et al., 1996](#)), but the assignment of the retrieved sediments to seismostratigraphic units is problematic. Nevertheless, they provide several key nuggets of precious information about the Stage 3 paleoenvironment:

- Sites 965 and 966, located roughly on the crest of the Eratosthenes Seamount, just south of Cyprus ([Fig. 2b](#)), recovered soil structures above the evaporites indicating exposure above sea level ([Robertson, 1998a, 1998b](#); [Maillard et al., 2011a](#); [Reiche et al., 2016](#)).
- ODP Sites 967 and 968, located at the base of the northern and southern slope of Eratosthenes Seamount ([Fig. 2b](#)), respectively,

revealed the presence, within the MSC interval, of calcareous turbidites with Cyprus-derived clasts and clays containing *Ammonia tepida*, *Cyprideis pannonica* and *pulmonate gastropods* (Blanc-Valleron et al., 1998; Robertson, 1998a,b; Reiche et al., 2016).

- Abundant *Cyprideis pannonica* specimens were also recovered from DSDP Sites 375 and 376 drilled on the crest of the Florence Rise, west of Cyprus (Fig. 2b; Hsü et al., 1978b).
- Abundant, well-preserved *Ammonia* tests and *Cyprideis* specimens are also known from Site 129A (Fig. 2b), occurring with dwarf planktonic foraminifera (Ryan et al., 1973).

All the evidence listed above suggest that a base-level fall leading to subaerial exposure occurred at some point(s) during Stage 3 in the Eastern Mediterranean (Ryan, 2009). However, it must be kept in mind that both the Florence Rise and Eratosthenes Seamount are likely to have been much more elevated during the Messinian than they are today because of Pliocene-Quaternary subsidence related to the Cyprus subduction zone (Robertson, 1998a, 1998b; Maillard et al., 2011a; Reiche et al., 2016).

Sites 375 and 376 display several discrete layers of primary and clastic gypsum interbedded in the *Cyprideis*-rich mudstones (McCulloch and De Deckker, 1989; Lugli et al., 2015). This succession shares several similarities with sites drilled in the Western Mediterranean (e.g. ODP 654A) and Ionian Basin (DSDP 374), where they have been correlated with the seismic Upper Unit (see subsections 4.5 and 4.6). This may suggest that a Western Mediterranean-like gypsum-bearing UU was also locally deposited in the easternmost abyss of the Mediterranean (see Günes, et al., 2018).

4.7.2 Levant continental margin

Evaporitic and non-evaporitic deposits are buried beneath PQ deposits (Yafo Formation) along the Levant continental margin, where they are mostly preserved within canyons carved underwater in pre-Messinian time (Druckman et al., 1995; Lugli et al., 2013). Within the Afq canyon, Druckman et al. (1995) distinguished three formations in the Messinian sequence: the evaporitic Mavqi'im Formation, 115 m-thick and mostly composed of anhydrite in places interbedded with micritic limestones; the Be'eri Formation, comprising gypsum; the Afq Formation, varying in thickness from 30 to 90 m and consisting of conglomerates, sandstones and marls interpreted as representing fluvial and lacustrine-marsh environments (Druckman et al., 1995). The Afq Fm. is only present in the deepest portions of the canyon where it overlies the Mavqi'im Fm. By contrast, the Be'eri gypsum is only found

along the canyon shoulders covered by the Pliocene, at elevations > 600 m with respect to the Mavqi'im Fm. Based on Sr values, Druckman et al. (1995) attributed the Mavqi'im Fm. to MSC Stage 1, the Be'eri Fm. to substage 3.1 and the Afq Fm. to the Lago-Mare phase. These authors also suggested that gypsum precipitation occurred under subaqueous conditions, with the water level ~600 m (i.e. the difference in altitude between the Mavqi'im and Be'eri fms.) higher during the deposition of the Be'eri Fm. Two base-level falls of approximately the same magnitude are thought to have occurred between the evaporitic phases and after Mavqi'im deposition. A lowstand phase was therefore in force during Afq deposition (Druckman et al., 1995).

However, combining stratigraphic, sedimentological and geochemical (Sr isotopes) considerations, Lugli et al. (2013) revealed the clastic nature of both the Mavqi'im and Be'eri evaporites and suggested the persistent drowning of the canyon(s), filled with turbidites (Lugli et al., 2013). Due to the presence of clastic evaporites, Gvirtzman et al. (2017) suggested that the Mavqi'im Formation is a condensed section encompassing MSC Stage 2 and early Stage 3, while the evaporite-free Afq Formation represents the Lago-Mare phase.

Ben Moshe et al. (2020) ascribed (at least part of) the Afq Fm. to the whole of Stage 3 as a wedge-shaped clastic complex lying on top of the Mavqi'im Fm. and with the basal surface corresponding to the correlative conformity of the MES developed landward, at the expense of the

Mavqi'im Fm (Fig. 8h). Ben Moshe et al. (2020) distinguished a lower sub-unit composed of clastic gypsum and with fore-stepping and down-stepping internal geometry typical of progradational wedges, and an upper sub-unit containing anhydrite fragments and marls with Lago-Mare fauna (e.g. *Cyprideis torosa*; Rosenfeld, 1977) and with seismic characteristics typical of a transgressive systems tract. Incisions are reported throughout the Afq Fm. at different depths, while erosional surfaces bound both sub-units (Ben Moshe et al., 2020). In particular, the surface capping the upper sub-unit and correlated to the M horizon or TES basinward (see subsection 4.7.1) shows dendritic drainage patterns of gullies and channels (Ben Moshe et al., 2020).

Ben Moshe et al. (2020) identify the variation of base level specifically during Stage 3 by analyzing the morphology of truncation surfaces bounding the Afq Formation on the continental margin of the Levant Basin. This suggests high amplitude fluctuations of base-level in the order of one hundred meters, with development of subaerial erosion surfaces and the deposition of clastics and incision by fluvial drainage systems that occurred during the lowstand phases, while aggradational units (of unknown lithological nature) accumulated during the highstand phases. According to their analysis, base level dropped down to a maximum 535 m during Afq deposition (i.e. below the maximum 430 m estimated paleodepth of the Sicily Sill; Garcia-Castellanos et al., 2009), implying hydrological disconnection between the Eastern and Western basins at various times during Stage 3. A regression to 615-885 m is proposed to have occurred at the top of the Afq Fm., pre-dating the abrupt refilling at the base of the Zanclean (e.g. Micallef et al., 2018, 2019; Garcia-Castellanos et al., 2020; Spatola et al., 2020).

4.8 Summary of the offshore Stage 3 record

Knowledge of the Stage 3 sequence offshore is mainly based on the integration of seismic interpretations and analysis of material recovered from fragmentary and unevenly distributed DSDP/ODP/industrial cores.

- MSC sediments are absent on the eroded continental shelves bordering the deep basins, except in the Messinian thalwegs and at their mouth. Here the PQ lies directly above the MES which, in turn, cuts through the pre-MSC deposits (Fig. 7e). A similar stratigraphic arrangement is found along the middle-upper slopes (Fig. 7d), although the presence of a thin, possibly incomplete UU in morphological depressions is sometimes postulated. Seamounts also lack MSC Stage 3 sediments and are strongly incised by the MES (Fig. 7g).
- The thick UU is widespread and roughly present everywhere in the abyssal plains from west of the Alborán volcanic arc to the eastern edge of the Ionian Basin (Fig. 2b). In the abyssal plains its seismic facies appears homogeneous, comprising parallel and relatively continuous high amplitude reflections (Figs. 7b-c). The UU pinches out towards the foot of continental slopes and seamounts (Figs. 7b, d-g), where it can be irregularly bedded or relatively well bedded (Lofi et al., 2011a, 2011b). The uppermost part of the Bedded Units (defined in depressions physically disconnected from the abyssal plains and, therefore, from the UU; e.g. CMD and Corsica Basin; Maillard et al., 2014; Thinon et al., 2016; Raad et al., 2021) shows seismic features comparable to those of the UU.
- Drill Sites revealed that the reflections of relatively high amplitude in seismic profiles correspond to gypsum and mudstone alternations with sporadic intercalations of massive to cross-bedded sandstones. Some mudstone interbeds contain low-diversity assemblages of benthic organisms (ostracods, foraminifera and diatoms) indicative of shallow to neritic environments. Except for dwarfed forms of planktonic foraminifera and the monospecific nannofossil assemblages described

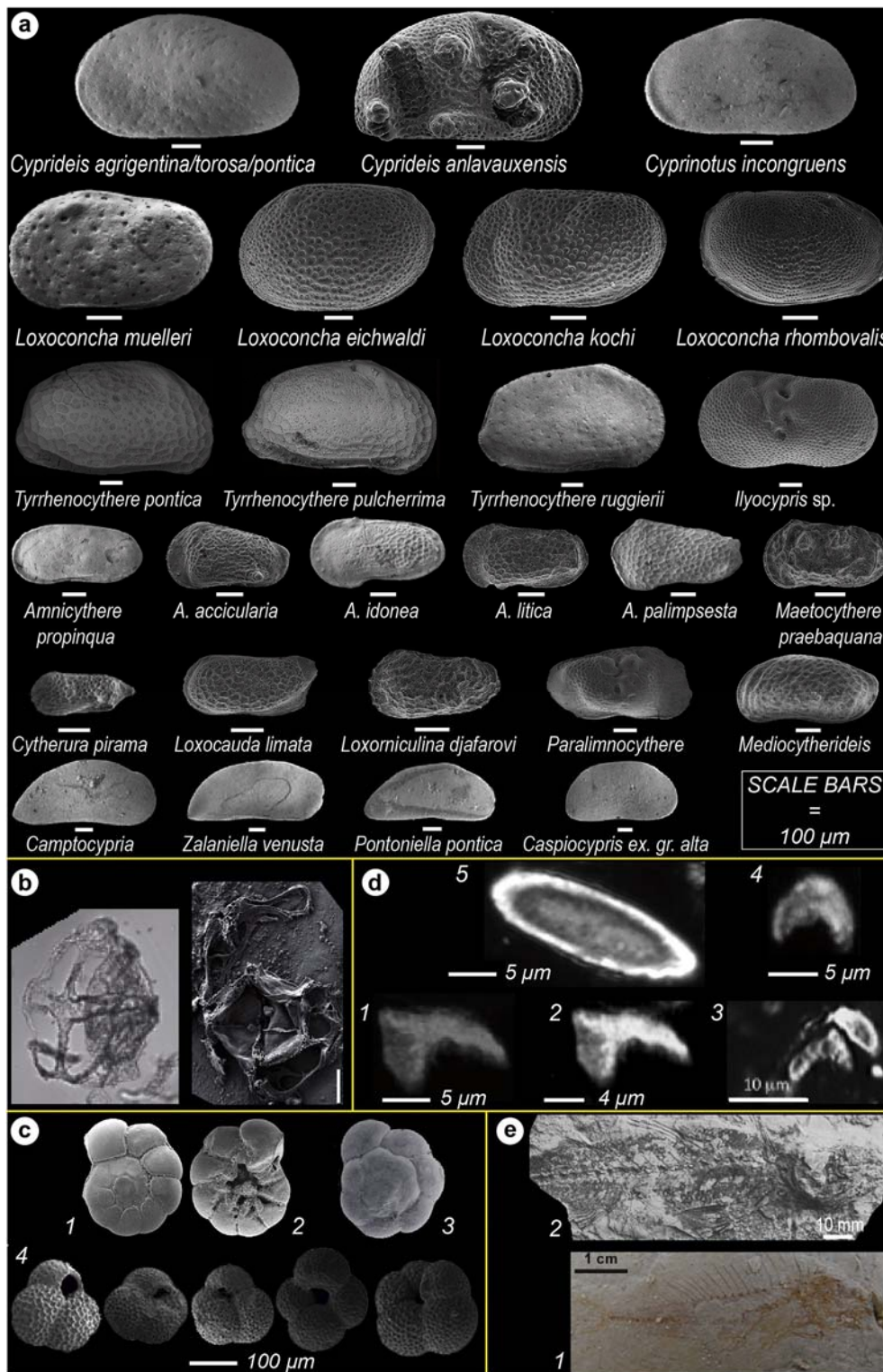


Fig. 9. Photomicrographs of the key micro- and macrofossils featuring Stage 3 sediments. (a) Scanning electron microscope (SEM) photographs of the more common Paratethyan ostracod species in substage 3.1 and 3.2 sediments (compiled from Stoica et al., 2016, Cosentino et al., 2018 and Sciuto et al., 2018). (b) Photomicrographs of the Paratethyan dinoflagellate cyst *Galea-cysta etrusca* under the optical microscope (left) and SEM (right) (modified from Do Couto et al., 2014 and Grothe et al., 2018). Scale=20 μ m. (c) SEM microphotographs of the euryhaline, shallow-water benthic foraminifera *Ammonia beccarii* (1-spiral side, 2-umbilical side) and *Ammonia tepida* (3-spiral side; Carnevale et al., 2019) and of the dwarf fauna of planktonic foraminifera from the Bajo Segura Basin (4; Corbí and Soria, 2016). (d) Photographs in polarized light (crossed nicols) of some specimens of *Ceratolithus acutus* (1-3) described in the Lagomare unit of Malaga (1-Do Couto et al., 2014), the Zorreras Mb. of Sorbas (2-Clauzon et al., 2015) and the Colombacci Fm. of the Northern Apennines (3-Popescu et al., 2017) and of destroyed (4) and intact (5) ascidian spicules of *Micrascidiscus* sp. (Golovina et al., 2019). Note that *C. acutus* specimens closely resemble ascidian spicules of *Micrascidiscus* sp., which may lead to misinterpretation of the *C. acutus* (see Golovina et al., 2019), and that pictures 1 and 2 are identical, despite they are attributed to samples taken from two different localities. (e) Articulated skeletons of marine fish from substage 3.1 mudstone horizons in Cyprus (1-*Aphanius crassicaudus*; Manzi et al., 2016a) and substage 3.2 deposits in Cava Serredi (2-*Mugil cf. cephalus*; Carnevale et al., 2018).

by Castradori (1998), the rest of planktonic foraminifera and nannofossils are largely regarded as reworked.

- The deep Levant Basin contains a ~1.8-2.0 km-thick MU (Figs. 8e-f), consisting of 6 to 7 seismic units depending on the resolution of the seismic employed. In high resolution seismic data, the lateral equivalent of part of the UU is identified as a ~100-m-thick, clastic-rich, anhydrite layer (Unit 7 of Gvirtzman 1207) offshore Israel, thickening to 300 m offshore Lebanon (Nahr Menashe complex, Madof et al., 2019). The Levant Basin still has major controversies concerning the timing of halite deposition (~50 kyr vs ~550 kyr; Manzi et al., 2018 vs Meilijson et al., 2019), the origin of the clastic accumulations overlying the halite (fluvial vs subaqueous) and the presence or absence of gypsum-mudstone cycles.
- Apart from the halite flow-related deformation, the Miocene/Pliocene boundary (i.e. UU/PQ transition) is conformable in intermediate (e.g. Balearic Promontory) and deep (WAB, EAB, Algero-Balearic, Liguro-Provençal, Tyrrhenian, Ionian and Levant) depocenters, while it shows signs of erosion on the shelf domain and along the upper-middle continental slopes and seamounts. Clear arguments of floor exposure at the M/P boundary are absent in all drill sites but 978A.

5. The paleontological perspective

Paleontological data have been used to define and identify Stage 3 sediments, but have also been a source of profound contention over the interpretation of its paleoenvironmental and paleohydrological nature. Biotic groups impacted by the evolution of the gateways linking the Mediterranean with the Atlantic, Indian Ocean and Paratethys include marine species (e.g. foraminifera, calcareous nannofossils, fish) and brackish water-species (ostracods, fish, mollusks and dinocysts endemic or with affinity to species of the Paratethys region) that were unable to migrate when these corridors were closed, and terrestrial species (e.g. mammals) that, conversely, got across the gateway during periods of exposure (see Colombero et al., 2017; Booth-Rea et al., 2018; Mas et al., 2018b). Analysis of these faunal datasets provides key insights into likely gateway dimensions and the timing of their opening, restriction and closure (e.g. Palcu et al., 2017). Furthermore, they are a key constraint on the water sources likely to have been affecting the Mediterranean during MSC Stage 3.

5.1 Ostracods

Ostracods are by far the most prolific faunal group during Stage 3. Brackish species are known from both land sections and deep-sea cores across the whole Mediterranean (see Fig. 2b for sites and references; Fig. 9a). Two characteristic biofacies are commonly distinguished: Biofacies 1 (Bonaduce and Sgarrella, 1999) or *Cyprideis* assemblage (Iaccarino and Bossio, 1999) consists of a monospecific population of *Cyprideis* species or of an oligotypic population dominated by *Cyprideis* species alongside rare specimens of *Tyrrhenocythere ruggierii*, *Loxococoncha kochi*, *Loxococoncha muelleri* and *Caspiocypris alta*; Biofacies 2 (Bonaduce and Sgarrella, 1999) or *Loxocorniculina djafarovi* assemblage (Iaccarino and Bossio, 1999) has a higher species diversity characterized by the abundant occurrence of truly Paratethyan species belonging to the genera *Amnicythere*, *Loxococoncha*, *Loxocauda*, *Cytheromorpha*, *Cyprinotus* and *Tyrrhenocythere* (see species names in Fig. 9a). The number of species reported in the onshore sections is variable, ranging from a dozen (e.g. Caruso et al., 2020) to more than sixty (e.g. Gliozzi et al., 2007; Grossi et al., 2008). This variability is not explained, but it may result from the application of different taxonomic concepts that resulted in the recognition of more or fewer species (Stoica et al., 2016) or from local environmental conditions that differed from basin to basin and resulted in different patterns of colonization. Compared to the onshore domain, the ostracod fauna offshore is

impoverished. Monospecific assemblages of *Cyprideis* sp. (Sites 372, 129A, 376, 654A, 967, 968; Ryan et al., 1973; Cita et al., 1990) or oligospecific assemblages dominated by *Cyprideis* and rare specimens of *Candona* sp. (Hole 974B, Iaccarino and Bossio, 1999) and *L. muelleri* (Hole 978, Iaccarino and Bossio, 1999) are the more widely reported. Interestingly, these assemblages are always associated with *Ammonia* sp. tests and, in some cases, with other species of shallow-water, euryhaline benthic foraminifera (see subsection 5.4). Only in Hole 975, close to the M/P boundary is a more heterotypic ostracod assemblage found (*Euxinocythere praebaquana*, *Amnicythere idonea*, *Leptocythere limbata*, *Loxocorniculina djafarovi*, *Candona* sp., and *Cyprideis* sp.; Iaccarino and Bossio, 1999) and lacking of euryhaline benthic foraminifera. The likely cause of the widespread barrenness of ostracods in most of the offshore samples is perhaps because environmental conditions in the deep basins (depth and/or salinity) were not suitable to permit population by this benthic fauna (see below for the ecological requirements; e.g. Hsü et al., 1978b in reference to Site 374). Finally, one must bear in mind that studying these organisms require much more material (some hundreds of grams) than the quantity of core sediments usually processed (i.e. ~10 cm³; Iaccarino and Bossio, 1999).

The paleoecology (salinity and depth ranges) of Stage 3 ostracods has been based on both observations of few species that still live in the Caspian and Black seas today and have affinities with the Stage 3 species and on the interpretation of sedimentological, geochemical and mineralogical data of the surrounding sediments (see Gliozzi and Grossi, 2008 and Grossi et al., 2008 for insights). Biofacies 1 is thought to represent

very shallow water environments (i.e. <15 m) with salinity fluctuating between mesohaline and hypersaline when the euryhaline *Cyprideis* is dominant. Instead, more stable oligo-mesohaline water is inferred when the other species are more abundant in Biofacies 1. The variegated Biofacies 2, on the other hand, is thought to represent somewhat deeper environments (up to 100 m) and less salty conditions (oligo-low mesohaline; Gliozzi and Grossi, 2008; Grossi et al., 2008; Caruso et al., 2020). Some authors consider the time when the Paratethyan ostracods arrived in the Mediterranean to be well constrained (e.g. Roveri et al., 2008a; Grossi et al., 2011; Cosentino et al., 2018) by the scarce occurrence of the first Paratethyan immigrant *Loxococoncha muelleri* 20 cm below the ash layer in the Colla di Votta section, which has a ²³⁸U-²⁰⁶Pb age of 5.5320 ± 0.0074 Ma (Cosentino et al., 2013), and in the chaotic deposits of the Adana Basin, ascribed to Stage 2 (Faranda et al., 2013). Instead, the first appearance of *Loxocorniculina djafarovi* has been considered to coincide with the biofacies 1-2 shift and to have occurred Mediterranean-wide synchronously at 5.40 Ma (Roveri et al., 2008a; Grossi et al., 2011; Cosentino et al., 2013). Roveri et al. (2008a) also showed Biofacies 2 diversity as increasing linearly through the Lago-Mare phase, reaching its maximum diversity just beneath the Miocene/Pliocene boundary and before disappearing in the Pliocene. Following the claimed synchronicity of the FO of both *Loxococoncha muelleri* and *Loxocorniculina djafarovi*, Roveri et al. (2008a) and Grossi et al. (2011) recognized one biozone in each biofacies: the *Loxococoncha muelleri* Biozone, spanning from 5.59 to 5.40 Ma, and the *Loxocorniculina djafarovi* Biozone, whose boundaries correspond respectively to the first (5.40 Ma) and last occurrence (5.33 Ma) of *L. djafarovi* in the Mediterranean. This biozonation, erected by Grossi et al. (2011), is often used for dating incomplete successions (e.g. Vera Basin; Stoica et al., 2016; Caruso et al., 2020). However, the first appearance of a diversified ostracod assemblage (including *Loxocorniculina djafarovi*) occurred in already cycle 3 of the Sicilian Upper Gypsum at Eraclea Minoa (Fig. 3a; Grossi et al., 2015), which has an astronomical age of 5.45 Ma (Van der Laan et al., 2006) or 5.47 Ma (Manzi et al., 2009). Furthermore, the sudden appearance of Biofacies 2 and its linear, upward increase in diversity have not been recognized in localities like Nijar and Malaga, where biofacies 1 and 2 are found stacked in more than one lithological (possibly precession-controlled) cycle in the Lago-Mare succession (Bassetti et al., 2006; Guerra-Merchán et al., 2010). These findings argue that the appearance of Paratethyan ostracods in the Mediterranean may

not have been synchronous, therefore casting serious doubts upon the biostratigraphic relevance of the Mediterranean ostracods.

Except for *Cyprideis* specimens, where species attribution is debated (see discussion in Stoica et al., 2016), the affinity of all other ostracod species observed in Mediterranean Stage 3 sediments (Fig. 9a) with those of the Eastern Paratethys basins (i.e. Dacian, Euxinic and Caspian) has been demonstrated in several publications (e.g. Ruggieri, 1967; Gliozzi et al., 2007; Stoica et al., 2016; Sciuto et al., 2018). Only Bassetti et al. (2003, 2006) have questioned the Paratethyan affinity by suggesting that species from the Northern Apennines and Nijar Basin have ambiguous affinities with Paratethyan fauna as described in the mainly Russian literature from the '60-'70s. However, these differences between the late Messinian Mediterranean and Paratethyan ostracods resulted from misidentifications and/or a different use of species nomenclature (Stoica et al., 2016). Recently acquired knowledge of the Pontian assemblages of the Dacian, Euxinic and Caspian basins now permit to trace the provenance of Mediterranean Stage 3 ostracod species from the entire Black Sea region (Stoica et al., 2016) and, for a few species, from the Dacian (Stoica et al., 2013; Lazarev et al., 2020), Caspian (Van Baak et al., 2016) and North Aegean (see references in Krijgsman et al., 2020a) basins.

The means by which the ostracods travelled from the Paratethys to and across the Mediterranean during Stage 3 is as crucial for reconstructing the Stage 3 paleoenvironment as it is poorly addressed in onshore studies or overlooked in seismic and computational studies. Two migratory mechanisms have been suggested:

- 1) the aerial dispersion of ostracods through the migration of aquatic birds (Benson, 1978; Caruso et al., 2020); this hypothesis was proposed because, in a Mediterranean concluded to have been desiccated, it was the only possible migration mechanism.

- 2) direct aqueous migration by the ostracods themselves (which are planktonic in the larval stage) through the establishment of similar paleoenvironmental conditions; by this mechanism, the dispersion of Paratethyan ostracod fauna from right across the Mediterranean requires E-W intraconnection and a Mediterranean water-level high enough to reach the marginal basins (Gliozzi et al., 2007; Stoica et al., 2016; Sciuto et al., 2018; Sciuto and Baldanza, 2020).

Finally, Carnevale et al. (2006a, 2006b, 2008, 2018) recognized the Paratethyan affinity of the Mediterranean Stage 3 species but, in view of their occurrence with *in-situ* species of marine fish, they suggested that Stage 3 ostracods descended from a Paratethyan stock that migrated into the Mediterranean well before the MSC and survived the extreme salinity conditions of Stage 1 and 2 in marginal, fresher water refugia. In this scenario the brackish water ostracod assemblages found in Stage 3 have no paleoecological significance for Stage 3 paleoenvironment (Carnevale et al., 2006a, 2006b, 2008, 2018). However, there are two, unflagged problems with this hypothesis: 1) the Mediterranean-Central Paratethys connection through the Trans-Tethyan gateway in Slovenia already closed in the early Tortonian (Kováč et al., 2007; Sant et al., 2017; Palcu et al., 2017); 2) No Paratethyan ostracod species have been found in the Mediterranean before the MSC (see Gliozzi et al., 2007).

5.2 Dinoflagellate cysts

Dinoflagellate cysts (dinocysts) are the fossil remains of unicellular protists that live in the upper water column of many water bodies (e.g. Zonneveld et al., 2013; Mudie et al., 2017). They can be used as paleoenvironmental indicators and for biostratigraphy, providing the ages of speciation and extinction events, as well as supplying evidence of age diagnostic dispersals of characteristic taxa/assemblages. Influxes of these microorganisms into a basin may occur as the result of interconnection with another basin and dinocysts can therefore be useful indicators of the open gateways between adjacent basins and the resultant changes in conditions (e.g. Grothe et al., 2018). In the case of the MSC, presence of *in situ* marine and/or Paratethys dinocyst assemblages in a marginal basin are likely to indicate the presence of Atlantic and/or

Eastern Paratethys water (respectively) in the Mediterranean and (relatively) high water level conditions (e.g. Pellen et al., 2017).

Palynological studies on the late Messinian Mediterranean dinocysts record are rather scarce, confined to a limited number of outcrops (Malaga Basin, Do Couto et al., 2014; Northern Apennines, Bertini, 2006; Popescu et al., 2007; Iaccarino et al., 2008; Cosentino et al., 2012; Pellen et al., 2017; Caltanissetta Basin, Londeix et al., 2007) and deep wells (976B, 977A, 978A and 134B, Popescu et al., 2015). These studies describe substage 3.1 as being barren of dinocysts. By contrast, substage

3.2 dinocyst assemblages are diverse particularly a few meters/tens of meters below the Miocene/Pliocene boundary and show recurrent vertical variation in abundance between brackish, Paratethyan-type taxa and marine stenohaline and euryhaline species. Taxa with Paratethyan affinities are largely considered to be autochthonous by all aforementioned authors. The extent to which reworking may have affected the marine assemblages is more controversial and debated between none (in Malaga and in the Apennines; Popescu et al., 2007; Do Couto et al., 2014; Pellen et al., 2017), partial (in the uppermost part of the Sicilian Upper Gypsum; Londeix et al., 2007) and total (in the Apennines; e.g. Bertini, 2006; Iaccarino et al., 2008; Cosentino et al., 2012). Given the extent of the implications (i.e. re-establishment of a Mediterranean-Atlantic flow or connection earlier than the Zanclean; e.g. Pellen et al., 2017), this is an issue that will require further clarification.

A key dinocyst influencing our understanding of the late Miocene Lago-Mare phase is *Galeacysta etrusca* (Fig. 9b; see Bertini and Corradini, 1998; Popescu et al., 2009 and Grothe et al., 2018 for more insights).

This species was originally described from sediments in the Mediterranean (Corradini and Biffi, 1988), but has since been discovered in much older deposits in Paratethys (Magyar et al., 1999a, 1999b). The earliest recorded occurrence of *Galeacysta etrusca* is in sediments from the Pannonian Basin dated at ~8 Ma (Magyar et al., 1999a, 1999b). It subsequently dispersed throughout Paratethys at ~6 Ma and was present in the Black Sea throughout the MSC interval (Grothe et al., 2014, 2018). Despite a Mediterranean-Eastern Paratethys connection that is thought to have been established at ~6.1 Ma (Krijgsman et al., 2010; Van Baak et al., 2016; Grothe et al., 2020), *G. etrusca* is not found in the Mediterranean during MSC Stages 1, 2 and 3.1 (5.97-5.42 Ma; Bertini,

2006, Londeix et al., 2007, Manzi et al., 2007, Iaccarino et al., 2008, Gennari et al., 2013) and is only reported in the uppermost part of the Lago-Mare phase, very close to the transition to the Pliocene (e.g. Bertini, 2006; Londeix et al., 2007; Popescu et al., 2007; Iaccarino et al., 2008; Cosentino et al., 2012; Pellen et al., 2017). This implies that *Galeacysta etrusca* may have migrated from Paratethys into the Mediterranean after 5.42 Ma or that environmental conditions in the Mediterranean and in its marginal basins were only suitable for this species (and more generally the whole dinocysts Paratethyan contingent) to proliferate in the uppermost Messinian. Several authors report multiple occurrences of *Galeacysta etrusca* within the Zanclean (e.g. Clauzon et al., 2005; Londeix et al., 2007; Popescu et al., 2007, 2015; Do Couto et al., 2014; Clauzon et al., 2015), but these interpretations are based on the use of an alternative stratigraphic model for the MSC sections (Fig. 4b; see Grothe et al., 2018 for details).

5.3 Diatoms

Among the fresh-brackish organisms found in Stage 3 sediments are also species of diatoms. To date (and to our knowledge), there are no onshore studies that have ever looked for these organisms. By contrast, two samples from DSDP Site 124 in the Algero-Balearic Basin (Fig. 2b) revealed the presence of littoral planktonic forms accompanied by brackish water, and even freshwater, euryhaline, benthonic, and epiphytic species in considerable numbers (Hajós, 1973). Diatoms of undisclosed paleoecological significance are also reported from the ~60 cm-thick mudstone bed between an anhydrite and halite bed in the last core of Site 134 (Ryan et al., 1973). According to Hajós (1973) and Ryan (2009), the diatoms found in these drill cores attest to an

extremely low salinity and a base level in the Balearic and Valencia basins below wave action. Further study of these indicative species and a wider distribution is required to apply this interpretation more generally.

5.4 Foraminifera

A reasonably diverse benthic and planktic foraminiferal assemblage containing no age-diagnostic taxa have been found co-occurring with the brackish Paratethyan fauna in both the onshore and offshore record throughout the Mediterranean (Fig. 2b for localities and references). The benthic foraminifera assemblage is dominated by euryhaline representatives of the genus *Ammonia*, which today dwell in marginal marine (lagoons, estuaries, fjords and deltas) and lacustrine environments at depths < 50 m and tolerate salinities of up to 50‰ (Milker and Schmiedl, 2012; Consorti et al., 2020). *Ammonia tepida* and *Ammonia beccari* (Fig. 9c) are by far the most abundant species in both onshore (see Fig. 2b for localities and references) and offshore (e.g. Site 968A, Blanc-Valleron et al., 1998; Sites 375, 376, 965-968, Orszag-Sperber, 2006) localities, where they co-occur with ostracods belonging to Bio-facies 1. Other commonly occurring benthic euryhaline taxa are *Elphidium* sp., *Cribolephidium excavatum*, *Haynesina* sp., *Nonion* sp., *Quinqueloculina* sp., *Discorbis* sp. and *Trichohyalus* sp., *Brizalina dentelata*, *Bulimina echinate* and *Bolivina* spp. (Ryan et al., 1973; Hsü et al., 1978a, 1978b; Rouchy et al., 2001, 2003, 2007; Iaccarino et al., 2008; Caruso et al., 2020). These species are frequently mixed with poorly preserved and older in age bathyal species (e.g. Caruso et al., 2020).

Planktic foraminifera are represented both by species whose last occurrence pre-dates the MSC (e.g. *Praeorbulina* spp., *Paragloborotalia partimlabiata*, *P. siakensis*, *Neogloquadrina atlantica praeatlantica*, *Globigerinoides subquadratus*, *Globorotalia saheliana*, *Globorotalia conomiozea*, *Acarinina* sp., *Hedbergella* sp.) and by taxa with extended biostratigraphic ranges (e.g. *Sphaeroidinellopsis seminulina*, *Turborotalia quinqueloba*, *Globorotalia mionumida*, *Globoturborotalita decoraperta*, *Neogloquadrina acostaensis*, *Neogloquadrina* spp., *Orbulina universa*, *Globigerinoides trilobus*, *Globigerinoides obliquus*, *Globorotalia scitula*, *Globigerina bulloides*, *G. Mediterranea* and *G. humerosa*; see Fig. 2b for references).

The mixing of foraminifera species with different ecological and salinity requirements and the widespread agreement that the brackish Paratethyan fauna are autochthonous (see subsection 5.1) has always complicated the interpretation of the origin of the foraminiferal assemblages. Among the benthic species, *Ammonia* taxa and the other benthic euryhaline taxa are generally considered autochthonous because they are typically well-preserved and their ecological and salinity requirements could be compatible with those of the Paratethyan ostracods.

The habitat of these benthic foraminifera today in environments both influenced by and disconnected from the open ocean indicates that the Stage 3 sediments in which they occur were deposited in a shallow-water environment subject to salinity fluctuations (Caruso et al., 2020 and references therein), but they do not provide insights into the water provenance. By contrast, the poor preservation, older age and low diversity of the bathyal taxa strongly suggest that these species are reworked (Bassetti et al., 2006; Iaccarino et al., 2008; Caruso et al., 2020). Their mode of life is also incompatible with the shallower water elements of the faunal assemblage. The planktic species which went extinct before the MSC are also undoubtedly reworked (Iaccarino et al., 2008; Caruso et al., 2020). It is more challenging to discriminate between *in situ* and reworked specimens of the long range Neogene taxa. Most of them are considered to be reworked because of their scarcity, their occurrence with *in-situ* brackish organisms and their poor preservation (e.g. Iaccarino et al., 2008; Caruso et al., 2020). A more complex controversy surrounds the long-range dwarf specimens (Fig. 9c) occurring in onshore substage 3.1 (di Tetto Fm. in the Trave section; Iaccarino et al., 2008) and Lago-Mare sediments (Upper Mb. of the Nijar Feos Fm., Fortuin and Krijgsman, 2003; Aguirre and Sánchez-Almazo, 2004;

Bassetti et al., 2006; Sorbas Basin, Roveri et al., 2019a; Bajo Segura Basin, Corbí and Soria, 2016; Colombacci Fm. in Northern Apennines localities, Casati et al., 1976; Colalongo et al., 1976; Rio and Negri, 1988; Popescu et al., 2007; Cyprus, Rouchy et al., 2001) and in some offshore localities (e.g. Sites 124, 125, 129A, 132, 134, 372, 376, 653, 974B, 975, 978; Cita, 1973; Cita et al., 1978; Kastens et al., 1987; Cita et al., 1990; Iaccarino and Bossio, 1999). This fauna is variably interpreted as:

- 1) reworked and size-sorted during transport, therefore lacking any paleoenvironmental significance (e.g. Kastens et al., 1987; Iaccarino and Bossio, 1999; Fortuin and Krijgsman, 2003; Bassetti et al., 2006);
- 2) *in situ* and indicating normal marine conditions (Aguirre and Sánchez-Almazo, 2004; Braga et al., 2006) or temporary Atlantic incursions (Rouchy et al., 2001);
- 3) *in situ* and indicative of high-stress environments (Keller and Abramovich, 2009), such as restricted and/or diluted marine environments (Corbí and Soria, 2016; Corbí et al., 2016, 2020). However, the paleoecological significance of dwarfism in foraminifer tests is not well understood and, given its potential implications for the Lago-Mare environment, it needs to be explored in greater detail.

5.5 Calcareous nannofossils and the *C. acutus* conundrum

Calcareous nannofossils are the fossil remains of coccolithophores, single-celled marine algae which dwell in the eutrophic and photic zone of the ocean (e.g. Ziveri et al., 2004). The potential recognition of marine calcareous nannofossils in marginal Stage 3 deposits would therefore have implications for the Mediterranean base-level and the hydrological riddle of MSC Stage 3. However, like foraminifera and dinocysts, the *in situ* versus reworking issue also impacts the nannoflora.

MSC Stage 3 is crossed by three important nannofossil bio-events astronomically calibrated in the ocean record: the top of *Discoaster quinqueramus* at 5.537 Ma, the base of *Ceratolithus acutus* at 5.36 Ma and the top of *Triquetrorhabdulus rugosus* at 5.231 Ma (Backman et al., 2012; Agnini et al., 2017). Most of the (few) studies that addressed the nannoflora component of Stage 3 deposits did not report taxa belonging to the biozones defined by these bio-events, but only taxa of Cenozoic and Cretaceous age, clearly physically reworked (e.g. Sites 132, 134, 653, 654A, 967A, 969B, Ryan et al., 1973; Hsü et al., 1978b; Müller et al., 1990; Castradori, 1998; Piedmont Basin, Trenkwalder et al., 2008; Violanti et al., 2009; Trave, Fonte dei Pulcini and Stingeti sections and Mondragone well in the Apennines, Cosentino et al., 2006, 2012, 2018; Iaccarino et al., 2008). An exception is the nannoflora observed in the uppermost Messinian sediments at Sites 978A, 975B and 967A (Levant Basin; Fig. 2b). Here, among the plethora of reworked and long-ranging Neogene taxa, Castradori (1998) reported the anomalous abundance of *Sphenolithus* spp (mostly *Sphenolithus gr abies/moriformis*). Although the assemblage points to the absence of a primary marine signature, the unlikely possibility that reworking and/or sorting lies behind the observed peak of *Sphenolithus* spp. led Castradori (1998) to conclude that at least one incursion of marine water occurred during the (uppermost) Lago-Mare.

By contrast, some authors (i.e. Popescu et al., 2007, 2015; Do Couto et al., 2014; Clauzon et al., 2015; Pellen et al., 2017) described the nannofossil assemblage the Lago-Mare LM Unit in Malaga, the Zorreras Member in Sorbas, the uppermost di Tetto/Colombacci Fm. in some Apenninic localities and offshore in the Alborán Basin as having good preservation and showing no erratic fluctuations, all characteristics that led to their interpretation as autochthonous and to the conclusion that these sediments were deposited in a Mediterranean already replenished of Atlantic water (Fig. 4b). In addition, these authors reported the low abundance, but continuous presence of the biostratigraphic markers for the Zanclean *Triquetrorhabdulus rugosus* and *Ceratolithus acutus* (Fig. 9d) below the formally defined Miocene/Pliocene boundary (Van Couvering et al., 2000) in several onshore and offshore Mediterranean (as well as Paratethyan) localities (see Popescu et al., 2017 for details and a

complete list of finding locations).

Such findings (especially that of *C. acutus*) are in sharp disagreement with most of the existing literature and have resulted in an important debate amongst the MSC community (e.g. Popescu et al., 2007, 2008 vs Roveri et al., 2008c and Stoica et al., 2016 vs Popescu et al., 2017), not only for their paleoenvironmental implications (i.e. presence of Atlantic water in the Mediterranean), but also for the chronostratigraphic re-percussions (Fig. 4b). The chronostratigraphic value of *C. acutus* lies in its short temporal distribution straddling the M/P boundary (astro-chronologically calibrated at 5.332 Ma; Van Couvering et al., 2000; Lourens et al., 2004). However, the corresponding biozone is established in oceanic areas (Zone CNPL1: 5.36–5.05 Ma; Backman et al., 2012; Agnini et al., 2017) and is considered not applicable to the Mediterranean region during the MSC due to the harsh physicochemical conditions that are unsuitable for marine biota (Di Stefano and Sturiale, 2010). The interpretation of these nanofossil assemblages in the westernmost areas of the Mediterranean has been countered with several observations: (1) the observation of these age-diagnostic taxa is often not replicated by other studies (e.g. Roveri et al., 2008a; Van Baak et al., 2015; Krijgsman et al., 2020b); (2) *Ceratolithus acutus* is very rare also in fully marine open-ocean sediments (e.g. Di Stefano and Sturiale, 2010); (3) despite being rare in the late Messinian Mediterranean, this species has never been documented together with other long-range taxa, generally predominant in the assemblage, in Stage 3 deposits (see discussion in Krijgsman et al., 2020b). Recently, Golovina et al. (2019) showed that the morphology and size of *C. acutus* overlaps with the shape and dimensions of destroyed ascidian spicules (i.e. calcareous elements produced by benthic tunicates; Fig. 9d), providing an explanation for erroneous identification of *C. acutus* in the Black Sea Basin (Golovina et al., 2019) and perhaps in the western Mediterranean Lago-Mare sediments as well.

5.6 Fish

Fossil fish remains provide information about salinity and depth and have been used to contradict the brackish nature of the Lago-Mare deposits by Carnevale et al. (2006a, 2006b, 2008, 2018) and Grunert et al. (2016). Euryhaline fish species inhabit marine to brackish environments and dominate settings with strong salinity variations while stenohaline fish have specific salinity requirements (marine, brackish, or freshwater) and cannot survive under different conditions. Demersal fish (i.e. those living in or immediately above the sea floor) have specific depth requirements, whereas pelagic fish occupy the water column within a wide range of depth variable from species to species. Fossil fish remains are found either as articulated or disarticulated skeletal parts, including teeth and otoliths, which are identified to the species level. Articulated fish skeletons typically indicate autochthonous deposition because of the difficulty in reworking and transporting intact skeletons. Otoliths and fish teeth are much more likely to be transported.

Otoliths and rare articulated skeletons (Fig. 9e) of marine and Paratethyan species have been reported from Stage 3 deposits, but commonly huge volumes of sediment are required to find even quite small numbers of these fossils (e.g. 20 tons from Moncucco, 6 tons from Cava Serredi, 700 kg from Capanne di Bronzo; Schwarzghans et al., 2020), much more than what is expected for normal marine deposits (i.e. < 30 kg; Agiadi et al., 2017; Karakitsios et al., 2017b).

Substage 3.1 sediments contain articulated skeletons (Fig. 9e) of the marine fish species *Lampanyctus licatae* and *Maurollicus muelleri*, and the shallow water, euryhaline species *Aphanius crassicaudus* in the Lower Feos Member in the Nijar Basin (de la Chapelle and Gaudant, 1987) and the marls of the first UG cycle in the Polemi Basin (Manzi et al., 2016a; Fig. 3a). Cava Serredi (Tuscany), Verduno and Moncucco (Piedmont) are the only other localities in which fish remains (only otoliths) in (claimed) substage 3.1 sediments are known (Carnevale et al., 2006a, 2008, 2018; Grunert et al., 2016).

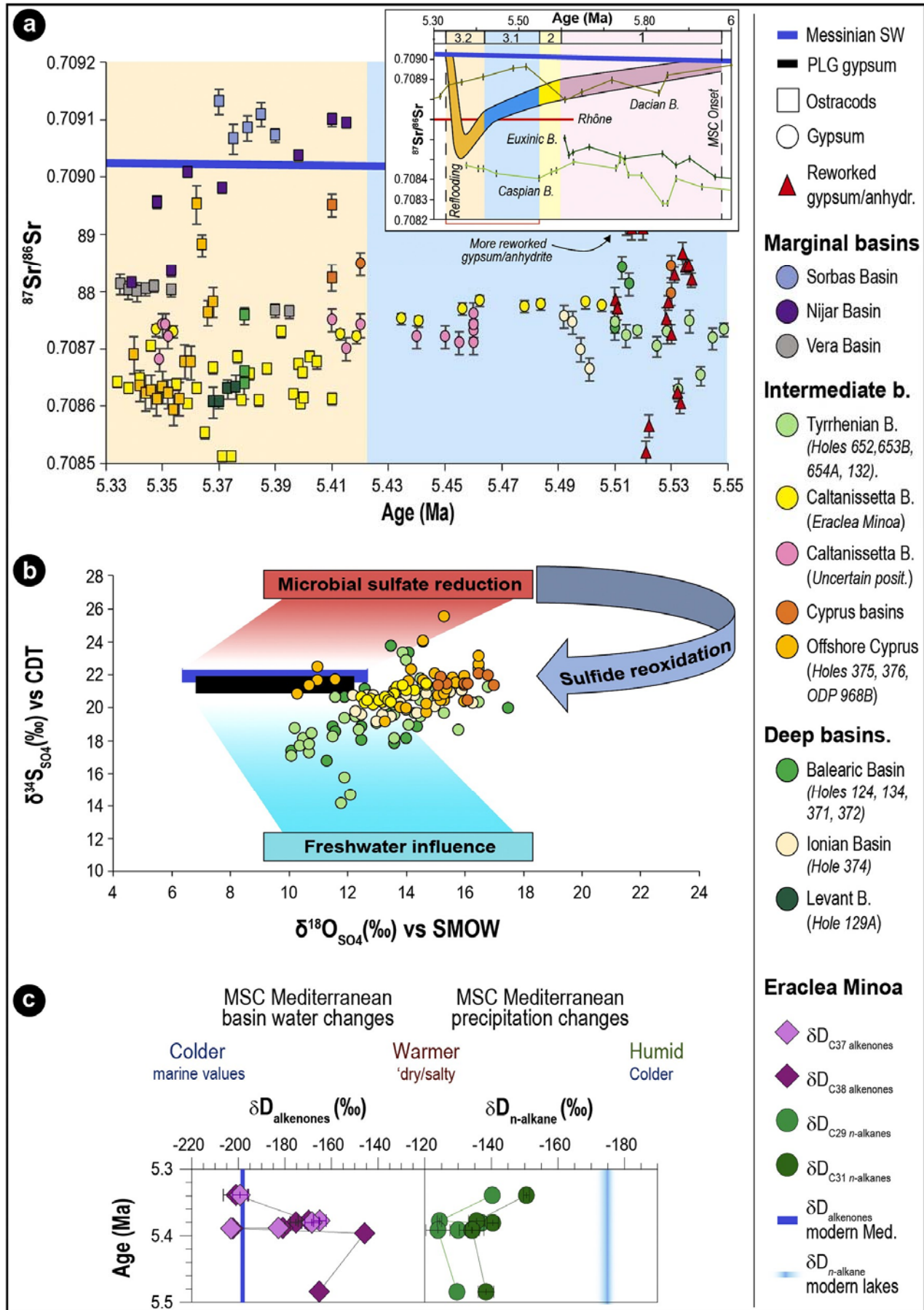
The more diverse and abundant ichthyofaunal record occurs in

substage 3.2 in a few marginal sections on the Italian peninsula (Ciabot Cagna in the Piedmont Basin; Cava Serredi and Podere Torricella in Tuscany; Capanne di Bronzo, La Vicenne and Ca' Ciuccio in thrust-top basins of the Northern and Central Apennines). The Lago-Mare fish remains mainly comprise otoliths of both euryhaline and stenohaline taxa indicative of marine, brackish, and freshwater habitats (Carnevale et al., 2018). Three articulated skeletons of the euryhaline marine taxa *Mugil cf. cephalus* (Fig. 9e), the marine Indo-Pacific species *Spratelloides gracilis* and of *Gobius* sp. have been identified at Cava Serredi in a horizon < 1 m below the Miocene/Pliocene boundary (Carnevale et al., 2006b). The dominant stenohaline families in these assemblages are Gobiidae, a family of demersal fish occupying shallow-water marine, brackish and freshwater environments, and Myctophidae, which are marine meso-pelagic fish that live below 200 m depth during the day, but feed at night in surface waters. A recent review of the Tortonian-Zanclean Gobiidae of the Mediterranean (Schwarzghans et al., 2020) showed that the otoliths of this family, described by Carnevale et al. (2006a, 2008, 2018) and Grunert et al. (2016) as belonging to marine Atlantic species, instead belong to brackish and freshwater species of Paratethyan affinity inhabiting sheltered prodelta environments. In fact, no normal marine demersal taxa were recognized in these assemblages by Schwarzghans et al. (2020). As for the Myctophidae, the vast majority of the taxa belonging to this family were recovered in Moncucco and Verduno from alluvial plain silty mudstones along with terrestrial mammals (Dela Pierre et al., 2011; Colombero et al., 2017 and references therein), pointing to a physically reworked origin. When ⁸⁷Sr/⁸⁶Sr isotope ratios are measured (Carnevale et al., 2008; Grunert et al., 2016), the resulting Sr-based age of the otoliths is > 7 Ma, therefore further arguing against their in-situ origin. Since the good preservation of the otoliths suggests they did not suffer physical reworking (Carnevale et al., 2006a, 2006b, 2008, 2018; Grunert et al., 2016), predators foraging in open marine settings and migrating to marginal environments are proposed as a way out of the enigma (Carnevale et al., 2008, 2018; Grunert et al., 2016; Colombero et al., 2017). However, Carnevale et al. (2006a) also rule out that so well preserved otoliths may have suffered post-mortem transport and action of the digestive acids in the stomach of predators. Rare findings of Myctophidae from Ciabot Cagna (3 species), Cava Serredi (1 species), Capanne di Bronzo (1 species) and Podere Torricella (6 species) (Carnevale et al., 2018) are all from sections where the host sediments have not been studied in sufficient detail to be clear about the *in situ* or reworked nature of the fossil assemblage. This lack of sedimentological uncertainty also extends to the stratigraphic position of many samples, because a stratigraphic log is provided for only a few sections (i.e. Ca' Ciuccio, Cava Serredi and Moncucco; Carnevale et al., 2006a, 2006b). What this stratigraphic information suggests is that euryhaline fish taxa are widespread throughout substage 3.2, whereas strictly Myctophidae, which are an oceanic, marine stenohaline species, only occur very close to the base of the Pliocene, plausibly corresponding to the uppermost lithological cycle in substage 3.2 (~5.35–5.33 Ma; Carnevale et al., 2018).

5.7 Summary of the Stage 3 paleontological record

The aquatic fossil record of MSC Stage 3 indicates that substage 3.1 in onshore sections is mostly barren, while diverse assemblages characterize substage 3.2 deposits. By contrast, the deep record as a whole contains relatively few, low diversity assemblages. This might be as a consequence either of the limited sample locations recovered from the offshore areas (see Fig. 2b) or because the environmental conditions in the intermediate-deep basins were less favorable for sustaining the life forms typical of the onshore domain. Nevertheless, the assemblages that are found in both marginal and deep locations comprise mixed brackish and marine species.

Brackish species are mostly represented by ostracods and dinocysts (and mollusks here not addressed because poorly studied; see Esu, 2007 and Guerra-Merchán et al., 2010). Prominent is the affinity of these late



(caption on next page)

Fig. 10. Isotopic record of MSC Stage 3 for the Mediterranean Basin. (a) Compilation of MSC Stage 3 $^{87}\text{Sr}/^{86}\text{Sr}$ isotope data sourced from ostracod valves and gypsum crystals (see Supplementary material 1 and subsection 6.1 for references). Data are plotted with the global $^{87}\text{Sr}/^{86}\text{Sr}$ seawater curve (McArthur et al., 2012). Error bars indicate analytical error, which is so small in some cases that no error bars are visible at this scale. To not complicate the figure, horizontal error bars have not been added for the sections/cores unprovided of a chronostratigraphic framework and for which age uncertainties are present (i.e. all but Nijar and Vera basins, Eraclea Minoa and onshore Cyprus; see Fig. 3). Note that none of the $^{87}\text{Sr}/^{86}\text{Sr}$ isotope ratios but one from Nijar plot on the ocean curve. In the inset is shown the Mediterranean Sr record for the entire MSC as well as the time-equivalent Eastern Paratethys record (modified after Andreetto et al., 2021). (b) Plot of $\delta^{34}\text{S}_{\text{SO}_4}$ and $\delta^{18}\text{O}_{\text{SO}_4}$ in Stage 3 gypsum and anhydrite beds from onshore and offshore localities (see Supplementary material 1 and subsection 6.2 for references). No measures are available from the marginal basins, where gypsum did not deposit during Stage 3. The dark blue and black rectangles represent the sulfate isotopic composition of the Global Messinian ocean and Stage 1 (PLG) evaporites, respectively. The light blue area represents the sulfate isotopic composition of mixtures of Messinian marine waters with non-marine sources. The red area represents the isotopic composition of the residual sulfate ion in a basin where marine Messinian sulfate is consumed by microbial sulfate reduction to produce H_2S . The arrow represents the isotope trajectory of dissolved sulfate resulting from the mixing of residual ^{34}S -enriched sulfate produced by MSR and ^{34}S -depleted sulfate produced by H_2S oxidation. All the published $\delta^{34}\text{S}_{\text{SO}_4}$ and $\delta^{18}\text{O}_{\text{SO}_4}$ values are provided corrected with the fractionation factors $\delta^{34}\text{S} = +1.65\text{‰}$ and $\delta^{18}\text{O} = +3.5\text{‰}$ to smooth the isotopic fractionation effects experienced by dissolved sulfate and to reason on values reproducing the isotopic composition at the time of gypsum precipitation. (c) δD isotopes of C_{29} and C_{31} -alkanes and C_{37} and C_{38} long chain alkenones recorded in the Stage 3 gypsums and marls of the Eraclea Minoa section (modified from Vasiliev et al., 2017). Blue lines indicate the values recorded in the present day lacustrine settings for the n -alkanes (Sachse et al., 2006) and in the alkenones from the Mediterranean in the recent times (Van der Meer et al., 2007). Error bars indicate standard errors of the mean.

Messinian Mediterranean brackish species with the same species that were simultaneously dwelling in the Eastern Paratethyan basins (Dacian, Euxinic and Caspian) and in the North Aegean. Since these organisms were not present in the Mediterranean at any time before the MSC, they are considered, with a broad consensus, as *in situ*. This conclusion is further corroborated by the mixing of adult and juvenile forms in the ostracod assemblages and by the good preservation of the specimens, which do not show typical evidence of physical reworking like abrasion, dissolution, or fragmentation. Still problematic is the time of their arrival in the Mediterranean and their likelihood as biostratigraphic tool. From our review it seems more likely that truly Paratethyan species of ostracods entered the Mediterranean already during substage 3.1, when they colonized intermediate-deep settings, while they entered the marginal basins at different times during substage 3.2. As for dinocysts, characteristic is their occurrence only in the uppermost Messinian. However, it must be noted that samples from the substage 3.1 interval are rarely processed for dinocysts, especially in age model-equipped sections (Fig. 3a). The route followed by the Paratethyan immigrants is equally contested and important for paleoenvironmental and paleohydrological interpretations. In view of a desiccated Mediterranean, their migration can only have taken place passively by means of aquatic migratory birds. Conversely, the homogeneity of the ostracod assemblages throughout the Mediterranean marginal basins is more indicative of the presence of a water body fed by Eastern Paratethys and connecting all Mediterranean subbasins, therefore implying relatively high water-level conditions (at least at times when ostracod-bearing sediments deposited; see Andreetto et al., 2021).

Marine assemblages are composed by foraminifera, nannofossils, dinocysts and calcareous nannofossils. Their reworked or *in situ* nature is in many cases contested but critical for paleoenvironmental interpretation. The picture that emerges from our review is that an open marine signature is questionable in the foraminifera, nannofossils, dinocyst and fish records, as well as in other biotic groups (e.g. corals, echinoids and mammals) here not tackled (and for which we refer the reader to Dominici et al., 2018 and Carnevale et al., 2019). All marine representatives of the above mentioned categories were reintroduced into the Mediterranean only at the beginning of the Pliocene and at the expense of the Paratethys species that, instead, disappeared. Collectively, these observations lead us to conclude that the marine model as conceived by Carnevale et al. (2006a, 2006b, 2008, 2018) and Grunert et al. (2016) has no foundation and therefore will not be further discussed.

6. The geochemical perspective

Variations in the water sources draining into the Mediterranean are expected to be reflected also in (geo)chemical properties of the paleodepositional environments. Important information about the nature of the connectivity framework of the Mediterranean can be gained by

interpreting geochemical signals that respond to the presence or absence of an exchange with a chemically-unique water body. Four main geochemical proxies have been applied so far to MSC Stage 3 sedimentary and paleontological records. These include both radiogenic (Sr isotope ratios) and stable isotopes (sulfate and oxygen) measured on fossils and minerals and hydrogen isotopes on molecular biomarkers. This section summarizes the dataset available for geochemical proxies (Fig. 10; Supplementary material 1) and its interpretation(s) for MSC Stage 3.

6.1 Strontium isotope ratios ($^{87}\text{Sr}/^{86}\text{Sr}$)

The available strontium isotope data for Stage 3 (Fig. 10a; Supplementary material 1) derive from measurements on both Ca-bearing fossils (ostracod valves, mollusk shells, fish otoliths; Fig. 9a) and minerals (calcite and gypsum), where Sr^{2+} dissolved in an aqueous solution substitutes Ca atoms due to their similar ionic radius (e.g. Hajj et al., 2017). Here we screen the available dataset and discuss only results that (1) reflect the original primary isotopic signal, i.e. the isotopic signal of the fluid at time of shell calcification or mineral precipitation, and (2) for which timing of mineral precipitation can be constrained. This screening excludes bulk carbonate samples (e.g. *Colombacci* limestones; Bassetti et al., 2004), which contain carbonate compounds of various and/or unknown provenance, measurements from mollusk shells and otoliths (e.g. Carnevale et al., 2008; Grunert et al., 2016; Roveri et al., 2019a), because they are made of mineral phases easily altered during diagenesis (e.g. aragonite; Marciano et al., 2015), and data coming from reworked material (e.g. all reworked gypsum or transported foraminifera). $^{87}\text{Sr}/^{86}\text{Sr}$ isotope ratios have also been measured by Müller and Mueller (1991) and Roveri et al. (2014b) on the halite beds recovered at Sites 134, 374 and 376 (Ryan et al., 1973; Hsü et al., 1978b). Although they provide interesting interpretative aspects, we do not consider these Sr measurements because the position of Sr in the crystal lattice of halite is unknown and the removal of all contaminants, that is not a straightforward procedure (see Meilijson et al., 2019), is not clear it was achieved by Müller and Mueller (1991) and Roveri et al. (2014b). As a matter of fact, there is no consistency between data generated from roughly the same interval in Core 134 by Müller and Mueller (1991) (0.708968) and Roveri et al. (2014b) (0.708800–0.708896). Added to this is the uncertainty over the provenance of halite in Sites 134 and 374 (see subsections 4.2 and 4.6.1), which violates both criteria mentioned above.

The general trend of the Mediterranean $^{87}\text{Sr}/^{86}\text{Sr}$ isotope ratio during the MSC deviates from the ocean curve towards the less radiogenic values of the major peri-Mediterranean rivers and Paratethys and returns abruptly to oceanic values at the Miocene/Pliocene boundary (Fig. 10a inset). This trend is regarded to reflect the progressive restriction of Mediterranean-Atlantic exchange and the relative increase in

the proportion of non-marine source waters (Topper et al., 2011; Roveri et al., 2014a). At first glance it seems that each MSC Stage was characterized by a well-defined range of Sr ratios (Fig. 10a inset), an observation that led Roveri et al. (2014b) to attribute a chronostratigraphic value to MSC $^{87}\text{Sr}/^{86}\text{Sr}$ ratios. A closer look, however, shows that MSC substages are anything but homogeneous with respect to $^{87}\text{Sr}/^{86}\text{Sr}$ ratios. At least in the marginal basins, local lithological differences in the catchments (each lithology carries a unique $^{87}\text{Sr}/^{86}\text{Sr}$ fingerprint; see subsection 8.1.1) explain the different Sr isotopic compositions from basin to basin (see Schildgen et al., 2014; Modestou et al., 2017; Andreetto et al., 2021), therefore arguing against the use of $^{87}\text{Sr}/^{86}\text{Sr}$ ratios for chronostratigraphic purposes in the MSC record.

Most of the data characterizing substage 3.1 (Fig. 10a) are from the Eraclea Minoa gypsum (Fig. 5h). These data define a narrow range of Sr isotope ratios between 0.708747 and 0.708793 (García-Veigas et al., 2018). Similar values were reported from both Eraclea Minoa and the nearby Siculiana Marina section (0.708710–0.708760; Keogh and Butler, 1999; Fig. 5i). The dominance of Sicily samples gives the appearance of a consistent Sr isotope signal for gypsum beds. However, data points from elsewhere (Cyprus, Manzi et al., 2016a; DSDPs 122, 371 and 372 in the Algero-Balearic Basin, ODPs 652, 653 and 654 in the Tyrrhenian Basin, DSDP 374 in the Ionian Basin; Müller et al., 1990; Müller and Mueller, 1991; Roveri et al., 2014b) display a wider range (from ~0.7087 to 0.708847; Fig. 10a) that may indicate a different hydrological regime for each basin (e.g. Müller et al., 1990; Müller and Mueller, 1991; Ryan, 2009). The one published Sr isotope value for ostracods found within one of the marl interbeds at Eraclea Minoa also has a lower value outside the typical Sicily gypsum range (Grossi et al., 2015). This suggests that a different hydrological regime may also have characterised precession minima stages of the precessional cycle.

The Sr isotope dataset for the Lago-Mare phase includes the lowest values measured on MSC sediments (~0.7085 from between gypsum VI and VII at Eraclea Minoa; Fig. 3a; Grossi et al., 2015) and the widest range of ratios spanning from 0.7085 to 0.7091, which is above coeval oceanic values (Fig. 10a). Again, the conspicuously high Sr isotope values in substage 3.2 come from two areas, the marginal basins of southern Spain (Andreetto et al., 2021 and references therein; Figs. 5a–c) and the intermediate Polemi Basin on Cyprus (McCulloch and De Deckker, 1989). The lower values are drawn from right across the intermediate-deep Mediterranean (Algero-Balearic, Sicily, Levant; Fig. 2a) and are therefore more likely to represent a Mediterranean-wide Sr isotope signal.

New Sr isotope data from Eastern Paratethys (i.e. Dacian and Caspian basins; Fig. 2b) are now available for the interval corresponding to MSC Stage 3 (inset Fig. 10a). The $^{87}\text{Sr}/^{86}\text{Sr}$ ratios of the Dacian Basin (0.708865–0.708982; Vasiliev et al., 2010; Grothe, 2016) are slightly lower than coeval ocean water (0.709020), but much higher than coeval Mediterranean values. However, the Dacian Basin is regarded as highly restricted from the Mediterranean throughout the MSC (Vasiliev et al., 2010). By contrast, the Caspian has very low values (0.708402 to 0.708473, Grothe et al., 2020) which are thought to reflect both the very low Sr isotope ratio of the Volga river (0.708020; Vasiliev et al., 2010 and references therein) and some input from the Mediterranean (Grothe et al., 2020).

6.2 Sulfate isotopes

Sulfur isotopic investigations have been carried out only on sulfate minerals (gypsum and more rarely anhydrite) of the MSC Stage 3 deposits with samples drawn from both onshore intermediate sequences (Caltanissetta Basin and Cypriot basins) and deep basinal records (Sites 122, 124, 125A, 132, 134, 372, 374, 375, 376, 652, 653, 654, 968, 969, 970; Fig. 10b; Fontes et al., 1973; Pierre, 1974, 1982; Pierre and Fontes, 1978; Ricchiuto and McKenzie, 1978; Pierre and Rouchy, 1990; Blanc-Valleron et al., 1998). Because the incorporation of dissolved sulfate into gypsum produces a nearly constant fractionation of $\delta^{18}\text{O}$ (+3.5‰) and

$\delta^{34}\text{S}$ (–1.65‰) at earth surface temperatures (Thode and Monster, 1965; Lloyd, 1968; Warren, 2016), $\delta^{18}\text{O}$ and $\delta^{34}\text{S}$ isotopic values measured in gypsum should be corrected with the above mentioned fractionation factors in order to reconstruct the sulfate isotopic composition of the basin waters at the time of gypsum formation.

The deep Mediterranean samples exhibit a wide range of $\delta^{34}\text{S}_{\text{SO}_4}$, but the majority of samples display $\delta^{34}\text{S}_{\text{SO}_4}$ values between 18 and 22‰, strongly indicative of a marine origin of the sulfate forming the gypsum (Fig. 10b; Fontes et al., 1973; Pierre, 1974, 1982; Pierre and Fontes, 1978; Pierre and Rouchy, 1990; Blanc-Valleron et al., 1998). The $\delta^{34}\text{S}_{\text{SO}_4}$ values lower than marine sulfate in the dataset are generally considered to represent a greater influence of continental sulfate input to the basin (Fig. 10b; Pierre, 1974; Pierre and Fontes, 1978; Pierre and Rouchy, 1990). By contrast, the data display $\delta^{18}\text{O}_{\text{SO}_4}$ isotopic values that deviate substantially from marine $\delta^{18}\text{O}_{\text{SO}_4}$ values towards higher values (Fig. 10). This is consistent with the influence of sulfate produced by reoxidation of reduced sulfur compounds generated by microbial sulfate reduction (MSR; Kaplan and Rittenberg, 1964; Brunner and Bernasconi, 2005; Sim et al., 2011; Leavitt et al., 2013). The microbial use of SO_4^{2-} leads to an equilibration of $\delta^{18}\text{O}_{\text{SO}_4}$ with ambient water oxygen, whereas the $\delta^{34}\text{S}_{\text{SO}_4}$ returns towards its initial value as a higher fraction of sulfide produced by MSR is re-oxidated. This mechanism has been suggested for Sites in the Algero-Balearic, Tyrrhenian and Ionian basins and offshore Cyprus (Pierre, 1974; Pierre and Fontes, 1978; Pierre and Rouchy, 1990). Although some authors have suggested that partial equilibration of sulfate oxygen toward $\delta^{18}\text{O}_{\text{H}_2\text{O}}$ values of the basin enriched in heavy oxygen isotopes by evaporation have led to an increase in $\delta^{18}\text{O}_{\text{SO}_4}$ values without significant changes in $\delta^{34}\text{S}_{\text{SO}_4}$ (Fontes et al., 1973; Pierre, 1974; Ricchiuto and McKenzie, 1978), this hypothesis seems highly unlikely as the abiotic equilibration between sulfate and water oxygen take about 20 Myr at normal marine pH (Lloyd, 1968; Longinelli and Craig, 1967; Turchyn et al., 2006). Moreover, the microbial sulfate reduction process is supported by the presence of pyrite at Sites 132, 654A and 968 (Pierre, 1982; Pierre and Rouchy, 1990; Blanc-Valleron et al., 1998) and the existence of filaments of possible microbial origin at Site 654A (Pierre and Rouchy, 1990).

The sulfate isotopic values reported by Longinelli (1979) and Pierre (1982) from the Upper Gypsum of Eraclea Minoa (Caltanissetta Basin, Sicily) are considerably more scattered than those from a recent study by García-Veigas et al. (2018; Fig. 10b). Such discrepancies are probably a consequence of different sample selection: García-Veigas et al. (2018) analyzed only pristine whitish selenite and balatino samples, while Longinelli (1979) and Pierre (1982) analyzed all types of gypsum-bearing samples such as “gypsiferous marl” and gypsum laminae intercalated in carbonate or diatomaceous intervals. These less pristine samples probably contain high quantities of ^{34}S -depleted solid sulfides or diagenetic gypsum formed by oxidation of sulfides (see Liu et al., 2017 for more details on this process) and are therefore unlikely to be representative of the primary gypsum facies. Once these data are excluded, the Eraclea Minoa sulfate values ($\delta^{18}\text{O}_{\text{SO}_4}$ from 12.4 to 14.6‰ and $\delta^{34}\text{S}_{\text{SO}_4}$ from 21.0 to 22.3‰) suggest a marine origin of the sulfate and stable redox conditions during gypsum deposition (Fig. 9.b; García-Veigas et al., 2018). Interestingly, the Eraclea Minoa sulfate values are in compliance with the isotopic values ($\delta^{18}\text{O}_{\text{SO}_4}$ 15.2 to 16.8‰; $\delta^{34}\text{S}_{\text{SO}_4}$ = 20.4 to 21.9‰) measured by Pierre (1982) in the Polemi Basin (Cyprus).

6.3 Hydrogen isotopes on molecular biomarkers

From the point of view of the application of organic geochemistry proxies, the Miocene Mediterranean Basin received little attention so far, with biomarker-based proxies that have been mostly applied to (a limited number of) pre-MSC sequences (Tzanova et al., 2015; Herbert et al., 2016; Mayser et al., 2017; Natalicchio et al., 2017, 2019; Vasiliev et al., 2019) and pre-Stage 3 sedimentary records (Lower Evaporites on Sicily, Andersen et al., 2001; Vena del Gesso Basin, Sinninghe Damsté

et al., 1995 and Vasiliev et al., 2017; Levant Basin, Meilijson et al., 2019). To date, only one study analyzed Stage 3 samples (Vasiliev et al., 2017). This study used compound specific hydrogen isotope (δD) analyses, measured on both terrestrial (long chain C_{29} and C_{31n} -alkanes; Sachse et al., 2006) and aquatic (alkenones; Englebrecht and Sachs, 2005) biomarkers from the gypsum beds of the Upper Gypsum at Eraclea Minoa to reconstruct the hydrological cycle during gypsum precipitation. Both δD_{C_{29n} -alkane and $\delta D_{alkenones}$ results (Fig. 10c) suggested that conditions in Sicily were significantly dryer than today, with highly enriched values of δD_{C_{29n} -alkanes (up to -125‰). The $\delta D_{alkenones}$ varied between values suggesting evaporative conditions (-125‰) and values typical for present-day $\delta D_{alkenones}$ in the Mediterranean ($+203\text{‰}$) (Vasiliev et al., 2017). No time-equivalent biomarker data from the open ocean settings are currently available. Instead, Vasiliev et al. (2017) compared their Mediterranean data with data from the Black Sea (DSDP 42B Hole 380 and Taman peninsula; Vasiliev et al., 2013, 2015). The Upper Gypsum δD_{n} -alkanes were more enriched when compared to their time equivalent deposits of the DSDP 42B 380 borehole of the Black Sea ($+180\text{‰}$). This probably reflects the more intracontinental position of the Black Sea which commonly translates into more depleted values for $\delta D_{precipitation}$ used by the vegetation, resulting in more depleted δD_{C_{29n} -alkanes. However, there is a 30 to 40‰ enrichment relative to present in the δD_{n} -alkanes (i.e. $\delta D_{precipitation}$) in both Mediterranean and Paratethys domains, indicating concurrent changes in both areas during the latest phase of the MSC.

Both the Mediterranean and Paratethyan samples contain $\delta D_{alkenones}$ with low values ($\sim -200\text{‰}$) (Fig. 10c) leading Vasiliev et al. (2017) to suggest that either the surface water from the Upper Gypsum was derived from the Black Sea, or that the Mediterranean and Paratethys were exchanging surface water during gypsum precipitation. Similarity between the relative contribution of the C_{37} , C_{38} and C_{39} alkenones at Eraclea Minoa and one of the Black Sea samples may suggest common alkenone producers for the two areas, again supporting the idea of a Mediterranean-Paratethys connection during Stage 3 (Vasiliev et al., 2017).

A final speculative insight from this biomarker dataset is that the relative contribution of alkenones found in the Upper Gypsum of Eraclea Minoa is strikingly similar to present-day open marine samples, even though *Emiliania huxleyi*, the principal ocean alkenone producer today, did not exist in the late Miocene. Vasiliev et al. (2017) suggested that this could imply the existence of a connection to the open ocean during Upper Gypsum deposition in Sicily (i.e. throughout Stage 3; Fig. 3a).

6.4 Oxygen isotopes

Oxygen stable isotope data ($\delta^{18}O$) are available from bulk samples (Rouchy et al., 2001, 2003, 2007; Pierre et al., 2006; Cosentino et al., 2012), gypsum (Pierre and Fontes, 1978; Ricchiuto and McKenzie, 1978; Lugli et al., 2007), mollusk shells (Carnevale et al., 2008; Grunert et al., 2016) and ostracod valves (Cosentino et al., 2012; Grossi et al., 2015).

For all the sub-basins for which there is latest Messinian data (e.g. Sites 974 and 975; Eraclea Minoa section, Sicily; Aghios Stefanos section, Corfu; Kalamaki section, Zakynthos; Pissouri Basin, Cyprus; Rouchy et al., 2001, Pierre et al., 2006), each has its own range of oxygen isotopic compositions and its own degree of variability. Values from above the Miocene/Pliocene boundary regain seawater values of 0.3 to 1 ‰ (e.g. Pierre et al., 2006).

In marginal marine settings and lakes, the controls over $\delta^{18}O$ are poorly constrained as oxygen does not respond simply to the freshwater flux, but to a combination of variables such as temperature, rainfall and evaporation (e.g. Placzek et al., 2011). Freshwater input may contribute to the signal, resulting in $\delta^{18}O$ more negative than seawater (0.3‰ to 0.8‰ SMOW; Dettman et al., 2004), but under prevailing evaporating conditions it is likely that the $\delta^{18}O$ will be primarily influenced by

evaporation, leading to $\delta^{18}O$ more positive than seawater (e.g. Dettman et al., 2004), making any data very difficult to interpret. Furthermore, the lack of a unique $\delta^{18}O$ signature for each water source makes oxygen isotopes a difficult tracer proxy to use.

6.5 Summary of the Stage 3 geochemical dataset

The variety of paleoenvironmental and connectivity proxies applied to MSC Stage 3 record provide valuable insights into the hydrological conditions during Stage 3. The more outstanding results from all discussed proxies are that:

- 1) Paleodepositional subaqueous environments where gypsum was precipitating and ostracods and biomarker-producers were thriving were strongly dominated by non-oceanic inputs;
- 2) An indisputable marine signal is absent and only regained above the M/P boundary.

Sulfate and oxygen isotopes are currently difficult to use for water provenance reconstruction because the non-marine sources (local and major rivers and Eastern Paratethys) that are likely to be of influence lack distinctive isotopic signatures and, especially for oxygen, respond to a combination of controls (e.g. temperature, rainfall, evaporation) with local variability. $\delta^{34}S_{SO_4}$ are claimed by several authors to be aevidence of the presence of an Atlantic inflow ($\delta^{34}S_{SO_4} = 22\text{‰}$; Turczyn and Schrag, 2004) in a Mediterranean strongly affected by non-marine waters (Manzi et al., 2009, 2016a; García-Veigas et al., 2018 among others). However, the same values can be obtained by means of the recycling of PLG deposits ($\sim 23\text{‰}$; Lu et al., 2001; Lugli et al., 2010; García-Veigas et al., 2018).

Similarities between the $\delta D_{alkenones}$ of the Upper Gypsum at Eraclea Minoa and coeval Black Sea sediments and δD_{n} -alkanes similar to present-day marine settings, suggest that Eastern Paratethys and the Atlantic were simultaneously contributing to the Mediterranean hydrological budget. $^{87}Sr/^{86}Sr$ isotope ratios are a useful water-mass tracer because each water body carries a unique Sr isotope fingerprint (see subsection 8.1.1). Our plotting of Stage 3 $^{87}Sr/^{86}Sr$ isotope values (Fig. 10a) highlights the large geographical variability of the values and the sharp division between Sr isotope ratios measured in marginal basins versus those in intermediate-deep water locations. This is only noticeable in substage 3.2, since no (or not enough) material suitable for Sr analysis is present in substage 3.1 deposits from the marginal basins. Some authors see this variability as an indication of isolated subbasins with unique hydrological conditions driven by their catchment rivers (e.g. Müller et al., 1990; Müller and Mueller, 1991; Ryan, 2009). If some degree of connection was present, it involved only neighbouring basins (e.g. Tyrrhenian subbasins; Müller et al., 1990; Müller and Mueller, 1991). A recent comparison of the Sr isotope record of the Spanish marginal basins of Sorbas, Nijar and Vera with the Sr isotope ratios likely to have typified the local riverine sources demonstrated that a local sources-mixed signal expected from an endorheic lake in that location is absent. In this instance mixing of intrabasin water sources with a non-marine Mediterranean water mass is used to explain the measured values (Andreetto et al., 2021). If this explanation is more widely applicable, then it may result in a re-interpretation of the spread of Sr isotope data from the latest Messinian interval.

To conclude, geochemical proxies have great potential to test the different scenarios, but data are currently too numerically and geographically limited to be robust.

7. Paleoenvironmental scenarios for freshening the salt giant: desiccated versus full Mediterranean

The riddle of the Mediterranean environmental and hydrological conditions during Stage 3 is a highly debated topic and it is key to understanding the means by which open marine conditions were restored

at the base of the Zanclean and on the potential impact that the Atlantic-Mediterranean re-connection had on the Atlantic and global climate (Flecker et al., 2015; Capella et al., 2019). In this chapter, the paleo-environmental scenarios, in terms of base-level position (desiccated or full Mediterranean) and hydrological configuration (connections to the Atlantic and/or Paratethys), proposed for the Mediterranean during Stage 3 are described, as well as the different timings of the reflooding (instantaneous, gradual, step-like increments). The low-salinity Stage 3 followed the hypersaline Stage 2 and the transition between the twolikely influences the plausibility of the various paleoenvironmental scenarios proposed for the terminal stage. We therefore first summarize the current understanding of the configuration of the Mediterranean during Stage 2 and the enduring controversies (see Roveri et al., 2014a for a more extensive review).

6.6 Stage 2 (5.59-5.55 Ma): formation of the Mediterranean salt giant

Numerical modelling based on hydrological budget calculations shows that in order to reach salinity levels compatible with halite saturation and to accumulate the substantial thicknesses of halite observed in the seismic profiles (Ryan, 1973; Haq et al., 2020), the Atlantic-Mediterranean gateway needs to have permitted inflow from the Atlantic, but may have completely blocked outflow (Blanc, 2002; Krijgsman and Meijer, 2008). Numerical models also showed that without Atlantic inflow into the Mediterranean Sea its base level is forced to drop on time scales in the order of a few thousand years by virtue of the basin's negative hydrological budget, where more water is lost to the atmosphere by evaporation than is received from rainfall and river runoff (e.g. Meijer and Krijgsman, 2005; Krijgsman and Meijer, 2008; Simon et al., 2017). The idea of a drawdown is supported by several arguments: (1) the widespread presence, from the margins to the slopes, of the Messinian Erosional Surface cutting through Stage 1 and pre-MSC deposits and canyon incisions following today's drainage networks (e.g. Chumakov, 1973; Clauzon, 1982; Lofi et al., 2005, 2011a, 2011b; Loget et al., 2006; Maillard et al., 2006, 2020; Estrada et al., 2011; Just et al., 2011; Urgeles et al., 2011; Amadori et al., 2018; Lymer et al., 2018; Cazzini et al., 2020; Figs. 5e, 7e); (2) their morphology

interpreted as subaerial in origin; (3) the clastic fans at the outlet of the valleys overlapped by Stage 3 deposits and interpreted as fluvial accumulations (e.g. Lofi et al., 2005; Maillard et al., 2006; Pellen et al., 2019). A number of studies have tried to quantify the magnitude of the sea-level fall by compensating for the isostatic vertical motion since the Messinian to obtain the original depth of the erosional features and Messinian deposits. However, this depends on the assumptions about when the drawdown occurred relative to the halite precipitation: before (e.g. Cartwright and Jackson, 2008; Bache et al., 2009, 2012), during (e.g. Ryan, 2008, 2009) or after (e.g. Ryan, 1978; Bertoni and Cartwright, 2007; Lofi et al., 2011a, 2011b). How shallow the Mediterranean became during Stage 2 is also a matter of disagreement. Estimates in the Western Mediterranean vary from a maximum drawdown of 2500 m (Ryan, 1976) to 1000-1500 m (Bache et al., 2012) in the Gulf of Lion, 800-1200 m in the Balearic promontory (Mas et al., 2018b) and 400 m in the Ebro delta region (Frey-Martinez et al., 2004). A later backstripping analysis of this delta yielded a drawdown of ~1300 m (Urgeles et al., 2011). East of the Sicily sill, backstripping studies estimated base-level drops of 1800-2000 m in the Ionian basin (Micallef et al., 2018, 2019; Camerlenghi et al., 2019; Spatola et al., 2020), 800-900 m in the Adriatic foredeep and Po plain (Ghielmi et al., 2013; Amadori et al., 2018), 800-1300 m (Ben-Gal et al., 2005), 600 (Druckman et al., 1995) and 800m (Cartwright and Jackson, 2008) in the Levant Basin.

None of these quantifications could unequivocally constrain the timing of the drawdown within the MSC sequence, but numerical modeling studies show that, if the blocking of the outflow was controlled by a tectonic uplift counteracted by inflow erosion across the Strait of Gibraltar, then the expected drawdown of the Mediterranean Sea should be moderate (< 400 m; and possibly harmonic) due to an equilibrium between incision and uplift before the complete blocking of inflow and larger (up to complete desiccation) only after tectonic uplift overcame incision rates (Garcia-Castellanos and Villaseñor, 2011). The same model suggests that the initiation of halite precipitation might overlap in time with the late primary gypsum deposition, right before the full disconnection from the Atlantic Ocean.

The interpretation of the deep evaporites and their associated seismic markers (erosional surfaces and deep engravings along the shelf-slope

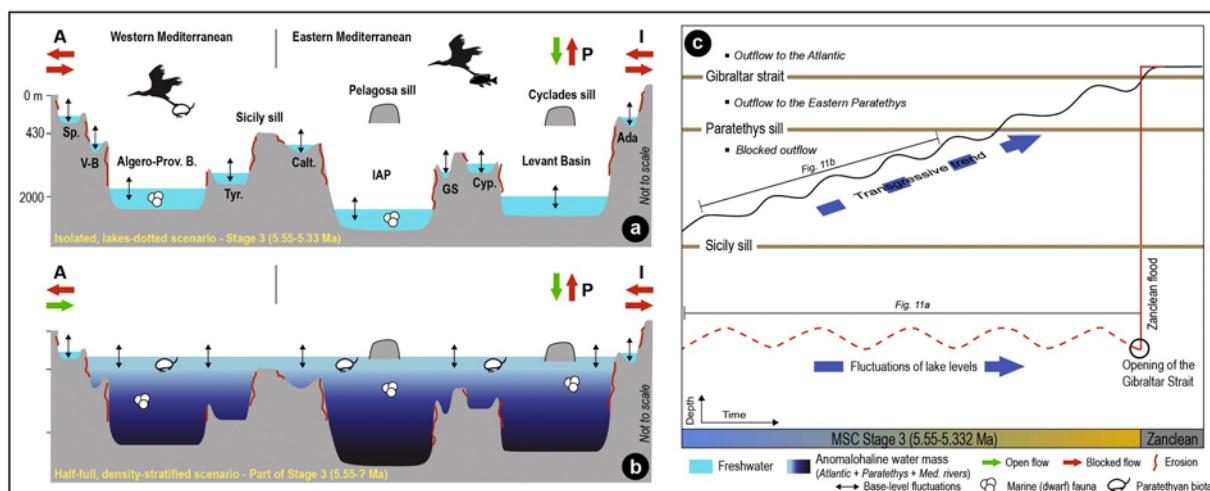


Fig. 11. (a), (b) Schematic W-E profiles across the Mediterranean Basin showing the contrasting paleoenvironmental, paleohydrological and paleoconnectivity interpretations proposed for Stage 3. When a water flow is present (green arrow) from and/or to an extra-Mediterranean water mass (i.e., A: Atlantic Ocean; I: Indian Ocean; P: Eastern Paratethys), the direction of the arrow gives the direction of flow. For simplicity, water added by the major and local rivers is not shown, but it adds to the hydrological budget at any time in each scenario. Note the main difference between the isolated (a) and density-stratified (b) scenario lies in the connectivity framework (Atlantic connection closed and negligible influence from the Paratethys in the isolated scenario; influence from both Atlantic and Paratethys in the density-stratified scenario), which affects the position of the base level of the Mediterranean water mass and its hydrochemistry (see extensive discussion in sub-section 7.2). Abbreviations: Sp.: SE Spain; V-B: Valencia Basin; Tyr: Tyrrhenian Basin; Calt: Caltanissetta Basin; IAP: Ionian Abyssal Plain; GS: Gulf of Sirt; Cyp: Cyprus; Ada: Adana Basin. See Fig. 2 for the geographic position of each basin. (c) Schematic plot showing the evolution of the Mediterranean base-level during Stage 3 according to both the isolated (red line) and half-full (black line) scenarios. The critical sills for controlling intra- and extra-Mediterranean connectivity are also shown.

systems) is not straightforward. Recently, it was suggested that the deep evaporitic facies and the seismic morphological features could have been produced without a significant drop of the Mediterranean base-level, therefore promoting the persistence of a relatively deep-water Mediterranean basin even during halite deposition (Lugli et al., 2013, 2015; Roveri et al., 2014b). For example, Roveri et al. (2014c) proposed that downslope flows of dense, hypersaline waters sourced from evaporation in shallower water areas could have generated both the observed shelf-slope erosion and have created a deep brine, supersaturated in the ions necessary for precipitating halite. These subaqueous hyperpycnal flows are consistent with the observed clastic evaporites that filled the Levant margin canyons (Lugli et al., 2013) and, more generally, with the widespread presence of Complex Units at the outlet of the MES drainage systems (see Lofi et al., 2005, 2011a, 2011b; Lofi, 2018). These sediments are dominated by reworked PLG that would have been exposed by a sea-level fall as little as 200 m (Lugli et al., 2010). However, the hypersaline environment that is presumed to be established by these hyperpycnal flows during the deposition of the RLG is in contrast with the occurrence of the Paratethyan ostracod *L. muelleri* within the clastic evaporites (RLG) in several marginal sections (e.g. Adana Basin, Faranda et al., 2013; Radeff et al., 2016, 2017). Whatever the state of Mediterranean base-level during Stage 2, the more commonly used chronostratigraphic model for the MSC (Fig. 1a; Roveri et al., 2014a) states that massive halite precipitation ceased at 5.55 Ma and was superseded by an environment that, with precession periodicity (Fig. 3a), cycled between gypsum precipitation and conditions that saw fresh-brackish organisms thriving. The question is whether these conditions cycled homogeneously in several isolated lakes or in basins largely connected to the same Atlantic and Eastern Paratethys-influenced water mass (Fig. 11).

6.7 Stage 3 (5.55-5.33 Ma): resumption of (upper) gypsum precipitation and Paratethys fauna invasion

6.7.1 An isolated Mediterranean dotted by sabkhas and lakes

The first and long-lasting paleoenvironmental interpretation of the evaporite-bearing UG/UU units and (possibly) time-equivalent evaporite-free units (e.g. LM Unit in Malaga, Sorbas and Zorerras Mb. in Sorbas, Feos Fm. in Nijar, Cassano Spinola Conglomerates in Piedmont, San Donato/Colombacci fms. in the Apennines, Handere Fm. in Turkey) envisaged their sedimentation in a Mediterranean mostly isolated from the Paratethys (which may have added water only to some basins in the Eastern Mediterranean) and totally isolated from the Atlantic where, in each subbasin, continental settings (e.g. alluvial plains, river channels, alluvial fans, playa lakes, sabkhas) alternated/interfingered with shallow, endorheic lakes (Figs. 11a, c; e.g. Ruggieri, 1962, 1967; Decima and Sprovieri, 1973; Decima and Wezel, 1973; Friedman, 1973; Hsü et al., 1973a, 1973b, 1973c; Hsü et al., 1978a, 1978b; Ryan et al., 1973; Selli, 1973; Sturani, 1973; Sissingh, 1976; Benson, 1978; Bossio et al., 1978; Cita et al., 1978, 1990; Ricchiuto and McKenzie, 1978; Ryan, 1978, 2008, 2009; Cita and Colombo, 1979; Orszag-Sperber and Rouchy, 1979; Ghibaudo et al., 1985; Müller et al., 1990; Benson and Rakic-El Bied, 1991; Benson et al., 1991; Müller and Mueller, 1991; Orszag-Sperber et al., 2000; Rouchy et al., 2001, 2003, 2007; Blanc, 2002; Lofiet al., 2005, Lofi et al., 2011b; Bassetti et al., 2006; Rouchy and Caruso, 2006; Bertoni and Cartwright, 2007; Comeselle and Urgeles, 2017; Amadori et al., 2018; Camerlenghi et al., 2019; Kartveit et al., 2019; Madof et al., 2019; Ben Moshe et al., 2020; Caruso et al., 2020; Cazzini et al., 2020; Raad et al., 2021). The full disconnection is also supported by observations that support an abrupt Zanclean reflooding (e.g. Blanc, 2002; Micallef et al., 2018, 2019; Garcia-Castellanos et al., 2020; Spatola et al., 2020), since a rapid outburst flood requires a large sea level difference prior to the flood that can only be developed in a scenario of a full Mediterranean-Atlantic disconnection (Garcia-Castellanos et al., 2009; Garcia-Castellanos and Villaseñor, 2011). Although rarely explicitly stated, all these studies must assume that:

- 1) all Paratethyan biota (and possibly other organisms of undisclosed provenance like diatoms) migrated passively via aquatic migratory birds across the entire Mediterranean (Fig. 11a; Benson, 1978; Benson and Rakic-El Bied, 1991; Caruso et al., 2020);
- 2) chemical and physical conditions (brackish water and water depth not exceeding 100 m; e.g. Hajós, 1973; Gliozzi and Grossi, 2008) that allowed alternated conditions suitable for gypsum to precipitate and Paratethyan biota and euryhaline benthic foraminifera to thrive were related to changes in the local freshwater budget;
- 3) The marine isotopic signals in UU/UG gypsum (Fig. 10) are entirely the reflection of the lithologies that are leached by continental waters in surficial and/or underground drainage areas (e.g. Ryan, 2009; Raad et al., 2021);
- 4) Stage 3 gypsum precipitated in extremely shallow-water (playa lakes) to completely dried environments (sabkhas) and the excessive sulfate necessary is completely derived from "clastic reworking, dissolution, re-precipitation and diagenesis of materials belonging to the PLG and halite of the previous MSC Stage 2" (Ryan, 2009).

Observations supporting a Mediterranean isolated throughout Stage 3 and only at the mercy of local freshwater inputs (Fig. 11a) are: (1) the lack of evidence for in situ marine fauna and flora in UU (e.g. Ryan et al., 1973; Hsü et al., 1978a; Cita et al., 1990; Ryan, 2009; Lofi et al., 2011a);

(2) the shallow-water mode of life and highly likely in-situ nature of ostracods and euryhaline, shallow-water benthic foraminifera observed in DSDP/ODP wells from intermediate and deep basins (e.g. Cita et al., 1978; Iaccarino and Bossio, 1999; Figs. 9a-c); (3) the bathymetric contrast (up to several hundred meters) between the late Messinian paleoenvironments and the marine Zanclean on top (e.g. Cita and Colombo, 1979; Bonaduce and Sgarrella, 1999; Caruso et al., 2020); (4) the presence of paleosols in Cyprus (Orszag-Sperber et al., 2000; Rouchy et al., 2001) and on the crest of the Eratosthenes seamount (Robertson, 1998a, 1998b); (5) the erosional features preserved both offshore on the continental shelves and lower-middle slope domain and interpreted in most seismic stratigraphic studies as the result of subaerial exposure (e.g. Lofi et al., 2005; Lofi et al., 2011b; Lymer et al., 2018; Ben Moshe et al., 2020); (6) the pinching out of the UU/BU units towards evaporite-free pre-Messinian structural highs (Figs. 7b-g; Figs. 8a, e; Ryan, 2009; Lymer et al., 2018; Camerlenghi et al., 2019; Raad et al., 2021); (7) the more abundant terrigenous clasts and reworked calcareous fossils in Stage 3 samples compared to the overlying, deep-water Pliocene (Ryannet al., 1973; Hsü et al., 1978b; Ryan, 2009); (8) the erosional nature of the M-reflector/TES/IMTS in the Levant Basin (Figs. 8e-g), by some linked to subaerial exposure of the Levant seafloor (e.g. Bertoni and Cartwright, 2007; Lofi et al., 2011a, 2011b; Maillard et al., 2011a) before the emplacement of deposits interpreted as fluvial from seismic observations (Bowman, 2012; Radeff et al., 2017; Leila et al., 2018; Kartveit et al., 2019; Madof et al., 2019). Furthermore, (9) isolated hydrological circuits with unique chemical composition are regarded by Camerlenghi et al. (2019) as the most plausible explanation for the W-E change in the MSC sedimentary expression in the deep basins, represented by the trilogy LU-MU-UU in the Algero-Balearic and Liguro-Provençal basins, missing the LU in the Tyrrhenian and (possibly) Ionian basins, by terrigenous deposits with hiatuses in the WAB and Adriatic foredeep and by halite, anhydrite and clastics in the Levant Basin (Interbedded and Argillaceous evaporites of Meilijson et al., 2019; Fig. 3b).

The main problems with the isolated scenario lasting throughout Stage 3 are: (1) it does not provide an explanation neither for the homogeneity of Paratethyan ostracod assemblages in the marginal basins (e.g. Gliozzi et al., 2007; Stoica et al., 2016), an aspect difficult to explain when fauna migration takes place passively via either birds or wind, nor for the biomarkers (Vasiliev et al., 2017), which cannot be transported effectively by aquatic birds; (2) it does not explain the mismatch between $^{87}\text{Sr}/^{86}\text{Sr}$ isotope ratios measured on marginal ostracods and Sr values expected from endorheic lakes fed with local

freshwaters (e.g. Andreetto et al., 2021); 3) it misses to substantiate, with geochemical arguments, the precipitation of gypsum in lakes, a process that is everything but straightforward (see Warren, 2016 for insights); 4) except for the salt-bearing basins, the source(s) of solutes which makes freshwater-fed endorheic lakes brackish and causes similar physico-chemical conditions to exist in each lake is also difficult to explain in the context of a Mediterranean only at the mercy of local rivers.

7.2.2. The half-full, density-stratified Mediterranean scenarios

An alternative concept to the isolated scenario envisages the Mediterranean connected with the Atlantic and/or the Eastern Paratethys and relatively full of water connecting the different subbasins (Fig. 11b). To our knowledge, this scenario was first developed by McCulloch and De Deckker (1989) on the basis of the similar $^{87}\text{Sr}/^{86}\text{Sr}$ ratios from marginal (Spain and Cyprus) and deep (Levantine and Algero-Balearic) basins. This intuition was a significant departure from the far more in vogue desiccated scenario (see conclusion of Hsü et al., 1973b), and for this was long overlooked. Sr isotope ratios lower than contemporary ocean water led McCulloch and De Deckker (1989) to conclude that a brackish water mass created by the mixing of water from the peri-Mediterranean rivers (e.g. Nile, Rhône and African rivers that no longer flow today, etc.; see Griffin, 2002 and Gladstone et al., 2007) with water of the Eastern Paratethys filled the Mediterranean, resembling the Caspian Sea today. This conclusion is consistent with the impoverished (or absent) marine fauna and flora of Stage 3 sediments and the enhanced assemblage of fresh-brackish water biota (see subsection 5.7; Figs. 9a-c), but is problematic as a viable origin for Stage 3 gypsum to precipitate at depth. Furthermore, climate models for the late Miocene fail to fill the Mediterranean Basin with fluvial and Paratethys waters alone (Gladstone et al., 2007; Marzocchi et al., 2016, 2019; Simon et al., 2017). A marine contribution is therefore required to fill the Mediterranean (Marzochiet al., 2016). In the event, the contribution is most likely to have derived from the Atlantic via the Gibraltar Corridor (Flecker et al., 2015; Booth-Rea et al., 2018; Krijgsman et al., 2018) either through a karst system (Krijgsman et al., 2018) or an emerged volcanic archipelago in the Alborán Basin (Booth-Rea et al., 2018). In fact, although an Indian Ocean contribution was proposed (Cita et al., 1978; Hsü et al., 1978a) and the possibility discussed (Ryan, 2009; Vai, 2016), palinspastic reconstructions concluded that the Neo-Tethys Mediterranean-Indian Ocean connection via southern Turkey and Iran already closed before the Tortonian (Rögl, 1998; Popov et al., 2004; Gargani et al., 2008; Bialik et al., 2019; Gülyüz et al., 2020), while a seaway via the Red Sea and Gulf of Aden, although not completely ruled out (e.g. Schütz, 1994; Bosworth et al., 2005; Gargani et al., 2008; Ryan, 2009), is highly contested (e.g. Meulenkamp and Sissingh, 2003; Segev et al., 2017).

In light of this, Roveri et al. (2014c), Gvirtzman et al. (2017), Vasiliiev et al. (2017), García-Veigas et al. (2018) and Grothe et al. (2020) suggested that the Mediterranean was likely density-stratified during this interval as a result of the simultaneous influx of isotopically-different marine and non-marine (major Mediterranean rivers and Eastern Paratethys) water sources (Fig. 11b). This connectivity framework resulted in a brackish layer carrying low-salinity (mostly Paratethyan) biota (Gliozzi et al., 2007; Stoica et al., 2016; Grothe et al., 2018, 2020; Figs. 9a-b) to lay on top of a more saline layer formed by Atlantic-derived seawater from which UU/UG gypsum (Figs. 5h-j, 7b-g, 8a-d), that facies analyses demonstrated to result from subaqueous deposition (Hardie and Lowenstein, 2004; Lugli et al., 2015), precipitated at intermediate and greater depths (e.g. García-Veigas et al., 2018). A dense, anoxic deep-water mass, possibly inherited from Stage 2, is envisaged at the bottom of the Mediterranean by Marzocchi et al. (2016) and García-Veigas et al. (2018), albeit without conclusive arguments, and by Gvirtzman et al. (2017) following the observation that the tilted halite body of the Levant Basin was simultaneously eroded landward and preserved basinward (Fig. 8f).

This scenario accounts for the erosive/non-depositional features

(Figs. 5e, 6a, e) and continental/lacustrine facies (Figs. 5a-b, d-g) widespread around the margins and shelves and suggestive of a Mediterranean base-level somewhat lower than the Atlantic level suggesting a one-way inflow from both the Atlantic and the Eastern Paratethys after Stage 2 (e.g. Marzocchi et al., 2016; Figs. 11b, c), a connectivity configuration that effectively translates in a half-full Mediterranean (e.g. Krijgsman and Meijer, 2008). Refilling as a result of persistent Atlantic inflow, in part perhaps because of the latest Messinian deglaciation (see subsection 2.2; Van der Laan et al., 2006; Hilgen et al., 2007), would have resulted in the establishment of two-way exchange first with the Paratethys at some point during the Lago-Mare phase and later, i.e. slightly before or at the Messinian/Zanclean boundary, with the Atlantic Ocean (Fig. 11c; Marzocchi et al., 2016). The moment the Mediterranean base-level reached the sill with the adjacent water body (Paratethys and Atlantic) and a two-way exchange was initiated, the density contrast will have prompted an enhanced inflow into the Mediterranean (Marzocchi et al., 2016). The overall transgressive trend leading to the Zanclean marine replenishment was accompanied by base-level fluctuations in the order of 400–100 m every precessional cycle (Fig. 11c; Fortuin and Krijgsman, 2003; Ben Moshe et al., 2020; Andreetto et al., 2021). These fluctuations are ascribed to switch in the Mediterranean

freshwater budget driven by the African summer monsoon and Atlantic winter storms (e.g. Marzocchi et al., 2015, 2019; Simon et al., 2017). Since higher freshwater discharge rates occur at precession minima times and their Stage 3 sedimentary expression is considered to be the mudstone intervals (Fig. 3a; Manzi et al., 2009), mudstone interbeds (both onshore and offshore; e.g. Figs. 5h-j) represent the highstand episodes (e.g. Manzi et al., 2009; Roveri et al., 2008a; Omodeo-Salé et al., 2012; Fig. 3), while continental facies onshore (e.g. conglomerates in the Apennines; Fig. 5g) and offshore (clastic beds in the Levant Basin) and gypsum beds (Algero-Balearic, Liguro-Provençal, CMD, Tyrrhenian, Caltanissetta, Ionian, Sirte and Polemi-Pissouri basins; Figs. 5h-j) represent the lowstand (e.g. Roveri et al., 2008a; Manzi et al., 2009; Meilijson et al., 2019; Fig. 3). If Atlantic was the major source of sulfate for Stage 3 gypsum (e.g. García-Veigas et al., 2018) and an intervening, relatively shallow (Sicily) sill was establishing Western and Eastern Mediterranean division during the MSC (e.g. García-Castellanos et al., 2009, 2020; Micallef et al., 2018), the presence of Stage 3 gypsum to the east of the Sicily sill (Fig. 2b) implies that the Mediterranean base level never dropped below the (maximum estimated) paleodepth of the sill (i.

e. ~430 m; García-Castellanos et al., 2009) during Stage 3 and Western and Eastern Mediterranean remained connected also during the arid (lowstand) phases of the precession cycles.

A Mediterranean step-wise refilled and at times filled with water up to the marginal belt agrees with: (1) Paratethyan biota being present only in intermediate-deeper settings during substage 3.1, but more widespread including marginal settings during substage 3.2; (2) the W-E homogeneity of Paratethyan ostracod assemblages around the Mediterranean marginal belt (Gliozzi et al., 2007; Stoica et al., 2016; Sciuto et al., 2018; Sciuto and Baldanza, 2020; Fig. 9a); (3) the presence, in marginal basins, of Paratethyan fish (Bannikov et al., 2018; Schwarzhans et al., 2020), dinocysts (e.g. Pellen et al., 2017; Fig. 9b) and bio-markers (Vasiliev et al., 2017; Fig. 10c); (4) the occurrence of a monospecific assemblage of abundant *Sphenolithus* spp. just below the M/P boundary at ODP Sites 978, 975 and 967 (Castradori, 1998); (5) the requirement of water from the Mediterranean to explain the Sr isotope ratios of ostracods that inhabited marginal subaqueous environments (Andreetto et al., 2021); (6) the Atlantic-like sulfate values (although variably diluted and affected by microbial processes; Fig. 10b) of the UU/UG gypsum beds (García-Veigas et al., 2018); (7) the presence of long chain alkenones in the Sicilian UG beds similar to those observed in present-day marine settings (Fig. 10c; Vasiliev et al., 2017).

Major problems also exist with the half-full stratified scenario: (1) it does not provide a proper mechanism for gypsum precipitation at several hundreds, or thousands, meters water depth; (2) it fails to explain how unquestionable shallow-water (< 50 m) benthic organisms

such as *Ammonia tepida* and *Cyprideis* sp. could survive at hundreds of meters of depth and beyond; (3) it does not provide an explanation for the high abundance of coarse-grained detritus at intermediate and deep-water locations, especially when compared to deep-water Pliocene samples, as well as for the broad absence of MSC deposits in the shelf domain; (4) a persistent Atlantic inflow without outflow seems to be a configuration that cannot be maintained stable for ~200 kyr. Indeed, models coupling the inflow of marine waters with the erosion of the gateway channel concluded that, if the Mediterranean level was lowered by at least several hundred meters below present sea level, any small overtopping of water from the Atlantic would inevitably trigger a fast refill of the basin that, if responsible for the erosion through the Alborán Basin, should have involved an unprecedented water discharge and be completed within a few years or less (García-Castellanos et al., 2020 and references therein). The scenario arising from Meilijson et al., 2019, Figs. 3b, 4a) is also problematic for a high base-level Mediterranean. In order to simultaneously reach precipitation of gypsum and halite in different basins sharing the same water, the water has to be of high salinity and stratified. Simon and Meijer (2017) demonstrated that this can be achieved with slow overturning circulation, but it is currently unclear how realistic this process is.

7.3 Demise of the MSC (5.33 Ma): the Zanclean marine replenishment

The conspicuous and abrupt transition to normal marine sediments in the Mediterranean is globally and historically important because it is the origin of the stratigraphic position of the Miocene/Pliocene boundary (Van Couvering et al., 2000). From an ocean perspective, it is not an ideal stratigraphic location being difficult to locate from biozonedata even in the adjacent Atlantic (Hodell et al., 2001; Krijgsman et al., 2004; Van den Berg et al., 2015). However, from a Mediterranean perspective it provides a clear and unambiguous end to the MSC and the restoration of normal marine conditions. All evidence show that the onset of the Zanclean marine replenishment followed a period of relative lowstand that exposed all the Mediterranean margins (see subsection 3.12; Figs. 6a-b, f) and kept intermediate and deep basins underwater (see subsection 4.8). Yet again, the key dispute concerns the exact depth of the Mediterranean base level preceding the Miocene/Pliocene transition.

Building on the isolated Mediterranean scenario, base level immediately before the early Zanclean was more than thousand kilometers below eustatic sea level (Fig. 10e; e.g. Hsü et al., 1973a; Blanc, 2002; Loget et al., 2006; García-Castellanos et al., 2009; Pérez-Asensio et al., 2012; García-Alix et al., 2016; Amadori et al., 2018; Micallef et al., 2018, 2019; Camerlenghi et al., 2019; Kartveit et al., 2019; Madof et al., 2019; Ben Moshe et al., 2020; Caruso et al., 2020; Cazzini et al., 2020; Mas and Fornós, 2020; Spatola et al., 2020). Hydrodynamic erosional models allowed a reinterpretation of the erosional features across the strait of Gibraltar (Campillo et al., 1992; Blanc, 2002) suggesting that a sudden breach of the Mediterranean-Atlantic divide at Gibraltar resulted in a vast cascade of Atlantic water that refilled the entire Mediterranean in less than 2 years (i.e. rates of ten meters per day) spilling first into the Western Mediterranean (see the extensive review in García-Castellanos et al., 2020) and then, after reaching the level of the Sicily sill, pouring into the Eastern Mediterranean (Micallef et al., 2018, 2019; Ben Moshe et al., 2020; Spatola et al., 2020). This concept of catastrophic refilling has led to terms such as “Zanclean flood” or “deluge”. Evidence supporting the catastrophic flood mechanism mostly comes from the seismic reflection dataset and includes: 1) the presence of >250 m deep and 390-km-long incisions on both sides of the Gibraltar Strait (García-Castellanos et al., 2020); 2) the detection of (allegedly) Pliocene-aged chaotic sedimentary bodies stretching for kilometers in the Alborán Basin (García-Castellanos et al., 2020 and references therein) and Ionian Basin at the foot of the Malta Escarpment (Micallef et al., 2018, 2019; Spatola et al., 2020; Fig. 8c). A further argument is the bathymetric jump of several hundred meters between the late Messinian and the early

Pliocene sediments (e.g. Caruso et al., 2020; Fig. 6d).

Instantaneous sea level rise is not the only possible refilling model. Bache et al. (2012) suggested the reflooding occurred in two steps at ~5.60 Ma, accompanied by a moderate (~500 m) rise, followed by a rapid rise of 600–900 m at around 5.46 Ma tracking the deposition of the deep basin evaporites and resulting from the collapse of the Gibraltar divide. There is also the reconnection model that follows from a Stage 3 Mediterranean that is already relatively full and with the base level possibly oscillating of 400–100 m with precessional frequency (Fig. 10h; Fortuin and Krijgsman, 2003; Ben Moshe et al., 2020; Andreetto et al., 2021). In this case, only a sea level rise of a few hundred meters is required to restore the Mediterranean to the Atlantic level (Fig. 10h), which was hypothesized to have occurred in the last pre-cessional cycle of the Messinian (Marzocchi et al., 2016; Fig. 3a).

In detail, the re-establishment of a fully marine faunal diversity and oceanic geochemistry (e.g. $^{87}\text{Sr}/^{86}\text{Sr}$ ratios and $\delta^{18}\text{O}$) occurred more gradually over one or more precessional cycles in the earliest Zanclean (e.g. Iaccarino et al., 1999; Pierre et al., 1998, 2006; Cipollari et al., 2013; Roveri et al., 2019a; Bulian et al., 2021). This suggests that stressed ecological conditions at first only suitable for opportunistic organisms to survive (e.g. Bulian et al., 2021) developed (or persisted) in the Mediterranean as marine replenishment occurred (e.g. Rouchy et al., 2003). One possible mechanism for achieving this may be the physico-chemical turnover in the water column triggered by the re-established two-way exchange with the Atlantic which, for reasons that are largely unknown, took time (at least one precession cycle; Pierre et al., 2006) to displace surficial Paratethyan water and restore normal marine conditions (Marzocchi et al., 2016).

8. Methods and proxies to better reconstruct base level and connectivity changes

Chronological uncertainty and spatial variability limit the use of both sedimentological and paleontological information to achieve a comprehensive and coherent basin-wide interpretation of the conditions and drivers of Stage 3 environments and water levels. Alternative methods are therefore required to clarify connectivity relationships and constrain base-level conditions. This section explores the principles and potential of geochemical, backstripping and numerical modelling techniques that could be used to further test existing hypotheses and enhance understanding of the complex environmental conditions experienced by the Mediterranean during the latest Messinian.

8.1 Geochemical proxies

Radiogenic strontium isotopes. Radiogenic strontium isotope ratio ($^{87}\text{Sr}/^{86}\text{Sr}$) is a widely applied geochemical tool in provenance studies, including the reconstruction of the hydrological circuit and connectivity of basins with little or null oceanic entries. Its potential to detect the provenance of the hydrological fluxes derives from the unique $^{87}\text{Sr}/^{86}\text{Sr}$ ratio that typifies each water source and from the negligible effects of isotopic fractionation during the liquid-solid transition (see Hajj et al., 2017).

Mineral phases precipitating in endorheic lakes uptake Sr with $^{87}\text{Sr}/^{86}\text{Sr}$ ratio that reflects the mixing of all feeding surficial and underground streams and whose $^{87}\text{Sr}/^{86}\text{Sr}$ fingerprint hinges on the composition and age of watershed bedrock (see Peucker-Ehrenbrink and Fiske, 2019; Andreetto et al., 2021 and references therein). When river water mixes with seawater such as in the oceans, semi-enclosed basins or estuaries, mineral phases uptake Sr with oceanic $^{87}\text{Sr}/^{86}\text{Sr}$ ratios because the high oceanic Sr concentration (~7.8 mg/l today; Veizer, 1989) masks the impact of the ~100 times lower concentrated continental Sr sources (~0.0780 mg/l; Palmer and Edmond, 1992). This is valid as long as a certain ratio of continental-marine water mixing is fulfilled, beyond which $^{87}\text{Sr}/^{86}\text{Sr}$ ratios deviate towards the $^{87}\text{Sr}/^{86}\text{Sr}$ ratios of the non-marine source(s) (Ingram and Sloan, 1992). For the

Mediterranean to attain non-marine $^{87}\text{Sr}/^{86}\text{Sr}$ ratios (like during the MSC), Topper et al. (2014) calculated a mixing of at least 1:4 (Atlantic: freshwater) to be required.

If Mediterranean subbasins hosted endorheic lakes (Figs. 10c, e), the $^{87}\text{Sr}/^{86}\text{Sr}$ isotope ratios measured on ostracod valves or gypsum crystals of each lake are expected to generate a scattered distribution by virtue of the different geology in the hinterland of each basin. By contrast, some degree of connection between different basins and the Mediterranean water mass (Figs. 10d, f) is expected to result in more homogeneous $^{87}\text{Sr}/^{86}\text{Sr}$ ratios because, although isotopically-different, local rivers mix with a water mass that has the same $^{87}\text{Sr}/^{86}\text{Sr}$ value and (much higher) Sr concentration for each basin (Andreetto et al., 2021). In this scenario, differences in the $^{87}\text{Sr}/^{86}\text{Sr}$ ratios between basins are likely the reflection of the different $^{87}\text{Sr}/^{86}\text{Sr}$ ratio of the local input in each basin (Andreetto et al., 2021). The application of numerical models assists to identify and quantify the different water sources feeding the basin(s) in question and (e.g. Placzek et al., 2011; Topper et al., 2011, 2014; Doebbert et al., 2014; Rossi et al., 2015b; Modestou et al., 2017; Grothe et al., 2020; Andreetto et al., 2021).

Sulfate isotopes. When sulfate-bearing minerals precipitate in a basin they uptake dissolved S and O with $\delta^{34}\text{S}_{\text{SO}_4}$ and $\delta^{18}\text{O}_{\text{SO}_4}$ isotopic composition that, once corrected for the fractionation effects during liquid-solid transition (see subsection 6.2), can be assimilated to that of the mother brine. The higher concentrated source of sulfate is seawater (with present-day $\delta^{34}\text{S}_{\text{SO}_4}$ 21.15 ‰ and $\delta^{18}\text{O}_{\text{SO}_4}$ 8.67 ‰, Johnston et al., 2014; with Messinian values of \sim 22 ‰ for the $\delta^{34}\text{S}_{\text{SO}_4}$ and \sim 9 ‰ for the $\delta^{18}\text{O}_{\text{SO}_4}$; Turchyn and Schrag, 2004; Markovic et al., 2016; Masterson et al., 2016). Significantly higher inputs from the \sim 1000 times less concentrated riverine freshwater (both surface and underground) with respect to the ocean water (more than 1:5 according to Lu et al., 2001) can modify the marine $\delta^{34}\text{S}_{\text{SO}_4}$ and $\delta^{18}\text{O}_{\text{SO}_4}$ isotopic composition of the mother brine (Utrilla et al., 1992; Lu et al., 2001) and have it deviated from that of the ocean (Lu et al., 2001). This deviation is normally towards lower values, because river-derived dissolved sulfate is generally depleted in heavy isotopes ^{34}S and ^{18}O compared to oceanic sulfate because these isotopes mainly come from the oxidation of ^{34}S -depleted pyrite (FeS_2) on the continents and to a lesser extent from the dissolution of older sulfate-bearing minerals (Claypool et al., 1980; Turchyn and Schrag, 2004; Burke et al., 2018). However, when marine sulfate is preferentially leached in the catchment, ^{34}S of the freshwater-dissolved sulfate and $[\text{SO}_4^{2-}]$ likely increase, therefore reducing the continental-marine mixing ratio necessary to deviate the resulting sulfate isotopic signature away from marine values.

Unfortunately, the sulfate isotopic composition is not provided for a number of major Mediterranean rivers (Burke et al., 2018) nor for the Eastern Paratethys and it is hardly assessed with the catchment-forming lithologies (Liu et al., 2017; Burke et al., 2018), making sulfate isotopes still an unsuitable tracer of non-marine water provenance in Mediterranean subbasins.

Deviation of $\delta^{34}\text{S}_{\text{SO}_4}$ and $\delta^{18}\text{O}_{\text{SO}_4}$ from the marine average can also be the result of isotopic fractionation during microbial sulfate reduction (MSR; Fritz et al., 1989; Berner, 1999). MSR produces ^{34}S -depleted hydrogen sulfide (\sim 0 to 70‰ lighter than initial sulfate; Brunner and Bernasconi, 2005; Sim et al., 2011; Leavitt et al., 2013) and induces the enrichment in ^{34}S and ^{18}O of the residual sulfate pool (Kaplan and Rittenberg, 1964; Thode and Monster, 1965; Turchyn et al., 2006; Wortmann et al., 2007). Therefore, if isotopically light H_2S produced by MSR leaves the system as a sulfide mineral (most likely pyrite), the resulting dissolved sulfate would have $\delta^{34}\text{S}_{\text{SO}_4}$ and $\delta^{18}\text{O}_{\text{SO}_4}$ isotopic signatures higher than the oceanic one (Brunner et al., 2005). However, if the MSR-produced H_2S is re-oxidized back to sulfate through abiotic or microbial sulfide oxidation, isotopically light sulfate will be brought back to the ^{34}S -enriched sulfate pool, producing little or no enrichment in ^{34}S observed in the resulting sulfate (Gomes and Johnston, 2017 and references therein; Pellerin et al., 2019). Slight deviations from marine $\delta^{18}\text{O}_{\text{SO}_4}$ and $\delta^{34}\text{S}_{\text{SO}_4}$ values of sulfate reflect both biological sulfur

cycling and/or freshwater riverine inputs (e.g. Utrilla et al., 1992; Luet al., 2001; Turchyn et al., 2009) (Fig. 10b). Untangling the relative importance of these processes is key to understanding the Mediterranean sulfur isotope record and gaining paleoenvironmental insights into Stage 3.

Hydrogen isotopes. Organic geochemistry biomarker-based tools can be used as independent proxies for reconstructing sea surface temperatures, relative changes in the basin hydrology and, indirectly, salinity. Basin water properties are reflected in a variety of life forms. Different types of organisms produce specific organic compounds that serve as molecular biomarkers. These large biomolecules record the changes in the hydrogen isotopic composition of the water used by different groups of biomarker producers (i.e. different organisms). The principle behind the method is to measure δD on biomarkers produced in Mediterranean Sea waters (e.g. alkenones, produced by a few species of haptophyte coccolithophores algae) during the MSC and compare the results with the δD signals retrieved from biomarkers produced in the open ocean ideally at the same time intervals. The influence of precipitation on the changes in hydrological budget can be monitored by measuring the δD of long chain *n*-alkanes (Sachse et al., 2006), biomarkers predominantly produced by higher terrestrial plants that rely on precipitation for plant growth, therefore reflecting the changes in the δD of the precipitation. The extreme base level drop(s) suggested for the Mediterranean during

the MSC would, in principle, indicate a negative precipitation (P) + runoff (R) – evaporation (E) ratio. Such a negative water budget ($E > P + R$) results in waters increasingly enriched in δD whereas, a positive water balance ($E < P + R$) results instead in a negative shift of δD values. The analysis of compound specific δD of alkenones, long and short chain *n*-alkanes can be used to constrain $E/(P+E)$ relationships.

8.2 Backstripping analyses

Backstripping uses paleobathymetry, sea level and sediment thickness to quantify the tectonic and isostatic components of subsidence. If tectonic subsidence or uplift history are known relative to the current position and depth of paleoshoreline markers, an inverse approach allows base level to be estimated. A number of approaches have been applied to the MSC, using erosional surfaces (e.g. Amadori et al., 2018), terraces (Micallef et al., 2018) or fluvial network characteristics (Urgeles et al., 2011) as paleoshoreline indicators. The relief on erosional features has also been used to estimate minimum base-level variation (Frey-Martinez et al., 2004).

Apart from the quantitative constraints on base level that backstripping provides, consideration of the regional implications of isostatic subsidence and the gravitational impact of redistributing water masses (such as in the cascading model of Roveri et al., 2014c; Fig. 10b) and evaporite precipitation is important in gateway regions like Gibraltar, which due to their shallow and restricted nature are exceptionally sensitive to vertical motions. Here, both flexural effects and gravitational effects on local sea level on the Atlantic side of the strait has the potential to influence Mediterranean-Atlantic connectivity driving paleo-environmental changes in the basin itself (Coulson et al., 2019).

8.3 Modelling

Numerical models can be used complementary to lab- and field-based studies, or to find answers to open questions by testing the physical plausibility of hypotheses and their compatibility with the available sedimentological/stratigraphic/paleontological/geochemical data, which have to constrain model results and not adjust to it. Foreexample, whether gypsum beds in marginal/intermediate basins can precipitate at the same time as the halite in deep basins is an intriguing question that circulates in the MSC literature (e.g. Van Couvering et al., 1976), but whether this is physically and geochemically possible is yet to be answered. In a first model analysis, Simon and Meijer (2017) found that the required stratification can indeed be achieved for specific

conditions including a slow overturning circulation. A different approach is needed to determine whether such slow circulation is to be expected or if other scenarios should be considered. A thermo-haline stratification that enables coeval precipitation of two evaporites for a considerable time span might also influence the degree of heterogeneity of other parameters, such as strontium concentration. Previous models showed the influence of the Atlantic Ocean and major rivers (Topper et al., 2014) and of evaporation (Flecker et al., 2002) on the Sr value of a basin with restricted oceanic inflow and assuming a homogeneous distribution of strontium throughout the water column (Flecker et al., 2002; Topper et al., 2011, 2014; Modestou et al., 2017), but it is uncertain if this holds true in conditions of water stratification. New insights into this behavior would have consequences for the way the strontium dataset (Fig. 10a) must be interpreted. Another loose end where the model approach can provide insight relates to the question whether a high water level could have been reached without an inflow from the Atlantic. Climate simulations conducted by Gladstone et al. (2007), Simon et al. (2017) and Marzocchi et al. (2019) indicate that this is not possible with today's bathymetry. A quantitative analysis exploring the Mediterranean water level reached in different situations (i.e. with or without an Atlantic or Paratethys in and outflow) and with information on the Mediterranean hypsometry that may be provided by isostatic restoration of the seafloor topography (flexural backstripping) could help understanding how the Messinian Salinity Crisis ended.

9. Certainties, open problems and future directions

Our understanding of the nature of MSC Stage 3 has evolved considerably over the last fifty years. However, there are still such disparate models for the paleoenvironmental conditions and basin connectivity that led to Stage 3 deposition and that express the challenges that the study of this interval presents: it is a relatively short interval and its sedimentary expression varies spatially. It is no surprise that the main point of contention lies in reconciling the observations from seismic profiles and well data, which are largely interpreted as favoring the desiccated scenario, with the sedimentological, paleontological and geochemical data from the marginal basins record, largely discontinuous and unaddressed from seismic-based and computational-based studies and mainly supporting the full-Mediterranean hypothesis. To a large extent this mismatch is the result of the lack of intersection of the two datasets. Some Stage 3 onshore localities are meticulously studied from the stratigraphic, sedimentological, paleontological and geochemical point of view, showing remarkably consistent and homogenous trends and patterns (as previously highlighted by Roveriet al., 2008a). However, changes at precessional and subprecessional scale are difficult to trace from one exposure to another and are well below the level of seismic resolution, making onshore-offshore correlation at this scale impossible. Even correlation between onshore sections is problematic since most of the stratigraphic sections are incomplete, with erosion surfaces at the bottom and/or top (i.e. the Miocene/Pliocene boundary), and this lack of stratigraphic continuity frustrates attempts to constrain ages by cyclostratigraphy. A future focus on strengthening the available chronostratigraphic framework (Fig. 3) and making it inclusive of the fragmented outcrops is required to better understand the paleoenvironmental and paleohydrological changes suffered by the Mediterranean marginal belt through time. The successful drilling of the three IODP proposals currently in the scheduling pool (see Camerlenghi and Aloisi, 2020), all of which propose to recover Stage 3 sediments, will also provide transformative information enabling far better offshore-onshore correlation and interpretation of currently enigmatic seismic data. In the meantime, re-evaluation of existing DSDP and ODP material, particularly through the application of more novel geochemical techniques and, where possible, access to material collected during industrial drilling would be helpful for understanding the deep Mediterranean Basin during this interval.

Extensive paleontological studies have established that Stage 3 contains *in situ* biota assemblages of Paratethyan provenance implying brackish water conditions. More problematic is the differentiation of *in situ* and reworked marine microfauna and flora and the paleoecological significance of dwarfism in marine calcareous microfossils/algae. These have important repercussions for the Mediterranean connectivity and base-level reconstruction. The geochemical dataset for Stage 3, particularly strontium isotopes and hydrogen isotopes on biomarkers, is both demonstrably valuable in providing key constraints on connectivity and environmental conditions, and frustratingly inadequate in terms of data distribution. It has great potential as a constraint on quantitative sensitivity analysis of the different hydrochemistry scenarios that follow from the endmember Stage 3 hypotheses, but substantially more data is required. An approach which combines geological, geochemical, geophysical and paleontological data with numerical modelling (e.g. climate simulations, backstripping analyses and paleoceanographic models) will provide a more accurate reconstruction of Mediterranean paleogeography and the processes that occurred during the final phase of the Messinian Salinity Crisis.

Data availability

The compilation of strontium, sulfate and hydrogen isotope data plotted in figure 9, as well as some of the available, and here not (graphically) shown, oxygen isotope values is accessible in separate excel spreadsheets (Supplementary material 1).

Declaration of Competing Interest

The authors whose names are listed immediately below certify that they have NO affiliations with or involvement in any organization or entity with any financial interest (such as honoraria; educational grants; participation in speakers' bureaus; membership, employment, consultancies, stock ownership, or other equity interest; and expert testimony or patent licensing arrangements), or non-financial interest (such as personal or professional relationships, affiliations, knowledge or beliefs) in the subject matter or materials discussed in this manuscript.

Acknowledgments

We thank the entire SALTGIANT community for many profitable workshops that inspired the development of this manuscript. This research was supported by the project SALTGIANT-Understanding the Mediterranean Salt Giant, a European project which has received funding from the European Union's Horizon 2020 research and innovation program, under the Marie Skłodowska-Curie [grant agreement No 765256]. We greatly thank the two reviewers Domenico Cosentino and William Ryan and the editor Alessandra Negri for the fruitful comments provided that led to a substantial improvement of the manuscript.

Appendix A. Supplementary data

Supplementary data to this article can be found online at <https://doi.org/10.1016/j.earscirev.2021.103577>.

References

- Abdel Aal, A., El Barkooky, A., Gerrits, M., Meyer, H., Schwander, M., Zaki, H., 2000. Tectonic evolution of the eastern Mediterranean Basin and its significance for hydrocarbon prospectivity in the ultra-deepwater of the Nile Delta. *Lead. Edge* 19, 1086–1102. <https://doi.org/10.1190/1.1438485>.
- Abdel-Fattah, M.I., 2014. Petrophysical characteristics of the messinian abu madi formation in the baltim east and north fields, offshore Nile delta, Egypt. *J. Pet. Geol.* 37 (2), 183–195.
- Agjadi, K., Antonarakou, A., Kontakiotis, G., Kafousia, N., Moissette, P., Cornee, J.-J., Manoutsoglou, E., Karakitsios, V., 2017. Connectivity controls on the late Miocene eastern Mediterranean fish fauna. *Int. J. Earth Sci.* 106, 1147–1159. <https://doi.org/10.1007/s00531-016-1355-7>.
- Agini, C., Monechi, S., Raffi, I., 2017. Calcareous nannofossil biostratigraphy: historical background and application in Cenozoic chronostratigraphy. *Lethaia* 50 (3), 447–463.
- Aguirre, J., Sanchez-Almazo, I.M., 2004. The Messinian post-evaporitic deposits of the Gafares area (Almeria-Nijar basin, SE Spain). A new view of the “Lago-Mare” facies. *Sediment. Geol.* 168, 71–95.
- Amadori, C., Garcia-Castellanos, D., Toscani, G., Sternai, P., Fantoni, R., Ghielmi, M., Di Giulio, A., 2018. Restored topography of the Po Plain-Northern Adriatic region during the Messinian base level drop-implications for the physiography and compartmentalization of the paleo-Mediterranean basin. *Basin Res.* 30 (6), 1247–1263. <https://doi.org/10.1111/bre.12302>.
- Andersen, N., Paul, H.A., Bernasconi, S.M., McKenzie, J.A., Behrens, A., Schaeffer, P., Albrecht, P., 2001. Large and rapid climate variability during the Messinian salinity crisis: evidence from deuterium concentrations of individual biomarkers. *Geology* 29, 799–802.
- Andreotto, F., Matsubara, K., Beets, C.J., Fortuin, A.R., Flecker, R., Krijgsman, W., 2021. High Mediterranean water-level during the Lago-Mare phase of the Messinian Salinity Crisis: insights from the Sr isotope records of Spanish marginal basins (SE Spain). *Paleogeogr. Paleoclimatol. Paleocool.* 562.
- Andrusov, D., 1890. Les Dreissenidae fossiles et actuelles d’Eurasie. *Geol. Min.* 25, 1–683 (in Russian).
- Arab, M., Rabineau, M., Deverchère, J., Bracene, R., Belhai, D., Roure, F., Marok, A., Bouyahiaoui, B., Granjeon, D., Andriessen, P., Sage, F., 2016. Tectonostratigraphic evolution of the eastern Algerian margin and basin from seismic data and onshore-offshore correlation. *Mar. Pet. Geol.* 77, 1355–1375. <https://doi.org/10.1016/j.marpetgeo.2016.08.021>.
- Arenas, C., Pomar, L., 2010. Microbial deposits in upper Miocene carbonates, Mallorca, Spain. *Paleogeogr. Paleoclimatol. Paleocool.* 297 (2), 465–485.
- Aufgebauer, A., McCann, T., 2010. Messinian to Pliocene transition in the deep part of the Sorbas Basin, SE Spain—a new description of the depositional environment during the Messinian Salinity Crisis. *Neues Jahrbuch für Geologie und Paläontologie—Abhandlungen* 259 (2), 177–195.
- Azdimouza, A., Poupeau, G., Rezqi, H., Asebriy, L., Bourgeois, J., Ait Brahim, L., 2006. Géodynamique des bordures méridionales de la mer d’Alboran; application de la stratigraphie séquentielle dans le bassin néogène de Boudinar Rif oriental. *Maroc. Bull. Inst. Sci. Rabat* 28, 9–18.
- Bache, F., Olivet, J.-L., Gorini, C., Rabineau, M., Baztan, J., Aslanian, D., Suc, J.-P., 2009. Messinian erosional and salinity crisis: view from the Provence basin (Gulf of Lions, western Mediterranean). *Earth Planet. Sci. Lett.* 286, 139–157.
- Bache, F., Popescu, S.-M., Rabineau, M., Gorini, C., Suc, J.-P., Clauzon, G., Olivet, J.-L., Rubino, J.-L., Melinte-Dobrinescu, M.C., Estrada, F., Londeix, L., Armijo, R., Meyer, B., Jolivet, L., Jouannic, G., Leroux, E., Aslanian, D., Reis, A.T.D., Mocochain, L., Dumurdžanov, N., Zagorchev, I., Lesić, V., Tomić, D., Namik Çağatay, M., Brun, J.-P., Sokoutis, D., Csato, I.T., Ucaruk, G., Çakır, Z., 2012. A two-step process for the reflooding of the Mediterranean after the Messinian Salinity Crisis. *Basin Res.* 24, 125–153. <https://doi.org/10.1111/j.1365-2117.2011.00521.x>.
- Backman, J., Raffi, I., Rio, D., Fornaciari, E., Palike, H., 2012. Biozonation and biochronology of Miocene through Pliocene calcareous nannofossils from low and middle latitudes. *Newsl. Stratigr.* 45, 221–244.
- Bannikov, A.F., Schwarzshans, W., Carnevale, G., 2018. Neogene Paratethyan croakers (Teleostei, Sciaenidae). *Riv. Ital. Paleontol. Stratigr.* 124, 535–571.
- Barra, D., Bonaduce, G., Sgarrella, E., 1998. Paleoenvironmental bottom water conditions in the early Zanclean of the Capo Rossello area (Agrigento, Sicily). *Boll. Soc. Paleontol. Ital.* 37, 61–88.
- Bassetti, M.A., Miculan, P., Lucchi, F.R., 2003. Ostracod faunas and brackish-water environments of the late Messinian Sapigno section (northern Apennines, Italy). *Paleogeogr. Paleoclimatol. Paleocool.* 198 (3–4), 335–352.
- Bassetti, M.A., Manzi, V., Lugli, S., Roveri, M., Longinelli, A., Lucchi, F.R., Barbieri, M., 2004. Paleoenvironmental significance of Messinian post-evaporitic lacustrine carbonates in the northern Apennines, Italy. *Sediment. Geol.* 172 (1–2), 1–18.
- Bassetti, M.A., Miculan, P., Sierro, F.J., 2006. Evolution of depositional environments after the end of Messinian Salinity Crisis in Nijar basin (SE Betic Cordillera). *Sediment. Geol.* 188–189, 279–295.
- Ben Moshe, L., Ben-Avraham, Z., Enzel, Y., Schattner, U., 2020. Estimating drawdown magnitudes of the Mediterranean Sea in the Levant basin during the Lago Mare stage of the Messinian Salinity Crisis. *Mar. Geol.* 106215 <https://doi.org/10.1016/j.margeo.2020.106215>.
- Ben-Gal, Y., Ben-Avraham, Z., Buchbinder, B., Kendall, C.G.S.C., 2005. Post-Messinian evolution of the Southeastern Levant Basin based on two-dimensional stratigraphic simulation. *Mar. Geol.* 221 (1–4), 359–379.
- Benson, R.H., 1978. The paleoecology of the ostracods of DSDP Leg 42A. In: Hsu, K., Montadert, L. (Eds.), *Initial Reports of the Deep-Sea Drilling Project*, 42. U.S. Government Printing Office, Washington, pp. 777–787.
- Benson, R.H., Rakic-El Bied, K., 1991. The Messinian parastratotype at Cuevas de Almazora, Vera Basin, SE Spain; refutation of the deep-basin, shallow-water hypothesis? *Microplaeontology* 37 (3), 289–302.
- Benson, R.H., Rakic-El Bied, K., Bonaduce, G., 1991. An important current reversal (influx) in the Rifian Corridor (Morocco) at the Tortonian-Messinian boundary: the end of Tethys Ocean. *Paleogeography* 6 (1), 165–192.
- Berner, R.A., 1999. Atmospheric oxygen over Phanerozoic time. *Proc. Natl. Acad. Sci.* 96, 10955.
- Bertini, A., 2006. The Northern Apennines palynological record as a contribute for the reconstruction of the Messinian paleoenvironments. *Sediment. Geol.* 188, 235–258.
- Bertini, A., Corradini, D., 1998. Biostratigraphic and paleoecological significance of Galeacysta etrusca in the “Lago-Mare” facies from the Mediterranean area (Neogene). *Dino NTNU Vitensk. Mus. Rapp. Bot. ser.* 6, 15–16. Abstract.
- Bertoni, C., Cartwright, J., 2007. Major erosion at the end of the Messinian Salinity Crisis: evidence from the Levant Basin, Eastern Mediterranean. *Basin Res.* 19, 1–18. Bessis, F., 1986. Some remarks on the study of subsidence of sedimentary basins. Application to the Gulf of Lions margin (Western Mediterranean). *Mar. Pet. Geol.* 3, 37–63.
- Bialik, O.M., Frank, M., Betzler, C., Zammit, R., Waldmann, N.D., 2019. Two-step closure of the Miocene Indian Ocean Gateway to the Mediterranean. *Sci. Rep.* 9 (1), 1–10. <https://doi.org/10.1038/s41598-019-45308-7>.
- Biscaye, P.E., Ryan, W.B.F., Wezel, F.C., 1972. Age and nature of the Pan-Mediterranean subbottom reflector M. *The Mediterranean Sea* 83–90.
- Blanc, P.L., 2002. The opening of the Plio-Quaternary Gibraltar Strait: assessing the size of a cataclysm. *Geodin. Acta* 15, 303–317.
- Blanc-Valleron, M.-M., Rouchy, J.-M., Pierre, C., Badaut-Trauth, D., Schuler, M., 1998. Evidence of Messinian nonmarine deposition at site 968 (Cyprus lower slope). In: *Proceedings of the Ocean Drilling Program, Scientific Results*, ODP Sci. Results 160, Texas, USA, pp. 43–445.
- Bonaduce, G., Sgarrella, F., 1999. Paleoeological interpretation of the latest Messinian sediments from southern Sicily (Italy). *Soc. Geol. Ital. Mem.* 54, 83–91.
- Booth-Rea, G., Ranero, R., Grevemeyer, I.C., 2018. The Alboran volcanic-arc modulated the Messinian faunal exchange and salinity crisis. *Sci. Rep.* 8 <https://doi.org/10.1038/s41598-018-31307-7>.
- Borsetti, A.M., Curzi, P.V., Landuzzi, V., Mutti, M., Ricci Lucchi, F., Sartori, R., Tomadin, L., Zuffa, G.G., 1990. Messinian and pre-Messinian sediments from ODP Leg 107 Sites 652 and 654 in the Tyrrhenian Sea: sedimentologic and petrographic study and possible comparisons with Italian sequences. In: Kastens, K.A., Masche, J., et al. (Eds.), *Proceedings of the Ocean Drilling Program, Scientific Results*, 107, pp. 169–186.
- Bossio, A., Esteban, M., Giannelli, L., Longinelli, A., Mazzanti, R., Mazzei, R., Ricci Lucchi, F., Salvadorini, G., 1978. Some aspects of the upper Miocene in Tuscany. In: *Messinian Seminar*, vol. 4. Pacini, Pisa, 88 pp.
- Bossio, A., Costantini, A., Lazzarotto, A., Liotta, D., Mazzanti, R., 1993. Rassegna delle conoscenze sulla stratigrafia del Neoaotoceno toscano. *Mem. Soc. Geol. Ital.* 49, 17–98.
- Bosworth, W., Huchon, P., Mc Clay, K., 2005. The Red Sea and Gulf of Aden Basins. *J. Afr. Earth Sci.* 43, 334–378.
- Bowman, S.A., 2012. A comprehensive review of the MSC facies and their origins in the offshore Sirt Basin, Libya. *Pet. Geosci.* 18, 457–469. <https://doi.org/10.1144/petgeo2011-070>.
- Braga, J.C., Martín, J.M., Riding, R., Aguirre, J., Sanchez-Almazo, I.M., Dinares-Turell, J., 2006. Testing models for the Messinian salinity crisis: the Messinian record in Almeria, SE Spain. *Sediment. Geol.* 188–189, 131–154. <https://doi.org/10.1016/j.sedgeo.2006.03.002>.
- Brolsma, M.J., 1975. Lithostratigraphy and Foraminiferal assemblages of the Miocene/Pliocene transitional strata at Capo Rossello and Eraclea Minoa (Sicily, Italy): Kon. Ned. Akad. Wetensch. Amsterdam Proc 78, 1–40.
- Brunner, B., Bernasconi, S.M., 2005. A revised isotope fractionation model for dissimilatory sulfate reduction in sulfate reducing bacteria. *Geochim. Cosmochim. Acta* 69, 4759–4771.
- Brunner, B., Bernasconi, S.M., Kleikemper, J., Schroth, M.H., 2005. A model for oxygen and sulfur isotope fractionation in sulfate during bacterial sulfate reduction processes. *Geochim. Cosmochim. Acta* 69, 4773–4785.
- Bulian, F., Sierro, F.J., Santiago, L., Jimenez-Espejo, F.J., Bassetti, M.A., 2021. Messinian West Alboran Sea record in the proximity 1 of Gibraltar: early signs of Atlantic-Mediterranean gateway restriction. *Mar. Geol.* 434.
- Burke, A., Present, T.M., Paris, G., Rae, E.C.M., Sandilands, B.H., Gaillardet, J., Peucker-Ehrenbrink, B., Fischer, W.W., McClelland, J.W., Spencer, R.G.M., Voss, B.M., Adkins, J.F., 2018. Sulfur isotopes in rivers: Insights into global weathering budgets, pyrite oxidation, and the modern sulfur cycle. *Earth Planet. Sci. Lett.* 496, 168–177.
- Butler, R.W.H., Likhovich, W.H., Grasso, M., Pedley, H.M., Ramberti, L., 1995. Tectonics and sequence stratigraphy in Messinian Basins, Sicily: constraints on the initiation and termination of the Mediterranean salinity crisis. *Geol. Soc. Am. Bull.* 107, 425–439.
- Butler, R.W.H., Maniscalco, R., Sturiale, G., Grasso, M., 2015. Stratigraphic variations control deformation patterns in evaporite basins: Messinian examples, onshore and offshore Sicily (Italy). *J. Geol. Soc.* 172, 113–124.

- Camerlenghi, A., Aloisi, V., 2020. Uncovering the Mediterranean Salt Giant (MEDSALT)- Scientific Networking as Incubator of Cross-disciplinary Research in Earth Sciences. *Eur. Rev.* 28 (1), 40–61. <https://doi.org/10.1017/S1062798719000255>.
- Camerlenghi, A., Accettella, D., Costa, S., Lastras, G., Acosta, J., Canals, M., Wardell, N., 2009. Morphogenesis of the SW Balearic continental slope and adjacent abyssal plain, Western Mediterranean Sea. *Int. J. Earth Sci.* 98, 735–750.
- Camerlenghi, A., Del Ben, A., Hübscher, C., Forlin, E., Geletti, R., Brancatelli, G., Micallef, A., Saule, M., Facchin, L., 2019. Seismic markers of the Messinian salinity crisis in the deep Ionian Basin. *Basin Res.* 12392. <https://doi.org/10.1111/bre.12392>.
- Cameselle, A.L., Urgeles, R., 2017. Large-scale margin collapse during Messinian early sea-level drawdown: the SW Valencia trough, NW Mediterranean. *Basin Res.* 29, 576–595. <https://doi.org/10.1111/bre.12170>.
- Cameselle, A.L., Urgeles, R., De Mol, B., Camerlenghi, A., Canning, J.C., 2014. Late Miocene sedimentary architecture of the Ebro Continental Margin (Western Mediterranean): implications to the Messinian Salinity Crisis. *Int. J. Earth Sci.* 103 (2), 423–440.
- Campillo, A.C., Maldonado, A., Mauffret, A., 1992. Stratigraphic and Tectonic evolution of the Western Alboran Sea late Miocene to recent. *Geo-Mar. Lett.* 12, 165–172.
- Capella, W., Flecker, R., Hernandez-Molina, F.J., Simon, D., Meijer, P.T., Rogerson, M., Sierro, F.J., Krijgsman, W., 2019. Mediterranean isolation preconditioning the Earth System for late Miocene climate cooling. *Sci. Rep.* 9 (1), 1–8. <https://doi.org/10.1038/s41598-019-40208-2>.
- Capella, W., Spakman, W., van Hinsbergen, D.J., Chertova, M.V., Krijgsman, W., 2020. Mantle resistance against Gibraltar slab dragging as a key cause of the Messinian Salinity Crisis. *Terra Nova* 32 (2), 141–150. <https://doi.org/10.1111/ter.12442>.
- Capellini, G., 1880. Gli strati a Congerie o la formazione gessosa solfifera nella provincia di Pisa e nei dintorni di Livorno. *Mem. R. Accad. Lincei., Cl. Sci. Fis. Mat. Nat.* 5, 1–64.
- Carbonnel, G., 1978. La zone a Loxoconcha djaffarovi Schneider (ostracodes, Mio' c'ene sup'erieur) ou le Messinien de la vallee du Rhone. *Rev. Micropaleontol.* 21 (3), 106–118.
- Carnevale, G., Landini, W., Sarti, G., 2006a. Mare versus Lago-mare: marine fishes and the Mediterranean environment at the end of the Messinian Salinity Crisis. *J. Geol. Soc.* 163 (1), 75–80. <https://doi.org/10.1144/0016-764904-158>.
- Carnevale, G., Caputo, D., Landini, W., 2006b. Late Miocene fish otoliths from the Colombacci Formation (Northern Apennines, Italy): implications for the Messinian 'Lago-mare' event. *Geol. J.* 41 (5), 537–555. <https://doi.org/10.1002/gj.1055>.
- Carnevale, G., Longinelli, A., Caputo, D., Barbieri, M., Landini, W., 2008. Did the Mediterranean marine reflooding precede the Miocene/Pliocene boundary? Paleontological and geochemical evidence from upper Messinian sequences of Tuscany, Italy. *Paleogeogr. Paleoclimatol. Paleocool.* 257, 81–105. <https://doi.org/10.1016/j.paleo.2007.09.005>.
- Carnevale, G., Dela Pierre, F., Natalicchio, M., Landini, W., 2018. Fossil marine fishes and the "Lago Mare" event: Has the Mediterranean ever transformed into a brackish lake? *Newsl. Stratigr.* 51, 57–72. <https://doi.org/10.1127/nos/2016/0343>.
- Carnevale, G., Gennari, R., Lozar, F., Natalicchio, M., Pellegrino, L., Dela Pierre, F., 2019. Living in a deep desiccated Mediterranean Sea: An overview of the Italian fossil record of the Messinian salinity crisis. *Boll. Soc. Paleontol. Ital.* 58, 109–140. <https://doi.org/10.4435/BSP.2019.04>.
- Cartwright, J.A., Jackson, M.P.A., 2008. Initiation of gravitational collapse of an evaporitic basin margin: the Messinian saline giant, Levant Basin, eastern Mediterranean. *Geol. Soc. Am. Bull.* 120, 399–413.
- Caruso, A., Pierre, C., Blanc-Valleron, M.M., Rouchy, J.M., 2015. Carbonate deposition and diagenesis in evaporitic environments: the evaporative and sulphur-bearing limestones during the settlement of the Messinian Salinity Crisis in Sicily and Calabria. *Palaeogeogr. Palaeoclimatol. Palaeoecol.* 429, 136–162. <https://doi.org/10.1016/j.palaeo.2015.03.035>.
- Caruso, A., Blanc-Valleron, M.M., Da Prato, S., Pierre, C., Rouchy, J.M., 2020. The late Messinian "Lago-Mare" event and the Zanclean Reflooding in the Mediterranean Sea: new insights from the Cuevas del Almanzora section (Vera Basin, South-Eastern Spain). *Earth Sci. Rev.* 200, 102993 <https://doi.org/10.1016/j.earscirev.2019.102993>.
- Casati, P., Bertozzi, P., Cita, M.B., Longinelli, A., Damiani, V., 1976. Stratigraphy and paleoenvironment of the Messinian "Colombacci" Formation in the periadriatic trough. *A pilot study. Memorie della Societa Geologica Italiana* 16, 17–3–195.
- Castradori, D., 1998. Calcareous nannofossils in the basal Zanclean of the Eastern Mediterranean Sea: remarks on paleoceanography and sapropel formation. In: Robertson, A.H.F., Emeis, K.C., Richter, C., Camerlenghi, A. (Eds.), *Proceedings of the Ocean Drilling Program. US Government Printing Office, Washington*, pp. 113–123. *Scientific Results* 160.
- Catalano, R., Valenti, V., Albanese, C., Accaino, F., Sulli, A., Tinivella, U., Morticelli, M.G., Zanolli, C., Giustiniani, M., 2013. Sicily's fold-thrust belt and slab roll-back: the SE. RI. PRO. seismic crustal transect. *J. Geol. Soc.* 170 (3), 451–464.
- Cazzini, F.F., Amadori, C., Bosino, A., Fantoni, R., 2020. New seismic evidence of the Messinian paleomorphology beneath Lake Maggiore area (Italy). *Ital. J. Geosci.* 139 (2), 195–211. <https://doi.org/10.33011/IJG.2019.26>.
- Chumakov, I.S., 1973. Pliocene and Pleistocene deposits of the Nile valley in Nubia and upper Egypt. In: Ryan, W.B.F., Hsu, K.J., et al. (Eds.), *Initial Reports of the Deep Sea Drilling Project*, 13. US Govern. Print. Office, Washington, DC, pp. 1242–1243.
- Cipollari, P., Cosentino, D., Giozzi, E., 1999. Extension-and compression-related basins in central Italy during the Messinian Lago-Mare event. *Tectonophysics* 315 (1–4), 163–185.
- Cipollari, P., Cosentino, D., Radeff, G., Schildgen, T.F., Faranda, C., Grossi, F., Giozzi, E., Smedile, A., Gennari, R., Darbas, G., Dudas, F.O., Gürbüz, K., Nazik, A., Ehtler, H., 2013. Easternmost Mediterranean evidence of the Zanclean flooding event and subsequent surface uplift: Adana Basin, southern Turkey. *Geol. Soc. Lond., Spec. Publ.* 372 (1), 473–494. <https://doi.org/10.1144/SP372.5>.
- Cita, M.B., 1973. Inventory of biostratigraphical findings and problems. *Init. Rep. Deep-Sea Drill. Proj.* 13 (2), 1045–1065.
- Cita, M.B., Colombo, L., 1979. Sedimentation in the latest Messinian at Capo Rossello (Sicily). *Sedimentology* 26, 497–522.
- Cita, M.B., Wright, R.C., Ryan, W.B.F., Longinelli, A., 1978. Messinian paleoenvironments. In: Hsü, K.J., Montadert, L., et al. (Eds.), *Initial Reports of the Deep Sea Drilling Project*, 42. U.S. Government Printing Office, Washington D.C., pp. 1003–1035.
- Cita, M.B., Santambrogio, S., Melillo, B., Rogate, F., 1990. Messinian Paleoenvironments: New Evidence from the Tyrrhenian Sea (ODP LEG 107). In: *Proceedings of the Ocean Drilling Program, Scientific Results*, 107, pp. 211–227.
- Clauzon, G., 1982. Le canyon messinien du Rho'ne: Une preuve decisive du "desiccated deep basin model" (Hsu, Cita et Ryan, 1973). *Bull. Soc. Geol. Fr.* 24, 231–246.
- Clauzon, G., Suc, J.-P., Gautier, F., Berger, A., Loutre, M.F., 1996. Alternate interpretation of the Messinian salinity crisis, controversy resolved? *Geology* 24, 363–366.
- Clauzon, G., Suc, J.P., Popescu, S.M., Marunteanu, M., Rubino, J.L., Marinescu, F., Melinte, M.C., 2005. Influence of Mediterranean sea-level changes on the Dacic Basin (Eastern Paratethys) during the late Neogene: the Mediterranean Lago Mare facies deciphered. *Basin Res.* 17 (3), 437–462. <https://doi.org/10.1111/j.1365-2117.2005.00269.x>.
- Clauzon, G., Suc, J.-P., Do Couto, D., Jouannic, G., Melinte-Dobrinescu, M.C., Jolivet, L., Quillev'ere, F., Le Bret, N., Mocochain, L., Popescu, S.-M., Martinelli, J., Domenech, R., Rubino, J.-L., Gumiaux, C., Warny, S., Bellas, S.M., Gorini, C., Bache, F., Rabineau, M., Estrada, F., 2015. New insights on the Sorbas Basin (SE Spain): the onshore reference of the Messinian salinity crisis. *Mar. Pet. Geol.* 66, 71–100. <https://doi.org/10.1016/j.marpetgeo.2015.02.016>.
- Claypool, G.E., Holser, W.T., Kaplan, I.R., Sakai, H., Zak, I., 1980. The age curves of sulfur and oxygen isotopes in marine sulfate and their mutual interpretation. *Chem. Geol.* 28, 199–260.
- Colalongo, M.L., Cremonini, G., Farabegoli, E., Sartori, R., Tampieri, R., Tomadin, L., 1976. Paleoenvironmental study of the "Colombacci" Formation in Romagna (Italy): the cella section. *Mem. Soc. Geol. Ital.* 16, 197–216.
- Colombero, S., Alba, D.M., D'Amico, C., Delfino, M., Esu, D., Giuntelli, P., Harzhauser, M., Mazza, P.P.A., Mosca, M., Neubauer, T.A., Pavia, G., Pavia, M., Villa, A., Carnevale, G., 2017. Late Messinian mollusks and vertebrates from Moncucco Torinese, north-western Italy. Paleontological and paleoclimatological implications. *Palaeontol. Electron.* 1–66, 20.1.10A.
- Comas, M.C., Zahn, R., Klaus, A., et al., 1996. *Proceedings of the Ocean Drilling Program, Initial Reports*, v. 161: College Station, Texas, Ocean Drilling Program.
- Comas, M.C., Platt, J.P., Soto, J.I., Watts, A.B., 1999. 44. The origin and tectonic history of the Alboran Basin: Insights from leg 161 results: *Proceedings of the Ocean Drilling Program. Sci. Res.* 161, 555–580.
- Consorti, L., Sabbatino, M., Parente, M., 2020. Insights on the paleoecology of Ammonia (Foraminifera, Rotalioidea) from Miocene carbonates of central and southern Apennines (Italy). *Palaeogeogr. Palaeoclimatol. Palaeoecol.* 110105 <https://doi.org/10.1016/j.palaeo.2020.110105>.
- Corbí, H., Soria, J.M., 2016. Late Miocene-early Pliocene planktonic foraminifer event-stratigraphy of the Bajo Segura basin: a complete record of the western Mediterranean. *Mar. Pet. Geol.* 77, 1010–1027. <https://doi.org/10.1016/j.marpetgeo.2016.08.004>.
- Corbí, H., Soria, J.M., Lancis, C., Giannetti, A., Tent-Manclús, J.E., Dinar'es-Turell, J., 2016. Sedimentological and paleoenvironmental scenario before, during, and after the Messinian Salinity Crisis: The San Miguel de Salinas composite section (western Mediterranean). *Mar. Geol.* 379, 246–266. <https://doi.org/10.1016/j.margeo.2016.05.017>.
- Corbí, H., Soria, J.M., Giannetti, A., Y'ebenes, A., 2020. The step-by-step restriction of the Mediterranean (start, amplification, and consolidation phases) preceding the Messinian Salinity Crisis (climax phase) in the Bajo Segura basin. *Geo-Mar. Lett.* 1–21. <https://doi.org/10.1007/s00367-020-00647-7>.
- Corn'ee, J.J., Munch, P., Achalhi, M., Merzeraud, G., Azdimousa, A., Quillev'ere, F., Melinte-Dobrinescu, M., Chaï, C., Ben Moussa, A., Lofi, J., Seranne, A., Moissette, P., 2016. The Messinian erosional surface and early Pliocene reflooding in the Alboran Sea: new insights from the Boudinar basin. *Morocco. Sediment. Geol.* 333, 115–129. <https://doi.org/10.1016/j.sedgeo.2015.12.014>.
- Corradini, D., Biffi, U., 1988. Etude des dinokystes a la limite Messinien-Pliocene dans la coupe Cava Serredi, Tos cane, Italie. *Bulletin des Centres de Recherche Exploration- Production Elf-Aquitaine* 12 (1), 221–236.
- Cosentino, D., Cipollari, P., Mastro, S.L., Giampaolo, C., 2005. High-frequency cyclicity in the latest Messinian Adriatic foreland basin: insight into paleoclimate and paleoenvironments of the Mediterranean Lago-Mare episode. *Sediment. Geol.* 178 (1–2), 31–53. <https://doi.org/10.1016/j.sedgeo.2005.03.010>.

- Cosentino, D., Federici, I., Cipollari, P., Gliozzi, E., 2006. Environments and tectonic instability in central Italy (Garigliano Basin) during the late Messinian Lago-Mare episode: new data from the onshore Mondragone 1 well. *Sediment. Geol.* 188, 297–317. <https://doi.org/10.1016/j.sedgeo.2006.03.010>.
- Cosentino, D., Gliozzi, E., Pionzi, G., 2007. The late Messinian Lago-Mare episode in the Mediterranean Basin: preliminary report on the occurrence of Paratethyan ostracod fauna from central Crete (Greece). *Geobios* 40 (3), 339–349. <https://doi.org/10.1016/j.geobios.2007.01.001>.
- Cosentino, D., Darbas, G., Gürbüz, K., 2010. The Messinian salinity crisis in the marginal basins of the peri-Mediterranean orogenic systems: examples from the central Apennines (Italy) and the Adana Basin (Turkey). *EGUGA* 2462.
- Cosentino, D., Bertini, A., Cipollari, P., Florindo, F., Gliozzi, E., Grossi, F., Lo Mastro, S., Sprovieri, M., 2012. Orbitally forced paleoenvironmental and paleoclimate changes in the late postevaporitic Messinian of the central Mediterranean Basin. *GSA Bull.* 124 (3–4), 499–516. <https://doi.org/10.1130/B30462.1>.
- Cosentino, D., Buchwaldt, R., Sampalmieri, G., Iadanza, A., Cipollari, P., Schildgen, T.F., Hinnov, L.A., Ramezani, J., Bowring, S.A., 2013. Refining the Mediterranean “Messinian gap” with high-precision U-Pb zircon geochronology, central and northern Italy. *Geology* 41, 323–326. <https://doi.org/10.1130/G33820.1>.
- Cosentino, D., Bracone, V., D’Amico, C., Cipollari, P., Esu, D., Faranda, C., Frezza, V., Gliozzi, E., Grossi, F., Gupperri, P., Iadanza, A., Kotsakis, D., Soulié-Marsche, I., 2018. The record of the Messinian salinity crisis in mobile belts: insights from the Molise allochthonous units (southern Apennines, Italy). *Paleogeogr. Paleoclimatol. Paleoecol.* 503, 112–130. <https://doi.org/10.1016/j.paleo.2018.04.028>.
- Coulson, S., Pico, T., Austermann, J., Powell, E., Moucha, R., Mitrović, J.X., 2019. The role of isostatic adjustment and gravitational effects on the dynamics of the Messinian salinity crisis. *Earth Planet. Sci. Lett.* 525, 115760.
- Dal Cin, M., Del Ben, A., Mocnik, A., Accaino, F., Geletti, R., Wardell, N., Zgur, F., Camerlenghi, A., 2016. Seismic imaging of late Miocene (Messinian) evaporites from western Mediterranean back-arc basins. *Pet. Geosci.* 22, 297–308. <https://doi.org/10.1144/petgeo2015-096>.
- De Benedetti, A., 1982. The problem of the origin of the salt deposits in the Mediterranean and of their relations to other salt occurrences in the Neogene formations of the contiguous regions. *Mar. Geol.* 49, 91–114. de la Chapelle, G., Gaudant, J., 1987. Découverte de deux nouveaux gisements de poissons fossiles messiniens dans le bassin de Nijar-Carboneras (Andalousie Orientale): Signification paléocéologique et implications paléogéographiques.
- de la Pena, L.G., Ranero, C.R.G., Racia, E., Booth-Rea, G., 2020. The evolution of the westernmost Mediterranean basins. *Earth Sci. Rev.* 103445.
- Decima, A., 1964. Ostracodi del Gen. *Cyprideis* JONES del Neogene e del Quaternario italiani. *Paleont. Italica*, 57, p. 81.
- Decima, A., Sprovieri, R., 1973. Comments on late Messinian microfaunas in several sections from Sicily. In: Drooger, C.W. (Ed.), *Messinian Events in the Mediterranean*. North-Holland Pub. Co, Amsterdam, pp. 229–234.
- Decima, A., Wezel, F.C., 1971. Osservazioni sulle evaporiti Messiniane della Sicilia centro-meridionale. *Rivista Mineraria Siciliana* 130–134, 172–187.
- Decima, A., Wezel, F.C., 1973. Late Miocene evaporites of the Central Sicilian Basin. In: Ryan, W.B.F., Hsu, K.J. (Eds.), *Initial Reports of the Deep Sea Drilling Project*, vol. 13. U.S. Gov. Print. Off, Washington, DC, pp. 1234–1240.
- Decima, A., Schreiber, B.C., McKenzie, J.A., 1988. The origin of “evaporitic” limestones: an example from the Messinian of Sicily (Italy). *J. Sediment. Petrol.* 58–2, 256–272.
- Del Olmo, W.M., 2011. The Messinian in the Gulf of Valencia and Alboran Sea (Spain): paleogeography and paleoceanography implications. *Rev. Soc. Geol. Esp.* 24, 1–22.
- Del Olmo, W.M., Martín, D., 2016. The Messinian record of Spanish onshore and offshore data (Atlantic Ocean and Western Mediterranean Sea). *Pet. Geosci.* 22 (4), 291–296. Dela Pierre, F., Bernardi, E., Cavagna, S., Clari, P., Gennari, R., Irace, A., Lozar, F., Lugli, S., Manzi, V., Natalicchio, M., Roveri, M., Violanti, D., 2011. The record of the Messinian salinity crisis in the Tertiary Piedmont Basin (NW Italy): The Alba section revisited. *Paleogeogr. Paleoclimatol. Paleoevol.* 310, 238–255. <https://doi.org/10.1016/j.paleo.2011.07.017>.
- Dela Pierre, F., Clari, P., Bernardi, E., Natalicchio, M., Costa, M., Cavagna, S., Lozar, F., Lugli, S., Manzi, V., Roveri, M., Violanti, D., 2012. Messinian carbonate-rich beds of the Tertiary Piedmont Basin (NW Italy): microbially-mediated products straddling the onset of the salinity crisis. *Paleogeogr. Paleoclimatol. Paleoevol.* 34, 78–93. <https://doi.org/10.1016/j.paleo.2012.05.022>.
- Dela Pierre, F., Clari, P., Natalicchio, M., Ferrando, S., Giustetto, R., Lozar, F., Lugli, S., Manzi, V., Roveri, M., Violanti, D., 2014. Flocculent layers and bacterial mats in the mudstone interbeds of the Primary Lower Gypsum unit (Tertiary Piedmont Basin, NW Italy): archives of paleoenvironmental changes during the Messinian salinity crisis. *Mar. Geol.* 335, 71–87. <https://doi.org/10.1016/j.margeo.2014.05.010>.
- Dela Pierre, F., Natalicchio, M., Lozar, F., Bonetto, S., Carnevale, G., Cavagna, S., Clari, P., Colombero, S., Violanti, D., 2016. The northernmost record of the Messinian salinity crisis (Piedmont Basin, NW Italy). *Geol. F. Trips* 8, 1–58. <https://doi.org/10.3301/GFT.2016.03>.
- Delrieu, B., Rouchy, J.M., Foucault, A., 1993. La surface d’érosion finmessinienne en Crête centrale (Grèce) et sur le pourtour méditerranéen: Rapports avec la crise de salinité méditerranéenne. *Comptes rendus de l’Académie des sciences. Série 2, Mécanique, Physique, Chimie, Sciences de l’univers, Sciences de la Terre* 316, no. 4, pp. 527–533.
- Dettman, D.L., Flessa, K.W., Roopnarine, P.D., Schone, B.R., Goodwin, D.H., 2004. The use of oxygen isotope variation in shells of estuarine mollusks as a quantitative record of seasonal and annual Colorado River discharge. *Geochim. Cosmochim. Acta* 68 (6), 1253–1263.
- Di Stefano, A., Sturiale, G., 2010. Refinements of calcareous nannofossil biostratigraphy at the Miocene/Pliocene Boundary in the Mediterranean region. *Geobios* 43 (1), 5–20.
- Do Couto, D., Popescu, S.-M., Suc, J.-P., Melinte-Dobrescu, M.C., Barhoun, N., Gorini, C., Jolivet, L., Poort, J., Jouanic, G., Auxietre, J.-L., 2014. Lago Mare and the Messinian salinity crisis: evidences from the Alboran Sea (S. Spain). *Mar. Pet. Geol.* 52, 57–76. <https://doi.org/10.1016/j.margeo.2014.01.018>.
- Doebbert, A.C., Johnson, C.M., Carroll, A.R., Beard, B.L., Pietras, J.T., Carson, M.R., Norsted, B., Throckmorton, L.A., 2014. Controls on Sr isotopic evolution in lacustrine systems: Eocene green river formation, Wyoming. *Chem. Geol.* 380, 172–189. <https://doi.org/10.1016/j.chemgeo.2014.04.008>.
- Dominici, S., Danise, S., Benvenuti, M., 2018. Pliocene stratigraphic paleobiology in Tuscany and the fossil record of marine megafauna. *Earth Sci. Rev.* 176, 277–310.
- Druschi, O., Maillard, A., Ochoa, D., Lofi, J., Chanier, F., Gaillier, V., Briaies, A., Sage, F., Sierro, F., Garcia, M., 2015. Messinian Salinity Crisis deposits widespread over the Balearic Promontory: insights from new high-resolution seismic data. *Mar. Pet. Geol.* 66, 41–54. <https://doi.org/10.1016/j.margeo.2014.09.008>.
- Druckman, Y., Buchbinder, B., Martinotti, G.M., Tov, R.S., Aharon, P., 1995. The buried Afik Canyon (eastern Mediterranean, Israel): a case study of a Tertiary submarine canyon exposed in Late Messinian times. *Mar. Geol.* 123 (3–4), 167–185.
- Drury, A.J., Westerhold, T., Hodell, D., Rohlf, U., 2018. Reinforcing the North Atlantic “backbone: revision and extension of the composite splice at ODP Site 982. *Clim. Past* 14 (3), 321–338.
- Emeis, K.-C., Robertson, A.H.F., Richter, C., et al., 1996. *Proc. ODP, Initial Reports*, 160: College Station, TX (Ocean Drilling Program).
- Englebrecht, A.C., Sachs, J.P., 2005. Determination of sediment provenance at drift sites using hydrogen isotopes and unsaturation ratios in alkenones. *Geochim. Cosmochim. Acta* 69, 4253–4265.
- Estrada, F., Ercilla, G., Gorini, C., Alonso, B., Vazquez, J.T., Garcia-Castellanos, D., Juan, C., Maldonado, A., Ammar, A., Elabbassi, M., 2011. Impact of pulsed Atlantic water inflow into the Alboran Basin at the time of the Zanclean flooding. *Geology* 39, 361–366.
- Esu, D., 2007. Latest Messinian “Lago-Mare” Lymnocypridae from Italy: close relations with the Pontian fauna from the Dacic Basin. *Geobios* 40 (3), 291–302. <https://doi.org/10.1016/j.geobios.2006.10.003>.
- Faranda, C., Gliozzi, E., Cipollari, P., Grossi, F., Darbas, G., Gürbüz, K., Cosentino, D., 2013. Messinian paleoenvironmental changes in the easternmost Mediterranean Basin: Adana Basin, southern Turkey. *Turk. J. Earth Sci.* 22 (5), 839–863. <https://doi.org/10.3906/yer-1205-11>.
- Feng, Y.E., Yankelzon, A., Steinberg, J., Reshef, M., 2016. Lithology and characteristics of the Messinian evaporite sequence of the deep Levant Basin, Eastern Mediterranean. *Mar. Geol.* 376, 118–131. <https://doi.org/10.1016/j.margeo.2016.04.004>.
- Feng, Y.E., Steinberg, J., Reshef, M., 2017. Intra-salt deformation: implications for the evolution of the Messinian evaporites in the levant basin, eastern Mediterranean. *Mar. Pet. Geol.* 88, 251–267.
- Fiduk, J.C., 2009. Evaporites, petroleum exploration, and the Cenozoic evolution of the Libyan shelf margin, central North Africa. *Mar. Pet. Geol.* 26 (8), 1513–1527.
- Flecker, R., de Villiers, S., Ellam, R.M., 2002. Modelling the effect of evaporation on the salinity-⁸⁷Sr/⁸⁶Sr relationship in modern and ancient marginal-marine systems: the Mediterranean Messinian Salinity Crisis. *Earth Planet. Sci. Lett.* 203, 221–233.
- Flecker, R., Krijgsman, W., Capella, W., de Castro Martins, C., Dmitrieva, E., Mayer, J.P., Marzocchi, A., Modestu, S., Ochoa, D., Simon, D., Tulbure, M., van den Berg, B., van der Schee, M., de Lange, G., Ellam, R., Govers, R., Gutjahr, M., Hilgen, F., Kouwenhoven, T., Lofi, J., Meijer, P., Sierro, F.J., Bachiri, N., Barhoun, N., Alami, A. C., Chacon, B., Flores, J.A., Gregory, J., Howard, J., Lunt, D., Ochoa, M., Pancost, R., Vincent, S., Yousfi, M.Z., 2015. Evolution of the late Miocene Mediterranean-Atlantic gateways and their impact on regional and global environmental change. *Earth Sci. Rev.* 150, 365–392. <https://doi.org/10.1016/j.earscirev.2015.08.007>.
- Fontes, J.-C., Letolle, R., Nesteroff, D., Ryan, W.B.F., 1973. Oxygen, Carbon, Sulfur and Hydrogen stable isotopes in carbonate and sulfate mineral phases of Neogene evaporites, sediments and in interstitial waters. Texas A.M University, O.D.P.C.S., TX, United States (Ed.). In: *Initial Reports of the Deep Sea Drilling Project, Covering Leg 13 of the Cruises of the Drilling Vessel Glomar Challenger Lisbon, Portugal to Lisbon, Portugal, August-October 1970*, United States, pp. 788–796.
- Fortuin, A.R., Krijgsman, W., 2003. The Messinian of the Nijar basin (SE Spain): sedimentation, depositional environments and paleogeographic evolution. *Sediment. Geol.* 160, 213–242.
- Fortuin, A.R., Kelling, J.M.D., Roep, T.B., 1995. The enigmatic Messinian-Pliocene section of Cuevas del Almanzora (Vera Basin, SE Spain) revisited-erosional features and strontium isotope ages. *Sediment. Geol.* 97, 177–201.
- Frey-Martinez, J.F., Cartwright, J.A., Burgess, P.M., Bravo, J.V., 2004. 3D seismic interpretation of the Messinian Unconformity in the Valencia Basin, Spain. *Geol. Soc. Lond. Mem.* 29 (1), 91–100.
- Friedman, G.M., 1973. Petrographic data and comments on the depositional environment of the Miocene sulfates and dolomites at Sites 124, 132, and 134, western Mediterranean Sea. In: Ryan, W.B.F., Hsu, K.J., et al. (Eds.), *Initial Reports of the Deep Sea Drilling Project* 13. U. S. Government Printing Office, Washington, pp. 695–708.
- Frigui, M., Youssef, M.B., Ouaja, M., 2016. Evidences of “Lago-Mare” episode around the Messinian-Pliocene boundary in eastern Tunisia (central Mediterranean). *J. Afr. Earth Sci.* 123, 57–74. <https://doi.org/10.1016/j.jafrearsci.2016.07.007>.

- Fritz, P., Basharmal, G.M., Drimmie, R.J., Ibsen, J., Qureshi, R.M., 1989. Oxygen isotope exchange between sulphate and water during bacterial reduction of sulphate. *Chem. Geol.* 79, 99–105.
- Gallais, F., Gutscher, M.A., Graindorge, D., Klaeschen, D., 2018. 12.B&E- Ionian Basin. In J. Lofi (Ed.), *Seismic Atlas of the Messinian salinity crisis markers in the Mediterranean sea*. Volume 2. - Memoires de la Societe geologique de France, n.s., 2018, t. 181, and Commission for the Geological Map of the World, pp. 41–44.
- García-Alix, A., Minwer-Barakat, R., Martín Suarez, E., Freudenthal, M., Aguirre, J., Kaya, F., 2016. Updating the Europe-Africa small mammal exchange during the late Messinian. *J. Biogeogr.* 43 (7), 1336–1348.
- García-Castellanos, D., Villasenor, A., 2011. Messinian salinity crisis regulated by competing tectonics and erosion at the Gibraltar arc. *Nature* 480, 359–363. <https://doi.org/10.1038/nature10651>.
- García-Castellanos, D., Estrada, F., Jimenez-Munt, I., Gorini, C., Fernandez, M., Verges, J., De Vicente, R., 2009. Catastrophic flood of the Mediterranean after the Messinian salinity crisis. *Nature* 462, 10. <https://doi.org/10.1038/nature08555>.
- García-Castellanos, D., Micallef, A., Estrada, F., Camerlenghi, A., Ercilla, G., Periañez, R., Abril, J.M., 2020. The Zanclean megaflood of the Mediterranean—Searching for independent evidence. *Earth Sci. Rev.* 201, 103061. <https://doi.org/10.1016/j.earscirev.2019.103061>.
- García-García, F., Corbí, H., Soria, J.M., Viseras, C., 2011. Architecture analysis of a river flood-dominated delta during an overall sea-level rise (Early Pliocene, SE Spain). *Sediment. Geol.* 237, 102–113.
- García-Veigas, J., Orti, F., Rosell, L., Ayora, C., Rouchy, J.M., Lugli, S., 1995. The Messinian salt of the Mediterranean: geochemical study of the salt from the Central Sicily Basin and comparison with the Lorca Basin (Spain). *Bull. Soc. Geol. Fr.* 166, 699–710.
- García-Veigas, J., Cendon, D.I., Gibert, L., Lowenstein, T.K., Artiaga, D., 2018. Geochemical indicators in Western Mediterranean Messinian evaporites: Implications for the salinity crisis. *Mar. Geol.* 403, 197–214. <https://doi.org/10.1016/j.margeo.2018.06.005>.
- Gargani, J., Moretti, I., Letouzey, J., 2008. Evaporite accumulation during the Messinian Salinity Crisis: the Suez rift case. *Geophys. Res. Lett.* 35 (2) <https://doi.org/10.1029/2007GL032494>.
- Gaullier, V., Chanier, F., Lymer, G., Vendeville, B., Maillard, A., Thion, I., Lofi, J., Sage, F., Loncke, L., 2014. Salt tectonics and crustal tectonics along the Eastern Sardinian margin, Western Tyrrhenian: new insights from the «METYSS 1» cruise. *Tectonophysics*. <https://doi.org/10.1016/j.tecto.2013.12.015>.
- Geletti, R., Zgur, F., Del Ben, A., Buriola, F., Fais, S., Fedi, M., Forte, E., Mocknik, A., Paoletti, V., Pipan, M., Ramella, R., Romeo, R., Romi, A., 2014. The Messinian Salinity Crisis: new seismic evidence in the West-Sardinian Margin and Eastern Sardo-Provençal basin (West Mediterranean Sea). *Mar. Geol.* 351, 76–90. <https://doi.org/10.1016/j.margeo.2014.03.019>.
- Gennari, R., Iaccarino, S.M., Di Stefano, A., Sturiale, G., Cipollari, P., Manzi, V., Roveri, M., Cosentino, D., 2008. The Messinian–Zanclean boundary in the Northern Apennine. *Stratigraphy* 5, 307–322.
- Gennari, R., Manzi, V., Angeletti, L., Bertini, A., Biffi, U., Ceregato, A., Rosso, A., 2013. A shallow water record of the onset of the Messinian salinity crisis in the Adriatic foredeep (Legnagnone section, Northern Apennines). *Paleogeogr. Paleoclimatol. Paleoevol.* 386, 145–164.
- Ghibaud, G., Clari, P., Perello, M., 1985. Litostratigrafia, sedimentologia ed evoluzione tettonico-sedimentaria dei depositi miocenici del margine sud-orientale del bacino terziario ligure-piemontese (Valli Borbera, Scriveria e Lemme). In memoria di Carlo Sturani. *Boll. Soc. Geol. Ital.* 104 (3), 349–397.
- Ghielmi, M., Minervini, M., Nini, C., Rogledi, S., Rossi, M., Vignolo, A., 2010. Sedimentary and tectonic evolution in the eastern Po-Plain and northern Adriatic Sea area from Messinian to Middle Pleistocene (Italy). *Rendiconti Lincei* 21 (1), 131–166. <https://doi.org/10.1007/s12210-010-0101-5>.
- Ghielmi, M., Minervini, M., Nini, C., Rogledi, S., Rossi, M., 2013. Late Miocene-Middle Pleistocene sequences in the Po Plain-Northern Adriatic Sea (Italy): the stratigraphic record of modification phases affecting a complex foreland basin. *Marine and Petroleum Geology, Special Issue: The Geology of the Peri-Adriatic Basin and of the Adriatic Sea* 42, 50–81. <https://doi.org/10.1016/j.margeo.2012.11.007>.
- Gignoux, M., 1936a. *Geologie stratigraphique*, 2^e édition. Masson, Paris.
- Gignoux, M., 1936b. *Geologie stratigraphique*, 2^e édition. Masson, Paris.
- Gillet, S., 1932. Essai de classification du Miocène supérieur et du Pliocène inférieur de Roumanie. La Transylvanie et le Banat. *Comptes Rendus Hebdomadaires des séances de l'Académie des sciences*. Séance 27 Décembre, 1932. Académie des Sciences, Paris.
- Gillet, S., 1933. Essai de classification du Miocène supérieur et du Pliocène inférieur de Roumanie. Le bassin dacique. *Comptes Rendus Hebdomadaires des séances de l'Académie des sciences*. 01/1933. Académie des Sciences, Paris.
- Gladstone, R., Flecker, R., Valdes, P., Lunt, D., Markwick, P., 2007. The Mediterranean hydrologic budget from a Late Miocene global climate simulation. *Paleogeogr. Paleoclimatol. Paleoevol.* 251 (2), 254–267. <https://doi.org/10.1016/j.paleo.2007.03.050>.
- Glozzi, E., 1999. A late Messinian brackish water ostracod fauna of Paratethyan aspect from the Vicenne Basin (Abruzzi, central Apennines, Italy). *Paleogeogr. Paleoclimatol. Paleoevol.* 151 (1–3), 191–208.
- Glozzi, E., Grossi, F., 2008. Late Messinian lago-mare ostracod paleoecology: a correspondence analysis approach. *Paleogeogr. Paleoclimatol. Paleoevol.* 264 (3–4), 288–295. <https://doi.org/10.1016/j.paleo.2007.03.055>.
- Glozzi, E., Ceci, M.E., Grossi, F., Ligios, S., 2007. Paratethyan ostracod immigrants in Italy during the Late Miocene. *Geobios* 40 (3), 325–337. <https://doi.org/10.1016/j.geobios.2006.10.004>.
- Golovina, L.A., Radionova, E.P., van Baak, C.G., Krijgsman, W., Palcu, D.V., 2019. A Late Maeotian age (6.7–6.3 Ma) for the enigmatic “Pebby Breccia” unit in DSDP Hole 380A of the Black Sea. *Paleogeogr. Paleoclimatol. Paleoevol.* 533, 109269. <https://doi.org/10.1016/j.paleo.2019.109269>.
- Gomes, M.L., Johnston, D.T., 2017. Oxygen and sulfur isotopes in sulfate in modern euxinic systems with implications for evaluating the extent of euxinia in ancient oceans. *Geochim. Cosmochim. Acta* 205, 331–359.
- Gorini, C., Lofi, J., Duval, C., Dos Reis, A.T., Guennoc, P., Lestrat, P., Mauffret, A., 2005. The Late Messinian salinity crisis and Late Miocene Tectonism: interaction and consequence on the physiography and post-rift evolution of the gulf of Lions margin. *Mar. Pet. Geol.* 22, 695–712.
- Griffin, D.L., 2002. Aridity and humidity: two aspects of the late Miocene climate of North Africa and the Mediterranean. *Paleogeogr. Paleoclimatol. Paleoevol.* 182 (1–2), 65–91.
- Grossi, F., Cosentino, D., Glozzi, E., 2008. Late Messinian Lago-Mare ostracods and paleoenvironments of the central and eastern Mediterranean Basin. *Boll. Soc. Paleontol. Ital.* 47 (2), 131–146.
- Grossi, F., Glozzi, E., Cosentino, D., 2011. Paratethyan ostracod immigrants mark the biostratigraphy of the Messinian Salinity Crisis. *Joannea Geologie und Paläontologie* 11, 66–68.
- Grossi, F., Glozzi, E., Anadon, P., Castorina, F., Voltaggio, M., 2015. Is *Cyprideis agrigentina* Decima a good paleosalinometer for the Messinian Salinity Crisis? Morphometrical and geochemical analyses from the Eraclea Minoa section (Sicily). *Paleogeogr. Paleoclimatol. Paleoevol.* 419, 75–89. <https://doi.org/10.1016/j.paleo.2014.09.024>.
- Grothe, A., 2016. *The Messinian Salinity Crisis: a Paratethyan perspective (Doctoral dissertation, University Utrecht)*.
- Grothe, A., Sangiorgi, F., Mulders, Y.R., Vasiliev, I., Reichart, G.-J., Brinkhuis, H., Stoica, M., Krijgsman, W., 2014. Black Sea desiccation during the Messinian Salinity Crisis: fact or fiction? *Geology* 42 (7), 563–566. <https://doi.org/10.1130/G35503.1>.
- Grothe, A., Sangiorgi, F., Brinkhuis, H., Stoica, M., Krijgsman, W., 2018. Migration of the dinoflagellate *Galeacysta etrusca* and its implications for the Messinian Salinity Crisis. *Newsl. Stratigr.* 51 (1), 73–91. <https://doi.org/10.1127/nos/2016/0340>.
- Grothe, A., Andreetto, F., Reichart, G.J., Wolthers, M., Van Baak, C.G., Vasiliev, I., Stoica, M., Sangiorgi, F., Middelburg, J.J., Davies, G.R., Krijgsman, W., 2020. Paratethys pacing of the Messinian Salinity Crisis: low salinity waters contributing to gypsum precipitation? *Earth Planet. Sci. Lett.* 532, 116029 <https://doi.org/10.1016/j.epsl.2019.116029>.
- Grunert, P., Harzhauser, M., Rosenthal, Y., Carnevale, G., 2016. Estuarine Lago Mare fauna from the Tertiary Piedmont Basin indicates episodic Atlantic/Mediterranean exchange during the final stage of the Mediterranean Salinity Crisis. *Paleogeogr. Paleoclimatol. Paleoevol.* 457, 70–79. <https://doi.org/10.1016/j.paleo.2016.06.005>.
- Guennoc, P., R'ehault, J.P., Thion, I., 2011. West-Corsica Margin: MSC basinal units. In: Lofi, J., et al. (Eds.), *Memoires de la Societe geologique de France and World' Geological Map Commission ed*, pp. 1–72.
- Guerra-Merchan, A., Serrano, F., Garcés, M., Gofas, S., Esu, D., Glozzi, E., Grossi, F., 2010. Messinian Lago-Mare deposits near the strait of Gibraltar (Malaga basin, S Spain). *Paleogeogr. Paleoclimatol. Paleoevol.* 285 (3–4), 264–276. <https://doi.org/10.1016/j.paleo.2009.11.019>.
- Guerra-Merchan, A., Serrano, F., Hlila, R., El Kadiri, K., de Galdeano, C.S., Garcés, M., 2014. Tectono-sedimentary evolution of the peripheral basins of the Alboran Sea in the arc of Gibraltar during the latest Messinian-Pliocene. *J. Geodyn.* 77, 158–170. <https://doi.org/10.1016/j.jog.2013.12.003>.
- Gülyüz, E., Durak, H., Ozkaptan, M., Krijgsman, W., 2020. Paleomagnetic constraints on the early Miocene closure of the southern Neo-Tethys (Van region; East Anatolia): Inferences for the timing of Eurasia-Arabia collision. *Glob. Planet. Chang.* 185, 103089. <https://doi.org/10.1016/j.gloplacha.2019.103089>.
- Günes, P., Aksu, A.E., Hall, J., 2018. Internal seismic stratigraphy of the Messinian evaporites across the northern sector of the eastern Mediterranean Sea. *Mar. Pet. Geol.* 91, 297–320. <https://doi.org/10.1016/j.margeo.2018.01.016>.
- Gvirtzman, Z., Reshef, M., Buch-Leviatan, O., Ben-Avraham, Z., 2013. Intense salt deformation in the Levant Basin in the middle of the Messinian salinity crisis. *Earth Planet. Sci. Lett.* 379, 108–119.
- Gvirtzman, Z., Reshef, M., Buch-Leviatan, O., Groves-Gidney, G., Karcz, Z., Makovsky, Y., Ben-Avraham, Z., 2015. Bathymetry of the Levant basin: interaction of salt-tectonics and surficial mass movements. *Mar. Geol.* 360, 25–39. <https://doi.org/10.1016/j.margeo.2014.12.001>.
- Gvirtzman, Z., Manzi, V., Calvo, R., Gavrieli, I., Gennari, R., Lugli, S., Reghizzi, M., Roveri, M., 2017. Intra-Messinian truncation surface in the Levant Basin explained by subaqueous dissolution. *Geology* 45 (10), 915–918. <https://doi.org/10.1130/G39113.1>.

- Hajj, F., Poszwa, A., Bouchez, J., Gu'erold, F., 2017. Radiogenic and "stable" strontium isotopes in provenance studies: a review and first results on archaeological wood from shipwrecks. *J. Archaeol. Sci.* 86, 24–49. <https://doi.org/10.1016/j.jas.2017.09.005>.
- Hajos, M., 1973. 34.5. The Mediterranean diatoms. In: *Proceedings of the Ocean Drilling Program: Initial report. Part A*, 944.
- Hallett, D., 2002. *Petroleum Geology of Libya*. Elsevier Inc., New York, 503 pp.
- Haq, B., Gorini, C., Baur, J., Moneron, J., Rubino, J.L., 2020. Deep Mediterranean's Messinian evaporite giant: how much salt? *Glob. Planet. Chang.* 184, 103052. <https://doi.org/10.1016/j.gloplacha.2019.103052>.
- Hardie, L.A., Lowenstein, T.K., 2004. Did the Mediterranean Sea dry out during the Miocene? A reassessment of the evaporite evidence from DSDP Legs 13 and 42A cores. *J. Sediment. Res.* 74, 453–461.
- Harzhauser, M., Neubaupper, T.A., Georgopoulou, E., Esu, D., D'Amico, C., Pavia, G., Giuntelli, P., Carnevale, G., 2015. Late Messinian continental and Lago-Mare gastropods from the Tertiary Piedmont Basin. NW Italy. *Boll. Soc. Paleontol. Ital.* 54, 1–53. <https://doi.org/10.4435/BSP1.2015.1>.
- Herbert, T.D., Lawrence, K.T., Tzanova, A., Peterson, L.C., Caballero-Gill, R., Kelly, C.S., 2016. Late Miocene global cooling and the rise of modern ecosystems. *Nat. Geosci.* 9, 843–847. <https://doi.org/10.1038/ngeo2813>.
- Hilgen, F.J., 1991. Astronomical calibration of Gauss to Matuyama sapropels in the Mediterranean and implication for the geomagnetic polarity time scale. *Earth Planet. Sci. Lett.* 104 (2–4), 226–244.
- Hilgen, F.J., Krijgsman, W., Langereis, C.G., Lourens, L.J., Santarelli, A., Zachariasse, W. J., 1995. Extending the astronomical (polarity) time scale into the Miocene. *Earth Planet. Sci. Lett.* 136, 495–510.
- Hilgen, F., Kuiper, K., Krijgsman, W., Snel, E., van der Laan, E., 2007. Astronomical tuning as the basis for high resolution chronostratigraphy: the intricate history of the Messinian Salinity Crisis. *Stratigraphy* 4 (2–3), 231–238.
- Hodell, D.A., Benson, R.H., Kent, D.V., Boersma, A., Rakic-el Bied, K., 1994. Magnetostratigraphic, biostratigraphic, and stable isotope stratigraphy of an Upper Miocene drill core from the Sale Briqueterie (northwest Morocco): a high-resolution chronology for the Messinian stage. *Paleoceanography* 9, 835–855.
- Hodell, D.A., Curtis, J.H., Sierro, F.J., Raymo, M.E., 2001. Correlation of late Miocene to early Pliocene sequences between the Mediterranean and North Atlantic. *Paleoceanography* 16, 164–178.
- Hsü, K.J., 1972. Origin of Saline Giants: a critical review after the discovery of the Mediterranean evaporite. *Earth-Sci. Rev.* 8, 371–396.
- Hsü, K.J., Ryan, W.B.F., Cita, M., 1973a. Late Miocene desiccation of the Mediterranean. *Nature* 242, 240.
- Hsü, K.J., Cita, M.B., Ryan, W.B.F., 1973b. The origin of the Mediterranean evaporites. In: Ryan, W.B.F., Hsü, K.J., et al. (Eds.), *Initial Reports of the Deep Sea Drilling Project*, 13. U. S. Government Printing Office, Washington, pp. 1203–1231.
- Hsü, K.J., Montadert, L., Bernoulli, D., Cita, M.B., Erikson, A., Garrison, R.G., Kidd, R.B., M'elieres, F., Müller, C., Wright, R., 1978a. History of the Mediterranean salinity crisis. In: Hsü, K.J., Montadert, L., et al. (Eds.), *Initial Reports of the Deep Sea Drilling Project*. U. S. Government Printing Office, Washington, DC.
- Hsü, K.J., Montadert, L., Bernoulli, D., Bizon, G., Cita, M., Erickson, A., Fabricius, F., Garrison, R.E., Kidd, R.B., M'elieres, F., Müller, C., Wright, R.C., 1978b. Initial reports of the deep sea drilling project: DSDP volume XLII Part 1.
- Iaccarino, S., Bossio, A., 1999. Paleoenvironment of uppermost Messinian sequences in the western Mediterranean (Sites 974, 975, and 978). In: *Proceedings of the Ocean Drilling Program, Scientific Results (Vol. 161, 529–541)*. College Station, TX: Ocean Drilling Program.
- Iaccarino, S.M., Cita, M.B., Gabori, S., Gruppini, G.M., 1999. 15. High-Resolution Biostratigraphy at the Miocene/Pliocene boundary in Holes 974b and 975b, Western Mediterranean. In: *Proceedings of the Ocean Drilling Program: Scientific Results, Vol. 161*, p. 197.
- Hsü, K.J., Ryan, W.B.F., Schreiber, B.C., 1973c. Petrography of a halite sample from Hole 134-Balearic Abyssal Plain. In: Ryan, W.B.F., Hsü, K.J., et al. (Eds.), *Initial Reports of the Deep Sea Drilling Project*, 13. U. S. Government Printing Office, Washington, pp. 708–711.
- Iaccarino, S.M., Bertini, A., Di Stefano, A., Ferraro, L., Gennari, R., Grossi, F., Lirer, F., Manzi, V., Menichetti, E., Ricci Lucchi, M., Taviani, M., Sturiale, G., Angeletti, L., 2008. The Trave section (Monte dei Corvi, Ancona, central Italy): an integrated paleontological study of the Messinian deposits. *Stratigraphy* 5 (3–4), 281–306.
- Ingram, B.L., Sloan, D., 1992. Strontium isotopic composition of estuarine sediments as paleosalinity-paleoclimate indicator. *Science* 255, 68–72.
- Jagger, L.J., Bevan, T.G., McClay, K.R., 2020. Tectono-stratigraphic evolution of the SE Mediterranean passive margin, offshore Egypt and Libya. *Geol. Soc. Lond., Spec. Publ.* 476 (1), 365–401.
- Johnston, D.T., Gill, B.C., Masterson, A., Beirne, E., Casciotti, K.L., Kna, A.N., Berelson, W., 2014. Placing an upper limit on cryptic marine sulphur cycling. *Nature* 513, 530–533.
- Jolivet, L., Augier, R., Robin, C., Suc, J.-P., Rouchy, J.-M., 2006. Lithospheric-scale geodynamic context of the Messinian Salinity Crisis. *Sediment. Geol.* 188–189, 9–33. <https://doi.org/10.1016/j.sedgeo.2006.02.004>.
- Just, J., Hübscher, C., Betzler, C., Lüdmann, T., Reicherter, K., 2011. Erosion of continental margins in the Western Mediterranean due to sea-level stagnancy during the Messinian Salinity Crisis. *Geo-Mar. Lett.* 31 (1), 51–64.
- Kaplan, I.R., Rittenberg, S.C., 1964. Microbiological fractionation of sulphur isotopes. *Microbiology* 34, 195–212.
- Karakitsios, V., Cornee, J., Tsourou, T., Moissette, P., Kontakiotis, G., Agiadi, K., Manoutsoglou, E., Triantaphyllou, M., Koskeridou, E., 2017a. Messinian salinity crisis record under strong freshwater input in marginal, intermediate, and deep environments: the case of the North Aegean. *Paleogr. Paleoclimatol. Paleoecol.* 485, 316–335. <https://doi.org/10.1016/j.palaeo.2017.06.023>.
- Karakitsios, V., Roveri, M., Lugli, S., Manzi, V., Gennari, R., Antonarakou, A., Triantaphyllou, M., Agiadi, K., Kontakiotis, G., Kafousia, N., de Rafelis, M., 2017b. A record of the Messinian salinity crisis in the eastern Ionian tectonically active domain (Greece, eastern Mediterranean). *Basin Res.* 29, 203–233. <https://doi.org/10.1111/bre.12173>.
- Kartveit, K.H., Ulsund, H.B., Johansen, S.E., 2019. Evidence of sea level drawdown at the end of the Messinian salinity crisis and seismic investigation of the Nahr Menashe unit in the northern Levant Basin, offshore Lebanon. *Basin Res.* 31 (5), 827–840. <https://doi.org/10.1111/bre.12347>.
- Kastens, K.A., Masclé, J., 1990. The geological evolution of the Tyrrhenian Sea: An introduction to the scientific results of ODP Leg 107. In: *Proceedings of the Ocean Drilling Program, Scientific Results (Vol. 107, No. 3)*, p. 26. College Station, TX (Ocean Drilling Program).
- Kastens, K.A., Masclé, J., Auroux, C., et al., 1987. Proc. ODP, Init. Repts., 107. College Station, TX (Ocean Drilling Program). <https://doi.org/10.2973/odp.proc.ir.107.1987>.
- Keller, G., Abramovich, S., 2009. Lilliput effect in late Maastriichtian planktic foraminifera: response to environmental stress: *Paleogeography. Paleoclimatol. Paleoecol.* 284, 47–62.
- Keogh, S.M., Butler, R.W.H., 1999. The Mediterranean water body in the late Messinian: interpreting the record from marginal basins on Sicily. *J. Geol. Soc.* 156 (4), 837–846.
- Kirkham, C., Berton, C., Cartwright, J., Lensky, N.G., Sirota, I., Rodriguez, K., Hodgson, N., 2020. The demise of a 'salt giant' driven by uplift and thermal dissolution. *Earth Planet. Sci. Lett.* 531, 115933 <https://doi.org/10.1016/j.epsl.2019.115933>.
- Kováč, M., Andreyeva-grigorovich, A., Bajraktarević, Z., Brzobohatý, R., Filipescu, S., Fodor, L., Harzhauser, M., Nagymarosy, A., Oszczytko, N., Pavlíč, D., Rogl, F., Saftić, B., Sliva, U., Studencka, B., 2007. Badenian evolution of the Central Paratethys Sea: paleogeography, climate and eustatic sea-level changes. *Geol. Carpathica* 58, 579–606.
- Krijgsman, W., Meijer, P.T., 2008. Depositional environments of the Mediterranean "Lower Evaporites" of the Messinian salinity crisis: constraints from quantitative analyses. *Mar. Geol.* 253 (3–4), 73–81. <https://doi.org/10.1016/j.margeo.2008.04.010>.
- Krijgsman, W., Hilgen, F.J., Raffi, I., Sierro, F.J., Wilson, D.S., 1999a. Chronology, causes, and progression of the Messinian salinity crisis. *Nature* 400, 652–655.
- Krijgsman, W., Hilgen, F.J., Marabini, S., Vai, G.B., 1999b. New paleomagnetic and cyclostratigraphic age constraints on the Messinian of the Northern Apennines (Vena del Gesso Basin, Italy). *Mem. Soc. Geol. Ital.* 54, 25–33.
- Krijgsman, W., Fortuin, A.R., Hilgen, F.J., Sierro, F.J., 2001. Astrochronology for the Messinian Sorbas basin (SE Spain) and orbital (precessional) forcing for evaporite cyclicity. *Sediment. Geol.* 140, 43–60.
- Krijgsman, W., Gabori, S., Hilgen, F.J., Iaccarino, S., Kaenel, E.D., Laan, E.V.D., 2004. Revised astrochronology for the Ain el Beida section (Atlantic Morocco): no glacio-eustatic control for the onset of the Messinian Salinity Crisis. *Stratigraphy* 1, 87–101.
- Krijgsman, W., Stoica, M., Vasiliev, I., Popov, V.V., 2010. Rise and fall of the Paratethys Sea during the Messinian Salinity Crisis. *Earth Planet. Sci. Lett.* 290 (1–2), 183–191. <https://doi.org/10.1016/j.epsl.2009.12.020>.
- Krijgsman, W., Capella, W., Simon, D., Hilgen, F.J., Kouwenhoven, T.J., Meijer, P.Th., Sierro, F.J., Tulbure, M.A., van den Berg, B.C.J., van der Schee, M., Flecker, R., 2018. The Gibraltar Corridor: watergate of the Messinian Salinity Crisis. *Mar. Geol.* 403, 238–246. <https://doi.org/10.1016/j.margeo.2018.06.008>.
- Krijgsman, W., Palcu, D., Andreotto, F., Stoica, M., Mandic, O., 2020a. Changing seas in the late Miocene Northern Aegean: a Paratethyan approach to Mediterranean basin evolution. *Earth Sci. Rev.* 103386 <https://doi.org/10.1016/j.earscirev.2020.103386>.
- Krijgsman, W., Stoica, M., Hoyle, T.M., Jorissen, E.L., Lazarev, S., Rausch, L., Bista, D., Alçiçek, M.C., Ilgar, A., van den Hoek Ostende, L.W., Mayda, S., Raffi, I., Flecker, R., Mandic, O., Neubauber, T.A., Wesselingh, F.P., 2020b. The myth of the Messinian Dardanelles: Late Miocene stratigraphy and paleogeography of the ancient Aegean-Black Sea gateway. *Paleogeogr. Paleoclimatol. Paleoecol.* 110033 <https://doi.org/10.1016/j.palaeo.2020.110033>.
- Van der Laan, E., Gabori, S., Hilgen, F.J., Lourens, L.J., 2005. Regional climate and glacial control on high-resolution oxygen isotope records from Ain El Beida (latest Miocene, NW Morocco): a cyclostratigraphic analysis in the depth and time domain. *Paleoceanography* 20. <https://doi.org/10.1029/2003PA000995>. PA1001.
- Van der Laan, E., Snel, E., de Kaenel, E., Hilgen, F.J., Krijgsman, W., 2006. No major deglaciation across the Miocene-Pliocene boundary: integrated stratigraphy and astronomical tuning of the Loulja sections (Bou Regreg area, NW Morocco). *Paleoceanography* 21. <https://doi.org/10.1029/2005PA001193>. PA3011.
- Laskar, J.J., Robutel, P., Joutel, F., Gastineau, M., Correia, A.C.M., Levrard, B., 2004. A long term numerical solution for the insolation quantities of the Earth. *Astron. Astrophys.* 428, 261–285.
- Lazarev, S., de Leeuw, A., Stoica, M., Mandic, O., van Baak, C.G.C., Vasiliev, I., Krijgsman, W., 2020. From Khersonian drying to Pontian "flooding": Late Miocene stratigraphy and paleoenvironmental evolution of the Dacian Basin (Eastern Paratethys). *Glob. Planet. Chang.* 103224 <https://doi.org/10.1016/j.gloplacha.2020.103224>.
- Leavitt, W.D., Halevy, I., Bradley, A.S., Johnston, D.T., 2013. Influence of sulfate reduction rates on the Phanerozoic sulfur isotope record. *Proc. Natl. Acad. Sci.* 110, 11244.

- Leila, M., Moscardello, A., Segvı́c, B., 2018. Depositional facies controls on the diagenesis and reservoir quality of the Messinian Qawasim and Abu Madi formations, onshore Nile Delta, Egypt. *Geol. J.* 54 (3), 1797–1813.
- Liu, J., Li, S., Zhong, J., Zhu, X., Guo, Q., Lang, Y., Han, X., 2017. Sulfate sources constrained by sulfur and oxygen isotopic compositions in the upper reaches of the Xijiang River, China. *Acta Geochimica* 36, 611–618.
- Lloyd, R.M., 1968. Oxygen isotope behavior in the Sulfate-Water System. *J. Geophys. Res.* 1896-1977 (73), 6099–6110.
- Lofi, J., 2018. Seismic Atlas of the Messinian salinity crisis markers in the Mediterranean sea. Volume 2 - M'emoires de la Societ'e geologique de France, n.s., 2018, t. 181, and Commission for the Geological Map of the World, 72 p. + DVD. <https://doi.org/10.10682/2018M ESSINV2>.
- Lofi, J., Gorini, C., Berne, S., Clauzon, G., Dos Reis, A.T., Ryan, W.B.F., Steckler, M.S., 2005. Erosional processes and paleo-environmental changes in the Western Gulf of Lions (SW France) during the Messinian Salinity Crisis. *Mar. Geol.* 217, 1–30. <https://doi.org/10.1016/j.margeo.2005.02.014>.
- Lofi, J., Sage, F., Deverc'h'ere, J., Loncke, L., Maillard, A., Gaullier, V., Thionin, I., Gillet, H., Guennoc, P., Gorini, C., 2011a. Refining our knowledge of the Messinian salinity crisis records in the offshore domain through multi-site seismic analysis. *Bulletin de la Societ'e geologique de France* 182 (2), 163–180.
- Lofi, J., Deverc'h'ere, J., Gaullier, V., Gillet, H., Gorini, C., Guennoc, P., Loncke, L., Maillard, A., Sage, F., Thionin, I., 2011b. Seismic atlas of the "Messinian Salinity Crisis" markers in the Mediterranean and Black seas. Commission for the Geological Map of the World and Memoires de la Societ'e Geologique de France. *Nouv. Ser.* 72.
- Loget, N., Davy, P., Van Den Driessche, J., 2006. Mesoscale fluvial erosion parameters deduced from modelling the Mediterranean sea-level drop during the Messinian (late Miocene). *J. Geophys. Res.* 111, F03005.
- Loncke, L., Gaullier, V., Mascle, J., Vendeville, B., Camera, L., 2006. The Nile deep-sea fan: An example of interacting sedimentation, salt tectonics, and inherited subsalt paleotopographic features. *Mar. Pet. Geol.* 23, 297–315. <https://doi.org/10.1016/j.marpetgeo.2006.01.001>.
- Londeix, L., Benzakour, M., Suc, J.P., Turon, J.L., 2007. Messinian paleoenvironments and hydrology in Sicily (Italy): the dinoflagellate cyst record. *Geobios* 40 (3), 233–250. <https://doi.org/10.1016/j.geobios.2006.12.001>.
- Longinelli, A., 1979. Isotope geochemistry of some Messinian evaporates: paleoenvironmental implications. *Paleogeogr. Paleoclimatol. Paleoeoc.* 29, 95–123.
- Longinelli, A., Craig, H., 1967. Oxygen-18 variations in sulfate ions in sea water and saline lakes. *Science* 156 (3771), 56–59.
- Lopez-Garrido, A.C., Sanz de Galdeano, C., 1999. Neogene sedimentation and tectonic-eustatic control of the Malaga basin, South Spain. *J. Pet. Geol.* 22 (1), 81–96.
- Loreto, M.F., Zitellini, N., Ranero, C.R., Palmiotto, C., Prada, M., 2020. Extensional tectonics during the Tyrrhenian back-arc basin formation and a new morpho-tectonic map. *Basin Res.* 33 (1), 138–158.
- Lourens, L., Hilgen, F., Shackleton, N.J., Laskar, J., Wilson, D., 2004. The Neogene period. In: Gradstein, F.M., Ogg, J.G., Smith, A.G. (Eds.), *A Geologic Time Scale 2004*. Cambridge Univ. Press, Cambridge, pp. 409–440.
- Lozano, D.O., 2016. Astrochronological Constraints on Margin to deep basin correlations across the Balearic Promontory and the Valencia basin (Doctoral dissertation, Universidad de Salamanca).
- Lu, F.H., 2006. Lithofacies and water-body record of Messinian evaporites in Nijar Basin, SE Spain. *Sediment. Geol.* 188, 115–130.
- Lu, F.H., Meyers, W.J., Schoonen, M.A., 2001. S and O (SO4) isotopes, simultaneous modeling, and environmental significance of the Nijar Messinian gypsum, Spain. *Geochim. Cosmochim. Acta* 65, 3081–3092.
- Lugli, S., Schreiber, B.C., Triberti, B., 1999. Giant polygons in the Realmonte mine (Agrigento, Sicily): evidence for the desiccation of a Messinian halite basin. *J. Sediment. Res.* 69, 764–771.
- Lugli, S., Bassetti, M.A., Manzi, V., Barbieri, M., Longinelli, A., Roveri, M., 2007. The Messinian "Vena del Gesso" evaporites revisited: characterization of isotopic composition and organic matter. In: Schreiber, B.C., Lugli, S., Babel, M. (Eds.), *Evaporites through Space and Time*. Special Publications, 285. Geological Society, London, pp. 143–154.
- Lugli, S., Manzi, V., Roveri, M., Schreiber, B.C., 2010. The Primary Lower Gypsum in the Mediterranean: a new facies interpretation for the first stage of the Messinian salinity crisis. *Paleogeogr. Paleoclimatol. Paleoeoc.* 297, 83–99. <https://doi.org/10.1016/j.paleo.2010.07.017>.
- Lugli, S., Gennari, R., Gvirtzman, Z., Manzi, V., Roveri, M., Schreiber, B.C., 2013. Evidence of clastic evaporites in the canyons of the Levant Basin (Israel): implications for the Messinian Salinity Crisis. *J. Sediment. Res.* 83, 942–954. <https://doi.org/10.2110/jsr.2013.72>.
- Lugli, S., Manzi, V., Roveri, M., Schreiber, B.C., 2015. The deep record of the Messinian salinity crisis: evidence of a non-desiccated Mediterranean Sea. *Paleogeogr. Paleoclimatol. Paleoeoc.* 433, 201–218. <https://doi.org/10.1016/j.paleo.2015.05.017>.
- Lyster, G., Lofi, J., Gaullier, V., Maillard, A., Thionin, I., Sage, F., Chanier, F., Vendeville, B.C., 2018. The Western Tyrrhenian Sea revisited: New evidence for a rifted basin during the Messinian Salinity Crisis. *Mar. Geol.* 398, 1–21. <https://doi.org/10.1016/j.margeo.2017.12.009>.
- Madof, A.S., Connell, S.D., 2018. Northern Levant Basin. In: Lofi, et al. (Eds.), *Atlas of the Messinian Salinity Crisis markers in the Mediterranean and Black Seas* M'emoires de la Societ'e geologique de France 179. World Geological Map Commission, pp. 6'0–62.
- Madof, A.S., Bertoni, C., Lofi, J., 2019. Discovery of vast fluvial deposits provides evidence for drawdown during the late Miocene Messinian salinity crisis. *Geology* 47 (2), 171–174. <https://doi.org/10.1130/G45873.1>.
- Magyar, I., Geary, D.H., Lantos, M., Müller, P., Suto-Szentai, M., 1999a. Integrated biostratigraphic, magnetostratigraphic and chronostratigraphic correlations of the Late Miocene Lake Pannon deposits. *Acta Geol. Hung.* 42 (1), 5–31.
- Magyar, I., Geary, D.H., Müller, P., 1999b. Paleogeographic evolution of the late miocene Lake Pannon in Central Europe. *Paleogeogr. Paleoclimatol. Paleoeoc.* 147 (3–4), 151–167.
- Maillard, A., Mauffret, A., 2006. Relationship between erosion surfaces and Late Miocene Salinity Crisis deposits in the Valencia Basin (northwestern Mediterranean): evidence for an early sea-level fall. *Terra Nova* 18 (5), 321–329. <https://doi.org/10.1111/j.1365-3121.2006.00696.x>.
- Maillard, A., Mauffret, A., 2011. Valencia through. In: Lofi, et al. (Eds.), *Atlas of the Messinian Salinity Crisis markers in the Mediterranean and Black Seas* M'emoires de la Societ'e geologique de France 179. World Geological Map Commission (72 pp.).
- Maillard, A., Mauffret, A., 2013. Structure and present-day compression in the offshore area between Alicante and Ibiza Island (Eastern Iberian Margin). *Tectonophysics* 591, 116–130.
- Maillard, A., Gorini, C., Mauffret, A., Sage, F., Lofi, J., Gaullier, V., 2006. Offshore evidence of polyphase erosion in the Valencia Basin (Northwestern Mediterranean): scenario for the Messinian Salinity Crisis. *Sediment. Geol.* 188–189, 69–91.
- Maillard, A., Hübscher, C., Benkheil, J., Tahchi, E., 2011a. Deformed Messinian markers in the Cyprus Arc: tectonic and/or Messinian Salinity Crisis indicators? *Basin Res.* 23, 146–170.
- Maillard, A., Lofi, J., Deverc'h'ere, J., Gaullier, V., Loncke, L., Sage, F., Thionin, I., Guennoc, P., Gillet, H., Gorini, C., 2011b. Synthesis. In: Lofi, J., D'everc'h'ere, J., et al. (Eds.), *Atlas of the Messinian Salinity Crisis Markers in the Offshore Mediterranean Domain*. CCGM & M'em. Soc. geol. Fr., n.s., 179, 72' p.
- Maillard, A., Driussi, O., Lofi, J., Briaes, A., Chanier, F., Hübscher, C., Gaullier, V., 2014. Record of the Messinian Salinity Crisis in the SW Mallorca area (Balearic Promontory, Spain). *Mar. Geol.* 357, 304–320. <https://doi.org/10.1016/j.margeo.2014.10.001>.
- Maillard, A., Gaullier, V., L'ezin, C., Chanier, F., Odonne, F., Lofi, J., 2020. New onshore/offshore evidence of the Messinian Erosion Surface from key areas: The Ibiza-Balearic Promontory and the Orsei-Eastern Sardinian margin. D'ecouverte de la surface d'erosion messinienne onshore/offshore dans deux lieux cl'es: le Promontoire Bal'earies (Ibiza) et la marge est-sarde (Orsei). *Bulletin de la Societ'e Ge'ologique de France* 191 (1). <https://doi.org/10.1051/bsgf/2020007>.
- Maniscalco, R., Casciano, C.I., Distefano, S., Grossi, F., Di Stefano, A., 2019. Facies analysis in the Second Cycle Messinian evaporites predating the early Pliocene reflooding: the Balza Soletta section (Corvillo Basin, central Sicily). *Ital. J. Geosci.* 138 (3), 301–316. <https://doi.org/10.3301/IJG.2019.06>.
- Manzi, V., Lugli, S., Ricci Lucchi, F., Roveri, M., 2005. Deep-water clastic evaporites deposition in the Messinian Adriatic foredeep (northern Apennines, Italy): did the Mediterranean ever dry out? *Sedimentology* 52, 875–902.
- Manzi, V., Roveri, M., Gennari, R., Bertini, A., Biffi, U., Giunta, S., Iaccarino, S.M., Lanci, L., Lugli, S., Negri, A., Riva, A., Rossi, M.E., Taviani, M., 2007. The deep-water counterpart of the messinian lower evaporites in the apennine foredeep: the fananello section (northern Apennines, Italy). *Paleogeogr. Paleoclimatol. Paleoeoc.* 251, 470–499.
- Manzi, V., Lugli, S., Roveri, M., Schreiber, B.C., 2009. A new facies model for the Upper Gypsum of Sicily (Italy): chronological and paleoenvironmental constraints for the Messinian salinity crisis in the Mediterranean. *Sedimentology* 56. <https://doi.org/10.1111/j.1365-3091.2009.01063.x>, 1937–1960.
- Manzi, V., Lugli, S., Roveri, M., Schreiber, B.C., Gennari, R., 2011. The Messinian CdB (Sicily, Italy) revisited. *Geol. Soc. Am. Bull.* 123, 347–370. <https://doi.org/10.1130/B30262.1>.
- Manzi, V., Gennari, R., Hilgen, F., Krijgsman, W., Lugli, S., Roveri, M., Sierro, F.J., 2013. Age refinement of the Messinian salinity crisis onset in the Mediterranean. *Terra Nova* 25 (4), 315–322.
- Manzi, V., Lugli, S., Roveri, M., Dela, Pierre F., Gennari, R., Lozar, F., Natalicchio, M., Schreiber, B.C., Taviani, M., Turco, E., 2016a. The Messinian salinity crisis in Cyprus: A further step towards a new stratigraphic framework for Eastern Mediterranean. *Basin Res.* 28, 207–236. <https://doi.org/10.1111/bre.12107>.
- Manzi, V., Gennari, R., Lugli, S., Minelli, N., Reghizzi, M., Roveri, M., Schreiber, B.C., 2016b. Comment on "Carbonate deposition and diagenesis in evaporitic environments: the evaporative and sulphur-bearing limestones during the settlement of the Messinian Salinity Crisis in Sicily and Calabria" by Caruso et al., 2015. *Palaeo3*, 429, 136e162. *Palaeogeogr. Palaeoclimatol. Palaeoeoc.* 459, 585–596.
- Manzi, V., Gennari, R., Lugli, S., Persico, D., Reghizzi, M., Roveri, M., Schreiber, B.C., Calvo, R., Gavrieli, I., Gvirtzman, Z., 2018. The onset of the Messinian salinity crisis in the deep Eastern Mediterranean basin. *Terra Nova* 30 (3), 189–198. <https://doi.org/10.1111/ter.12325>.
- Manzi, V., Argnani, A., Corcagnani, A., Lugli, S., Roveri, M., 2020. The Messinian salinity crisis in the Adriatic foredeep: evolution of the largest evaporitic marginal basin in the

- Mediterranean. *Mar. Pet. Geol.* 115, 104288 <https://doi.org/10.1016/j.marpetgeo.2020.104288>.
- Marcano, M.C., Frank, T.D., Mukasa, S.B., Lohmann, K.C., Taviani, M., 2015. Diagenetic incorporation of Sr into aragonitic bivalve shells: Implications for chronostratigraphic and paleoenvironmental interpretations. *Depositional Record* 1 (1), 38–52. <https://doi.org/10.1016/j.marpetgeo.2020.104288>.
- Markovic, S., Paytan, A., Li, H., Wortmann, U.G., 2016. A revised seawater sulfate oxygen isotope record for the last 4Myr. *Geochim. Cosmochim. Acta* 175, 239–251. Marsaglia, K.M., Tribble, J.S., 1999. Petrography and mineralogy of the uppermost Messinian section and the Pliocene/Miocene boundary at Site 975, Western Mediterranean Sea. In: *Proc. ODP, Sci. Results*, Vol. 161, pp. 3–20. Ocean Drilling Program College Station, TX.
- Martin-Suarez, E., Freudenthal, M., Krijgsman, W., Fortuin, R., 2000. On the age of the continental deposits of the Zorreras Member (Sorbas Basin, SE Spain). *G'ebios* 33, 505–512.
- Marzocchi, A., Lunt, D.J., Flecker, R., Bradshaw, C.D., Farnsworth, A., Hilgen, F.J., 2015. Orbital control on late Miocene climate and the North African monsoon: insight from an ensemble of sub-precessional simulations. *Clim. Past* 11 (10), 1271–1295. <https://doi.org/10.5194/cpd-11-2181-2015>.
- Marzocchi, A., Flecker, R., Van Baak, C.G.C., Lunt, D.J., Krijgsman, W., 2016. Mediterranean outflow pump: an alternative mechanism for the Lago-mare and the end of the Messinian Salinity Crisis. *Geology* 44, 523–526. <https://doi.org/10.1130/G37646.1>.
- Marzocchi, A., Flecker, R., Lunt, D.J., Krijgsman, W., Hilgen, F.J., 2019. Precessional drivers of late Miocene Mediterranean sedimentary sequences: African summer monsoon and Atlantic winter storm tracks. *Paleoceanogr. Paleoclimatol.* 34 (12), 1980–1994. <https://doi.org/10.1029/2019PA003721>.
- Mas, G., 2013. Definició i caracteritzac'io de la Formac'io ses Olles (Lago mare, messin'ia terminal) a l'illa de Mallorca (illes balears, mediterrania Occidental). *Bolleti de l'Historia Natural de Balears* 56, 20'9–231.
- Mas, G., 2015. El registre estratigr'afic del Messin'ia terminal i del Plioc'ene a l'illa de Mallorca. Relacions amb la crisi de salinitat de la Mediterrania. PhD Tesis. Universitat de les Illes Balears. <http://www.tdx.cat/handle/10803/375904>.
- Mas, G., Fornos, J.J., 2020. The messinian salinity crisis in Mallorca: New insights for a western mediterranean stratigraphic scenario. *Mar. Pet. Geol.* 104656 <https://doi.org/10.1016/j.marpetgeo.2020.104656>.
- Mas, G., Bisconti, M., Torres-Roig, E., Juarez, J., Saca'eres, J., 2018a. The last whale of the Messinian. First record of a mysticete cetacean from the Mediterranean Messinian Salinity Crisis. In: *1st Paleontological Virtual Congress. Book of Abstracts—Paleontology in the Virtual Era*, Vol. 97.
- Mas, G., Maillard, A., Alcover, J.A., Fornos, J.J., Bover, P., Torres-Roig, E., 2018b. Terrestrial colonization of the Balearic Islands: New evidence for the Mediterranean sea-level drawdown during the Messinian Salinity Crisis. *Geology* 46 (6), 527–530. <https://doi.org/10.1130/G40260.1>.
- Masterson, A.L., Wing, B.A., Paytan, A., Farquhar, J., Johnston, D.T., 2016. The minor sulfur isotope composition of Cretaceous and Cenozoic seawater sulfate. *Paleoceanography* 31, 779–788.
- Mather, A., Martin, J.M., Harvey, A.M., Braga, J.C., 2001. A Field Guide to the Neogene Sedimentary Basins of the Almeria Province, South-East Spain., 186-189. Blackwell Science, Oxford.
- Mayser, J.P., Flecker, R., Marzocchi, A., Kouwenhoven, T.J., Lunt, D.J., Pancost, R.D., 2017. Precession driven changes in terrestrial organic matter input to the Eastern Mediterranean leading up to the Messinian Salinity Crisis. *Earth Planet. Sci. Lett.* 462, 199–211. <https://doi.org/10.1016/j.epsl.2017.01.029>.
- McArthur, J.M., Howarth, R.J., Shields, G.A., 2012. Strontium isotope stratigraphy. In: *Gradstein, F.M., Ogg, J.G., Schmitz, M.D., Ogg, G.M. (Eds.), The Geological Time Scale 2012*. Elsevier B.V., Oxford, pp. 127–144.
- McCulloch, M.T., De Deckker, P., 1989. Sr isotope constraints on the Mediterranean environment at the end of the Messinian salinity crisis. *Nature* 342, 62–65.
- McKenzie, J.A., 1999. From desert to deluge in the Mediterranean. *Nature* 400, 613–614.
- McKenzie, J.A., Evans, N., Hodell, D., Aloisi, G., Vasconcelos, C., 2017. Subsurface dolomite formation during post-depositional flow of sulphate-bearing fluids from underlying salt giants: Early Pliocene example at DSDP Leg 42A, Site 374, Ionian Abyssal Plain. *EGUGA* 10166.
- Medaouri, M., D'everch'ere, J., Graindorge, D., Bracene, R., Badji, R., Ouabadi, A., Yelles, K., Bendib, F., 2014. The transition from Alboran to Algerian basins (Western Mediterranean Sea): chronostratigraphy, deep crustal structure and tectonic evolution at the rear of a narrow slab rollback system. *J. Geodyn.* 77, 186–205. <https://doi.org/10.1016/j.jog.2014.01.003>.
- Meijer, P.T., Krijgsman, W., 2005. A quantitative analysis of the desiccation and re-filling of the Mediterranean during the Messinian Salinity Crisis. *Earth Planet. Sci. Lett.* 240 (2), 510–520.
- Meilijson, A., Steinberg, J., Hilgen, F., Bialik, O.M., Waldmann, N.D., Makovsky, Y., 2018. Deep-basin evidence resolves a 50-year-old debate and demonstrates synchronous onset of Messinian evaporite deposition in a non-desiccated Mediterranean. *Geology* 46 (3), 243–246. <https://doi.org/10.1130/G39868.1>.
- Meilijson, A., Hilgen, F., Sepúlveda, J., Steinberg, J., Fairbank, V., Flecker, R., Waldmann, N.D., Spaulding, S.A., Bialik, O.M., Boudinot, F.G., Illner, P., Makovsky, Y., 2019. Chronology with a pinch of salt: integrated stratigraphy of Messinian evaporites in the deep Eastern Mediterranean reveals long-lasting halite deposition during Atlantic connectivity. *Earth-Sci. Rev.* 194, 374–398. <https://doi.org/10.1016/j.earscirev.2019.05.011>.
- Melinte-Dobrinescu, M.C., Suc, J.-P., Clauzon, G., Popescu, S.-M., Armijo, R., Meyer, B., Biltekin, D., Çagatay, M.N., Ucakus, G., Jouannic, G., Fauquette, S., Çakir, Z., 2009. The Messinian salinity crisis in the Dardanelles region: Chronostratigraphic constraints. *Paleogeogr. Paleoclimatol. Paleoevol.* 278, 24–39. <https://doi.org/10.1016/j.paleo.2009.04.009>.
- Merzeraud, G., Achalhi, M., Cornee, J.J., Münch, P., Azdimousa, A., Moussa, A.B., 2019. Sedimentology and sequence stratigraphy of the late-Messinian-Early Pliocene continental to marine deposits of the Boudinar basin (North Morocco). *J. Afr. Earth Sci.* 150, 205–223. <https://doi.org/10.1016/j.jafrearsci.2018.11.002>.
- Meulenkamp, J.E., Sissingh, W., 2003. Tertiary paleogeography and tectonostratigraphic evolution of the Northern and Southern Peri-Tethys platforms and the intermediate domains of the African-Eurasian convergent plate boundary zone. *Paleogeogr. Paleoclimatol. Paleoevol.* 196 (1-2), 209–228.
- Meulenkamp, J.E., Dermizakis, M., Georgiades-Dikeoulia, E., Jonkers, H.A., Boger, A., 1979. Field Guide to the Neogene of Crete. Publication of the Department of Geology and Paleontology, University of Athens, A, 32, pp. 1–32.
- Micallef, A., Camerlenghi, A., Garcia-Castellanos, D., Cunarro Otero, D., Gutscher, M.-A., M.A., Barreca, G., Spatola, D., Facchin, L., Geletti, R., Krastel, S., Gross, F., Urlaub, M., Sulli, A., Basilone, L., Basilone, G., 2018. Evidence of the Zanclean megaflood in the eastern Mediterranean Basin. *Sci. Rep.* 8, 1–8. <https://doi.org/10.1038/s41598-018-19446-3>.
- Micallef, A., Camerlenghi, A., Georgiopoulos, A., Garcia-Castellanos, D., Gutscher, M.-A., Lo Iacono, C., Huvenne, V.A.I., Mountjoy, J.J., Paull, C.K., Le Bas, T., Spatola, D., Facchin, L., Accettella, D., 2019. Geomorphic evolution of the Malta Escarpment and implications for the Messinian evaporative drawdown in the eastern Mediterranean Sea. *Geomorphology* 327, 264–283. <https://doi.org/10.1016/j.geomorph.2018.11.012>.
- Milker, Y., Schmiedl, G., 2012. A taxonomic guide to modern benthic shelf foraminifera of the western Mediterranean Sea. *Palaeontol. Electron.* 15 (2), 1–134. <https://doi.org/10.26879/271>.
- Mocnik, A., Camerlenghi, A., Del Ben, A., Geletti, R., Wardell, N., Zgur, F., 2014. The Messinian Salinity Crisis in the West-Mediterranean Basins: comparison between two rifted margins. In: *Proceedings of the 33rd GNGTS Conference*, Bologna, Vol. 1, pp. 156–163.
- Mocnik, A., Del Ben, A., Camerlenghi, A., Geletti, R., Saule, M., 2018. 12. Ionian Basin. In: *J. Lofi (Ed.), Seismic Atlas of the Messinian salinity crisis markers in the Mediterranean sea. Volume 2. - Mémoires de la Société géologique de France, n.s., 2018, t. 181, and Commission for the Geological Map of the World*, pp. 41–44.
- Modestou, S., Simon, D., Gutjahr, M., Marzocchi, A., Kouwenhoven, T.J., Ellam, R.M., Flecker, R., 2017. Precessional variability of ⁸⁷Sr/⁸⁶Sr in the late miocene sorbas basin: An interdisciplinary study of drivers of interbasin exchange. *Paleoceanography* 32 (6), 531–552.
- Montadert, L., Letouzey, J., Mauffret, A., 1978. Messinian event: seismic evidence. In: Hsu, K.J., Montadert, L., et al. (Eds.), *Initial Reports of the Deep Sea Drilling Project*, 1. US Government Printing Office, Washington, DC, pp. 1037–1050.
- Mudie, P.J., Marret, F., Mertens, K.N., Shumilovskikh, L., Leroy, S.A., 2017. Atlas of modern dinoflagellate cyst distributions in the Black Sea Corridor: from Aegean to Aral Seas, including Marmara, Black, Azov and Caspian Seas. *Mar. Micropaleontol.* 134, 1–152.
- Müller, D.W., Mueller, P.A., 1991. Origin and age of the Mediterranean Messinian evaporites: implications from Sr isotopes. *Earth Planet. Sci. Lett.* 107 (1), 1–12.
- Müller, D.W., Mueller, P.A., McKenzie, J.A., 1990. Strontium isotopic ratios as fluid tracers in Messinian evaporites of the Tyrrhenian Sea (western Mediterranean Sea). In: *Proceedings of the Ocean Drilling Program, Scientific Results (Vol. 107, 603- 614)*. College Station, Tex.: Ocean Drill. Program.
- Natalicchio, M., Birgel, D., Peckmann, J., Lozar, F., Carnevale, G., Liu, X., Hinrichs, K.-U., Dela Pierre, F., 2017. An archaeal biomarker record of paleoenvironmental change across the onset of the Messinian salinity crisis in the absence of evaporites (Piedmont Basin, Italy). *Org. Geochem.* 113, 242–253.
- Natalicchio, M., Dela Pierre, F., Birgel, D., Brumsack, H., Carnevale, G., Gennari, R., Gier, S., Lozar, F., Pellegrino, L., Sabino, M., Schnetger, B., Peckmann, J., 2019. Paleoenvironmental change in a precession-paced succession across the onset of the Messinian salinity crisis: insight from element geochemistry and molecular fossils. *Paleogeogr. Paleoclimatol. Paleoevol.* 518, 45–61. <https://doi.org/10.1016/j.paleo.2019.01.009>.
- Nesteroff, W.D., 1973. Un mod'ele pour les evaporites messiniennes et bassins profonds avec depot' d'evaporites lagunaires. In: *Drooger, C.W. (Ed.), Messinian Events in the Mediterranean*. North-Holland Publ. Co., Amsterdam, pp. 68–81.
- Netzeband, G., Hübscher, C., Gajewski, G., 2006. The structural evolution of the Messinian evaporites in the Levantine Basin. *Mar. Geol.* 230, 249–273.
- Ochoa, D., Sierro, F.J., Lofi, J., Maillard, A., Flores, J.A., Suarez, M., 2015. Synchronous onset of the Messinian evaporite precipitation: First Mediterranean offshore evidence. *Earth Planet. Sci. Lett.* 427, 112–124. <https://doi.org/10.1016/j.epsl.2015.06.059>.
- Ochoa, D., Sierro, F.J., Hilgen, F.J., Cortina, A., Lofi, J., Kouwenhoven, T., Flores, J.A., 2018. Origin and implications of orbital-induced sedimentary cyclicity in Pliocene well-logs of the

- Western Mediterranean. *Mar. Geol.* 403, 150–164. <https://doi.org/10.1016/j.margeo.2018.05.009>.
- Odin, G.S., Vai, G.B., Cosca, M., Tateo, F., Hunziker, J.C., 1997. Integrated stratigraphy of the Maccaronese section. In: Montanari, A., Odin, G.S., Coccioni, R. (Eds.), *Miocene Stratigraphy: An Integrated Approach: Developments in Paleontology and Stratigraphy*, 15. Elsevier Science B.V., Amsterdam, Netherlands, pp. 531–545.
- Ogniben, L., 1955. Le argille scagliose del Crotonese. *Memorie e Note dell'Istituto di Geologia Alicanta di Napoli* 6, 1–72.
- Omodeo-Sale, S., Gennari, R., Lugli, S., Manzi, V., Roveri, M., 2012. Tectonic and climatic control on the Late Messinian sedimentary evolution of the Nijar Basin (Betic Cordillera, Southern Spain). *Basin Res.* 24, 314–337. <https://doi.org/10.1111/j.1365-2117.2011.00527.x>.
- Orszag-Sperber, F., 2006. Changing perspectives in the concept of “Lago-Mare” in Mediterranean Late Miocene evolution. *Sediment. Geol.* 188, 259–277. <https://doi.org/10.1016/j.sedgeo.2006.03.008>.
- Orszag-Sperber, F., Rouchy, J.M., 1979. Le Miocene terminal et le Pliocène inférieur au sud de Chypre, livret-guide, 5e séminaire sur le Messinien. *Chypre*, 60 p.
- Orszag-Sperber, F., Rouchy, J.M., Blanc-Valleron, M.M., 2000. La transition Messinien-Pliocène en Méditerranée orientale (Chypre): la période du Lago-Mare et sa signification. *Comptes Rendus de l'Académie des Sciences-Séries IIA-Earth and Planet. Sci.* 331 (7), 483–490.
- Orszag-Sperber, F., Caruso, A., Blanc-Valleron, M.M., Merle, D., Rouchy, J.M., 2009. The onset of the Messinian salinity crisis: insights from Cyprus sections. *Sediment. Geol.* 217 (1–4), 52–64. <https://doi.org/10.1016/j.sedgeo.2009.03.006>.
- Palcu, D.V., Golovina, L.A., Vernyhovora, Y.V., Popov, S.V., Krijgsman, W., 2017. Middle Miocene paleoenvironmental crises in Central Eurasia caused by changes in marine gateway configuration. *Glob. Planet. Chang.* 158, 57–71. <https://doi.org/10.1016/j.gloplacha.2017.09.013>.
- Palmer, M.R., Edmond, J.M., 1992. Controls over the strontium isotope composition of river water. *Geochim. Cosmochim. Acta* 56 (5), 2099–2111.
- Pellen, R., Popescu, S.-M., Suc, J.-P., Melinte-Dobrinescu, M.C., Rubino, J.-L., Rabineau, M., Marabini, S., Loget, N., Casero, P., Cavazza, W., Head, M.J., Aslanian, D., 2017. The Apennine foredeep (Italy) during the latest Messinian: Lago Mare reflects competing brackish and marine conditions based on calcareous nanofossils and dinoflagellate cysts. *Geobios* 50, 237–257. <https://doi.org/10.1016/j.geobios.2017.04.004>.
- Pellen, R., Aslanian, D., Rabineau, M., Suc, J.-P., Gorini, C., Leroux, E., Blanpied, C., Silenziario, C., Popescu, S.M., Rubino, J.L., 2019. The Messinian Ebro River incision. *Glob. Planet. Chang.* 181, 102988. <https://doi.org/10.1016/j.gloplacha.2019.102988>.
- Pellerin, A., Antler, G., Holm, S.A., Findlay, A.J., Crockford, P.W., Turchyn, A.V., Jørgensen, B.B., Finster, K., 2019. Large sulfur isotope fractionation by bacterial sulfide oxidation. *Sci. Adv.* 5 eaaw1480-eaaw1480.
- Pérez-Asensio, J.N., Aguirre, J., Schmied, G., Civis, J., 2012. Impact of restriction of the Atlantic-Mediterranean gateway on the Mediterranean Outflow Water and eastern Atlantic circulation during the Messinian. *Paleoceanography* 27 (3). <https://doi.org/10.1029/2012PA002309>.
- Peucker-Ehrenbrink, B., Fiske, G.J., 2019. A continental perspective of the seawater 87Sr/86Sr record: A review. *Chem. Geol.* 510, 140–165. <https://doi.org/10.1016/j.chemgeo.2019.01.017>.
- Pierre, C., 1974. Contribution à l'étude sédimentologique et isotopique des évaporites messiniennes de la Méditerranée; implications géodynamiques. Thesis, University of Paris.
- Pierre, C., 1982. Teneurs en isotopes stables (18O, 2H, 13C, 34S) et conditions de genèse des évaporites marines: A l'occasion de quelques milieux actuels et au Messinien de la Méditerranée, Ecole Normale Supérieure. Université de Paris Sud Orsay, p. 262.
- Pierre, C., Fontes, J.-C., 1978. Isotope Composition of Messinian sediments from the Mediterranean Sea as indicators of paleoenvironments and diagenesis, in: Texas A M University, O.D.P.C.S., TX, United States (Ed.), Initial reports of the Deep Sea Drilling, covering Leg 42 of the cruises of the drilling Vessel Glomar Challenger Malaga Spain to Istanbul Turkey. April–May 1975. University of California. Scri Institution of Oceanography. National Science Foundation. National Ocean Sediment Coring Program, pp. 635–650.
- Pierre, C., Rouchy, J.M., 1990. Stable isotope composition of carbonates in the Tyrrhenian Sea, Sulemont to Pierre, C.; Rouchy, JM (1990): Sedimentary and diagenetic evolution of Messinian evaporites in the Tyrrhenian Sea (ODP Leg 107, Sites 652, 653, and 654): petrographic, mineralogical, and stable isotope records. In: Kastens, K.A., Mascle, J., et al. (Eds.), Proceedings of the Ocean Drilling Program, Scientific Results, College Station, TX (Ocean Drilling Program), 107, pp. 187–210. <https://doi.org/10.2973/odp.proc.sr.107.131.1990>. PANGAEA.
- Pierre, C., Rouchy, J.M., Blanc-Valleron, M.-M., 1998. Sedimentological and stable isotope changes at the Messinian-Pliocene boundary in the eastern Mediterranean. In: Robertson, A.H.F., Emeis, K.-C., Richter, C., Camerlenghi, A. (Eds.), Proc. ODP, Sci. Res., vol. 160. Ocean Drilling Program, College Station, TX, pp. 3–8.
- Pierre, C., Caruso, A., Blanc-Valleron, M.M., Rouchy, J.M., Orszag-Sperber, F., 2006. Reconstruction of the paleoenvironmental changes around the Miocene-Pliocene boundary along a West-East transect across the Mediterranean. *Sediment. Geol.* 188, 319–340. <https://doi.org/10.1016/j.sedgeo.2006.03.011>.
- Placzek, C.J., Quade, J., Patchett, P.J., 2011. Isotopic tracers of paleohydrologic change in large lakes of the Bolivian Altiplano. *Quat. Res.* 75 (1), 231–244. <https://doi.org/10.1016/j.yqres.2010.08.004>.
- Polonia, A., Torelli, L., Mussoni, P., Gasperini, L., Artoni, A., Klaeschen, D., 2011. The Calabrian Arc subduction complex in the Ionian Sea: Regional architecture, active deformation, and seismic hazard. *Tectonics* 30 (5).
- Popescu, S.M., Melinte, M.C., Suc, J.P., Clauzon, G., Quillevère, F., Sütö-Szentai, M., 2007. Earliest Zanclean age for the Colombacci and uppermost Di Tetto formations of the “latest Messinian” northern Apennines: New paleoenvironmental data from the Maccaronese section (Marche Province, Italy). *Geobios* 40 (3), 359–373. <https://doi.org/10.1016/j.geobios.2006.11.005>.
- Popescu, S.-M., Melinte, M.-C., Suc, J.-P., Clauzon, G., Quillevère, F., Sütö-Szentai, M., 2008. Marine reflooding of the Mediterranean after the Messinian Salinity Crisis predates the Zanclean GSSP. Reply to the “Comment on ‘Earliest Zanclean age for the Colombacci and uppermost Di Tetto formations of the ‘latest Messinian’ northern Apennines: new paleoenvironmental data from the Maccaronese section (Marche Province, Italy)’” by Popescu et al. (2007). *Geobios* 40 (359–373) authored by Roveri et al. *Geobios* 41, 657–660.
- Popescu, S.M., Dalesme, F., Jouannic, G., Escarguel, G., Head, M.J., Melinte-Dobrinescu, M.C., Sütö-Szentai, M., Bakrac, K., Clauzon, G., Suc, J.P., 2009. Galeacysta etrusca complex: dinoflagellate cyst marker of Paratethyan influges to the Mediterranean Sea before and after the peak of the Messinian Salinity Crisis. *Palynology* 33 (2), 105–134.
- Popescu, S.-M., Dalibard, M., Suc, J.-P., Barhoun, N., Melinte-Dobrinescu, M.C., Bassetti, M.A., Deaconu, F., Head, M.J., Gorini, C., Do Couto, D., Rubino, J.-L., Auxietre, J.-L., Floodpage, J., 2015. Lago Mare episodes around the Messinian-Zanclean boundary in the deep southwestern Mediterranean. *Mar. Pet. Geol.* 66, 55–70. <https://doi.org/10.1016/j.marpetgeo.2015.04.002>.
- Popescu, S.M., Melinte-Dobrinescu, M.C., Suc, J.P., Do Couto, D., 2017. Ceratolithus acutus (= C. armatus), calcareous nanofossil marker of the marine reflooding that terminated the Messinian salinity crisis: Comment on “Paratethyan ostracods in the Spanish Lago-Mare: More evidence for interbasinal exchange at high Mediterranean sea level” by. *Paleogeogr., Paleoclimatol., Paleoecol.* 441, 854–870. <https://doi.org/10.1016/j.paleo.2016.07.011>.
- Popov, S.V., Rogl, F., Rozanov, A.Y., Steininger, F.F., Shcherba, I.G., Kovac, M., 2004. Lithological-paleogeographic maps of Paratethys-10 maps late Eocene to Pliocene.
- Popov, S.V., Shcherba, I.G., Ilyina, L.B., Nevenskaya, L.A., Paramonova, N.P., Khondkarian, S.O., Magyar, I., 2006. Late Miocene to Pliocene paleogeography of the Paratethys and its relation to the Mediterranean. *Paleogeogr. Paleoclimatol. Paleoecol.* 238 (1–4), 91–106.
- Raad, F., Lofi, J., Maillard, A., Tzevahirtzian, A., Caruso, A., 2021. The Messinian Salinity Crisis deposits in the Balearic Promontory: an undeformed analog of the MSC Sicilian basins? *Mar. Pet. Geol.* 104777. <https://doi.org/10.1016/j.marpetgeo.2020.104777>.
- Radeff, G., Cosentino, D., Cipollari, P., Schildgen, T.F., Iadanza, A., Strecker, M.R., Darbas, G., Gurbuz, K., 2016. Stratigraphic architecture of the upper Messinian deposits of the Adana Basin (southern Turkey): implications for the Messinian salinity crisis and the Taurus petroleum system. *Ital. J. Geosci.* 135, 408–424. Radeff, G., Schildgen, T.F., Cosentino, D., Strecker, M.R., Cipollari, P., Darbas, G., Gürbüz, K., 2017. Sedimentary evidence for late Messinian uplift of the SE margin of the Central Anatolian Plateau: Adana Basin, southern Turkey. *Basin Res.* 29, 488–514. <https://doi.org/10.1111/bre.12159>.
- Reiche, S., Hübscher, C., Ehrhardt, A., 2016. The impact of salt on the late Messinian to recent tectonostratigraphic evolution of the Cyprus subduction zone. *Basin Res.* 28 (5), 569–597. <https://doi.org/10.1111/bre.12122>.
- Ricchiuto, T.E., McKenzie, J.A., 1978. Stable Isotopic investigation of Messinian sulfate samples from DSDP. LEG 42. Eastern Mediterranean Sea. In: Texas A M University, O.D.P.C.S., TX, United States (Ed.), Initial reports of the Deep Sea Drilling covering Leg 42 of the cruises of the drilling vessel Glomar Challenger. Malaga, Spain to Istanbul, Turkey. April–May 1975. University of California. Scri Institution of Oceanography, National Science Foundation. National Ocean Sediment Coring Program, pp. 657–660.
- Rio, D., Negri, A., 1988. Calcareous nanofossils (Monticino Quarry, Faenza). In: De Giuli, C., Vai, G.B. (Eds.), Fossil Vertebrates in the Lamone Valley, Romagna Apennines. Field Trip Guidebook of the International Workshop “Continental faunas at the Miocene/Pliocene boundary”, Faenza, pp. 55–57.
- Robertson, A.H.F., 1998a. Late Miocene paleoenvironments and tectonic settings of the southern margin of Cyprus and the Eratosthenes Seamount. In: Robertson, A.H.F., Emeis, K.C., Richter, C., Camerlenghi, A. (Eds.), Proc. ODP, Sci. Res., vol. 160. Ocean Drilling Program, College Station, TX, pp. 453–463.
- Robertson, A.H., 1998b. Tectonic significance of the Eratosthenes Seamount: a continental fragment in the process of collision with a subduction zone in the eastern Mediterranean (Ocean Drilling Program Leg 160). *Tectonophysics* 298 (1–3), 63–82.
- Robertson, A.H.F., Eaton, S., Follows, E.J., Payne, A.S., 1995. Depositional processes and basin analysis of Messinian evaporites in Cyprus. *Terra Nova* 7, 233–253.
- Roca, E., Guimera, J., 1992. The Neogene structure of the eastern Iberian margin: structural constraints on the crustal evolution of the Valencia trough (western Mediterranean). *Tectonophysics* 203, 203–218.
- Roep, Th.B., Van Harten, D., 1979. Sedimentological and ostracodological observations on Messinian post-evaporite deposits in some southeastern Spanish basins. *Annales Geologiques des Pays Helleniques* 3, 1037–1044.

- Roep, T.B., Dabrio, C.J., Fortuin, A.R., Polo, M.D., 1998. Late highstand patterns of shifting and steing coastal barriers and washer-fans (Late Messinian, Sorbas Basina, SE Spain). *Sediment. Geol.* 116, 27–56.
- Rogli, F., 1998. Paleogeographic considerations for Mediterranean and Paratethys[†] seaways (Oligocene to Miocene). *Ann. Naturhist. Mus. Wien* 99 A, 27931[†] 0. Rosenfeld, A., 1977. The sieve pores of *Cyprideis torosa* (Jones, 1850) from the Messinian Maqv'im Formation in the coastal plain and continental shelf of Israel as an indicator of paleoenvironment. *Isr. J. Earth Sci.* 26, 89993.
- Rossi, M., 2017. Outcrop and seismic expression of stratigraphic patterns driven by accommodation and sediment sully turnarounds: Implications on the meaning and variability of unconformities in syn-orogenic basins. *Mar. Pet. Geol.* 87, 112–127. <https://doi.org/10.1016/j.marpetgeo.2017.03.032>.
- Rossi, M., Rogledi, S., 1988. Relative sea-level changes, local tectonic setting and basin margin sedimentation in the interference zone between two orogenic belts: seismic stratigraphic examples from Padan foreland basin, northern Italy. In: *Fan Delatas: Sedimentology and Tectonic Settings*, pp. 368–384.
- Rossi, M., Minervini, M., Ghielmi, M., Rogledi, S., 2015a. Messinian and Pliocene erosional surfaces in the Po Plain-Adriatic Basin: Insights from allostratigraphy and sequence stratigraphy in assessing play concepts related to accommodation and gateway turnarounds in tectonically active margins. *Marine Petroleum Geol. The Messinian events and hydrocarbon exploration in the Mediterranean* 66, 192–216. <https://doi.org/10.1016/j.marpetgeo.2014.12.012>.
- Rossi, C., Vilas, L., Arias, C., 2015b. The Messinian marine to nonmarine gypsums of Jumilla (Northern Betic Cordillera, SE Spain): Isotopic and Sr concentration constraints on the origin of parent brines. *Sediment. Geol.* 328, 96–114. <https://doi.org/10.1016/j.sedgeo.2015.08.007>.
- Rouchy, J.M., 1982. La crise évaporitique messinienne de Méditerranée: nouvelles propositions pour une interprétation génétique. Thesis, Mem. p. 280. Mus. Natn. Hist. Nat., Paris.
- Rouchy, J.M., Caruso, A., 2006. The Messinian salinity crisis in the Mediterranean basin: a reassessment of the data and an integrated scenario. *Sediment. Geol.* 188, 35–67. <https://doi.org/10.1016/j.sedgeo.2006.02.005>.
- Rouchy, J.M., Orszag-Sperber, F., Blanc-Valleron, M.M., Pierre, C., Rivièrè, M., Combourieu-Nebout, N., Panayides, I., 2001. Paleoenvironmental changes at the Messinian-Pliocene boundary in the eastern Mediterranean (southern Cyprus basins): significance of the Messinian Lago-Mare. *Sediment. Geol.* 145 (1–2), 93–117.
- Rouchy, J.M., Pierre, C., Et-Touhami, M., Kerzazi, K., Caruso, A., Blanc-Valleron, M.M., 2003. Late Messinian to Early Pliocene paleoenvironmental changes in the Melilla Basin (NE Morocco) and their relation to Mediterranean evolution. *Sediment. Geol.* 163 (1–2), 1–27.
- Rouchy, J.M., Caruso, A., Pierre, C., Blanc-Valleron, M.M., Bassetti, M.A., 2007. The end of the Messinian salinity crisis: evidences from the Chelif Basin (Algeria). *Paleogeogr. Paleoclimatol. Paleocool.* 254 (3–4), 386–417. <https://doi.org/10.1016/j.paleo.2007.06.015>.
- Roveri, M., Manzi, V., Bassetti, M.A., Merini, M., Ricci Lucchi, F., 1998. Stratigraphy of the Messinian post-evaporitic stage in eastern-Romagna (northern Apennines, Italy). *G. Geol.* 60, 119–142.
- Roveri, M., Bassetti, M.A., Ricci Lucchi, F., 2001. The Mediterranean Messinian salinity crisis: an Apennines foredeep perspective. *Sediment. Geol.* 140, 201–214.
- Roveri, M., Boscolo Gallo, A., Rossi, M., Gennari, R., Iaccarino, S.M., Lugli, S., Manzi, V., Negri, A., Rizzini, F., Taviani, M., 2005. The Adriatic foreland record of Messinian events (central Adriatic sea, Italy). *GeoActa* 4 (139), 158.
- Roveri, M., Bertini, A., Cosentino, D., Di Stefano, A., Gennari, R., Gliozzi, E., Grossi, F., Iaccarino, S.M., Lugli, S., Manzi, V., Taviani, M., 2008a. A high-resolution stratigraphic framework for the latest Messinian events in the Mediterranean area. *Stratigraphy* 5 (3–4), 323–342.
- Roveri, M., Lugli, S., Manzi, V., Schreiber, B.C., 2008b. The Messinian Sicilian stratigraphy revisited: new insights for the Messinian salinity crisis. *Terra Nova* 20 (6), 483–488. <https://doi.org/10.1111/j.1365-3121.2008.00842.x>.
- Roveri, M., Bertini, A., Cipollari, P., Cosentino, D., Di Stefano, A., Florindo, F., Gennari, R., Gliozzi, E., Grossi, F., Iaccarino, S., Lugli, S., Manzi, V., 2008c. Comment on "Earliest Zanclean age for the Colombari and uppermost Di Tetto formations of the "latest Messinian" northern Apennines: new palaeoenvironmental data from the Maccarone section (Marche Province, Italy)" by Popescu et al. (2007) *Geobios* 40 (359–373). *Geobios* 41, 669–675.
- Roveri, M., Gennari, R., Lugli, S., Manzi, V., 2009. The Terminal Carbonate Complex: the record of sea-level changes during the Messinian salinity crisis. *GeoActa* 8 (63), 63–77.
- Roveri, M., Flecker, R., Krijgsman, W., Lofi, J., Lugli, S., Manzi, V., Sierro, F.J., Bertini, A., Camerlenghi, A., De Lange, G., Govers, R., Hilgen, F.J., Hübscher, C., Meijer, P.Th., Stoica, M., 2014a. The Messinian salinity crisis: past and future of a great challenge for marine sciences. *Mar. Geol.* 349, 113–125. <https://doi.org/10.1016/j.margeo.2014.02.002>.
- Roveri, M., Lugli, S., Manzi, V., Gennari, R., Schreiber, B.C., 2014b. High resolution strontium isotope stratigraphy of the Messinian deep Mediterranean basins: implications for marginal to central basins correlation. *Mar. Geol.* 349, 113–125. <https://doi.org/10.1016/j.margeo.2014.01.002>.
- Roveri, M., Manzi, V., Bergamasco, A., Falcieri, F., Gennari, R., Lugli, S., 2014c. Dense shelf water cascading and Messinian canyons: a new scenario for the Mediterranean salinity crisis. *Am. J. Sci.* 314, 751–784. <https://doi.org/10.2475/05.2014.03>.
- Roveri, M., Gennari, R., Persico, D., Rossi, F.P., Lugli, S., Manzi, V., Reghizzi, M., Taviani, M., 2019a. A new chronostratigraphic and paleoenvironmental framework for the end of the Messinian salinity crisis in the Sorbas Basin (Betic Cordillera, southern Spain). *Geol. J.* 54 (3), 1617–1637. <https://doi.org/10.1002/gj.3256>.
- Roveri, M., Gennari, R., Ligi, M., Lugli, S., Manzi, V., Reghizzi, M., 2019b. The synthetic seismic expression of the Messinian salinity crisis from onshore records: implications for shallow-to deep-water correlations. *Basin Res.* 31 (6), 1121–1152. <https://doi.org/10.1111/bre.12361>.
- Roveri, M., Lugli, S., Manzi, V., Reghizzi, M., Rossi, F.P., 2020. Stratigraphic relationships between shallow-water carbonates and primary gypsum: insights from the Messinian succession of the Sorbas Basin (Betic Cordillera, Southern Spain). *Sediment. Geol.* 105678 <https://doi.org/10.1016/j.sedgeo.2020.105678>.
- Ruggieri, G., 1962. La serie marine pliocenica e quaternaria della Val Marecchia: Atti Accad. Sci. Lett. Arti Palermo 19, 1–169.
- Ruggieri, G., 1967. The Miocene and later evolution of the Mediterranean sea. Adams and Ager (Eds.). In: *Aspects of Tethyan Biogeography: Syst. Ass. Publ.* 7, p. 238.
- Ryan, W.B.F., 1973. Geodynamic implications of the Messinian crisis of salinity. In: Drooger, C.W. (Ed.), *Messinian Events in the Mediterranean*. North-Holland Publ. Co., Amsterdam, Netherlands, pp. 26–38.
- Ryan, W.B.F., 1976. Quantitative evaluation of the depth of the western Mediterranean before, during and after the late Miocene salinity crisis. *Sedimentology* 23, 791–813.
- Ryan, W.B.F., 1978. Messinian badlands on the southeastern margin of the Mediterranean Sea. *Mar. Geol.* 27, 349–363.
- Ryan, W.B.F., 2008. Modeling the magnitude and timing of evaporative drawdown during the Messinian salinity crisis. *Stratigraphy* 5, 227–243.
- Ryan, W.B.F., 2009. Decoding the Mediterranean salinity crisis. *Sedimentology* 56 (1), 95–136.
- Ryan, W.B.F., Hsü, K.J., Cita, M.B., Dumitrica, P., Lort, P., Maync, W., Nesteroff, W.D., Pautot, P., Stradner, H., Wezel, F.C., 1973. In: Ryan, W.B.F., Hsü, K.J. (Eds.), *Initial Reports of the Deep Sea Drilling Project, Vol. 13*. U.S. Government Printing Office, Washington, DC, p. 1447.
- Sabat, F., Gelabert, B., Rodriguez-Perea, A., Gimenez, J., 2011. Geological structure and evolution of Majorca: implications for the origin of the Western Mediterranean. *Tectonophysics* 510, 217–238.
- Sabato Ceraldi, T., Kamel, M., Mason, T., Poole, A., Hossack, J., Slack, J., Fraser, A., 2010. Messinian seismic facies in offshore Sirt Basin Libya and implications for sub-Messinian seismic imaging. In: Paper presented at TOG 2008-Technology of Oil and Gas, Forum and Exhibition, 21-23 October, Tripoli.
- Sachse, D., Radke, J., Gleixner, G., 2006. δD values of individual n-alkanes from terrestrial plants along a climatic gradient - implications for the sedimentary biomarker record. *Org. Geochem.* 37, 469–483.
- Sage, F., Von Gronfeld, G., Vervec[†] h'ere, J., Gaullier, V., Maillard, A., Gorini, C., 2005. A record of the Messinian salinity crisis on the western Sardinia margin, northwestern Mediterranean. *Mar. Pet. Geol.* 22, 757–773.
- Sampalmieri, G., Iadanza, A., Cipollari, P., Cosentino, D., Lo Mastro, S., 2010. Paleoenvironments of the Mediterranean Basin at the Messinian hypersaline/hyposaline transition: evidence from natural radioactivity and microfacies of post-evaporitic successions of the Adriatic sub-basin. *Terra Nova* 22 (4), 239–250. <https://doi.org/10.1111/j.1365-3121.2010.00939.x>.
- Sant, K., Palcu, V., Mandic, D., Krijgsman, O., 2017. Changing seas in the Early-Middle Miocene of Central Europe: a Mediterranean approach to Paratethyan stratigraphy. *Terra Nova* 29 (5), 273–281.
- Schildgen, T.F., Cosentino, D., Frijia, G., Castorina, F., Dudas, F.O., Iadanza, A., Sampalmieri, G., Cipollari, P., Caruso, A., Bowring, S.A., Strecker, M.R., 2014. Sea level and climate forcing of the Sr isotope composition of Late Miocene Mediterranean marine basins. *Geochem. Geophys. Geosyst.* 15, 2964–2983. <https://doi.org/10.1002/2014GC005332>.
- Schmalz, R.F., 1969. Deep-water evaporite deposition, a genetic model. *Am. Assoc. Pet. Geol. Bull.* 53, 798–823.
- Schreiber, B.C., 1997. Field trip to Ercadea Minoa: Upper Messinian. "Neogene Mediterranean Paleooceanography", Excursion Guide Book Palermo-Caltanissetta-Agrigento-Erice (Sicily), 24-27 September 1997, pp. 72–80.
- Schütz, K.I., 1994. Structure and stratigraphy of the Gulf of Suez, Egypt, in Interior Rift Basins, edited by S. M. Landon. AAPG Mem. 59, 57–96.
- Schwarzans, W., Agiadi, K., Carnevale, G., 2020. Late Miocene-Early Pliocene evolution of Mediterranean gobies and their environmental and biogeographic significance. *Riv. Ital. Paleontol. Stratigr.* 126 (3).
- Sciuto, F., Baldanza, A., 2020. Full restoration of marine conditions after the late Messinian Mediterranean Lago-Mare phase in Licodia Eubea and Villafranca Tirrena areas (east Sicily). *Carnets de géologie*.
- Sciuto, F., Baldanza, A., Temani, R., Privitera, G., 2018. New reports of Paratethyan ostracods affinity from the Mediterranean Basin (Sicily, Italy). *Paleontologia Electronica* 21 (1), 1. <https://doi.org/10.26879/800>.
- Segev, A., Avni, Y., Shahar, J., Wald, R., 2017. Late Oligocene and Miocene different seaways to the Red Sea-Gulf of Suez rift and the Gulf of Aqaba-Dead Sea basins. *Earth Sci. Rev.* 171, 196–219. <https://doi.org/10.1016/j.earscirev.2017.05.004>.
- Selli, R., 1954. Il Bacino del Metauro. *Giorn. Geol.* 24, 1–294.
- Selli, R., 1960. Il Messiniano Mayer-Eymar 1867. Proposta di un neostratotipo. *Giornale di Geologia* 28, 1–33.
- Selli, R., 1973. An outline of the Italian Messinian. In: Drooger, C.W. (Ed.), *Messinian Events in the Mediterranean*, pp. 150–171. Amsterdam (Kon. Nedl. Akad. Wetensch.).
- Sgarrella, F., Sprovieri, R., Di Stefano, E., Caruso, A., 1997. Paleooceanographic conditions at the base of the Pliocene in the Southern Mediterranean Basin. *Riv. Ital. Paleontol. Stratigr.* 103, 207–220.
- Sgarrella, F., Sprovieri, R., Di Stefano, E., Caruso, A., Sprovieri, M., Bonaduce, G., 1999.

- The Capo Rossello Bore-Hole (Agrigento, Sicily): cyclostratigraphic and paleoceanographic reconstructions from quantitative analyses of the Zanclean foraminiferal assemblages. *Ital. Paleontol. Stratigr.* 105, 303–322.
- Sierro, F.J., Flores, J.A., Civis, J., Gonzà, J.A., France, G., 1993. Late Miocene globorotaliid event-stratigraphy and biogeography in the NE-Atlantic and Mediterranean. *Mar. Micropaleontol.* 21 (1–3), 143–167.
- Sim, M.S., Bosak, T., Ono, S., 2011. Large sulfur isotope fractionation does not require disproportionation. *Science* 333, 74–77.
- Simon, D., Meijer, P.T., 2017. Salinity stratification of the Mediterranean Sea during the Messinian crisis: A first model analysis. *Earth Planet. Sci. Lett.* 479, 366–376.
- Simon, D., Marzocchi, A., Flecker, R., Lunt, D.J., Hilgen, F.J., Meijer, P.T., 2017. Quantifying the Mediterranean freshwater budget throughout the late Miocene: New implications for sapropel formation and the Messinian Salinity Crisis. *Earth Planet. Sci. Lett.* 472, 25–37.
- Sinninghe Damst'e, J.S., Frewin, N.L., Kenig, F., De Leeuw, J.W., 1995. Molecular indicators for palaeoenvironmental changes in a Messinian evaporitic sequence (Vena del Gesso, Italy). I: Variations in extractable organic matter of ten cyclically deposited marl beds. *Org. Geochem.* 23, 471–483.
- Sissingh, W., 1976. Aspects of late Cenozoic evolution of the South Aegean ostracode fauna. *Paleogeogr., Paleoclimatol., Paleocool.* 20, 131–146.
- Snel, E., Marunt'eanu, M., Meulenkamp, J.E., 2006. Calcareous nannofossil biostratigraphy and magnetostratigraphy of the upper Miocene and lower Pliocene of the Northern Aegean (Orphanic Gulf-Strimon Basin areas), Greece. *Paleogeogr. Paleoclimatol. Paleocool.* 238 (3–4), 125–150. <https://doi.org/10.1016/j.paleo.2006.03.022>.
- Soria, J.M., Caracuel, J.E., Y'ebenes, A., Fernandez, J., Viseras, C., 2005. The stratigraphic record of the Messinian salinity crisis in the northern margin of the Bajo Segura basin (SE Spain). *Sediment. Geol.* 179 (3), 225–247. <https://doi.org/10.1016/j.sedgeo.2005.05.011>.
- Soria, J.M., Caracuel, J.E., Corbì, H., Dinar'es-Turell, J., Lancis, C., Tent-Manclús, J.E., Y'ebenes, A., 2007. Estratigrafía y biomagnetostratigrafía del Messiniense en la seccion del Garruchal (Cuenca del Bajo Segura). Implicaciones para la Crisis de Salinidad del Mediterraneo. *Geogaceta* 41, 21' 5–218.
- Soria, J.M., Caracuel, J.E., Corbì, H., Dinar'es-Turell, J., Lancis, C., Tent-Manclús, J.E., Y'ebenes, A., 2008a. The Bajo Segura basin (SE Spain): implications for the Messinian Salinity Crisis in the Mediterranean margins. *Stratigraphy* 5, 259–265.
- Soria, J.M., Caracuel, J.E., Corbì, H., Dinar'es-Turell, J., Lancis, C., Tent-Manclús, J.E., Viseras, C., Y'ebenes, A., 2008b. The Messinian-Early Pliocene stratigraphic record in the southern Bajo Segura basin (Betic Cordillera, Spain). Implications for the Mediterranean salinity crisis. *Sediment. Geol.* 203, 267–288.
- Spatola, D., del Moral-Erencia, J.D., Micallef, A., Camerlenghi, A., Garcia-Castellanos, D., Gupta, S., Bohorquez, P., Gutscher, M.A., Bertoni, C., 2020. A single-stage mega-flood at the termination of the Messinian salinity crisis: geophysical and modelling evidence from the eastern Mediterranean Basin. *Mar. Geol.* 106337 <https://doi.org/10.1016/j.margeo.2020.106337>.
- Stampfli, J., Hocker, C.F.W., 1989. Messinian paleorelief from a 3D seismic survey in the Tarrasco concession area (Spanish Mediterranean Sea). *Geologie in Mijnbouw* 68, 201–210.
- Stoica, M., Lazar, I., Krijgsman, W., Vasiliev, I., Jipa, D., Floroiu, A., 2013. Palaeoenvironmental evolution of the East Carpathian foredeep during the late Miocene-early Pliocene (Dacian Basin; Romania). *Glob. Planet. Chang.* 103, 135–148. <https://doi.org/10.1016/j.gloplacha.2012.04.004>.
- Stoica, M., Krijgsman, W., Fortuin, A., Gloizzi, E., 2016. Paratethyan ostracods in the Spanish Lago-Mare: More evidence for intra-basinal exchange at high Mediterranean sea level. *Paleogeogr. Paleoclimatol. Paleocool.* 441, 854–870. <https://doi.org/10.1016/j.paleo.2015.10.034>.
- Strasser, A., Hilgen, F.J., Heckel, P.H., 2006. Cyclostratigraphy-concepts, definitions, and applications. *Newsl. Stratigr.* 42 (2), 75–114.
- Sturani, C., 1973. A fossil eel (*Anguilla* sp.) from the Messinian of Alba (Tertiary Piedmont Basin). Palaeoenvironmental and paleogeographic implications. In: *Messinian Events in the Mediterranean*. K. Nederl. Akad. Wetensch, Amsterdam, pp. 243–255.
- Suarez-Gonzalez, P., Arenas, C., Benito, M.I., Pomar, L., 2019. Interplay between biotic and environmental conditions in presalt Messinian microbialites of the western Mediterranean (Upper Miocene, Mallorca, Spain). *Paleogeogr. Paleoclimatol. Paleocool.* 533, 109–242.
- Suc, J.-P., Do Couto, D., Melinte-Dobrinescu, M.C., Macalet, R., Quill'ever'e, F., Clauzon, G., Csato, I., Rubino, J.-L., Popescu, S.-M., 2011. The Messinian salinity crisis in the Dacic Basin (SW Romania) and early Zanclean Mediterranean-Paratethys high sea-level connection. *Paleocool.* 310, 256–272. <https://doi.org/10.1016/j.paleo.2011.07.018>.
- Suc, J.-P., Popescu, S.-M., Do Couto, D., Clauzon, G., Rubino, J.-L., Melinte-Dobrinescu, M.C., Quillever'e, F., Brun, J.-P., Dumurd'zanov, N., Zagorchev, I., Lesi'c, V., Tomi'c, D., Sokoutis, D., Meyer, B., Macalet, R., Rifejl, H., 2015. Marine gateway vs. fluvial stream within the Balkans from 6 to 5 Ma. *Mar. Pet. Geol.* 66 (1), 231–245. <https://doi.org/10.1016/j.marpetgeo.2015.01.013>.
- Thinon, I., Guennoc, P., Serrano, O., Maillard, A., Lasseur, E., R'ehault, J.P., 2016. Seismic markers of the Messinian Salinity Crisis in an intermediate-depth basin: data for understanding the Neogene evolution of the Corsica Basin (Northern Tyrrhenian Sea). *Mar. Pet. Geol.* 77, 1274–1296. November 2016. <https://doi.org/10.1016/j.marpetgeo.2016.02.017>.
- Thode, H.G., Monster, J., 1965. Sulfur-Isotope Geochemistry of Petroleum, Evaporites, and Ancient Seas. In: Young, A., Galley, J.E. (Eds.), *Fluids in Subsurface Environments*. American Association of Petroleum Geologists, p. 0.
- Topper, R.P.M., Meijer, P.T., 2015. The precessional phase lag of Messinian gypsum deposition in Mediterranean marginal basins. *Paleogeogr. Paleoclimatol. Paleocool.* 417, 6–16.
- Topper, R.P.M., Flecker, R., Meijer, P.T., Wortel, M.J.R., 2011. A box model of the Late Miocene Mediterranean Sea: implications from combined 87Sr/86Sr and salinity data. *Paleoceanography* 26. <https://doi.org/10.1029/2010PA002063>. PA3223.
- Topper, R.P.M., Lugli, S., Manzi, V., Roveri, M., Meijer, P.T., 2014. Precessional control of Sr ratios in marginal basins during the Messinian salinity crisis? *Geochem. Geophys. Geosyst.* 15–5, 1926–1944. <https://doi.org/10.1002/2013GC005192>.
- Trenkwalder, S., Violanti, D., D'Atri, A., Lozar, F., Dela Pierre, F., Irace, A., 2008. The Miocene/Pliocene boundary in the Early Pliocene Mediterranean Sea surface temperatures during the Late Miocene provide a climate context for evolutionary transitions in Africa and Eurasia. *Earth Planet. Sci. Lett.* 419, 71–80. <https://doi.org/10.1016/j.epsl.2015.03.016>.
- Turchyn, A.V., Schrag, D.P., 2004. Oxygen Isotope Constraints on the Sulfur Cycle over the Past 10 Million Years. *Science* 303, 2004.
- Turchyn, A.V., Sivan, O., Schrag, D.P., 2006. Oxygen isotopic composition of sulfate in deep sea pore fluid: evidence for rapid sulfur cycling. *Geobiology* 4, 191–201.
- Turchyn, A.V., Schrag, D.P., Coccioni, R., Montanari, A., 2009. Stable isotope analysis of the Cretaceous sulfur cycle. *Earth Planet. Sci. Lett.* 285, 115–123.
- Tzanova, A., Herbert, T.D., Peterson, L., 2015. Cooling Mediterranean Sea surface temperatures during the Late Miocene provide a climate context for evolutionary transitions in Africa and Eurasia. *Earth Planet. Sci. Lett.* 419, 71–80. <https://doi.org/10.1016/j.epsl.2015.03.016>.
- Urgeles, R., Camerlenghi, A., Garcia-Castellanos, D., De Mol, B., Garces, M., Verges, J., Haslam, I., Hardman, M., 2011. New constraints on the Messinian sealevel drawdown from 3D seismic data of the Ebro margin, western Mediterranean. *Basin Res.* 23, 123–145. <https://doi.org/10.1111/j.1365-2117.2010.00477.x>.
- Utrilla, R., Pierre, C., Orti, F., Pueyo, J.J., 1992. Oxygen and sulphur isotope compositions as indicators of the origin of Mesozoic and Cenozoic evaporates from Spain. *Chem. Geol.* 102, 229–244.
- Vai, G.B., 1997. Chapter E3 Cyclostratigraphic estimate of the messinian stage duration. In: Montanari, A., Odin, G.S., Coccioni, R. (Eds.), *Miocene Stratigraphy: An Integrated Approach*. *Dev. Paleontol. Stratigr.* 15, 463–476.
- Vai, G.B., 2016. Over half a century of Messinian salinity crisis. *Bol. Geol. Min.* 127 (2), 625–641.
- Van Baak, C.G.C., Radionova, E.P., Golovina, L.A., Raffi, I., Kuiper, K.F., Vasiliev, I., Krijgsman, W., 2015. Messinian events in the Black Sea. *Terra Nova* 27, 433–441. <https://doi.org/10.1111/ter.12177>.
- Van Baak, C.G., Stoica, M., Grothe, A., Aliyeva, E., Krijgsman, W., 2016. Mediterranean-Paratethys connectivity during the Messinian salinity crisis: The Pontian of Azerbaijan. *Glob. Planet. Chang.* 141, 63–81. <https://doi.org/10.1016/j.gloplacha.2016.04.005>.
- Van Baak, C.G., Krijgsman, W., Magyar, I., Sztano, O., Golovina, L.A., Grothe, A., Hoyle, T.M., Mandic, O., Patina, I.S., Popov, S.V., Radionova, E.P., Stoica, M., Vasiliev, I., 2017. Paratethys response to the Messinian salinity crisis. *Earth Sci. Rev.* 172, 193–223. <https://doi.org/10.1016/j.earscirev.2017.07.015>.
- Van Couvering, J.A., Berggren, W.A., Drake, R.E., Aguirre, E., Curtis, G.H., 1976. The terminal Miocene event. *Mar. Micropaleontol.* 1, 263–286.
- Van Couvering, J.A., Castradori, D., Cita, M.B., Hilgen, F.J., Rio, D., 2000. The base of the Zanclean Stage and of the Pliocene Series. *Episodes* 23, 179–187.
- Van den Berg, B.C.J., Sierro, F.J., Hilgen, F.J., Flecker, R., Larrasoana, J.C., Krijgsman, W., Flores, J.A., Mata, M.P., Martín, E.B., Civis, J., Gonzalez-Delgado, J. A., 2015. Astronomical tuning for the upper Messinian Spanish Atlantic margin: disentangling basin evolution, climate cyclicity and MOW. *Glob. Planet. Chang.* 135, 89–103.
- Van der Meer, M.T.J., Baas, M., Rijpstra, I.C., Marino, G., Rohling, E.J., Sinninghe Damste, J.S., Schouten, S., 2007. Hydrogen isotopic compositions of long-chain alkenones record freshwater flooding of the Eastern Mediterranean at the onset of sapropel deposition. *Earth Planet. Sci. Lett.* 262, 594–600.
- Van Hinsbergen, D.J., Meulenkamp, J.E., 2006. Neogene supradetachment basin development on Crete (Greece) during exhumation of the South Aegean core complex. *Basin Res.* 18 (1), 103–124.
- Vasiliev, I., Reichart, G.-J., Davies, G.R., Krijgsman, W., Stoica, M., 2010. Strontium isotope ratios of the Eastern Paratethys during the Miocene/Pliocene transition; Implications for interbasinal connectivity. *Earth Planet. Sci. Lett.* 292, 123–131. <https://doi.org/10.1016/j.epsl.2010.01.027>.
- Vasiliev, I., Reichart, G.J., Krijgsman, W., 2013. Impact of the Messinian Salinity Crisis on Black Sea hydrology - insights from hydrogen isotopes on molecular biomarkers. *Earth Planet. Sci. Lett.* 362, 272–282. <https://doi.org/10.1016/j.epsl.2012.11.038>.
- Vasiliev, I., Reichart, G.-J., Grothe, A., Sinninghe Damst'e, J.S., Krijgsman, W., Sangiorgi, F., Weijers, J.W.H., van Rooij, L., 2015. Recurrent phases of drought in the upper Miocene of the Black Sea region. *Paleogeogr. Paleoclimatol. Paleocool.* 423, 18–31.
- Vasiliev, I., Mezger, E.M., Lugli, S., Reichart, G.J., Manzi, V., Roveri, M., 2017. How dry was the Mediterranean during the Messinian salinity crisis? *Paleogeogr. Paleoclimatol. Paleocool.* 471, 120–133. <https://doi.org/10.1016/j.paleo.2016.03.022>.

paleo.2017.01.032.

Vasiliev, I., Karakitsios, V., Bouloubassi, I., Agiadi, K., Kontakiotis, G., Antonarakou, A., Triantaphyllou, M., Gogou, A., Kafousia, N., de Rafelis, M., Zarkogiannis, S.,

Kaczmar, F., Parinos, C., Pasadakis, N., 2019. Large sea surface temperature, salinity, and productivity preservation changes preceding the onset of the Messinian Salinity Crisis in the eastern Mediterranean Sea. *Paleoceanogr. Paleoclimatol.* 34, 182–202.

<https://doi.org/10.1029/2018PA003438>.

Veizer, J., 1989. Strontium isotopes in seawater through time. *Annu. Rev. Earth Planet. Sci.* 17 (1), 141–167.

Violanti, D., Trenkwalder, S., Lozar, F., Gallo, L.M., 2009. Micropaleontological analyses of the Narzole core: biostratigraphy and paleoenvironment of the late Messinian and early Zanclean of Piedmont (Northwestern Italy). *Boll. Soc. Paleontol. Ital.* 48, 167–181.

Warren, J.K., 2016. *Evaporites: A geological compendium*. Springer.

Winterberg, S., Picotti, V., Willett, S.D., 2020. Messinian or Pleistocene valley incision within the Southern Alps. *Swiss J. Geosci.* 113 (1), 1–14. <https://doi.org/10.1186/s00015-020-00361-7>.

Wortmann, U.G., Chernyavsky, B., Bernasconi, S.M., Brunner, B., Bottcher, M.E., Swart, P.K., 2007. Oxygen isotope biogeochemistry of pore water sulfate in the deep biosphere: Dominance of isotope exchange reactions with ambient water during microbial sulfate reduction (ODP Site 1130). *Geochim. Cosmochim. Acta* 71, 4221–4232.

Zachariasse, W.J., van Hinsbergen, D.J.J., Fortuin, A.R., 2008. Mass wasting and uplift on Crete and Karpathos (Greece) during the Early Pliocene related to beginning of South Aegean left-lateral, strike slip tectonics. *Geol. Soc. Am. Bull.* 120, 976–993.

Zachariasse, W.J., van Hinsbergen, D.J., Fortuin, A.R., 2011. Formation and fragmentation of a late Miocene supradetachment basin in central Crete: implications for exhumation mechanisms of high-pressure rocks in the Aegean forearc. *Basin Res.* 23 (6), 678–701. <https://doi.org/10.1111/j.1365-2117.2011.00507.x>.

Ziveri, P., Baumann, K.H., Bockel, B., Bollmann, J., Young, J., 2004. Present day coccolithophore-biogeography in the Atlantic Ocean. In: *Coccolithophores: From Molecular Processes to Global Impact*. Springer Verlag, pp. 403–428.

Zonneveld, K.A., Marret, F., Versteegh, G.J., Bogus, K., Bonnet, S., Bouimtarhan, I., Crouch, I.E., Esper, O., 2013. Atlas of modern dinoflagellate cyst distribution based on 2405 data points. *Rev. Paleobot. Palynol.* 191, 1–197.

Annex B

A comprehensive and updated compilation of the seismic stratigraphy markers in the Western Mediterranean Sea

Bellucci Massimo^{1,2,3}, Pellen Romain², Leroux Estelle¹, Bache François⁴, Garcia Marga⁵, Do Couto Damien⁶, **Raad Fadi**⁷, Blondel Simon^{3,9}, Rabineau Marina², Gorini Christian⁶, Moulin Maryline¹, Maillard Agnès⁸, Lofi Johanna⁷, Del Ben Anna³, Camerlenghi Angelo⁹, Poort Jeffrey⁶, Aslanian Daniel¹

1 IFREMER, Géosciences Marines, Plouzané, France

2 Univ. Brest, Laboratoire Géosciences Océan, UMR 6538 IUEM - CNRS, Plouzané, France

3 Dipartimento di Matematica e Geoscienze, Università di Trieste, Italy

4 GNS Science, PO Box 30-368, Lower Hutt, New Zealand

5 Univ. Barcelona, now at IEO, Cadiz, Spain

6 Sorbonne Université, CNRS, Institut des Sciences de la Terre de Paris, ISTeP, Paris, France

7 Géosciences Montpellier, CNRS, Université de Montpellier, Université des Antilles – Bâtiment 22, Université de Montpellier 2, Place E. Bataillon, Montpellier Cedex 05, 34095, France

8 Géosciences Environnement Toulouse (GET), Observatoire Midi Pyrénées, Université de Toulouse, CNRS, IRD, 14 avenue E. Belin, Toulouse, F-31400, France

9 Istituto Nazionale di Oceanografia e di Geofisica Sperimentale OGS, Trieste, Italy

Abstract

The Western Mediterranean Sea is a natural laboratory to address questions about the formation and evolution of continental margins and the relationship between surface and deep processes. The evaporites deposited during the late Miocene's Messinian Salinity Crisis (MSC) strongly impact its sedimentological and geomorphological evolution. Hereafter, we present a compilation of some of the main regional seismic stratigraphic markers throughout all the Western Mediterranean Sea. We provide in xyz format (z in second twt) the original, not interpolated, points interpretation of the following horizons: i) Acoustic basement, ii) Base and Top of the MSC salt, also known as Mobile Unit (MU), iii) base Pliocene and iv) Seafloor. The

available reflection seismic dataset, coming from a collaboration between French, Spanish, Algerian and Italian research institutes, covers most of the Western Mediterranean sub-basins with the exception of the Ligurian Basin. This compilation is currently the most comprehensive and updated available in literature and provides a useful contribution to the scientific community working in sedimentary, tectonics and geodynamics studies in Western Mediterranean Sea.

Brief dataset history

Since the 1960s the Western Mediterranean Sea has been exploited by reflection seismic surveys, both with academic and industrial objectives. Although some surveys are relatively old, new processing techniques have allowed a good improvement of quality. The results gave a great variability of available data, with strong differences in resolution and quality. In the Western Mediterranean area (Fig. 1), a first industrial and academic reflection seismic compilation was made by Mauffret, (1976), Gorini, (1993) and Maillard, (1993), complemented by Bache, (2008), Garcia *et al.*, (2011), Leroux, (2012), Driussi, (2014) and Pellen, (2016). The last three aforementioned authors digitalized a dense seismic grid in the Valencia and Menorca basins as well as the Balearic Promontory. Over the years the dataset has grown, thanks to collaborations between several French and foreign institutes and industry, such as the GDR “Margins” (Groupement de Recherches 'Marges') followed by Action Marges, which had the objectives to better understand the processes that control the formation and evolution of continental margins (e.g. Berne & Gorini, 2005).

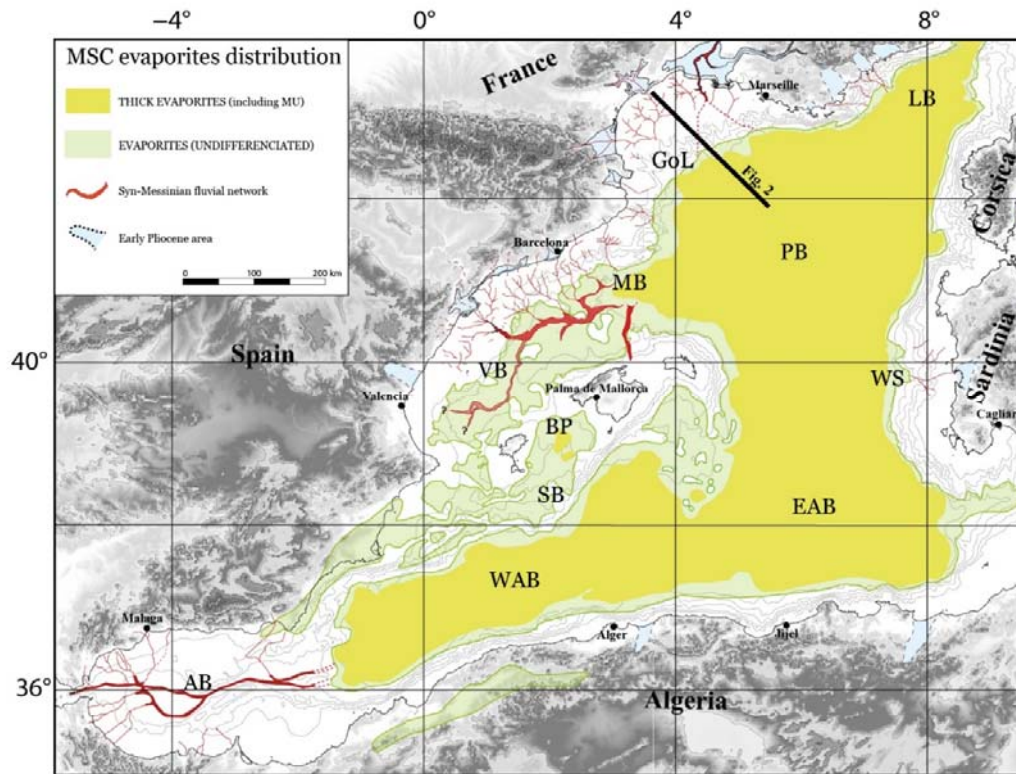


Figure 8.1. Extension map of the MSC evaporites in the Western Mediterranean Sea (modified after Rabineau et al., 2015 and Pellen et al., 2019). LB: Ligurian basin; GoL: Gulf of Lion margin; PB: Provençal basin; WS: western Sardinian margin; EAB: eastern Algerian basin; WAB: western Algerian basin; AB: Alboran basin; SB: south Balearic margin; BP: Balearic Promontory; VB: Valencia basin; MB: Menorca basin. Black line indicates the approximate position of the profile is shown in figure 2.

Within this framework, we could undertake multidisciplinary studies through a collaboration between the University of Brest, Ifremer, Sorbonne University, University of Montpellier, University of Toulouse, University of Barcelona, Consejo Superior de Investigaciones Científicas (CSIC), TOTAL, IFP Energies Nouvelles and Bureau de Recherches Géologiques et Minières (BRGM).

More recently, we added some new lines to the dataset coming from the Italian institutions thanks to the close collaboration with OGS (National Institute of Oceanography and Applied Geophysics) and the University of Trieste. To this date, this work provides the largest and most comprehensive stratigraphic markers compilation available to the scientific community across the Mediterranean Sea.

Stratigraphic markers presentation

This work provides the interpretation of several stratigraphic markers, below briefly described and referred (Fig. 2). We provide xyz files, where x is the longitude, y the latitude and z the depth in second twt. The coordinates are not projected and the datum/ellipsoid is the WGS84 (EPSG 4326).

The Top acoustic **Basement** is interpreted in all the geomorphological domains, from the shelf to the deep basin (Fig. 3). It coincides with the deepest continuous, high amplitude and positive polarity (SEG normal polarity) reflector in the sedimentary column. It separates the chaotic seismic facies of the substratum from the stratified seismic facies of the sedimentary column (Fig. 2). In the Alboran and Valencia basins it corresponds to the Base of the Tertiary, or Oligocene unconformity (e.g. Do Couto *et al.*, 2014; Pellen *et al.*, 2016; Etheve *et al.*, 2016).

The **Base of salt** marker is interpreted only in the deep basin, where the MSC Salt is observed (Fig. 4). It corresponds to the base MU (Mobile Unit), from Lofi *et al.*, (2011) and base MUM (Messinian upper megasequence) in the deep basin, from Gorini *et al.*, (2015). The MU is absent elsewhere in our study area (*i.e.* Valencia and Alboran basins). It is imaged as a strong reflector characterized by high amplitude and negative polarity (Fig. 2).

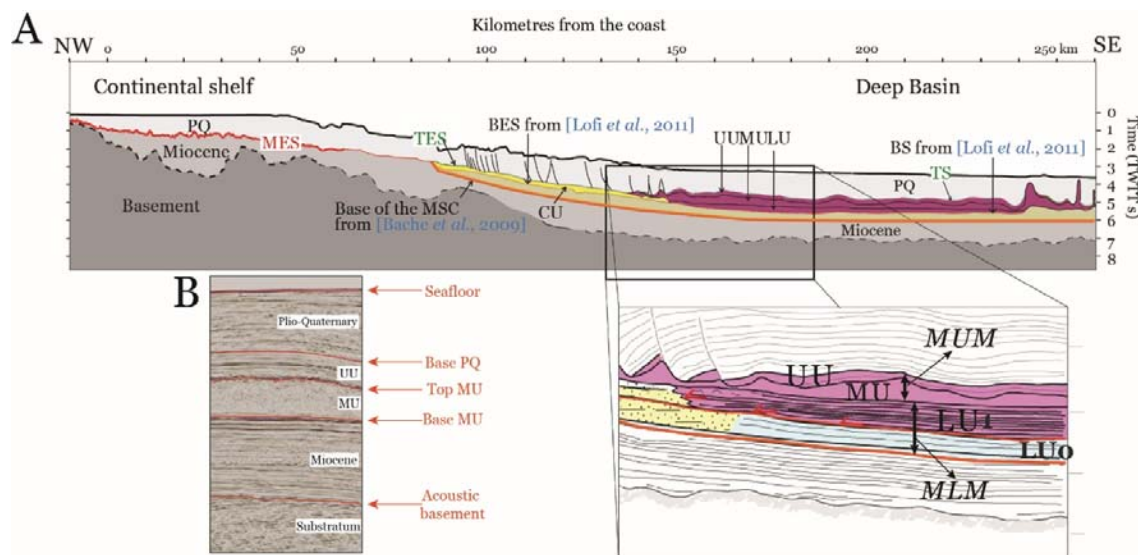


Figure 8.2. A) Synthesis of offshore stratigraphic markers on a profile crossing the Gulf of Lion margin (location figure 1). PQ: Plio-Quaternary sequence; MSC: Messinian Salinity Crisis. LU: Lower Unit; MU: Mobile Unit; UU: Upper Unit; MES: Margin Erosion Surface; TES/TS: Top (Erosion) Surface; BES/BS: Bottom (Erosion) Surface; CU: Complex Unit. MLM: Messinian Lower Megasequence; MUM: Messinian Upper Megasequence; LU0: erosion on the shelf and detrital deposits in the basin. The base of the PQ sequence corresponds to the MES on the shelf, to the top of MSC detrital units on the slope and to the top of UU in the basin (modified after Leroux *et al.*, 2019). B) Seismic zoom representing seismic units facies and reflectors provided in this work.

The **Top of salt** marker is interpreted only in the deep basin, where the Messinian Salt is observed (Fig. 5). It corresponds to the top MU from Lofi *et al.*, (2011) and Gorini *et al.*, (2015). It is imaged as a strong reflector characterized by high amplitude and positive polarity overlying a usually transparent or chaotic (depends on seismic resolution) seismic facies unit interpreted as salt (Fig. 2).

The **Base of the Plio-Quaternary (PQ)** sequence marker is interpreted in all the geomorphological domains, from the shelf to the deep basin (Fig. 6). It corresponds, according to Lofi *et al.*, (2011), to the MES (Marginal Erosional Surface) on the shelf and upper margin where no MSC units are present, to the TES/TS on the slope and margin and to the top of UU in the deep basin. According to Gorini *et al.*, (2015), it corresponds to the top MUM (Fig. 2). In the Gulf of Lion margin, we consider the base of the PQ unit as the Top M2 reflector (from Bache, 2008) and in the Valencia and Menorca basins the S30 reflector (from Pellen, 2016). It is imaged as a strong reflector characterized by high amplitude and positive polarity. It corresponds to the end of the Messinian Salinity Crisis, dated at 5.33 Ma (Krijgsman *et al.*, 1999a) (Fig. 2).

The **seafloor** marker is interpreted in all the available dataset (Fig. 7). It is imaged as a strong reflector characterized by high amplitude and positive polarity (Fig. 2).

Isobath maps

Below, we show the data distribution as provided in xyz format, illustrating the isobath map for each stratigraphic marker. The maps are projected in Mercator, using GMT software (Wessel and Smith, 1995). The data come from interpretation of seismic lines and digitalization from published isobath maps.

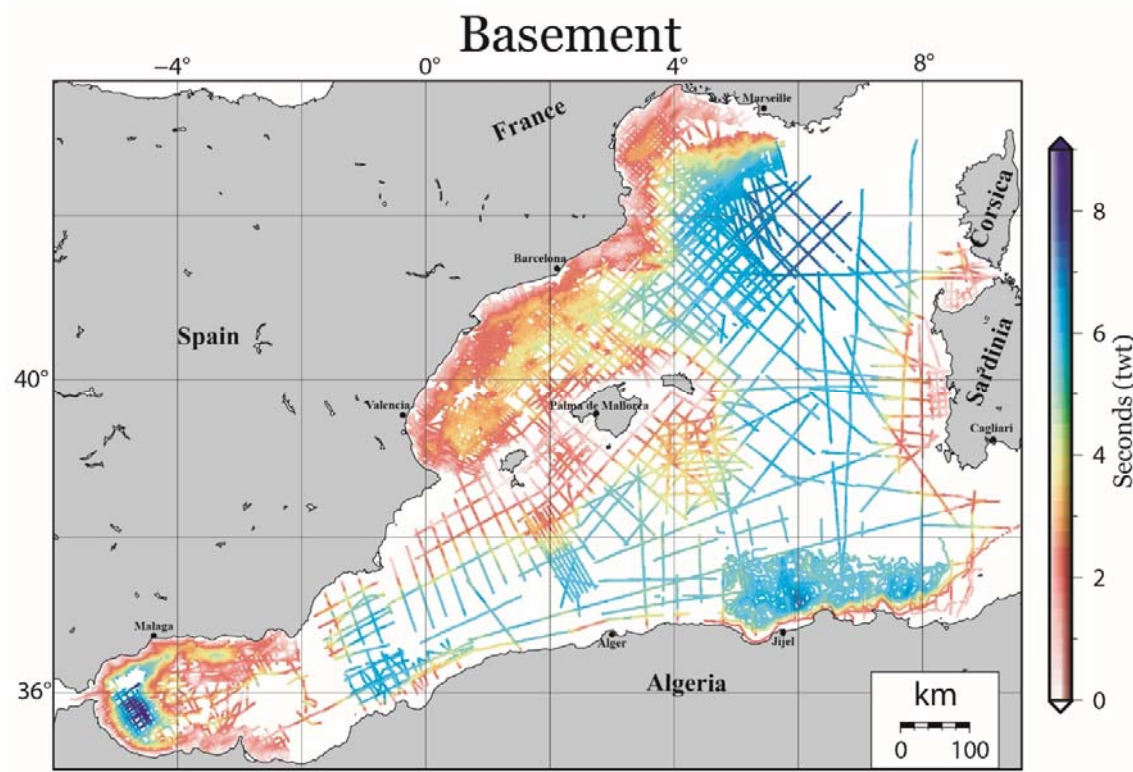


Figure 3. Acoustic basement isobath map. The NE Algerian margin interpretation comes from Arab, (2016).

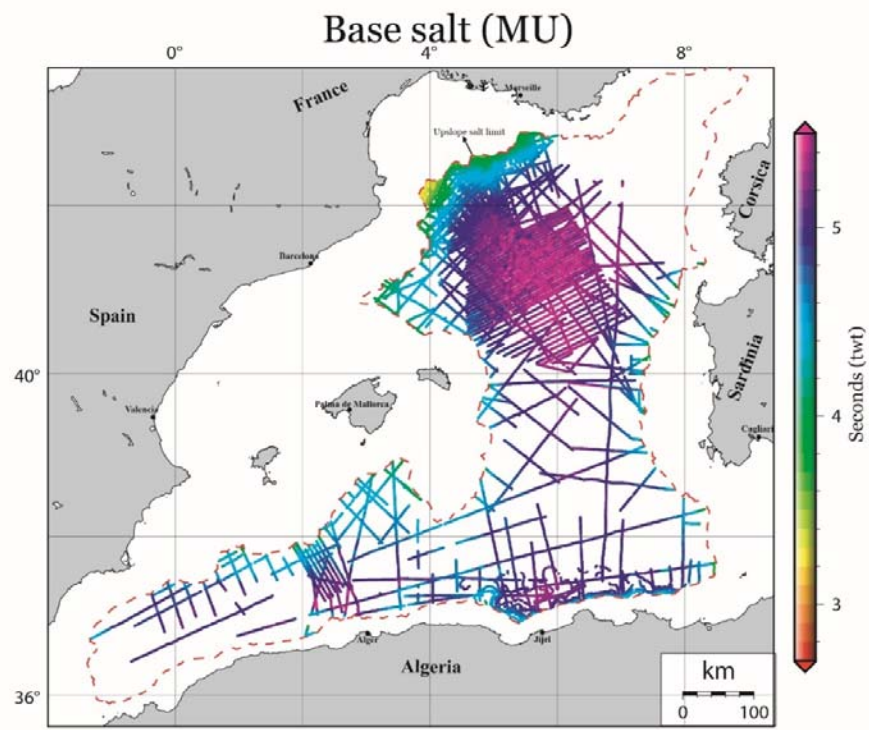


Figure 4. Base salt (Base MU) isobath map. The NE Algerian margin interpretation comes from Arab, (2016). Upslope salt (MU) limit is from Bellucci et al., (2021).

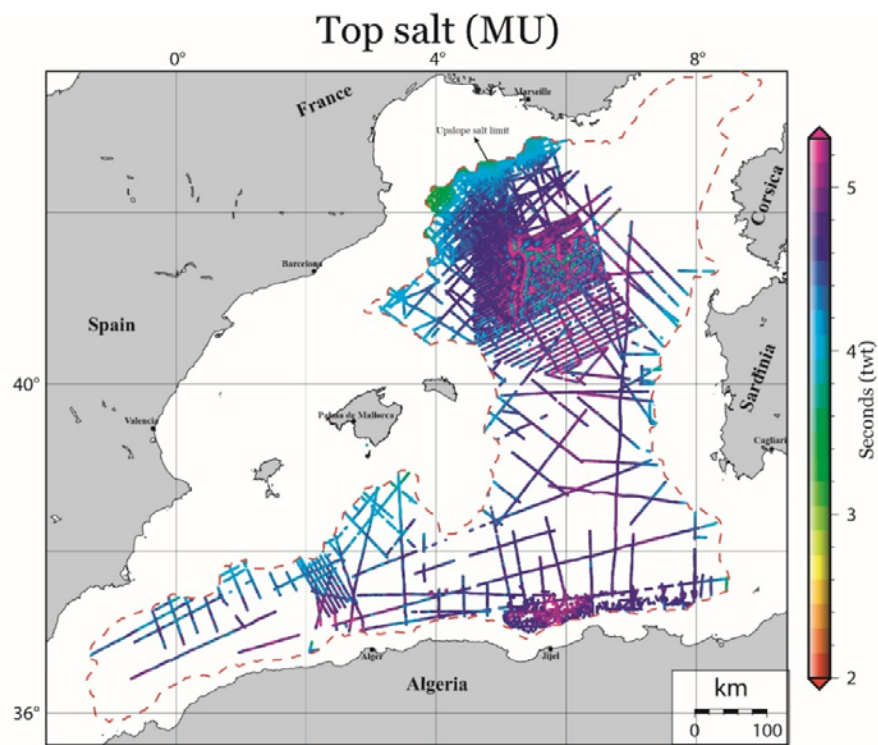


Figure 5. Top salt (Top MU) isobath map. The NE Algerian margin interpretation comes from Arab, (2016). Upslope salt (MU) limit is from Bellucci et al., (2021).

Base Plio-Quaternary

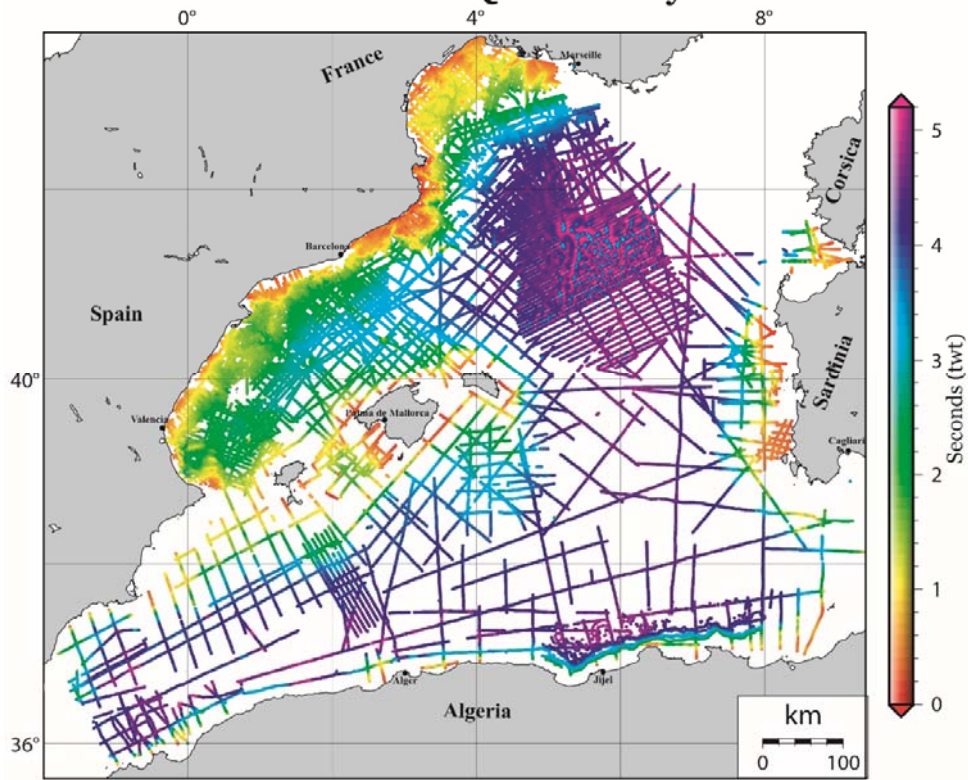


Figure 6. Base Plio-Quaternary isobath map. The NE Algerian margin interpretation comes from Arab, (2016).

Seafloor

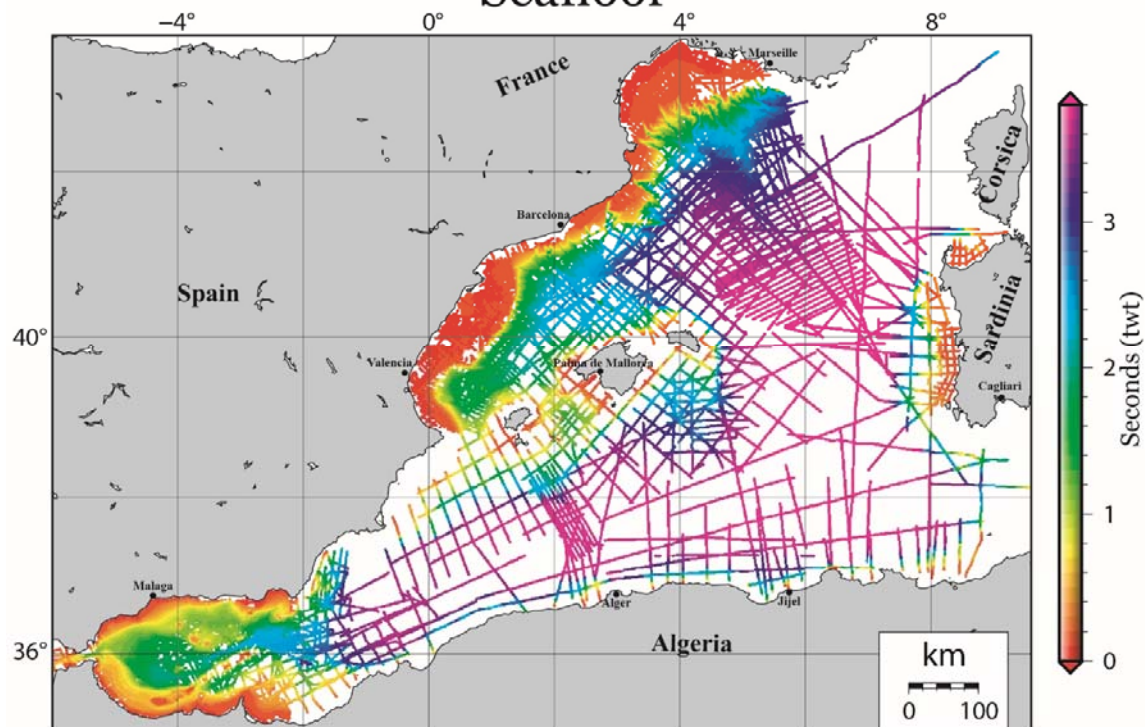


Figure 7. Seafloor isobath map.

Authors' contribution:

This project was designed by DA and realised by MB with active participation of RP. The data organisation and setting up was made by JP.

Seismic interpretation for this data compilation

Alboran basin: the interpretation was made by DDC during his PhD (Do Couto, 2014) with the collaboration of CG and JP.

Algerian deep basin: the interpretation was made by MB during his PhD under the supervision and collaboration of DA, MR, MM, EL and RP. The western part was interpreted by AM.

Balearic Promontory and South Balearic margin: the South Balearic margin interpretation was made by MB during his PhD with the collaboration and supervision of RP, DA, MR, MM and EL. The interpretation in the south of Menorca and between Mallorca and Ibiza was made by FR (Raad *et al.*, 2020) during his PhD under the supervision of AM and JL.

Gulf of Lion: the interpretation was made by MR, FB and EL during their PhD (Rabineau, 2001; Bache, 2008; Leroux, 2012) with the supervision and collaboration of MR, CG and DA.

Liguro-Provençal basin: the interpretation was made by MB, EL, FB and RP during their PhD (Bache, 2008; Leroux, 2012; Pellen, 2016) with the collaboration of MR, CG, DA and MM.

North-East Algerian margin: the interpretation was made by MB and RP during their PhD and Post-Doc, respectively, with the supervision and collaboration of MR, DA, MM and EL. The interpretation was complemented by digitalisation from the thesis of Arab, (2016).

Valencia and Menorca basins: the interpretation was made by RP during his thesis (Pellen, 2016) under the supervision of MR and DA. The Catalan margin was interpreted by MG Post-Doc (Garcia *et al.*, 2011) with the collaboration of DA, MB and AM.

Western Sardinian margin: the interpretation was made by MB during his PhD with the collaboration and supervision of ADB, EL, MR, RP, MM and DA. The north Sardinian margin was supplemented by interpretation of AM.

Data organisation and supply

Alboran basin: refer to Do Couto, (2014) for the data source.

Algerian deep basin: AC provided part of the dataset. Refer to Leroux *et al.*, (2019) for other data source.

Balearic Promontory and South Balearic margin: refer to Driussi, (2014), Dal Cin *et al.*, (2016); Pellen, (2016) and Raad *et al.*, (2020). Additional data by SIGEOF Spanish site and Schlumberger.

Gulf of Lion: refer to Gorini, (1993), Maillard, (1993), Rabineau, (2001), Lofi, (2002), Bache, (2008) and Leroux, (2012).

Liguro-Provençal basin: refer to Gorini, (1993), Maillard, (1993), Rabineau, (2001), Bache, (2008), Leroux, (2012), Geletti *et al.*, (2014), Bellucci, (M2, 2017).

North-East Algerian margin: refer to Arab, (2016) and Leroux *et al.*, (2019).

Valencia and Menorca basins: refer to Maillard, (1993), Garcia *et al.*, (2011), Driussi, (2014) and Pellen, (2016). Additional data by SIGEOF Spanish site and Schlumberger.

Western Sardinian margin: refer to Geletti *et al.*, (2014), Dal Cin *et al.*, (2016) and Bellucci, (M2, 2017). Additional data by VIDEPI Italian site.

References associated to the data compilation

- Arab, M. (2016). Analyse des systèmes pétroliers de l'offshore algérien oriental: Quantification, modélisation stratigraphique et thermique (Doctoral dissertation, Université de Bretagne Occidentale (UBO); Université des Sciences et Technologie Houari Boumedienne (USTHB), Alger, Algérie; Université Bretagne Loire). <https://tel.archives-ouvertes.fr/tel-01459675>
- Bache, F. (2008). Evolution Oligo Miocène des marges du micro océan Liguro-Provençal (Doctoral dissertation, Université de Bretagne Occidentale). <https://tel.archives-ouvertes.fr/tel-00326616>
- Bellucci, M., Aslanian, D., Moulin, M., Rabineau, M., Leroux, E., Pellen, R., Poort, J., Del Ben, A., Gorini, C., Camerlenghi, A. (2021). Salt morphologies and crustal segmentation

relationship: new insights from well-known salt-bearing margins, *Earth-Science Reviews* ,
11th Jan 2021

- Bellucci, M., Del Ben, A., Geletti, R., Forlin, E., Rabineau, M., Leroux, E., Aslanian D. & Pellen, R. (Master thesis, 2017). Interpretation of seismic profiles in the Western Mediterranean Sea. .
- Berne, S., & Gorini, C. (2005). The Gulf of Lions: An overview of recent studies within the French 'Margins' programme. *Marine and petroleum geology*, 22(6-7), 691-693.
- Dal Cin, M., Del Ben, A., Mocnik, A., Accaino, F., Geletti, R., Wardell, N., Zgur F., & Camerlenghi, A. (2016). Seismic imaging of Late Miocene (Messinian) evaporites from Western Mediterranean back-arc basins. *Petroleum Geoscience*, 22(4), 297-308.
- Do Couto, D., Popescu, S. M., Suc, J. P., Melinte-Dobrinescu, M. C., Barhoun, N., Gorini, C., & Auxietre, J. L. (2014). Lago Mare and the Messinian salinity crisis: evidence from the Alboran Sea (S. Spain). *Marine and Petroleum Geology*, 52, 57-76. <https://tel.archives-ouvertes.fr/tel-01148777>
- Driussi, O. (2014). Évolution de la région Baléares (Méditerranée occidentale) du néogène à l'actuel: aspects géodynamiques et paléo-environnementaux (Doctoral dissertation, Université de Toulouse, Université Toulouse III-Paul Sabatier). <https://tel.archives-ouvertes.fr/tel-01118302>
- Etheve, N., de Lamotte, D. F., Mohn, G., Martos, R., Roca, E., & Blanpied, C. (2016). Extensional vs contractional Cenozoic deformation in Ibiza (Balearic Promontory, Spain): Integration in the West Mediterranean back-arc setting. *Tectonophysics*, 682, 35-55.
- Garcia, M., Maillard, A., Aslanian, D., Rabineau, M., Alonso, B., Gorini, C., & Estrada, F. (2011). The Catalan margin during the Messinian Salinity Crisis: Physiography, morphology and sedimentary record. *Marine Geology*, 284(1-4), 158-174.
- Geletti, R., Zgur, F., Del Ben, A., Buriola, F., Fais, S., Fedi, M., Forte E., Mocnik A., Paoletti V., Pipan M., Ramella R., Romeo R., & Romi, A. (2014). The Messinian Salinity Crisis: new seismic evidence in the West-Sardinian Margin and Eastern Sardo-Provençal Basin (West Mediterranean Sea). *Marine Geology*, 351, 76-90.
- Gorini C. (1993) Géodynamique d'une marge passive: le Golfe du Lion (Méditerranée Occidentale). Doctorat, Université Paul Sabatier, Toulouse, 256 pp.
- Gorini, C., Montadert, L., & Rabineau, M. (2015). New imaging of the salinity crisis: Dual Messinian lowstand megasequences recorded in the deep basin of both the eastern and western Mediterranean. *Marine and Petroleum Geology*, 66, 278-294.

- Krijgsman, W., Hilgen, F. J., Raffi, I., Sierro, F. J., & Wilson, D. S. (1999a). Chronology, causes and progression of the Messinian salinity crisis. *Nature*, 400(6745), 652-655.
- Leroux, E. (2012). Quantification des flux sédimentaires et de la subsidence du bassin Provençal (Doctoral dissertation, Université de Bretagne occidentale-Brest). <https://tel.archives-ouvertes.fr/tel-00790852>
- Leroux, E., Aslanian, D., Rabineau, M., Gorini, C., Rubino, J.-L., Poort, J., Suc, J.-P., Bache, F. and Blanpied, C., et al. (2019). Atlas of the stratigraphic markers in the western mediterranean with focus on the Messinian, Pliocene and Pleistocene of the Gulf of Lion. CGMW (Commision for the Geological Map of the World) editor, 73p + CD.
- Leroux, E., Rabineau, M., Aslanian, D., Gorini, C., Molliex, S., Bache, F., Robin C., Droz L., Moulin M., Poort J., Rubino J.P., & Suc, J. P. (2017). High-resolution evolution of terrigenous sediment yields in the Provence Basin during the last 6 Ma: relation with climate and tectonics. *Basin Research*, 29(3), 305-339.
- Lofi, J. (2002). La crise de salinité messinienne: conséquences directes et différées sur l'évolution sédimentaire de la marge du Golfe du Lion. Diss. Lille 1. www.theses.fr/2002LIL10034
- Lofi J., Déverchère, J., Gaullier, V., Gillet, H., Gorini, C., Guennoc, P., Loncke, L., Maillard, A., Sage, F., Thion, I., (2011a). Seismic atlas of the “messinian salinity crisis” markers in the mediterranean and black seas. *Comm. Geol. Map World Mem. SoC. Géol. de France, Nouvelle Sér.* 72.
- Lofi, J. (2018). Seismic Atlas of the Messinian Salinity Crisis markers in the Mediterranean Sea-Volume 2 (Vol. 181, pp. 1-72). Société Géologique de France.
- Maillard, A. (1993). Structure et riftogénèse du golf de Valence (Méditerranée Occidentale) (Doctoral dissertation, Atelier national de reproduction des thèses).
- Mauffret, A., 1976, Étude géodynamique de la marge des îles Baléares (Thèse d'État thesis), Univ. Paris VI.
- Pellen, R. (2016). Géodynamique et impact de la crise d'érosion et de salinité Messinienne sur les transferts sédimentaires (bassins de Valence et Adriatique) (Doctoral dissertation, Université Bretagne Loire). <https://tel.archives-ouvertes.fr/tel-01651341>
- Pellen, R., Aslanian, D., Rabineau, M., Leroux, E., Gorini, C., Silenziario, C., Blanpied C., & Rubino, J. L. (2016). The Minorca Basin: a buffer zone between the Valencia and Liguro-Provençal Basins (NW Mediterranean Sea). *Terra Nova*, 28(4), 245-256.

- Pellen, R., Aslanian, D., Rabineau, M., Suc, J. P., Gorini, C., Leroux, E., Blanpied, C., Silenziario, C., Popescu, S.M. & Rubino, J. L. (2019). The Messinian Ebro River incision. *Global and Planetary Change*, 181, 102988.
- Raad, F., Lofi, J., Maillard, A., Tzevahirtzian, A., & Caruso, A. (2021). The Messinian Salinity Crisis deposits in the Balearic Promontory: an undeformed analog of the MSC Sicilian basins? *Marine and Petroleum Geology*, 124, 104777.
- Rabineau, M. (2001). Un modèle géométrique et stratigraphique des séquences de dépôts quaternaires sur la marge du Golfe du Lion: enregistrement des cycles climatiques de 100 000 ans (Doctoral dissertation, Université de Rennes1). <https://tel.archives-ouvertes.fr/tel-00136517>
- Rabineau, M., Cloetingh S., Kuroda J., Aslanian D., Droxler A., Gorini C., Garcia-Castellanos D., Nolet G., Moscariello A., Hello Y., Burov E., Sierro F., Lirer F., Roure F., Pezard P., Mart Y., Camerlenghi A., and the GOLD and DREAM Working Groups, Probing connections between deep earth and surface processes in a land-locked ocean basin transformed into a giant saline basin: the Mediterranean DREAM-GOLD project, *Marine & Petroleum Geology*, Special Vol. , 2015.
- SIGEOF – Sistema de Informacion Geofisica IGME https://info.igme.es/sigeof/default.html?ambito=BD_GEOF_SIS_SEGY
- VIDEPI Project <https://www.videpi.com/videpi/videpi.asp>
- Wessel, P., & Smith, W. H. (1995). New version of the generic mapping tools. *Eos, Transactions American Geophysical Union*, 76(33), 329-329.

Annex C

Mapping in the Western Mediterranean

In this annex I briefly present the results of a mapping campaign that I initiated in the Western Mediterranean area in collaboration with colleagues from the University of Lille and from Ifremer institute. We put together the interpretation of the key horizons in the area, deriving from a widespread seismic dataset that each of the participants worked on. In addition, I digitalized and added to this compilation some maps published in literature by Leroux et al. (2019).

The overall horizons put together are shown below in Figure 1. Note that this is still a preliminary work that I would like to develop and improve by bringing more data and interpretation. The ideal objective would be to put available in open access the interpretation of the key horizons in the whole Western Mediterranean area and, why not one day, the Eastern Mediterranean.

Data courtesy to:

- Shaza Haidar and Jacques Déverchère for the seismic interpretation in the eastern Algerian Basin
- Gaia Travan and Virginie Gaullier for the seismic interpretation in the central Algerian Basin on the African margin
- Agnes Maillard for the seismic interpretation in the Valencia, Provencal and Algerian Basin

The data on the Balearic Promontory derives from the interpretation done during my thesis. I also re-interpreted some re-processed old industrial seismic dataset (see chapter 3, section 3.1.1.1) in most of the Western Mediterranean area. The data shown in the Gulf of Lions and in the Alboran Basin are taken from the published Atlas of Leroux et al. (2019). For the mapping of the bathymetry (Figure 2), I integrated the EMODNET dataset (www.emodnet-bathymetry.eu) to the overall compilation.

All maps will be presented in time. The depth in meters of the horizons is not yet calculated at this point of the work.

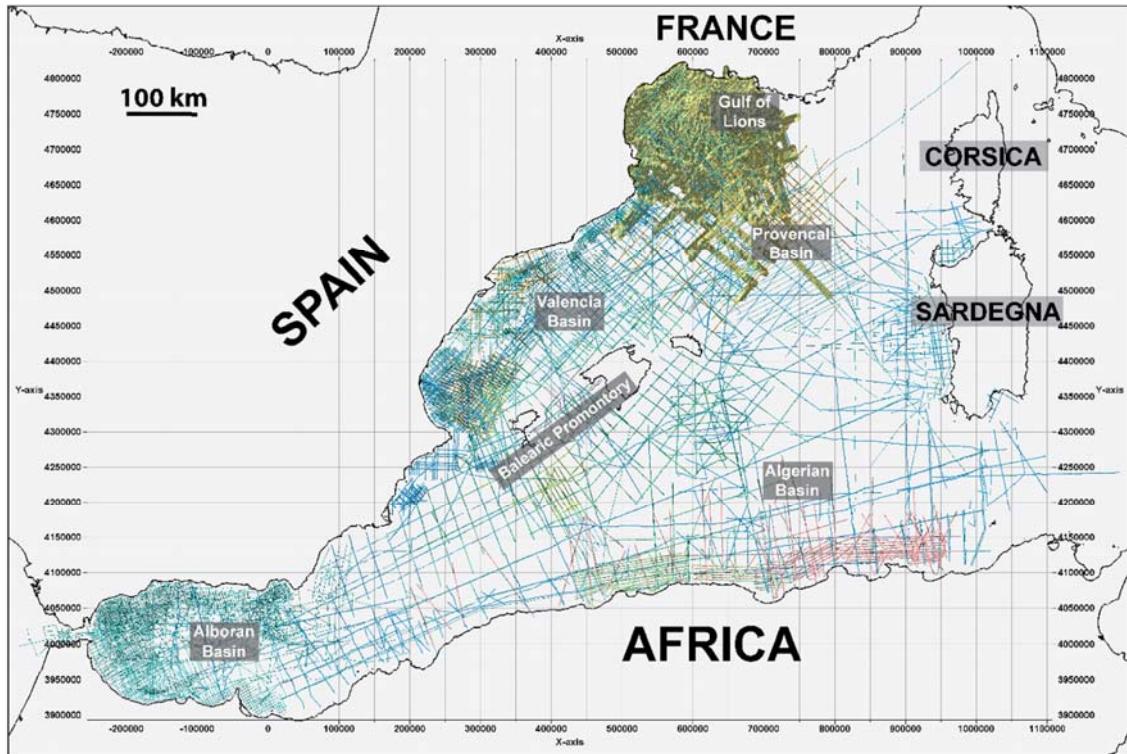


Figure 1. Location of the seismic-derived horizons used in the compilation for the mapping project.

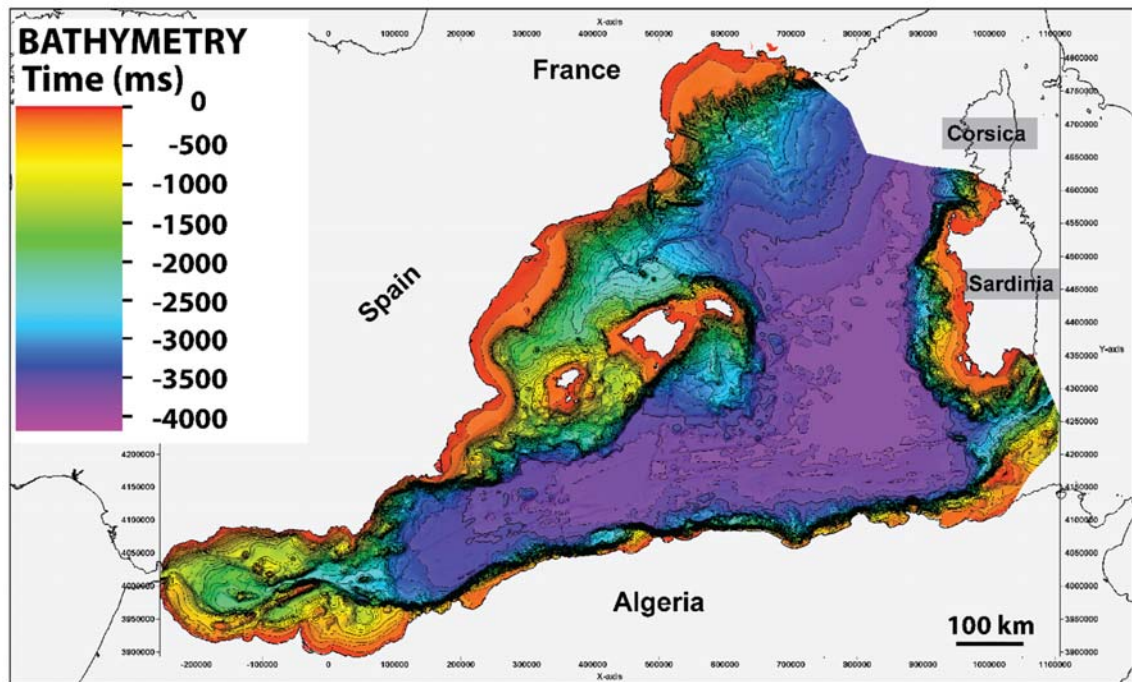


Figure 2. Bathymetric map (in time) of the Western Mediterranean derived from the interpolation of the data shown in Figure 1, integrated with the EMODNET dataset available online (www.emodnet-bathymetry.eu).

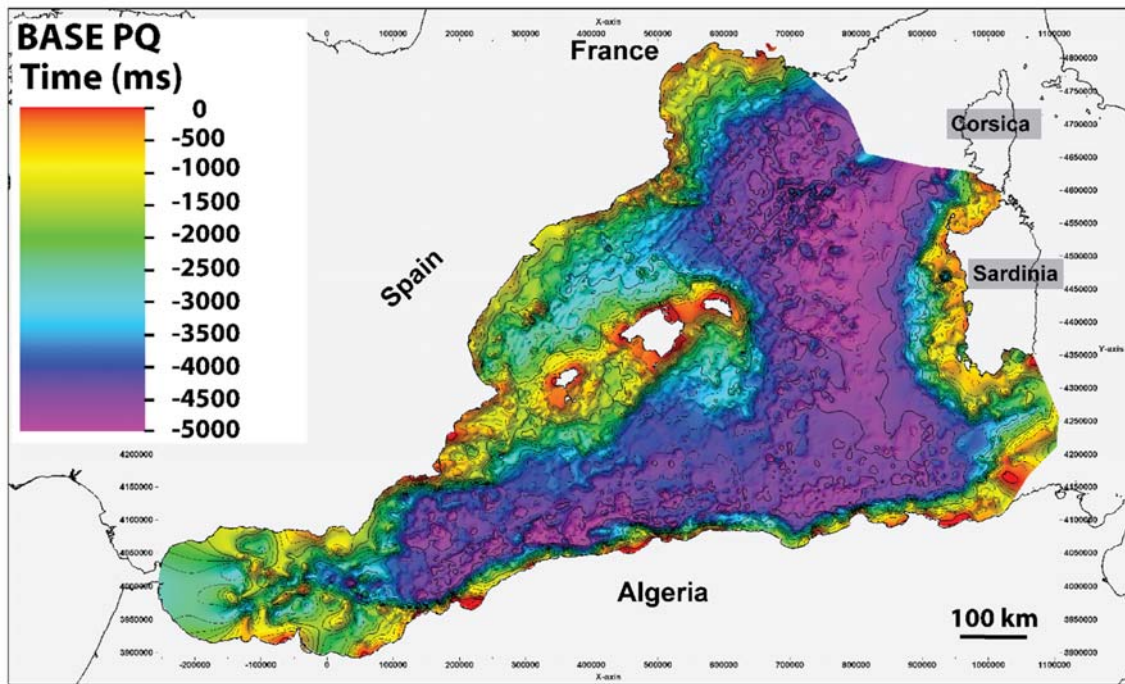


Figure 3. Depth (in time) of the base PQ unit. The data in the west Alboran Basin is still not integrated and included in the mapping at the time of creation of the maps.

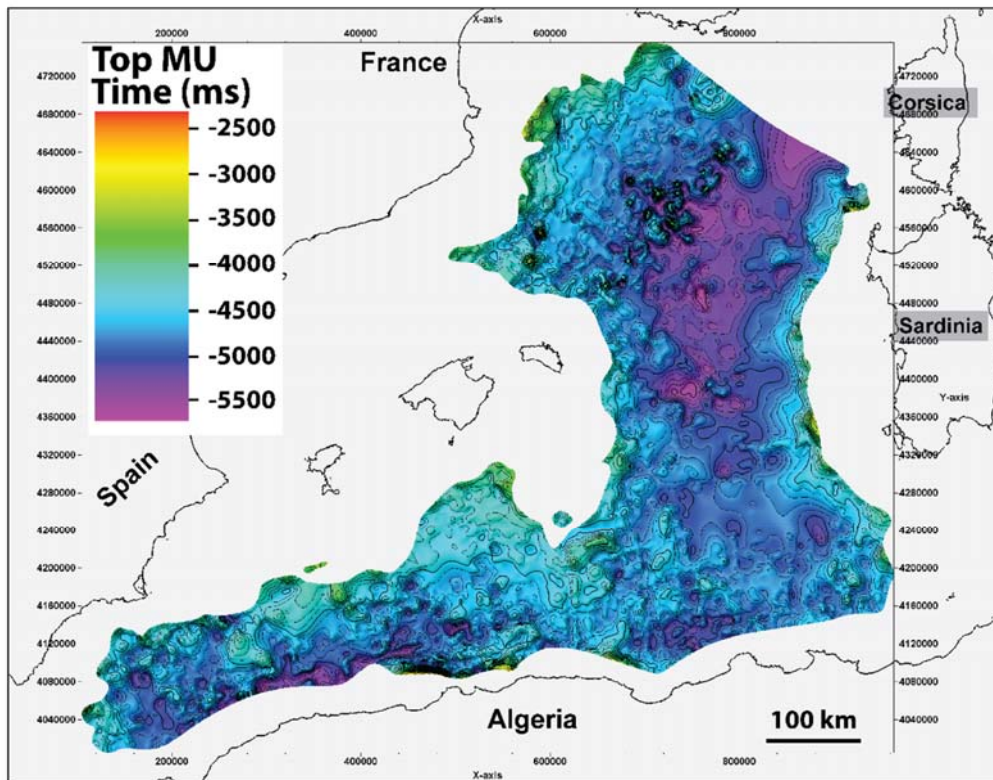


Figure 4. Depth (in time) of the top of the MSC salt unit, also known as Mobile Unit. The high irregularity of the surface is due to the salt tectonics.

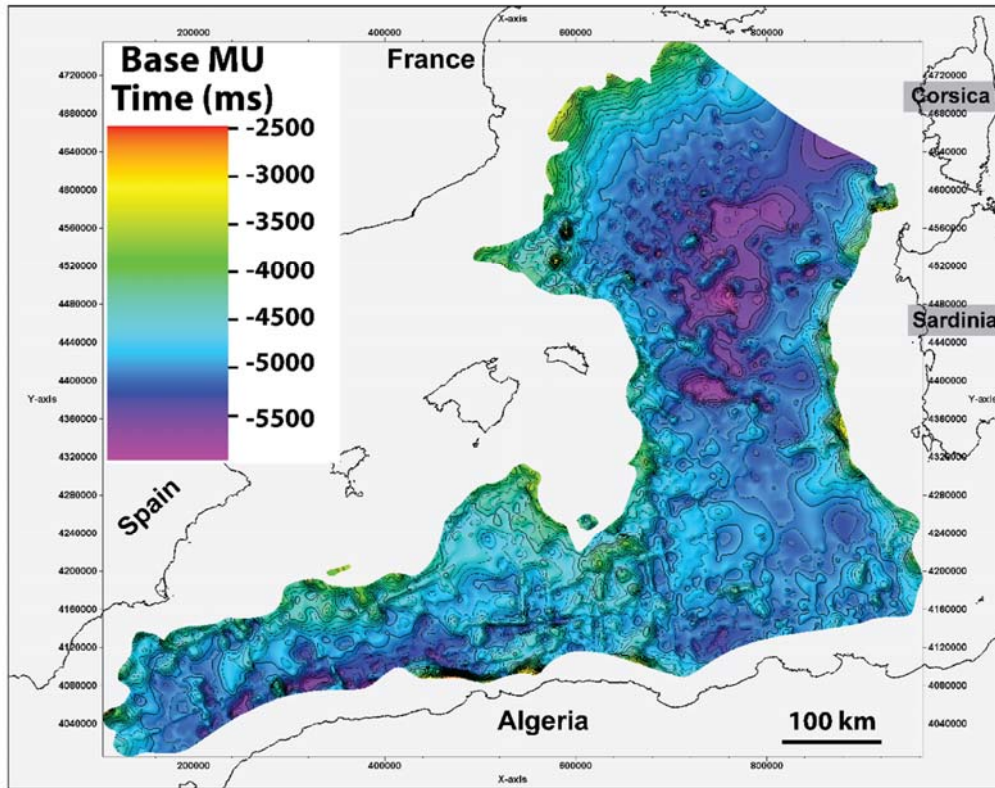


Figure 5. Depth (in time) of the base of the MSC salt unit, also known as Mobile Unit. Note how the base salt is more regular than the top salt horizon shown in Figure 4.

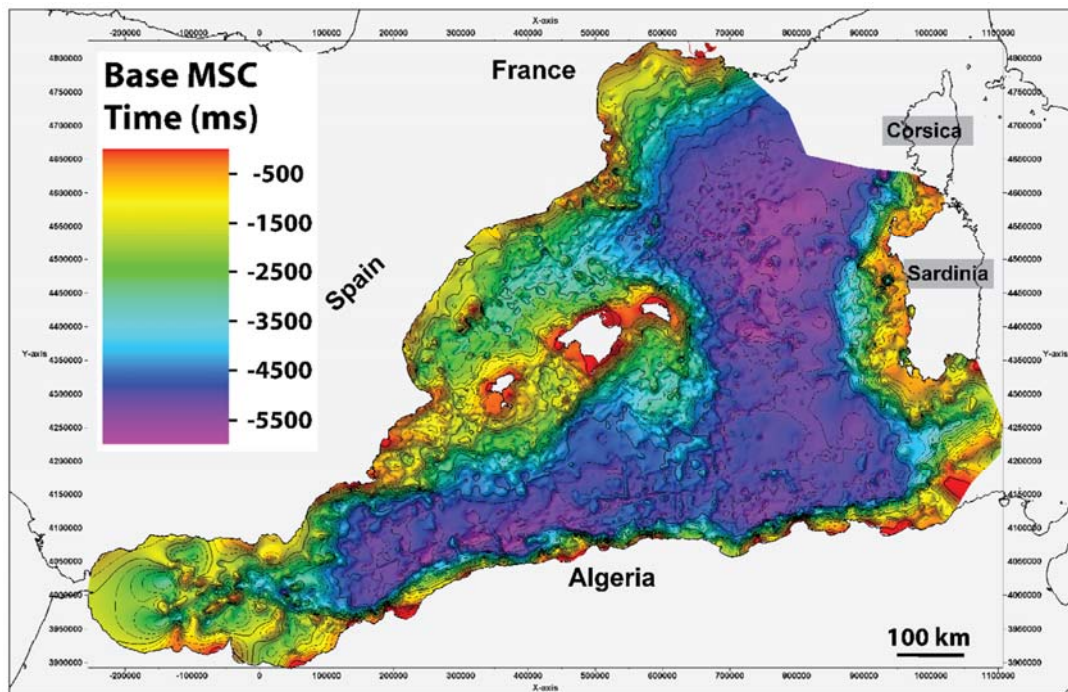


Figure 6. Depth (in time) of the base MSC horizon. In the deep basin, the horizon corresponds to the base of the Mobile Unit; in the intermediate basins it corresponds to the base of the Upper Unit or the Bedded Unit; on the slopes and margins it corresponds to the Messinian Erosion Surface.

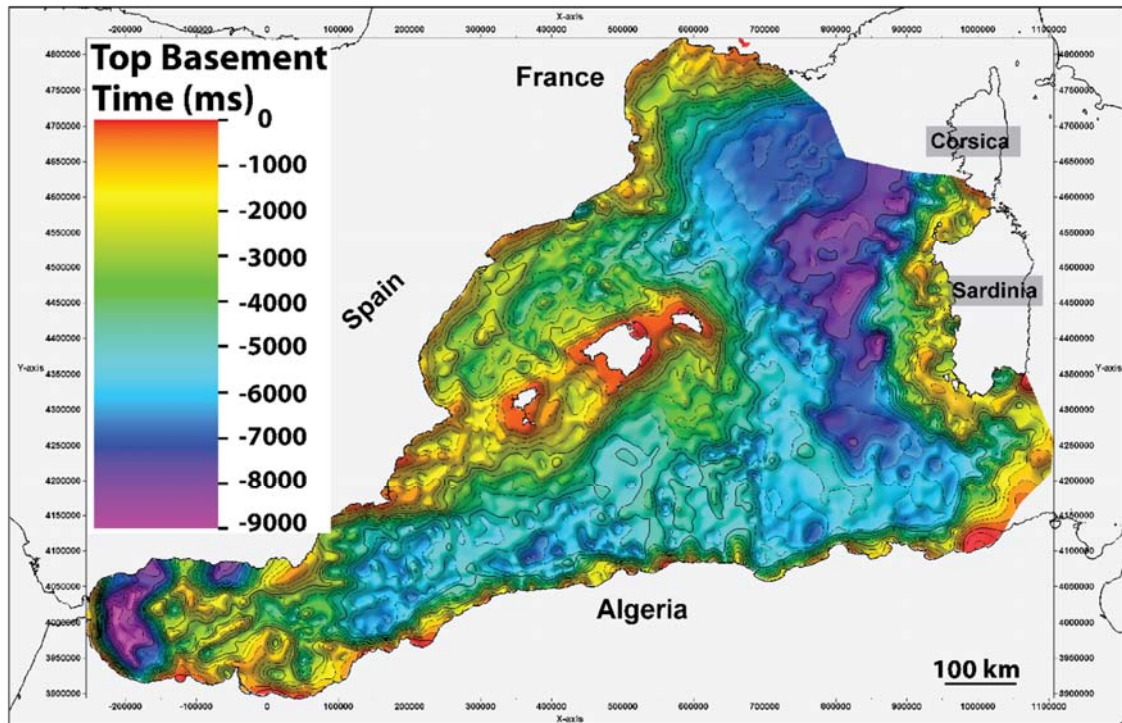


Figure 7. Depth (in time) of the top of the acoustic basement. The irregular morphology on the west Sardinia margin is due to artefacts in the provided dataset and needs to be revised.